New polymer-ruthenium cyclopentadienyl-porphyrin conjugates for photodynamic therapy of cancer

Adhan Pilon[1], José Almeida[2], Maria Rangel[3], Ana M. G. Silva[2], M. Helena Garcia [1], Andreia Valente [1]

[1] Centro de Química Estrutural, Faculdade de Ciências da Universidade de Lisboa, Campo Grande, 1749-016 Lisboa, Portugal.

[2] LAQV/REQUIMTE, Departamento de Química e Bioquímica da Faculdade de Ciências da Universidade do Porto, 4169-016 Porto, Portugal.

[3] LAQV/REQUIMTE, Instituto de Ciências Biomédicas de Abel Salazar, Universidade do Porto, 4050-313 Porto, Portugal

INTRODUCTION

During the last years, our group has developed new ruthenium(II) complexes with potential application in cancer chemotherapy.[1] In this presentation we will disclose our recent advances in a novel family of compounds with the core **[$Ru^{II}(\eta^5\text{-}C_5H_5)(CO)(bipy)$]** where bipy is a bipyridine containing two **polymeric chains** chain end functionalized with a **porphyrin** for application in photodynamic therapy of cancer. Photodynamic therapy is an alternative therapy for the treatment of cancer, based on the interaction between a photosensitizing (PS), light and oxygen, which when reacted form reactive oxygen species (ROS), such as singlet oxygen, leading to cell death.

SYNTHESIS AND CHARACTERIZATION

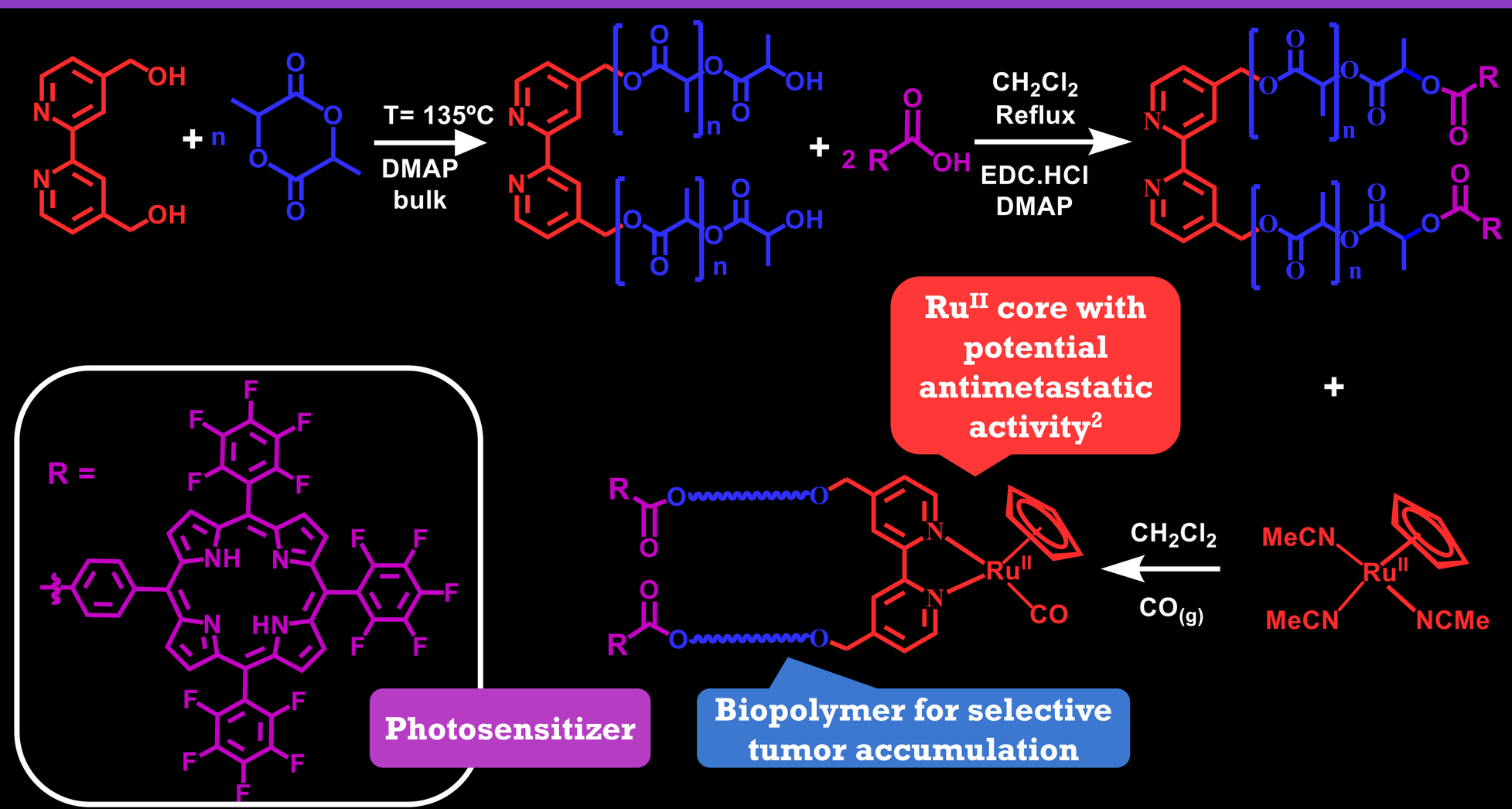

Figure 1. Reaction scheme for the synthesis at the new polymer-ruthenium cyclopentadienyl-porphyrin conjugate.

SINGLET OXYGEN GENERATION

Figure 2. Graphic showing the $^1O_2$ formation over time.

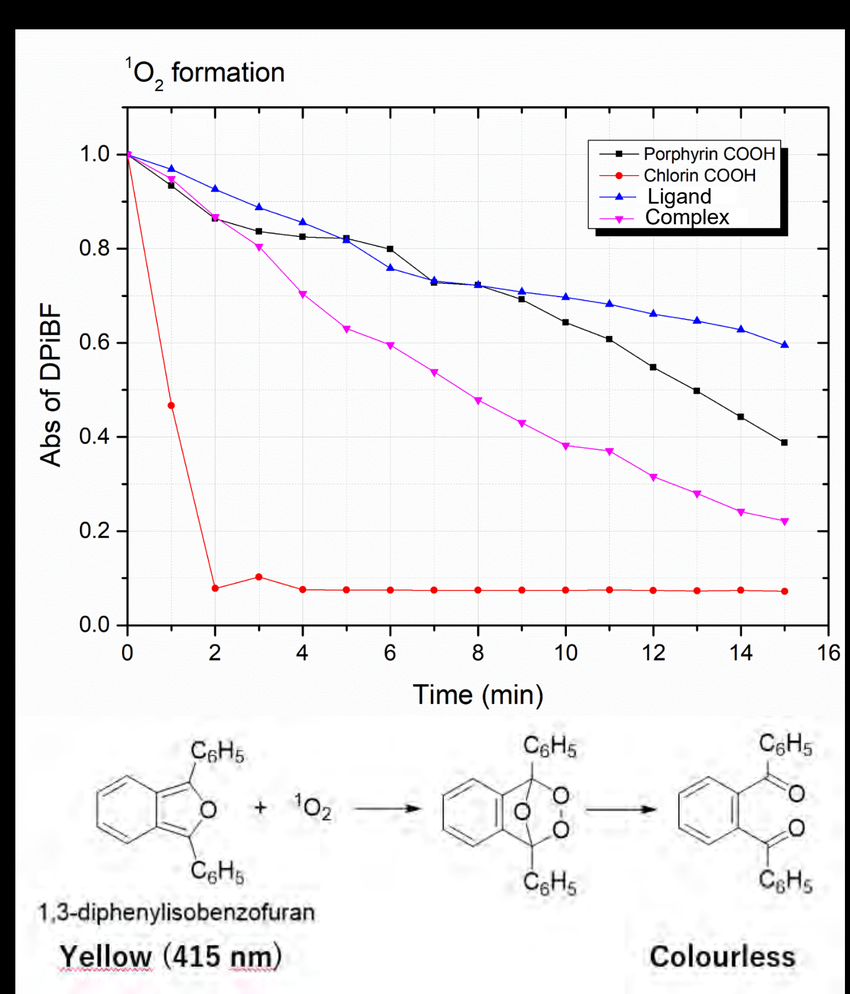

The $^1O_2$ formation for the new polymer-Ru^{II} cyclopentadienyl-porphyrin conjugate surpassed porphyrin.

PHOTOPHYSICAL STUDIES

Figure 3. Spectrum of absorbance and fluorescence of macromolecular ligand and complex

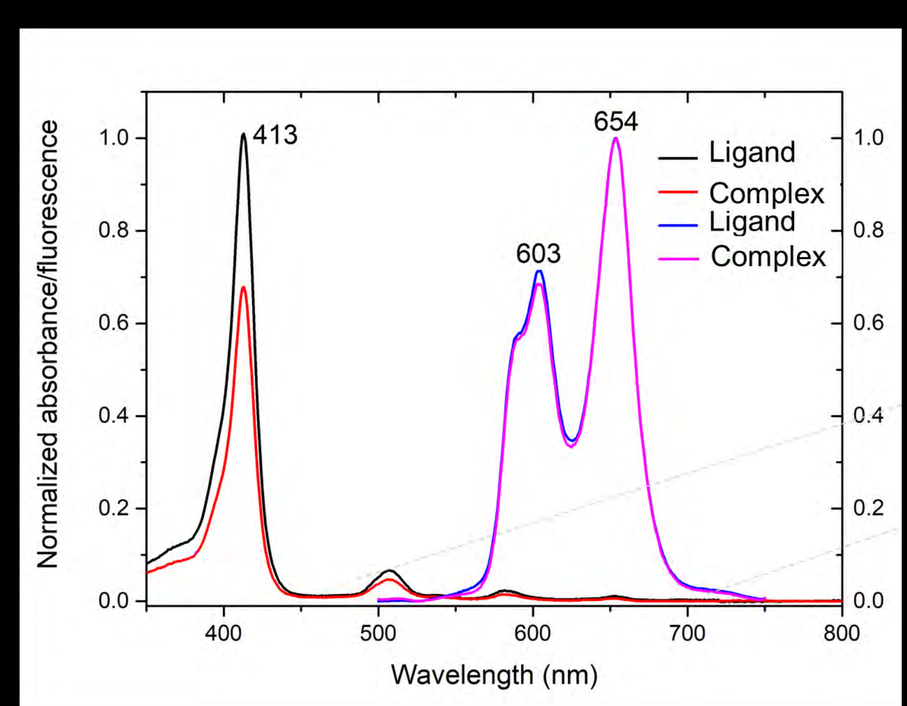

Absorbance in the therapeutic window.

CONCLUSIONS

It was possible to synthesize and purify a high molecular weight complex containing a core with **antimetastatic properties[2]**, a **Biopolymer** and a **photosensitizer** with adequate photochemical properties.

Funding:
Centro de Química Estrutural is funded by Fundação para a Ciência e Tecnologia (FCT) – project UID/QUI/00100/2019. This work was also financed by FCT within the scope of the project PTDC/QUI-QIN/28662/2017.

References:

[1] T. S. Morais, A. Valente, A. I. Tomaz, F. Marques, M. H. Garcia, Future Med. Chem. 2016, 8, 527-544.

[2] N. Mendes, F. Tortosa, A. Valente, F. Marques, A. Matos, T. S. Morais, A. I. Tomaz, F. Gärtner, M. H. Garcia, Anti-cancer Agents in Med. Chem. 2017, 17, 126-136.

IDENTIFICATION OF **TOXIC** COMPOUNDS USED TO **KILL** DOMESTIC ANIMALS IN FORENSIC CONTEXT

Ana Patrícia Abreu,[1] Andrea Alexandre,[2] Maria João Caldeira,[2] Alexandra M. M. Antunes[1]

[1]Centro de Química Estrutural (CQE), Instituto Superior Técnico (IST), ULisboa, Avenida Rovisco Pais, 1049-001 Lisboa
[2]Laboratório de Polícia Científica da Polícia Judiciária (LPC/PJ), Novo edifício Sede da Polícia Judiciária, Rua Gomes Freire 1169-007 Lisboa

TÉCNICO LISBOA

CQE Química Estrutural

05 BIOMOL

POLICIA JUDICIÁRIA

INTRODUCTION

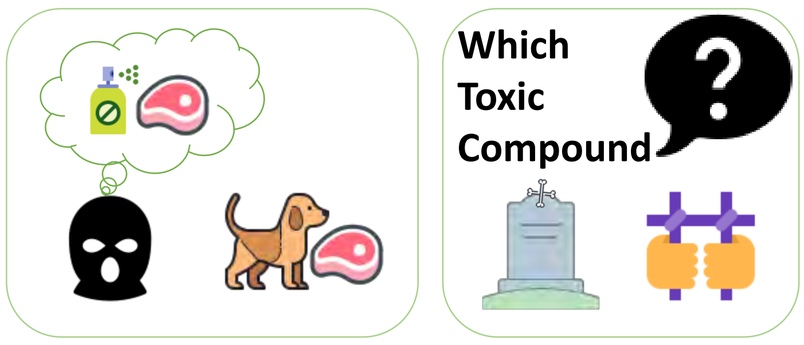

Killing animals by poisoning, is unfortunately a frequent criminal behavior. However, most of these criminal offenses are not conveniently penalized due to the unavailability of standard methodologies for the identification of chemical compounds suspected to have caused the intoxication.

OBJECTIVES

Using high resolution mass spectrometry (HRMS)-based methodologies, this work has as objective the identification of the poisoning substance in material collected from poisoned baits found in public places.

METODOLOGY

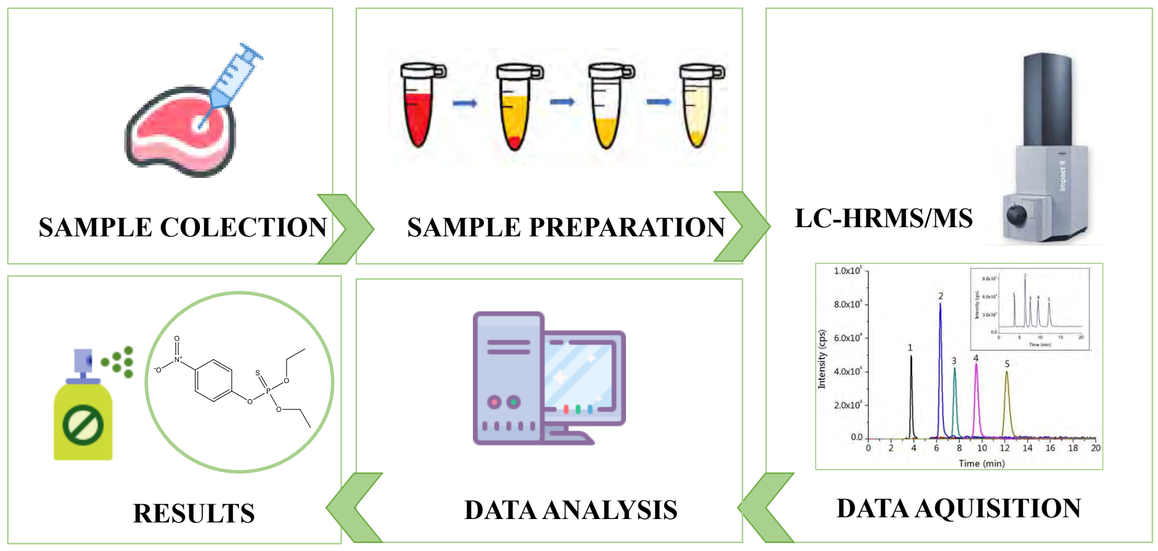

RESULTS

CASE STUDY 1 . RESIDUES FOUND IN A DOG BOWL

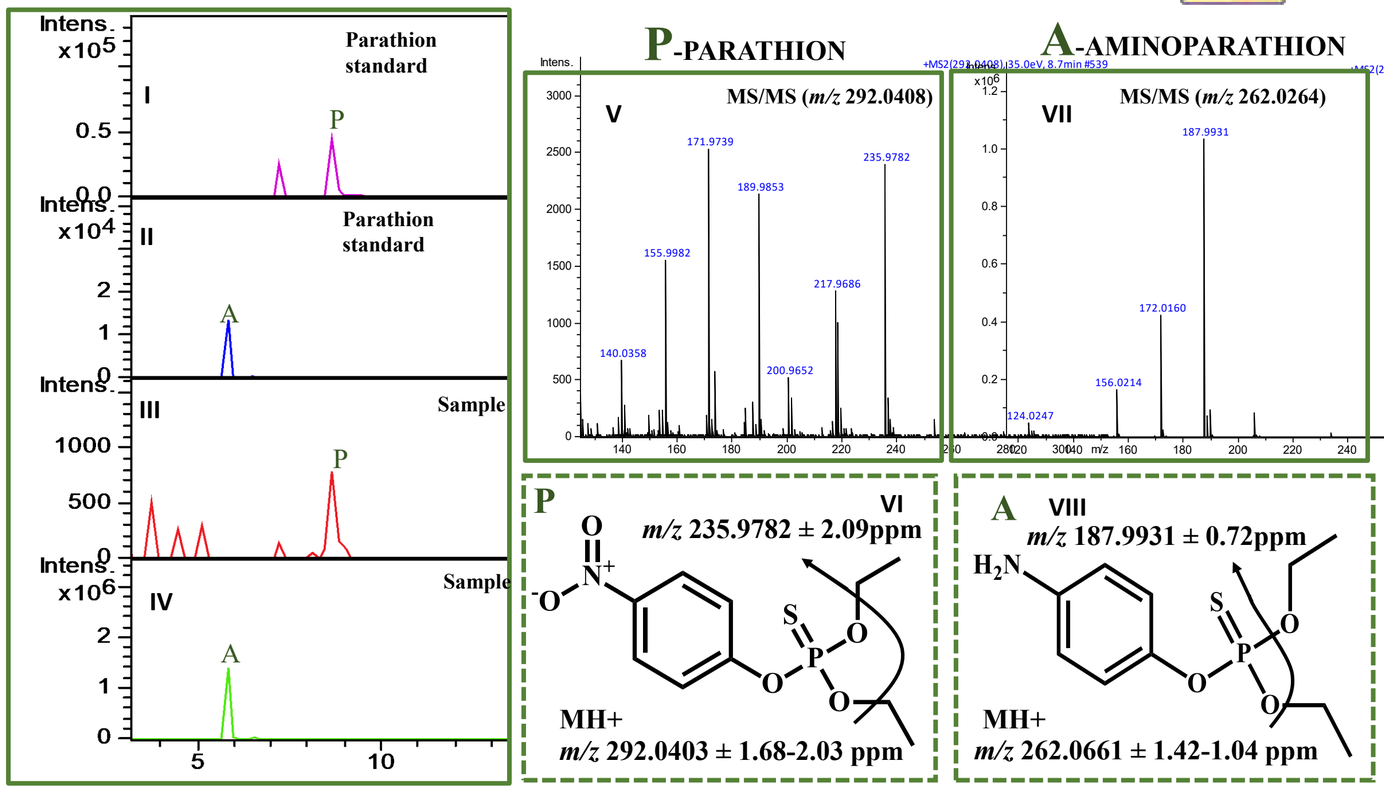

Figure 1: **I**) Extracted ion chromatogram at *m/z* 292.0403 of parathion standard; **II)** Extracted ion chromatogram at *m/z* 262.0661 of parathion standard, corresponding to the protonated molecule of aminoparathion; **II**) Extracted ion chromatogram at *m/z* 292.0403 obtained for the sample; **IV)** Extracted ion chromatogramat *m/z* 262.0661 obtained for the sample; **V)** Tandem mass spectrum of the protonated molecule of parathion; **VI)** Parathion structure, showing one of the fragment ions obtained; **VII)** Tandem mass spectrum obtained for the protonated molecule of aminoparathion; **VIII)** Structure of aminoparathion, showing one of the fragment ions obtained.

The identification of parathion and its metabolite amino-parathion in a forensic sample was based on identical Tr and tandem mass spectrum obtained for the sample and parathion standard.

Although parathion sale is currently forbidden, it continues to be widely used for criminal purposes.

CASE STUDY 2 . A MEAT BAIT FOUND IN A BACKYARD

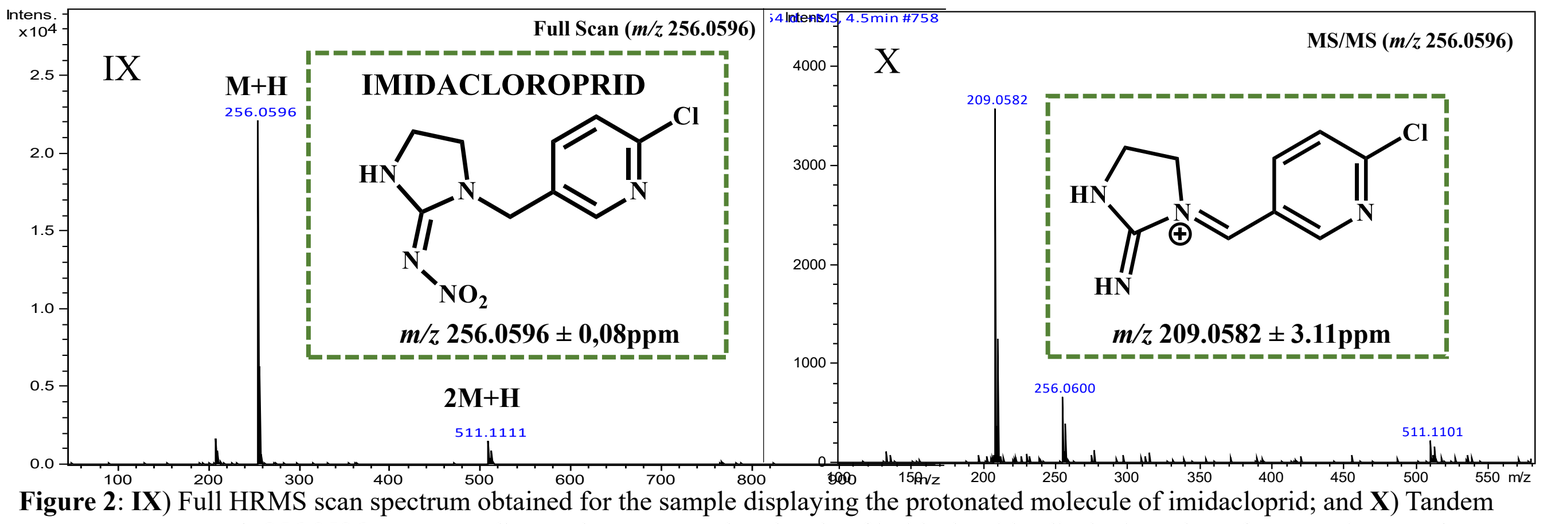

Figure 2: **IX**) Full HRMS scan spectrum obtained for the sample displaying the protonated molecule of imidacloprid; and **X**) Tandem mass spectrum at m/z 256.0596, corresponding to the protonated molecule of imidaclopride, displaying a base fragment ion at *m/z* 209.0582 ± 3.11ppm.

The identification of the insecticide imidacloprid in this sample was possible based on the accuracy obtained for the protonated molecule and fragment ions obtained in the HRMS full scan and MS/MS spectra, respectively.

CONCLUSION

Poisoning episodes of domestic animals present a major investigational problem for toxicologists and forensic laboratories. Accidental toxic disasters are difficult to prevent and control, but of greater concern are cases of illegal and deliberated use of poisons.

Funding:
Centro de Química Estrutural is funded by Fundação para a Ciência e Tecnologia – project UID/QUI/00100/2019.

FCT Fundação para a Ciência e a Tecnologia

Synthesis and characterization of rGO/M 2wt%-N co-doped (M=Co, Fe, Mn, Ni, Cu and Rh) as abiotic electrocatalyst for oxygen reduction reaction

Alves A. C.[1], Correia J. P[1], Dubois L.[2], Zebda A.[3]

[1] Grupo de Eletroquímica Interfacial, Centro de Química e Bioquímica, Centro de Química Estrutural, Faculdade de Ciências da Universidade de Lisboa, Campo Grande 016, 1749-016 Lisboa, Portugal; [2] Université Grenoble Alpes, CEA, CNRS, INAC, Grenoble 38000, France; [3] UGA-Grenoble 1/CNRS/INSERM/TIMC-IMAG UMR 2252, Grenoble, 38000, France.

Background and Introduction

The development of **new** and **non-precious metal electrocatalyst** based on transition metals for the oxygen reduction reaction (ORR) is the key to improve the energy conversion technology.

Strategy:

Increase the catalytic sites by an atom dispersion over a conductive and large surface area.

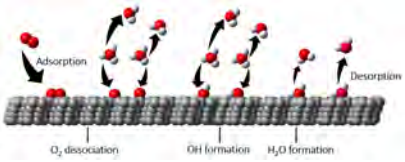

Main goals:

Synthesis of a 2 wt% single-atom transition metal catalyst supported in nitrogen-reduced graphene oxide;

Electrochemical evaluation of ORR by linear sweep voltammetry (LSV) with a rotating disc electrode in PBS pH 7.4 and 0.1 KOH solutions.

Methods

Extra exfoliation of graphene

Incorporation of defects

Co-doping with N and metal

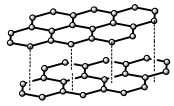

(i) Exfoliation of graphene
(ii) Incorporation of metals
(iii) Insertion of nitrogen

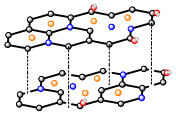

Physical Characterization by

XPS
Raman
AFM

Electroreduction of oxygen, evaluated by LSV with a glassy carbon rotating disc electrode in PBS pH 7.4 and 0.1 M KOH pH 13 solutions (10 mV/s, 400 to 2400 rpms).

Electrocatalysts & Oxygen Reduction Reaction – Discussion and results

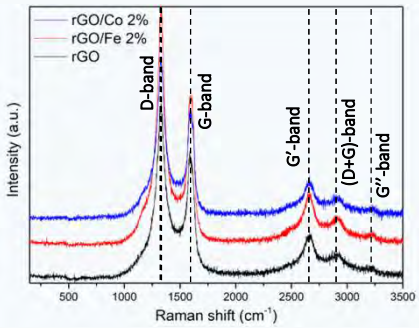

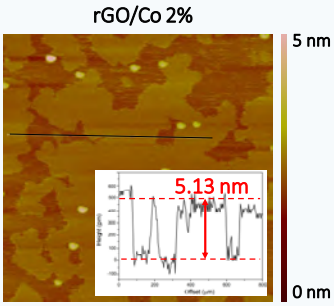

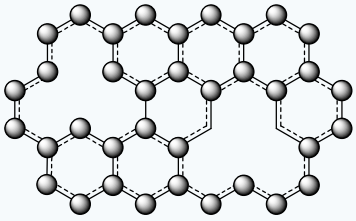

Raman spectra of rGO and its derivates and AFM measurements confirm the **incorporation of defects** in the graphene structure.

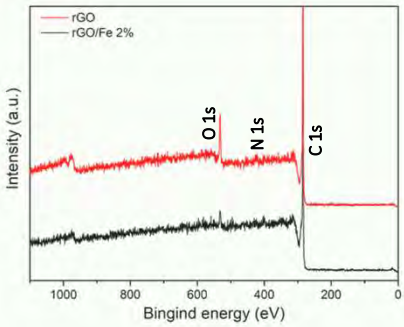

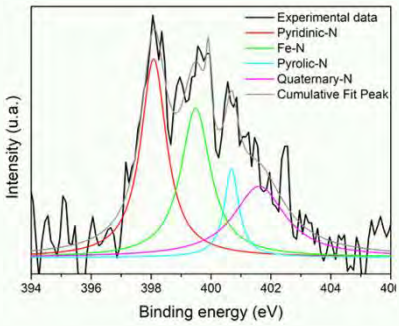

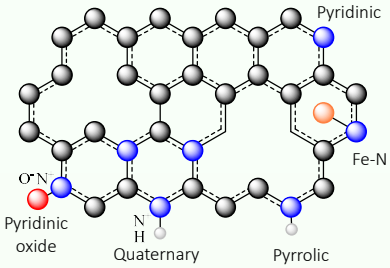

XPS general spectrum and high-resolution N 1s core level spectrum of rGO/Fe 2% show the **co-doping with nitrogen** and **metal**.

PBS pH 7.4 and 1600 rpms

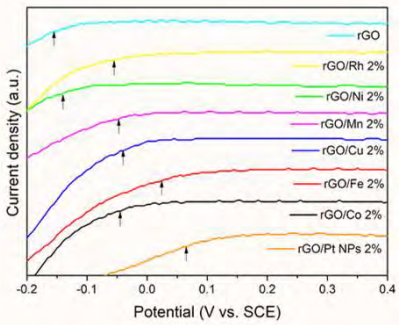

Catalyst	E_{onset}/ V	$E_{1/2}$/ V	J_{lim} /mA cm^{-2}	Nr of e$^-$
rGO/Fe 2%	0.025	-0.022	-0.7334	3.17
rGO/Co 2%	-0.045	-0.190	-0.5704	2.69
rGO/Mn 2%	-0.050	-0.335	-0.5602	3.74
rGO/Cu 2%	-0.040	-0.215	-0.8047	2.66
rGO/Ni 2%	-0.140	-0.310	-0.6672	2.78
rGO/Rh 2%*	-0.055	-0.260	-0.6570	2.58
rGO	-0.155	-0.385	-0.7283	-
rGO/Pt NPs 2%*	0.065	-0.230	-0.7996	1.60

0.1M KOH rGO/Co 2%

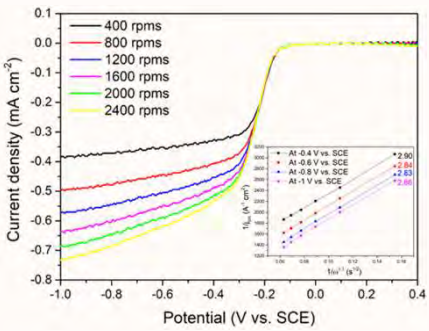

Current & Future work

- Incorporation of porphyrins in the rGO structure and its electrochemical and physical characterization.
- Synthesis of new electrocatalyst with 10% wt (or more!) of transition metal and their characterization by AFM, Raman, XPS and ICP.
- Electrochemical oxidation of glucose in both neutral and alkaline media in the presence of rGO/M 10%.

Funding:

Centro de Química Estrutural is funded by Fundação para a Ciência e Tecnologia – project UID/Multi/00612/2019.

References:

Jorio. A; Saito, R.; Dresselhaus, M.S.; Dresselhaus, G. *Raman spectroscopy in graphene related systems* (2011). Weinheim, Germany: Wiley-VCH, 3-13;

Ferrero, G.A.; Diez, N.; Sevilla, M.;Fuertes, A. B. *ACS Appl. Energy Mater.* (2018), *1(11)*, 6560-6568.

Ferrero, G.A.; Diez, N.; Sevilla, M.; Fuertes, A.B. *Microporous and Mesoporous Materials* (2019), *278*, 280-288

The influence of glaze on the tribological properties of zirconia dental pieces obtained by subtractive and additive manufacturing

BIOMAT RESEARCH GROUP

A.C. Branco[1], M. Polido[2], R.Colaço[2,3], C.G. Figueiredo-Pina[2,3,4], A.P. Serro[1,2]

[1] Centro de química estrutural, Instituto Superior Técnico, Universidade de Lisboa, Av. Rovisco Pais, 1049-001 Lisboa, Portugal;

[2] Centro de investigação Interdisciplinar Egas Moniz , Instituto Universitário Egas Moniz, Quinta da Granja, Monte de Caparica, 2829-511 Caparica, Portugal;

[3] IDMEC e Departamento de Engenharia Mecânica, Instituto Superior Técnico, Universidade de Lisboa, Av. Rovisco Pais, 1049-001 Lisboa, Portugal;

[4] Centro de Física e Engenharia de Materiais Avançados, Instituto Superior Técnico, Universidade de Lisboa, Av. Rovisco Pais, 1049-001 Lisboa, Portugal

CQE Química Estrutural

FCT Fundação para a Ciência e a Tecnologia

Background

- Ceramic based prosthetic materials are highly used for the repairing/replacing a damaged/missing tooth, due to their suitable mechanical and aesthetic properties, chemical stability and biocompatibility [1-3].
- Subtractive manufacturing (SM) is commonly used to obtain core pieces by removing surplus material from ceramic blocks.
- Robocasting is an Additive manufacturing (AM) technique that involves the production of 3D structures by depositing materials in a layer-by-layer manner based on a 3D model, with minimum materials' waste and production time relatively to the conventional manufacturing methods [4].
- Generally, ceramic restorations are coated with a ceramic glaze paste, which is applied over the surface in order to improve their aesthetic properties.

Subtractive Manufacturing vs **Additive Manufacturing**

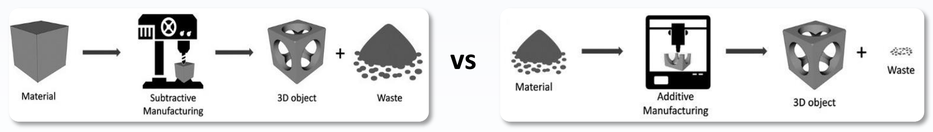

Objectives

- Evaluate the potential of an additive manufacturing (AM) technique (Robocasting) to produce reliable zirconia dental structures. AM samples properties are compared with those of SM samples.
- Study the influence of glazing on the tribological performance of the samples.

Materials and Methods

Materials

- SM samples were produced from Yttria (3% mol) - stabilized zirconia blocks Ice Zirkon Translucent [Zirkonzahn].
- AM samples were produced from a paste containing 350 g of ZrO_2 (yttria (3% mol)-stabilized zirconia powder Zpex [Tosoh]), 75.6 g of water, 8.75 g of corn syrup, 10.5 g of fructose, 0.84 g of Zusoplast C92, 0.105 g of Dolapix CE 64.

Methods

- Zirconia samples produced by both methods were sintered at 1500ºC, polished to obtain the same surface finishing and glazed.
- Density, porosity, Vickers hardness, toughness and roughness measurements were performed.
- Chewing simulation tests against dental human cusps were carried out in artificial saliva, before and after glazing.
- The counter-faces' wear was quantified and the wear mechanisms investigated.

Results and Discussion

Zirconia Samples Characterization

	SM	AM
Density (g/cm³)	6.06 ± 0.02	5.88 ± 0.10
Superficial porosity (%)	0.10 ± 0.03	3.92 ± 1.85
Hardness (HV)	1400 ± 16	1175 ± 29
Fracture toughness (MPa.m$^{1/2}$)	5.6 ± 0.6	4.5 ± 0.7
Linear roughness (nm)	243 ± 9	241 ± 16

Dental Cusps Wear Rate

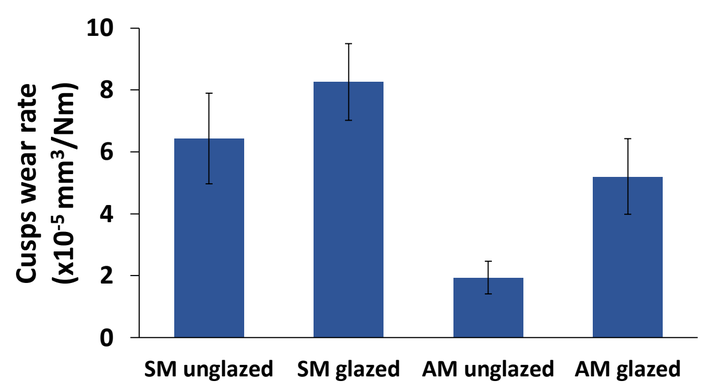

Dental Cusps after Wear Tests

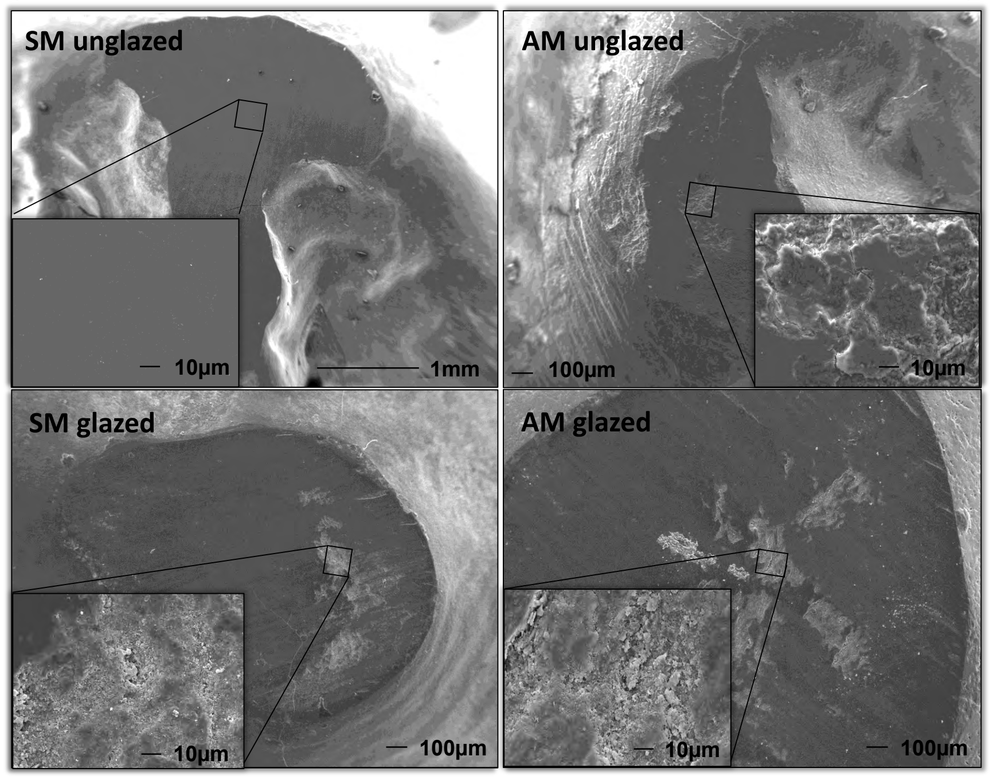

- SM unglazed cusps have a polished appearance without almost any signs of scratches
- AM unglazed cusps present some delamination and adhered dental particles
- SM/AM glazed cusps present scratches, delamination and adhered dental & glaze particles

Zirconia Unglazed Samples after Wear Tests

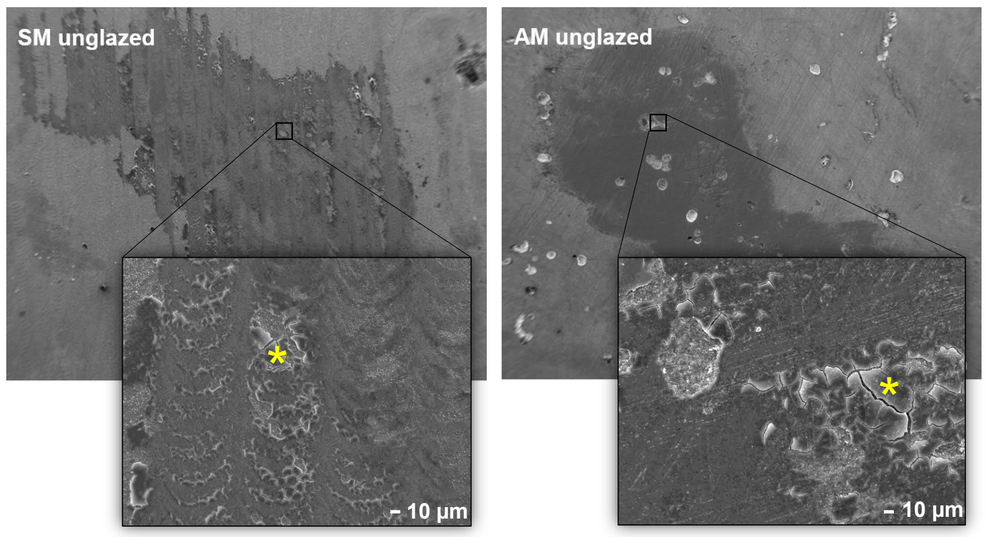

- Both SM and AM unglazed zirconia did not not suffer visible wear during chewing simulation
- SM unglazed zirconia presents a thick layer of adhered dental material over machining marks
- AM unglazed zirconia presents pores in which the worn dental particles preferentially adhered

Zirconia Glazed Samples after Wear Tests

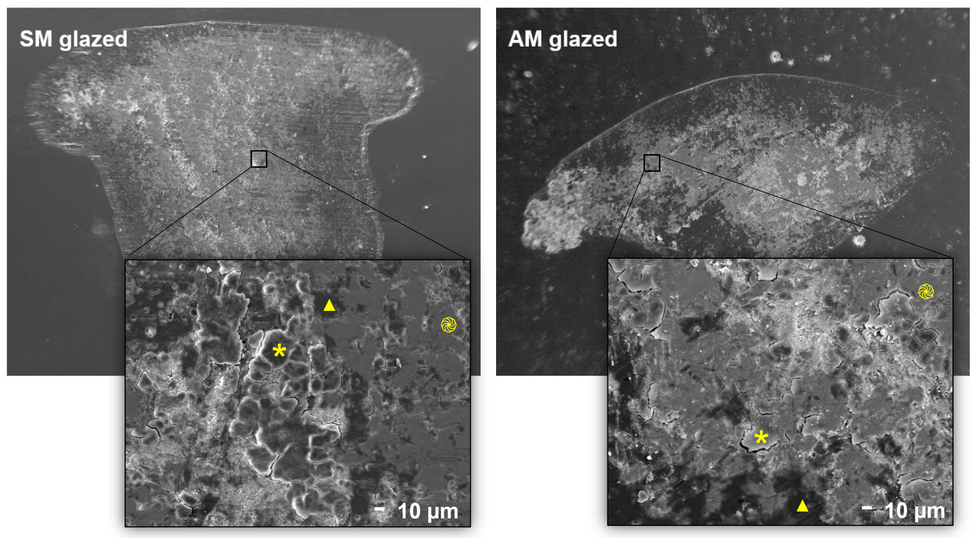

In both SM and AM glazed zirconia:

- Glaze suffered wear, leaving some zones of zirconia exposed
- Dental particles from the cusps wear adhered to zirconia/glaze
- Some parts of the glaze coating did not suffer wear

Zirconia
Dental Particles
Glaze

Conclusions

Additive manufacturing seems to be a promising technique to produce zirconia dental pieces.

Funding

Centro de Química Estrutural is funded by Fundação para a Ciência e Tecnologia – project UID/QUI/00100/2019.

To Fundação para a Ciência e Tecnologia for funding through Projects 3D-DentalPrint (02/SAICT/unit 2016/023940) and the projects UID/QUI/00100/2013, UID/BIM/04585/2016 and UID/EMS/50022/2019 (LAETA) from CQE, CiiEM and IDMEC respectively.

References

[1] Pollington S, Noort R Van. An update of ceramics in dentistry. J Clin Dent 2011.

[2] Denry I, Kelly JR. Emerging Ceramic-based Materials for Dentistry 2014.

[3] Hisbergues M, Vendeville S, Vendeville P. Zirconia: Established facts and perspectives for a biomaterial in dental implantology. J Biomed Mater Res - Part B Appl Biomater 2009;88:519–29.

[4] Galante R, Figueiredo-pina C.G., Serro A.P. Additive manufacturing of ceramics for dental applications: A review, Dent Mater 2019; 35:825-846.

Sustainable synthesis of important intermediates for the pharmaceutical industry from biomass resources

Fernandes A. C., Caetano J. A. T., Isca V. M. S.

The development of sustainable and green processes for the synthesis of pharmaceutical substances continues to be one of the main challenges for the pharmaceutical industry.
In this communication we present the one-pot conversion of carbohydrates into a variety of important intermediates for the pharmaceutical industry with good overall yields. [1-3]

Synthesis of 5-HMF

5-Hydroxymethylfurfural (5-HMF) is a sustainable and versatile precursor for the pharmaceutical industry and also for the petrochemical industry and biofuel chemistry. 5-HMF can be obtained selectively from fructose in 100% yield using $HReO_4$ as catalyst and DMSO as solvent.[1]

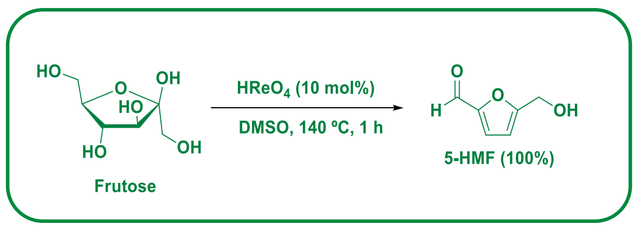

Synthesis of HMF from different carbohydrates

5-HMF was also obtained in 78% and in 66% yields from inulin and sucrose, respectively. In contrast, only 20% yield of 5-HMF was formed from glucose.

Synthesis of Levulinic Acid (LA)

LA is a useful precursor for the pharmaceutical industry, biofuel industry and food industry.
The reaction of fructose in 1,4-dioxane catalyzed by $HReO_4$ at 140 °C during 1 h gave LA with 100% yield.[1]

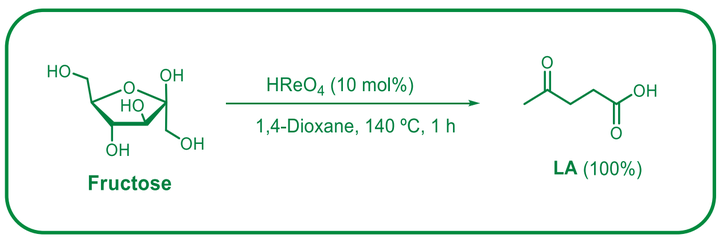

Synthesis of LA from different carbohydrates

LA can also be obtained in excellent yields from inulin (97%) and sucrose (85%) and in moderate yield (50%) from glucose.

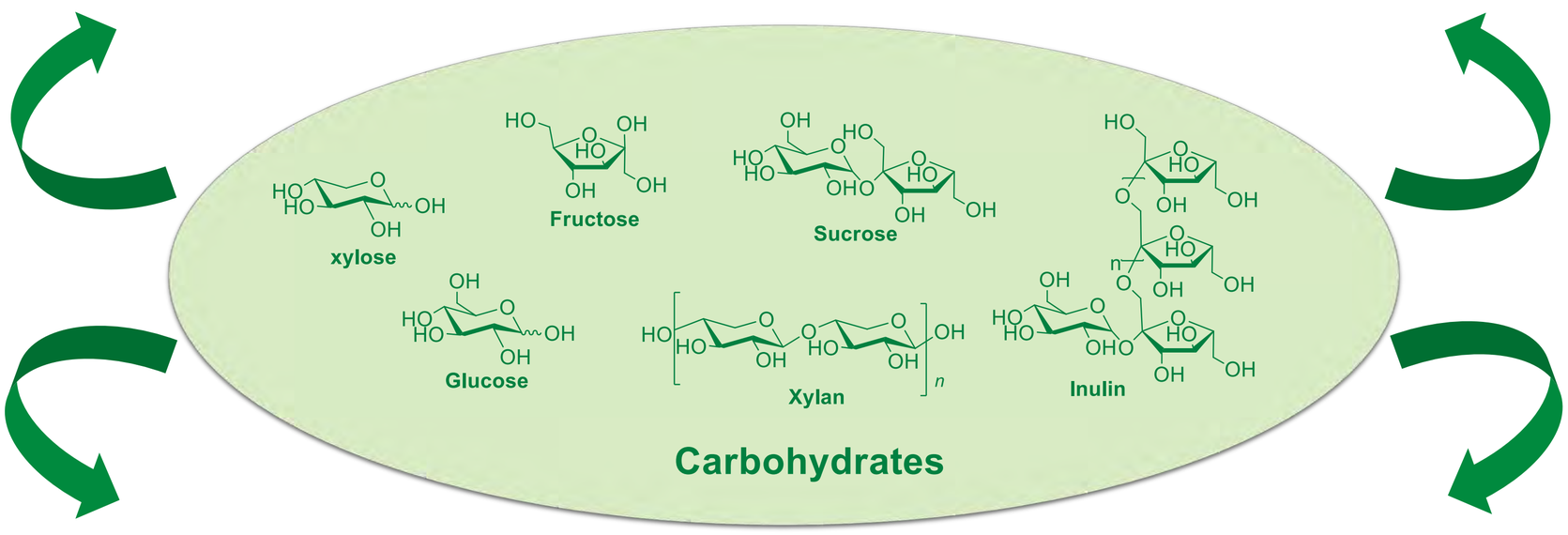

One-pot synthesis of amines from carbohydrates

Furfurylamines are important intermediates in the synthesis of pharmaceuticals such as antiseptic agents, antihypertensives and diuretics.
We developed a novel one-pot process for the synthesis of furfurylamines from carbohydrates. This chemical transformation involves three consecutive reactions, including the conversion of xylose to furfural, followed by *in situ* reaction of furfural with aniline to form the imine and the selective reduction of imine by the silane, giving the furfurylamines with moderate to good overall yields (55-80%).[2]

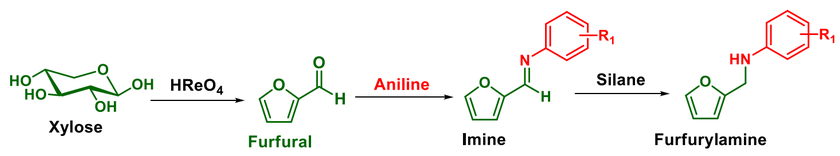

one-pot three-reaction process

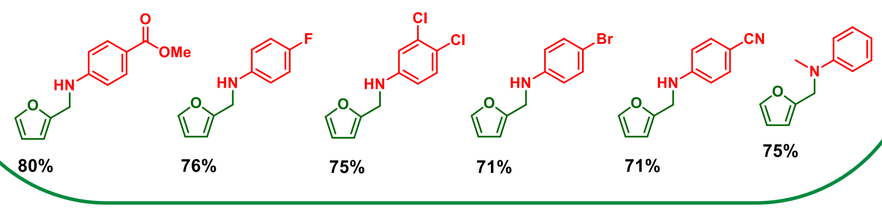

One-pot synthesis of α-aminophosphonates from carbohydrates

α-Aminophosphonates are amino acid analogues, which have found a wide range of applications in the areas of industrial, agricultural, and medicinal chemistry.
In our group, we developed the first methodology for the sustainable synthesis of heteroatom compounds, containing N and P atoms, from biomass resources catalyzed by $HReO_4$. This one-pot multi-reaction process allows the conversion of xylose and xylan into a large variety of α-aminophosphonates with moderate to good overall yields.[3]

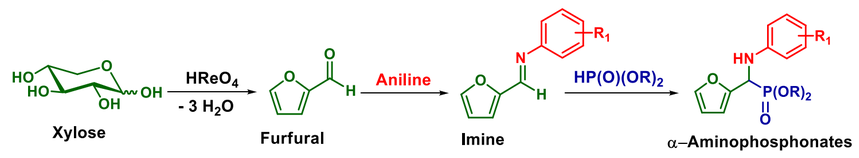

one-pot three-reaction process

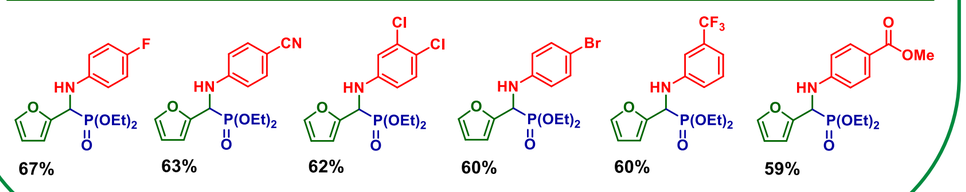

05 BIOMOL

Funding:
This work was supported by project UID/QUI/00100/2019.

Acknowledgements:
ACF (IF/00849/2012) acknowledges FCT for the "Investigador FCT" Program.

References:
1. Bernardo, J. R.; Oliveira, M. C.; Fernandes, A. C. *Mol. Catal.* 2019, *465*, 87.
2. Caetano, J. A. T.; Fernandes, A. C. *Green Chem*. 2018, *20*, 2494.
3. Isca, V. M. S.; Fernandes, A. C. *Green Chem*. 2018, *20*, 3242.

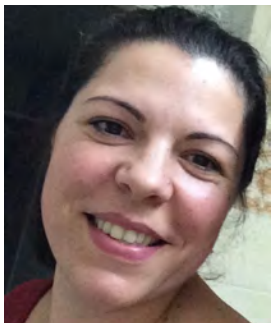

Microporous materials for the storage and therapeutical release of H_2S

Ana C. Fernandes[a,b,*], Beatriz Cambaio [b], Mary Batista[b], Fernando Antunes[b], Moisés Pinto[c], João Rocha[a], Luís Mafra[a], João Pires[b]

*acfernandes@fc.ul.pt

[a] CICECO, Departamento de Química, Universidade de Aveiro, Aveiro, Portugal
[b] Centro de Química Estrutural e Centro de Química e Bioquímica, Faculdade de Ciências, Universidade de Lisboa, Lisboa, Portugal
[c] CERENA, Instituto Superior Técnico, Universidade de Lisboa, Lisboa, Portugal

CQE Days Spring Meeting 2019

CAUTION H_2S

MAIN THERAPEUTICAL APPLICATIONS OF HYDROGEN SULFIDE

Long known as a toxic gas[1], hydrogen sulfide (H_2S) is also a biological signaling molecule that is produced by organisms ranging from bacteria to man.

In 2005, a paper in Science drew attention to its beneficial physiological effects[2].

Despite numerous studies reporting various biological effects of hydrogen sulfide in physiology and diseases in different organs/tissues, little is known about the signaling mechanisms underlying the H_2S effects.[3]

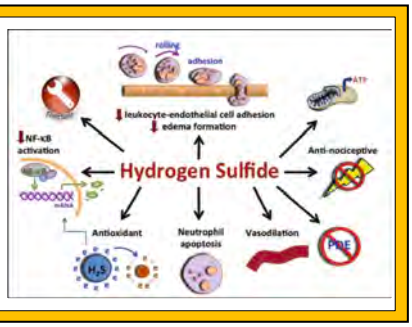

ADSORBENT MATERIALS

Zeolites

4A

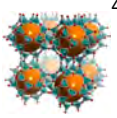

Y

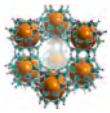

Carbon

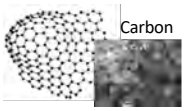

Materials	A_{BET} (m^2g^{-1})	Notes
4A	—	Zeolite
4A-Chi	—	Zeolite 4A modified with chitosan
Y	835	Zeolite
TG@Carbon	467	Activated carbon obtained by thermal activation at 700ºC
CG@Carbon	1111	Activated carbon obtained by chemical activation at 700ºC
CCG@Carbon	—	CG@Carbon modified with chitosan

BIOCOMPATABILITY

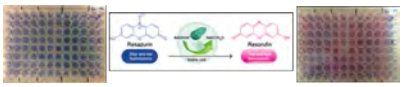

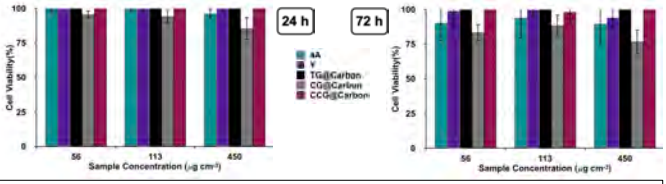

Figures above present the results for materials toxicity in HeLa cells.
After 24 h cells have 100% viability when exposed to all the materials, excepted for chemically activated carbon (CG@Carbon).
Increasing the exposure time of cells to the materials up to 72h, lead to a slight decrease on the viability. Carbon modification with chitosan presented higher biocompatibility.

ADSORPTION

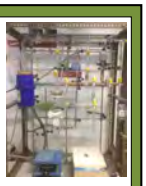

Materials	Adsorbed H_2S ($mmol_{H2S}/g_{sample}$)
4A	3.1
4A-Chi	0.3
Y	4.4
TG@Carbon	1.5
CG@Carbon	3.1
CCG@Carbon	0.4

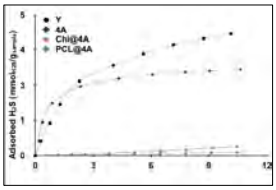

Zeolites Y and 4A adsorbed high amounts of H_2S.
The modification of 4A with Chitosan and PCL polymers didn't improve de H_2S adsorption. It seemed the polymers created a coating preventing the gas to enter the zeolite pores.

Activated carbon obtained by chemical activation presented a higher capacity to adsorb H_2S, comparing to the carbon obtained by thermal activation. Its adsorption capacity was similar to zeolite 4A. The carbon modification with chitosan also lead to a decrease on the capacity on the H2S adsorption.

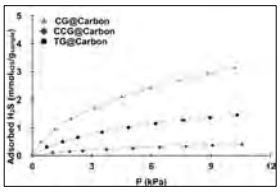

Liquid Phase
Methylene Blue Method

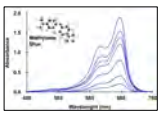

Methylene Blue reacts with H_2S, deceasing it absorbance. In this way, it is possible to quantify the content of H_2S released from the materials.

Materials	Released H_2S (mg_{H2S}/g_{sample})
4A	13.4
4A-Chi	0.3
4A-PCL	1.2
Y	25.8
TG@Carbon	—
CG@Carbon	—
CCG@Carbon	—

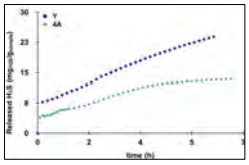

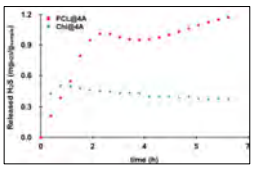

From the studied materials, zeolites are the ones that release a higher content of H_2S. Zeolite Y continues to release H_2S even after 7h.
4A modified with PCL and Chitosan not only presented a decrease in its H_2S adsorption capacity, but also it did not had the capacity to release the gas after being adsorbed.

Zeolite and carbon materials present an enhanced biocompatibility with HeLa cells, even after 72h of exposure.
Commercial zeolites 4A and Y present high H_2S adsorption capacity. Carbon obtained by chemical activation present a similar adsorption capacity to 4A, it seemed that chemical activation originates carbons with higher adsorption capacity for H_2S than thermal activation.
The introduction PCL and chitosan, both on 4A and CG@Carbon, decreased the materials capacity to adsorb H_2S.
Although carbons have the capacity to adsorb H_2S, they are not able to release it.
Zeolites not only are able to adsorb and then slowly release H_2S, but also present an enhanced biocompatibility with HeLa cells, which suits them to be used as vehicles for drug delivery.

06 CE

Funding:
Fundação para a Ciência e Tecnologia (FCT) funds Centro de Química Estrutural by project UID/QUI/00100/2019; and Centro de Química e Bioquímica by project UID/Multi/00612/2019.

FCT also funds PTDC/MED-QUI/28721/2017.

Ana C. Fernandes and Mary Batista thank FCT by the Post-doc Grants SFRH/BPD/115953/2016 and SFRH/BPD/84542/2012.

References:

[1] Li Q., Lancaster J.R., Nitric Oxide, 35, 21 (2013).

[2] Blackstone E., Morrison M., Roth M.B., Science, 308, 5721 (2005).

[3] Yi-Chun Zhu, *Hydrogen Sulfide and its Therapeutic Applications*, (2013) 83-107, Springer.

Nanostructures for CO_2 removal, fuels production and development of new energy sources

Ana C. Ferreira[1,2], Fábio Vieira[1,2], Ricardo Silva[1,2], António P. Gonçalves[2], Joaquim Branco[1,2]

[1]Centro de Química Estrutural and [2]Centro de Ciências e Tecnologias Nucleares, Instituto Superior Técnico, Universidade de Lisboa
Campus Tecnológico e Nuclear, Estrada Nacional 10 ao km 139,7, 2695-066 Bobadela-Loures, Portugal

The **main goals of Laboratory of Catalysis** covers: i) the production of value-added chemicals and fuels, such as hydrocarbons, methanol or syngas, using **major gaseous pollutants (e.g. CO_2, CH_4, N_2O)** as raw materials; ii) the development, preparation and characterization of **nanostructured intermetallic compounds containing the *f*-block elements (lanthanides, Th and U), bimetallic oxides, metal borides, pnictides and chalcogenides** with specific functionalities and applications in environment and energy.
For catalytic studies, different heterogeneous systems using transition metals and *f*-block elements as massic or supported (SiO_2 or Al_2O_3) catalysts were tested, either at atmospheric pressure or under high-pressure conditions. On the other hand, pnictides (e.g. $CoSb_3$) and chalcogenides (e.g. Cu_3SbS_4 and $Cu_{12}Sb_4S_{13}$) were prepared using unsual approaches, such as electrospinning and solvothermal method.

For catalytic studies, different heterogeneous systems using transition metals and ***f*-block elements as massic or supported (SiO_2 or Al_2O_3) catalysts** were tested, either at atmospheric pressure or under high pressure conditions.

On the other hand, **chalcogenides** (e.g. Cu_3SbS_4 and $Cu_{12}Sb_4S_{13}$) and **pnictides** (e.g. $CoSb_3$) were prepared using unusual approaches, such as electrospinning and solvothermal method.

Methanation of CO_2

Very **active and selective nanostrutured bimetallic nickel-lanthanide or actinide oxides** to production of CH_4. Yield to CH_4 ($L_{CH_4}/m^2_{Ni}.h$) is significant higher when compared to the reference catalysts.

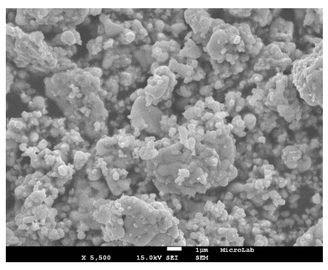

Intermetallic precursors

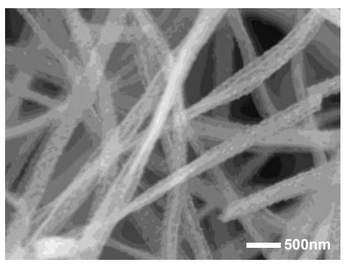

Nanofibers of bimetallic oxides

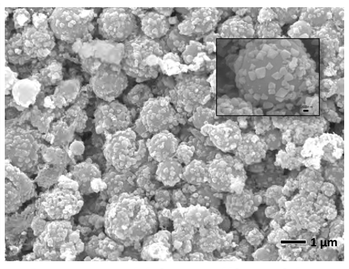

Supported bimetallic oxides

Nanostrutured bimetallic nickel-lanthanide or actinide oxides present a remarkable stability in the gaseous stream for at least 60 h, which was also confirmed by the low carbon deposition measured after reaction (< 1 %).

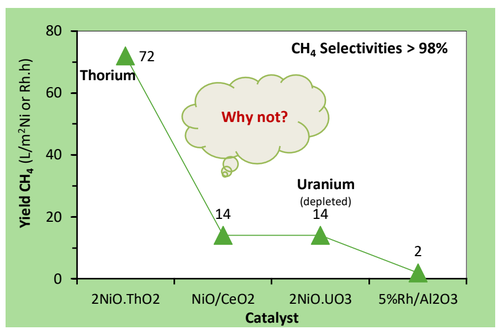

Methanation of CO_2 over bimetallic nickel-actinide oxides at 350 °C

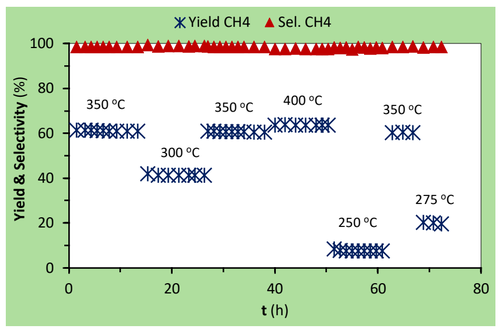

Stability of the bimetallic nickel-thorium oxide in the gaseous stream

This work has a **strong societal impact** since it contributes to the **reduction/removal of major greenhouse gases**, namely CO_2, contributing to alleviating **global climate changes** and contributing to the **development of more clean and efficient industrial processes**, targeting the production of value-added products (e.g. CH_4) that can be used as fuel or fuel precursors.

New objectives includes the development of new **nanoporous/nanofoams *f*-block element based catalysts** that can economical be competitive when compared to the present state of art used by the industry.

Materials for Energy

$Cu_{12}Sb_4S_{13}$ (Tetrahedrite)

- High symmetric crystal struture (cubic) with a large unit cell.
- Intrinsically low termal conductivity.
- Existence as a mineral with **environmentally friendly** and earth abundant element of sulfur.

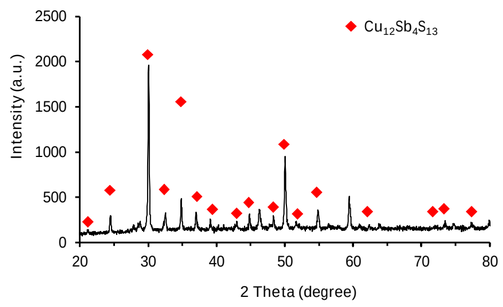

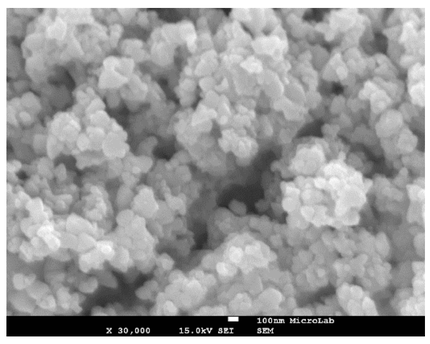

Cu_3SbS_4 (Famatite)

- Thermopower.
- Potential *p*-type thermoelectric material.

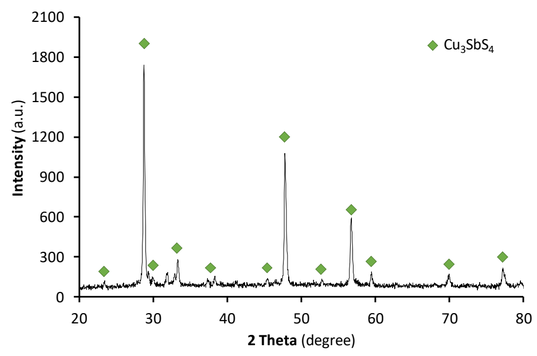

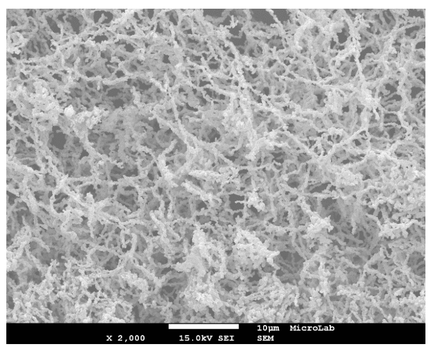

Skutterudite ($CoSb_3$)

- High-efficiency thermoelectric device application.
- The high thermal conductivity of the binary skutterudite needs to be reduced to further increase its efficiency.
- Techniques to improve the thermal and electrical properties of the skutterudite to enhance its thermoelectric efficiency: **nanostructured compound and lanthanides filling** (La, Ce, Pr, Eu, Yb).

$La_{0.5}Co_4Sb_{12}$

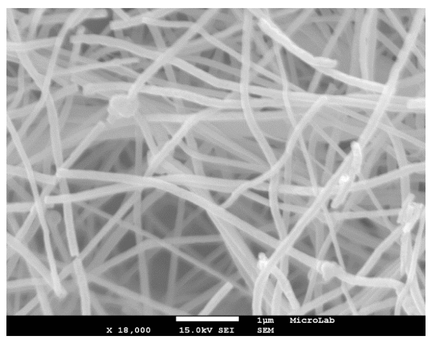

$CoSb_3$

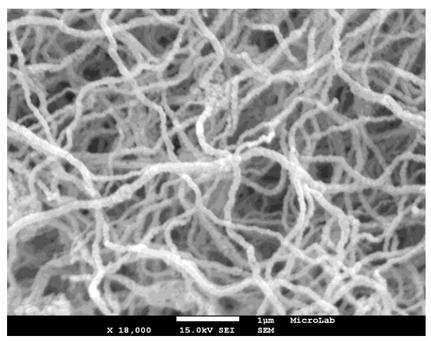

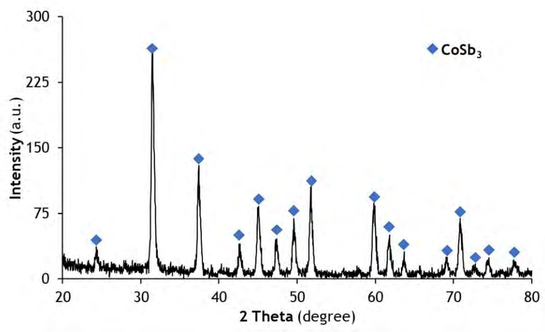

Funding:
Centro de Química Estrutural is funded by Fundação para a Ciência e Tecnologia – project UID/QUI/00100/2019.
Centro de Ciências e Tecnologias Nucleares is funded by Fundação para a Ciência e Tecnologia – project UID/Multi/04349/2019,
Ana C. Ferreira (postdoc grant)

References:

Joaquim B. Branco, Ana C. Ferreira, T. Almeida Gasche, João P. Leal, *Nano-Structures & Nano-Objects 15*, **2018**, 75-83.
Joaquim B. Branco, Ana C. Ferreira, *Eur. J. Inorg. Chem.* **2019**, 1039–1045.
Ana C. Ferreira, Joaquim B. Branco, *Inter. J. Hydrogen Energy 44*, **2019**, 6505-6513.
Ana C. Ferreira, Joaquim B. Branco, *Intermetallics 108*, **2019**, 32-38.

Synthesis and characterization of a new family of ruthenium(II) complexes with phenanthroline **derivate** ligands for anticancer applications

Margarida P. Pereira[1,2], João Franco Machado[1,2,3], M. Fátima M. Piedade[2,4], M. Helena Garcia[1,2], Tânia S. Morais[1,2,*]

[1] Centro de Química Estrutural, Faculdade de Ciências, Universidade de Lisboa, Portugal | [2] Departamento de Química e Bioquímica, Faculdade de Ciências, Universidade de Lisboa, Portugal | [3] Centro de Ciências e Tecnologias Nucleares, Instituto Superior Técnico, Universidade de Lisboa, Portugal | [4] Centro de Química Estrutural, Instituto Superior Técnico, Universidade de Lisboa, Portugal

*Email: tsmorais@fc.ul.pt

Introduction

Cancer is the second leading cause of death worldwide (9.6 million deaths in 2018). Cisplatin is still one of the most commonly used drugs in cancer chemotherapy, however show broad and severe side effects. Our group has been developing new **ruthenium(II) complexes** with higher cytotoxicity than cisplatin against several cancer cell lines (e.g. ovarian, breast, colon and prostate).[1] One of these compounds was evaluated in an orthotopic triple negative breast cancer mouse model, revealing **significant capacity to suppress tumour growth** and to **inhibit the development of metastases**, without presenting the common side-effects of cisplatin.[2]

Herein, we report the synthesis and characterization of a new family of complexes of formula **$[Ru(\eta^5\text{-}C_5H_5)(PPh_3)(NN)][CF_3SO_3]$**, in which NN corresponds to phenanthroline-derived ligands (Scheme 1).

Synthesis

Ru(II) complexes were synthesized according to Scheme 1, with yields of **43 to 85%** upon purification by recrystallization.

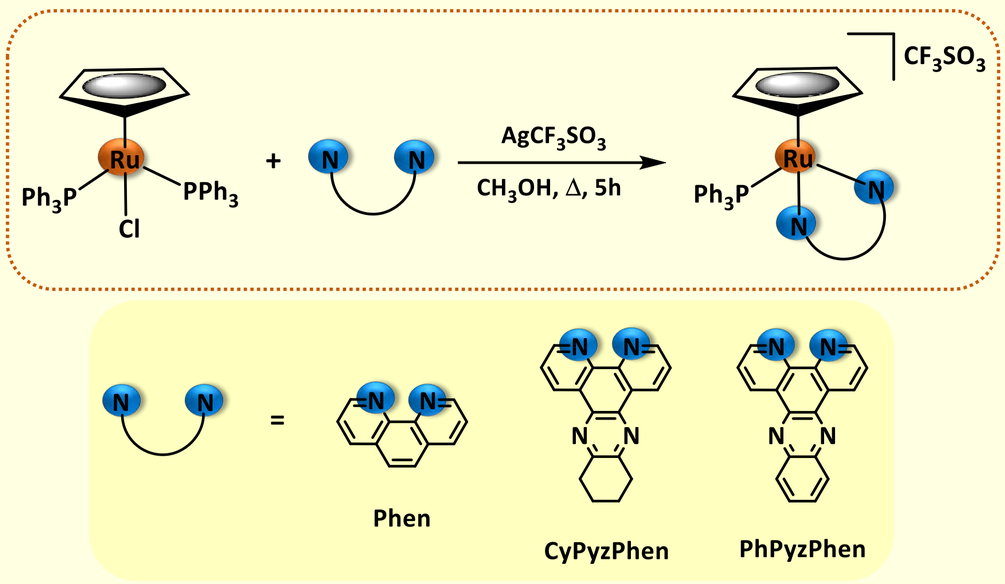

Scheme 1. Reaction scheme for the synthesis of **$[Ru(\eta^5\text{-}C_5H_5)(PPh_3)(NN)][CF_3SO_3]$** complexes, where NN = to phenanthroline-derived ligands.

X-Ray Diffraction

X-ray diffraction studies were performed and the results support the proposed structures for the complexes. As example, the $[Ru(PPh_3)_2(phen)][CF_3SO_3]$ complex crystalized in monoclinic crystal system, space group P 21/n, with one cationic complex molecule and one $CF_3SO_3^-$ as a counter ion in the asymmetric unit.

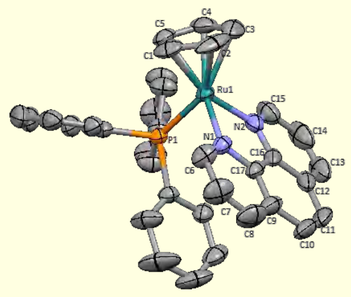

Figure 1. Molecular diagram depicting the cationic moiety of the $[Ru(PPh_3)_2(phen)][CF_3SO_3]$ complex.

Stability Assays

The stability of the Ru(II) complexes in dimethyl sulfoxide over 24 hours was determined by UV-Visible spectrophotometry. **All compounds revealed to be stable**, and therefore suitable for further biological assays, namely test their anticancer activity in different human cell lines.

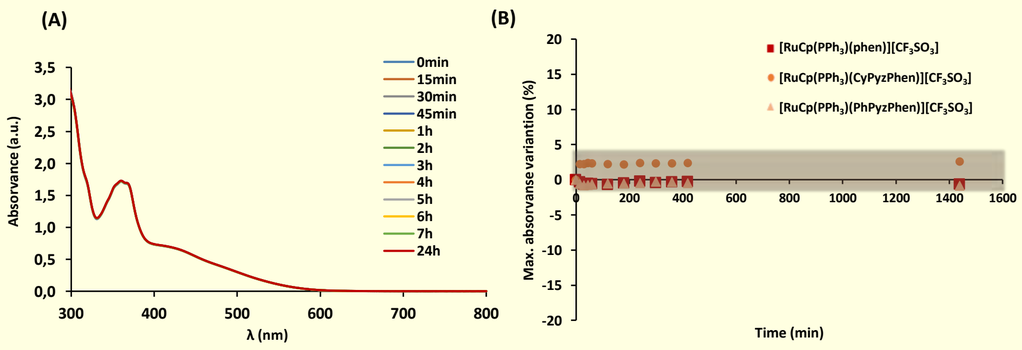

Figure 2. Evaluation of the stability of $[RuCp(PPh_3)(PhPyzPhen)][CF_3SO_3]$ complex over 24h in DMSO **(A)**. Absorbance variation percentage along time (0 min to 1440 min) **(B)**.

Structural Characterization

NMR analysis are in good agreement with the proposed structures for all the compounds.

In general, in ^1H NMR spectrum, upon coordination of the ligand to the metal center a deshielding is observed in the cyclopentadienyl and phenanthroline signals. Also, a deshielding is observed in the signal of ^{31}P NMR after coordination of phenanthroline-derived ligand.

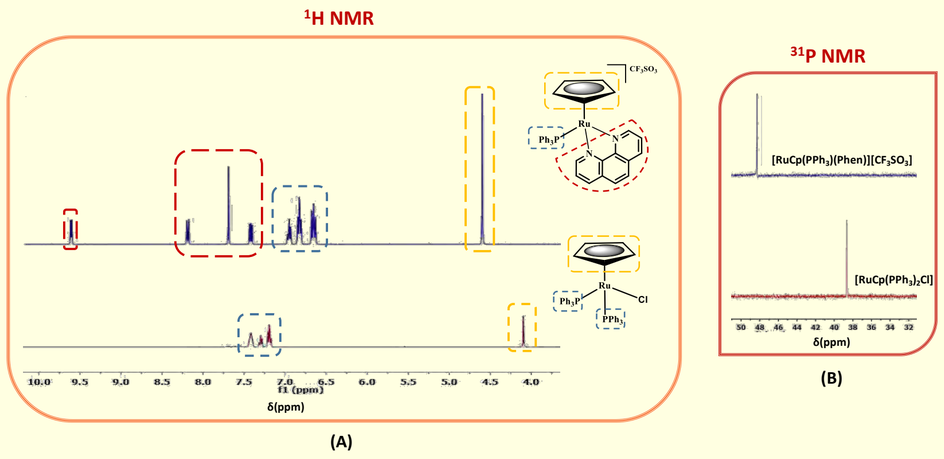

Figure 3. ^1H NMR **(A)** and $^{31}P\{^1H\}$ NMR **(B)** spectra of the $[RuCp(PPh_3)(Phen)][CF_3SO_3]$ complex (blue) and its precursor $[RuCp(PPh_3)_2Cl]$ (red) in $(CD_3)_2CO$ (RT).

UV-Visible Studies

$[Ru(PPh_3)_2(CyPyzPhen)][CF_3SO_3]$ show an intense absorption band in the UV region with maximum circa 250-280 nm, characteristic of **π→π* transitions** of the aromatic fragments. A second broad less intense band between 370 and 445 nm is observed too, corresponding to a metal to ligand charge transfer band (**MLCT**).

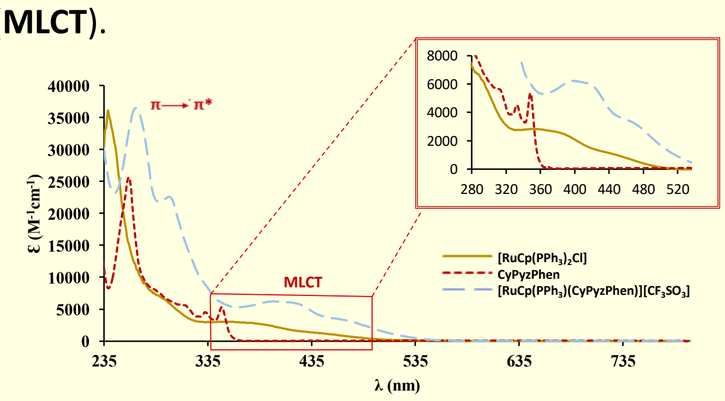

Figure 4. Electronic spectra of $[RuCp(PPh_3)(CyPyzPhen)][CF_3SO_3]$, its precursor $[RuCp(PPh_3)_2Cl]$ and free ligand CyPyzPhen in dichloromethane.

Conclusions

- A **new** family of complexes of formula **$[Ru(\eta^5\text{-}C_5H_5)(PPh_3)(NN)][CF_3SO_3]$** (NN = phenanthroline-derived ligands) was synthesized with high purity.
- All complexes were **structurally characterized** by NMR, FT-IR, UV-Vis and elemental analysis.
- **2** structures were determined by **single crystal X-ray diffraction** studies.
- The **stability** of the complexes supports their suitability to proceed to **further biological assays**, namely testing their anticancer activity in different human cell lines.

Centro de Química Estrutural is funded by Fundação para a Ciência e Tecnologia (FCT) – project UID/QUI/00100/2019.

T.S.Morais acknowledges the CEECIND 2017 Initiative for the project CEECIND/00630/2017 (acknowledging FCT, as well as POPH and FSE-European Social Fund).

J. F. Machado thanks FCT for his doctoral grant (SFRH/BD/135915/2018).

References:

[1] Morais TS, Valente A *et al.*, Future Med. Chem., 8 (**2016**) 527-544.

[2] Mendes N, Tortosa F *et al.*, AntiCancer Agents in Med. Chem. 17 (**2017**) 126-136.

Synthesis of Theobromine Isonucleosides as Potential Cholinesterase Inhibitors

Margarida P. Pereira,[1,2] Eduardo C. de Sousa,[1] Anne Loesche,[3] René Csuk,[3] and Nuno M. Xavier[1,2]

[1] *Centro de Química e Bioquímica, Faculdade de Ciências, Universidade de Lisboa, Ed. C8, 5º Piso, Campo Grande, 1749-016 Lisboa, Portugal*

[2] *Centro de Química Estrutural, Faculdade de Ciências, Universidade de Lisboa; margaridamags1992@gmail.com; nmxavier@fc.ul.pt*

[3] *Bereich Organische Chemie, Martin-Luther-Universität Halle-Wittenberg, Kurt-Mothes-Str. 2, D-06120 Halle (Saale), Germany*

11 HC

Funding:

Centro de Química Estrutural is funded by Fundação para a Ciência e Tecnologia – project UID/QUI/00100/2019.

Introduction

Isonucleosides are regioisomers of nucleosides in which a nucleobase is linked to the sugar moiety at a non-anomeric position. These groups of molecules have attracted significant interest in the investigation of nucleoside analogs with therapeutic potential, namely in the context of anticancer and antiviral drug research.[1,2]

In a previous work,[3] a isonucleoside comprising a theobromine unit linked to a methyl glucoside moiety (**A**) was shown to be a good inhibitor of acetylcholinesterase with a K_i value of 4.3 μM. The activity of this compound motivated the synthesis of novel analogs, which are presented in this poster.

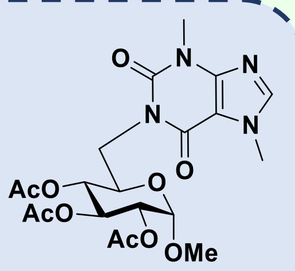

A

K_i (AChE) = 4.3 μM

Theobromine 3′-*O*-Benzyl Xylofuranos-5′-yl Isonucleoside and *N*-Isonucleosidyl Sulfonamide

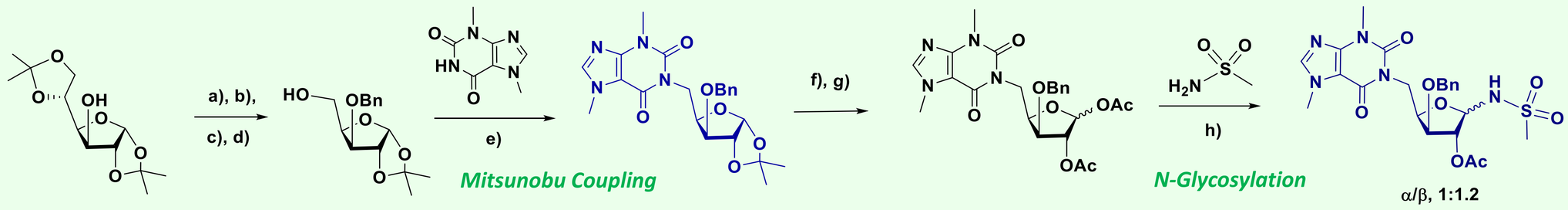

Scheme 1. Reagents and conditions: (a) BnBr, NaH; (b) AcOH 60% aq.; (c) $NaIO_4$; (d) $NaBH_4$, EtOH/H_2O; (e) PPh_3, DEAD, 57%; (f) TFA/H_2O; (g) Ac_2O,py, 61%; (h) $BF_3.Et_2O$, 30%.

Theobromine 3′-*O*-Dodecyl Xylofuranos-5′-yl Isonucleoside

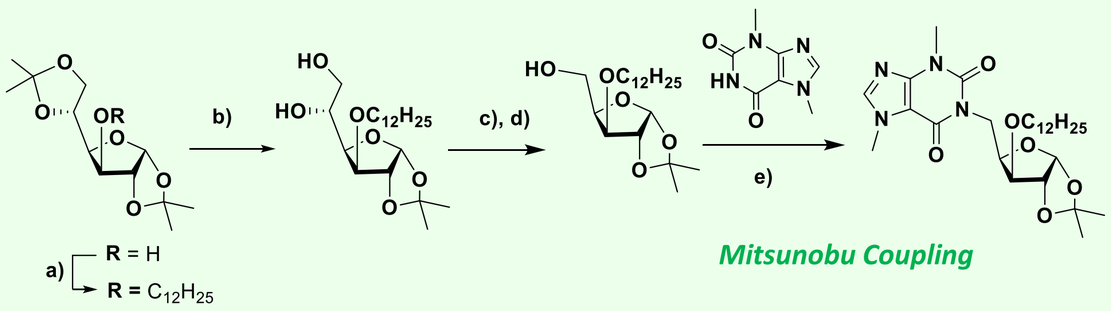

Scheme 2. Reagents and conditions: (a) $C_{12}H_{25}Br$, NaH, 93%; (b) AcOH 70% aq. , 78%; (c) $NaIO_4$, 79%; (d) $NaBH_4$, EtOH/H_2O, 81%; (e) PPh_3, DEAD, 44%.

Theobromine 3′-*O*-Dodecyl Xylofuranos-5′-yl *N*-Isonucleosidyl Derivatives

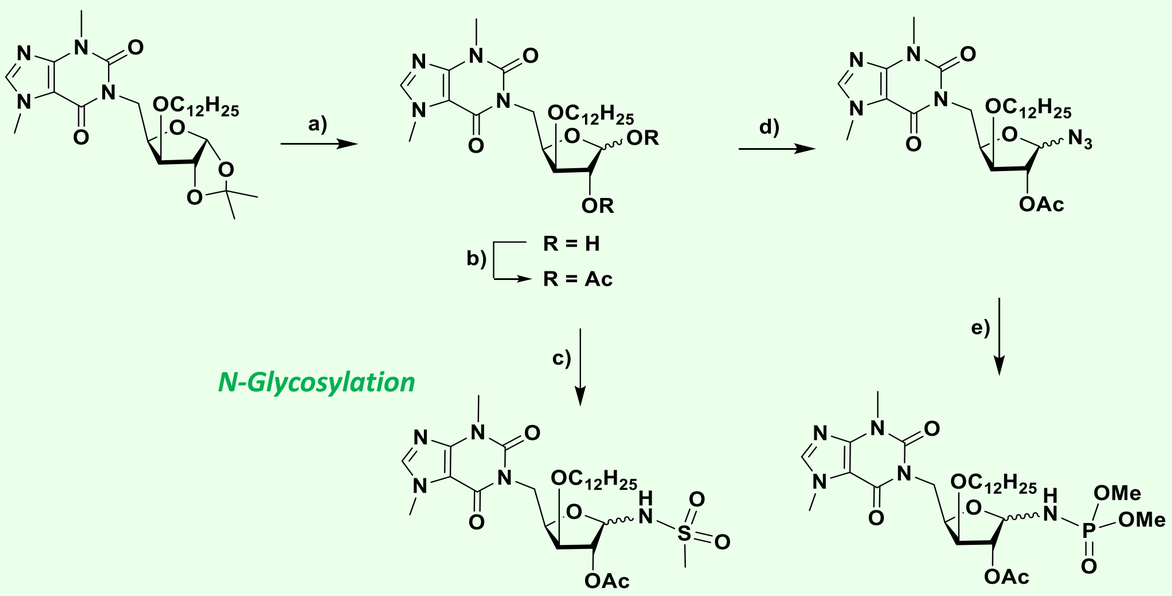

Scheme 3. Reagents and conditions: (a) TFA 70% aq., 83%; (b) Ac_2O, py, 69%; (c) $CH_3SO_2NH_2$, $BF_3{\cdot}Et_2O$, 81%; (d) $TMSN_3$, TMSOTf, 86%; (e) $P(OMe)_3$, 56%.

Cholinesterase Inhibitory Activities

Compounds	AChE	BChE
	K_i (μM) (% Inhibition)[a]	
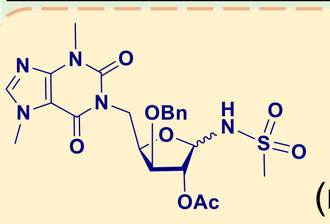	6.6 ± 0.2 [K_i' > 200] (mixed-type)	> 100 (19%)

[*Galantamine.HBr* , **AChE**: K_i = 0.5 μM; **BChE:** K_i = 9.4 μM]

Compounds	AChE	BChE
	K_i (μM) or % Inhibition[a]	
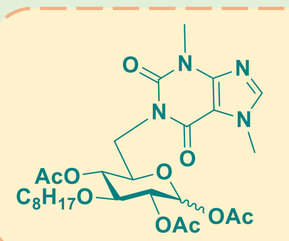	3.1 ± 0.2 [K_i' > 100] (mixed-type)	5.4 ± 0.3 [> 60] (mixed-type)
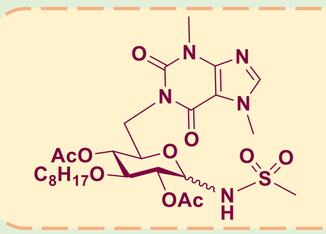	% I = 28	% I = 53

[*Galantamine.HBr* , **AChE**: K_i = 0.2 μM; **BChE:** K_i = 2.4 μM]

[a] %-Inhibition at 50 μM.

Theobromine 3′-*O*-Octyl Glucopyran-6′-yl Isonucleoside and *N*-Isonucleosidyl Sulfonamide

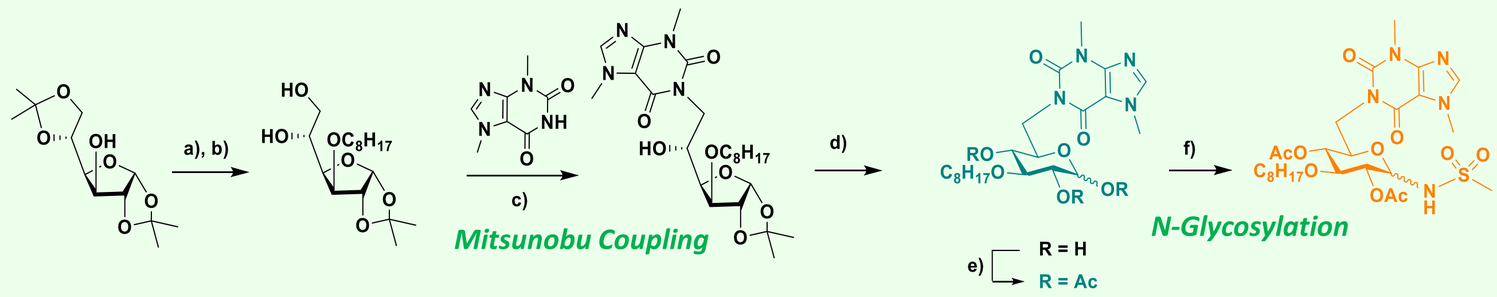

Scheme 4. Reagents and conditions: (a) $C_8H_{17}Br$, NaH, DMF; (b) AcOH 70% aq. , 88%; (c) PPh_3, DEAD, 16%; (d) TFA 60% aq., 87% ; (e) Ac_2O, py, 84%; (f) $CH_3SO_2NH_2$, $BF_3{\cdot}Et_2O$, 38%.

Conclusions

- Novel theobromine isonucleosides based on pyranose and furanose templates and *N*-isonucleosidyl derivatives were synthesized by efficient methodologies.
- The ability of some compounds to display inhibition of cholinesterases with K_i values at single digit micromolar concentrations demonstrates their potential interest as anti-Alzheimer's disease agents.

References:

[1] Yu, H.-W.; Zhang, H.-Y.; Yang, Z.-J.; Min, J.-M.; Ma, L.-T.; Zhang, L.-H. Pure Appl. Chem. 70 (**1998**) 435–438.

[2] Solke, K. F.; Huang, J.-L.; Russell, J. W.; Whiterock, V. J.; Sundeen, J. E.; Stratton, L. W.; Clark, J. M. Antiviral Res. 23 (**1994**) 219–224.

[3] Batista, D.; Schwarz, S.; Loesche, A.; Csuk, R.; Costa, P. J.; Oliveira, M. C.; Xavier, N. M. Pure Appl. Chem. 88 (**2016**) 363–379.

Chemical and Thermal Study of the *Catostylus tagi* for the development of a new biopolymer

A.R.P. Gonçalves[1], M.J.V. Lourenço[1], J.C. Bordado[2], R. Galhano dos Santos[2], L. S. Gordo[3]

[1] Centro de Química Estrutural - CQE, [2] Centro de Recurso Naturais e Ambiente - CERENA, [3] Centro de Ciências do Mar e do Ambiente - MARE

INTRODUCTION: *Catostylus tagi* (*Cnidaria*, *Scyphozoa*) is a jellyfish that can be readily found in the Tagus estuary as it has one of its most important and large populations. The body of this species of jellyfish has about 97% water making them quite fragile as they have less than 5% of solid organic matter [1]. The research conducted is a preliminary study into the possibility of using this species of jellyfish in the development of new biopolymers for marine applications.

METHODS: The specimens were collected between May and June 2018, in the region of São João da Talha. After washing with distilled water and lyophilization, the jellyfishes were characterized using SEM, FTIR-ATR, DSC and TGA.

RESULTS AND DISCUSSION: The SEM images revealed in the mesoglea zone a porous network composed of collagen fibers, allowing most of the water present in these animals to be considered free water. The FTIR-ATR of the lyophilized *C. tagi*, revealed the relevant peaks of collagen, the largest component of these animals. The DSC characterization of this species presents a pick transition at 200 °C that can be related to decomposition of the smallest collagen fibers. On the other hand, the degradation of the collagen takes place at 300 °C in the TGA analysis, but it was not possible to define the total degradation of the jellyfish since at the end of the experiment, 15% of the total mass sample still remained [2].

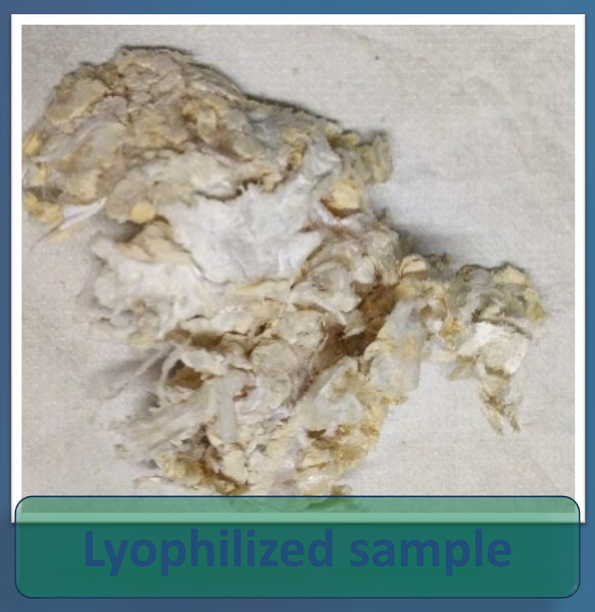

Lyophilized sample

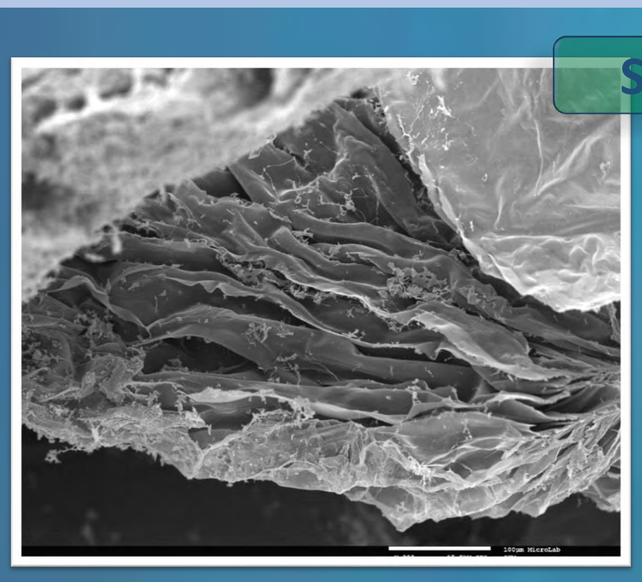

SEM

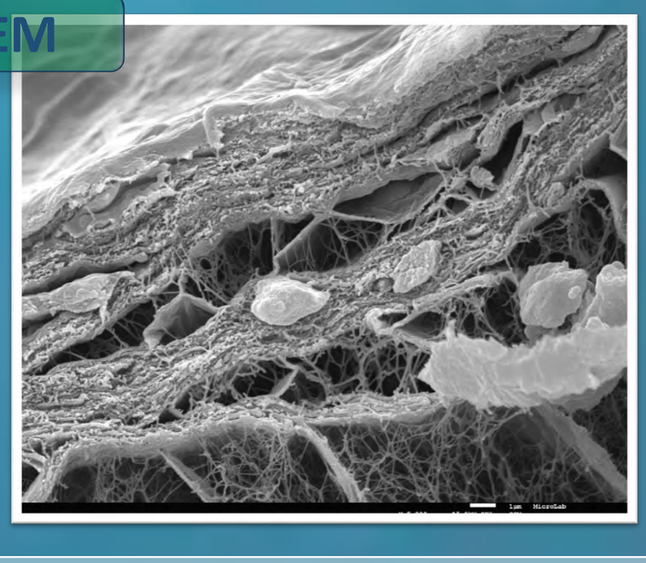

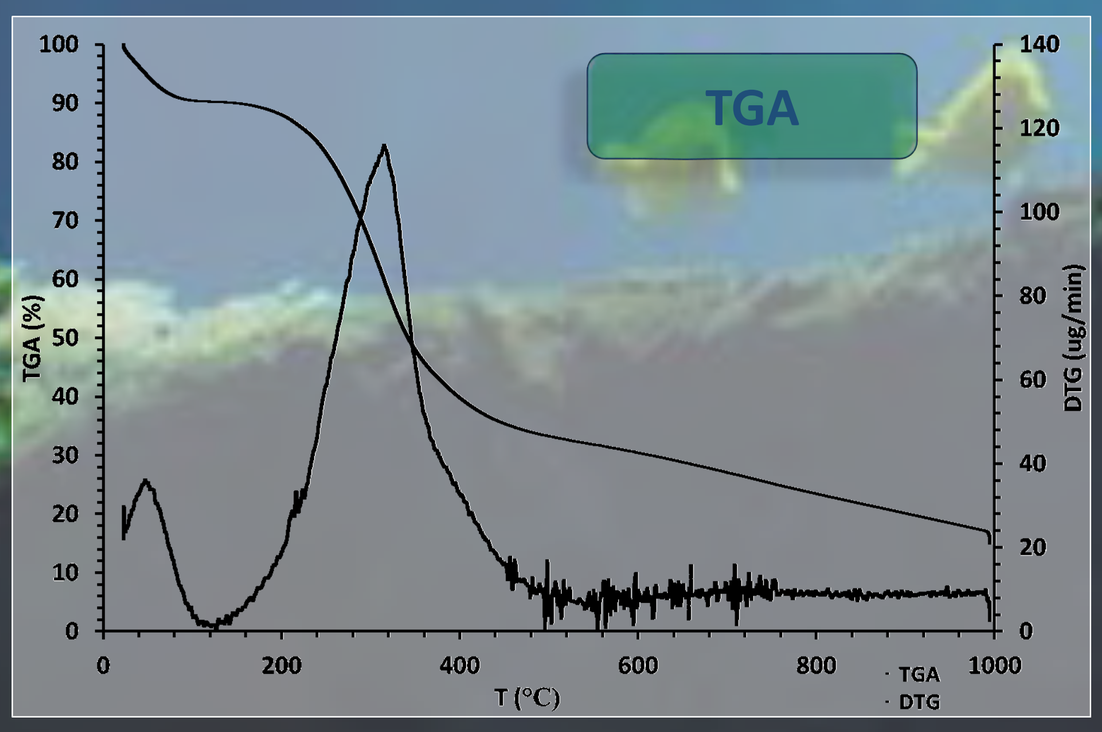

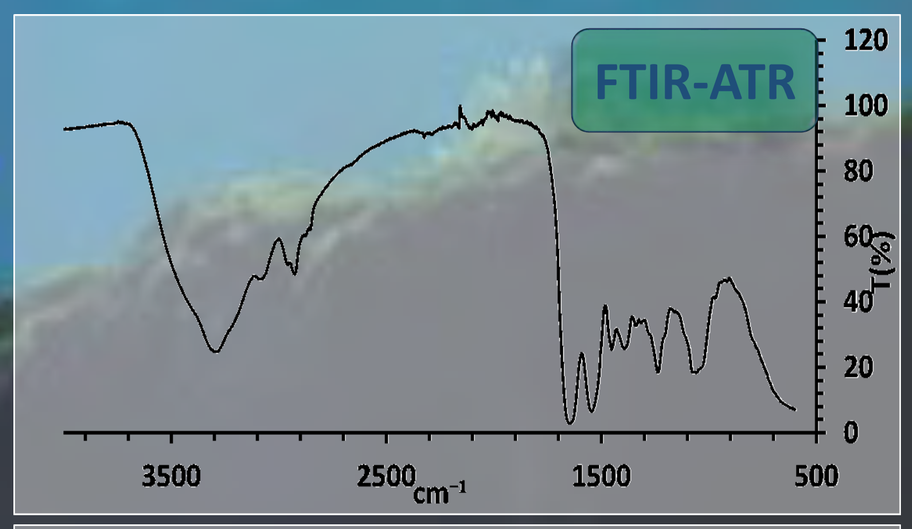

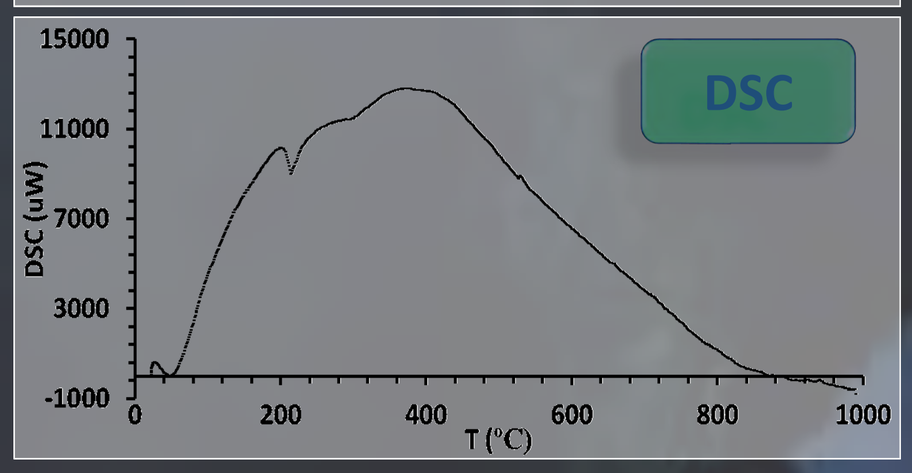

CONCLUSIONS: It was observed that the lost of water, of the lyophilized samples, led to a remarkable increase of the mechanical properties due to the strong interactions between the fibers and the mesoglea membranes. Such effect may be the result from the high closeness of those fibers, making the lyophilized jellyfish almost insoluble in most common organic solvents[3]. This behavior makes this species a potential additive to the development of a new biopolymer.

CQE Química Estrutural

FCT
MINISTÉRIO DA CIÊNCIA, TECNOLOGIA E ENSINO SUPERIOR

10 MTFT

Funding:
Centro de Química Estrutural is funded by Fundação para a Ciência e Tecnologia – project UID/QUI/00100/2019, CERENA - FCT-UID/ECI/04028/2019 and MARE – Centro de Ciências do Mar e do Ambiente , funded by FCT - Fundação para a Ciência e Tecnologia.

References:

[1] A. Mayer, The Carnegieins Stitutioonf Washington, Vol.III (1910).
[2] A.R.P. Gonçalves, "Desenvolvimento de novos polímeros biocompatíveis para a utilização em ambiente aquático", Master Thesis, Faculdade de Ciências da Universidade de Lisboa, 2019.
[3] J. Zhu et al., Journal of the Mechanical Behavior of Biomedical Materials, Vol.6 (2012) 63 – 73.

Corresponding Autor:
argoncalves@fc.ul.pt

Innovative Materials for Nitric Oxide Adsorption and Therapeutic Releases

Rosana V. Pinto[1,2], Ana Sofia Oliveira[2], Moisés L. Pinto[1], João Pires[2]

[1] CERENA, Departamento de Engenharia Química, Instituto Superior Técnico, Universidade de Lisboa, 1049-001 Lisboa.
[2] Centro de Química Estrutural e Centro de Química e Bioquímica, Departamento de Química e Bioquímica, Faculdade de Ciências da Universidade de Lisboa, Ed. C8, Campo Grande, 1749-016 Lisboa.

CQE Química Estrutural

06 CE

Motivation

- Nitric oxide (NO) is a gaseous molecule with well-known therapeutic properties, being a strong vasodilator, antibacterial, tumor repressor and promotes wound healing.
- Existent NO donors are limited due to their high solubility, instability and release toxic degradation products.
- Porous materials stands as a new system for NO release, storing NO by chemisorption. Previous results for zeolites and titanosilicates [1] demonstrated high capacity to store NO however their release kinetics in biological media are not sufficiently slow for most potential applications (most of them release almost all stored NO in the first hour).

Objectives

- Obtain longer release rates by covering the porous solids with a biopolymer (polycaprolactone (PCL)) without compromising the following requirements:

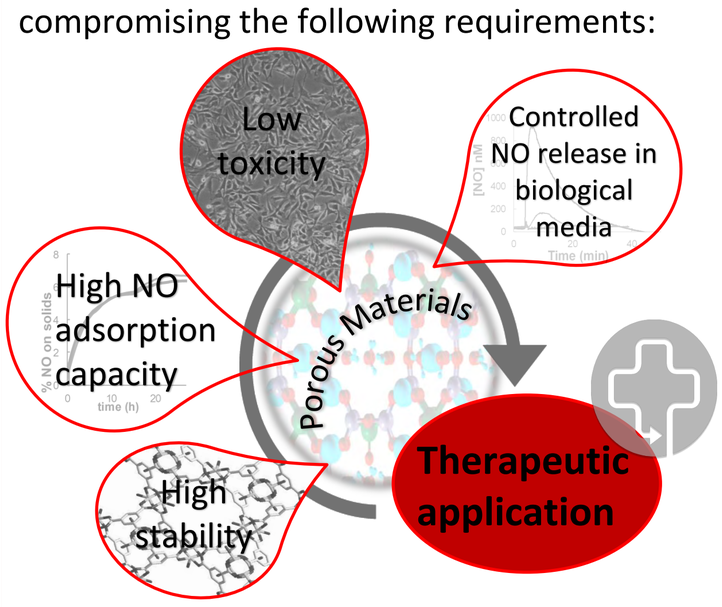

- Develop PCL/zeolite composite films to be used as transdermal patches for wound healing treatment.

Materials

- PCL/zeolite microcomposites particles were prepared using the oil in water solvent evaporation method.
- PCL/zeolite microcomposites were compressed in disks and melted at 100 ºC to form the films.

Composite materials designation	Description
PCL/4A [2:1] 1200	PCL and Zeolite 4A films at 2:1 w/w with microparticles obtained under stirring at 1200 rpm.
PCL/4A [2:1] 600	PCL and Zeolite 4A films at 2:1 w/w with microparticles obtained under stirring at 600 rpm.
PCL/4A [8:5]	PCL and Zeolite 4A films at 8:5 w/w with microparticles obtained under stirring at 1200 rpm.

Materials Characterization

Infrared Spectroscopy

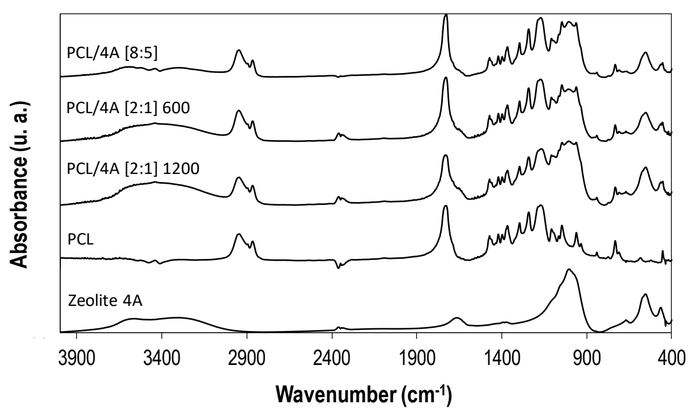

Termogravimetry

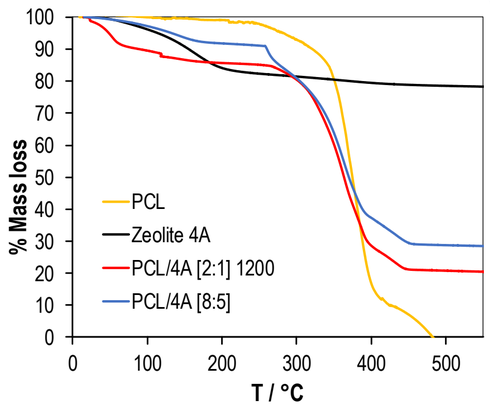

Contact angle

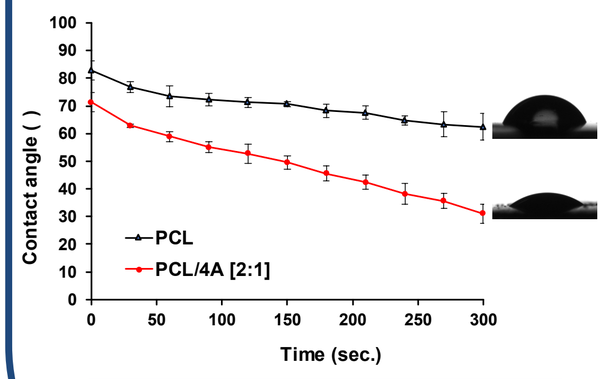

Zeolite 4A confers higher hydrophilicity to the PCL films.

SEM/EDS

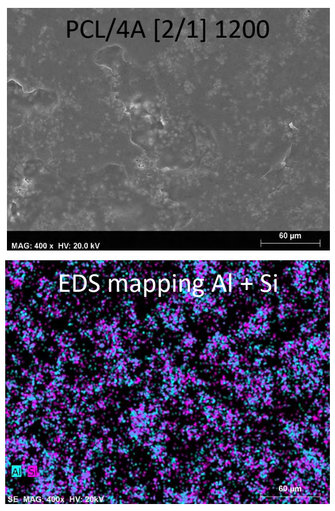

Zeolite 4A (which contains Al and Si in its composition) is uniformly distributed over the film.

Results

NO adsorption/release

1. Gaseous phase

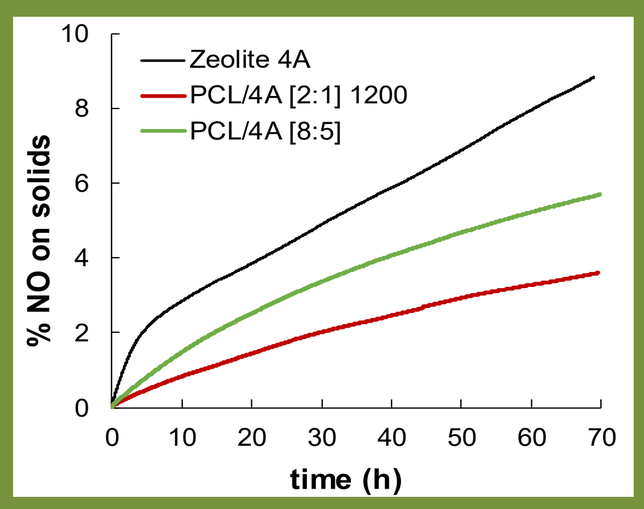

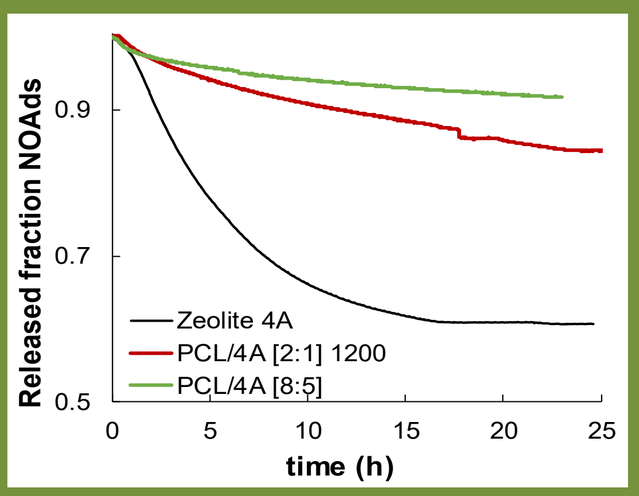

- Composite PCL/4A films feature high storage capacity and a slower NO release rate.

2. Liquid phase

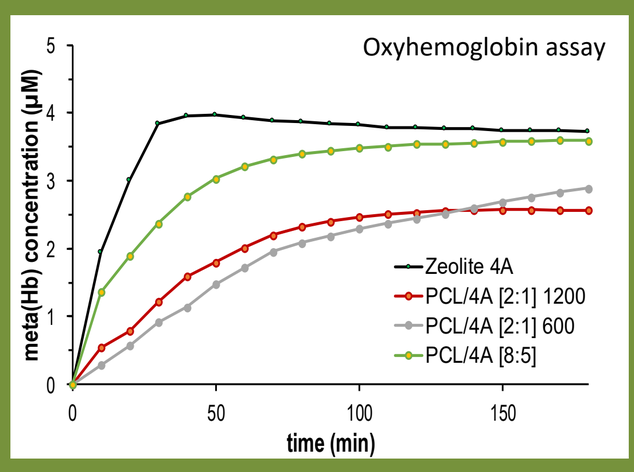

- Longer and controlled NO release rates were achieved with composite PCL/4A films in PBS at 25 °C.

Conclusions

- Moderate hydrophilicity of the composite films facilitates slower NO release rates.
- Composite PCL/Zeolite indicated slower and a controlled NO release comparing with the release profile of the adsorbent.
- Uniform distribution of the adsorbent through the film ensures the target release of pure NO.
- This new composite formulation pave the way for the design of new NO delivery systems with potential application as transdermal patches for wound healing treatments.

Funding:
Centro de Química Estrutural is funded by Fundação para a Ciência e Tecnologia (FCT) – project UID/QUI/00100/2019.
The work was financed by FCT through projects IF/00993/2012/CP0172/CT0013 and PTDC/MED-QUI/28721/2017. This work was developed in the scope of the Projects UID/MULTI/00612/2019 (CQB), UID/ECI/04028/2019 (CERENA).

TECNICO LISBOA · Ciências ULisboa · FCT Fundação para a Ciência e a Tecnologia

References:
[1] Pinto, R. V.; Pinto, M. L. Chapter 14 - Nanoporous Materials: New Generation of Nitric Oxide Donors. In Therapeutic Application of Nitric Oxide in Cancer and Inflammatory Disorders; Morbidelli, L., Bonavida, B., Eds.; Academic Press, 2019; pp 277–305.

New sustainable approaches to the synthesis of 1,2- and 1,4-naphthoquinones

Ana Catarina Sousa[1,2], Lígia O. Martins[3], M. Paula Robalo[1,2]

[1] Área Departamental de Engenharia Química, Instituto Superior de Engenharia de Lisboa, Instituto Politécnico de Lisboa,1959-007 Lisboa, Portugal.
[2] Centro de Química Estrutural, Instituto Superior Técnico, Universidade de Lisboa,1049-001 Lisboa, Portugal.
[3] Instituto de Tecnologia Química e Biológica, Universidade Nova de Lisboa, 2780-15 Oeiras, Portugal.

Importance

Naphthoquinones are a very important class of organic compounds in pharmaceutical chemistry due to their extremely rich redox and acid-base properties. Quinone cores are known to be electron transporters and quinone redox cycling, that yields “reactive oxygen species" (ROS), is important for many biological oxidative processes that are essential to living organisms. The predominant scaffold in nature is the naphthalene 1,4-dione (Figure 1) whose different derivatives exhibit a wide range of biological activities and pharmacological properties including anti-inflammatory, antibacterial, antitumor and other chemotherapeutic agents. However, also the 1,2-dione isomers have a very important role in the development of new substances for medical purposes with a wide range of derivatives exhibiting significant therapeutic properties.[1-3]

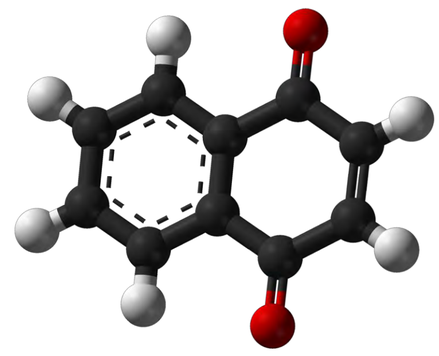

Figure 1. 1,4-naphthoquinone

Synthesis

The synthesis of naphthoquinone frameworks is quite-well documented, and some strategies involve the use of natural naphthoquinones as starting materials, which involves their extraction from plants using organic solvents. On the other hand, other traditional methods/protocols involve as first step the oxidation of the hydronaphthoquinone core with chemical oxidants such as H_2O_2, Fremy’s salt [$(KSO_3)_2NO$], chromium trioxide or other chemical oxidants.[2] Although there are reports of new environmentally friendly methodologies[4], it is still a challenge to explore new sustainable synthetic routes for these compounds, that assume importance in the field of both synthetic and medicinal chemistry.

Methodologies

In pursuit of our research interest devoted to exploiting environmentally friendly protocols to obtain original compounds or to improve known reactions, we report herein two methodologies, a biocatalytic and a microwave irradiation process, to obtain phenylamino 1,2- and 1,4-naphtoquinones derivatives, respectively, with different substituents at the 4-position of the phenylamine ring.

Biocatalysis

CotA-laccase is a copper containing oxidoreductase isolated from *Bacillus subtillis*. The active site contains four copper ions responsible for the oxidation of substrates with concomitant reduction of oxygen to water.

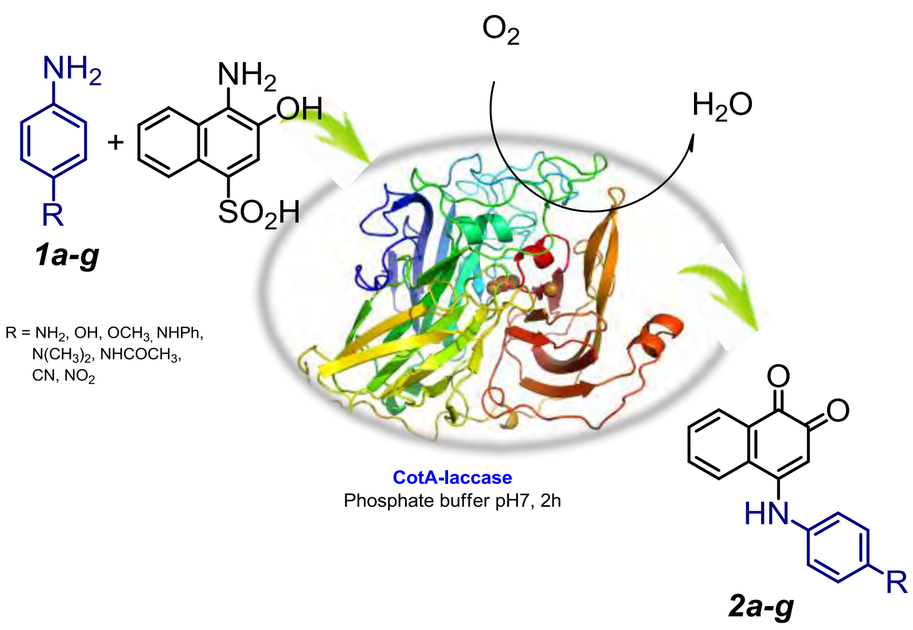

Figure 2. Synthetic route for 1,2-naphthoquinone derivatives catalysed by CotA-laccase

The enzyme promotes the formation of the *ortho*-naphthoquinone intermediate that subsequently underwent nucleophilic addition by the different *p*-substituted primary aromatic amines (*1a-g*). Reactions are complete in less than 2 hours and reasonable to good yields (54 - 78 %) are provided.

Microwave irradiation

Microwave radiation is nowadays considered as a powerful option in the field of sustainable pharmaceutical synthesis specially due to shorter reaction times, lower energy consumption and higher product yield.

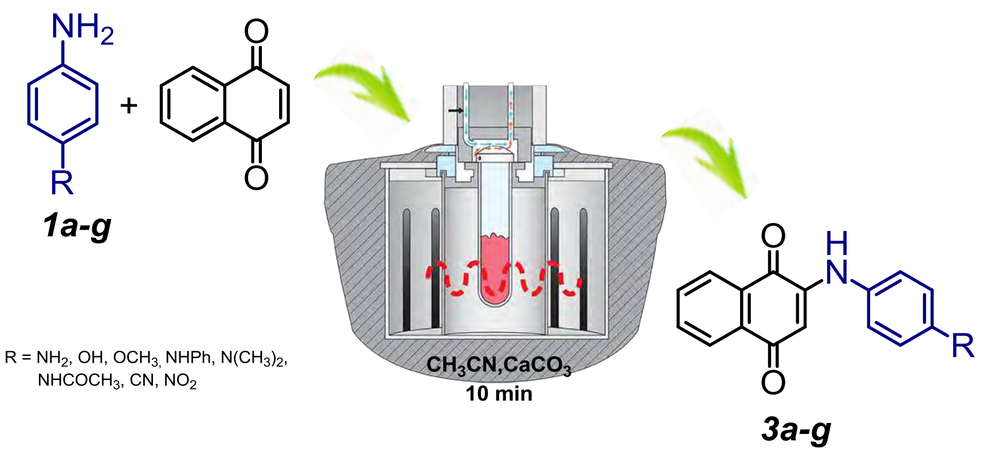

Figure 3. Synthesis of 1,4-naphthoquinone derivatives using microwave irradiation

Reactions were conducted in acetonitrile (2 mL) in the presence of catalytic amounts of $CaCO_3$ and 4-arylamino-1,4-naphthoquinone (*3a-g*) were obtained after 10 min in good yields (up to 80%).

Conclusions

Two environmentally benign protocols, Biocatalysis and Microwave irradiation, have been implemented towards the synthesis of 1,2- and 1,4- naphthoquinone derivatives as target molecules with good to excellent yields. The presented methodologies are in accordance with the principles of Green Chemistry and can be faced as sustainable alternatives to the synthesis of these classes of compounds.

05 BIOMOL

Funding:
Centro de Química Estrutural is funded by Fundação para a Ciência e Tecnologia – project UID/QUI/00100/2019. Authors gratefully acknowledge financial support from FCT PTDC/BBB-B/0122/2014, RECI/QEQ-IN/0189/2012 and the IST-UTL NMR and MS Networks for facilities.

References:

1. Qiu, H-Y, Wang, P, Lin, H, Tang, C, Zhu, H, Yang, Y, Chem Biol Drug Des, 91 (**2018**) 681-690.
2. López, J, Cruz, F, Alcaraz, Y, Delgado, F, Vázque, M, Med Chem Res, 24 (**2015**) 3599–3620.
3. Tandon, V, Kumar, S, Expert Opin Ther Patents 23 (**2013**) 1087-1108.
4. Peralta, L, López, L, Belmares, S, Cruz, A, Herrera, R, González, C, Formatex, (**2015**) 542-550.

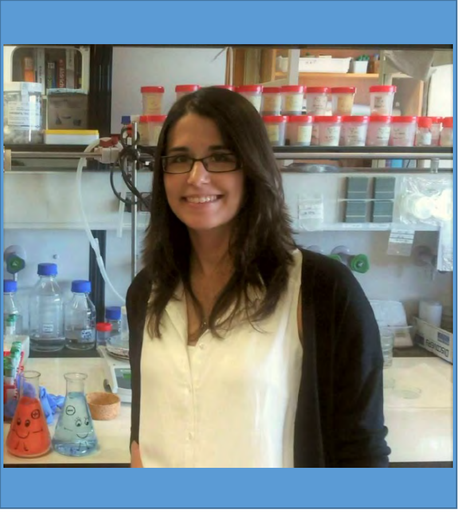

Poly(ionic liquid)/ionic liquid membranes with fluorosulfonyl derivative anions: characterization and CO_2/H_2 separation

Andreia S.L. Gouveia, Liliana C. Tomé and Isabel M. Marrucho

CQE Química Estrutural

09 MET

Introduction

Despite the recognized potential of biohydrogen (bioH_2) for sustainable development, there are still challenges to be overcome regarding its production and purification, such as the elimination of CO_2, N_2, and other impurities (H_2O and H_2S), so that an enriched H_2 stream can be obtained for efficient energy generation [1].

Ionic liquids (ILs) have been used as a successful platform to design novel task-specific materials for CO_2 separation [2]. Moreover, different studies have been unveiling that the use of poly(ionic liquid)s (PILs) and their composites (PIL–IL) is a powerful strategy to design improved CO_2 separation membranes [2]. In this work, PIL–IL membranes of pyrrolidinium-based PILs containing $[TFSAM]^-$, $[FSI]^-$ and $[TSAC]^-$ anions were prepared by the incorporation of ILs containing the same anions. The composite membranes as well as the pure PIL and IL components were characterized by different techniques (TGA, DSC, FT-IR and Raman) and their CO_2/H_2 separation performance was evaluated using the time-lag method at biohydrogen production conditions.

Experimental Section

Time-Lag Equipment

Temperature: **303 K**
Feed pressure: **1 bar**

Solution-Diffusion Mechanism

$$P = D \times S$$

Permeation cell

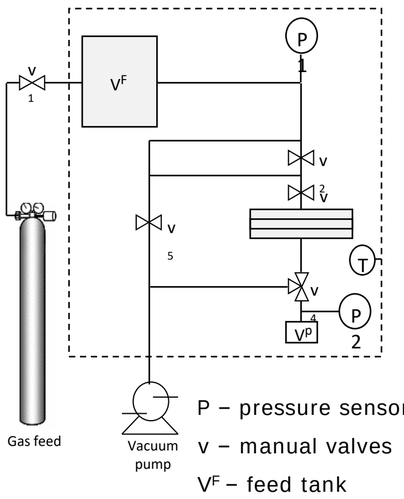

P – pressure sensors
v – manual valves
V^F – feed tank
V^P – permeate tank
T – thermostatic air bath

PIL–IL Composite Membranes

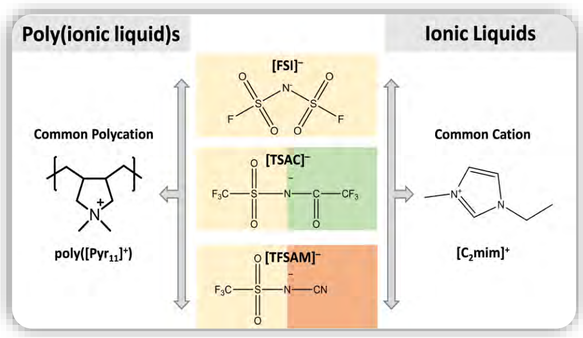

Chemical structures of the PILs and ILs used in this work.

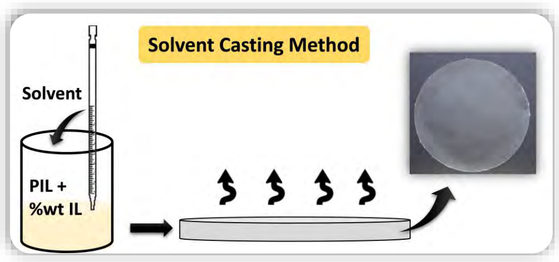

Results and Discussion

Thermogravimetric Analysis (TGA)

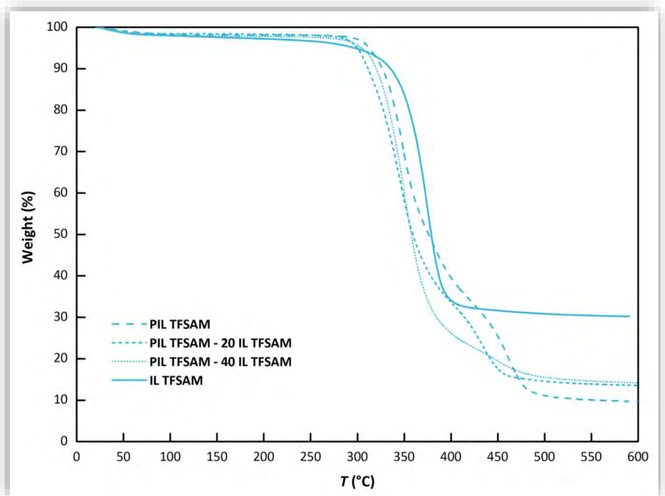

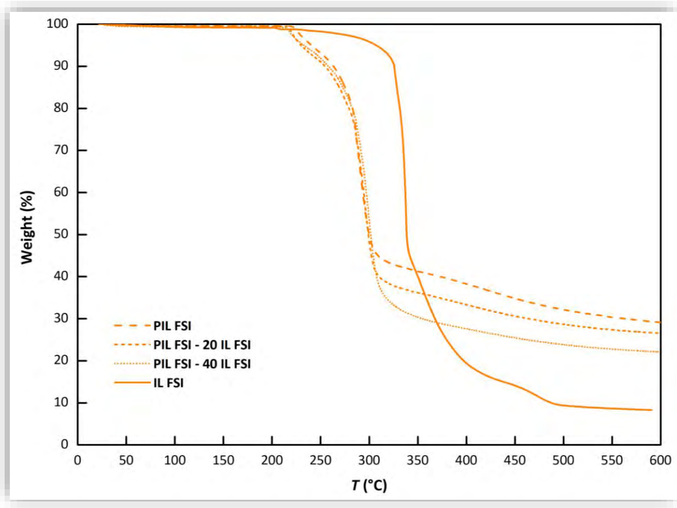

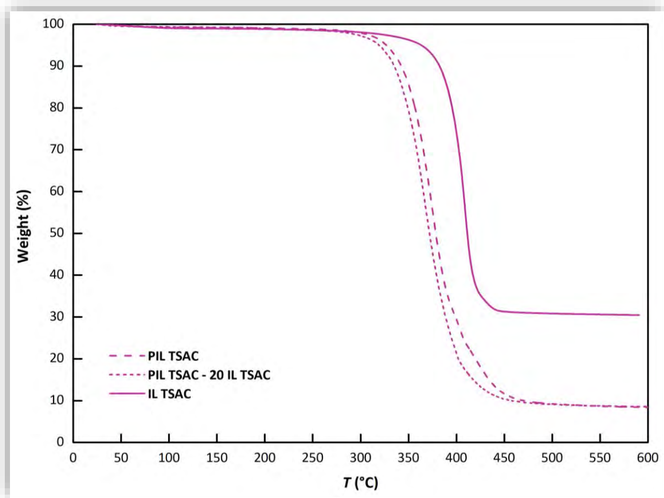

From the TGA results, different trends were observed for degradation temperatures of the PIL–IL composites with the addition of free IL. In fact, the thermal stability of the prepared PIL–IL membranes not always follows a simple mixing rule.

CO_2/H_2 Separation Performance

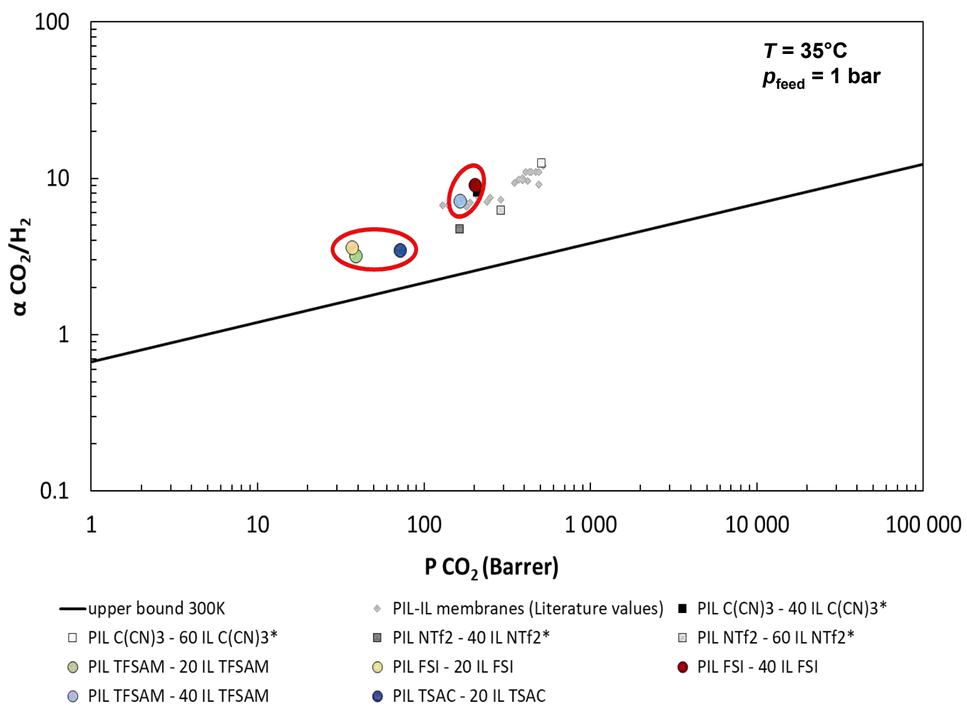

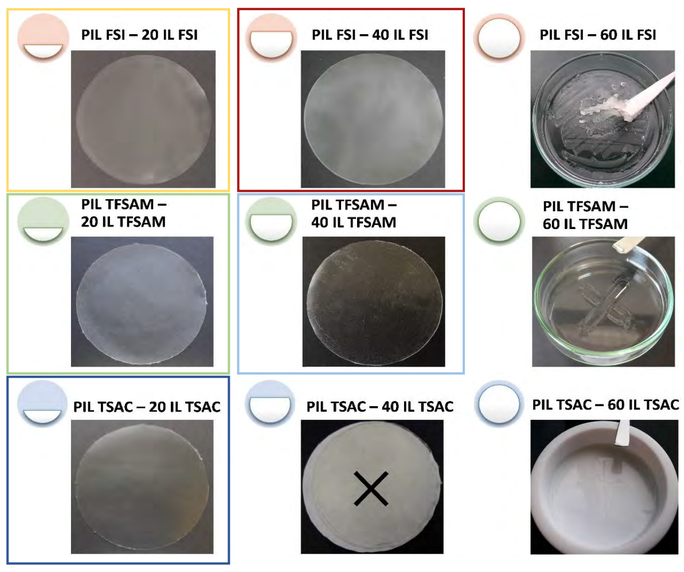

Higher CO_2/H_2 selectivities were obtained for both PIL FSI– 40 $[C_2mim][FSI]$ (α = 9.0) and PIL TFSAM– 40 $[C_2mim][TFSAM]$ (α = 7.1) compared to those of reported composites containing the conventional $[NTf_2]^-$ anion (PIL NTf_2 – 40 $[C_2mim][NTf_2]$ (α = 6.5) and PIL NTf_2 – 60 $[Pyr_{14}][NTf_2]$ (α = 6.3).

Conclusions

- PILs and ILs containing anions based on fluorosulfonyl derivatives were synthesized and characterized.
- PIL–IL membranes were prepared and their CO_2 and H_2 permeation properties were studied.
- The prepared PIL-IL membranes revealed CO_2/H_2 separation performances above the upper bound.

Funding:
Centro de Química Estrutural is funded by Fundação para a Ciência e Tecnologia – project UID/QUI/00100/2019.
This work was supported by FCT through the project PTDC/CTM-POL/2676/2014.
Andreia S.L. Gouveia is grateful to FCT for her Doctoral research grant (SFRH/BD/116600/2016).

References:
[1] Merkel T.C.; Zhou M.; Baker R.W., J. Memb. Sci., 389 (2012) 441–450.
[2] Tomé L.C.; Marrucho, I. M., Chem. Soc. Rev., 45 (2016) 2785.

FCT Fundação para a Ciência e a Tecnologia

Poly(vinyl alcohol) hydrogels for cartilage replacement:
Impact of processing conditions on the materials properties

Andreia S. Oliveira[1,2,5], Oumar Seidi[3], Rogério Colaço[2], Ana P. Serro[1,4]

andreia.oliveira@tecnico.ulisboa.pt

[1] CQE, IST - Universidade de Lisboa, Av. Rovisco Pais 1, 1049-001 Lisboa, Portugal
[2] IDMEC, IST - Universidade de Lisboa, Av. Rovisco Pais 1, 1049-001 Lisboa, Portugal
[3] ISBS - École supérieure d'ingénieurs de Paris-Est Créteil, 71 Rue Saint-Simon, 94000 Créteil
[4] CiiEM, Instituto Universitário Egas Moniz, Quinta da Granja, Monte de Caparica, 2829-511 Caparica, Portugal

CQE Química Estrutural

09 MET

INTRODUCTION

Over the past few years, hydrogels have demonstrated their potential as promising materials to be used as replacement options for cartilage damaged tissues. In particular, hydrogels made of poly(vinyl alcohol) (PVA) have attracted much attention due to their similarities to native tissue. PVA hydrogels are biocompatible, present a high swelling capacity and have a rubbery and elastic nature. In addition, PVA is easy to process and manipulate and is stable at human body temperature.

OBJECTIVE

The aim of this study was to evaluate the effect of the preparation conditions on the swelling capacity, microstructure, mechanical properties and thermotropic behavior of PVA-based materials.

MATERIALS

PVA solution at 15% w/v in DD water

Dissolution — 6 h — 95 ºC

Processing strategies

Cast-drying method (CD)

Drying temperature: 20ºC OR 30ºC

SAMPLES: CD 20 and CD 30.

Freeze-thawing method (FT)

Nº of cycles: 15

Freeze time / Thawing time: 21h / 3h OR 23h / 1h

SAMPLES: FT 21-3 and FT 23-1.

METHODS

Swelling ratio

Samples dried at 60ºC until reach the equilibrium.

$$\%SR = \frac{Weight_{water}}{Weight_{dry\ hydrogel}} \times 100$$

Differential scanning calorimeter

DSC (200 F3 Maia, NETZSCH).

Samples dried at 60ºC for 8 days.

Degree of crystallinity $\%DC = \frac{\Delta H_f}{\Delta H_{f^*}} \times 100$

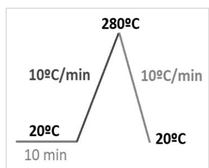

Scanning electron microscopy

FEG-SEM (JSM−7001F, JEOL).

Samples lyophilized for 50 h and coated with 20nm of Au/Pd.

Compression

Texturometer (TA.XT Express Texture Analyzer, Stable Micro Systems). Uniaxial mode.

Performed at 25ºC. Limit: F = 50N.

Tensile

Limit: Until it break. Performed at room temperature.

RESULTS AND DISCUSSION

Swelling

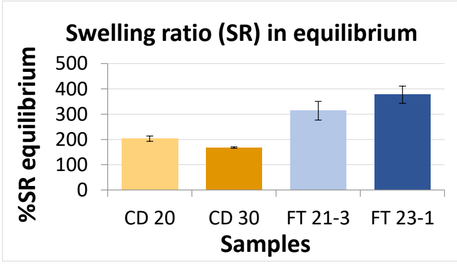

CD samples present lower swelling ratios than FT samples.

Thermotropic behaviour

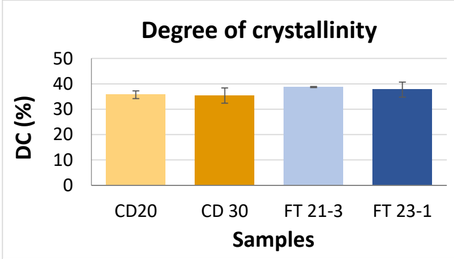

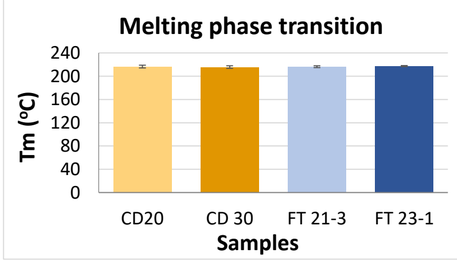

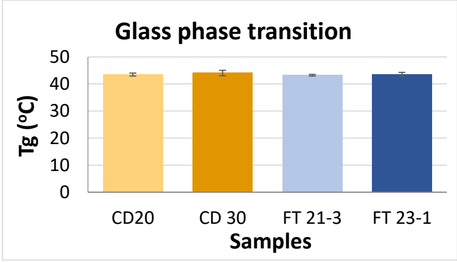

Thermotropic behavior almost was not affected by the materials preparation conditions.

Microstructure

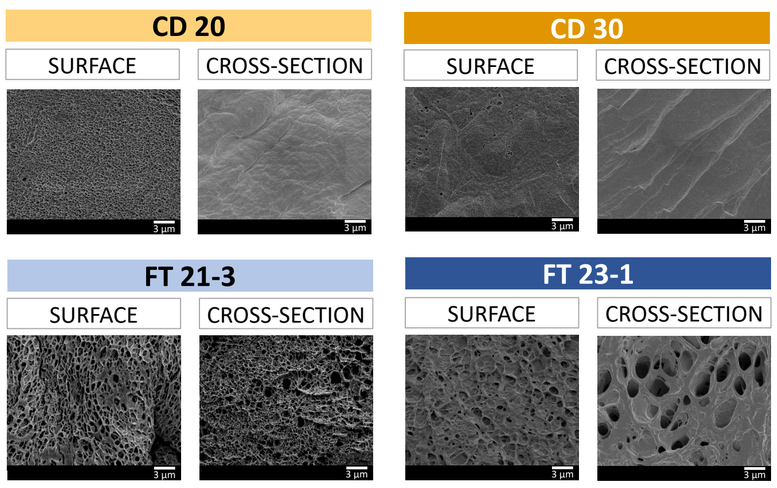

CD samples are less porous than FT samples.

Mechanical Properties: Compression

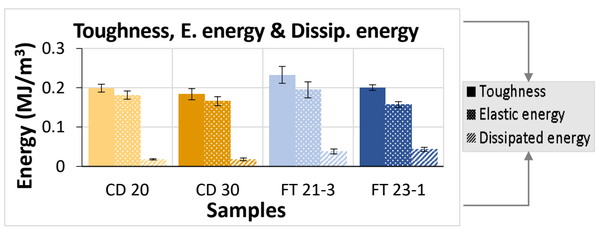

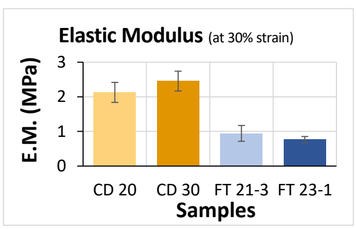

CD samples are more rigid and dissipate less energy.

Mechanical Properties: Tensile

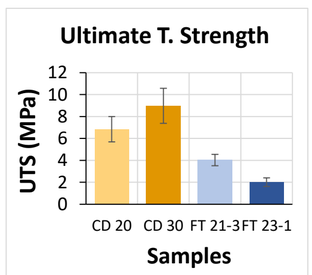

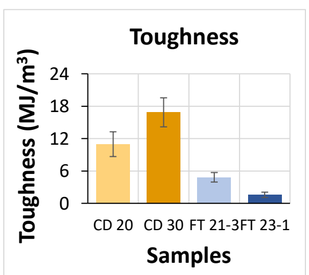

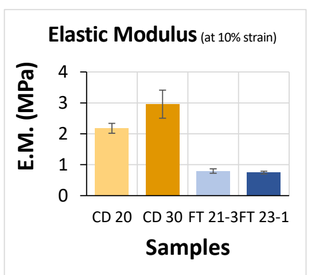

CD samples have higher ultimate tensile strength and toughness.

CONCLUSION

The results demonstrate that the mechanical properties of PVA hydrogels are strongly determined by the preparation conditions. The CD method allowed to obtain hydrogels with greater mechanical resistance and with promising characteristics for cartilage substitution.

Funding:

This work was supported and funded by Fundação para a Ciência e a Tecnologia, I.P., through the PhD grant PD/BD/128140/2016 (MIT - Portugal program), the research project PTDC/CTM-CTM/29593/2017, and the unit projects UID/QUI/00100/2019 (CQE), UID/BIM/04585/2019 (CiiEM) and UID/EMS/50022/2019 (IDMEC).

Acknowledgements:

To Kuraray Group for providing the PVA powder.

Keywords:

poly(vinyl alcohol), hydrogel, cartilage replacement.

Optimization of metal loaded hierarchical zeolite structures MOR, BEA, and MFI for catalytic oxidation reactions

Leonardo Ansari[1,2], Ana P. Carvalho[3], Luísa Martins[2], Angela Martins[1,3*]

[1] ADEQ, ISEL-IPL, Rua Conselheiro Emídio Navarro, 1959-007 Lisboa, Portugal

[2] CQE, Complexo I, IST, Universidade de Lisboa, Av. Rovisco Pais, 1049-001 Lisboa, Portugal

[3] CQB and CQE, Faculdade de Ciências, Universidade de Lisboa, 1749-016 Lisboa, Portugal

amartins@deq.isel.ipl.pt

CQE Química Estrutural

01 CCC
06 CE

Introduction

In this work hierarchical zeolite structures MFI, BEA and MOR (**Figure 1**) were prepared by desilication procedures, followed by acid treatment.

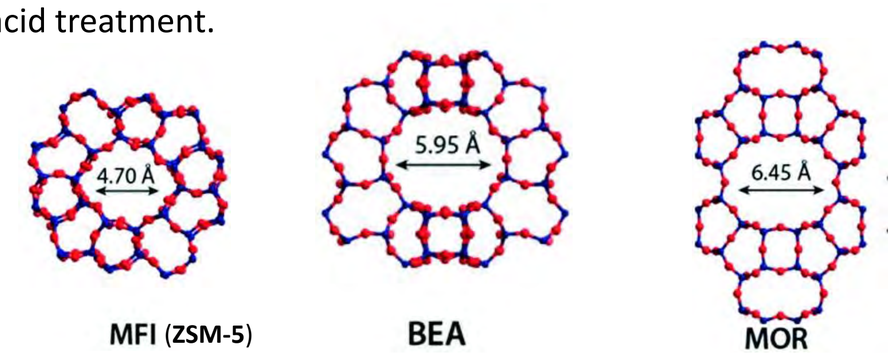

Figure 1. Zeolite structures studied .

The catalytic behavior of metal loaded (Fe) hierarchical zeolites structures) was explored in the oxidation of 1-phenylethanol into acetophenone (**Figure 2**). The metal was introduced by mechanochemical grinding using a ball mill and the catalytic reaction was performed using microwave radiation as a heating source.

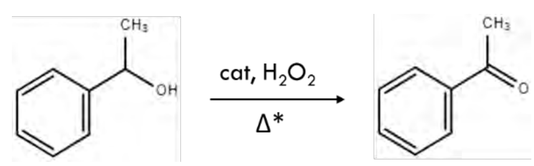

Figure 2. Oxidation of 1-phenilethanol into acetophenone under microwave heating.

Experimental Procedure

- **Preparation of the hierarchical zeolites**:

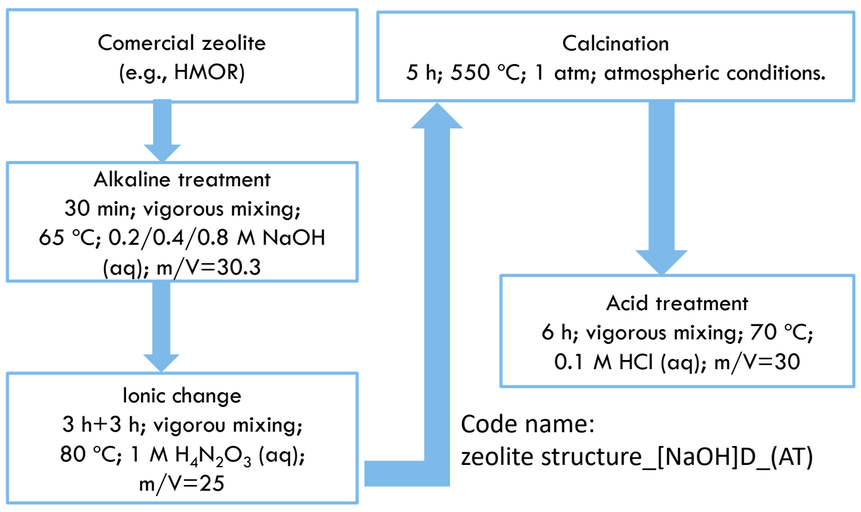

- **Immobilization of Iron in zeolite support**:

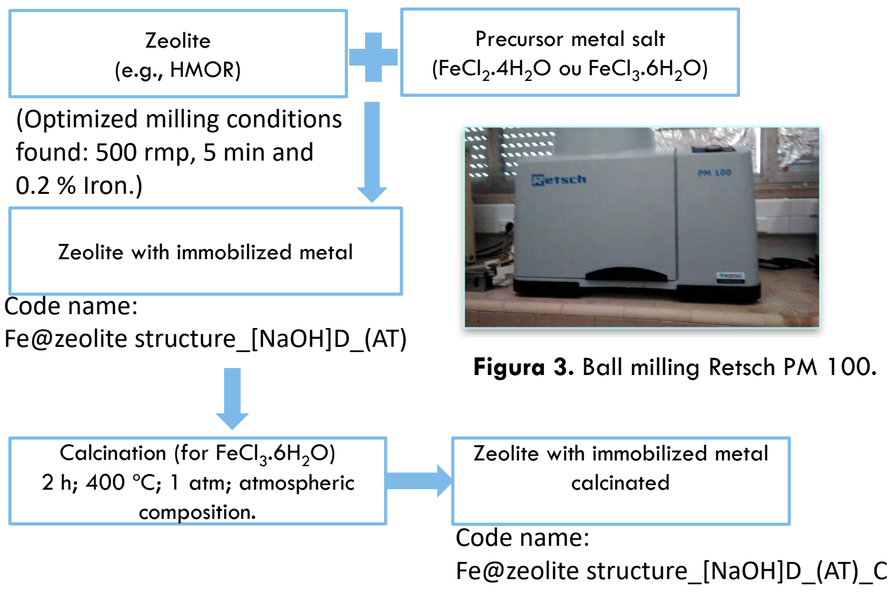

Figura 3. Ball milling Retsch PM 100.

- **Characterization methods:**

X-Ray Diffraction – Analytical X'Pert PRO with X'Celerator detector with an angular scan (2 θ) ranging between 5 and 40, with a step of 0,017º and a time/step of 20s.

Adsorption of N_2 at -196 °C – Micromeritics ASAP 2010; m_{sample} = 50 mg ; degasification at T=150 ° C, for 2 h under vacuum better than 10^{-2} Pa.

Results

- Characterization:

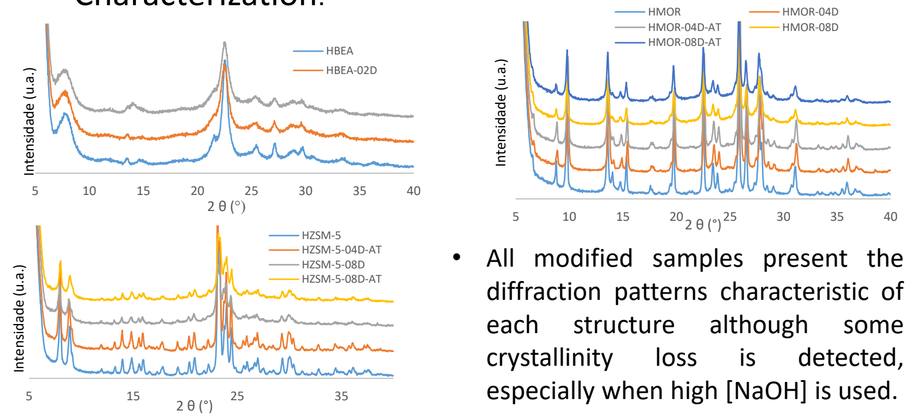

Figure 4. Diffraction patterns of parent and modified supports.

- All modified samples present the diffraction patterns characteristic of each structure although some crystallinity loss is detected, especially when high [NaOH] is used.

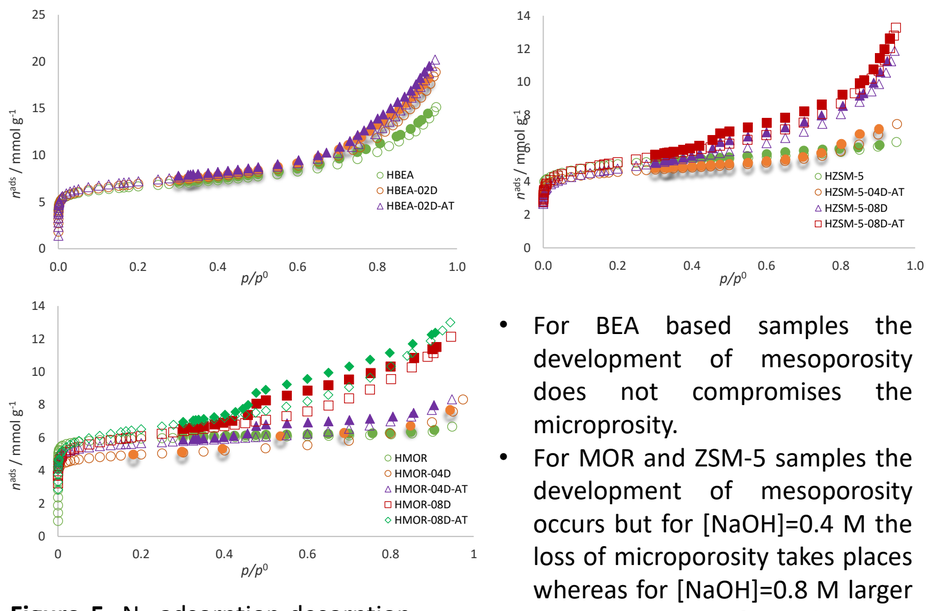

Figure 5. N_2 adsorption-desorption isotherms at -196 °C for parent and modified supports.

- For BEA based samples the development of mesoporosity does not compromises the microprosity.
- For MOR and ZSM-5 samples the development of mesoporosity occurs but for [NaOH]=0.4 M the loss of microporosity takes places whereas for [NaOH]=0.8 M larger micropores are formed during treatments.

- **Catalytic tests:**

The catalytic tests were performed in a microwave reactor under previously optimized conditions: 100 °C, 600 rpm and 50 min.

Figure 6. Microwave reactor, Anton Paar.

Product analysis - Gas Chromatograph FISONS Instruments. Nitromethane was used as internal standard.

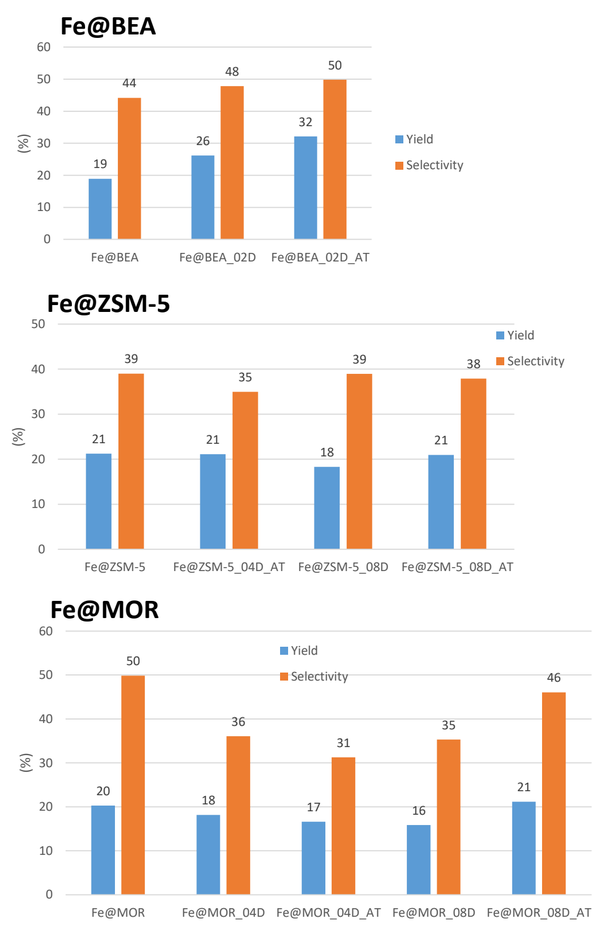

Figure 7. Product yield and selectivity for parent and modified Fe@ZSM-5, BEA and MOR.

- For Fe@BEA samples both alkaline and alkaline + acid treatment led to an increase in yield and product selectivity.
- For Fe@ZSM-5 the treatments does not seem to affect the catalytic behaviour.
- For Fe@MOR distinct behaviour are observe according to the [NaOH], besides lower selectivities and yields were found:
- For 0.4 M there is a continuous decrease for D and AT sample
- For 0.8M upon AT an important recover of selectivity and product yield is verified

Conclusions

- Hierarchical zeolite supports were successfully prepared exhibiting micro + mesoporosity with good crystallinity.
- The treatments affect the catalytic behaviour distinctively for each support.
- Fe@BEA catalysts present the most promising catalytic behaviour so far.

Funding:
Centro de Química Estrutural is funded by Fundação para a Ciência e Tecnologia – project UID/QUI/00100/2019, UID/MULTI/00612/2019 and PTDC/QEQ/ERQ/1648/2019

References:
[1] Grau-Atienza A., Campos R., Serrano E., Ojeda M., Romero A., Garcia-Martinez, J. Luque R. ChemCatChem 6 (2014) 3530-3539.

FCT Fundação para a Ciência e a Tecnologia

Synthesis of metallo-macrocycle and coordination polymers with pyridine based amido-carboxylate ligand and their catalytic activities towards Henry and Knoevenagel reactions

Anirban Karmakar, Guilherme M. D. M. Rúbio, M. Fátima C. Guedes da Silva and Armando J. L. Pombeiro

CQE Química Estrutural

01 CCC, SYNCat

Introduction

Coordination polymers (CPs) are compounds consisting of inorganic metal ions and organic linkers, which have attracted a significant interest recently.[1] The rapid development in this field is due to their attractive structures and topologies, as well as to their uses in various areas, *e.g.*, catalysis, nonlinear optics, gas storage and separation and magnetism.[1] On the other hand, the synthesis of metallo-macrocyclic (MMC) molecules using metal-directed self-assembly is a current area of research activity.[2]

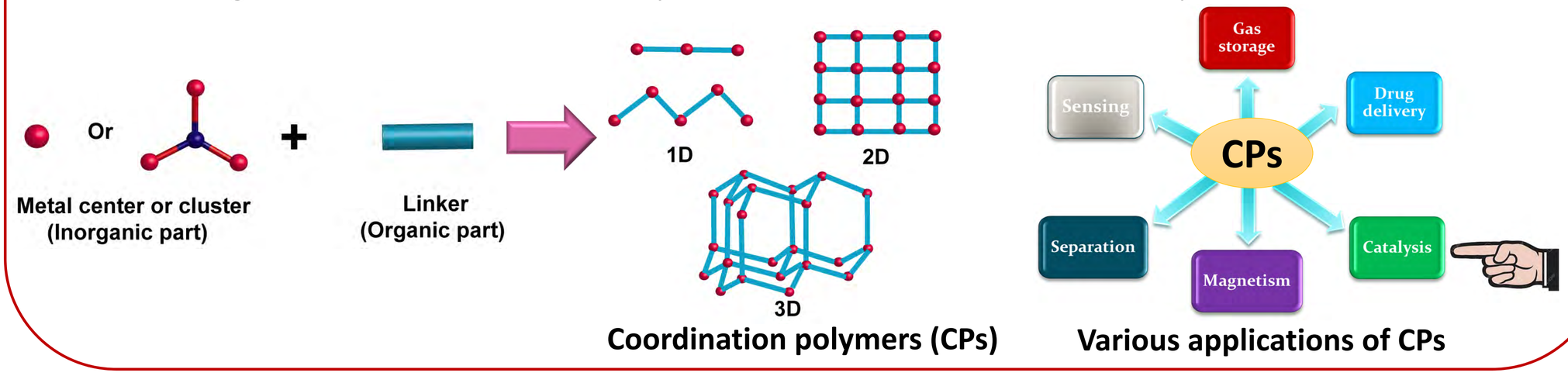

Synthesis and Structures of Metallo-macrocycle and Coordination polymers

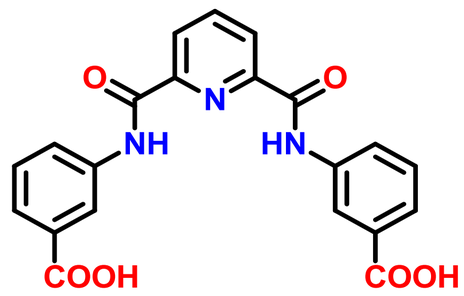

3,3'-{(pyridine-2,6-dicarbonyl)bis (azanediyl)}dibenzoic acid (H_2L)

$Zn(NO_3)_2.6H_2O$, DMF:MeOH, NH_4OH, 70°C, 48h

$Cd(NO_3)_2.6H_2O$, DMF:1,4-Dioxane, NH_4OH, 70°C, 48h

$Sm(NO_3)_3.6H_2O$, DMF:H_2O, 70°C, 48h

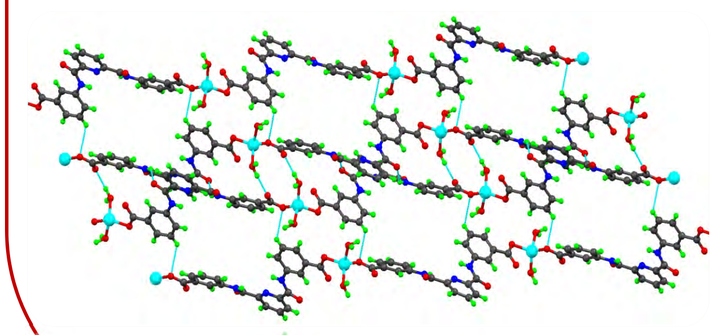

Zn(II)-CP (1)

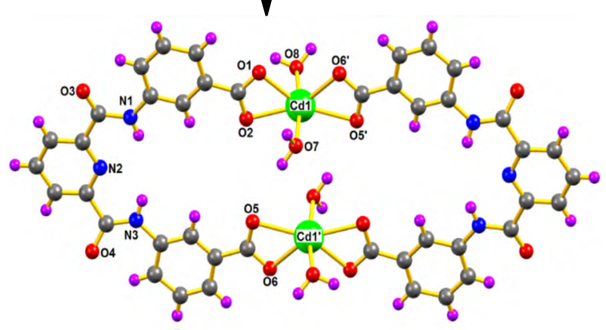

Cd(II)-MMC (2)

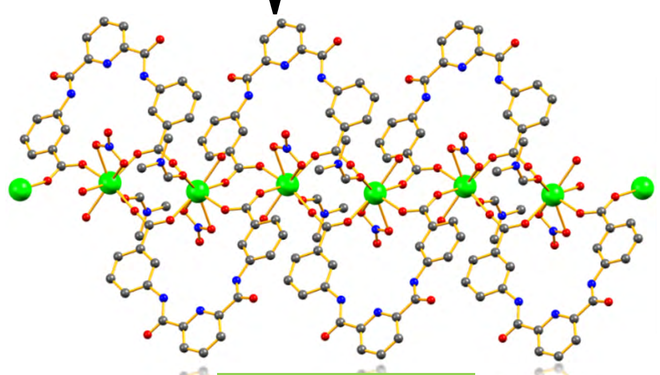

Sm(III)-CP (3)

Catalysis, Size selectivity and Recycling

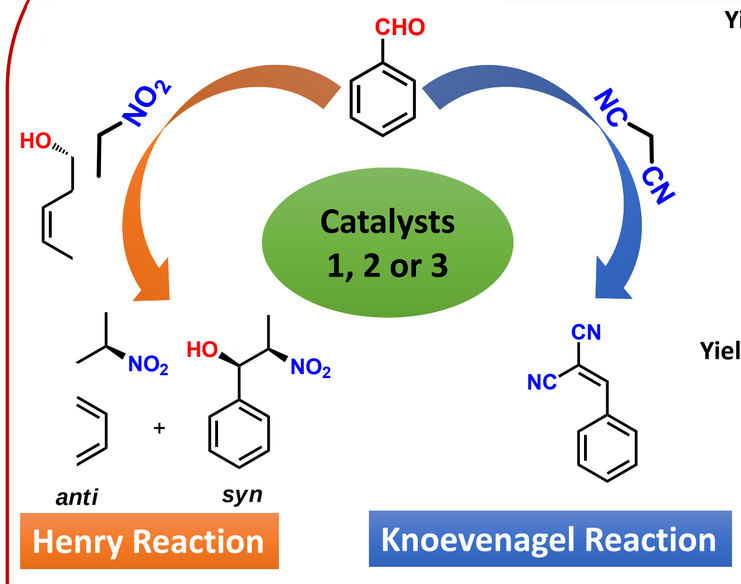

Yield *vs.* time plot for Henry reaction

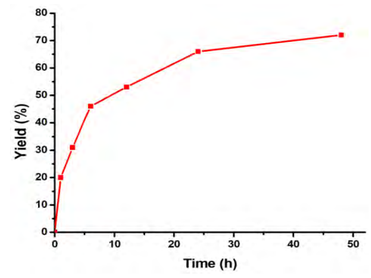

Yield *vs.* time plot for Knoevenagel reaction

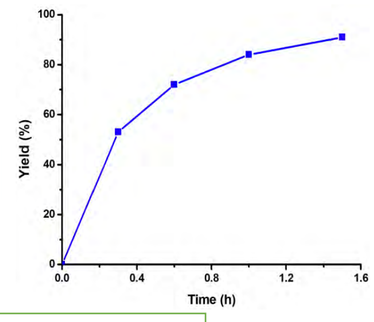

Catalysts	Yield for Henry Reaction[a]	Selectivity for Henry reaction (*syn*:*anti*)	Yield for Knoevenagel Reaction[b]
1	72	62:38	91
2	66	67:33	84
3	61	60:40	73

[a]Reaction conditions: 3.0 mol% of catalyst, benzaldehyde (52 µL, 0.5 mmol), nitroethane (0.2 mL, 2.6 mmol) and water (1.0 mL) for 48h at 70°C. [b]Reaction conditions: 2.0 mol% of catalyst, solvent (THF) 1 mL, malononitrile (66 mg, 1.0 mmol) and benzaldehyde (52 µL, 0.5 mmol) for 1.5h at 50°C.

Henry and Knoevenagel condensation reactions of substrates with different sizes catalyzed by catalyst 1

Entry	Aldehyde	Nitroalkane	Yield(%)	Entry	Active methylene compound	Yield(%)
1	Benzaldehyde	Nitromethane	79	6	Malononitrile	91
2	Benzaldehyde	Nitroethane	72	7	Ethylcyanoacetate	73
3	Benzaldehyde	Nitropropane	61	8	Tert-butyl cyanoacetate	45
4	1-Naphthaldehyde	Nitroethane	53	9	Malononitrile	82
5	9-Anthraldehyde	Nitroethane	37	10	Malononitrile	67

PXRD and FT-IR curves of 1, before and after Henry and Knoevenagel reactions

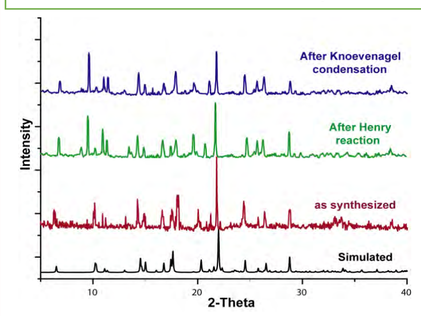

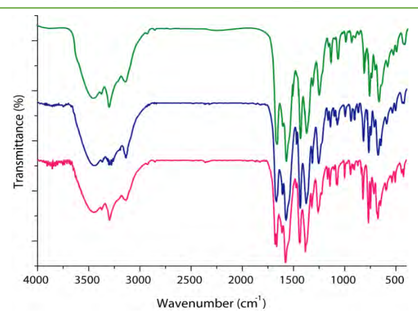

Effect of catalyst recycling on Henry and Knoevenagel reactions

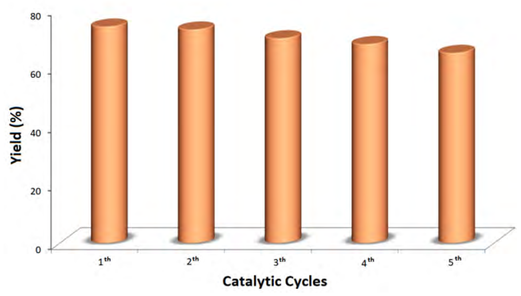

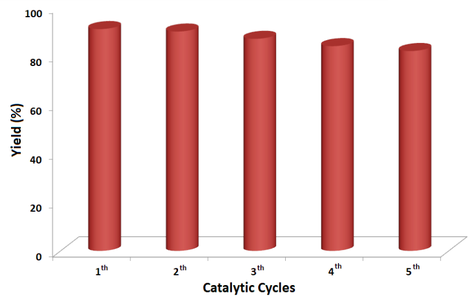

Funding:

Centro de Química Estrutural is funded by Fundação para a Ciência e Tecnologia – project UID/QUI/00100/2019. A. Karmakar expresses his gratitude to the FCT and Instituto Superior Técnico for a post-doctoral fellowship (Ref. No. SFRH/BPD/76192/2011) and for Scientific Employment contract (Contrato No: IST-ID/107/2018) under Decree-Law no. 57/2016, of August 29.

References:

1. (*a*) A. Karmakar, M. F. C. Guedes da Silva, A. J. L. Pombeiro, *Dalton Trans.* **2014**, *43*, 7795–7810; (*b*) A. Karmakar, M. F. C. Guedes da Silva, S. Hazra, A. J. L. Pombeiro *New J. Chem.* **2015**, *39*, 3004-3014; (*c*) A. Paul, A. Karmakar, M. F. C. Guedes da Silva, A. J. L. Pombeiro *RSC Adv.* **2015**, *5*, 87400-87410.
2. A. Karmakar, G. M. D. M. Rúbio, M. F. C. Guedes da Silva, A. J. L. Pombeiro, *Chemistry Open*, **2018**, *7*, 865 –877.

FCT Fundação para a Ciência e a Tecnologia

Effect of alkyl substituent's on the biological activity of benzimidazole-based Schiff base copper(II) complexes

Anup Paul,[1] Sallemuthu Anbu,[1] Gunjan Sharma,[2] Maxim L. Kuznetsov,[1] Biplob Koch,[2] M. Fátima C. Guedes da Silva,[1] Armando J. L. Pombeiro[1]

[1]*Centro de Química Estrutural, Instituto Superior Técnico, Universidade de Lisboa, Av. Rovisco Pais, 1049-001 Lisboa. Portugal.*

[2]*Departments of Zoology, Faculty of Science, Banaras Hindu University, Varanasi - 221 005 (U.P.) India.*

CQE Química Estrutural

CCC-1

Background

The majority of platinum based drugs used for cancer treatment have numerous and severe side-effects and this lead to the exploration of non-platinum metal based drugs. Amongst all the metal complexes, Schiff base Copper(II) complexes are regarded as a promising anticancer drug alternative and the design of improved antitumour agents occupies a significant place in cancer chemotherapy.[1-3]

In view of this, we have reported a new benzimidazole-based Schiff base copper(II) complexes (1-3) by varying the N-alkyl substituents' and their anti cancer properties (Fig. 1).

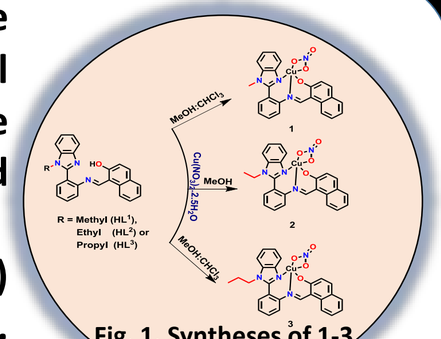

Fig. 1. Syntheses of 1-3.

Results

DNA interaction studies

Fig. 2. DNA titration profile of 1.

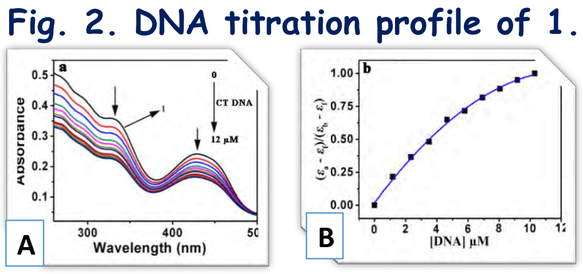

- The absorption titration profiles of 1-3 suggests intercalation between the complexes and DNA. As a representation only the titration profile of 1 is presented here [Fig. 2 (A)].
- The binding constant (K_b) of the complexes 1-3 with CT DNA, was found to be 3.45(±0.23) × 10^5 M^{-1} (*1*), 3.33 (±0.18) × 10^5 M^{-1} (*2*), 3.15 (±0.16) × 10^5 M^{-1} (*3*). The non-linear plot for 1 is shown in [Fig. 2 (B)].

Fig. 2. Ethidium Bromide (EB) Displacement Assays of 1

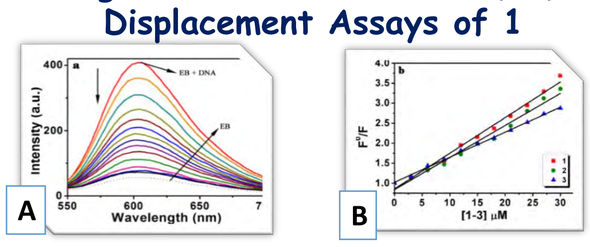

- The competitive binding studies of the complexes 1-3 to DNA, *via* the EB displacement technique led leads to quenching of the emission intensity by 82, 77 and 68%, respectively. For 1 is shown here [Fig. (A)].
- The calculated K_q values for the complexes 1-3 are 3.3 × 10^5, 2.8 × 10^5 and 1.8 × 10^5, respectively. The Stern-Volmer plot is shown in [Fig. (B)].

Molecular docking

Fig. 3. DNA titration profile of 1.

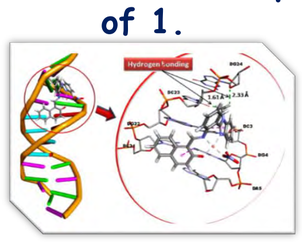

- The docking experiments revealed that the complexes interact with B-DNA (PDB ID: 1BNA) to the G-C rich intercalation site of the minor groove with relative binding energy of -341.83 (1, Shown in Fig. 3), -302.5 (2) and -301.9 (3) kJ mol^{-1}.
- The binding affinity follows the order 1 > 2 > 3.

Cytotoxicity studies MTT assay

Table 1

Compounds	Incubation time (24 h)		
	IC_{50} (μM)		
	A-549	MDA-MB-231	HeLa
1	16.7 ± 0.29	29.58 ± 1.17	32.66 ± 0.58
2	24.0 ± 1.99	31.92 ± 0.73	33.79 ± 0.36
3	29.1 ± 1.12	46.03 ± 1.12	45.27 ± 0.65

- The cytotoxicities of complexes 1-3 against three different human cancer cell lines, A-549 (lung carcinoma), MDA-MB-231 (breast cancer) and HeLa (cervical cancer) cancer cells, were evaluated (Table 1).
- Complex 1 exhibits a significant inhibitory effect on proliferation of the A-549 cancer cells and is found to be more potent than the widely used drug cisplatin (IC_{50} = 27.2 ± 1.71 μM) under similar experimental condition.

- In control cells, a uniform level of blue fluorescence nucleus was seen for treated cells, early apoptotic cells with deep blue fluorescence (yellow circle) for late apoptotic cells with fragmented nucleus (blue circle) and for necrotic cells with red fluorescence (red circle), observed upon increasing the concentration of the drug administration (15 and 18 μM) [Fig. 4].

Fig. 4. Nuclear morphology using FIs

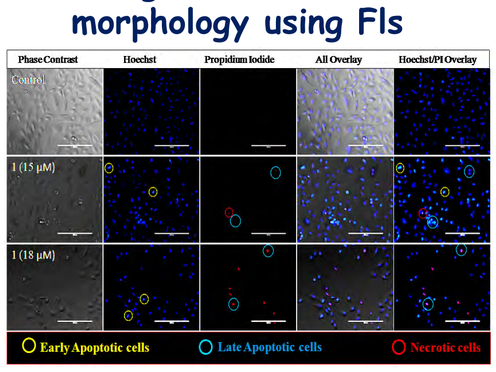

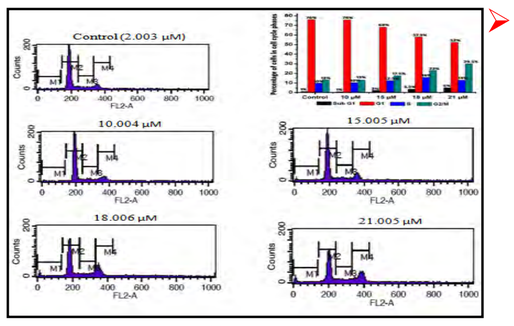

Fig. 5. Cell cycle analysis by flow cytometry

- FACS histogram shows the percentage of sub-G1 (apoptotic cell death) cells slightly increased from 1% to 5% in treated group as compared to control. Upon increasing the concentration of complex 1 (10-21 μM), a significant increase from 13% to 30% was observed in G2/M phase of cell cycle, a decrease from 76% to 52% was observed in G1 phase clearly indicating the cell cycle arrest at the G2/M phase [Fig. 5].

- In DNA fragmentation assay [Fig. 6] control DNA do not have any detectable ladder pattern, whereas the introduction of 1 (15 μM) caused a remarkable appearance of DNA fragmentation/ladder pattern. The effect becomes more prominent at higher concentrations 18 and 21 μM (lanes 4 and 5, respectively), comparable to etoposide, a known DNA damaging agent.

Fig. 6. DNA fragmentation

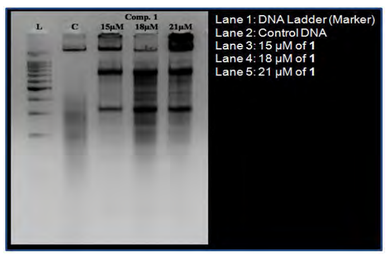

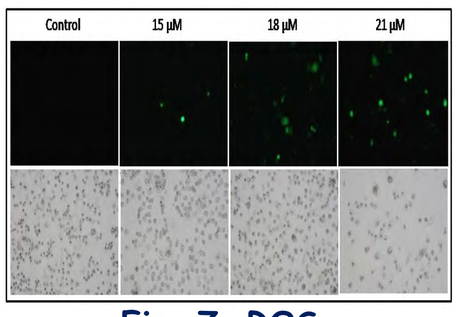

Fig. 7. ROS

- As shown in Fig. 7, after 24 h treatment, the complex under study induces an elevated level of ROS generation in a dose dependent manner. These results demonstrate that complex 1 may induce apoptotic pathways mediated by ROS.

Conclusions

- Three new N-alkyl substituted benzimidazole-based Schiff base copper(II) complexes (1-3) were synthesised and their anti-cancer properties were evaluated.
- They effectively bind to DNA through intercalative mode, in the order of 1 > 2 > 3 and the binding of the complexes to DNA minor groove through intercalative mode has been rationalized by molecular docking studies
- The complexes exhibit *in vitro* cytotoxic activity against lung (A-549), breast (MDA-MB-231) and cervical (HeLa) cancer cell lines, with potency of 1 (with the shortest alkyl substituent, i.e., methyl) being even higher than that of the widely used drug cisplatin (IC_{50} = 27.2 ± 1.71 μM) against lung cancer (A-549) cell line. The greater antiproliferative activity of the complex 1 was further proved by morphologic, cell cycle, DNA fragmentation and ROS studies.

Funding:
Centro de Química Estrutural is funded by Fundação para a Ciência e Tecnologia – project UID/QUI/00100/2019.

FCT Fundação para a Ciência e a Tecnologia

References:

1. A. Paul, S. Anbu, G. Sharma, M. L. Kuznetsov, B. Koch, M. F. C. Guedes da Silva, A. J. L. Pombeiro, Dalton Trans. 15 (2015) 19983-19996.
2. A. Paul, R.K. Gupta, M. Dubey, G. Sharma, B. Koch, G. Hundal, M. S. Hundal, D. S. Pandey, RSC Adv. 4 (2014) 41228-41236.
3. R. K. Gupta, G. Sharma, R. Pandey, A. Kumar, B. Koch, P-Z Li, Q. Xu, D. S. Pandey, *Inorg. Chem.* *52* (2013) 13984–13996.

Acknowledgment
A. Paul acknowledges financial support from FCT for post-doctoral fellowship (SFRH/BPD/88450/2012).

CQE Days
Spring Meeting 2019

Synthesis and structures of Al(III), Fe(III) and Cu(II) formazanates

Atash V. Gurbanov,[1,2] M. Fátima C. Guedes da Silva,[1] Kamran T. Mahmudov,[1,2] Armando J.L. Pombeiro[1]

[1] *Centro de Química Estrutural, Instituto Superior Técnico, Universidade de Lisboa, Av. Rovisco Pais, 1049–001 Lisboa, Portugal*
[2] *Department of Chemistry, Baku State University, Z. Xalilov Str. 23, Az 1148 Baku, Azerbaijan*

Formazans have been attracted much attention due to their optical properties, *E/Z* isomerization, analytical and biomedical applications, etc. [1,2]. Attachment of substituents to formazan moiety allows to improve their properties and control/direct reactivity. In fact, cooperation of optical and redox properties makes them attractive ligands for coordination chemistry. However, the number of publications devoted to structurally characterized formazan complexes is very limited. Herein we have synthesized a new formazan ligand namely sodium 2-(2-((*E*)-cyano((*E*)-(2-sulfonatophenyl)diazenyl)methylene)hydrazineyl)benzenesulfonate (Na_2HL) and its Al(III), Fe(III) and Cu(II) (Scheme). The synthesized Al(III), Fe(III) and Cu(II) formazanates were characterized by IR, elemental analysis, ESI-MS, and single crystal X-ray diffraction.

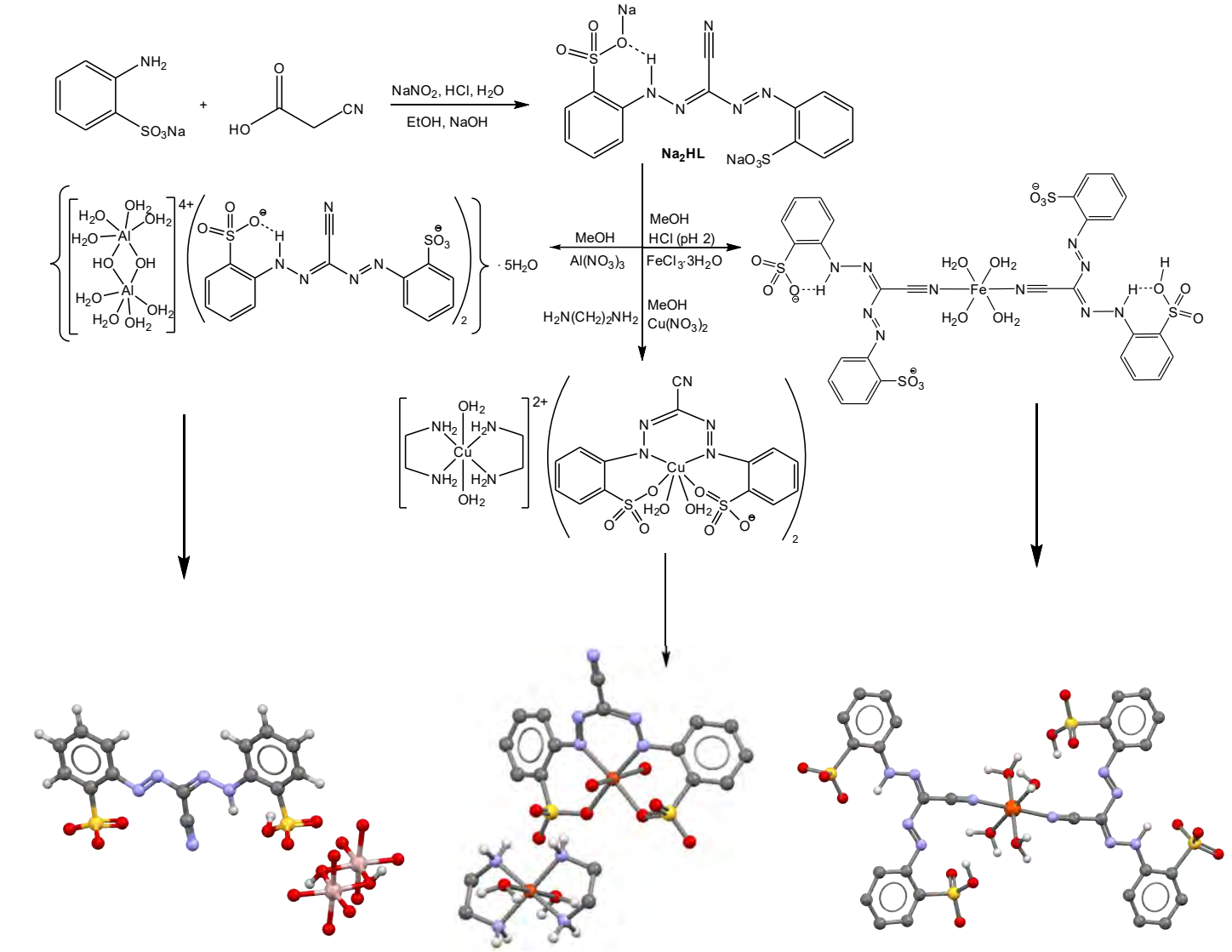

Scheme: Synthesis and structures of a formazan ligand and its Al(III), Fe(III) and Cu(II) complexes.

Keywords: Formazan; Al(III), Fe(III) and Cu(II) complexes, X-ray analysis.
Acknowledgements: AVG acknowledges the Fundação para a Ciência e a Tecnologia and Instituto Superior Técnico (DL 57/2016 and L 57/2017 Program, Contract no: IST-ID/110/2018).
Funding: This work was supported by projects UID/QUI/00100/2013 and UID/QUI/00100/2019 Fundação para a Ciência e a Tecnologia (FCT).

References:

[1] (*a*) A. W. Nineham, *Chem. Rev.,* 1955, 55, 355; (*b*) Y. Yu. Karabach and M. N. Kopylovich, ''Synthesis, applications and coordination chemistry of formazans'', in ''Ligands: Synthesis, Characterization and Role in Biotechnology'', P. Gawryszewska and P. Smoleński (eds.) Nova Science Publishers (New York), Chapter 8, 2014, pp. 249–274.
[2] (*a*) J. B. Gilroy, P. O. Otieno, M. J. Ferguson, R. McDonald and R. G. Hicks, *Inorg. Chem.,* 2008, **47**, 1279; (*b*) J. B. Gilroy, B. O. Patrick, R. McDonald and R. G. Hicks, *Inorg. Chem.,* 2008, **47**, 1287; (*c*) S. M. Barbon, J. T. Price, P. A. Reinkeluers and J. B. Gilroy, *Inorg. Chem.,* 2014, **53**, 10585; (d) S. Hong, L. M. R. Hill, A. K. Gupta, B. D. Naab, J. B. Gilroy, R. G. Hicks, C. J. Cramer and W. B. Tolman, *Inorg. Chem.,* 2009, **48**, 4514; (*e*) J. B. Gilroy, M. J. Ferguson, R. McDonald, B. O. Patrick and R. G. Hicks, *Chem. Commun.,* 2007, 126; (*f*) M.-C. Chang, T. Dann, D. P. Day, M. Lutz, G. G. Wildgoose, E. Otten, *Angew. Chem., Int. Ed.,* 2014, **53**, 4202; (g) M.-C. Chang, P. Roewen, R. Travieso-Puente, M. Lutz and E. Otten, *Inorg. Chem.,* 2015, **54**, 379.

Ocean Acidification - Study of the carbonate system in seawaters from the Portuguese Coast

Bárbara Anes, C. M. Oliveira, R.B. Silva, M. F. Camões

The **carbonate system** is one of the most important and complex systems in the **oceans**. Increasing concentrations of CO_2 in the atmosphere is followed by its dissolution in **seawater** with consequent **acidification.**

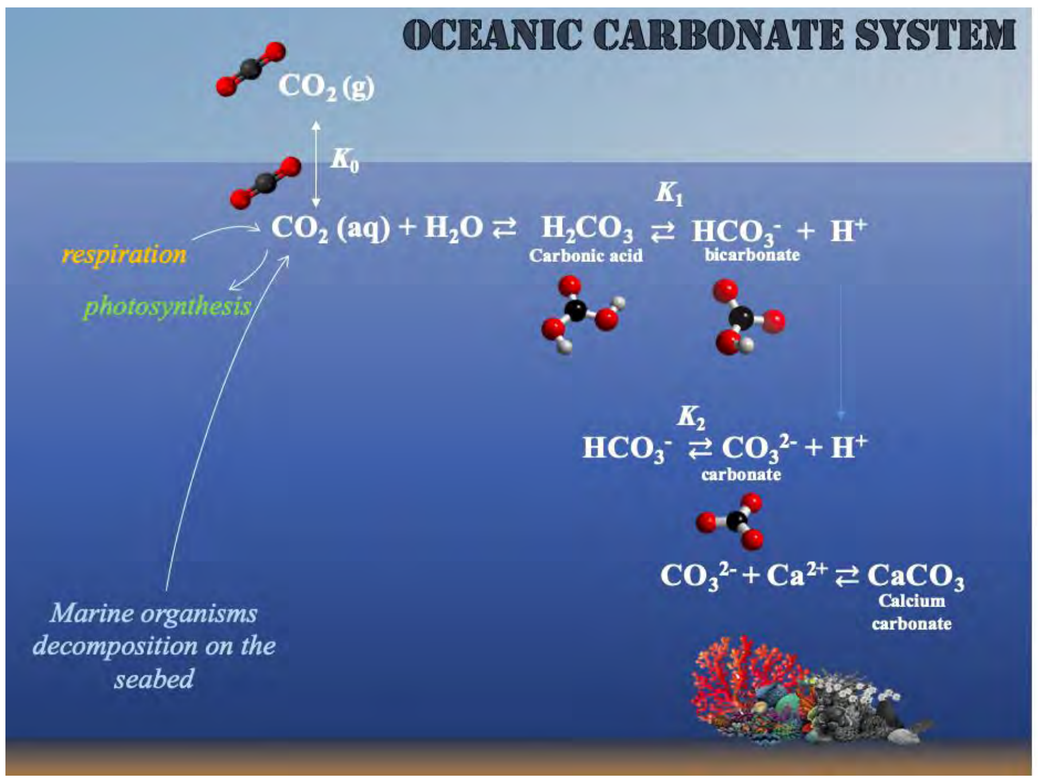

essential for shells and skeletons of many marine organisms

SAMPLE LOCATION

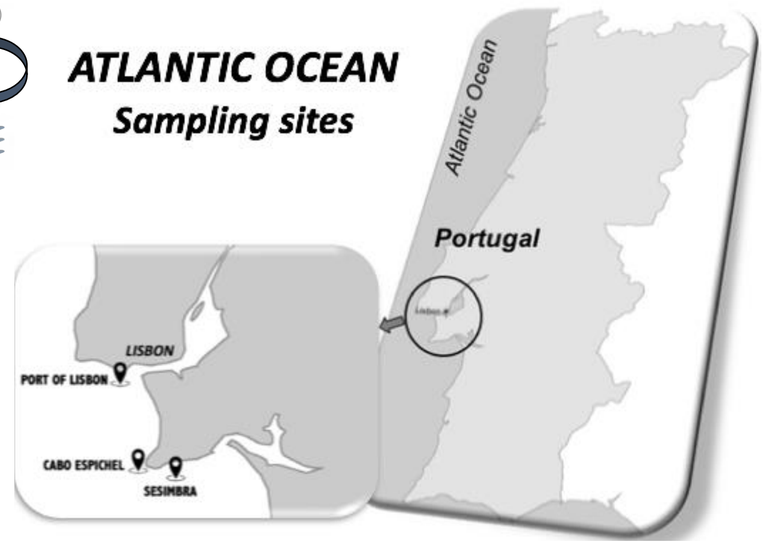

CARBONATE SYSTEM MASTER VARIABLES ⇨ knowing 2 variables makes it possible to determine the other 2

➢ **pH** Seawater $I \approx 0.67$ mol kg^{-1} ⇒ HIGH IONIC STRENGTH REFERENCE BUFFER SOLUTIONS
(proper choice of calibration standards)

$$pH = -\lg\left(\frac{a_{H^+}}{a^0}\right)$$

TRIS.TRIS HCl in Artificial Seawater

Buffer Solutions Composition (mol kg^{-1})	Reference pH ± U
0.03 TRIS-0.05 TRIS-HCl in ASW	7.8521 ± 0.0072
0.04 TRIS-0.04 TRIS-HCl in ASW	8.0756 ± 0.0071
0.05 TRIS-0.03 TRIS-HCl in ASW	8.2966 ± 0.0071

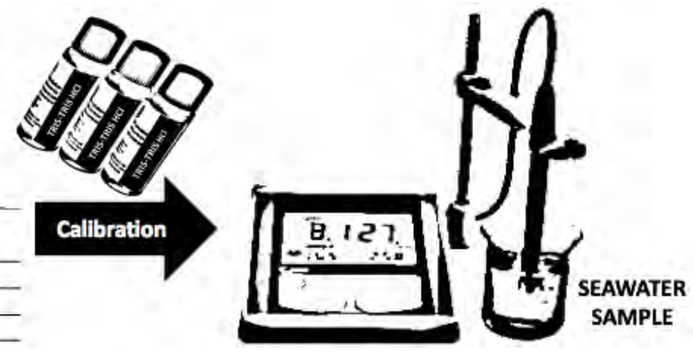

➢ **Total Alkalinity**

$$TA = [HCO_3^-] + 2\,[CO_3^{2-}]$$

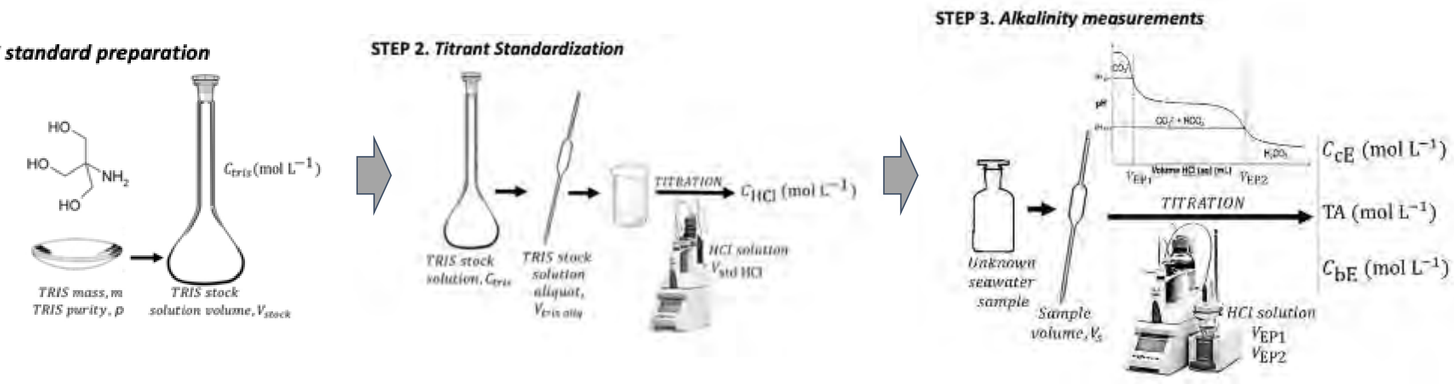

➢ ***p*CO$_2$**

$$p_{CO_2} = \frac{[CO_2]}{K_0}$$

➢ **DIC** $DIC = CO_2 = [HCO_3^-] + [CO_3^{2-}] + [CO_2]$

RESULTS ⇒ TARGET 14.3 FROM THE 2030 AGENDA

Equilibrium constants of carbonic acid: pK_1 = 5.844 ± 0.010; pK_2 = 8.935 ± 0.047

	Port of Lisbon	Cabo Espichel	Sesimbra	OSIL
Coordinates	ϕ = 38º 38'.0 N L = 009º 20'.0 W	ϕ = 38º 23'.0 N L = 009º 16'.2 W	ϕ = 38º 24'.5 N L = 009º 06'.2 W	---
pH	8.265 ± 0.019	8.210 ± 0.019	8.195 ± 0.019	8.192 ± 0.019
TA/mol L^{-1}	2423 ± 70	2432 ± 70	2428 ± 78	2423 ± 80
[HCO_3^-]/mol L^{-1}	1822 ± 64	1805 ± 63	1814 ± 73	1813 ± 73
[CO_3^{2-}]/mol L^{-1}	301 ± 10	313 ± 9	307 ± 10	305 ± 10
[CO_2]/μmol L^{-1}	6.91 ± 0.44	7.77 ± 0.49	8.09 ± 0.53	8.14 ± 0.54
DIC /μmol L^{-1}	2130 ± 63	2126 ± 63	2129 ± 72	2427 ± 71
*p*CO$_2$/μatm	244 ± 16	274 ± 18	285 ± 19	287 ± 19

Results reported with expanded uncertainty, *U'* for a confidence level of 95% (*k*=2)

CONCLUSIONS

- ✓ pH measurement in seawater requires TRIS-TRIS HCl solutions in ASW for calibration of measurement equipment ⟹ Associated uncertainty below target value (<0.02)
- ✓ TA is measured with *U'* =1.5%. Method allows the determination of [HCO_3^-] and [CO_3^{2-}] with *U'* < 4%
- ✓ Uncertainty propagation for the other variable of Carbonate System: *U'*(DIC) = 3%; *U'*(*p*CO_2) = 7%

RESULTS NECESSARY FOR COMPARISON PURPOSES, LONG-TERM TRENDS OR SPATIAL VARIATIONS

CQE Química Estrutural

06 CE

Funding:
Centro de Química Estrutural is funded by Fundação para a Ciência e Tecnologia – project UID/QUI/00100/2019. The authors wish also to acknowledge FCT for supporting their research, namely through the PhD Scholarship SFRH/BD/111437/2015

FCT Fundação para a Ciência e a Tecnologia

References:

Stum, W., & Morgan, J. J. (1996). *Aquatic Chemistry - Chemical Equilibria and Rates in Natural Waters* (3rd ed.). New York: John Wiley & Sons Inc.

Millero, F. J. (2013). *Chemical Oceanography* (4th Editio). Boca Raton, FL: CRC Press.

Mojica Prieto, F. J., & Millero, F. J. (2002). *Geochimica et Cosmochimica Acta*, *66*(14), 2529–2540.

Anes, B., Bettencourt da Silva, R. J. N., Oliveira, C., & Camões, M. F. (2019). *Talanta*, *193*, 118–122.

Synthesis and photocatalytic application of novel diethylenetriamine modified titanate nanotubes for emergent pollutants degradation

B. Barrocas[1], M. Conceição Oliveira[2], O.C. Monteiro[1]

[1] Centro de Química Estrutural and Centro de Química e Bioquímica, Faculdade de Ciências, Universidade de Lisboa, 1749-016 Lisboa, Portugal
[2] Centro de Química Estrutural, Instituto Superior Técnico, ULisboa, 1049-001 Lisboa, Portugal

Introduction

Pharmaceuticals and personal care products (PPCPs) disposal has become very problematic nowadays. These emergent pollutants are resistant to conventional treatments and even at very low concentrations, they may impose toxicity at all biological hierarchy levels. Photocatalysis is attractive for several applications including for removal of pollutants from wastewater and/or air[1].

Here, new hybrid nanomaterials, were obtained through sensitization of titanate nanotubes (TNT) and titanium dioxide nanoparticles (TiO_2) with diethylenetriamine (DETA) to produce DETA-TNT and DETA-TiO_2 materials, respectively. The photocatalytic ability of the sensitized materials for the diclofenac degradation was evaluated. Secondary products were identified and quantified using LC-HR-ESI/MS. Reusability potential was evaluated in successive degradations using visible light. The sensitized samples demonstrated excellent catalytic reusability ability, without loss of chemical stability and photocatalytic performance.

Experimental[2,3]

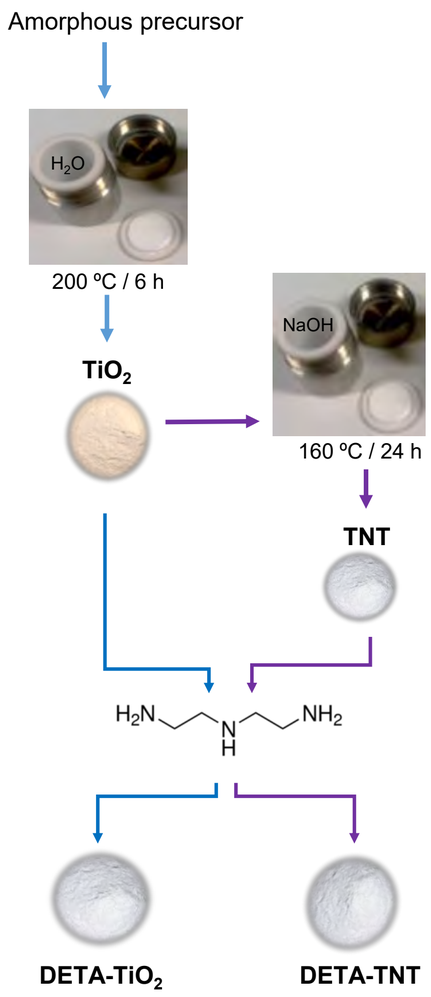

Photocatalytic experiments

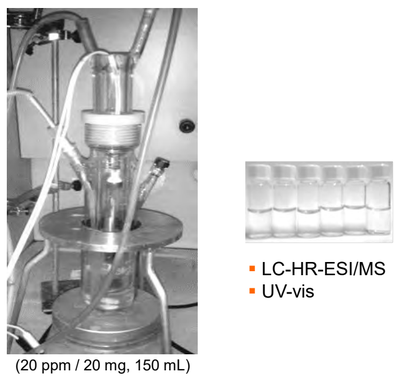

Results and discussion

XRD

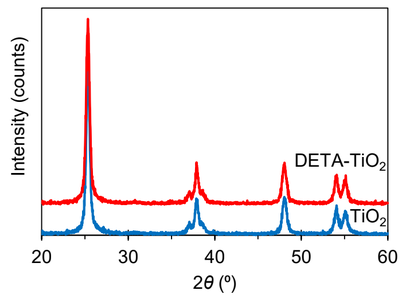

TiO_2 and DETA-TiO_2

- Both XRD patterns match with the TiO_2 *anatase* phase;
- No secondary phases of *rutile* or *brookite* were observed, nor alterations in the crystalline structure of TiO_2 after sensitization with DETA

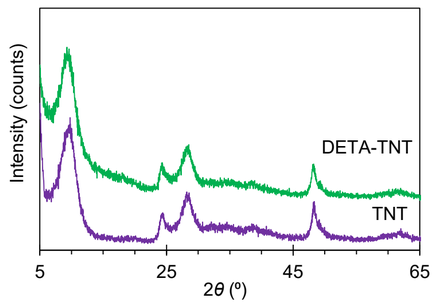

TNT and DETA-TNT

- XRD patterns are in agreement with the existence of a $Na_xH_{2-x}Ti_3O_7$ ($0 \leq x \geq 2$) titanate layered structure;
- it is perceptible a slightly shift, for lower 2θ values, of the peak at 2θ ~10º after DETA sensitization

presence of some amine molecules in the interlayers

TEM

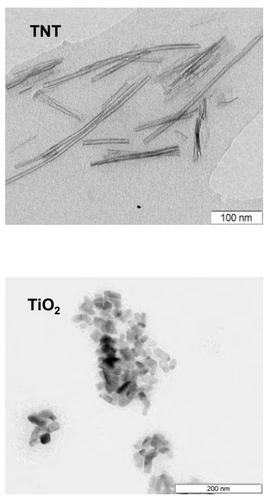

- No differences were obtained in the TiO_2 and TNT morphology after DETA modification.

B.E.T. surface area

Sample	$A_{B.E.T.}$ (m^2g^{-1})
TiO_2	60.08
DETA-TiO_2	58.62
TNT	177.88
DETA-TNT	118.41

PL

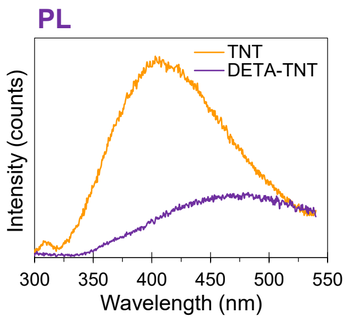

- lower recombination rate of the e^-/h^+ pairs of the DETA modified samples

DRS

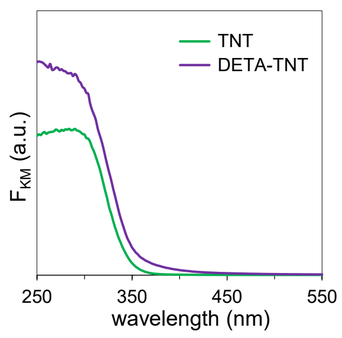

- For the DETA-TNT sample, a clearly shift to the red and an increase in the absorption intensity were observed
- No significative differences were observed in the optical behavior of the TiO_2 and DETA-TiO_2 samples.

Valence Band spectra

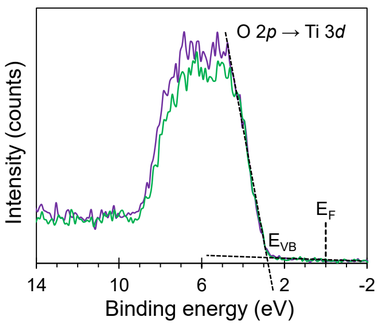

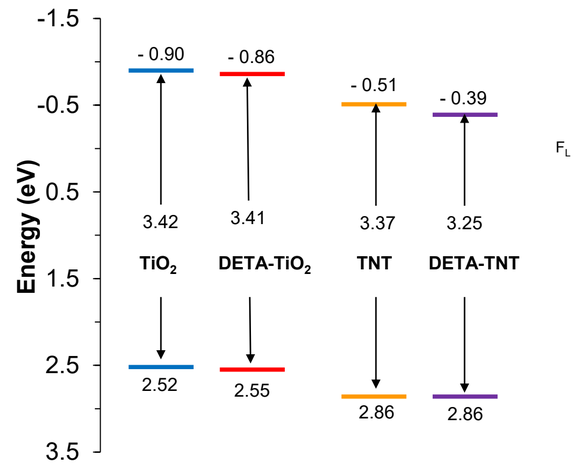

Pollutants photocatalytic degradation

Diclofenac

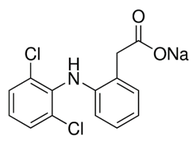

UV-vis radiation

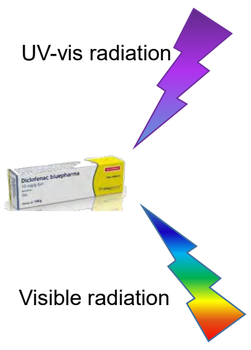

Visible radiation

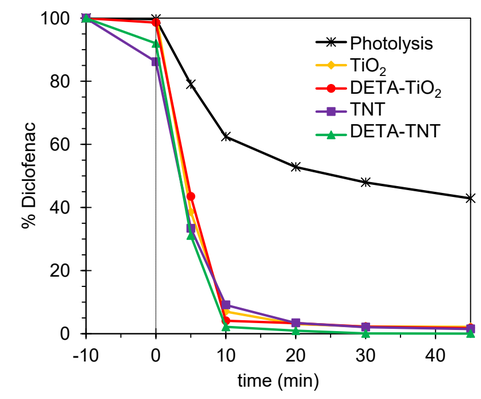

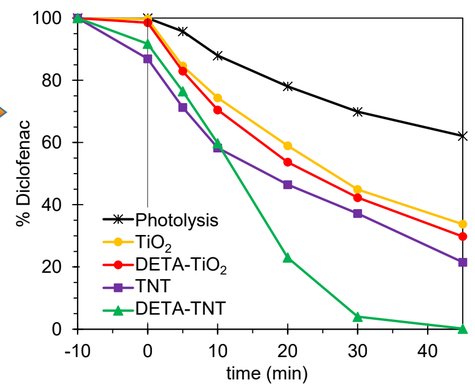

By-products formation/degradation

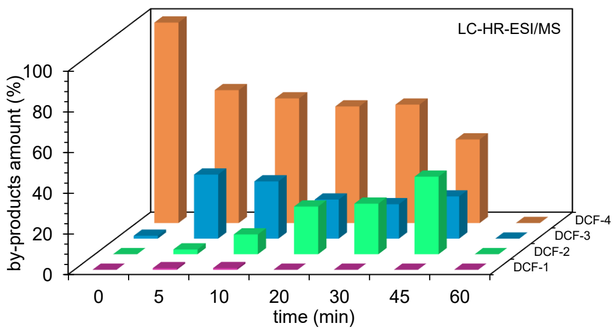

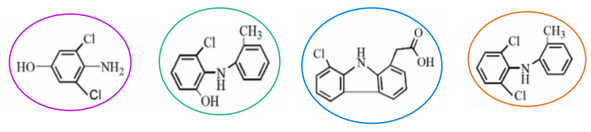

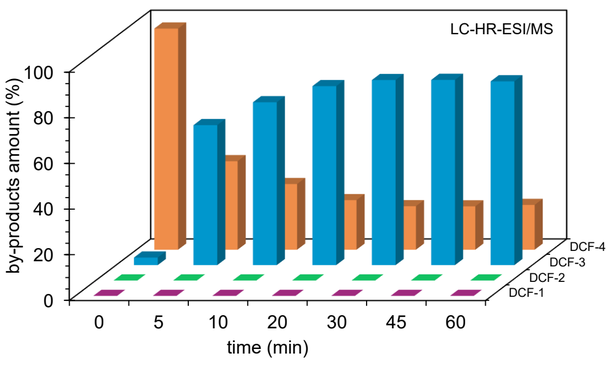

UV-vis irradiation

- All the TNT and TiO_2 samples show catalytic activity for diclofenac photodegradation;
- No significative differences were observed in TNT and TiO_2 photocatalytic activity;
- All diclofenac (20 ppm) was degraded using DETA-TNT as photocatalyst, after 10 min of irradiation;
- All by-products were removed using DETA-TNT as catalyst after 60 min of irradiation.

Visible irradiation

- TNT and TiO_2 samples show photocatalytic activity for diclofenac degradation;
- The best catalytic performance was achieved using DETA-TNT sample;
- All diclofenac has been degraded using DETA-TNT as photocatalyst, after 45 min of irradiation;
- After 60 min of irradiation, there are two by-products in solution, indicating that more time is required to complete the degradation under visible light.

Reusability experiments (visible radiation)

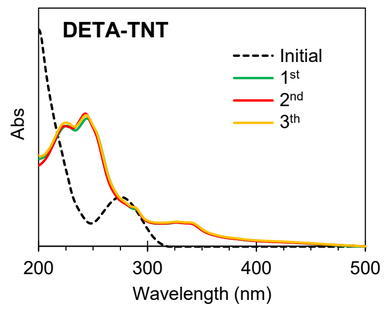

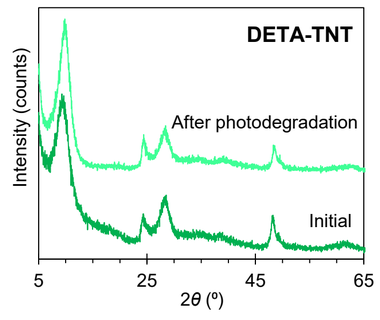

- DETA-TNT catalyst presents a excellent catalytic performance, after three reuses.
- XRD results evidenced a high stability of the DETA-TNT catalyst after 3 consecutive degradations with visible light.

Conclusions

- Nanocrystalline titanate nanotubes and TiO_2 nanoparticles sensitized with DETA were successful prepared.
- The best catalytic results, for diclofenac photodegradation, were obtained using DETA-TNT, within 10 and 45 min of UV-vis and visible light irradiation, respectively.

06 CE

Funding:
Centro de Química Estrutural is funded by Fundação para a Ciência e Tecnologia (FCT) – project UID/QUI/00100/2019.
This work was also supported by FCT projects: UID/MULTI/00612/2019, IF/01210/2014 and LISBOA-01-0145-FEDER-022125.
B. Barrocas acknowledge FCT for her PhD grant: SFRH/BD/101220/2014.

References:
1. Kaneko M., Okura I. (Eds.), Photocatalysis: Science and Technology, Biological and Medical Physics Series, Springer, Berlin 2010.
2. Ylhäinen E.K., Nunes M.R., Silvestre A.J., Monteiro O.C., J. Mater. Sci. 47 (2012) 4305–4312.
3. Barrocas B., Neves M.C., Conceição Oliveira M., Monteiro O.C., Environ. Sci.: Nano 5 (2018) 350-361.

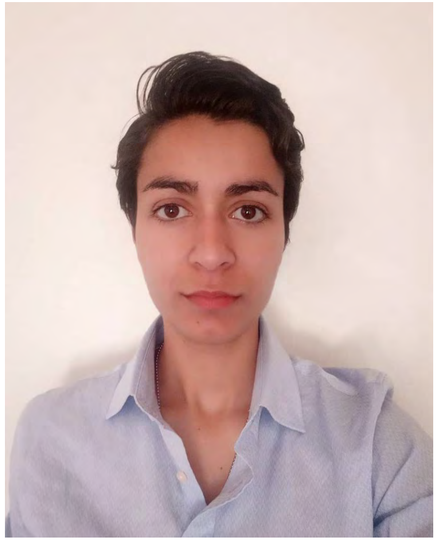

Thermal Stability of Choline Chloride-Ethylene Glycol Eutectic Mixtures: What DSC Tells Us

Beatriz Estevens Castelo Branco[1,2], Filomena Martins[1,2], Hermínio Diogo[3]

[1] Centro de Química e Bioquímica, Faculdade de Ciências, Universidade de Lisboa, Edif. C8, Campo Grande 1749-016 Lisboa, Portugal
[2] Centro de Química Estrutural, Faculdade de Ciências, Universidade de Lisboa, Edif. C8, Campo Grande 1749-016 Lisboa, Portugal
[3] Centro de Química Estrutural, Instituto Superior Técnico, Universidade de Lisboa, Avenida Rovisco Pais, 1049-001 Lisboa, Portugal

Email: beatrizestevenscb@hotmail.com

CQE Química Estrutural

09 MET

Introduction

Deep Eutectic Systems (DES) have known a huge expansion in recent years[1,2] as alternative solvents to conventional organic solvents, due to the simplicity of preparation, low melting points and low toxicities, which potentiate a wide variety of technological applications that span, among others, from the extraction and solubilization of some biomolecules to CO_2 capture.

A deep eutectic solvent consists of two or more components that liquefy upon interaction through hydrogen bonding and Van der Waals interactions. At a molecular level, these physical interactions considerably lower the melting temperature of the mixture (relative to pure components) by stabilizing the liquid phase at room temperature.

In this work, the thermal behaviour of two compositions of the eutectic mixture choline chloride (ChCl)/ethylene glycol (eg) - 1:2 and 1:9 – was explored by differential scanning calorimetry (DSC) and, complementarily, also by hot stage microscopy (HSM) and nuclear magnetic resonance (NMR).

Results

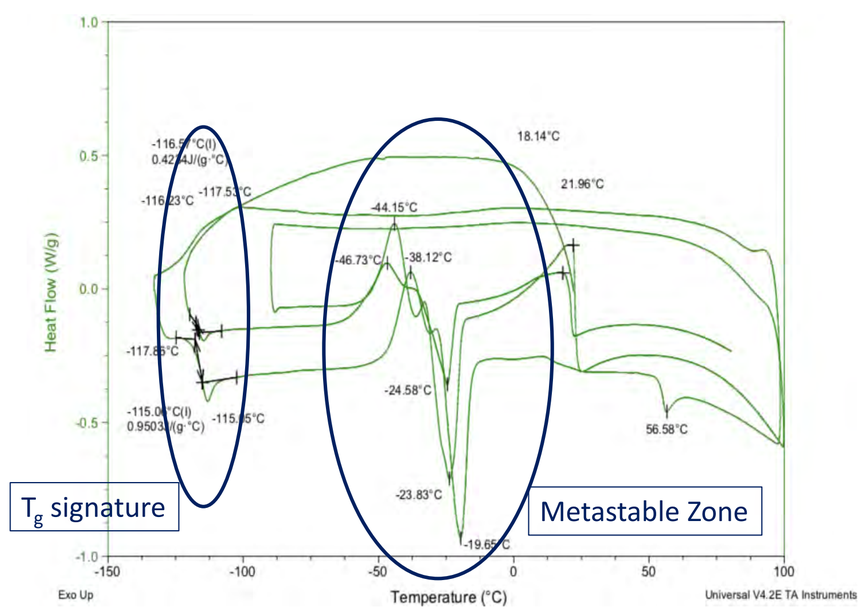

Figure 1: Thermogram of heat flow (W/g) *vs*. temperature (°C) of a liquid sample from the eutectic mixture ChCl/Eg 1:9.

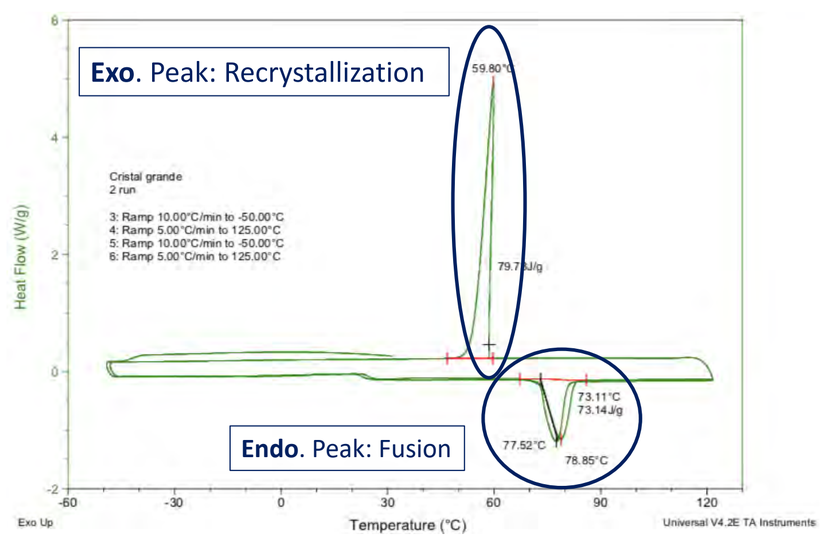

Figure 2: Thermogram of heat flow (W/g) *vs*. temperature (°C) of a needle sample, from the eutectic mixture ChCl/Eg 1:2.

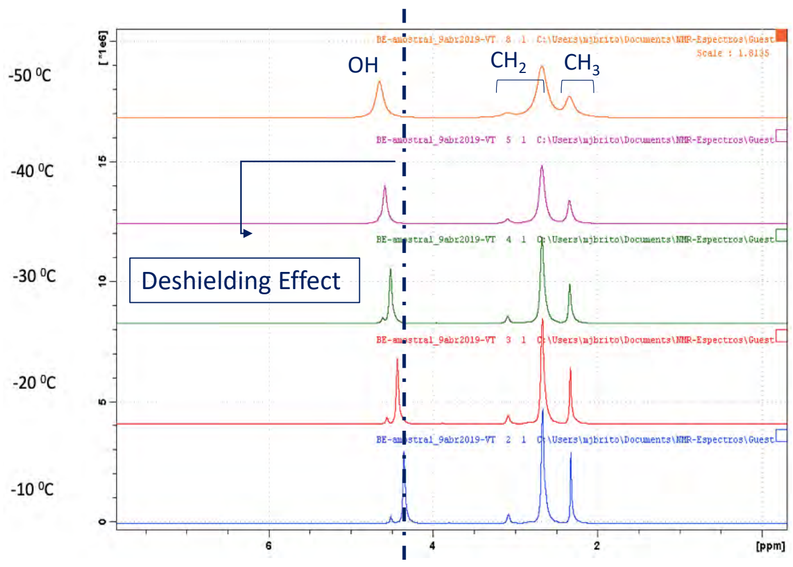

Figure 3: ^{1}H NMR (400,13 MHz, external solvent reference acetone-d_6) spectra of an eutectic mixture ChCl/Eg 1:9 monitored at -10, -20, -30, -40 and -50 °C.

Materials & Methods

DSC 2920 - TA Instruments
- ChCl/Eg 1:9; Needles 1:2
  - T∈[-130, 100] °C

Bruker 400 MHz NMR, B-ACS 60, 400 UltraShield
- ChCl/Eg 1:9
  - T∈[-50, -10] °C

Olympus Microscope BX51
- Needles of ChCl/Eg 1:2
  - T∈[-50, -10] °C

Conclusions

- 1:2 and 1:9 ChCl/Eg eutectic mixtures were assessed in the temperature range -130 °C to 100 °C by DSC and also tracked by HSM using polarized light. The 1:9 mixture showed a reproducible metastable phase at low temperatures (at ~ -20 °C), as well as a glass-transition temperature (at ~ -115 °C) – Fig. 1. 1:2 needles registered a well-defined fusion temperature, at around +78 °C, and simultaneously a recrystallization temperature at ~ 60 °C observed upon cooling – Fig. 2.
- Preliminary ^{1}H and ^{13}C NMR experiments were also carried out (Fig. 3) to tentatively rationalize the observed thermal events detected during 1:9 DSC analysis, but no structural modification was perceived in the selected temperature range, unlike what is suggested by the calorimetric results (Fig. 1).
- HSM data confirmed the calorimetric analysis of the 1:2 needles with the observation of the progressive loss of crystallinity before the fusion process (Fig. 4).
- The results gathered, suggest the need for a systematic study of the thermodynamic properties of these systems at a molecular level over time.

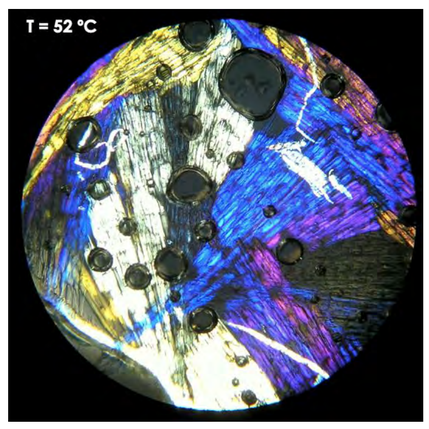

Figure 4: Image captured after DSC analysis of 1:2 needles, obtained by HSM using polarized light, at 52 °C (150x).

Funding:
Centro de Química Estrutural is funded by Fundação para a Ciência e Tecnologia – project UID/QUI/00100/2019.
Centro de Química e Bioquímica is funded by Fundação para a Ciência e Tecnologia – project UID/QUI/00612/2019.

References:

1. Smith, E. L., Abbott, A. P., Ryder, K.S., *Chem. Rev.* 114 (2014) 11060–11082.
2. Liu, P., Hao, J.-W, Mo, L.-P., Zhang, Z.-H., *RSC Adv.* 5 (2015) 48675–48704.

FCT Fundação para a Ciência e a Tecnologia

Synthetic Cathinones: Metabolite Profile by High Resolution Mass Spectrometry

Beatriz Teixeira Lopes[1,2], Maria João Caldeira[3], Helena Gaspar[2], Alexandra M.M. Antunes[1]

[1]Centro de Química Estrutural (CQE), Instituto Superior Técnico (IST), ULisboa, Avenida Rovisco Pais, 1049-001 Lisboa
[2]University of Lisbon, Faculty of Sciences, BioISI – Biosystems & Integrative Sciences Institute, Campo Grande, C8, 1749-016 Lisboa, Portugal
[3]Laboratório de Polícia Científica da Polícia Judiciária (LPC/PJ), Novo edifício Sede da Polícia Judiciária, Rua Gomes Freire 1169-007 Lisboa

Introduction

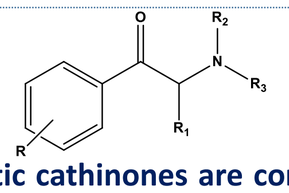

Synthetic cathinones are commonly abused new psychoactive substances (NPS)[1]. The rapid speed at which new NPS enter the market difficults the response from authorities with toxicological studies and analytical methodologies suitable for the identification and quantification of parent NPS and their metabolites in biofluids[2].

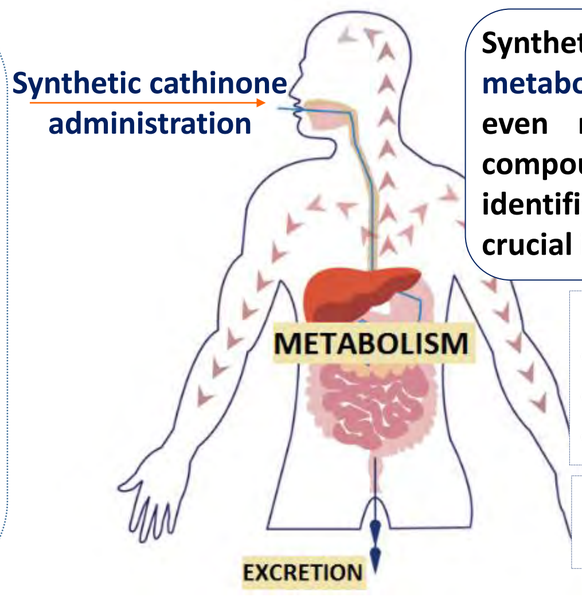

Synthetic cathinones may undergo extensive metabolism in the body, leading to low or even negligible content of the parent compound in urine. Therefore, the identification of urinary metabolites is crucial in a forensic context[3].

Phase I (Biotransformation)
- Oxidation
- Reduction
- Hydrolysis

Phase II (Conjugation)
- Glucuronidation.

Objective

This work was aimed at characterizing by high resolution mass spectrometry (HRMS) the Phase I and Phase II metabolite profiles of several synthetic psychoactive cathinones (*e.g.* α-PVP and 4Cl-PVP) upon *in vitro* incubation in rat and human liver microsomes.

Methodology

***In vitro* metabolism studies**

Rat/Human liver microsome + Alamethicin

Cathinone

Phase I co-factor : **NADPH**
Phase II co-factor : **UPDGA**

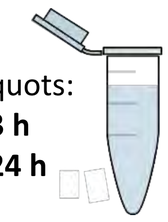

Aliquots:
- **3 h**
- **24 h**

LC-HRMS/MS

Isotope Cluster Analysis Targeted Approach

Alamethicin-induced microsomes were used for identification of glucuronide metabolites.

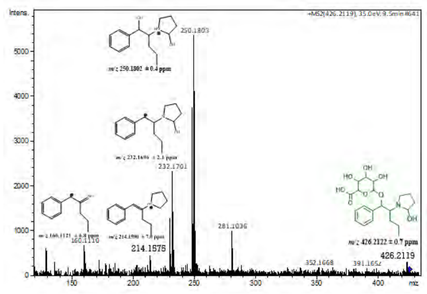

Metabolite profile identification

Results

HRMS Isotope cluster, tandem HRMS profiles and targeted search approaches were used for the identification of multiple metabolites.

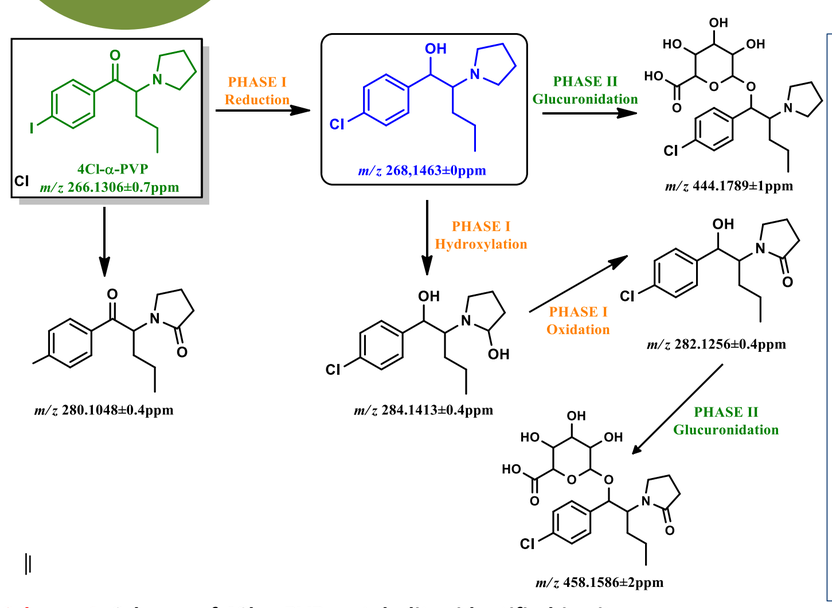

Scheme 1. Scheme of 4Cl-α-PVP metabolites identified *in vitro*.

Multiple Phase I and II metabolite of 4-Cl-α-PVP, were for the first tie identified.

This cathinone was recently introduced in the NPS market.

Figure 1 displays the tandem HRMS spectrum obtained for one of the Phase I metabolites identified for this cathinone.

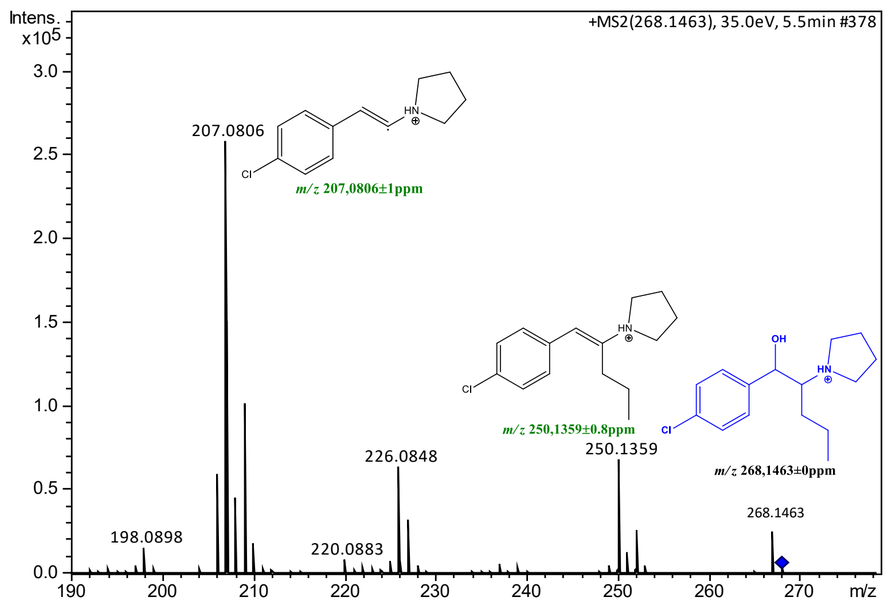

Figure 1. Tandem high resolution mass spectrum, obtained by ESI (+), and proposed fragmentation mechanisms for the new 4Cl-α-PVP-metabolite.

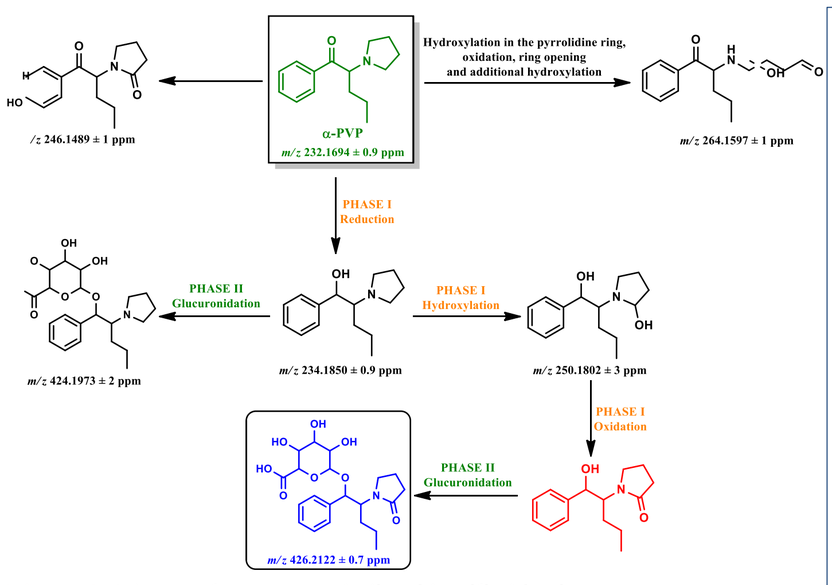

Scheme 2. Scheme of α-PVP metabolites identified *in vitro*.

For α-PVP, it was consistently identified in rat and human microsome incubations one previously uncharacterized Phase II metabolite of this cathinone.

The tandem HRMS of the protonated molecule of this new adduct presents fragment ions fully compatible with the structure ascribed (Figure 2).

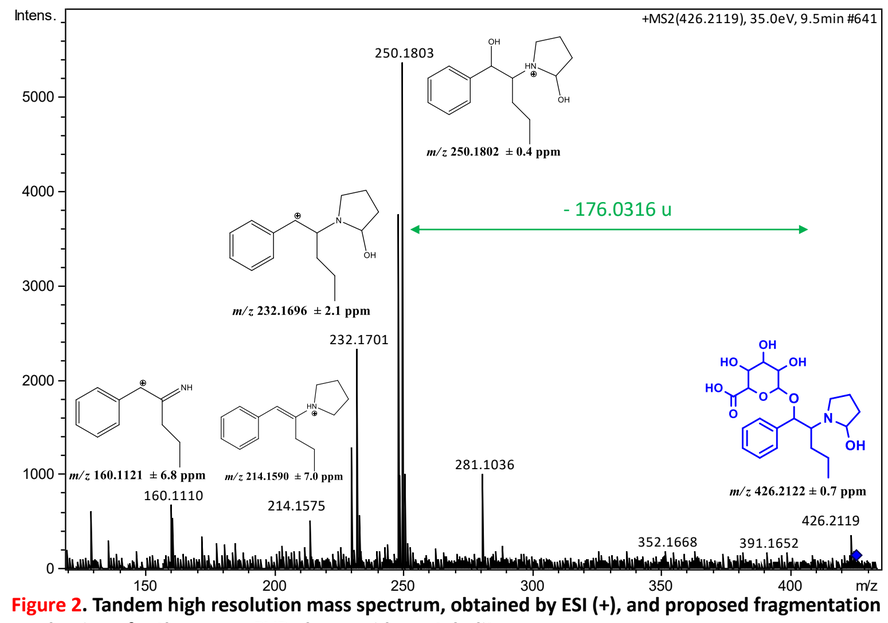

Figure 2. Tandem high resolution mass spectrum, obtained by ESI (+), and proposed fragmentation mechanisms for the new α-PVP-glucuronide-metabolite.

Conclusion

Using this approach, not only a new Phase II metabolite of drug of abuse α-PVP was identified but also multiple Phase I and II metabolites of the new NPS, 4-Cl-α-PVP, were fully characterized.
These metabolites are now available to be used as standards in a forensic context.

05 BIOMOL

Funding:
Centro de Química Estrutural is funded by Fundação para a Ciência e Tecnologia – project UID/QUI/00100/2019.
FCT is also aknowledged for projects RECI/QEQ-MED/0330/2012, CEECIND/02001/2017 and UID/Multi/04046/2013.

References:
[1]M. Prosser, J., & S. Nelson, L. (2012). The Toxicology of Bath Salts: A Review of Synthetic Cathinones. J. Med. Toxicol., 8(33), 42. [2]United Nations Office on Drugs and Crime (2013) World Drug Report 2013. United Nations, Vienna. [3]Negreira, N., Erratico, C., Kosjek, T., L. N. van Nuijs, A., Heath, E., Neels, H., & Covaci, A. (2015). In vitro Phase I and Phase II metabolism of α-pyrrolidinovalerophenone (α-PVP), methylenedioxypyrovalerone (MDPV) and methedrone by human liver microsomes and human liver cytosol. Anal Bioanal Chem, 407(19), 5803-5816.

Modeling Preferential Solvation in Acetonitrile-Water Mixtures Using Kinetic Probes

Beatriz Pena[1,2*], Luís Moreira[1-3], Filomena Martins[1,2]

[1] Centro de Química e Bioquímica, Faculdade de Ciências, Universidade de Lisboa, Ed. C8, Campo Grande 1749-016 Lisboa, Portugal.
[2] Centro de Química Estrutural, Faculdade de Ciências, Universidade de Lisboa, Ed. C8, Campo Grande 1749-016 Lisboa, Portugal.
[3] Instituto Superior de Educação e Ciências, Alameda Linhas de Torres 179 1750-142 Lisboa, Portugal.

*Email: beabtcpena@gmail.com

CQE Química Estrutural

09 MET

Introduction

- Acetonitrile-water (MeCN/water) mixtures are widely used for several physicochemical purposes and have been extensively studied using different methods[1].
- Our research group has been interested in the application of quantitative structure-property relationships to the study of tertiary alkyl halides' reactivity in different media.
- We have studied the reaction of 3-Cl-3-methylpentane (Fig. 1) in MeCN/water mixtures and the obtained -log *k* *vs*. x_{water} curve revealed some interesting aspects (Fig. 2), most probably related to preferential solvation phenomena.
- Several models have been developed to explain/quantify preferential solvation, like the Bosch and Rosés' model, originally applied to binary mixtures[2] and later extended to ternary mixtures[3],and the El Seoud's model[4].
- Both models consider the existence of preferential solvation phenomena in which solvent 1 (S1) can be replaced by solvent 2 (S2) or by a binary complex formed by both solvents (S1S2) – see equilibria equations.
- The preferential solvation is quantified considering 2 constants (derived from the models): $f_{2/1}$ which quantifies the preferential solvation ability ratio of S2/S1 and $f_{12/1}$, quantifying S1S2/S2 ratio.
- Bosch and Rosés' model, postulates the formation of S1S2 only in the solute's (I) cybotactic region.
- Conversely, El Seoud's model, considers that S1S2 is formed only in the bulk mixture, throughout an equilibrium which is quantified outside the context of the studied process. In the case of MeCN/water binary mixtures, at 25.0 °C, *K* = 10.08[4].
- The observed property (*Y*), in our case -log *k* (proportional to $\Delta^{\neq}G$), is considered to result from the sum of the Y_i values (for S1, S2 and S1S2) multiplied by the respective molar fractions in the cybotatic region (x_i^*).
- $Y_1, Y_2, Y_{12}, f_{2/1}$ and $f_{12/1}$ values are determined by experimental curve fitting.

Bosch and Rosés' Equilibria Equations

$$\mathrm{I(S1)_m + mS2 \rightleftharpoons I(S2)_m + mS1}$$

$$\mathrm{I(S1)_m + \frac{m}{2}S2 \rightleftharpoons I(S1S2)_m + \frac{m}{2}S1}$$

El Seoud's Equilibria Equations

$$\mathrm{S1 + S2 \rightleftharpoons S1S2}$$

$$\mathrm{I(S1)_m + mS2 \rightleftharpoons I(S2)_m + mS1}$$

$$\mathrm{I(S1)_m + mS1S2 \rightleftharpoons I(S1S2)_m + mS1}$$

Model Equation

$$Y = Y_1x_1^* + Y_2x_2^* + Y_{12}x_{12}^*$$

Experimental Procedure

- Solvent mixtures were prepared by mass. Substrate concentration was 0.01 mol dm^{-3}. Kinetic measurements were carried out on an automated conductance bridge. Reactions were followed, at 25.0 °C, up to 90% of the apparent plateau. Experimental values of -log *k* for 11 binary mixtures were determined using a previously designed spreadsheet[5]. Values for the pure solvents were calculated using a 3rd degree polynomial curve. Table curve 2D and 3D programs were used to perform the adjustments.

Results and Discussion

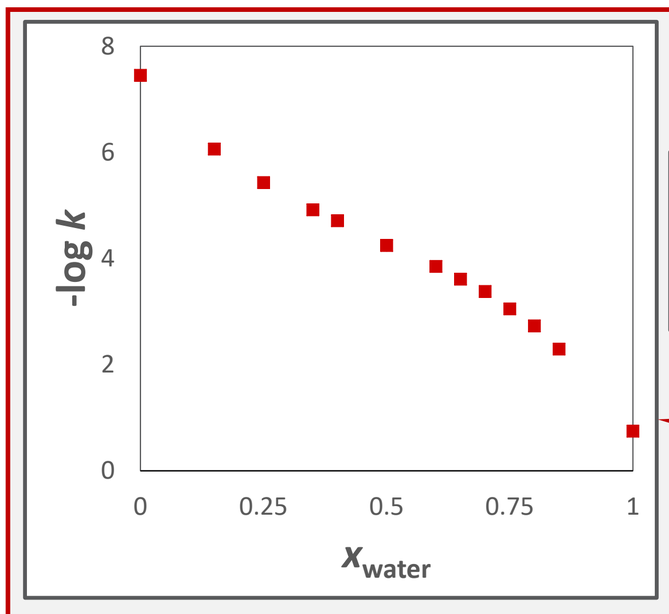

Figure 1

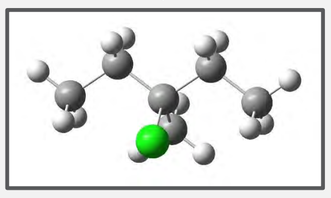

Figure 2

Table 1

Statistics and properties	Bosch and Rosés' model	El Seoud's model
s_{fit}	0.03	0.03
R^2	0.9997	0.9998
F	7801	9361
-log k_{water}	$0.74_{\pm0.03}$	$0.74_{\pm0.03}$
-log k_{MeCN}	$7.46_{\pm0.03}$	$7.46_{\pm0.03}$
-log $k_{water\text{-}MeCN}$	$4.47_{\pm0.17}$	$7.86_{\pm0.85}$
$f_{MeCN/water}$	$0.88_{\pm0.17}$	$0.41_{\pm0.07}$
$f_{water\text{-}MeCN/water}$	$3.95_{\pm0.33}$	$4.91_{\pm0.70}$

- The statistical figures of merit (s_{fit}, R^2 and F) show that both models are adequate to model the experimental data (Table 1).
- Bosch and Rosés' model predicts a value of -log $k_{water\text{-}MeCN}$ which corresponds to a $\Delta^{\neq}G$ = 99 kJ/mol (similar to the average result for a 1:1 mixture) and the corresponding value for El Seoud's model is $\Delta^{\neq}G$ = 118 kJ/mol, representing an increase of about 22% regarding the average result for a 1:1 mixture.
- Bosch and Rosés' model predicts a preferential solvation order (with an approximate relative magnitude) of water-MeCN (5) >> water (1) ≈ MeCN (1).
- Results for El Seoud's model lead to the following order: water-MeCN (10) >> water (2) > MeCN (1).

Funding:
Centro de Química Estrutural is funded by Fundação para a Ciência e Tecnologia – project UID/QUI/00100/2019 and Centro de Química e Bioquímica by Fundação para a Ciência e a Tecnologia – projects UID/MULTI/00612/2013 and UID/MULTI/00612/2019

FCT Fundação para a Ciência e a Tecnologia

References:

1. Marcus, Y., J. Phys. Org. Chem. 25 (2012) 1072–1085.
2. Bosch, E., Rosés, M., J. Phys. Org. Chem. 9 (1996) 403–410.
3. Nunes, N., Ventura, C., Martins, F., Leitão, R. E., J. Phys. Chem. B 113 (2009) 3071-3079.
4. Silva, P. L., Bastos, E. L., El Seoud, O. A., Phys. Chem. B 111 (2007) 6173-6180.
5. Moreira, L., Martins, F., Leitão, R. E., J. Chem. Educ. 83 (2006) 1879-1883

Green method for the production inverse spinels

Beatriz M. Santos,[1] Rute F. C. Faustino,[1] Ana P. C. Ribeiro[1]

Beatriz Santos

Rute Faustino

INTRODUCTION

Spinel is a common structural arrangement shared by many oxides of the transition metals with formula AB_2O_4. An **inverse spinel** is an alternative arrangement where the divalent ions swap with half of the trivalent ions so that the M(II) now occupy octahedral sites i.e. $B(AB)O_4$.

In this work, the preparation methods, materials characterization, and magnetic properties of inverse spinel materials, such as $ZrFe_2O_3$, $NiFe_2O_3$, by hydrothermal method.

The synthetic procedure includes the use of water and room temperature, and the purification is by thermal activation. The final materials are magnetic and can have potential applications in catalysis.

INVERSE SPINELS STRUCTURE

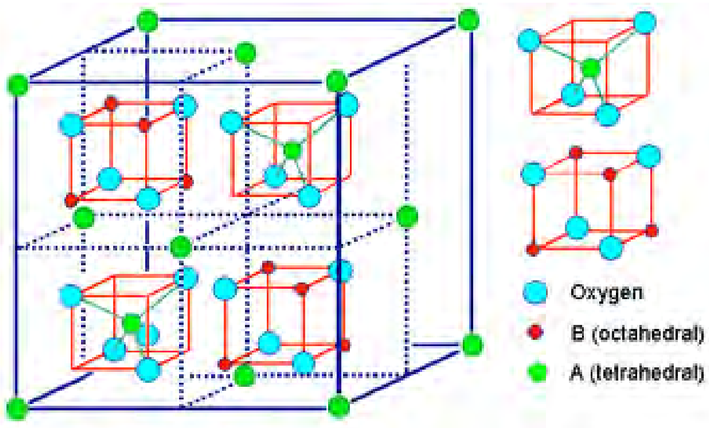

The metals used were manganese and zirconia.

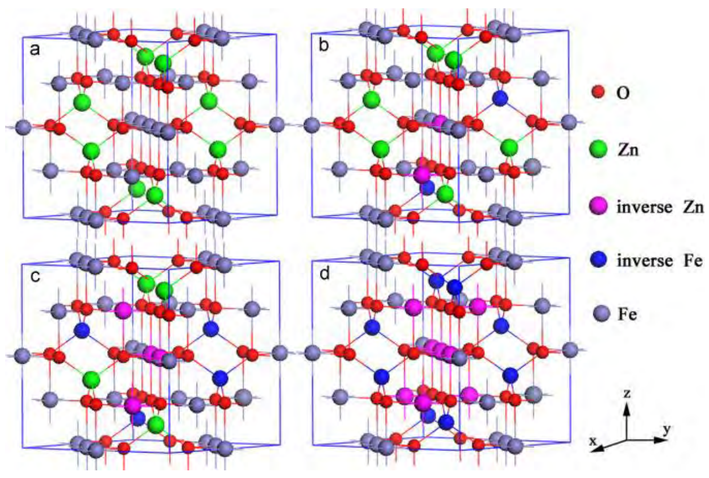

SYNTHESIS

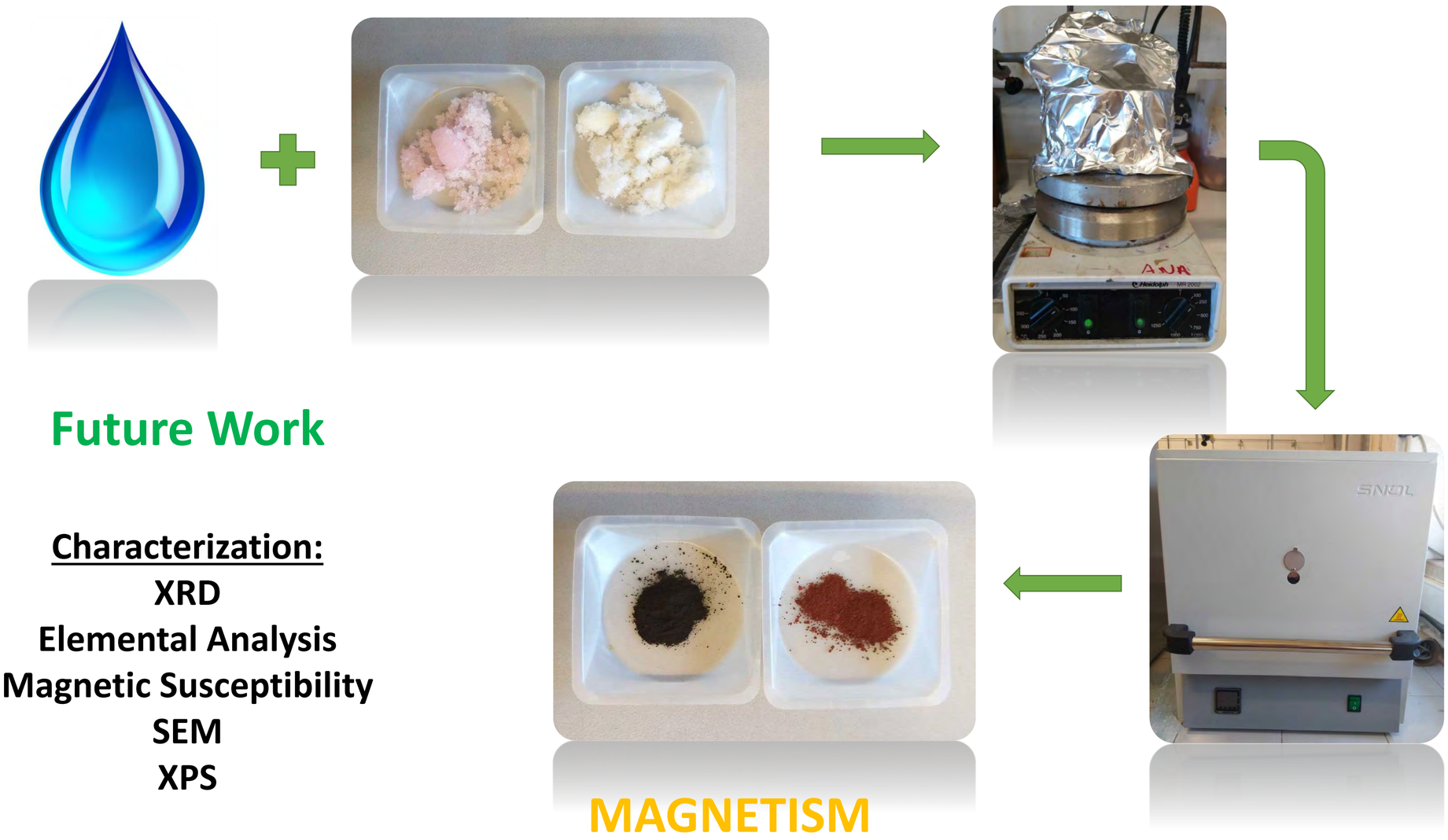

Future Work

Characterization:

XRD
Elemental Analysis
Magnetic Susceptibility
SEM
XPS

MAGNETISM

Zirconia

Before

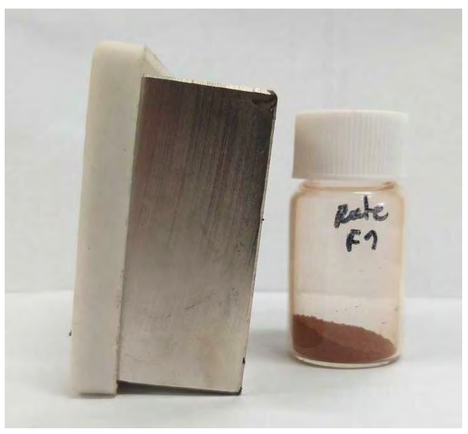

Non magnetic

After

Magnetic

Manganese

Before

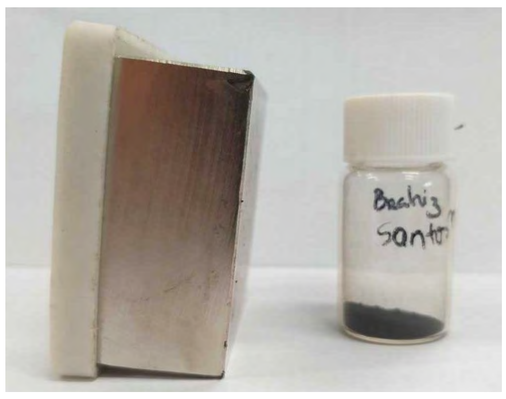

Non magnetic

After

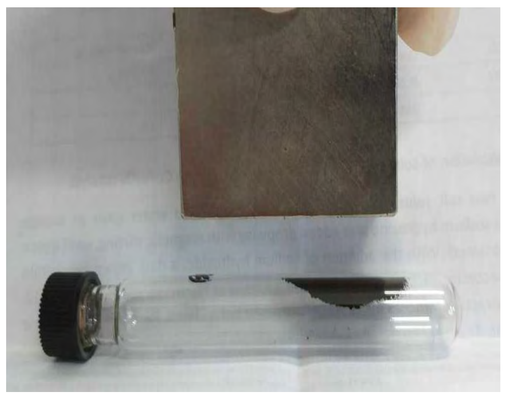

Magnetic

SynCat

Funding:
Centro de Química Estrutural is funded by Fundação para a Ciência e Tecnologia – project UID/QUI/00100/2019.

Ln-based Compounds Applications in Magnetism and Optical Sensing

Bernardo Monteiro,[1,2] Joaquim Marçalo,[1,2] João P. Leal,[1,2] Joana T. Coutinho,[2] Laura C.J. Pereira,[2] Manuel Almeida,[2] Cláudia C.L. Pereira,[3] Tiago Moreira,[3] Mani Outis,[3] César T. Laia,[3] Filipe A.A. Paz,[4] Ricardo F. Mendes,[4] José J. Baldovi[5]

[1] Centro de Química Estrutural, Instituto Superior Técnico, Universidade de Lisboa; [2] Centro de Ciências e Tecnologias Nucleares, Instituto Superior Técnico, Universidade de Lisboa; [3] REQUIMTE, Dep. de Química, Universidade Nova de Lisboa; [4] CICECO, Instituto de Materiais de Aveiro, Universidade de Aveiro; [5] MPSD, Max Planck Institute for the Structure and Dynamics of Matter

CQE Química Estrutural

02 IOARC

Funding:

We thank the Fundação para a Ciência e a Tecnologia (FCT) for financial support through the UID/Multi/04349/2019 project (C2TN), UID/QUI/00100/2019 (CQE), UID/QUI/50006/2013 (LAQV-REQUIMTE), grants to J.T.C. (SFRH/BD/84628/2012) and C.C.L.P. (SFRH/BPD/108959/2015) and contract to BM (contract nº IST-ID/077/2018). We thank the EU for project "SunStorage" (POCI-01-0145-FEDER-016387), funded by European Regional Development Fund (ERDF) and co-financed by the ERDF under the PT2020 Partnership Agreement (POCI-01-0145-FEDER – 007265), through COMPETE 2020 - Operational Programme for Competitiveness and Internationalization (OPCI), COST Action CA15128 MOLSPIN and ERC-2014-CoG-647301 DECRESIM) and the Spanish MINECO (Unit of excellence "Maria de Maeztu" MDM-2015-0538). J.J.B. thanks the EU for a Marie Curie Fellowship (H2020-MSCA-IF-2016-751047).

FCT Fundação para a Ciência e a Tecnologia

Magnetism

The field of Ln-based single-molecule magnets (SMMs) is one of the hottest research areas in Molecular Nanomagnetism. Nevertheless, the study of the magnetic properties of Layered Lanthanide Hydroxides (LLHs) still remains largely unexplored, with the exceptions of our recent investigations in Dy layered compounds, belonging to the $Ln_8(OH)_{20}Cl_4.nH_2O$ series (Figure 1). In this work, three LLHs, with the general formula $Ln_8(OH)_{20}Cl_4{\cdot}nH_2O$ (Ln = Tb, Ho, Er), were prepared and magnetically characterized both as pure compounds and diluted within a yttrium diamagnetic matrix, LYH:xLn, LYH:0.044Tb, LYH:0.045Ho, and LYH:0.065Er.

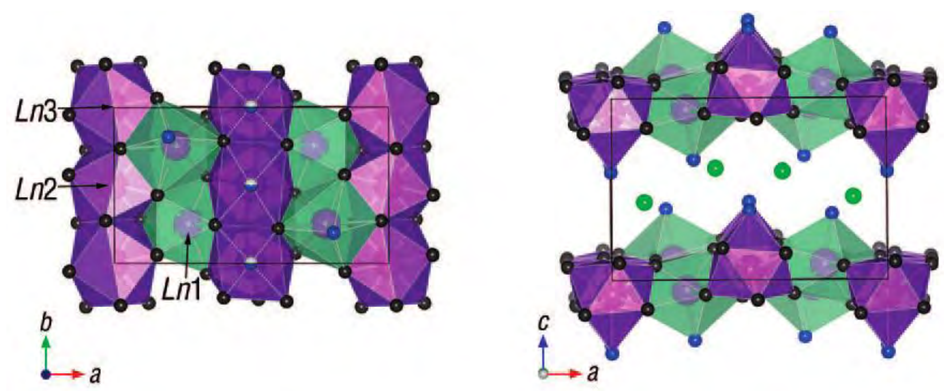

Figure 1. $Ln_8(OH)_{20}Cl_4{\cdot}nH_2O$ unit with: Ln – purple, hydroxyls – grey, water oxygen – blue, chloride - green. The 8-fold dodecahedron and 9-fold monocapped square antiprism are in light green and purple, respectively

As it can be observed in Figure 2, the χT curves can be successfully reproduced by using the Radial Effective Charge (REC) model in the SIMPRE software package.

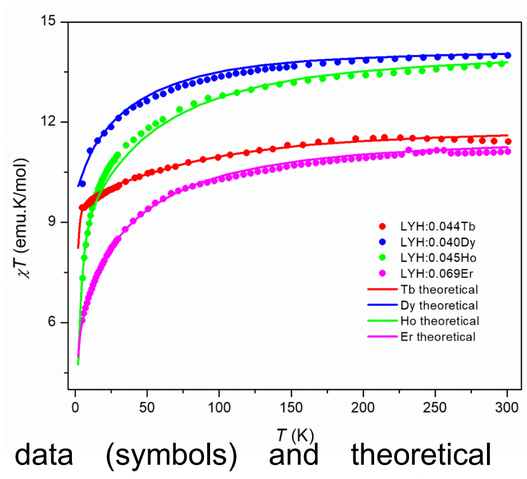

Figure 2. Experimental data (symbols) and theoretical simulation (lines) of the temperature dependence of the magnetic susceptibility of the LYH:xLn compounds.

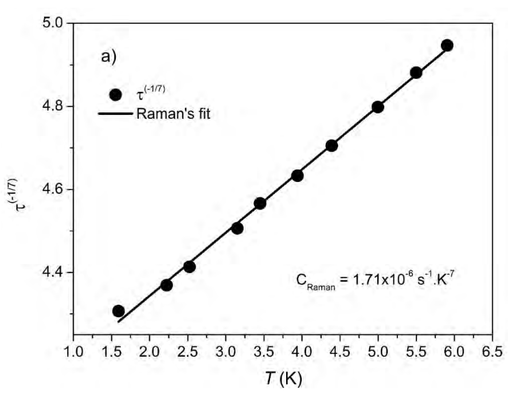

The Raman process was the more adequate to interpret the relaxation magnetic behavior of the $Ln_8(OH)_{20}Cl_4{\cdot}nH_2O$, Figure 3.

Figure 3. Plot of the temperature dependence of the relaxation time as $\frac{1}{n_R\sqrt{\tau}}\,vs.\,T$ for $Tb_8(OH)_{20}Cl_4{\cdot}6H_2O$.

Highlight

These results highlight the presence of significant interactions between the Ln centers. A clearer slow relaxation behavior is observed in the LYH:xLn solid solutions. *Semi-empirical* calculations successfully allowed to access the Ln electronic configurations and the respective contributions to the slow relaxation behavior of these LLHs showing a diversity of magnetic behaviors.

Optical Sensing

Methanol is extremely toxic so the development of a fast, efficient and low-cost methods for methanol quantification and detection in mixtures of ethanol/methanol is, therefore, pertinent to ensure food safety. Based on the interaction of trihexyltetradecylphosphonium cation $(P_{6,6,6,14})+$ with the β-diketonate (1,1,1,2,2,3,3-heptafluoro-7,7-dimethyloctane-4,6-dionate - FOD) of an Europium(III) complex, $[P_{6,6,6,14}][Eu(FOD)_4]$, we present and discuss an equilibrium reaction with $NaOPhMe_3$ (Figure 4) with pronounced solvent effect between ethanol and methanol on Eu(III) luminescence.

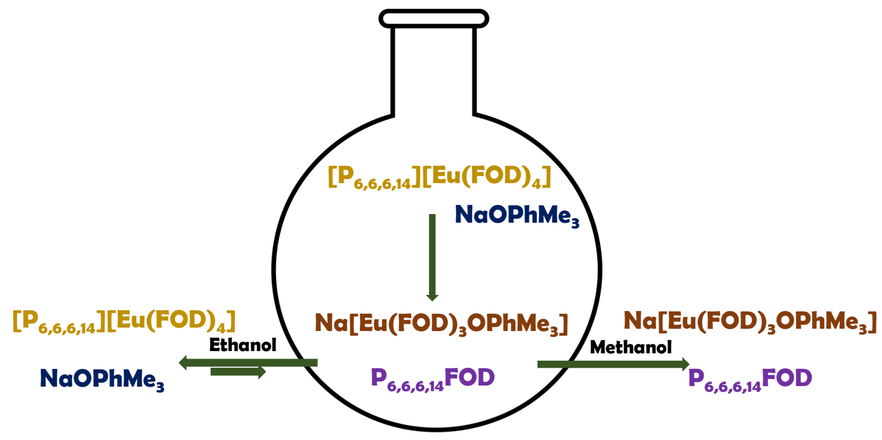

Figure 4. Solvent dependent equilibrium with pronounced solvent effect on Eu(III) emission.

A ratiometric method was used to calculate the ratio of the fluorescence intensities by adding different amounts of methanol in ethanol and correlate the methanol concentration with the normalized intensity of the $^5D_0$ $^7F_0$ transition, Figure 5.

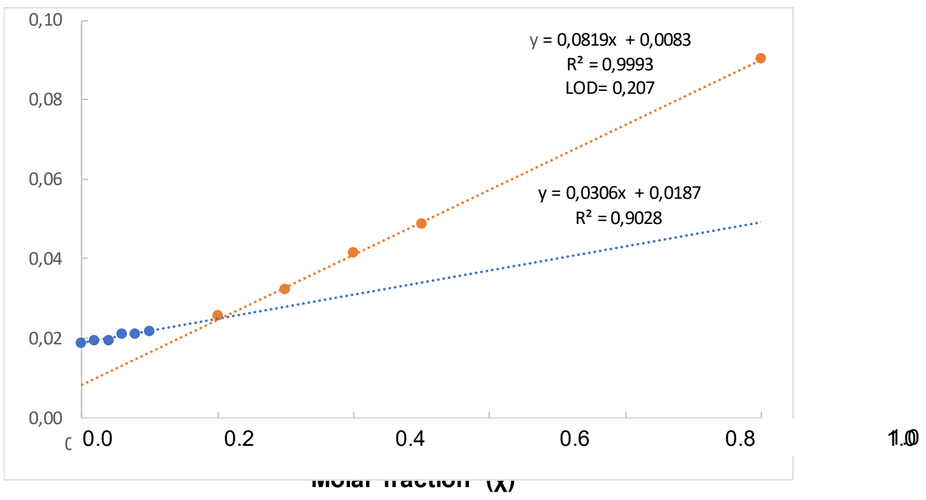

Figure 5. Calibration curve for methanol estimation in ethanol/methanol mixtures. χ molar fraction of methanol in ethanol

Highlight

The methanol-sensing studies showed that the resulting mixture of the reaction between $[P_{6,6,6,14}][Eu(FOD)_4]$ and $NaOPhMe_3$ can be used as a sensitivity, highly reproducible, fast and low-cost ratiometric method to determine the methanol content in methanol/ethanol mixtures from as low as 15 % (w/w).

Development of consolidation products to carbonate stones from built heritage

B. Sena da Fonseca, A.P. Ferreira Pinto, S. Piçarra, M.F. Montemor

CQE Química Estrutural

MATsoft

Introduction

Carbonate stones are extensively present in monumental and non-monumental constructions having an outstanding cultural and architectural value. Conservation interventions, involving consolidation of stone, are often required due to their advanced state of degradation that threat the cultural value and significance of built heritage. However, the existing consolidation products, based in alkoxysilanes, present some limitations and often show a reduced efficacy or even potential to accelerate degradation phenomena. The most commonly cited drawbacks and the reasons behind their poor performance are:

- Tendency to crack
- Lack of chemical affinity with carbonate substrates

The project aims at developing new consolidation products with improved characteristics, particularly regarding these recognized weaknesses.

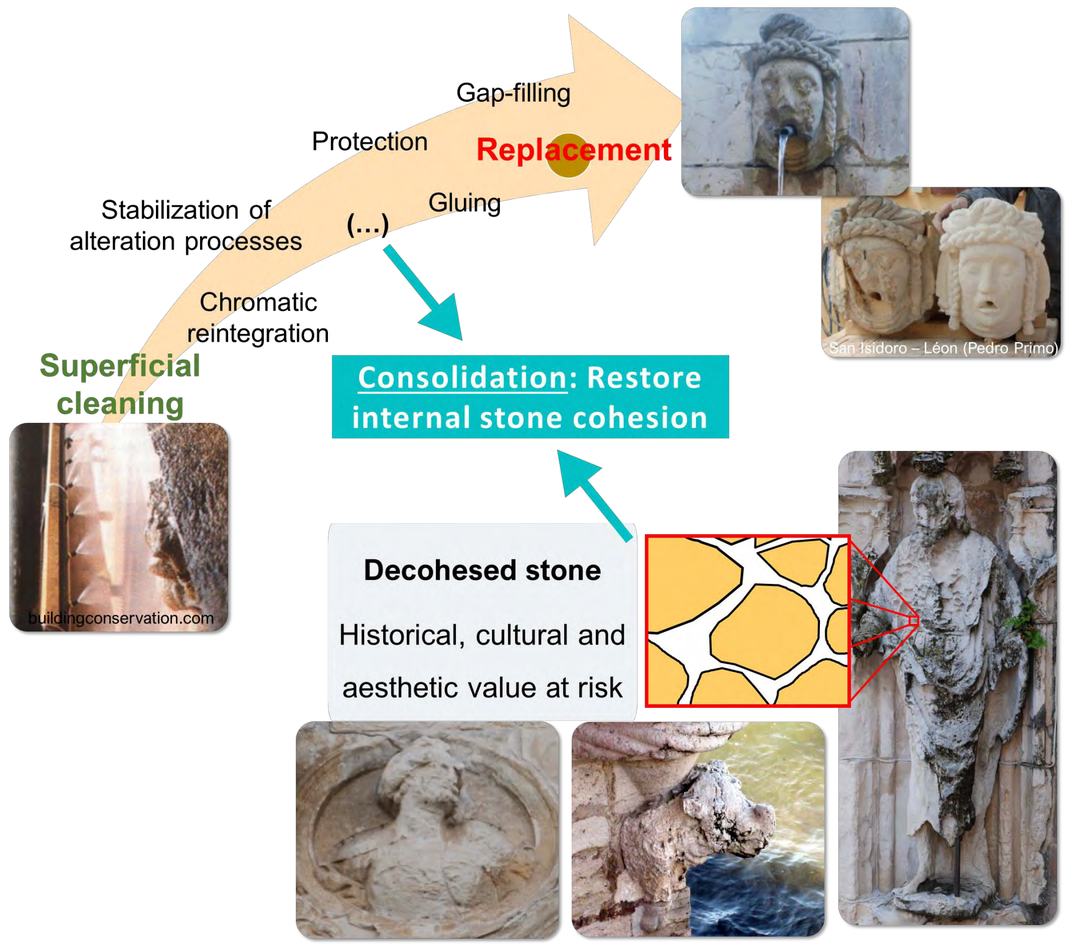

Strategies

Optimized TEOS-based formulation

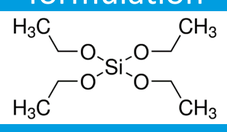

Organic acid solution

- Flexible hydrophilic polymer (LPfp)

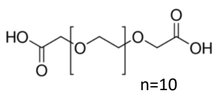

- Organically modified alkoxysilanes (LPam)

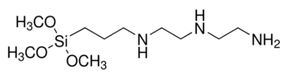

- Tartaric acid (LPoa)

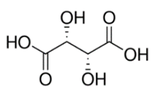

Appropriate gelling time Within 6-7 days

Stone application Capillary absorption 3 hours

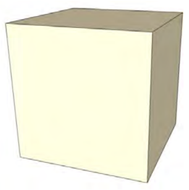

Ançã stone

Good penetration capacity >30 mm

Results

Xerogels

LPfp

Silicate material with low tendency to crack during gelling and aging steps (in relation to commercial consolidants)

LPam

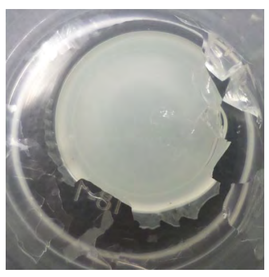

Translucent ORMOSIL with low tendency to crack during gelling and aging steps

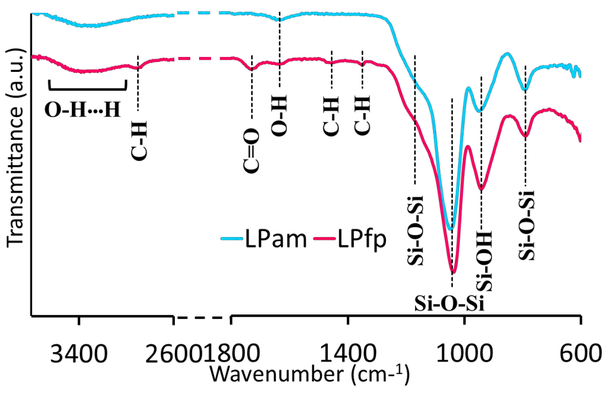

Calcite crystal / powder

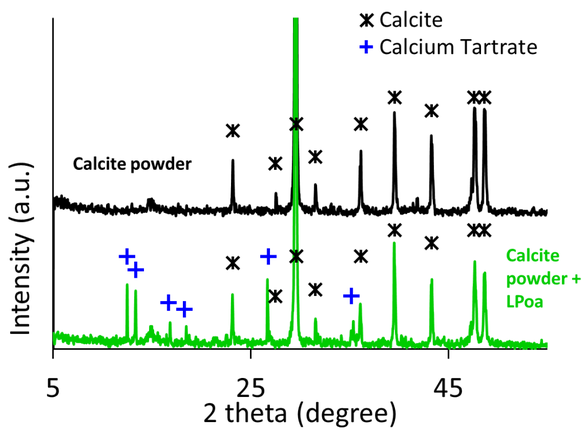

LPoa

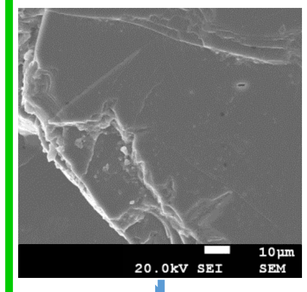

Calcite surface

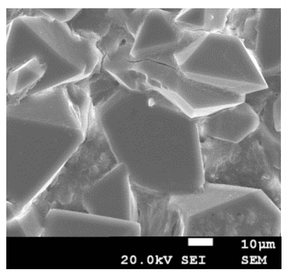

Conversion layer after contact with calcite (calcium tartrate)

Efficacy (drilling resistance)

Stone cohesion increments:

→ all treatments

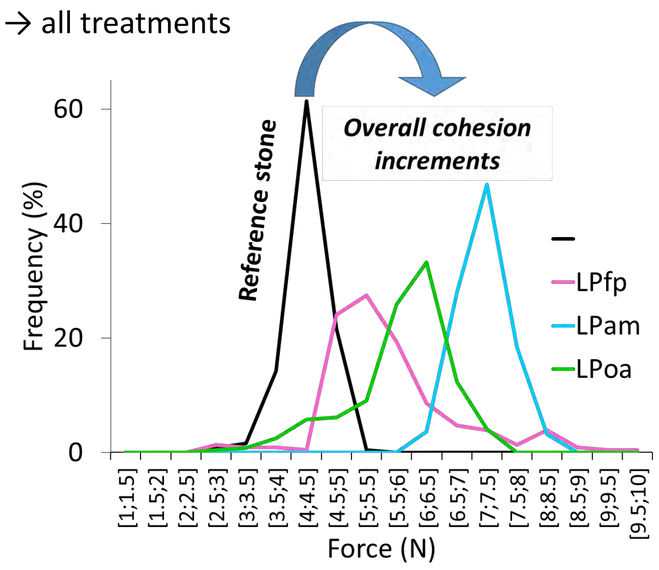

Alkoxisilane-based products: Silicate/ ORMOSIL material bridging/covering calcite grains bonding them at the contact points.

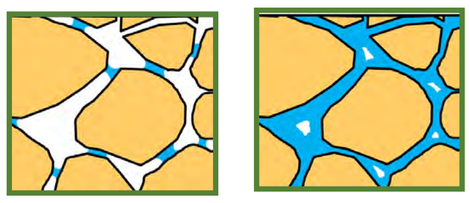

Conversion layer: Interlocking effect of newly formed crystals within stone pores.

Superficial hard layers (harmful side effect):

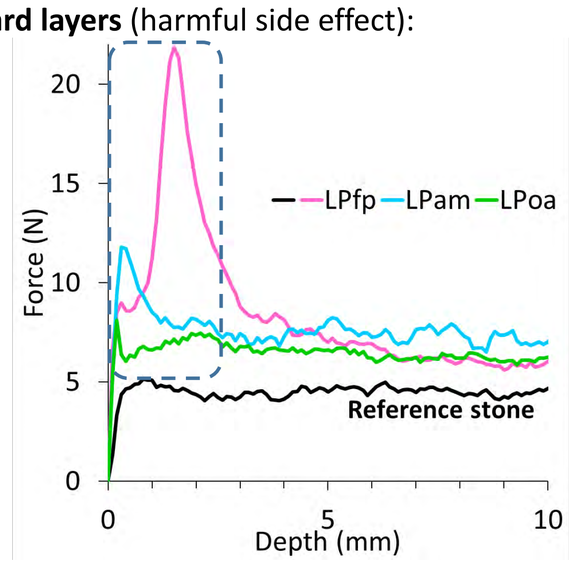

Final Remarks

All the formulations demonstrated potential to be applicable into porous carbonate stones and to increment their cohesion. Even so, the solutions with improved chemical affinity with the substrate caused the higher overall increment but still some tendency to create potentially harmful hard layers. In the sequence of the promising results achieved, further improvements will be pursuit by tailoring the reactional parameters of the formulations as well as to test other formulation paths.

Funding:
Centro de Química Estrutural and project NanoCStoneH are funded by Fundação para a Ciência e Tecnologia – UID/QUI/00100/2019 and PTDC/ECI-EGC/29006/2017, respectively.

FCT Fundação para a Ciência e a Tecnologia

CHARACTERIZATION OF ATMOSPHERIC AEROSOL OF A MEDIUM SIZE CITY IN BRAZIL

Bruno T. Franzin[1,3], Fernando L. Fertonani[1,2], Cristina M. R. R. Oliveira[3]

[1] São Paulo State University (Unesp), Institute of Chemistry-IQ, Department of Analytical Chemistry, Araraquara, SP, Brazil, CEP:14800-060

[2] São Paulo State University (Unesp), Institute of Biosciences, Humanities and Exact Sciences (Ibilce), Department of Chemistry and Environmental Sciences, São José do Rio Preto, SP, Brazil, CEP:15054-000

[3] Centro de Química Estrutural- Faculdade de Ciências da Universidade de Lisboa, C8 Campo Grande, 1749-016 Lisboa, Portugal

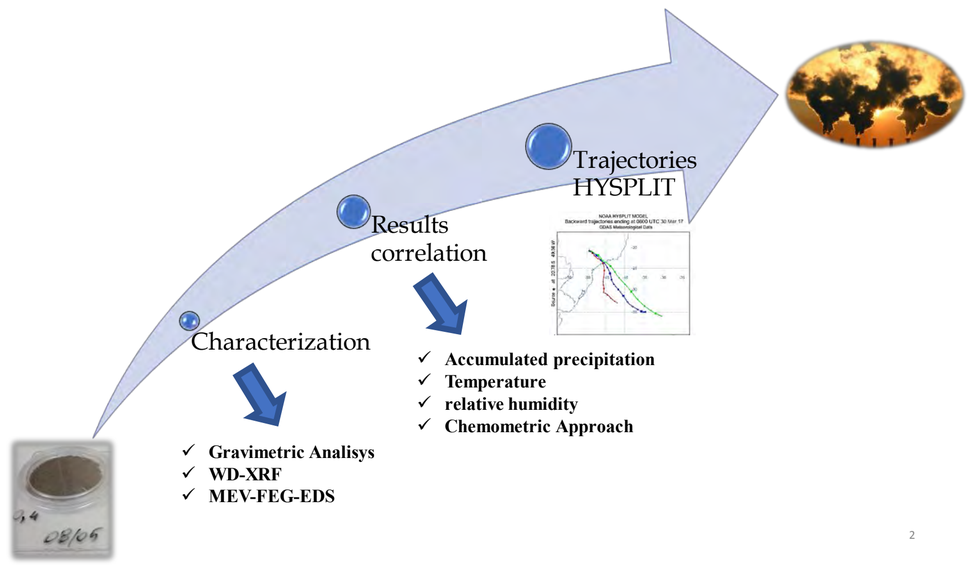

Fig. 1. São Paulo State map - Sampling site (black pin)

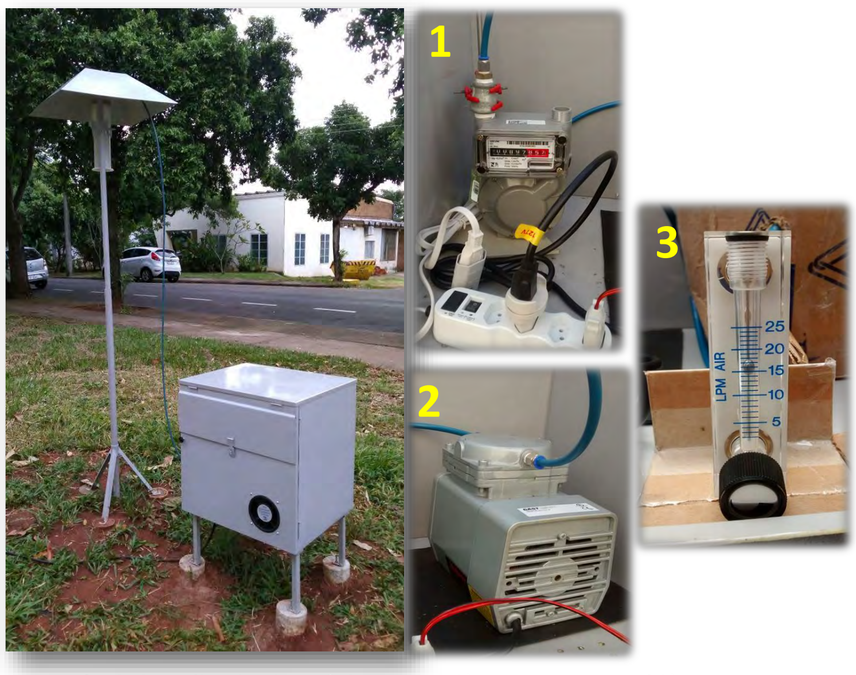

Fig. 2. Sampling Station. 1) Gas meter, 2) Vacum Pump and 3) Rotameter :

Fig. 4. Manufatured Gent type Sampler

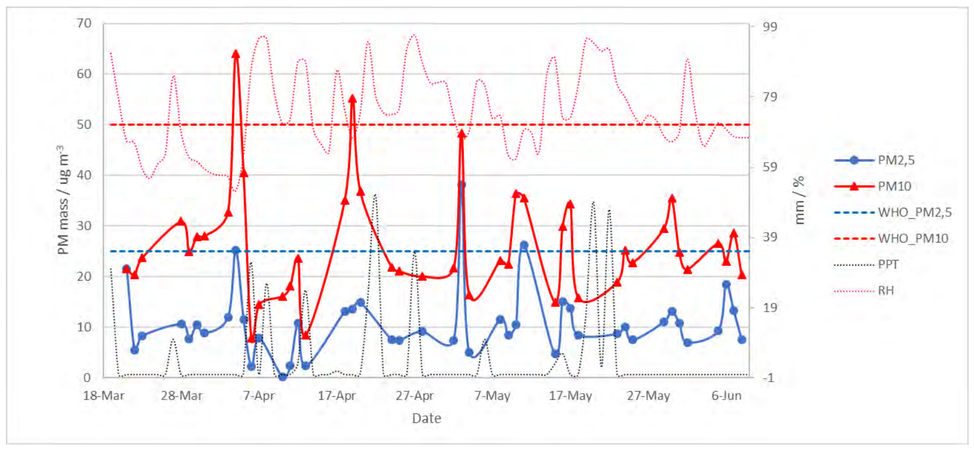

Fig. 3. Aerosol mass profile, meteorological data and daily maximum values (WHO), red: coarse fraction (PM_{10}); blue: fine fraction ($PM_{2.5}$); accumulated precipitation (PPT) and relative humidity (RH)

Table 1: General statistic of massic profile and meteorological data in the sampling period

	PM_{10} / µg m^{-3}	$PM_{2.5}$ / µg m^{-3}	T / ºC	RH[1] / %	WS[2] / m s^{-1}	PPT[3] / mm
Mean	24.54	10,88	24,37	74,40	2,05	338
Maximum	64,00	38,11	28,99	96,75	3,29	51
Minimum	7,79	0,19	18,55	52,18	1,12	0
SD[4]	11.02	6,78	2,15	11,46	0,39	11,37
CV[5] %	41.51	62,37	8,81	15,40	18,98	3,36

[1] Relative humidity, [2]Wind speed [3]Accumulated precipitation; [4] Standard deviation; [5] Coefficient of variation

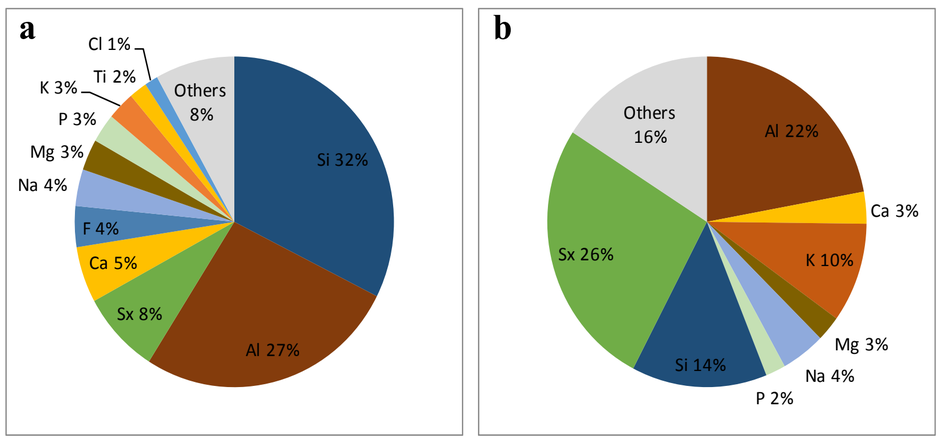

Fig. 5. Relative average distribution of the main components of the fractions: a) $PM_{10-2.5}$ and b) $PM_{2.5}$

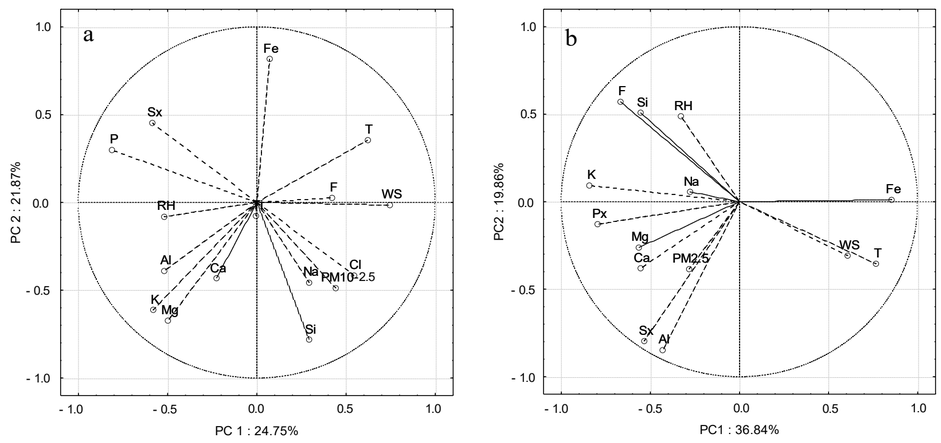

Fig. 7. Graph of loadings a) $PM_{10-2.5}$ and b) $PM_{2.5}$. WS: wind speed; T: temperature; RH: relative humidity, $PM_{10-2.5}$ and $PM_{2.5}$ mass concentrations

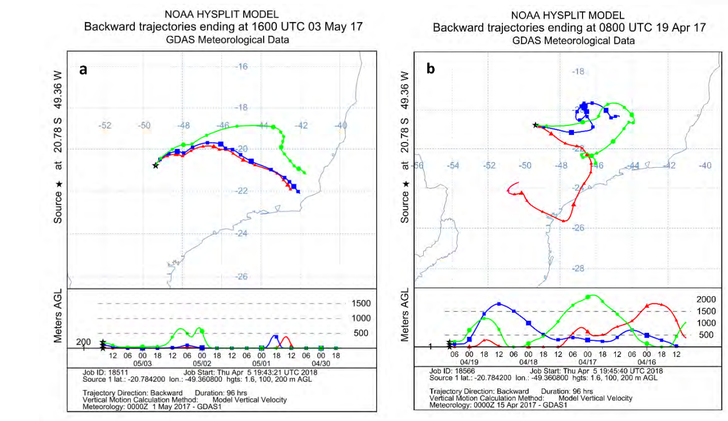

Fig. 6. HYSPLIT model backward trajectories, arriving in sampling site: a) May 03, 2017 and b) April 19, 2017 - Red lines: 1.6 m; Blue: 100 m and Green: 200 m

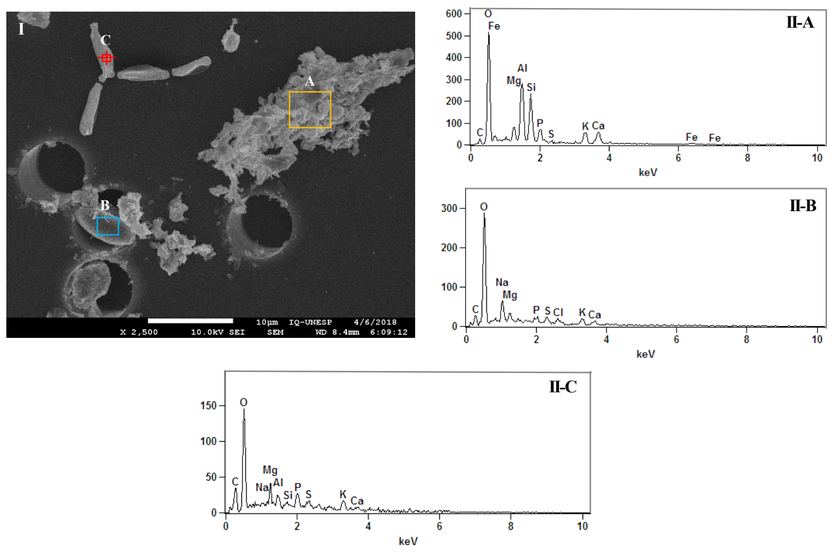

Fig. 8. I- SEM-FEG images of the $PM_{10-2.5}$ sample of April 19, 2017; II - EDS, regions bounded by the A-orange rectangle, B-blue, and C-red, dot determination

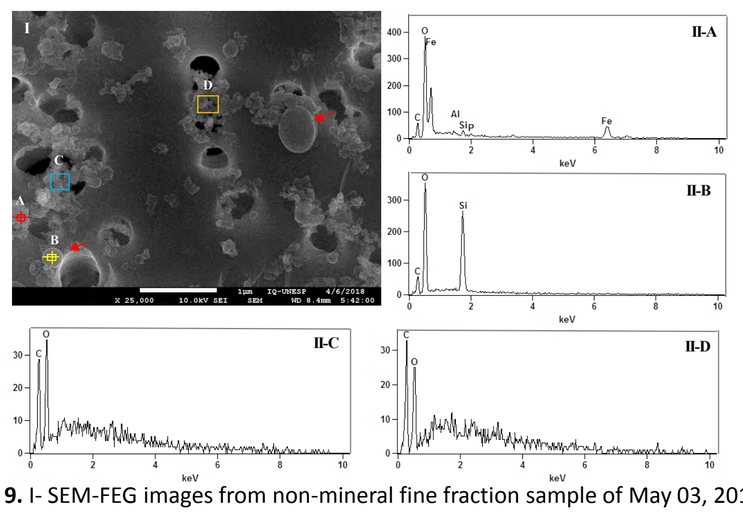

Fig. 9. I- SEM-FEG images from non-mineral fine fraction sample of May 03, 2017 and II- EDS spectra obtained from the regions bounded by red (A) and yellow (B) targets and blue (C) and orange (D) rectangles.

CQE Química Estrutural

06 CE

FCT Fundação para a Ciência e a Tecnologia

Funding:

Centro de Química Estrutural is funded by Fundação para a Ciência e Tecnologia – project UID/QUI/00100/2019, Coordenação de Aperfeiçoamento de Pessoal de Nível Superior - CAPES (Scholarship) and PROPG – UNESP Foundation´s (Brazil).

References:

1. WHO - World Health Organization. Air Quality Guidelines - Global Update 2005 Copenhagen: WHO, 2006.

2. Cruz, Lícia P. S., Elisvan R. Mota, Vânia P. Campos, Franciele O. Santana, Sâmeque R. Luza, Daniela F. Santos. J. Braz. Chem. Soc. 30 (2019) 904-914.

3. UN - Report Towards a pollution-free planet. Report of the Executive Director. United Nations Environment Assembly of the United Nations Environment Programme Third session Nairobi, 4–6 December 2017.

4. Bulbul G, Shahid I, Chishtie F, Shahid Mz, Hundal RA, Zahra F, Shahzad M. Aerosol and Air Quality Research 18 (2018) 188-199.

5. González, L.T., Longoria-Rodríguez, F.E., Sánchez-Domínguez, M., Leyva-Porras, Cr., Acuña-Askar, K., Kharissov, B.I., Arizpe-Zapata, A., Alfaro-Barbosa, J.M. J. Environ. Sci. 74 (2018) 32-49.

Evaluation of tannins as green corrosion prevention inhibitors in AA2024-T3 aluminium alloy used in aerospace industry

C. Sofia Proença[1], B. Serrano[2], M. E. Araújo[1], J. Correia[1]

[1)]Centro de Química e Bioquímica, Centro de Química Estrutural, Faculdade de Ciências, Universidade de Lisboa
Campo Grande, 1749-016 Lisboa, Portugal
[2)] Força Aérea Portuguesa, Estado-Maior da Força Aérea
2614-506 Amadora, Portugal

CQE Química Estrutural

FCT Fundação para a Ciência e a Tecnologia

G 06 CE
G 11 HC

Abstract

Corrosion is a major problem that affects many metals and alloys. The costs and consequences caused by corrosion are of such importance that justifies a comprehensive study in relation to its causes, mechanisms of identification, detection and development of methods of prevention and protection. The former conventional pre-treatment of AA2024-T3 aluminium alloy involves formulations containing chromium (VI) but REACH restricts the use of hexavalent chromium, due to the negative impact of these compounds in environment and human health. In recent years there has been an increased interest in developing new corrosion protection alternatives.

The objective of this study is to evaluate the anticorrosion character imparted by vegetable tannins, both hydrolyzable and condensed, in the AA2024-T3 alloy, and compare it with that obtained with tartaric acid based bath, which is used in the anodizing of this aluminium alloy widely used in aerospace industry (e.g. AIRBUS).

The corrosion resistance of the treated samples was monitored by potentiodynamic polarization assays and electrochemical impedance spectroscopy analysis.

Experimental

All the aluminium substrate panels (AA2024-T3) were submitted to the following sequence: cleaning, water rinsing, deoxiding, water rinsing, anodizing and sealed. The corrosion resistance of the treated samples was monitored by potentiodynamic polarization assays and Electrochemical Impedance Spectroscopy analysis.

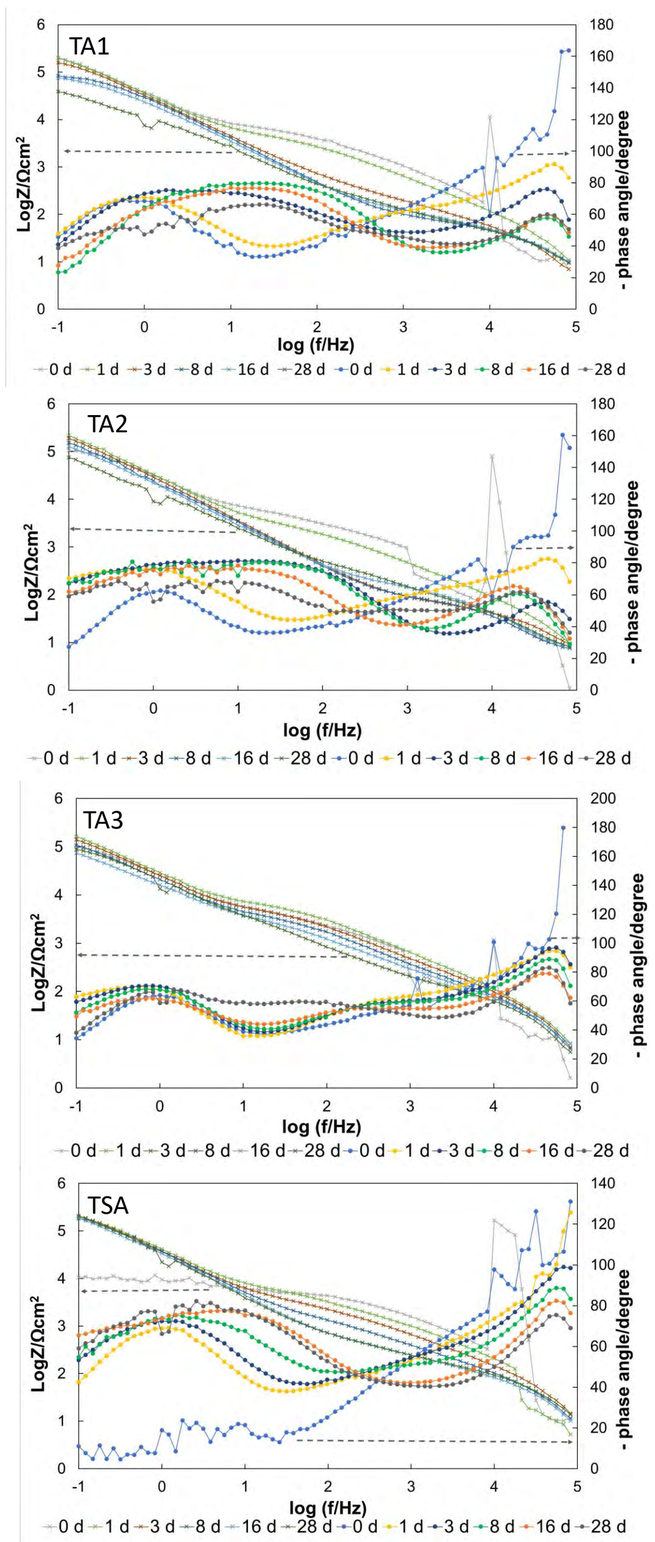

Bode plot for different green inhibitors, before anodising and sealed films in 0,5M NaCl.

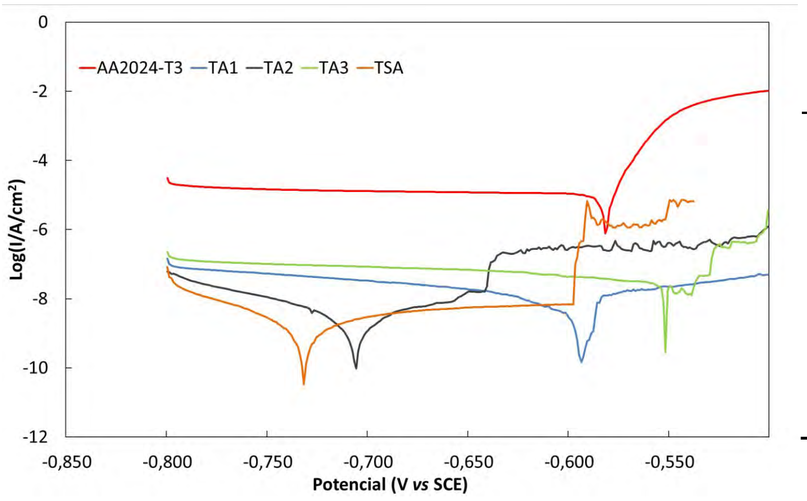

Tafel Plots for different green inhibitors.

	E_{corr} (V *vs* SCE)	I_{corr} (A/cm²)
AA2024-T3	-0.581	1.00×10^{-5}
TA1	-0.594	5.1×10^{-9}
TA2	-0.706	1.3×10^{-9}
TA3	-0.552	5.0×10^{-8}
TSA	-0.732	1.3×10^{-9}

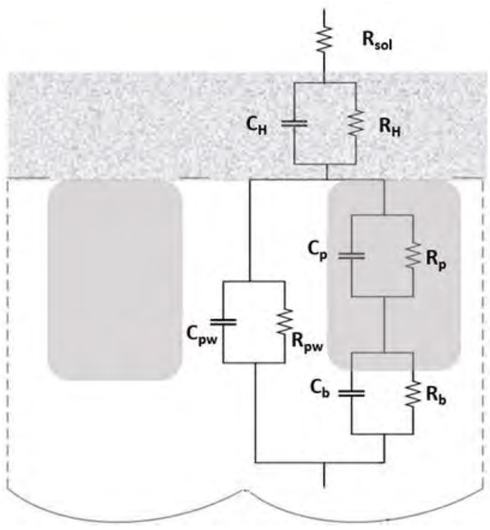

- R_{sol} Electrolyte resistance
- R_H Hidrataded layer resistance
- C_H Hidratated porous layer capacitance
- R_l Layer resistance
- C_p Porous layer capacitance
- R_p Porous layer resistance
- C_b Barrier layer capacitance
- R_b Barrier layer resistance
- C_{pw} Pore walls capacitance
- R_{pw} Pore walls resistance

Physical representation of the equivalent circuit used for interpretation of impedance behaviour.

Conclusion

The conversion coatings formed on the aluminium alloy revealed that the use of these tannins, despite the differences in their chemical structures, provide a good corrosion protection, making this pre-treatment a promising alternative for chromium (VI) based chemical conversion coatings. A discussion aiming to correlate the performance of these materials with their chemical class will be presented.

Funding:
Centro de Química Estrutural is funded by Fundação para a Ciência e Tecnologia – project UID/QUI/00100/2019 and project UID/Multi/00612/2019

References:

[1] González J. *et al*, Journal of applied Electrochemistry, 1999, 29, 229-238.
[2] Rubio M. *et al*, Electrochemica Acta, 2009, 54, 4789-4800.
[3] Arenas M. *et al*, Electrochemica Acta, 2010, 55, 8704-8708.
[4] Boisier G. *et al*, JES, 2008, 155, C521- C529.

Acknowledgements

Ciências ULisboa
Força Aérea Portuguesa
FCT Fundação para a Ciência e a Tecnologia

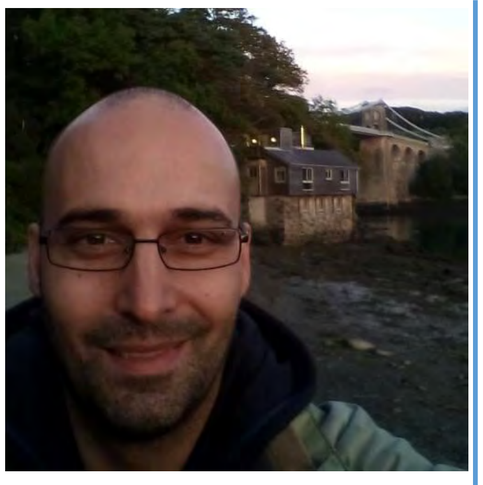

Insights on the occurrence and transport of Pt and Rh in Tagus estuary region, SW Europe: from urban into the aquatic system.

Carlos E. Monteiro and Margarida Correia dos Santos

CQE Química Estrutural

G06 CE

Rationale

Platinum-group elements (PGE), i.e. platinum (Pt), palladium (Pd), rhodium (Rh), iridium (Ir), osmium (Os), and ruthenium (Ru), have low concentrations in the Earth's crust (< 0.50 ng g^{-1}) and due to increasing concentrations in different environmental compartments, they are considered contaminants of emerging environmental concern, particularly in aquatic systems. Owing to their excellent properties, over the past years PGE worldwide demand and uses in a large variety of technology-based industries have increased. The automobile industry *per se* is responsible for nearly 50 % of global demand and in turn resulting in one of the main sources of PGE to the environment, from degradation and abrasion of automotive catalytic converters. However, other source emissions, such as industrial catalysts and medical uses, cannot be disregarded. As a consequence, the widespread and increase of PGE in different environmental compartments have been observed. Their biogeochemical cycling in aquatic systems, namely in estuaries and coastal areas, remains unclear and potential hazardousness needs to be assessed.

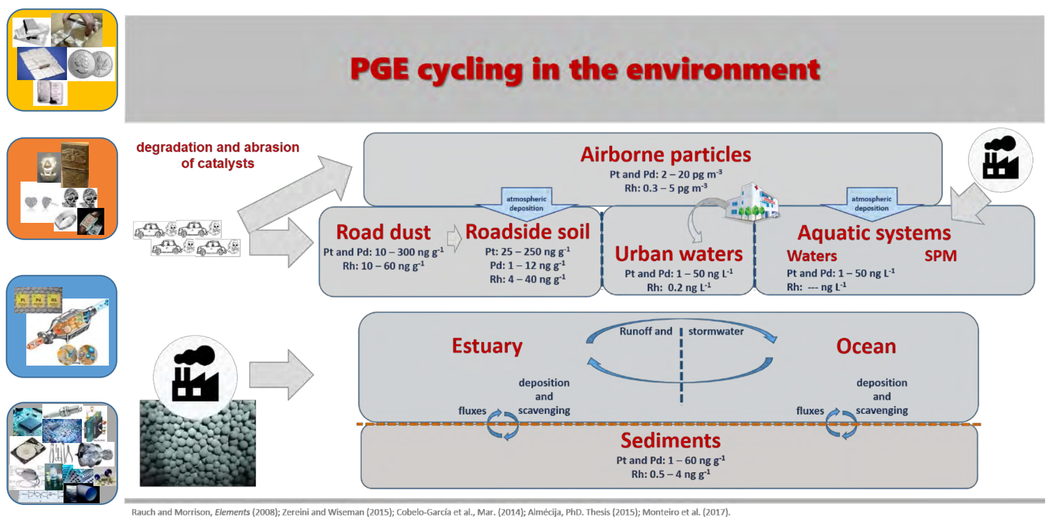

Rauch and Morrison, *Elements* (2008); Zereini and Wiseman (2015); Cobelo-García et al., Mar. (2014); Almécija, PhD. Thesis (2015); Monteiro et al. (2017).

Methods

Several analytical techniques have been proposed to quantify PGE in different matrices, such ICP-MS or AAS. Voltammetry has also been pointed out as a suitable technique for Pt and Rh determination, due to fast analysis and being less expensive. Adsorptive Cathodic Stripping Voltammetry (AdCSV) has been optimised and used for Pt and Rh quantification (Monteiro et al., 2017).

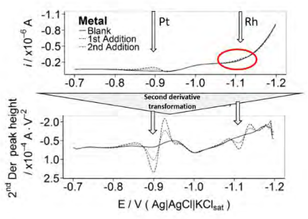

Samples preparation

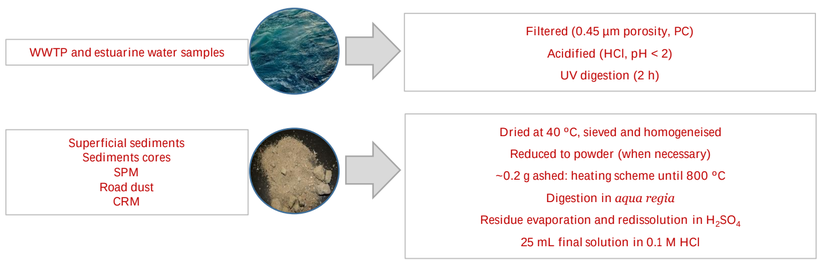

Additionally, a multi-method approach has been used to characterise ancillary parameters used in data interpretation.

Study area – the Tagus estuary

Estuaries are transition areas between the land and the ocean that can be greatly impacted with anthropogenic pressures. Therefore, the Tagus estuary is an ideal setting for PGE studies due to surrounding highly urbanised and industrialised areas, with considerably high traffic, as well adjacent to the Atlantic Ocean. Furthermore, the Tagus estuary is largely controlled by the hydrodynamic, which may affect distribution and fate of PGE at a regional scale.

A natural laboratory:

320 km²
Several channels and islands
Intense urban sprawl
(3 M inhabitants)
Industrialised areas

Land – Estuary – Ocean

- Rivers and streams
- Motorway bridge
- Bridge gullypots
- Industrial area
- Natural Reserve area
- WWTP
- Tank collectors

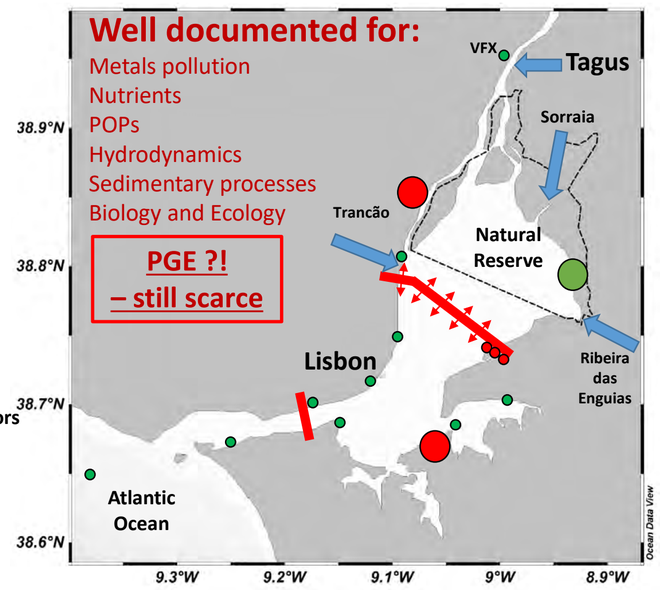

Pt and Rh distribution in superficial sediments

Pt background: 0.51 ng g^{-1} **Rh background:** 0.27 ng g^{-1}

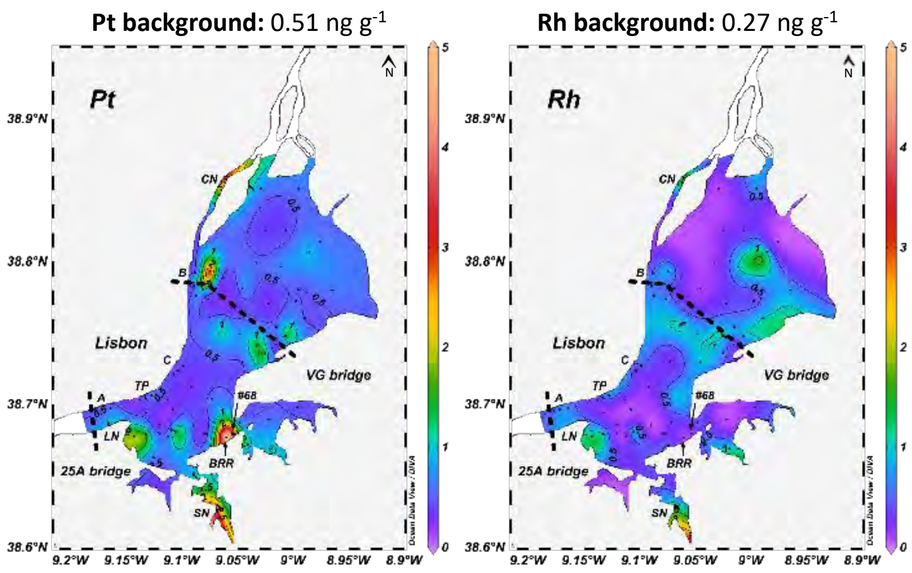

Monteiro et al., *in revision*

Range of concentrations found: 0.18 – 5.1 ng Pt g^{-1} and 0.02 – 1.5 ng Rh g^{-1}

Lowest concentrations found mainly in the central areas of the estuary

Increase of concentrations nearby VG bridge and industrialised areas (BRR, SN, LN and CN)

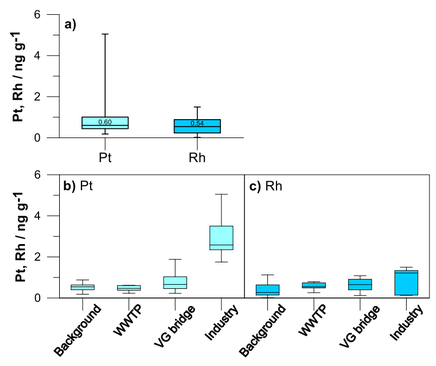

Based on the Pt and Rh spatial distribution (Fig. 2), four sections were outlined (Fig. 3):

(i) ***Background*** of Pt and Rh, comprising the stations considerably distant from potential sources

(ii) ***Waste- and pluvial waters discharge sites*** from the northern margin (Lisbon region)

(iii) ***Motorway bridges***, in particular *VG bridge*

(iv) ***Industrialised areas***

Pt and Rh signature in WWTP

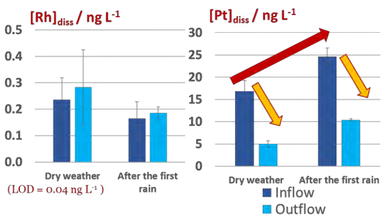

WWTP process does not seem to affect dissolved Rh concentrations, whereas it decreases dissolved Pt concentrations

Rh concentrations were similar while heavy rain flushes urban Pt into the estuary

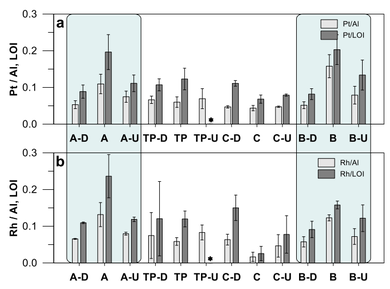

Higher signatures at the discharge sites in the estuary compared to the control stations

Urban drainage of Pt and Rh into the estuary

Pt and Rh imprint in sediments of industrial areas

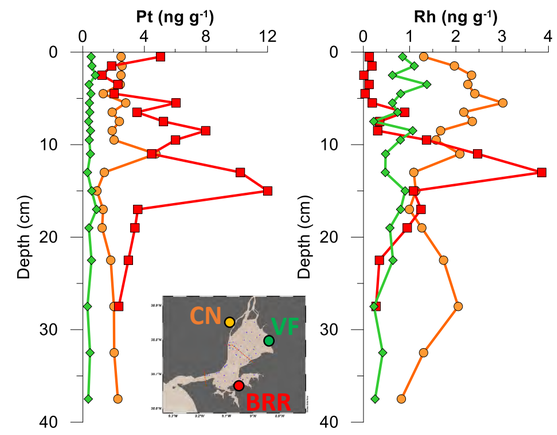

VF: no significant variation for Pt (0.30 – 0.90 ng g^{-1})
Rh higher than the background (0.23 – 1.4 ng g^{-1})

CN: minor variations higher than the background in the estuary
For Pt: 0.92 – 4.7 ng g^{-1}
For Rh: 0.23 – 1.4 ng g^{-1}

BRR: larger variation along the core
For Pt: 1.3 – 12 ng g^{-1}
For Rh: 0.01 – 3.9 ng g^{-1}

Present and historical sources of Pt; Rh minimum at top layers
Highest concentrations between 10- and 15-cm depth

BRR Hotspot

Ongoing work

Geochemical analysis and data interpretation

Variables	Pt	Rh
Al	**0.627**	**0.819**
Si	**-0.608**	**-0.833**
Fe	0.400	**0.738**
Mn	**0.681**	**0.882**
OC	**0.661**	**0.832**
HgT	**0.598**	**0.919**
MeHg	**0.720**	**0.677**
pH	-0.199	-0.423
Eh	-0.076	0.016
Pt	**1**	**0.625**
Rh	**0.625**	**1**

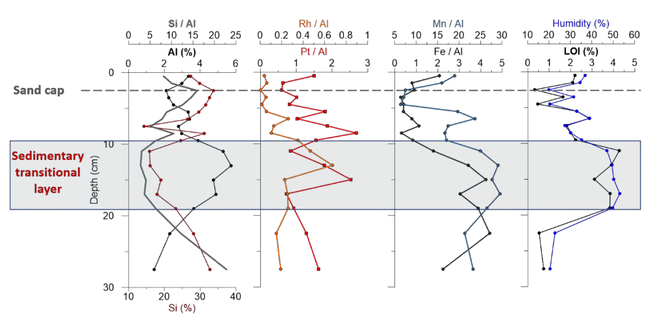

Ongoing and future work

Pt and Rh speciation under relevant environmental conditions
effect of ionic strength on the dissolution from road dust; truly dissolved vs. nanoparticles characterisation

Pt and Rh in the water column under tidal influence
effect of neap and spring tides on the distribution and fate

Modelling at a regional scale
a pratical tool to predict the distribution, fate and possible impacts

Funding:
Centro de Química Estrutural is funded by Fundação para a Ciência e Tecnologia – project UID/QUI/00100/2019.

FCT funded PhD grant SFRH/BD/111087/2015.

FCT funded projects: REEuse – PTDC/QEQ-EPR/1249/2014.

PROFLUX – PTDC/MAR/102748/2008.

COST Action TD1407 – NOTICE

FCT Fundação para a Ciência e a Tecnologia

References:

S. Rauch, G.M. Morrison, Environmental Relevance of the Platinum-Group Elements, Elements. 4 (2008) 259 LP-263. http://elements.geoscienceworld.org/content/4/4/259.abstract.

F. Zereini, C.L.S. Wiseman, Platinum Metals in the Environment, Springer Berlin Heidelberg, Berlin, Heidelberg, 2015. doi:10.1007/978-3-662-44559-4.

A. Cobelo-García, D.E. López-Sánchez, J. Schäfer, J.C.J. Petit, G. Blanc, A. Turner, Behavior and fluxes of Pt in the macrotidal Gironde Estuary (SW France), Mar. Chem. 167 (2014) 93–101. doi:10.1016/j.marchem.2014.07.006.

C. Almécija, Geochemical behaviour and sources of platinum group elements in anthropogenically-impacted sediments, PhD. Thesis, 2015.

C.E. Monteiro, A. Cobelo-Garcia, M. Caetano, M. M. Correia dos Santos, 2017. Improved voltammetric method for simultaneous determination of Pt and Rh using second derivative signal transformation – application to environmental samples. Talanta 175, 1–8. doi:10.1016/j.talanta.2017.06.067

C.E. Monteiro, M. M. Correia dos Santos, A. Cobelo-Garcia, P. Brito, and M. Caetano. Platinum and Rhodium in Tagus Estuary, SW Europe: sources and spatial distribution. *in revision.*

Supported semiconductor nanocatalysts for environmental remediation and radiation sensing

Catarina Santos, André Lima, O.C. Monteiro, V.C. Ferreira

Centro de Química Estrutural e Centro de Química e Bioquímica, Faculdade de Ciências, Universidade de Lisboa, Campo Grande, 1749-016 Lisboa, Portugal

Ciências ULisboa | CQB Centro de Química e Bioquímica

CQE Química Estrutural

06 Chemistry for the Environment - Chem4Env

Introduction

The modification of fibers has been widely explored towards the development of materials with specific and advantageous properties. This takes advantage from the possibility of imparting the properties of the NPs (or molecules) to the fibers, resulting in the preparation of a novel composite or hybrid material. Successful examples are the attachment of Ag, TiO_2 or BiOCl NPs to textile fibers for antibacterial, UV protection, self-cleaning and photocatalytic purposes, and the coating of fabrics with a hydrophobic layer (molecules or polymers) for water repellency and stain free fabrics. [1-4] In this work, several approaches for fibers modification are exploited towards the preparation of materials displaying photocatalytic and radiation sensing/protection responses

Experimental details

In situ fibers modification

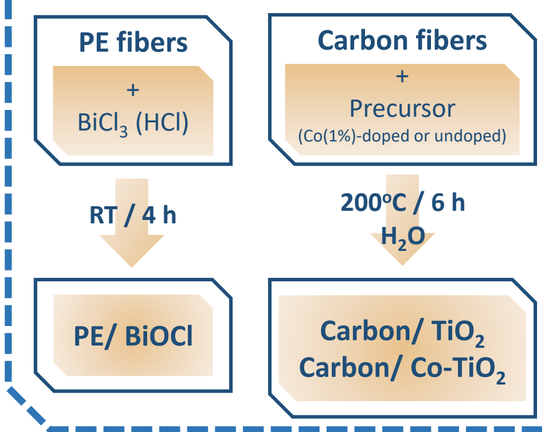

Dye removal

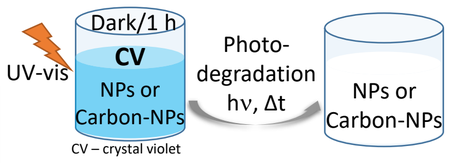

Radiation sensing

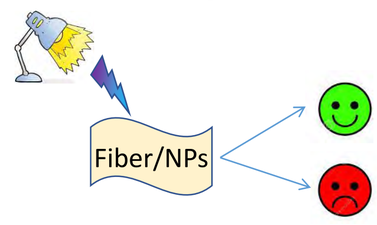

Characterization

XRD

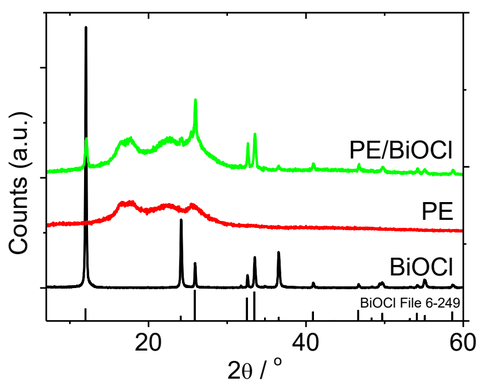

DRS

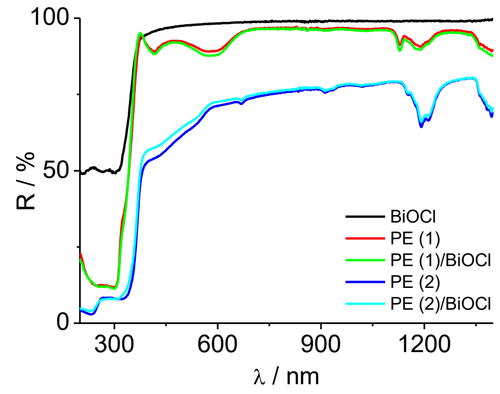

FTIR

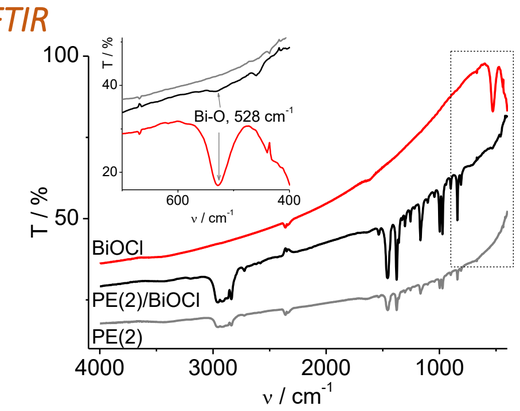

- PE(1) ≠ PE(2)
- BiOCl and PE absorbs in the UV ⟶ DRS did not allow the NPs detection

- BiOCl NPs:
  - crystalline and show typical BiOCl diffraction peaks
  - clearly detected on the PE surface by XRD and FTIR

Optical response

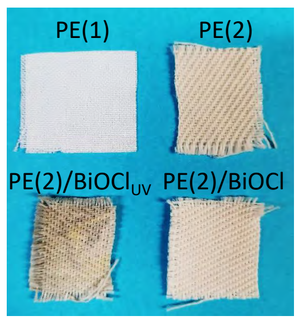

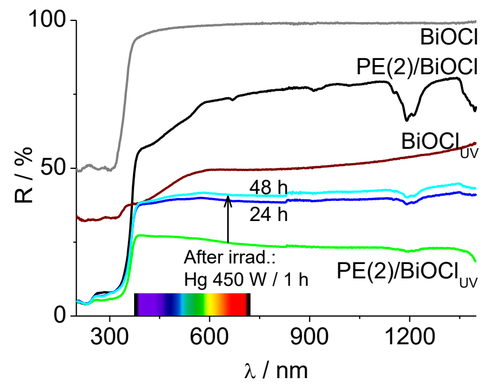

Sample	Conditions	After irradiation*	% recovery @ 650 nm	
			24 h	*48 h*
Hg 450W / 1h	Wet	-48.8	14.3	16.2
Xe-Hg 300W / 4h	Wet	-41.8	0.8	3.9
	Dry	-36.8	2.4	1.6
Xe-Hg 300W / 4h #	Wet	-31.7	1.8	3.8
Sun	Wet	-43.1	6.8	6.1
	Dry	-32.7	5.1	6.9

*- compared with as prepared PE(2)/BiOCl; # - with glass filter

- Self-sensibilisation of BiOCl under light irradiation
  - Optical response intensity in wet samples:
    - Hg 450 W > Sun ≈ Xe-Hg 300 W > Xe-Hg 300 W (w/ filter)
    - Faster recovery for Hg 450 W irradiated wet samples

Characterisation

DRS

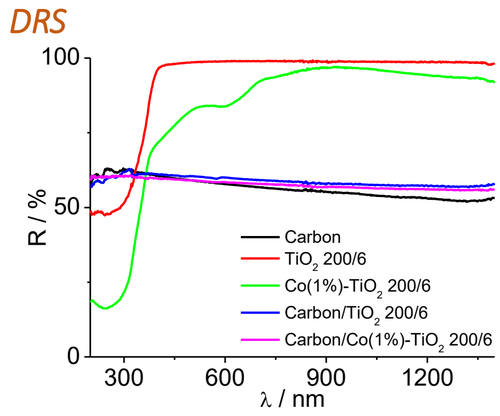

Sample	E_g / eV	d / nm
TiO_2 200/6	3.05	17.3
Co(1%)-TiO_2 200/6	1.59/3.11	15.6

DRX

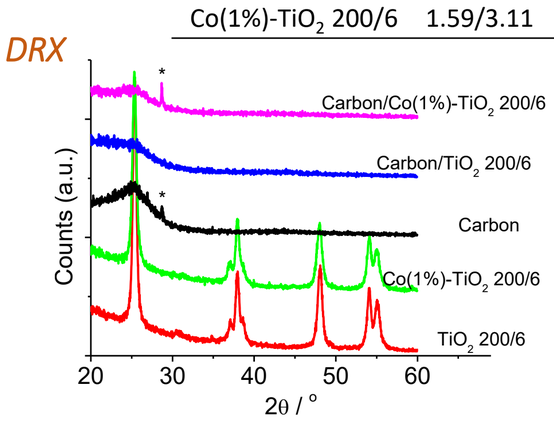

- TiO_2 & Co-TiO_2 NPs: crystalline *anatase* phase with ca. 16 nm
- Co-doping shifts the band-gap energy and absorption range

Pollutants removal

Adsorption

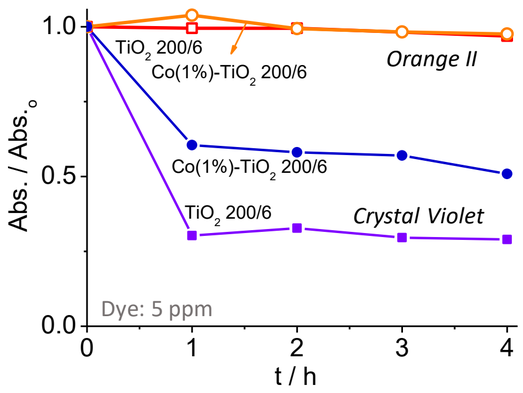

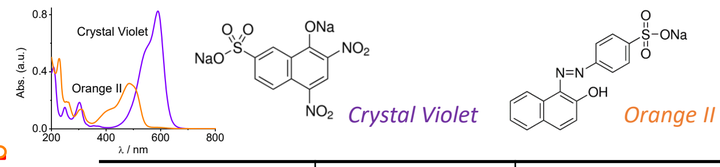

Adsorption: t = 4 h	Crystal Violet		Orange II	
Sample	TiO_2	Co-TiO_2	TiO_2	Co-TiO_2
Abs. (a.u.)	0.2389	0.4195	0.3183	0.3002
$m_{catalyst}$ / g	0.0198	0.0197	0.0199	0.0201
Dye ads. / mg g^{-1}	1.833	1.317	0	0.047

- *Low adsorption ability: of TiO_2 and Co-TiO_2*
  - Crystal violet > Orange II

Photodegradation under UV-vis radiation

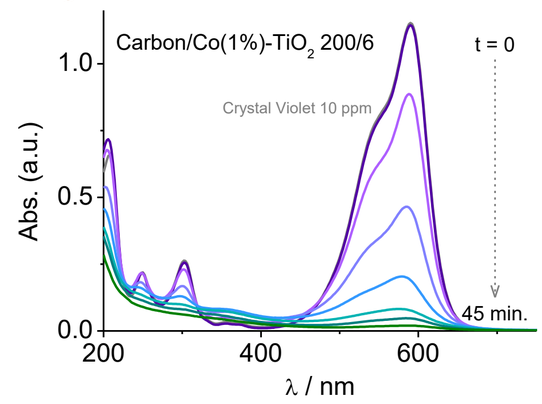

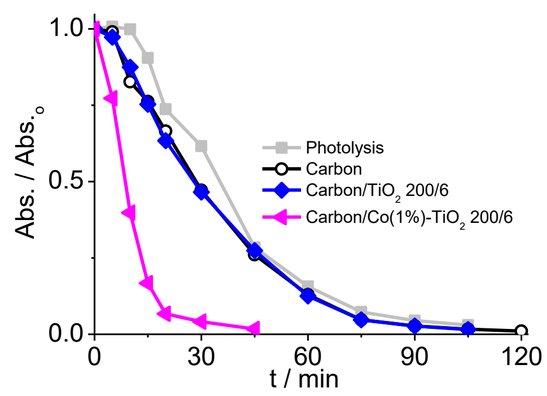

- No effect of TiO_2 attachment – possibly no NPs immobilised on acid-treated Carbon
- Fast CV degradation with Carbon/Co-TiO_2 – successful immobilisation of NPs on plasma-treated Carbon

Conclusions

Polyester fibers were successfully modified with BiOCl NPs as shown by XRD and FTIR. Those NPs are crystalline and can be self-sensitised by light irradiation by oxygen vacancies formation. The degree of sensitisation depends on the conditions (*e.g.* wet/dry) and radiation source (energy), as well as the reversible process. Pristine TiO_2 NPs absorb in the UV range and show a good crystallinity with typical *anatase* phase. The cobalt doping did not affect the NPs crystallinity and those show absorption extended to the visible range. Although no NPs have been detected on the Carbon fibers surface by the characterisation techniques, the good photocatalytic response obtained towards crystal violet degradation clearly shows that Co(1%)-TiO_2 NPs were immobilised on plasma-treated Carbon fibers.

Funding:

Support for this work was provided by FCT through UID/MULTI/00612/2019.

V.C. Ferreira acknowledges financial support from Fundação para a Ciência e a Tecnologia, scholarship: SFRH/BPD/77404/2011 and Marc Ponsa from Polisilk for supplying the PE fibers.

Centro de Química Estrutural is funded by FCT project UID/QUI/00100/2019.

FCT Fundação para a Ciência e a Tecnologia

References:

1. A.K. Yetisen, H. Qu, A. Manbachi, H. Butt, M.R. Dokmeci, J.P. Hinestroza, M. Skorobogatiy, A. Khademhosseini, S.H. Yun, ACS Nano 10 (2016) 3042–3068.
2. V.C. Ferreira, A.J. Goddard, O.C. Monteiro, J. Photochem. Photobiol. A 357 (2018) 201–212.
3. X. Zhou, Z. Zhang, X. Xu, F. Guo, X. Zhu, X. Men, B. Ge, ACS Appl. Mater. Interfaces 5 (2013) 7208–7214.
4. J. Molina, M.F. Esteves, J. Fernández, J. Bonastre, F. Cases, Eur. Polym. J. 47 (2011) 2003–2015

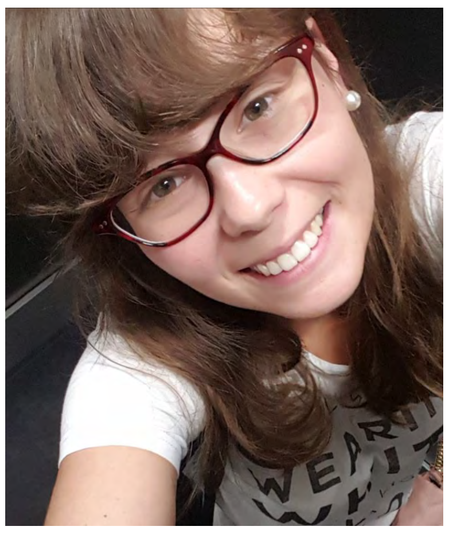

Sulfalene: A Case Study on the Polymorphism of APIs

Cátia S. D. Lopes*, Carlos E. S. Bernardes, Manuel E. Minas da Piedade

Centro de Química e Bioquímica e Centro de Química Estrutural, Faculdade de Ciências, Universidade de Lisboa, 1749-016 Lisboa, Portugal

***csolopes@fc.ul.pt**

SCOPE

An **active pharmaceutical ingredient** (**API**) can crystallize in different packings – **Polymorphism.** Different polymorphs can have dissimilar physical properties (e.g. fusion point, solubility). Hence, **each polymorph** should be regarded as a **unique material**. Despite not being fully understood from a fundamental point of view, **recrystallization from solution,** is the election method to prepare and isolate an API. As consequence during this procedure unforeseen polymorphs can emerge, leading to dangerous health situations (e.g. Ritonovir [1]).

Sulfalene (SL, Figure 1) is an antibiotic and, until now, only one crystalline sctructure was identified [2].

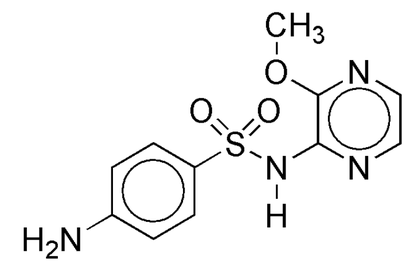

Figure 1. Molecular structure of **s**ulfalene.

AIM: Systematic study of crystallization in sulfalene to assess the existence of different solid forms.

RESULTS

Morphology

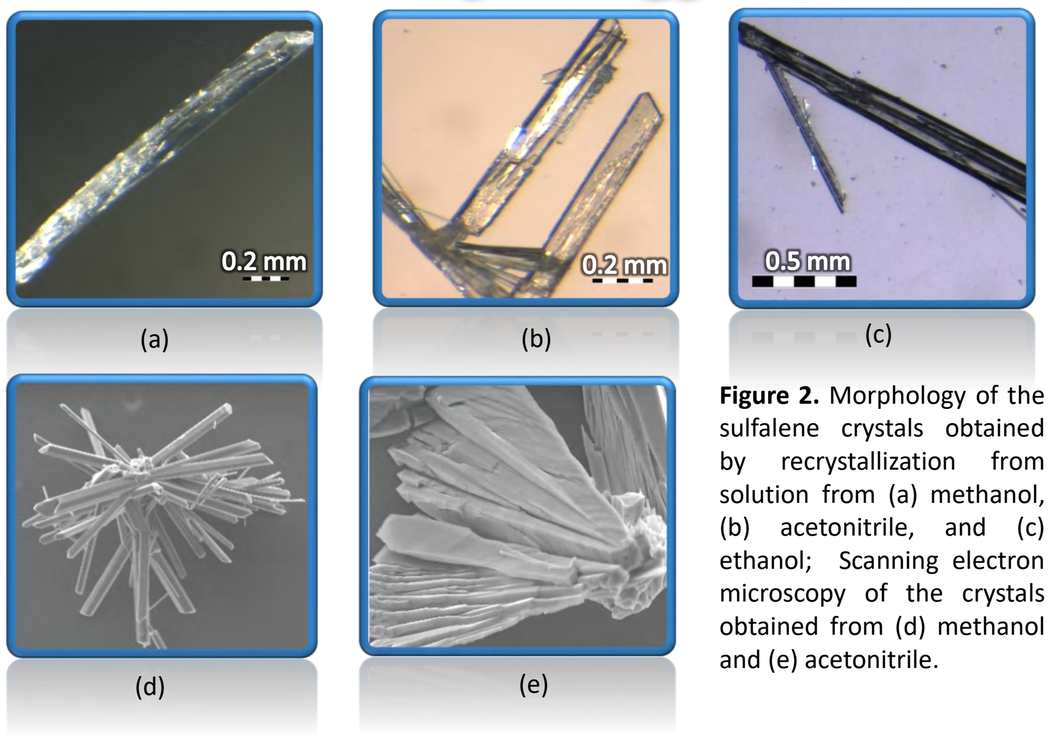

Figure 2. Morphology of the sulfalene crystals obtained by recrystallization from solution from (a) methanol, (b) acetonitrile, and (c) ethanol; Scanning electron microscopy of the crystals obtained from (d) methanol and (e) acetonitrile.

Solubility and Crystallization Curves

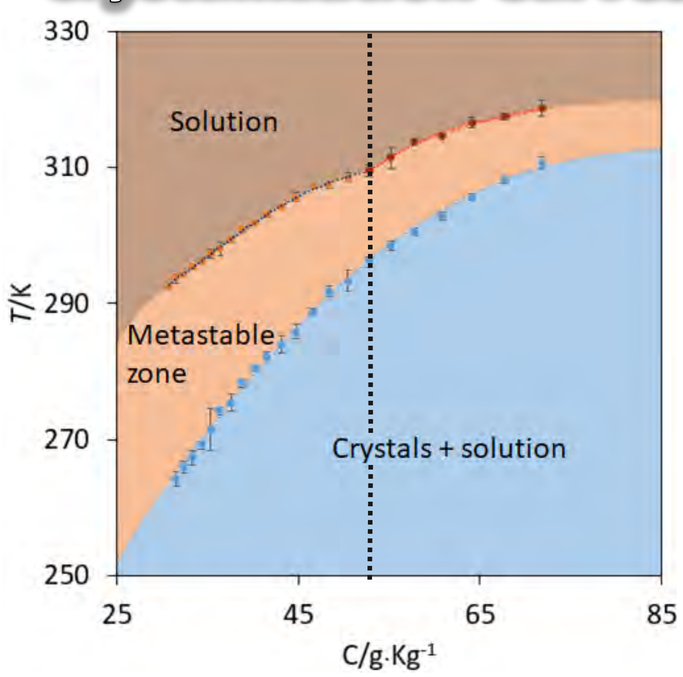

Figure 3. Temperature versus concentration phase diagram of sulfalene in methanol. The blue and orange dots correspond, respectively, to the crystallization and solubilization curves. It is possible to distinguish two different zones in the solubilization curve, before and after 53 g·Kg^{-1}, which suggests that two different phases of SL could be prepared under those conditions.

Crystalline Structure

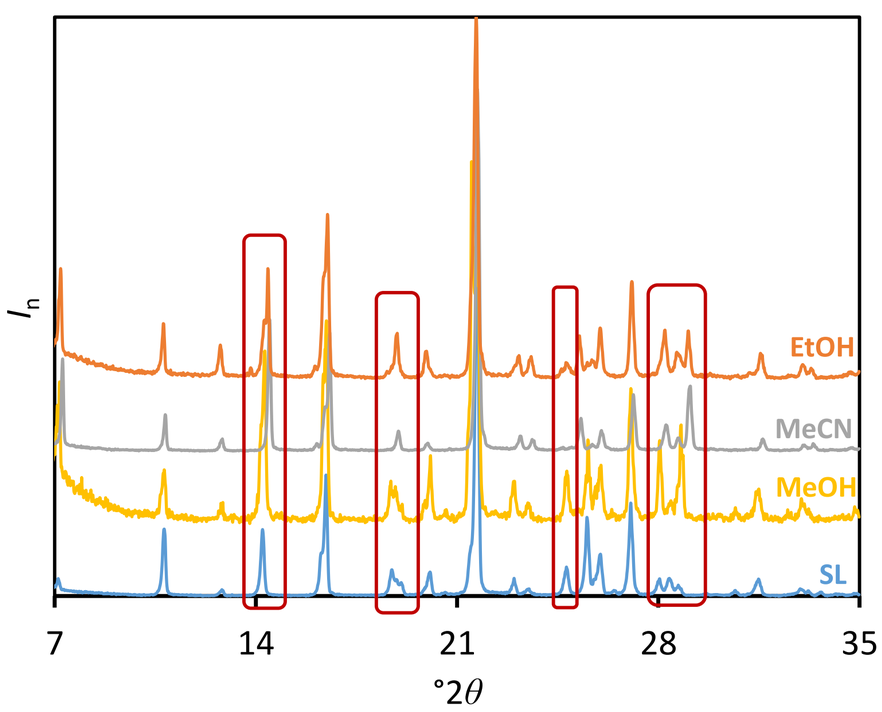

Figure 4. Diffractograms obtained by powder X-ray diffraction (PXRD) for the recrystallizations of Sulfalene (SL, in blue) from methanol (MeOH, in yellow), acetonitrile (MeCN, in grey) and ethanol (EtOH, in orange). The areas signaled in red highlight the 2θ values where the diffractograms present differences. All the diffractograms were normalized to the peak of highest intensity.

Energetics

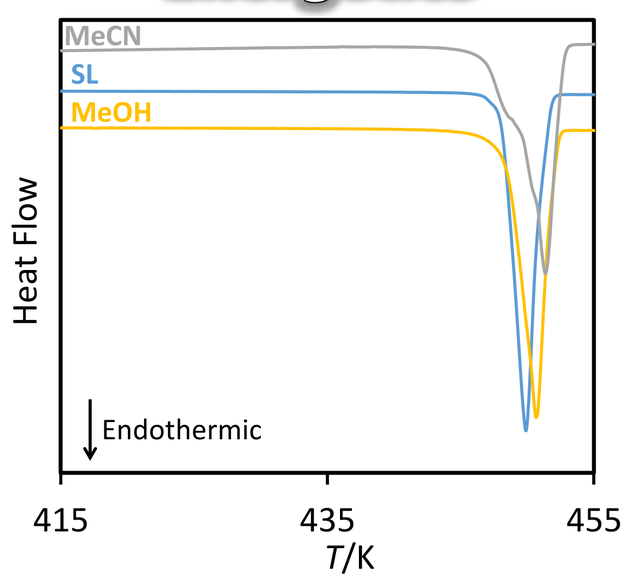

Figure 5. Thermograms obtained by differential scanning calorimetry (DSC) for the recrystallizations of Sulfalene (SL, in blue) from methanol (MeOH, in yellow) and acetonitrile (MeCN, in grey). All thermograms were normalized relative to the mass of the sample used. No other thermal events were detected prior to the fusion of the samples.

Conclusions

- Crystallization from several solvents leads to crystals with similar morphology (Figure 2), but the PXRD and DSC data suggest the preparation of different phases (Figures 4 and 5).
- Different polymorphs can be prepared from methanol by cooling crystallization, by changing the initial solution concentration (Figure 3).

CQE Química Estrutural

09 MET

Funding:
Centro de Química Estrutural is funded by FCT project UID/QUI/00100/2019. This work was supported by Fundação para a Ciência e a Tecnologia (FCT), Portugal through Projects PTDC/QUI-OUT/28401/2017(LISBOA-01-0145-FEDER-028401) and UID/MULTI/00612/2013. A PhD and Post-Doctoral grants from FCT are also gratefully acknowledged by C. S. D. Lopes (SFRH/BD/128794/2017) and C. E. S. Bernardes (SFRH/BPD/101505/2014), respectively.

FCT Fundação para a Ciência e a Tecnologia

MONTELUKAST METABOLISM – MASS SPECTROMETRY APPROACH IN METABOLIC STUDIES

C. F. Marques[1, 2], G. C. Justino[1], M. M. Marques[1]

[1] Centro de Química Estrutural, Instituto Superior Técnico, Universidade de Lisboa, Lisboa, Portugal
[2] Coimbra Institute for Clinical and Biomedical Research, Faculty of Medicine, University of Coimbra, Coimbra, Portugal
catiafmarques@tecnico.ulisboa.pt

BACKGROUND AND OBJECTIVE

Montelukast (MTK), a cysteine leukotriene receptor antagonist, is a drug used in **asthma management** in children and adults. Recently repurposed for **other therapeutic applications** (*e.g.* anti-inflammatory agent in the central nervous system, chemopreventive and adjuvant in cancer therapy and preventive agent in cardiovascular risk settings), **MTK metabolism is poorly understood**. To date, only five phase 1 and two phase 2 MTK metabolites have been identified and no association between metabolites and the adverse effects has been established. (1–4)

Taking into account the potential new applications of MTK, our initial goal was to evaluate the *in vitro* metabolism of MTK.

METHODOLOGY

Different incubations were performed at 37°C and different incubation times were tested. Products were analyzed by high performance liquid chromatography coupled to high-resolution electrospray ionization tandem mass spectrometry – QqTOF.

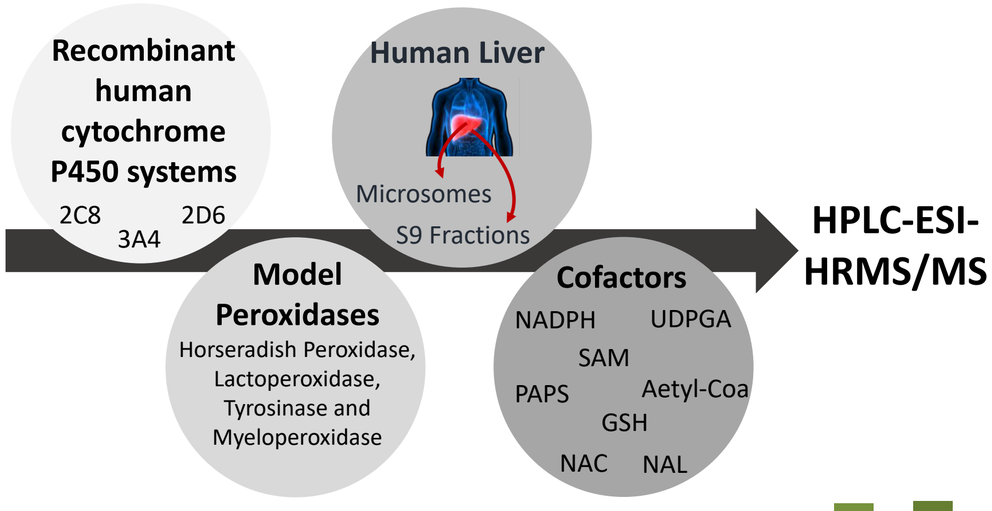

RESULTS

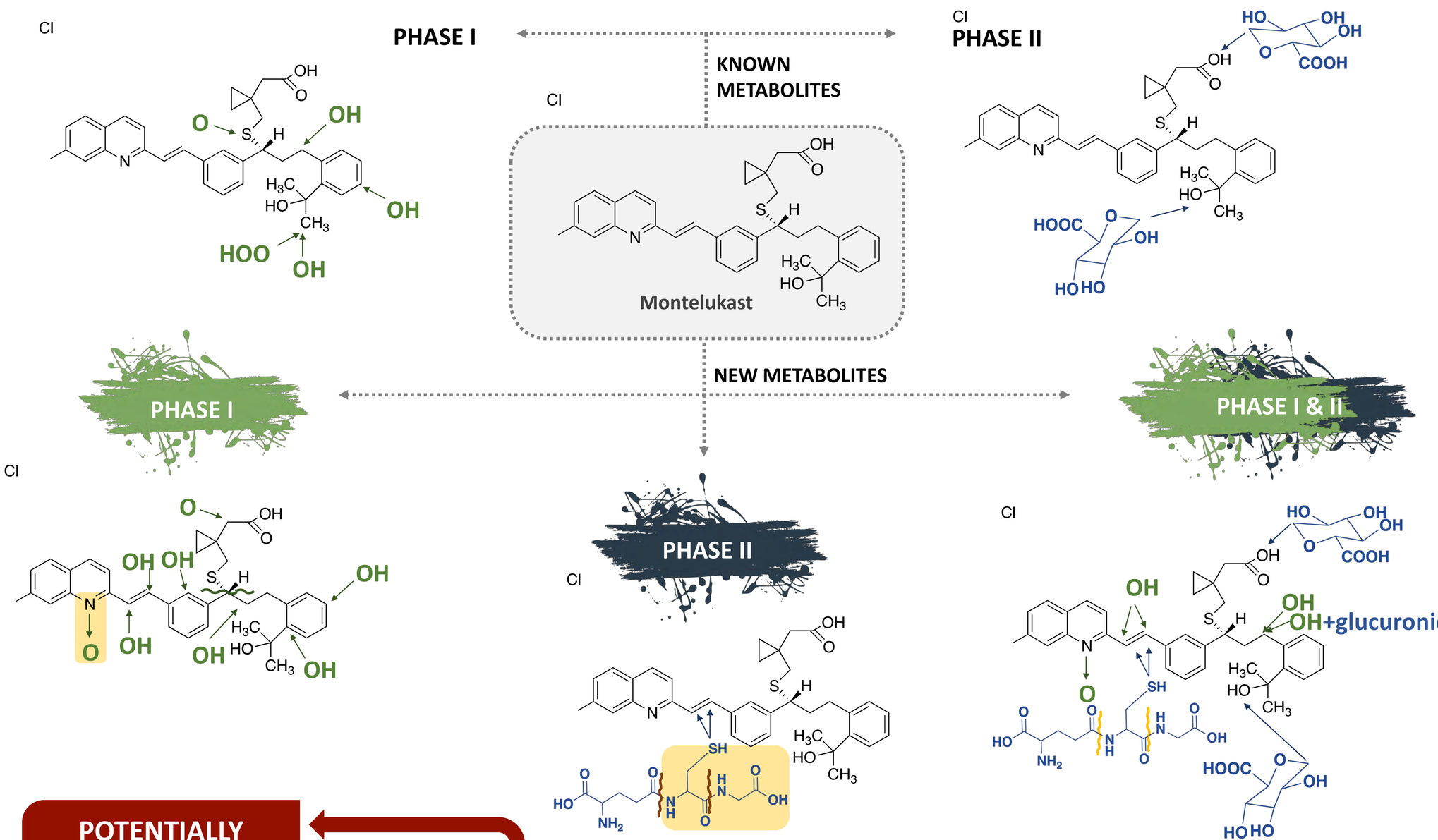

POTENTIALLY REACTIVE METABOLITE

biologically relevant thiyl radicals is plausible *in vivo*, with **NO NEED FOR BIOACTIVATION**.

MTK APPEARS TO BIND GLUTATHIONE AND CYSTEINE, both under **metabolic and non-metabolic conditions**

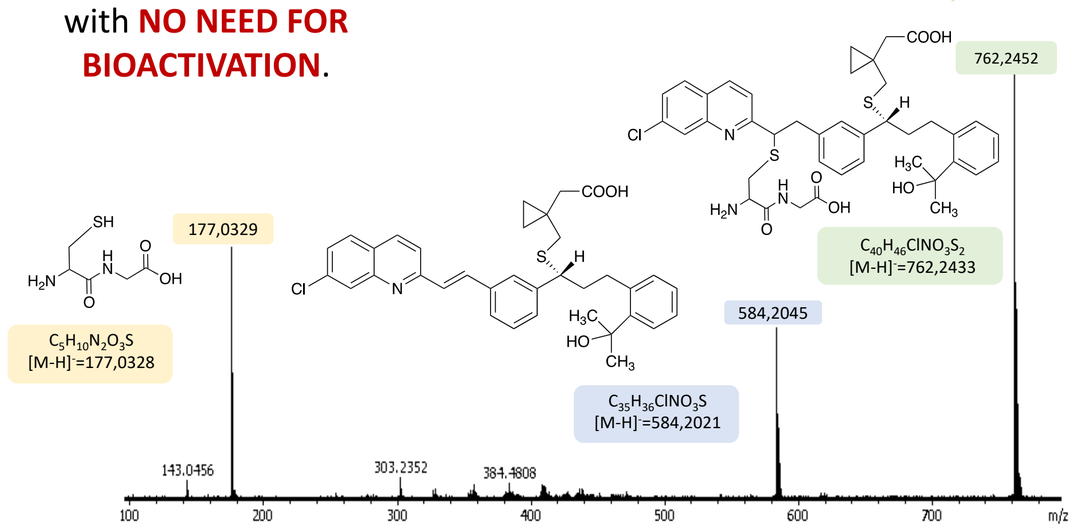

FINAL REMARKS

- With the exception of CYP2D6, all the biological systems were responsible for MTK metabolism.
- The metabolic ability of other human fractions will be tested to access the metabolite profiles in other organs.
- Further studies with MTK plus cofactors and other biomolecules will be conducted.
- Potentially reactive MTK metabolites will be explored and characterized.

05 BIOMOL

Funding:
Centro de Química Estrutural is funded by Fundação para a Ciência e Tecnologia (FCT, Portugal) – project UID/QUI/00100/2019. We thank FCT for funding through projects PTDC/QUI-QAN/32242/2017 and SAICTPAC/0019/2015 and for a PhD fellowship (PD/BD/143128/2019).

References:

1. Marschallinger J, Schäffner I, Klein B, Gelfert R, Rivera FJ, Illes S, et al. Structural and functional rejuvenation of the aged brain by an approved anti-asthmatic drug. *Nat Commun*. 2015;6:8466.
2. Tsai MJ, Wu PH, Sheu CC, Hsu YL, Chang WA, Hung JY, et al. Cysteinyl Leukotriene Receptor Antagonists Decrease Cancer Risk in Asthma Patients. *Sci Rep*. 2016;6:23979.
3. Ingelsson E, Yin L, Bäck M. Nationwide cohort study of the leukotriene receptor antagonist montelukast and incident or recurrent cardiovascular disease. *J Allergy Clin Immunol*. 2012;129(3):702-707.
4. De Oliveira Cardoso J, Oliveira RV, Lu JBL, Desta Z. In vitro metabolism of montelukast by cytochrome P450S and UDP-glucuronosyltransferases. *Drug Metab Dispos*. 2015;43(12):1905–16.

A WORKFLOW FOR DRUG METABOLISM MS STUDIES WITH DATA-INDEPENDENT ANALYSIS

C. F. Marques, P.F. Pinheiro, M.M. Marques, M.C. Oliveira, G.C. Justino

Centro de Química Estrutural, Instituto Superior Técnico, Universidade de Lisboa, Lisboa, Portugal

catiafmarques@tecnico.ulisboa.pt

CQE Química Estrutural

CQE MASS SPECTROMETRY

05 BIOMOL

BACKGROUND AND OBJECTIVE

Drug metabolism studies involve repetitive experiments where the target compounds are incubated with enzymes/cells/tissues of interest in order to understand their metabolic profile. An exhaustive study of possible metabolites must thereafter be performed, and a metabolite database created and updated using proprietary software such as Bruker's TASQ (Target Analysis for Screening and Quantitation), that is designed for metabolomics and not for drug metabolic profiling. However, with the advancement of IT tools, new software has been developed to help in data processing based on metabolite databases. Software as MZmine 2[1] and TASQ are two examples of how automation can help users in expedite data processing.

We present here the workflow for a complete identification of drug metabolites by HRMS using data-independent acquisition and data-independent processing.

WORKFLOW

REACTION MIX INCUBATION

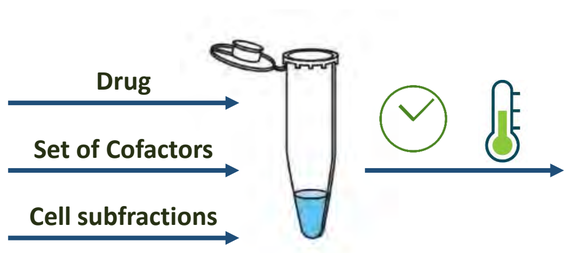

HRMS DATA ACQUISITION

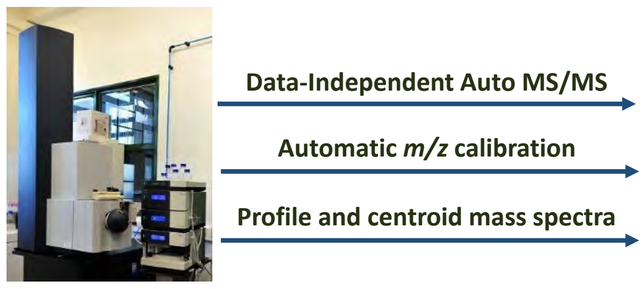

UPLC-ESI-HRMS (QqTOF) (Bruker Impact II)

MANUAL DATA PROCESSING

- Tentative identification of major peaks in full chromatogram
- Chromatogram extraction for known compounds
- No background subtraction

AUTOMATIC DATA PROCESSING

- Automatic chromatogram extraction (noise threshold dependent)
- Unique peak identification based on *m/z* and RT
- Automatic sample-control pairing

RESULTS

MANUAL DATA PROCESSING

Manual Chromatogram Extraction & Peak Picking

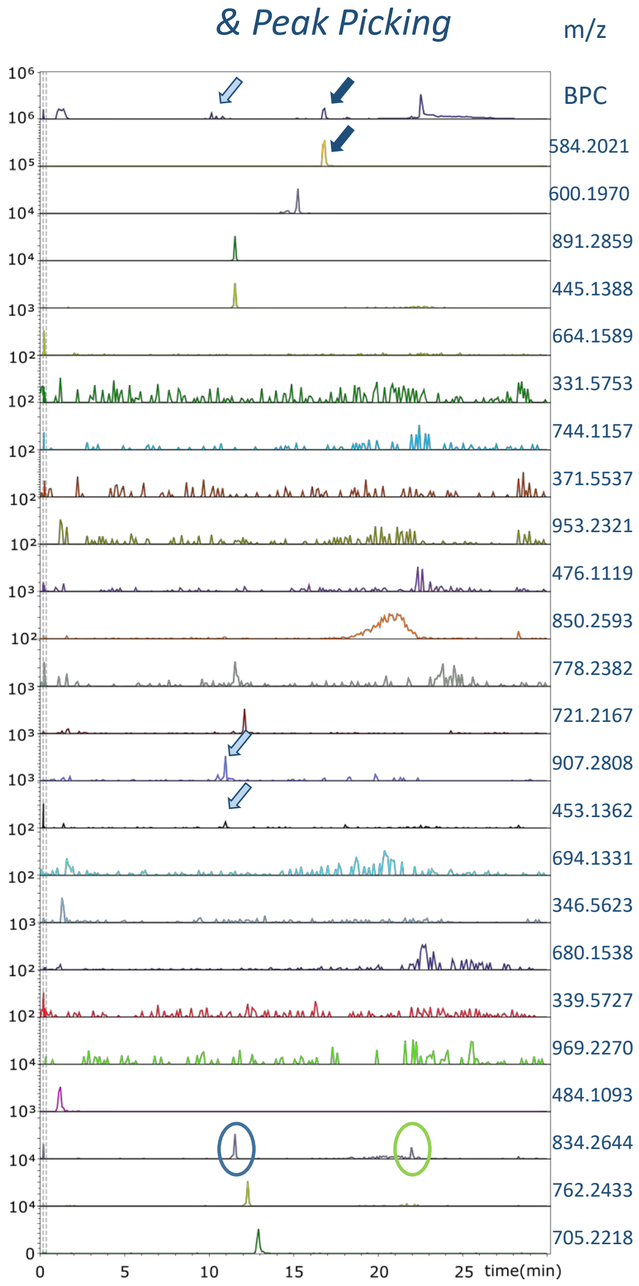

AUTOMATIC DATA PROCESSING

MZmine 2

Status		Average	
Control	Sample	*m/z*	RT
●	●	584.2024	16.77
●	●	600.1975	15.24
●	●	891.2640	11.51
●	●	445.1419	11.50
●	●	*664.1*	
●	●	*331.5*	
●	●	*744.1*	
●	●	*371.5*	
●	●	*953.2*	
●	●	*476.1*	
●	●	*850.2*	
●	●	*778.2*	
●	●	721.2164	11.93
●	●	907.2781	10.86
●	●	453.1586	11.39
●	●	*694.1*	
●	●	*346.5*	
●	●	*680.1*	
●	●	*339.5*	
●	●	*969.2*	
●	●	*484.1*	
●	●	834.2651	11.50
●	●	762.2407	12.15
●	●	705.2208	12.87

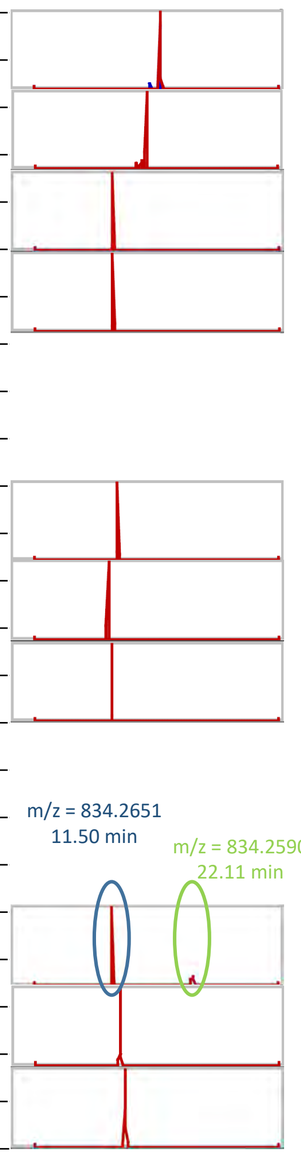

Automated mass detection (above specificed noise level)

⇩

Automated chromatogram extraction for all detected masses (above minimum height with minimum RT span and maximum 0.005 ppm *m/z* tolerance)

⇩

Retention time normalization and alignment between all chromatograms (below specified RT tolerance)

⇩

Isotopic peak grouping into one single hit per base *m/z*

⇩

Paired peak list

FINAL REMARKS

MANUAL PROCESSING
- 2 relevant peaks in BPC
- 24 searched compounds
  - 13 not found
  - 10 found
  - 1 below confidence level
- Manual peak isotope profile confirmation

AUTOMATIC PROCESSING
- 10 relevant peaks identified
- Ions within same mass range with different RT are identified
- No false positives
- No lost peaks

OTHER PROS OF AUTOMATED PROCESSING
- Reduced analysis time per sample
- Batch programmable

CONS OF AUTOMATED PROCESSING
- Actually none. If you read it this far, congratulations, you are a winner.

Funding:

Centro de Química Estrutural is funded by Fundação para a Ciência e Tecnologia (FCT, Portugal) – project UID/QUI/00100/2019. We thank FCT for the PhD fellowships SFRH/BD/110945/2015 (PFP) and SFRH/BD/143128/2019 (CFM). This work was also supported by grant LPCC/NRS – Terry Fox 2015-17 from Liga Portuguesa Contra o Cancro, and projects SAICTPAC/0019/2015, PTDC/QUI-QAN/32242/2017 and UID/QUI/00100/2019, funded by national funds through FCT and when appropriate co-financed by FEDER under the PT2020 Partnership Agreement.

References:

1. T. Pluskal, S. Castillo, A. Villar-Briones, M. Orešič, MZmine 2: Modular framework for processing, visualizing, and analyzing mass spectrometry-based molecular profile data, *BMC Bioinformatics* 11:395 (2010).

FCT Fundação para a Ciência e a Tecnologia

SOLVENT-FREE SYNTHESIS OF COPPER BENZENE-1,3,5-TRICARBOXYLATE $Cu_3(BTC)_2(H_2O)_3.10H_2O$ AND $Cu_2(OH)(BTC)(H_2O).2H_2O$ BY BALL MILLING

Célia Aissani [1,2,*], Elisabete C. B. A. Alegria [1,3], Ana P. C. Ribeiro [1]

[1] Coordination Chemistry and Catalysis, CQE-Instituto Superior Técnico, Lisbon, Portugal

[2] Chemistry departement, Faculty of Sciences and Engeneering, Sorbonne Université, Paris, France

[3] ADEQ-ISEL-Instituto Politécnico de Lisboa, Lisbon, Portugal

* Corresponding author : celia.aissani@etu.upmc.fr

CQE Química Estrutural

01 Coordination Chemistry and Catalysis

TÉCNICO LISBOA

SCIENCES SORBONNE UNIVERSITÉ

Introduction

Making compound synthesis easier and less energy consuming is possible with ball milling, representing a fundamental perspective for a greener and sustainable chemistry. However, modifying some parameter in ball milling experiments [1] tend to show their potential influence on the obtained substances. A systematic study was made to investigate the effect of various ball milling conditions on the production of two MOFs, $Cu_3(BTC)_2(H_2O)_3.10H_2O$ and $Cu_2(OH)(BTC)(H_2O).2H_2O$. The number of spheres, the rotation per minute (rpm) and initial mass of starting materials were found to be determining for the structure of the final compounds.

Strategy

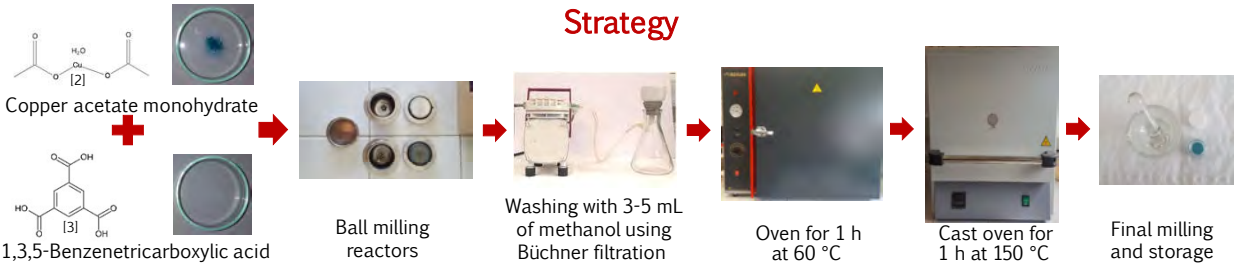

Figure 1 Synthesis procedure, inspired by [1]

First two set of experiments was done with $m(Cu(OAc)_2.H_2O)$ was about 0,3535g and $m(H_3BTC)$ 0,225g and the following milling conditions :

Sample	Number of spheres	Stirring time (min)
1	5	10
2	10	10
3	5	60
4	10	60
5	5	30
6	10	30

Sample	Number of spheres	rpm
7	5	1000
8	10	1000
9	5	1500
10	10	1500
11	5	2000
12	10	2000

A third set of experiments was done with $m(Cu(OAc)_2.H_2O)$ was about 1,7675g and $m(H_3BTC)$ 1,125g and the following milling conditions :

Sample	Number of spheres	rpm
13	5	500
14	10	500
15	5	1500

Results

All the samples were observed with a microscope (Figure 2) and analyzed by ATR (Figure 3). Compounds A, B and C, have been synthesized. A was obtained by samples 1, 3, 5, 13, 14 and 15 ; B from 2, 4, 6, 8, 10 and 12 ; C from 7, 9 and 11.

A comparison with the reported spectra [1] has lead to an attribution of 2 of the 3 compounds (Figure 3). Product C has probably an intermediate structure.

Hence, the stirring time had no effect on the final compound. Only the number of spheres, the rotation per minute and the starting mass of materials had an influence on the obtained compound.

A : $Cu_3(BTC)_2(H2O)_3.10H_2O$

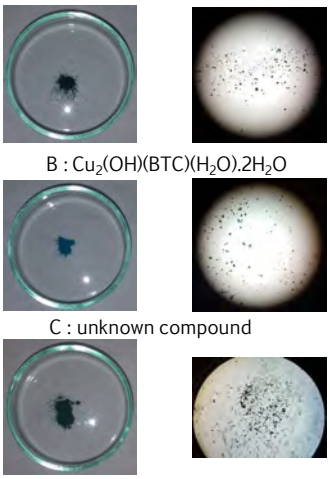

B : $Cu_2(OH)(BTC)(H_2O).2H_2O$

C : unknown compound

Figure 2 Pictures and microscopic observations of the obtained compounds

A : $Cu_3(BTC)_2(H_2O)_3.10H_2O$

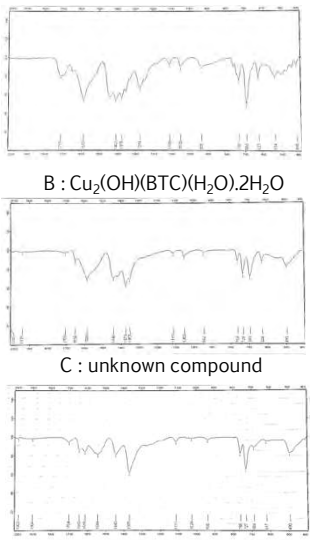

B : $Cu_2(OH)(BTC)(H_2O).2H_2O$

C : unknown compound

Figure 3 IR spectra of the obtained compounds

Conclusion

A solvent-free synthesis is possible by ball milling. The process will be investigated in the future for the production of MOFs based on other transition metals.

In future work, the produced MOFs will be complexed with TiO2 and tested in photo-catalysis (Figure 4).

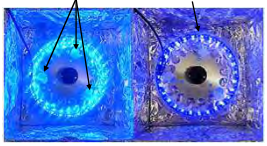

Figure 4 Photo-catalysis montage with blue and violet light

Fundings

Centro de Química Estrutural is funded by Fundação para a Ciência e Tecnologia – projects PTDC/QUI-QIN/29778/2017, UID/QUI/00100/2019 and PTDC/QEQ-ERQ/1648/2014. Erasmus + also contributed to this project.

FCT Fundação para a Ciência e a Tecnologia

Erasmus+

References

[1] Siew, W.Y. ; Abu Bakar, N.H.H. ; Abu Bakar M., Inorg. Chim. Acta [Online] *2019* (482) 53-61.

[2] https://www.spectrumchemical.com/OA_MEDIA/H_C1370.gif

[3] https://upload.wikimedia.org/wikipedia/commons/thumb/8/87/Trimesic_acid.svg/916px-Trimesic_acid.svg.png

Keywords

Ball milling, mechanochemistry metal organic framework, green chemistry

Ionic composition and balances of seawaters from different locations, assessed by Ion Chromatography

C. M. Oliveira, Bárbara Anes, R.B. Silva, M. F. Camões

Accurate characterization of the composition of seawater is required to understand chemical changes occurring in the ocean and their impact on marine ecosystems.
The different concentration ranges of major and minor ions represent a big challenge to the analysis of seawater samples by ion chromatography.

EQUIPMENT

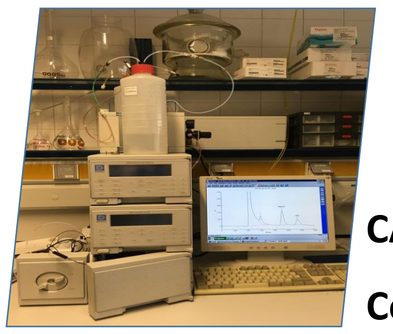

CATIONS:

Conductimetric detection

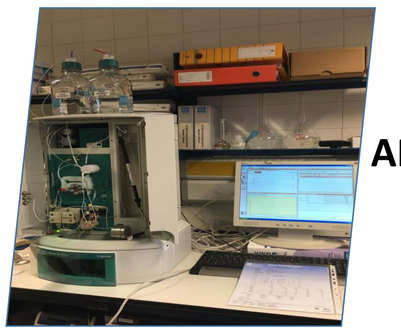

ANIONS: Conductimetric and UV-VIS detections

SAMPLING SITES

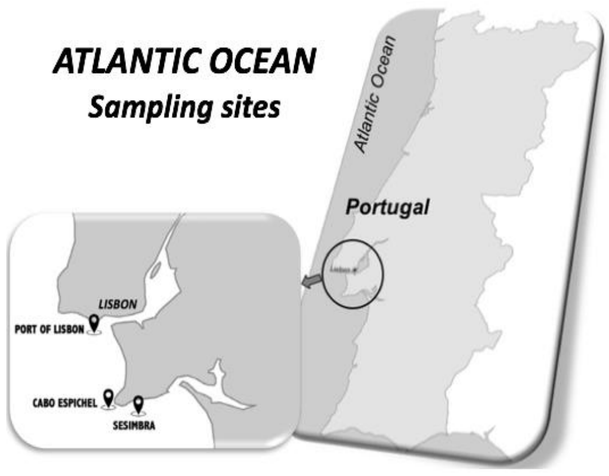

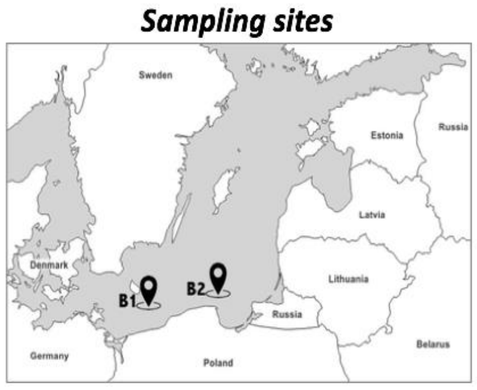

ION MASS CONCENTRATION IN THE ANALYSED SAMPLES

$(c \pm U)$ / g L^{-1}

Ion	Atlantic Ocean			Baltic Sea	
	Port of Lisbon	Cabo Espichel	Sesimbra	Position 1	Position 2
Na^+	11.04 ± 0.33	11.01 ± 0.35	11.99 ± 0.36	2.282 ± 0.076	2.273 ± 0.075
K^+	0.41 ± 0.12	0.42 ± 0.15	0.45 ± 0.12	0.084 ± 0.029	0.085 ± 0.029
Mg^{2+}	1.28 ± 0.13	1.31 ± 0.17	1.43 ± 0.13	0.261 ± 0.033	0.248 ± 0.033
Ca^{2+}	0.433 ± 0.063	0.416 ± 0.081	0.449 ± 0.064	0.107 ± 0.016	0.101 ± 0.016
Cl^-	19.7 ± 1.9	19.5 ± 2.2	21.4 ± 2.2	4.06 ± 0.51	4.09 ± 0.64
Br^-	0.066 ± 0.026	0.067 ± 0.026	0.067 ± 0.032	0.0140 ± 0.0090	0.0140 ± 0.0090
SO_4^{2-}	2.73 ± 0.15	2.65 ± 0.15	3.11 ± 0.28	0.565 ± 0.087	0.585 ± 0.110
Salinity	35.6‰	35.4‰	38.6‰	7.4‰	7.3‰
Hardness (g L^{-1})	6.33 ± 0.56	6.42 ± 0.73	7.00 ± 0.56	1.34 ± 0.14	1.27 ± 0.14
Mg^{2+}/ Ca^{2+}	2.94 ± 0.52	3.14 ± 0.74	3.18 ± 0.54	2.44 ± 0.48	2.46 ± 0.51

IONIC BALANCE PARAMETERS FOR EACH SEAWATER SAMPLE

Ionic balance/ meq L^{-1}

	Atlantic Ocean			Baltic Sea	
	Port of Lisbon	Cabo Espichel	Sesimbra	Position 1	Position 2
Cations	617 ± 18	618 ± 21	673 ± 19	128 ± 4	127 ± 4
Anions	613 ± 54	607 ± 62	668 ± 62	126 ± 18	128 ± 15
Charge balance	4.2 ± 57	10.5 ± 66	5.2 ± 65	1.8 ± 19	-1.2 ± 15

CONCLUSIONS

- The principle of constant proportions was observed for the tested samples.
- Results of seawater samples from the Portuguese Coast match the expected values for seawater hardness (≥ 6 g L^{-1}), having the characteristics of very hard water. The low total hardness of Baltic Sea water can be explained by the relevant influence of river discharges.
- Mg^{2+}/ Ca^{2+} ratios found for all the Portuguese Coast samples are very similar and slightly larger than those of Baltic Sea.
- A small but consistent "excess" of positive charges in the ionic balance can be explained by the presence of, not quantified, HCO_3^- and CO_3^{2-}.

CQE Química Estrutural

06 CE

Funding:
Centro de Química Estrutural is funded by Fundação para a Ciência e Tecnologia – project UID/QUI/00100/2019. FCT also supported the research, through the PhD Scholarship SFRH/BD/111437/2015

FCT Fundação para a Ciência e a Tecnologia

References:

Bettencourt da Silva, Ricardo J.N., and M. Filomena Camões. 2010. *Analytical Letters* 43 (7): 1257–66.

Gros, Nataša, M. F. Camões, Cristina Oliveira, and M. C.R. Silva. 2008. *Journal of Chromatography A* 1210 (1): 92–98.

JCGM (Working Group 1). 2008. "Evaluation of Measurement Data — Guide to the Expression of Uncertainty in Measurement." *International Organization for Standardization Geneva ISBN*. Vol. 50.

Whitfield, M, and D Jagner. 1981. *Marine Electrochemistry: A Practical Introduction*. A Wiley Interscience Publication. Wiley.

The ciliopathy-involved protein KIAA0753 functional interactions with the regulator of centrosome positioning TBCCD1

Ferreira DC[1,2], Carmona B[1,2,3], Nolasco S[3,4], Marinho HS[1,2] and Soares H[1,2,3]

[1] Centro de Química Estrutural, Faculdade de Ciências da Universidade de Lisboa; [2] Centro de Química e Bioquímica, Faculdade de Ciências da Universidade de Lisboa; [3] Escola Superior de Tecnologia da Saúde de Lisboa, Instituto Politécnico de Lisboa; [4] Centro de Investigação Interdisciplinar em Sanidade Animal (CIISA), Faculdade de Medicina Veterinária, Universidade de Lisboa

Background

Cilia are slender protuberances found in eukaryotic cells, consisting of a microtubule (MT)-based ciliary axoneme, which confer motility and sensory functions. These organelles have a centriole/basal body, which can be derived from the centrosome and that nucleates/assembles the ciliary axoneme. Centrosomes are composed of a pair of centrioles, surrounded by the pericentriolar matrix, and are the major microtubule organizers in animal cells, participating in a variety of processes (1). Centriolar satellites are cytoplasmic granules located around the centrosome. These structures play essential roles in centrosome assembly and primary cilium formation through the delivery of centriolar/centrosomal components from the cytoplasm to the centrosome (2). Mutations in genes encoding centrosome and/or centriolar satellite components and regulators lead to various human disorders, such as microcephaly and ciliopathies.

Ciliopathies are a group of rare diseases, typified by often overlapping clinical manifestations, such as infertility, brain and skeletal developmental problems and blindness. Previous work from our group, using a BioID approach, characterized the interactome of a new centrosomal TBCC domain-containing human protein (TBCCD1) involved in correct positioning of the centrosome and cilia biogenesis. Among the identified proteins, there were several well-known proteins encoded by ciliopathy genes, e.g. centrosomal and centriolar satellites protein KIAA0753 (also known as OFIP and Moonraker). The *ofip* gene is mutated in the Joubert syndrome and related disorders, a heterogenous group of ciliopathies defined by hypotonia, developmental delay, abnormal eye movements and breathing abnormalities (3).

Objectives

Our main objective is to study the role of the protein Moonraker, in association with the proteins TBCCD1 and OFD1, in the development of primary cilia. Additionally, we will also investigate if TBCCD1 interacts with this protein for being a component of the OFD1/Moonraker/FOR20 complex or if the interaction with these proteins involves another mechanism.

Results

1. Depletion of KIAA0753 in centrosome and MT cytoskeleton

In hTERT-RPE-1 cells, knockdown of KIAA0753 affects the centrosome by increasing the distance between the centrioles (shown in the figure below).

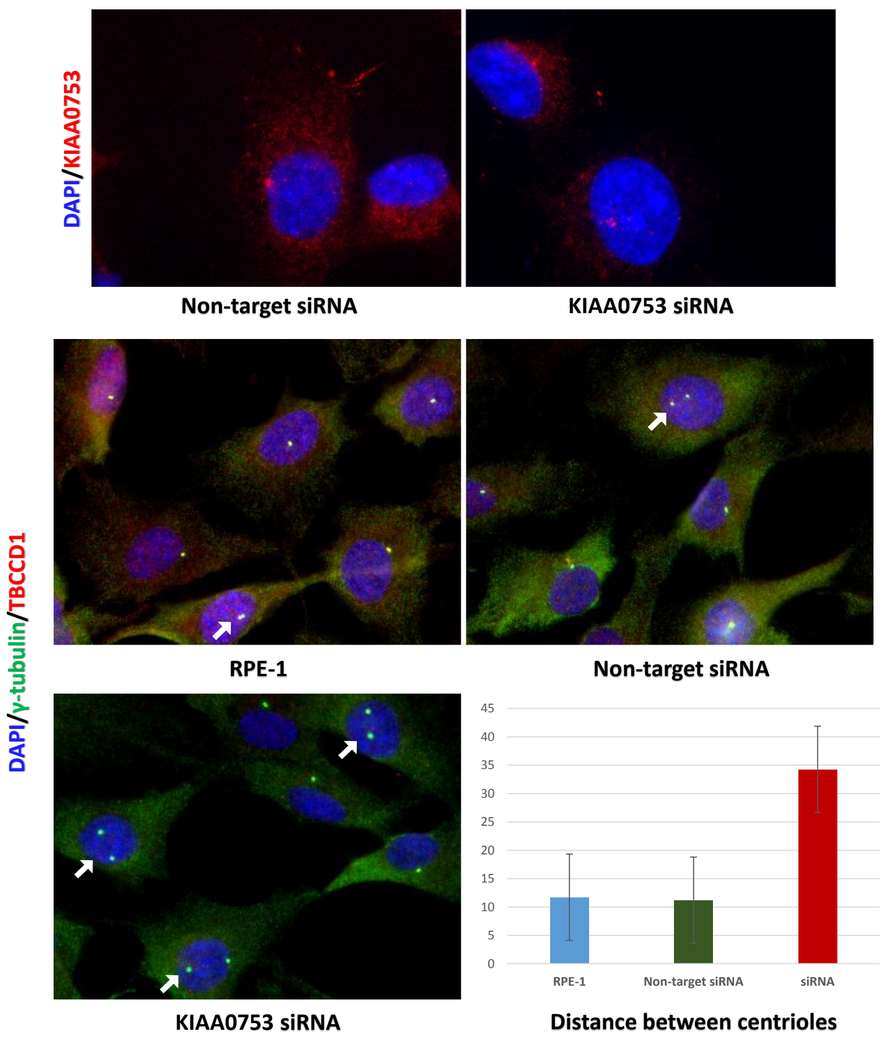

KIAA0753 depletion by siRNAs assays affected the organization of the MT cytoskeleton, possibly compromising cell polarity and cell migration.

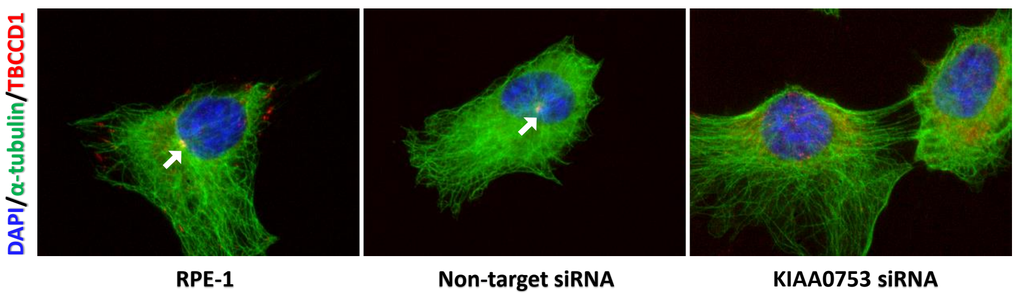

2. KIAA0753 localization in ciliated RPE1 cells

KIAA0753 accumulates in the proximal region of primary cilia.

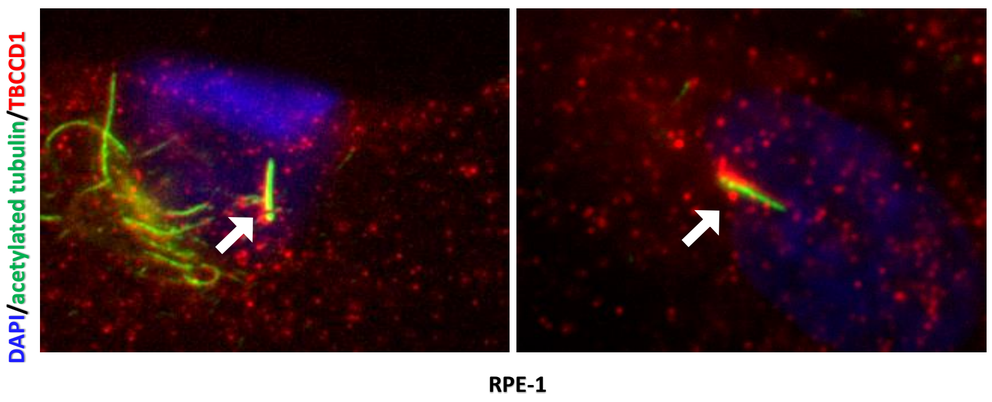

3. Impact of TBCCD1 levels in KIAA0753 and PCM1

Knockdown and overexpression of TBCCD1 affects the levels of KIAA0753, as well as its localization at the centrosome. The depletion of TBCCD1 also causes an alteration of the PCM1-containing pericentriolar satellites pattern next to the centrioles.

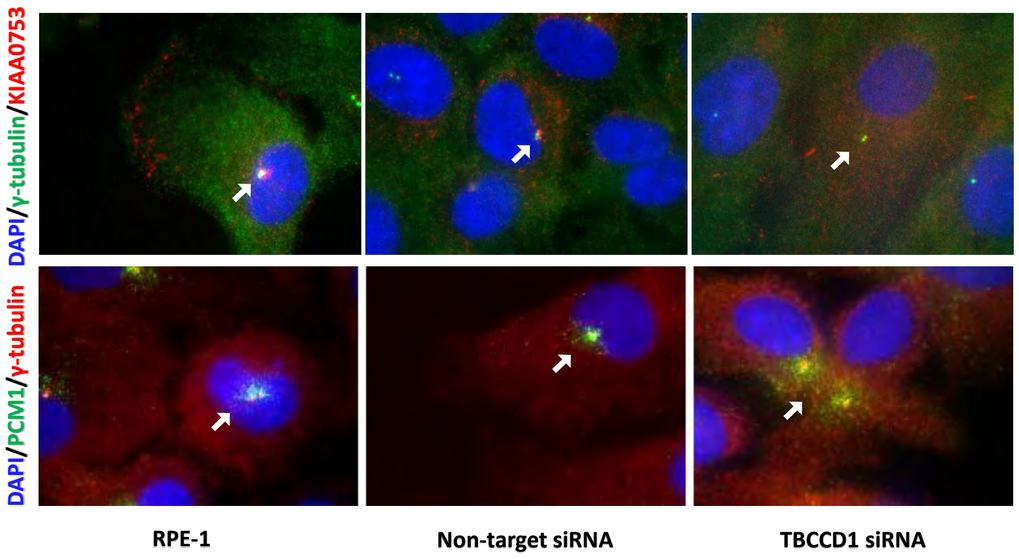

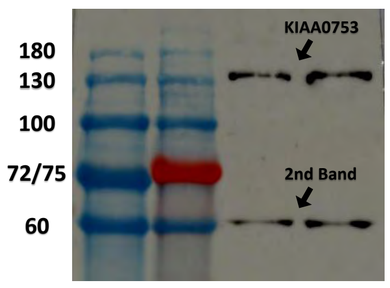

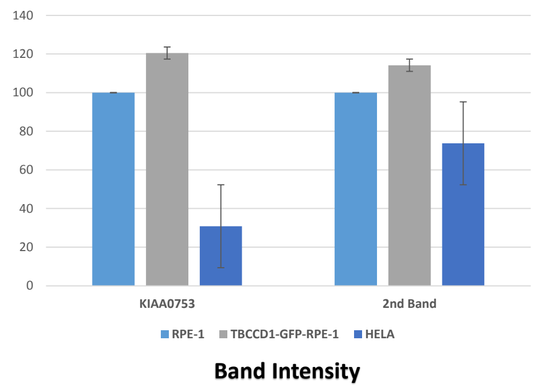

4. Impact of TBCCD1 overexpression in cilia biogenesis

TBCCD1-GFP-RPE-1 has more difficulty producing primary cilia, doubling it's size when they do (shown in the figure below).

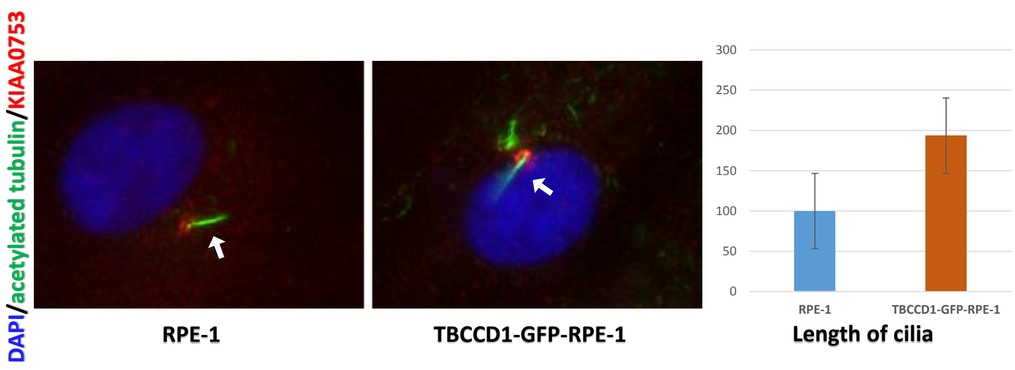

Conclusion

These results support KIAA0753's role in cytoskeleton organization and ciliogenesis, which implicates it in ciliopathies. They also point to a new functional interaction between TBCCD1 and KIAA0753, as it's suggested that TBCCD1 plays a role in the recruitment of KIAA0753 to the centrosome, and strongly support that *tbccd1* is a new ciliopathy gene.

CQE Química Estrutural

05 BIOMOL

Funding:
CQE (Centro de Química Estrutural) is funded by Fundação Fundação para a Ciência e Tecnologia (FCT, Portugal) – project UID/QUI/00100/2019 and CQB PEst-OE/QUI/UI0612/2013, Fundação para a Ciência e a Tecnologia; IPL/2016/TBCCentro_ESTeSL+ IPL/2017/CILIOPAT/ESTeSL, Instituto Politécnico de Lisboa (given to HS)

FCT Fundação para a Ciência e a Tecnologia

References:

1. Bettencourt-Dias M, Hildebrandt F, Pellman D, Woods G, Godinho SA. Centrosomes and cilia in human disease. Trends Genet. 27 (2011) 307-15.
2. Hori A, Toda T. Regulation of centriolar satellite integrity and its physiology. Cell Mol Life Sci. 74(2017) 213-229.
3. Stephen J, Vilboux T, Mian L, Kuptanon C, Sinclair CM, Yildirimli D, Maynard DM, Bryant J, Fischer R, Vemulapalli M, Mullikin JC; NISC Comparative Sequencing Program, Huizing M, Gahl WA, Malicdan MCV, Gunay-Aygun M. Mutations in KIAA0753 cause Joubert syndrome associated with growth hormone deficiency. Hum Genet. 136 (2017) 399-408

Diclofenac sustained release using an LbL coated silicon-based hydrogel

Diana Silva[1], Hermínio C. de Sousa[2], Maria Helena Gil[2], Carmen Alvarez-Lorenzo[3], Ana Paula Serro[1,4] and Benilde Saramago[1]

[1.] CQE, Instituto Superior Técnico, Universidade de Lisboa, Lisboa, Portugal
[2.] CIEPQPF, Departamento de Engenharia Química, Universidade de Coimbra, Coimbra, Portugal
[3.] Departamento de Farmacología, Farmacia y Tecnología Farmacéutica, R+D Pharma Group (GI-1645), Facultad de Farmacia and Health Research Institute of Santiago de Compostela (IDIS), Universidade de Santiago de Compostela, Santiago de Compostela, Spain
[4.] CIIEM, Instituto Universitário Egas Moniz, Caparica, Portugal.

Introduction

Although eye drops remain the primary dosage form for ocular therapy due to their easiness of administration by the patient himself, they provide low drug bioavailability. **Soft contact lenses** (SCLs) have raised great interest as potential drug vehicles for ocular therapy due to their biocompatibility and prolonged contact time with the eye. Nevertheless, they usually lead to an initial burst and a fast drug release.

The main **objective** of this work was to develop LbL coated therapeutic lenses loaded with the anti-inflammatory drug diclofenac (DCF).

Methods

TRIS/NVP/HEMA 40:40:20 w/w

Polymerization: Oven 60ºC, 24 h

STEP 1. DRUG LOADING

DCF, 1 mg/mL (38 h, 4ºC) in a 3 mL volume (NaCl 130 mM)

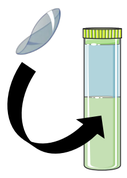

STEP 2. SURFACE MODIFICATION

- Initial layer PEI (Polyethylenimine) to bond to the hydrogel
- Cross linker Genipin (24 h, 36ºC)
- Triple layer **Alginate** (ALG) / **Chitosan** (CHI) / **Hyaluronate** (HA)

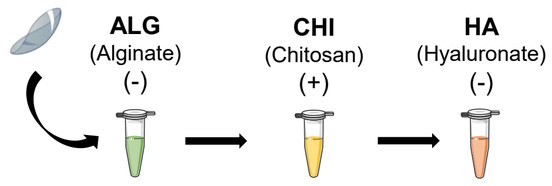

Results

I. Drug release

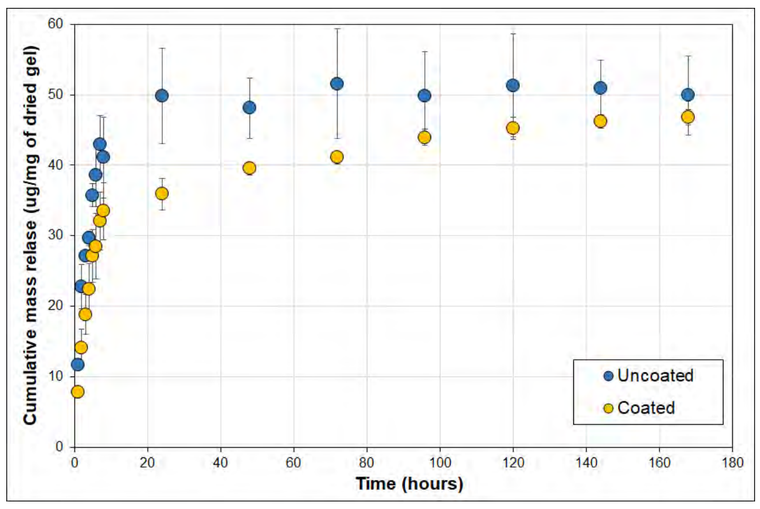

✓ The coating leads to a decrease in the initial drug burst and ensures a controlled drug release in sink conditions.

II. Optical Irritation

Hen's Egg Test – Chorioallantoic Membrane (HET-CAM) Test Method

✓ No haemorrhage, vascular lysis or coagulation was observed

III. Characterization

Property	Uncoated	Coated
Contact angle(º) (captive bubble)	35±5	32±3
Ionic Permeability (cm^2/s)	$5x10^{-7}$±$0.2x10^{-7}$	$4x10^{-7}$±$0.5x10^{-7}$
Swelling ratio (%) (DCF solution)	119±1	-
Transmittance (%) (400 – 700 nm)	99.4±0.5	95±2
Refraction index	1.417±0.002	1.356±0.004
Roughness (nm)	20±9	6±2
Layer thickness (nm)	-	~40

✓ Properties suitable for soft contact lenses

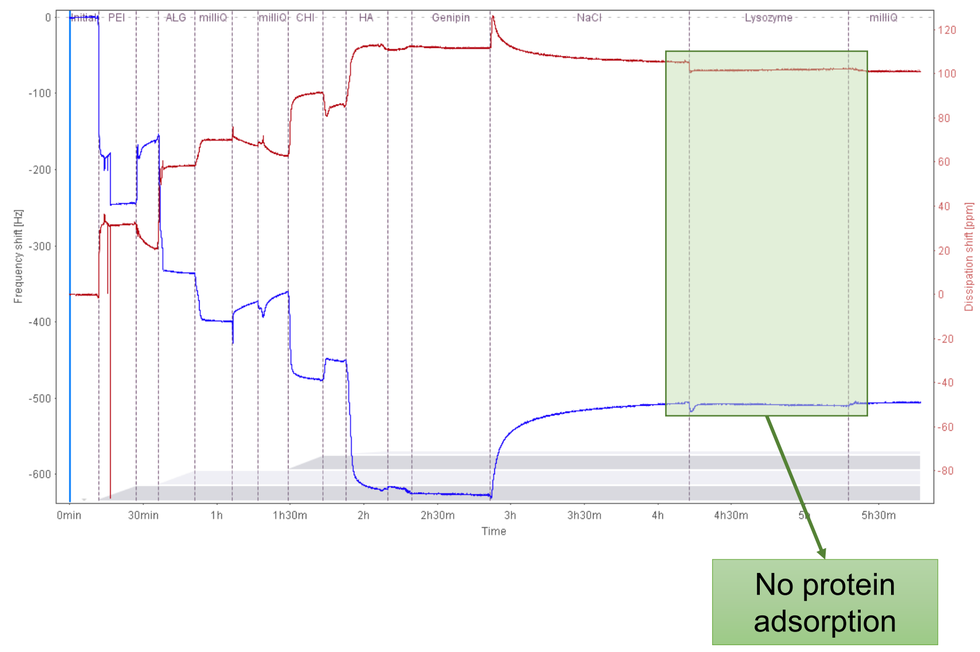

✓ The coating was stable, and did not adsorb lysozyme (tear fluid protein), showing antifouling properties.

Conclusions

- The coated hydrogel presents adequate characteristics to be used in therapeutic contact lenses.
- DCF release was significantly enhanced by the presence of the coating.
- The coated hydrogel shall not induce optical irritation.

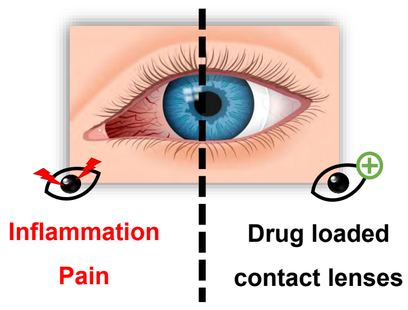

09 MET

Funding:
Centro de Química Estrutural is funded by Fundação para a Ciência e Tecnologia – project UID/QUI/00100/2019. This work was supported by Diana Silva PhD Grant (PD/BD/114088/2015) from Fundação para a Ciência e a Tecnologia (FCT) and project (STReoSTRAT) PTDC/CTM-BIO/3640/2014. This work was also partially funded by Spanish MINECO (SAF2017-83118-R), Agencial Estatal de Investigación (AEI) and FEDER.

Sustainable Iron(II) scorpionate for the synthesis of cyclic carbonates

Erivaldo J.C. Lopes, Ana Paula C. Ribeiro,
Luísa Margarida D.R.S. Martins

CQE Química Estrutural

01 Coordination Chemistry and Catalysis (CCC)

Funding:
Centro de Química Estrutural is funded by Fundação para a Ciência e Tecnologia – project UID/QUI/00100/2019

References:
Goodrich, P. Nimal Gunaratne, H. Q., Jacquemin, J., Jin, L., Lei, Y., Seddon, K.R. *ACS Sustainable Chem. Eng.*, *5* (7), (**2017**) , 5635–5641.

FCT Fundação para a Ciência e a Tecnologia

Introduction

The climate change issue is one of the main concern nowadays. Carbon dioxide have a significant contribution in this problematic, so, in order to reduce the release of carbon dioxide to the atmosphere, processes that use CO_2 as chemical feedstock, such as the one depicted in Sch. 1, have been developed.

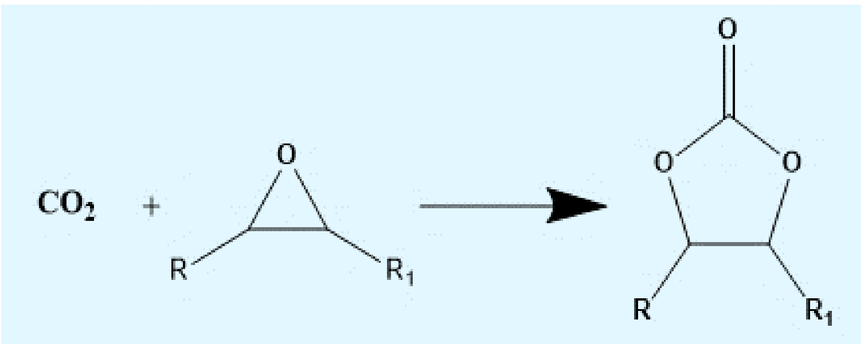

Sch. 1: Process to produce a cyclic carbonate by reacting CO_2 and epoxide.

Recently, other processes have been developed, see Sch. 2. They don't use CO_2 directly; CO_2 is required to treat the side product NH_3 to recycle the initial urea used in the process.

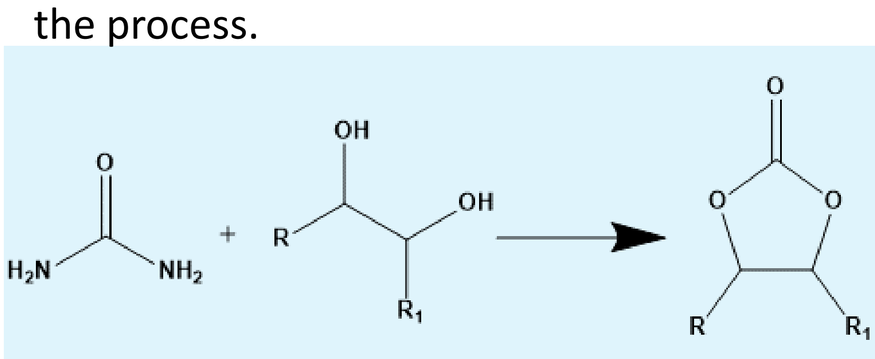

Sch. 2: Process to produce cyclic carbonate by reacting urea with 1,2-diol.

This poster presents selected results of the these processes catalyzed by the iron(II) scorpionate $[FeCl_2\{\kappa^3\text{-}HC(pz)_3\}]$ (pz = pyrazolyl) complex.

Procedure

The process uses temperatures from 80 to 150˚C during several hours.

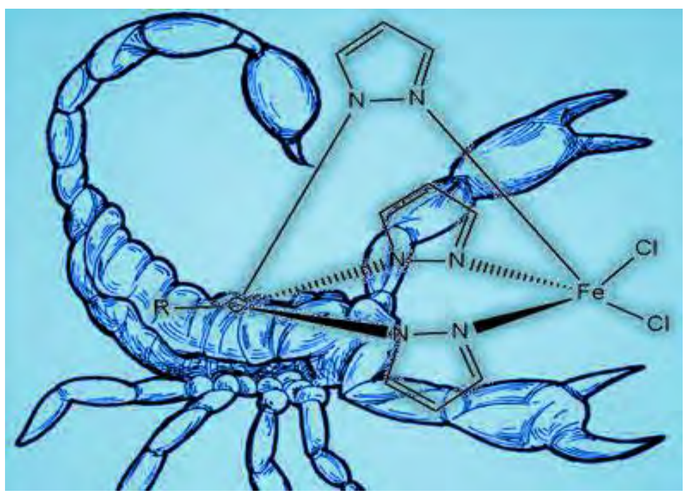

Fig. 1: The structure of iron(II) scorpionate catalyst.

Substrates tested

Table 1. Selected substrates and corresponding products for the cycloaddition of CO_2 to epoxides (Sch. 1).

Substrate	Product
	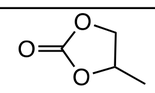
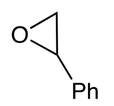	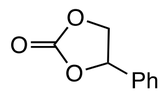
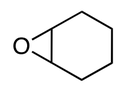	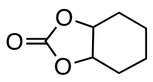

For the production of a cyclic carbonate by reacting urea with a 1,2-diol, the chosen substrate was 1,2–cyclohexanediol.

Results

Table 2. Selected data[a] for the cycloaddition of CO_2 to epoxides catalyzed by $[FeCl_2\{\kappa^3\text{-}HC(pz)_3\}]$ in THF.

Entry	Epoxide	Product	Yield /% [b]
1		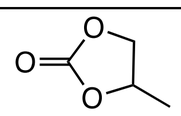	6.5
2	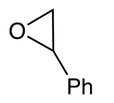	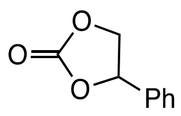	6.1
3	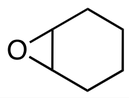	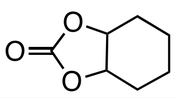	5.3

[a] Reaction conditions: epoxide (5 mmol), $[Bu_4N]Br$ (3% mol *vs.* epoxide), $[FeCl_2\{\kappa^3\text{-}HC(pz)_3\}]$ (0.5 %mol *vs.* epoxide), THF (2.5 mL), CO_2 (8 bar), 24 h, 80 ºC. [b] Yield determined by ^{1}HNMR.

Table 3. Selected data[a] for the synthesis of cyclic carbonates from organic precursors catalyzed by $[FeCl_2\{\kappa^3\text{-}HC(pz)_3\}]$ in THF.

Entry	Temperature	Time	Yield /% [b]
1	80 ºC	6 h	12.3
2	150 ºC	6 h	26.2
3	150 ºC	24 h	34.8

[a]Reaction conditions: 1,2-cyclohexane diol (5 mmol), $[FeCl_2\{\kappa^3\text{-}HC(pz)_3\}]$ (0.5 %mol *vs.* epoxide), 30mg ureia, THF (2.5 mL), 6 h, 150 ºC. [b]Yield determined by ^{1}HNMR.

Future work

- Test other substrates.
- Improve the tested procedures.
- Mechanistic studies.
- Assessment of the CO_2 utilization.

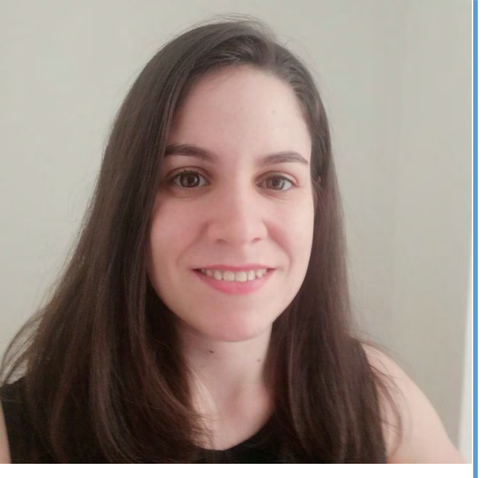

Polymorphism Study in Fumaric Acid

Filipa Bernardes, Carlos E. S. Bernardes
Centro de Química Estrutural, Faculdade de Ciências Universidade de Lisboa, 1749-016 Lisboa.

Scope

- Fumaric acid (FA, Scheme 1) is a compound widely used in the food industry, in medicine, and as starting material in several chemical processes [1].
- Almost no energetic and structural studies are available in the literature for this compound. A search at the Cambridge Crystallographic Data Centre (CCDC) reveals four communications reporting its single crystal structure of FA, published between 1925 and 1966.
- Until now, two polymorphs (i.e. materials where the packing of FA molecules is different) were identified, but a recent study [2], revealed that the X-ray powder pattern (XRPD) predicted based on the known single crystal structures does not correspond to the experimentally observed for the compound.

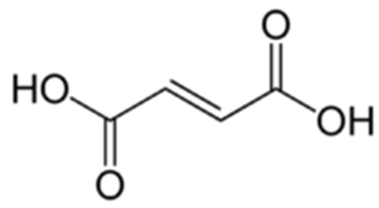

Scheme 1: Fumaric Acid (FA)

AIM

Investigate the polymorphism in fumaric acid based on recrystallization studies, and characterization of the precipitated materials by X-ray diffraction and differential scanning calorimetry (DSC).

Results

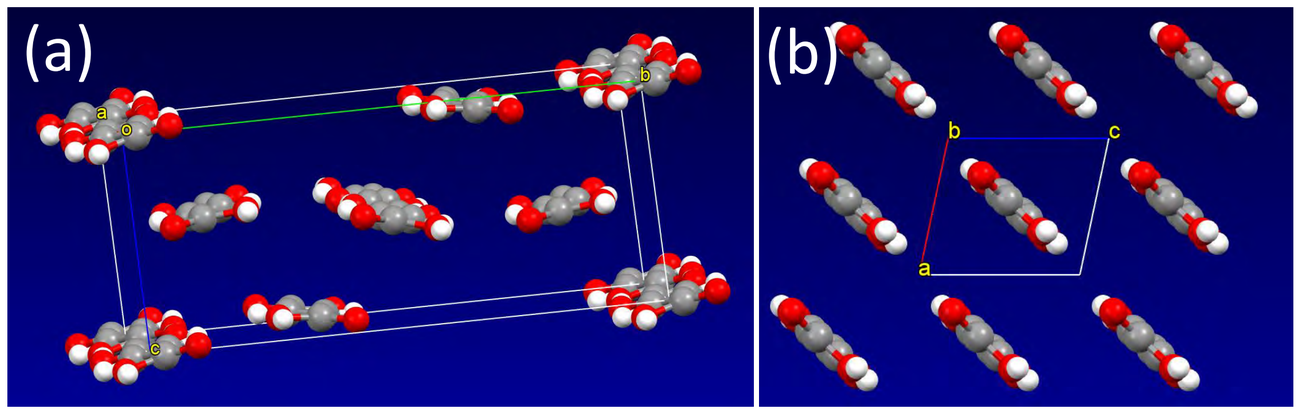

Figure 1. Single crystal structure of the two polymorphs of FA: **(a)** form α (redetermined in this work); **(b)** phase β (CCDC).

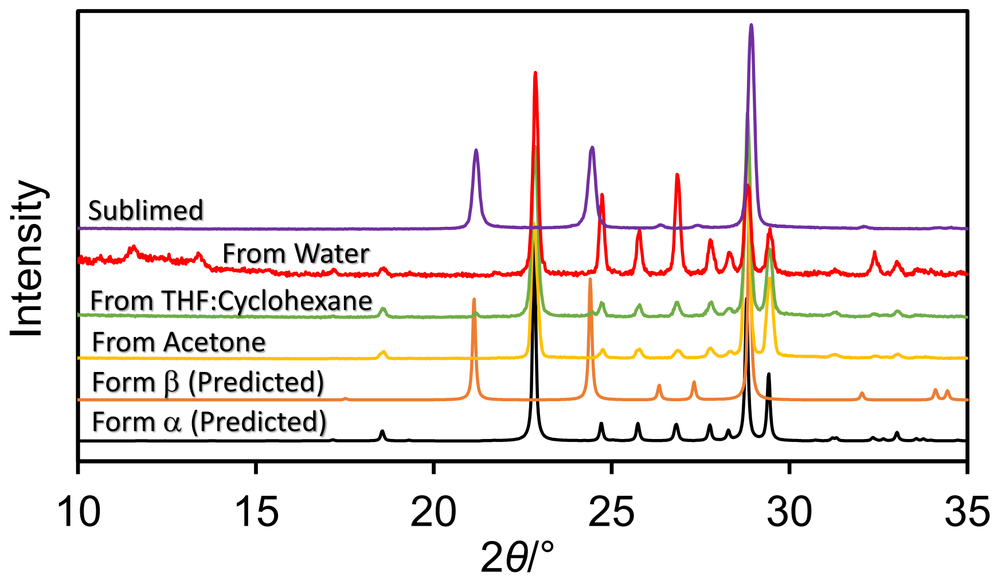

Figure 2. Comparison of the XRPD predicted for FA based on the single crystal data of form α and β, with the patterns found for the compound after recrystallization acetone, water, THF:Cyclohexane mixture, and by sublimation..

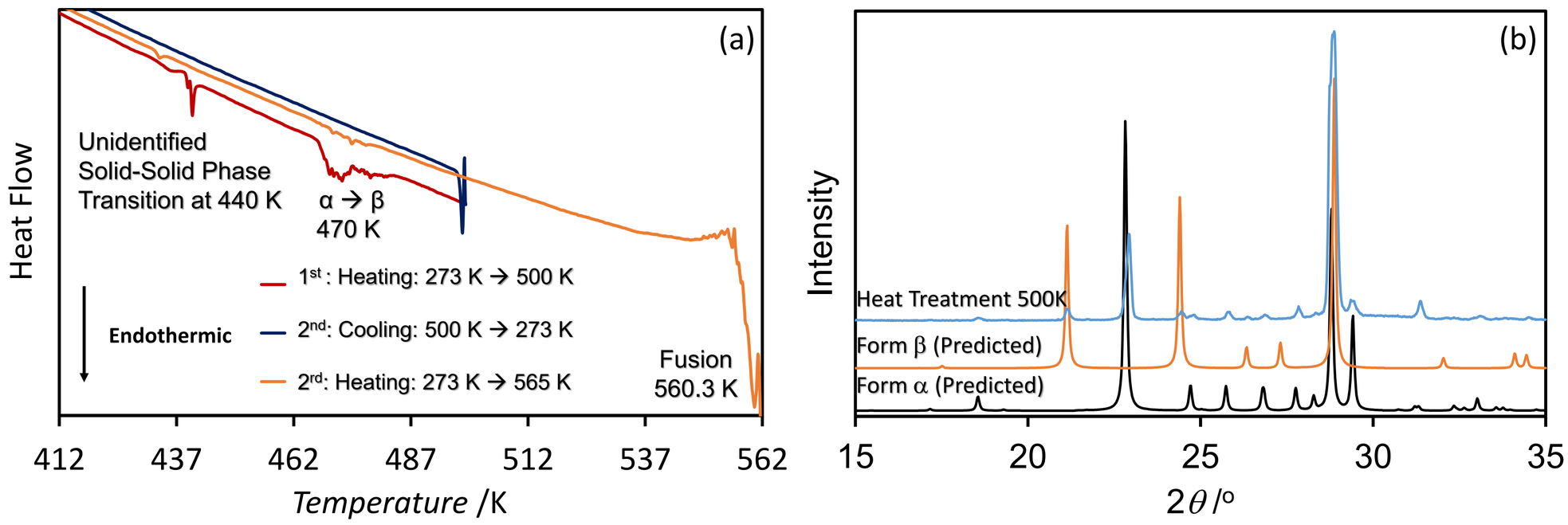

Figure 3. (a) Thermograms obtained by Differential Scanning Calorimetry (DSC), for a sample of FA form α, submitted to a sequence of heating and cooling runs. (b) Comparison between the predicted XRPD for the polymorphs of FA with that found for a sample heated to 500 K.

Conclusions

- Recrystallization of FA from acetone leads to the precipitation of form α, while a mixture of THF:Cyclohexane produces a mixture of phases α and β. A pure sample of form β was only obtained by sublimation (Figure 2).
- When water is used as a solvent, two diffraction peaks between 10 and 15 °2θ, are observed. This suggests that, besides crystals of phase α, a new polymorph was obtained (Figure 2).
- To the best of our knowledge, two previously unreported phase transitions at 440 K and 470 K, were observed in the DSC traces (Figure 3a). The thermal event at 470 K was assigned to a transition to the β phase (Figure 3b).

CQE Química Estrutural

9 MET

FCT Fundação para a Ciência e a Tecnologia

Funding:
Centro de Química Estrutural is funded by Fundação para a Ciência e Tecnologia – project UID/QUI/00100/2019.
This work was also supported by Fundação para a Ciência e a Tecnologia (FCT), Portugal through Projects PTDC/QUI-OUT/28401/2017 (LISBOA-01-0145-FEDER-028401) and UID/MULTI/00612/2013.
A Post-Doctoral grant from FCT is also gratefully acknowledged by C.B. (SFRH/BPD/101505/2014)

References:

[1] R. K. Das, S. K. Brar, M.Verma; "Chapter 8 - Fumaric Acid: Production and Application Aspects"; *Platform Chemical Biorefinery: Future Green Industry*; **2016**, 133-157.
[2] C.E.S. Bernardes, unpublished results.

Targeting Epigenetics in Cancer: Design and biological evaluation of EZH2 inhibitors

Filipa Ramilo-Gomes,[1,2] Sharon D. Bryant,[3] Riccardo Martini,[4] Thierry Langer,[4] Sheraz Gul,[5] Luís Sobral,[6] M. Matilde Marques,[1] Rita C. Guedes[2]

[1] Centro de Química Estrutural, Instituto Superior Técnico, Universidade de Lisboa, Av. Rovisco Pais, 1049-001 Lisboa, Portugal;
[2] iMed.ULisboa, Faculdade de Farmácia, Universidade de Lisboa, Av. Prof. Gama Pinto, 1649-003 Lisboa, Portugal;
[3]Inte:Ligand Software Entwicklungs und Consulting, Mariahilferstrasse 74B, 1070 Vienna, Austria;
[4]Department of Pharmaceutical Chemistry, Faculty of Life Sciences, University of Vienna, Althanstraße 14, A-1090 Vienna, Austria;
[5]Fraunhofer IME-SP, Schnackenburgallee 114, 22525 Hamburg, Germany;
[6]Hovione Farmaciência SA, Sete Casas, 2674-506, Loures, Portugal

CQE Química Estrutural

05 BIOMOL

INTRODUCTION

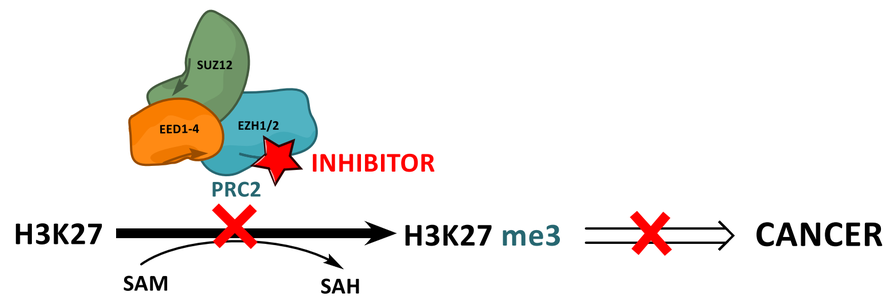

- Enhancer of Zest Homolog 2 (EZH2) is the catalytic subunit of PRC2;
- Some cancer types with poor prognosis are related to overexpression and gain of function mutations of EZH2.
- Thus, the inhibition of EZH2 appears as an opportunity for anticancer therapy.

METHODS/RESULTS

PHARMACOPHORE GENERATION → **PHARMACOPHORE VALIDATION** →

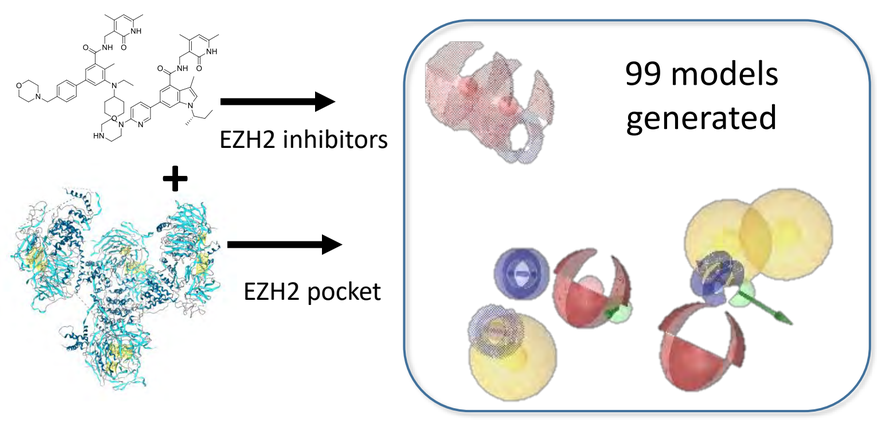

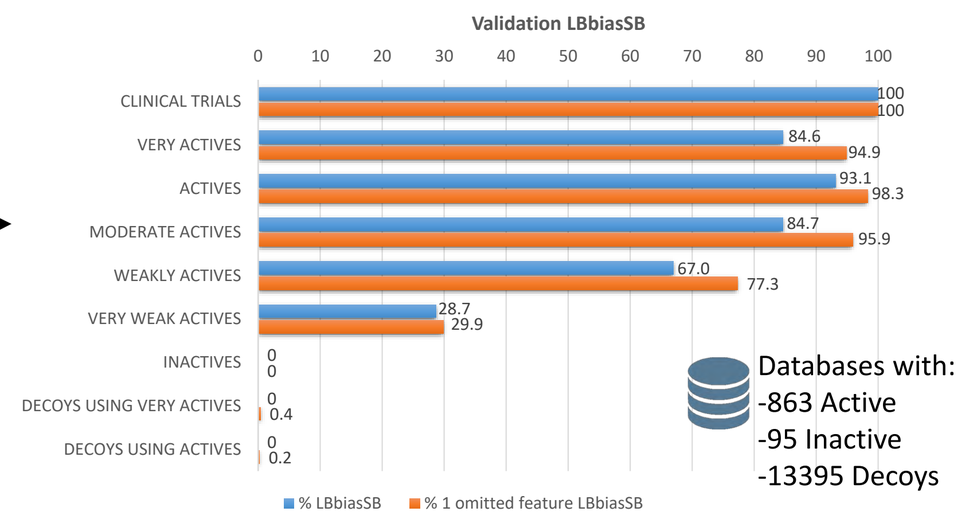

Databases with:
-863 Active
-95 Inactive
-13395 Decoys

PHARMACOPHORE USAGE

VIRTUAL SCREENING

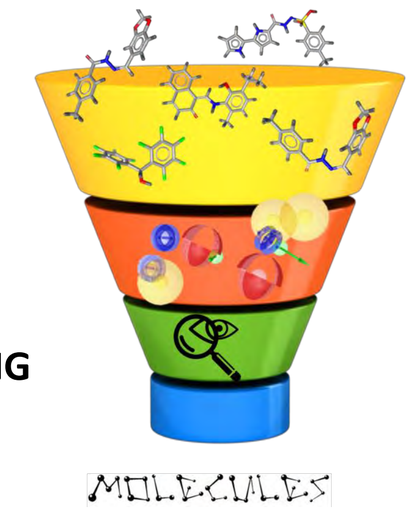

NCI;
In house;
Drugbank,
Chemotheca;
Pathogenbox

92hits of 273138

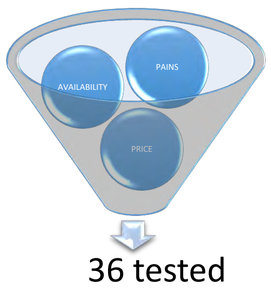

36 tested

***DE NOVO* DESIGN**

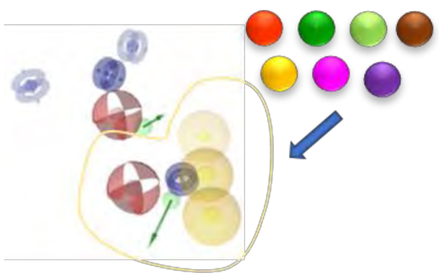

New core scaffold. For derivatization by SYNTHESIS

173hits

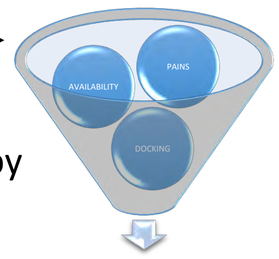

24 tested

BIOLOGICAL EVALUATION

EZH2 INHIBITION
ALPHALISA

H3K27me3 Cell imaging assay
HIGH CONTENT SCREENING
- Quantification of total H3
- Quantification of H3K27me3
- Quantification of nucleus (nº of cells)

METABOLISM
CYP450: -CYP2C9, -CYP2C19, -CYP2D6, -CYP3A4, -CYP1A2

OFF-TARGET
KINASE: -AURORA B, -PDE4C
CARDIOTOX: -hERG
EPIGENETICS: -SIRT7, -HDAC4, -HDAC6, -HDAC8, -HDAC9

TOXICITY
- MCF7
- hTERT
- OCI-LY 19
- Hep G2
- U-2 OS
- HEK 293

CONCLUSIONS

- Promising **EZH2 inhibitors** with **clean and safe** off-target and **ADME-Tox profiles** were found;
- **Pharmacophore models** were shown to be helpful in **finding new small molecule inhibitors** of this target;
- Additionally, computational methods proved to be important in **designing new scaffolds** of EZH2 inhibitors.

Funding:
Centro de Química Estrutural is funded by Fundação para a Ciência e Tecnologia – project UID/QUI/00100/2019. This work was supported by PD/BD/128320/2017 and also projects UID/DTP/04138/2013, PTDC/QUI-QAN/32242/2017, and SAICTPAC/0019/2015. This communication is based upon work from COST Action CA15135, supported by COST.

FCT Fundação para a Ciência e a Tecnologia

Comet, I., Rising, E. M., Leblanc, B.; Helin, K. Nature Rev Cancer 2016, 16, 803.

Kim, K. H. & Roberts, C. W. M. Targeting EZH2 in cancer. Nat Med. 2016, 22, 128–134

LigandScout Molecular Design Software from InteLigand GmbH (http://www.inteligand.com).

Evaluation of the vapor pressure of deep eutectic solvents for desulfurization applications

Filipa Lima[1,2,3], Armando Silvestre[2], Luís Branco[3], Isabel Marrucho[1]

[1]IST, Universidade de Lisboa; [2]CICECO-Universidade de Aveiro; [3]Solchemar Lda

CQE Química Estrutural

09 MET

FRAMEWORK

In recent years, Deep Eutectic Solvents (DES) have attracted a lot of attention due to their potential in green chemistry combined with their easy and simple preparation. In addition, the wide range of available compounds for their preparation has boosted the application of DES in various fields.

Removal of sulfur and nitrogen compounds from fossil fuels is one of those applications, since emissions of SOx and NOx represent one of the main current concerns related to air pollution. Over the last years, DES have been intensively explored as alternative solvents to remove those sulfur- and nitrogen-containing compounds from fuels [1,2].

Regarding separation technology, there is an important feature that stands out, which is the vapor pressure of the extractant (in this case – DES), and should be as low as possible. During the last years, DES have been largely compared to ionic liquids, which are known for their negligible vapor pressure. However, in the case of DES, depending on its constitution, it is to be expected that this is not always the case.

In this work, the vapor pressure of several DES was accessed through head-space gas chromatography mass spectrometry (HS-GC-MS).

OUR GOLD…

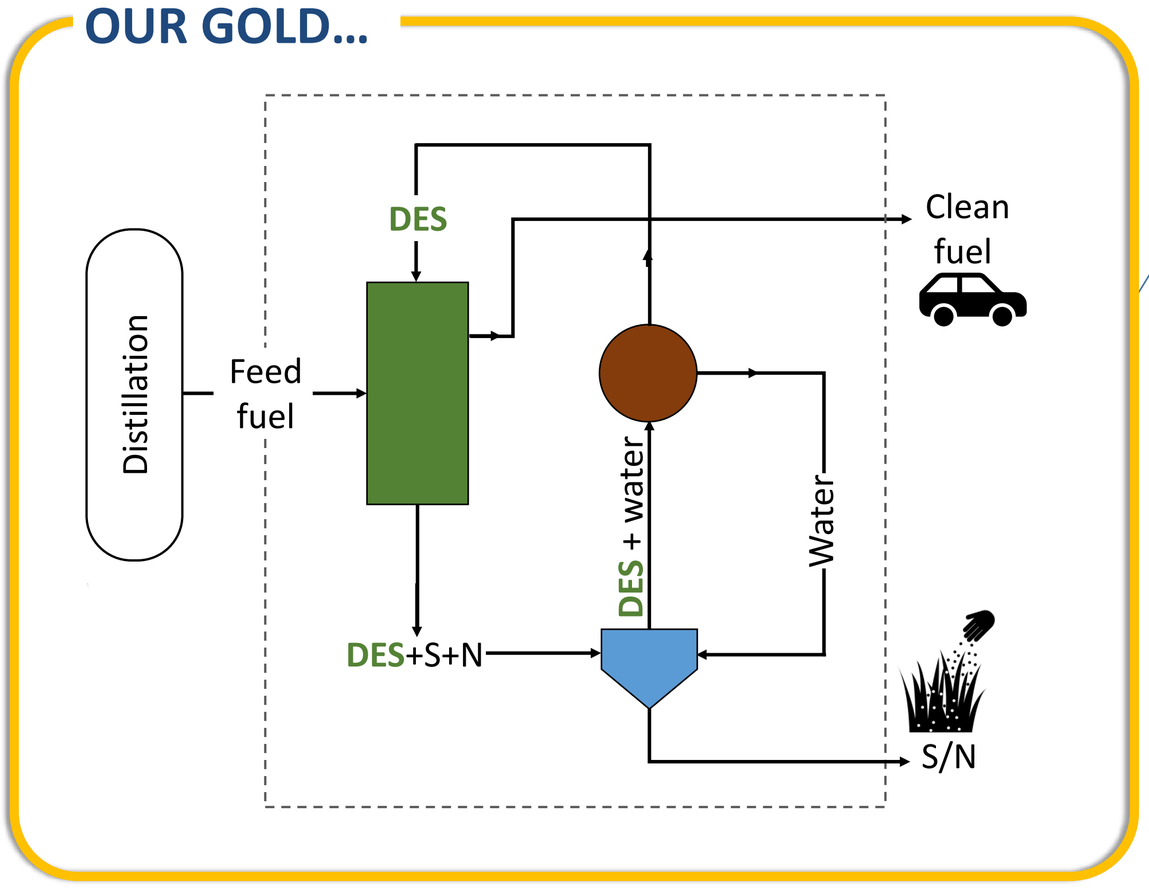

…we did it!

But…

What is, in fact, the volatility of our DES?

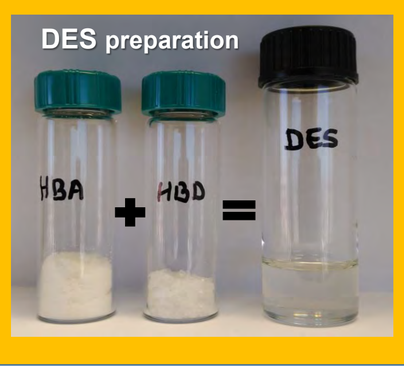

DES VAPOR PRESSURE

1) Vapor pressures of pure compounds *VERSUS* Partial pressure of the DES constituents:

- The partial vapor pressure of each DES constituent is lower than the vapor pressure of each pure compound;
- Our DES is less volatile than sulfolane.

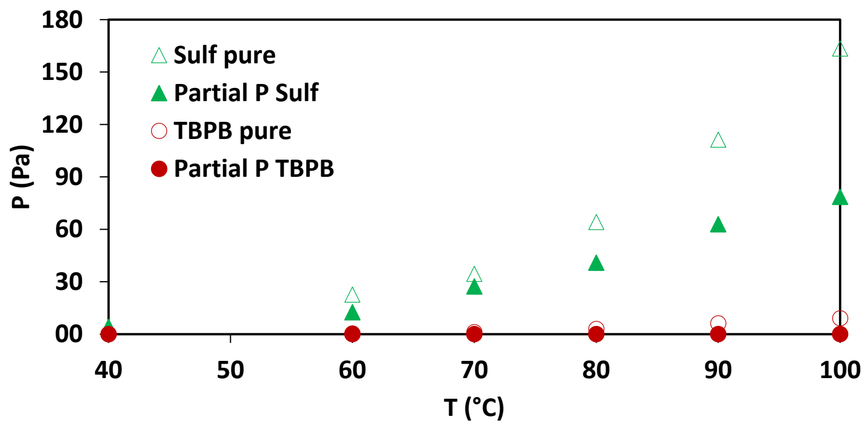

Figure 1: Vapor pressures of pure tetrabutylphosphonium bromide (TBPB) and pure sulfolane (Sulf) and partial vapor pressures of TBPB and Sulf in the DES TBPB:Sulf (1:4), determined by HS-GC-MS, between 40 °C and 100 °C.

2) Ideal mixture behavior? No!

- The calculated vapor pressures using the Roult's law ($P_i = x_i P_i^{vap}$) are over predicted for both DES constituents, indicating that TBPB:Sulf (1:4) DES is a non-ideal mixture;
- As the measured vapor pressures are lower than the ideal pressures, the activity coefficients will be lower than 1, which means that the interactions between HBA-HBD are more attractive than the interactions between HBA-HBA or HBD-HBD.

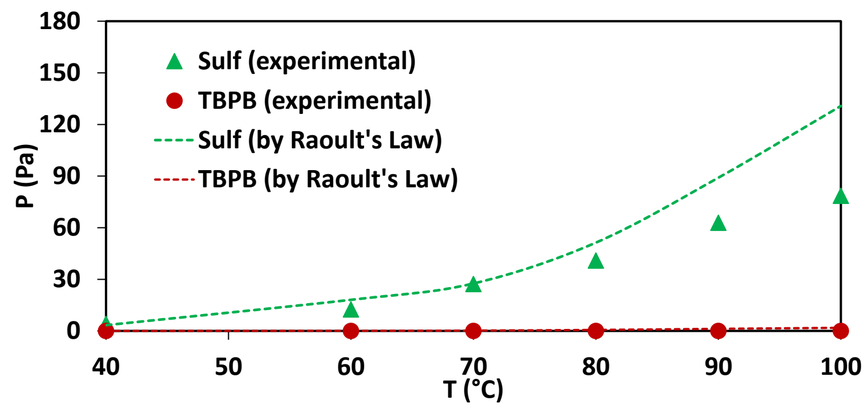

Figure 2: Partial vapor pressures of the DES TBPB:Sulf (1:4) constituents. Experimental data determined by HS-GC-MS (symbols); calculated vapor pressure using Raoult's law for ideal mixture behavior (lines).

3) Total vapor pressure of TBPB:Sulf at different molar ratios, at 60 °C:

- The increase in the amount of TBPB present in the DES leads to the decrease of the total vapor pressure of the DES, as expected;
- Interestingly, this effect was very noticeable in a specific mole fraction of TBPB (0.1). This is coincident with the eutectic point of our DES.

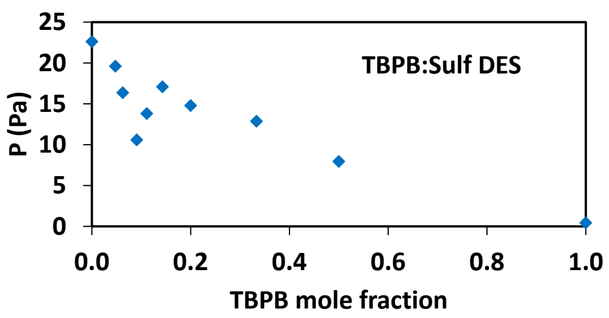

Figure 3: Total vapor pressure of TBPB:Sulf at different molar ratios.

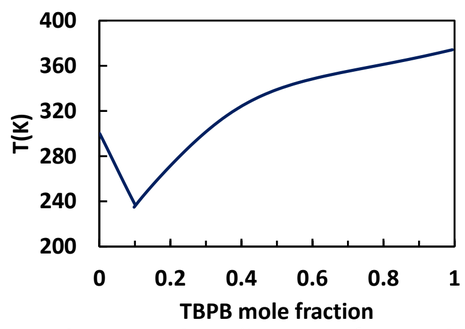

Figure 4: SLE diagram of TBPB:Sulf predicted by PC-SAFT.

FINAL REMARKS

- The total vapor pressure of TBPB:Sulf DES is lower than the vapor pressure or pure sulfolane;
- The TBPB:Sulf (1:4) DES is not an ideal mixture;
- The interactions between HBA-HBD in the DES are more attractive than the HBA-HBA and HBD-HBD interactions.

Funding:

Filipa Lima is grateful for the financial support of FCT for the PhD grant PD/BDE/114355/2016. This work was supported by CQE project (UID/QUI/00100/2019), the Associate Laboratory CICECO, Aveiro Institute of materials (UID/CTM/50011/2013), the Associated Laboratory for Green Chemistry, LAQV-REQUIMTE (UID/QUI/50006/2013) and Solchemar company.

FCT Fundação para a Ciência e a Tecnologia

References:

[1] F. Lima, J. Gouvenaux, L.C. Branco, A.J.D. Silvestre, I.M. Marrucho, , Fuel. 234 (2018) 414–421.

[2] M.C. Ali, Q. Yang, A.A. Fine, W. Jin, Z. Zhang, H. Xing, Q. Ren, Green Chem. 18 (2016) 157–164.

A Challenge, a Team, a Project: TARGTUB

Filomena Martins,[1,2] Susana Santos, [1,2] Marina Reis,[1-3] Catarina Faria,[1,2] Rodrigo Almeida,[1,2] Joaquim Marquês,[1,2] Diogo Vila-Viçosa,[1,4] Bruno Victor, [1,4] Pedro Lopes, [1,4] Ruben Leitão[1,2,5], Maria Soledade Santos[1,2], Diogo Latino,[1,2] Miguel Viveiros,[6] Jorge Ramos,[6] Diana Machado,[6] Miguel Machuqueiro[1,4]

[1]Centro de Química e Bioquímica, Faculdade de Ciências, Universidade de Lisboa, Ed. C8, Campo Grande 1749-016 Lisboa, Portugal.
[2]Centro de Química Estrutural, Faculdade de Ciências, Universidade de Lisboa, Edif. C8, Campo Grande 1749-016 Lisboa, Portugal.
[3] Instituto Superior de Educação e Ciências, Alameda Linhas de Torres 179 1750-142 Lisboa, Portugal.
[4]BIOISI, Faculdade de Ciências da Universidade de Lisboa, Campo Grande, 1749-016 Lisboa, Portugal
[5]ADEQ, ISEL-IPL, Rua Conselheiro Emídio Navarro, 1959-007 Lisboa, Portugal.
[6]Unidade de Microbiologia Médica, Instituto de Higiene e Medicina Tropical, Universidade Nova de Lisboa, 1349-008 Lisboa, Portugal

Tuberculosis (TB) is still one of the top 10 causes of death worldwide and the main cause of mortality from a single infectious agent, the *Mycobacterium tuberculosis* (*Mtb*) bacillus.[1] Treatment misuse has led to the upsurge of multidrug-resistant tuberculosis (MDR-TB), taken as resistance to at least isoniazid (INH) and rifampicin (RIF), first-line antituberculars, and to extensively drug-resistant TB (XDR-TB), a form of TB that answers to even fewer drugs.

Alarming numbers (2017)

- 10.0 million new cases
- 1.3 million deaths
- ~ 2 billion people infected with latent TB
- 4.1 % of new cases are RIF-resistant or multidrug resistant (MDR)
- From these 6.2% are XDR
- XDR-TB confirmed in 121 countries

Fact

Isoniazid (first synthesized in 1952) is one of the two most effective drugs to treat TB and is part of **all** WHO multidrug recommended regimens

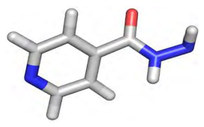

Problem

- *Mtb* has become increasingly resistant to INH and attempts to develop INH-based compounds to by-pass the problem and improve drug activity have **failed**
- So far, only 2 new drugs have received conditional approval for treatment of MDR-TB

Challenge

Is it possible to develop new , QSAR-oriented INH derivatives, rationally modified to upturn INH activity and, simultaneously, circumvent MDR-TB?

TARGTUB

Team

Multidisciplinary, with a wide range of backgrounds spanning from machine learning techniques molecular modeling and simulation, to organic synthesis, interfacial chemistry, biophysics and microbiology

Results from previous projects[2,3]

- Synthesis of 5 new compounds more active than INH against H37Rv *Mtb*
- From these, 3 are more effective than INH against the most frequent mutation conferring INH resistance, *katG* S315T
- Top compound is an INH derivative with a C_{10} alkyl chain (INH-C_{10})

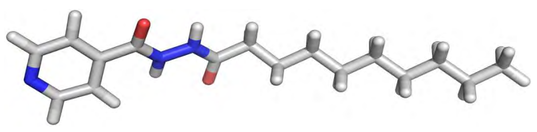

- Kinetic and computational studies of INH and INH-C_{10} indicate that the observed values of minimum inhibitory concentrations in various *Mtb* resistant strains result from the interplay of high membrane permeability and high reactivity (**Fig. 1**)

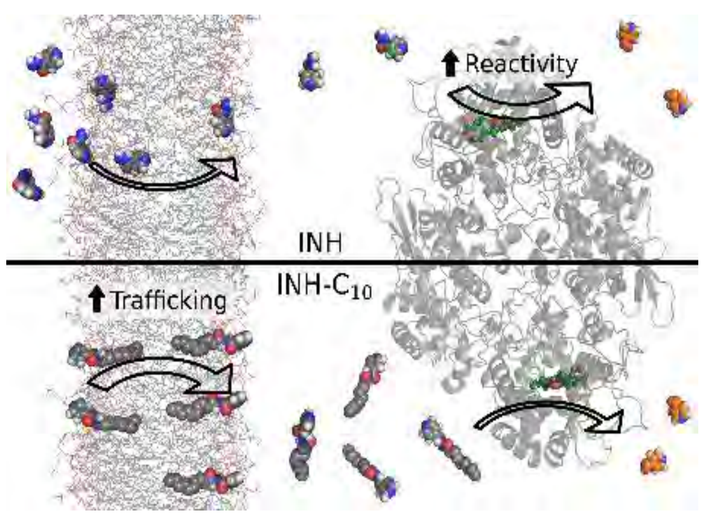

Figure 1: Overall scheme illustrating INH and INH-C_{10} trafficking (in a POPC membrane) and reactivity (in KatG).

Goals

To develop a new drug lead against MDR-TB, through in silico design of compounds, structurally similar to those that scored higher against S315T *Mtb*, followed by synthesis, and *in vitro* studies to assess their potential as anti-TB drug candidates

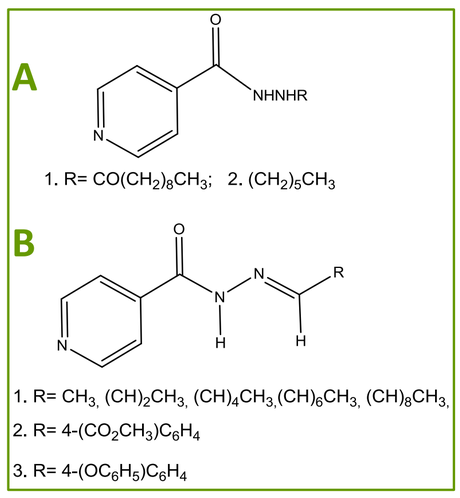

So far

- **Quantum mechanics** calculations to assess the ability of INH derivatives to spontaneously **form the IN• radical** (formed in the first step of INH activation in KatG), have been carried out and suggest that compounds INH-**A2** and INH-**B** facilitate the formation of the radical by comparison with INH
- **MD simulations of permeability rates** of compounds INH-**A1** (≡ INH-C_{10}) & INH-**A2**, as well as of higher order INH-**B1**, lead to permeability rates significantly higher than that of INH
- Compounds INH-**A** and INH-**B** have been **synthesized** (new ones fully characterized). **Biophysical studies** and **biological evaluation** of some of these derivatives will follow soon

CQE Química Estrutural

09 MET

Funding:
Centro de Química e Bioquímica is funded by Fundação para a Ciência e Tecnologia – project UID/QUI/00612/2019.
This work is funded by Fundação para a Ciência e Tecnologia – project PTDC/MED-QUI/29036/2017

FCT Fundação para a Ciência e a Tecnologia

References:

1. "Global tuberculosis report 2018". World Health Organization. Accessed May 2, 2019.
2. Martins, F., Santos, S., Ventura, C., *et al*. *Eur. J. Med. Chem*. 81 (2014), 119–138.
3. Vila-Viçosa, D., Victor, B., Ramos, J., *et al.*, *Mol. Pharmaceutics* 14 (2017) 4597–4605

Dye sensitized solar cells based on porphyrins

Gabriel F. Gika,[1,2] Francisco M. Ferraz,[1,2] Joana M. D. Calmeiro,[1,3] Leandro M. O. Lourenço,[3] Cláudia C. L. Pereira,[2] João P. C. Tomé[1]

[1] Centro de Química Estrutural (CQE), Departamento de Engenharia Química, Instituto Superior Técnico, Universidade de Lisboa, 1049-001 Lisboa, Portugal.
[2] LAQV-REQUIMTE, Departamento de Química, Faculdade de Ciências e Tecnologia, Universidade NOVA de Lisboa, 2829-516 Caparica, Portugal.
[3] QOPNA & LAQV-REQUIMTE, Department of Chemistry, University of Aveiro, 3810-193 Aveiro, Portugal.

gabriel.gika@tecnico.ulisboa.pt

Abstract: Dye sensitized solar cells (DSSC, Figure 1) have been representing a new promising method for the conversion of visible light, in a wide range of light in indoor and outdoor conditions, enabling the conversion of both artificial and natural lights into electrical energy to powered a broad range of electric devices.[1] This technology demands two main requirements: a) efficient charge generation at the semiconductor-dye interface; and b) efficient charge transport by the semiconductor and the electrolyte reduction ability.[2]

The selected semiconductor for the photoelectrode is mostly being titanium dioxide (TiO_2) due to its availability, low cost and non-toxic properties. In terms of dyes, there is the possibility of modifying its optical properties and consequently their corresponding DSSC's conversions/efficiencies. This can be done by simple dye structural modifications. At the same time, carriers transport properties can be improved by optimizing the semiconductor and the electrolyte composition.[3]

In the present work we are using free-base and metal coordinated porphyrins due to their unique optical properties and large possibility of structural modifications. These compounds are macrocycles with a highly conjugated aromatic system, which allow strong absorptions. They have been applied in natural and synthetic structures, being studied in different fields, such as: medicine, sensing and electron transfer applications.[4,5] The last application has drawn their use in light-harvesting devices.[6,7]

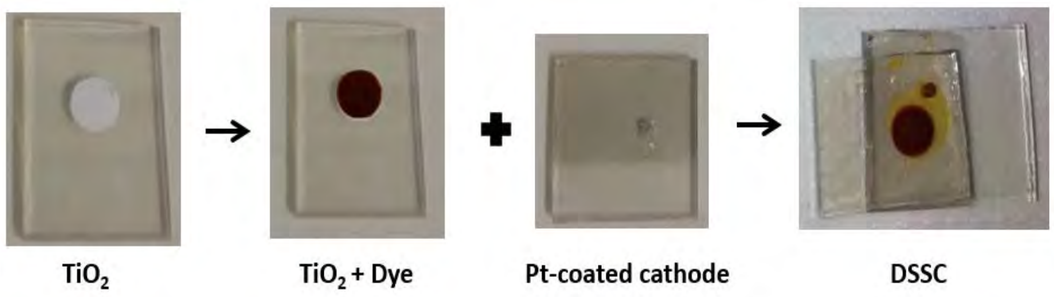

Figure 1 – Schematic representation of DSSC prototype preparation.

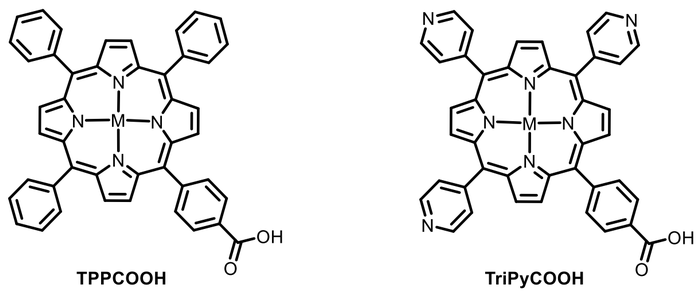

Figure 2 – Free base and metal-porphyrins used as dyes in our solar cells.

Results and Discussion

Evaluation of the photosensitizer properties of TPPCOOH and TriPyCOOH

Table 1 – Measurements of the efficiency of dye synthetized solar cells after the deposition of the dye in methanol.

	Voc[a)] (V)	η (%)	Jsc[b)] (mA/cm^2)	FF[c)]
N719	0,55	3,94	10,68	65,58
H_2TPPCOOH	0,22	0,1	0,9	52,82
NiTPPCOOH	0,23	0,035	0,32	45,91
H_2TriPyCOOH	0,22	0,044	0,42	45,09
ZnTriPyCOOH	0,4	1,75	7,33	57,8

a) Voc – open circuit voltage factor b) JSC – short circuit current c) FF – Filling

Depending on the type of dye used, the overall efficiency of the DSSCs may vary:

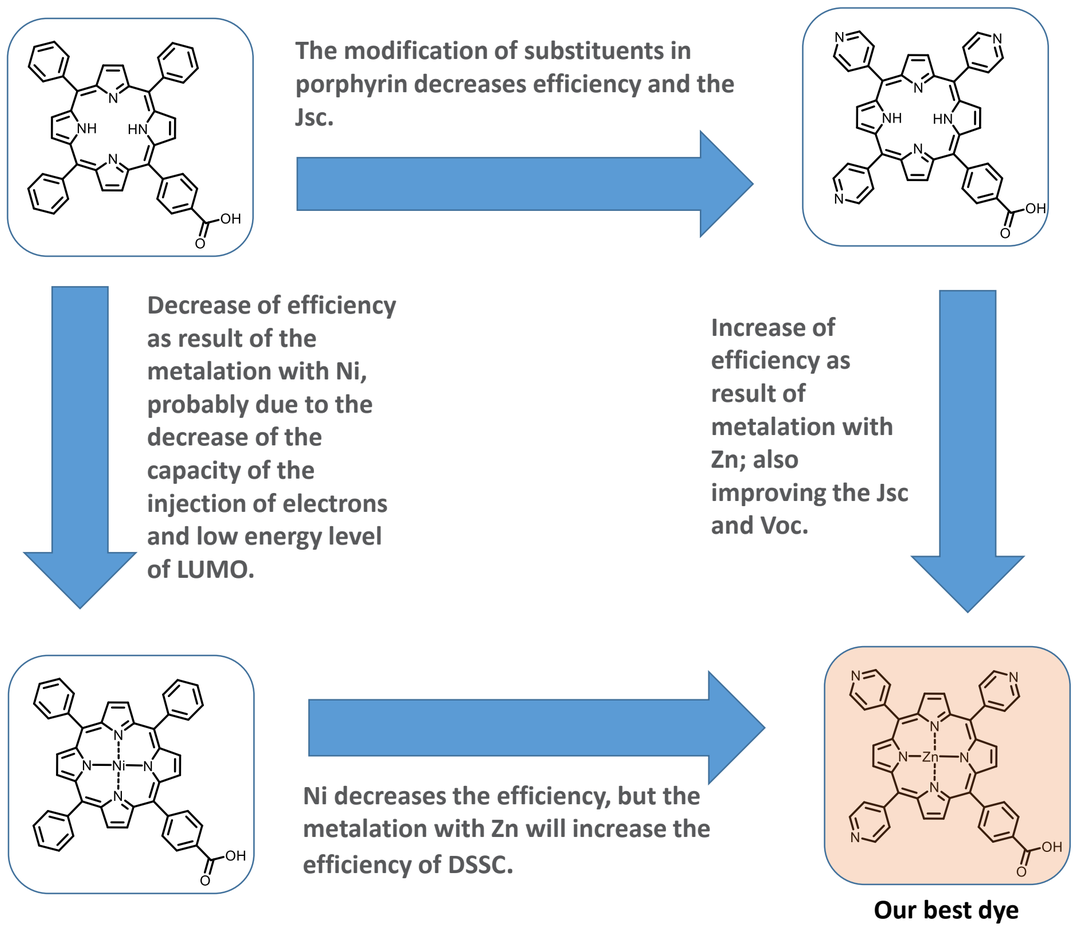

Behavior of DSSC after light soaking

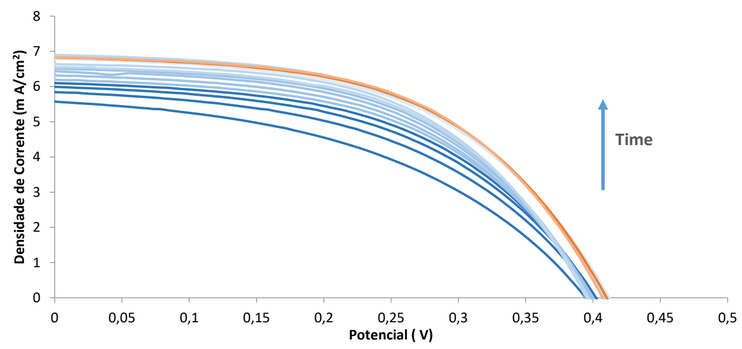

Figure 3 – I-V curve of ZnTriPyCOOH with time intervals of 15 seconds for blue lines and orange lines after 15 minutes.

As the DSSC was exposed to light, it was possible to observe the increase in the different parameters, as well as in the efficiency of the cell. When it was decided to stop exposure of the DSSC to light after 10 measurements, to see the impact of the dark on the cells under such conditions, no change was observed in the parameters of the first measurement. However, in the following, an increase in the parameter measured in the DSSC was noticed. This behaviour is also observed in some examples of the literature, but the true reason for such behaviour is not yet known.

Conclusions

- It was possible to see that the different structure of porphyrins influences the results of the DSSC. Exposure of DSSC to light appears to have a catalytic effect on ZnTriPyCOOH.
- The insertion of Zn in the porphyrin's nucleus influences the results obtained in a positive way. But, on the other hand, Ni negatively influences cell results when compared to free base porphyrin.
- In certain cases, even when the light has been turned off, the cell behaves in the same way as under light exposure. For this reason, and due to technical limitations, it would be interesting to develop further work on the characterization of these DSSC to better understand the results obtained.

01 CCC

Funding:
This work was supported by FCT/MEC financing CQE (FCT UID/QUI/0100/2019), Green Chemistry LAQV (FCT UID/QUI/50006/2019), QOPNA (FCT UID/QUI/00062/2019) research units, and to the projects P2020-PTDC/QEQ-SUP/5355/2014 and P2020-PTDC/QUI-QOR/31770/2017, through national founds (PIDDAC) and where applicable co-financed by the FEDER-Operational Thematic Program for Competitiveness and Internationalization-COMPETE 2020, within the PT2020 Partnership Agreement. J. Calmeiro was been granted (BI/UI51/7965/2017) by UAveiro.

References:

1. Grätzel, M., J. Photochem. Photobiol. C 4 (2003) 145–153.
2. Sharma, K., Sharma, V., Sharma, S. S., Nanoscale Res. Lett. 13 (2018) 381.
3. Nazeerudin, Md. K., Baranoff, E., Grätzel, M., Sol. Energy 85 (2011) 1172–1178.
4. Lourenço, L. M. O., Hausmann, A., Schubert, C., Neves, M. G. P. M. S., Cavaleiro, J. A. S., Torres, T., Guldi, D. M., Tomé, J. P. C., ChemPlusChem 80 (2015) 832–838.
5. Lourenço, L. M. O., Sousa, A., Gomes, M. C., Faustino, M. A. F., Almeida, A., Silva, A. M. S., Neves, M. G. P. M. S., Cavaleiro, J. A. S., Cunha, Â., Tomé, J. P. C., Photochem. Photobiol. Sci. 14 (2015) 1853–1863.
6. Li, L., Diau, E. W., Chem. Soc. Rev. 42 (2013) 291-304.
7. Higashino, T., Imahori, H., Dalton Trans. 44 (2015) 448-463.

Studying the PEG family

M.C.M. Sequeira[1], H. M. N. T. Avelino[1,2], F.J. P. Caetano[1,3], J. M. N. A. Fareleira[1]

[1] *Centro de Química Estrutural, Instituto Superior Técnico, Universidade de Lisboa, Portugal*
[2] *Instituto Superior de Engenharia de Lisboa, IPL, Portugal*
[3] *Departamento de Ciências e Tecnologia, Universidade Aberta, Lisboa, Portugal*

GOAL

Realisation of experimental measurements of thermophysical properties of a homologous series of ethylene (DiEG,TriEG,TeEG) and polyethylene glycols (PEG 600,PEG 400 and PEG 200) and the development of correlation methods.

Influence of molecular mass in density at constant pressure

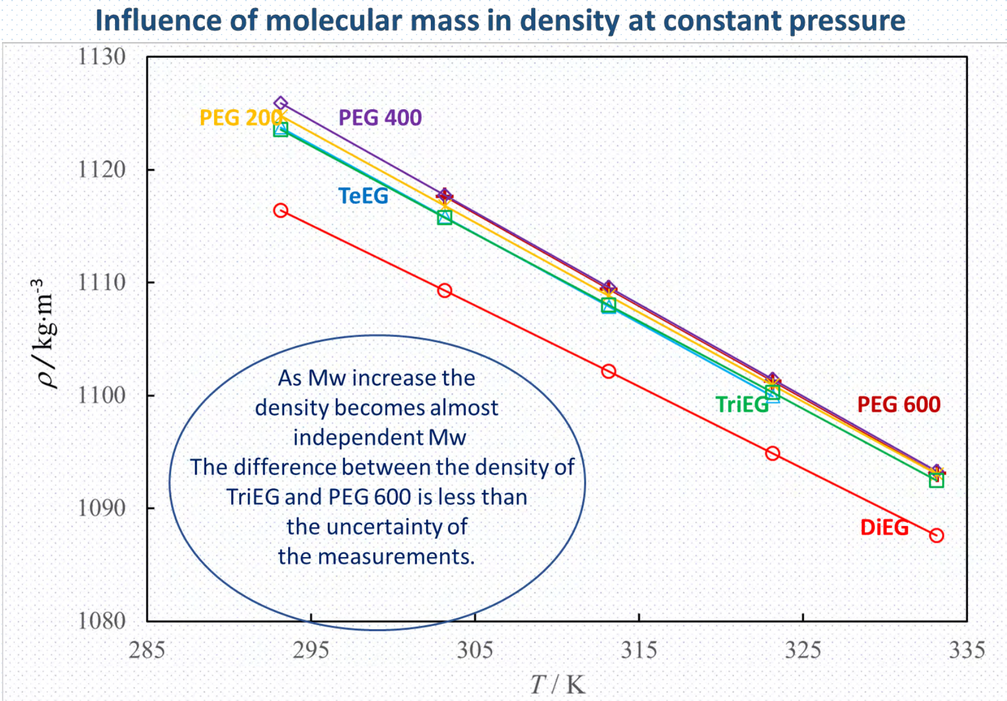

Influence of molecular mass in viscosity at constant pressure

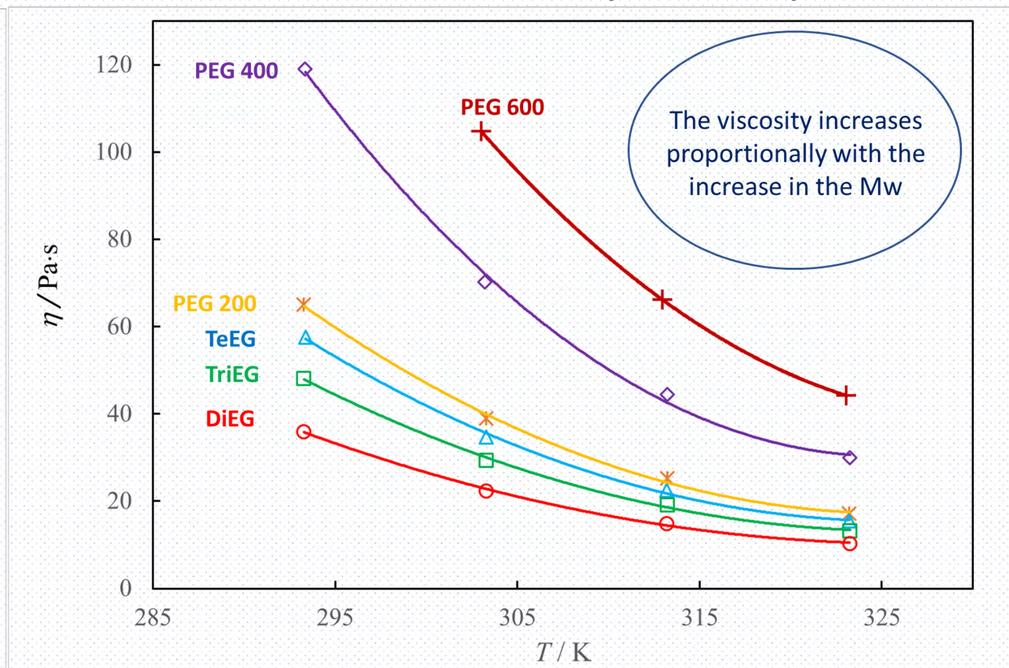

Influence of molecular mass in viscosity when the pressure increases at constant temperature

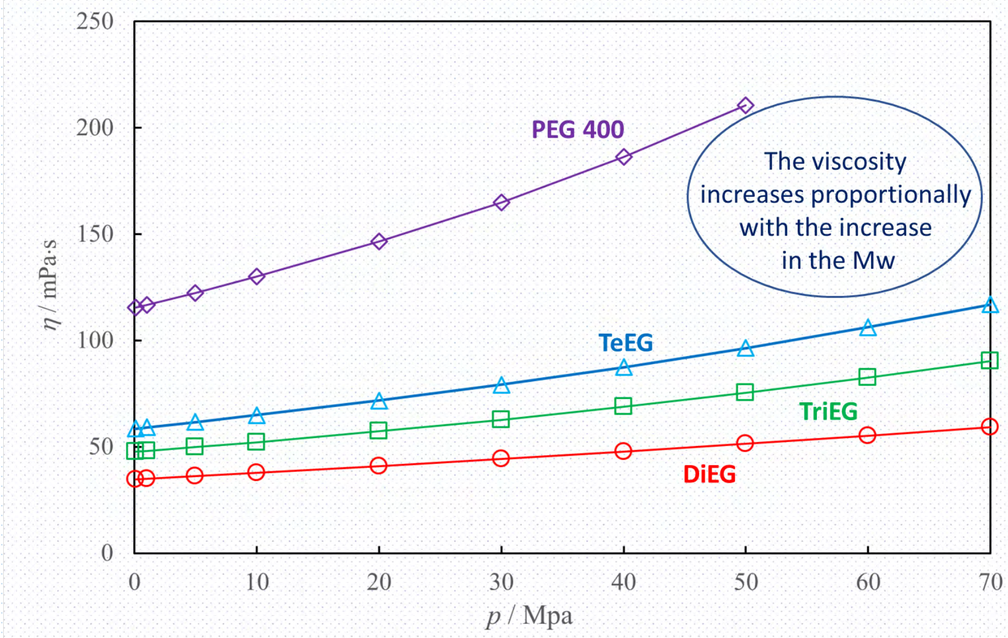

Viscosity of PEG 400 at high pressures Panoramic View

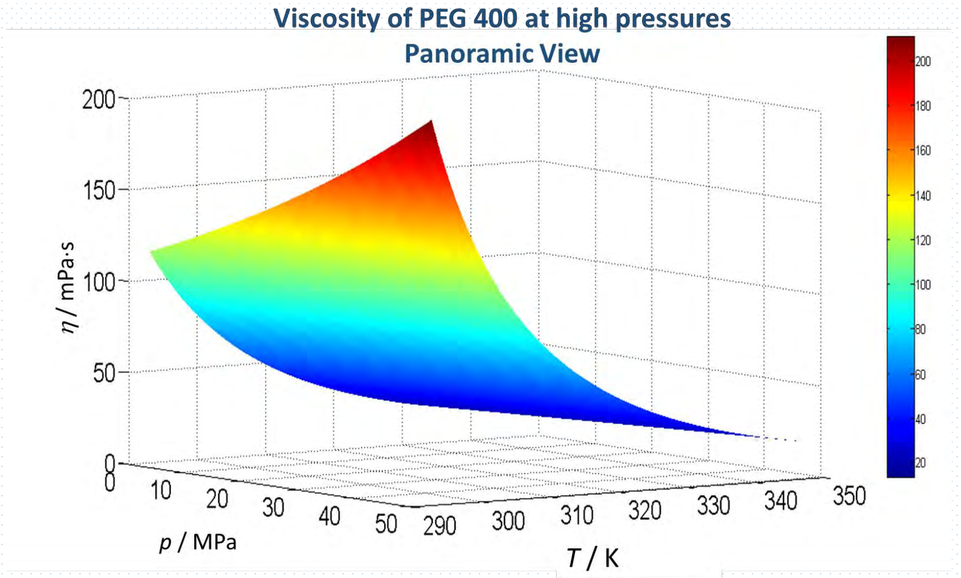

Hard-Spheres Correlation of series of ethylene (DiEG,TriEG,TeEG) and polyethylene glycol (PEG 400)

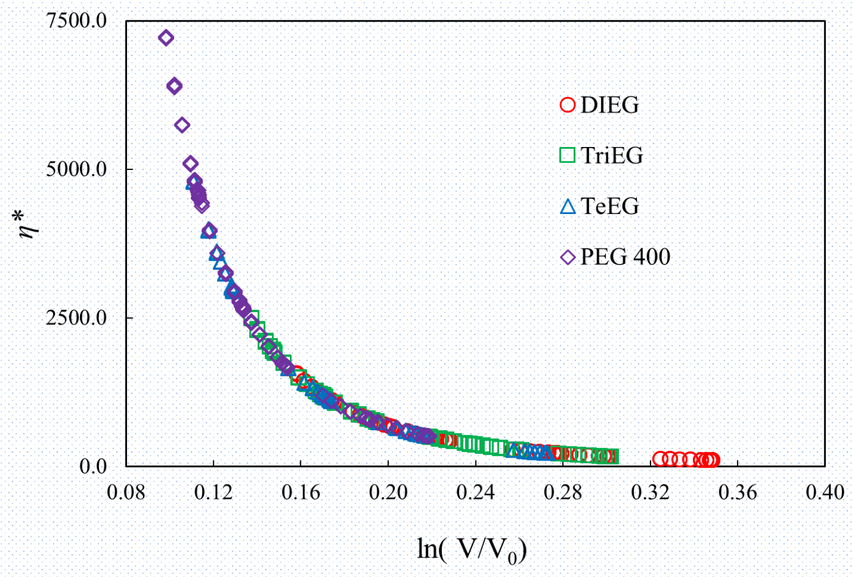

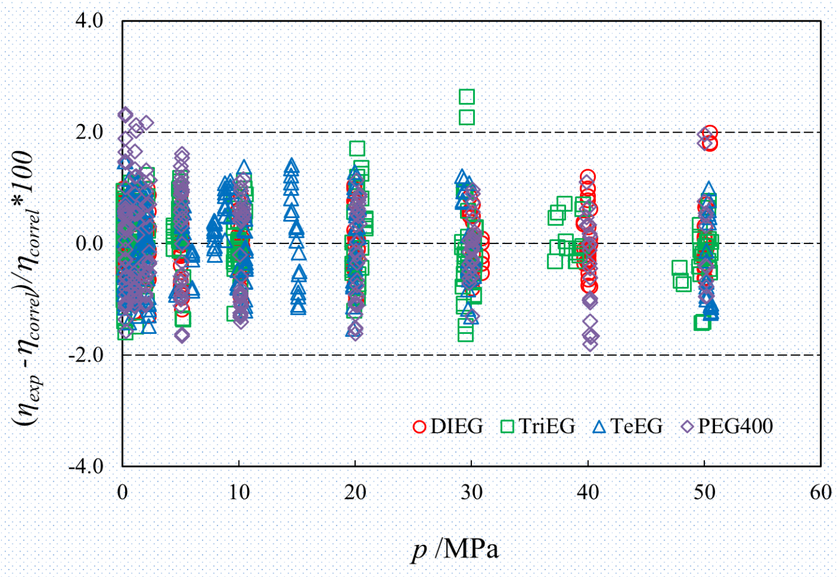

One the curve, one equation, allow interpolating the viscosity of any ethylene or PEG 400 in the pressure and temperature with accuracy about 2%.

Newtonian Behaviour of PEGs

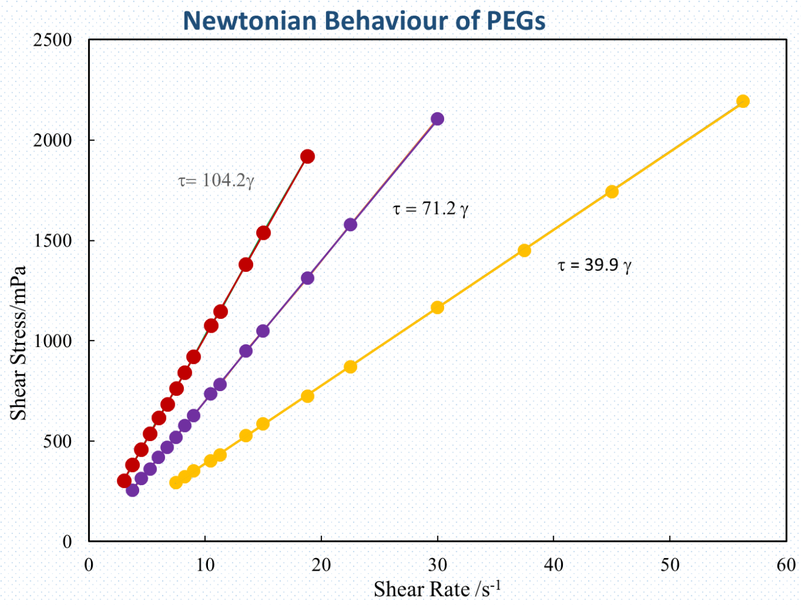

Work in progress:

- Viscosity and density measurements of PEG 200 at high pressure
- Self-diffusivity measurements of DiEG, TriEG and TeEG.
- Introduction of self-diffusion data in hard-spheres viscosity correlation.
- Analyse the relation of the present results with those obtained before for CO_2 saturated PEG mixtures. Aim: to predict the viscosity of the mixtures.
- Determination of the pressure-viscosity and temperature-viscosity coefficients - important to characterize lubricants.

CQE Química Estrutural

09 MET

Funding:
Centro de Química Estrutural is funded by Fundação para a Ciência e Tecnologia – project UID/QUI/00100/2019.

FCT Fundação para a Ciência e a Tecnologia

References:

[1] T. Welton, Proc. R. Soc. A 471 20150502. (**2015**).
[2] C.J. Clarke, W.C. Tu, O. Levers, A. Bröhl, J.P. Hallett, Chem. Rev. 118 (**2018**) 747–800.

[3] D.J. Heldebrant, H.N. Witt, S.M. Walsh, T. Ellis, J. Rauscher, P.G. Jessop, Green Chem. 8 (**2006**) 807–815.

[4] M.F.V. Pereira, H.M.N.T. Avelino, F.J.P. Caetano, J.M.N.A. Fareleira, Fluid Phase Equilib. 480 (**2019**) 87–97.

[5] Avelino, H.M.N.T; Diogo, J.C.F..; Caetano, F.J.P.; Fareleira, J.M.N.A.. *J. Chem. Eng. Data*, *60* (12), **2015,** 3696–3702.

[6] Avelino, H.M.N.T., Fareleira, J.M.N.A., Gourgouillon D., Igreja, J. M.; Nunes da Ponte, M. *J. of Supercritical Fluids* 128 (**2017**) 300–307.

[7] Gourgouillon D., Avelino, H.M.N.T., Fareleira, J.M.N.A., Nunes da Ponte, M., J. Supercritical Fluids, 13, (**1998**)177-185.

[8] Sequeira, M. C. M., M.F.V. Pereira, H.M.N.T. Avelino, F.J.P. Caetano, J.M.N.A. Fareleira, *Fluid Phase Equilib*. (available online in 25 may 2019.

USE OF WASTEWATER IN THE IRRIGATION OF EDIBLE VEGETABLES:EVALUATION OF THE RISK OF CONTAMINATION BY TOXIC METALS

Hugo F. Silva[1,2] ,Nelson A. Silva[1,2] ,José Coelho[1,2] ,M. Paula Robalo[1,2] ,Manuel J. Matos[2,3]

1 CQE Química Estrutural

2 ISEL ADEQ Área Departamental de Engenharia Química

3 it 25 YEARS instituto de telecomunicações

06 CE

CQE Days Spring Meeting 2019

INTRODUCTION 1

The use of treated water from Wastewater Treatment Plants (WWTP) for irrigation presents challenges that need to be clarified and then overcome. One of the challenges is the use of treated water from WWTP for the irrigation of vegetables. The use of treated water for lawn watering of gardens and golf courses poses the challenge of the proliferation of microorganisms that can cause diseases in humans and domestic animals. However, the use of treated water for gardening raises the question of the contamination of vegetables by toxic metals and other harmful compounds to humans [1].

In this study, our concern is about the contamination of vegetables by toxic metals, namely cadmium, chromium, nickel and lead. Regarding this concern, our group implemented a research project in which synthetic treated water was used for controlled irrigation of cabbage (*Brasissica oleracea*) and lettuce (*Lactuca sativa*).

Cultivation Conditions

Concentration:

Metals	1/3 VLE	2/3VLE	VLE
Cd	1	2	3
Cr	4	5	6
Ni	7	8	9
Pb	10	11	12
ALL	13	14	15
Ø	16	17	

Synthetic waters with 1/3 ELV, 2/3 ELV and ELV (Emission Limit Value) were used for irrigation.

ELV is the maximum discharge concentration of the metals allowed in the legislation, DL 236/98.

Microwave extraction

CEM SP Discover

Microwave extraction parameters:

Temperature: 80 ºC

Power: 100 W;

Total time: 3min;

Solvent: Methanol (2 mL/g sample)

DPPH free radical scavenging method

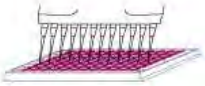

To each microplate well add:

Sample: 30 µL lettuce extract solution + 270 µL DPPH solution 100 µM; A blank and control reaction was done

40 min

T.amb /dark

Absorbance **λ=515nm** (BIOTek Synergy 2).

DPPH Cabagge Leaves results

Concentration:

DPPH expressed asTrolox equivalent antioxidant capacity (TEAC) in µg TEAC/mg FW (Fresh Weight - Extract)

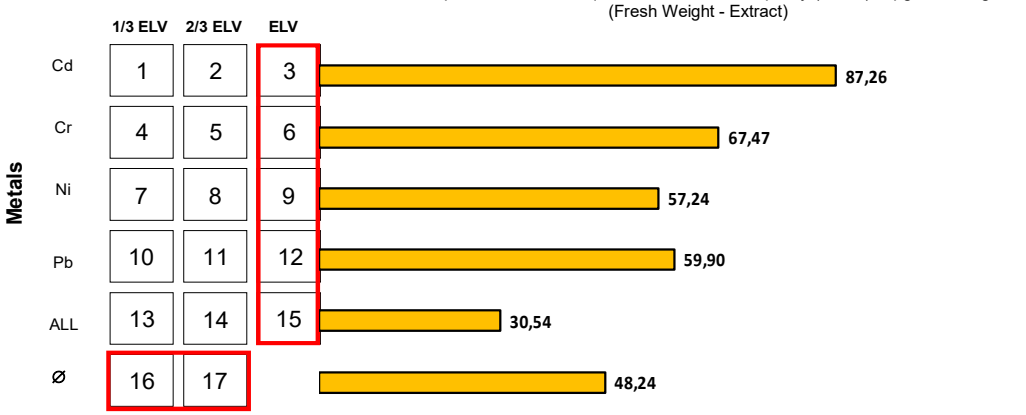

- In what the efficiency of the microwave extraction it concerns it was concluded that it was equivalent for all cabbage samples with and without contamination (~ 1,7%).
- On the other hand, the obtained results showed that, in fact, the antioxidant capacity of the studied samples increases when they are irrigated with contaminated solutions of the individual metals (with respect to the blank samples).
- This evidence may be due to the vegetables metabolism reaction in the presence of heavy metals, with the respective increase in antioxidant capacity.
- Additionally, the most significant response was obtained when the samples were irrigated with cadmium synthetic solutions.

Funding:
Centro de Química Estrutural is funded by Fundação para a Ciência e Tecnologia – project UID/QUI/00100/2019.

FCT Fundação para a Ciência e a Tecnologia

References

[1] N. Amin, A. Hussain, S. Alamzeb, S. Begum, Food Chemistry 2013, 136, 1515–1523.

[2] R. Apak, S. Gorinstein, V. Böhm, K. M. Schaich, M. Özyürek, K. Güçlü, Pure Appl. Chem 2013, 85, 957–998.

[3] A. Blainski, G. C. Lopes, J. C. P. De Mello, Molecules 2013, 18, 6852–6865.

[4] Commission Regulation (EC) No. 1881/2006

Email: hsilva@deq.isel.ipl.pt

Tetracopper(II) Cores Driven by an Unexplored Trifunctional Aminoalcohol Sulfonic Acid for Mild Catalytic C-H Functionalization of Alkanes

Inês F.M. Costa, Marina V. Kirillova, Vânia André, Tiago. A. Fernandes, Alexander M. Kirillov

Centro de Química Estrutural, Instituto Superior Técnico, Universidade de Lisboa, Av. Rovisco Pais, 1049-001 Lisboa, Portugal; inesfmcosta@outlook.com

Introduction

Cu-containing complexes represent an interesting class of compounds capable of functionalizing C–H bonds in rather inert substrates such as alkanes.[1-3] Considering the growing interest in the development of effective and single-step protocols for the oxidative transformation of saturated hydrocarbons, the main objectives of the present work were the synthesis and characterization of new multicopper(II) coordination compounds using H_3bes as a primary N,O ligand source, and the catalytic application of the obtained compounds in the mild oxidation and carboxylation of alkanes to form value-added products.

Due to its structure with three different functionalities, versatile multidentate nature, stability, and aqueous solubility, N,N-bis(2-hydroxyethyl)-2-aminoethanesulfonic acid (H_3bes) was selected as main building block.

Results (Synthesis)

Three novel tetracopper(II) coordination compounds namely $[Cu_4(\mu\text{-Hbes})_3(\mu\text{-}H_2\text{bes})(\mu\text{-ba})]\cdot 2H_2O$ (**1**), $[Cu_4(\mu\text{-Hbes})_3(\mu\text{-}H_2\text{bes})(\mu\text{-fhba})]\cdot 2H_2O$ (**2**), and $[Cu_4(\mu\text{-Hbes})_3(\mu\text{-}H_2\text{bes})(\mu\text{-thba})]\cdot 2H_2O$ (**3**) were easily generated from $Cu(NO_3)_2$, a trifunctional aminoalcohol sulfonic acid (H_3bes) as a principal building block, and a benzene carboxylic acid as a supporting ligand (i.e., benzoic (Hba), 4-hydroxybenzoic (Hfba), or 3-hydroxybenzoic (Hthba) acid).[1] The obtained microcrystalline products, were isolated and fully characterized by FTIR (Fourier-Transform Infrared Spectroscopy), elemental analysis, ESI-MS (Electrospray Ionisation Mass Spectrometry), and single-crystal X-ray diffraction methods (Figures 1 and 2).

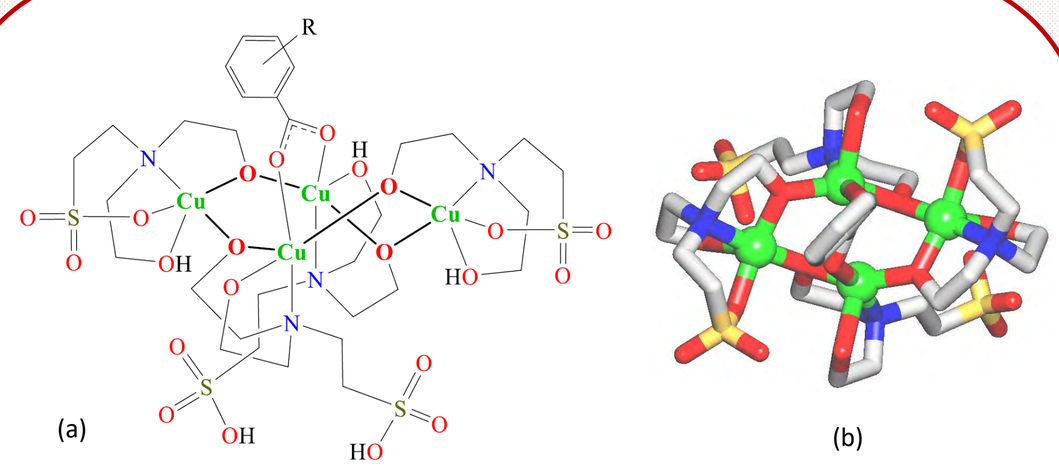

Figure 1. (a) General Formula of **1**–**3**; R = H (**1**), 4-OH (**2**) and 3-OH (**3**). (b) Crystal structure of **2**.

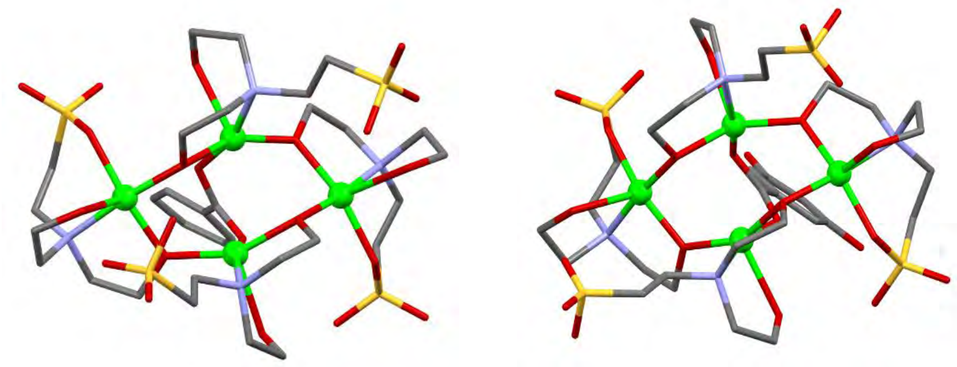

Figure 2. Crystal Structures of compounds **1** (left) and **3** (right).

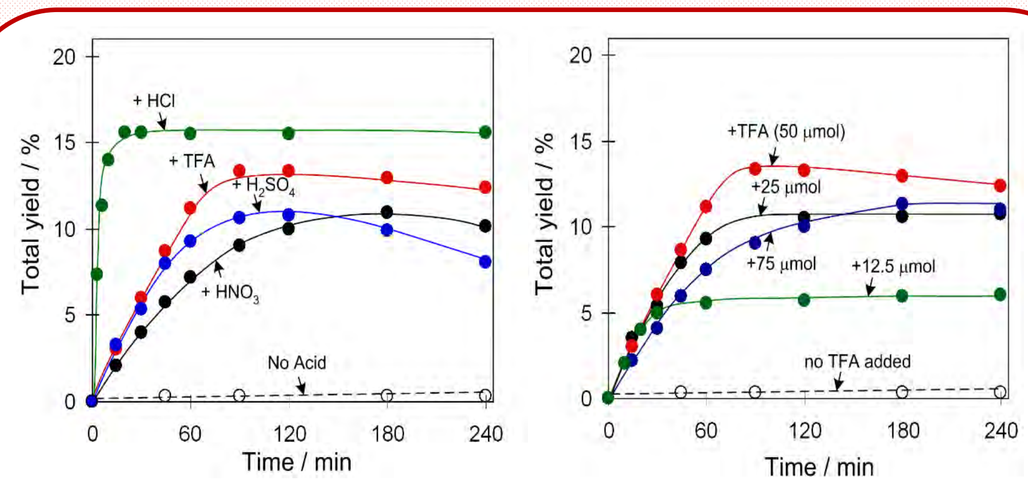

Figure 3. Effect of acid promoter type (left) and loading (right) on the total yield of products (cyclohexanol and cyclohexanone) in C_6H_{12} oxidation with H_2O_2.

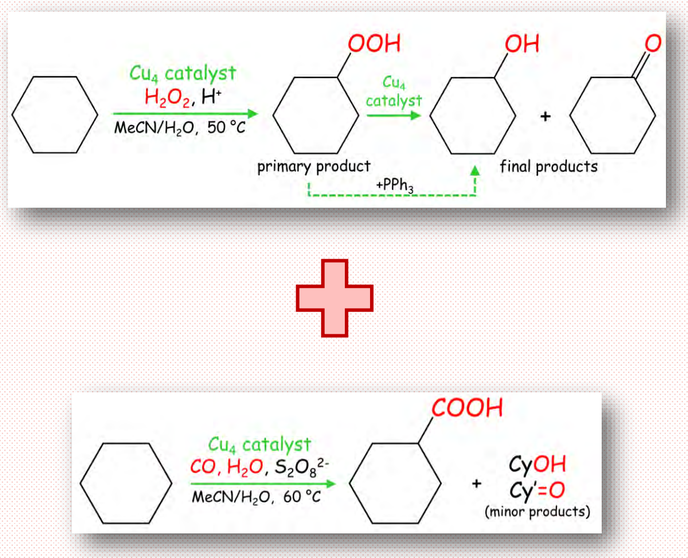

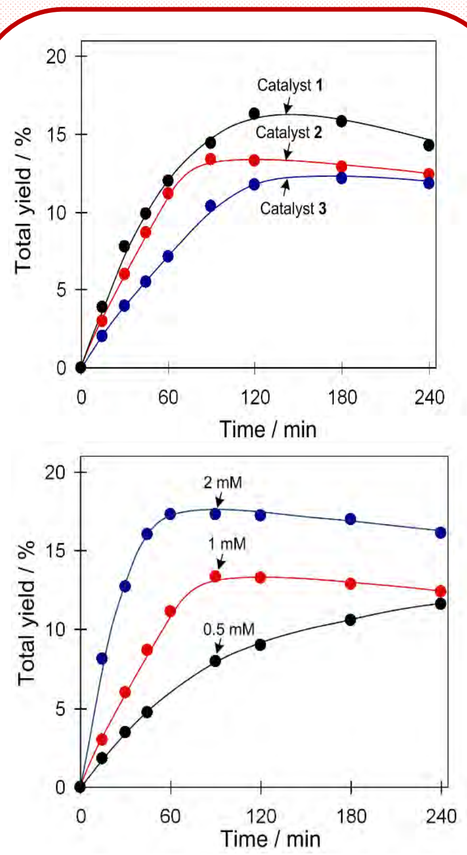

Figure 4. Effect of catalyst type (top) and catalyst loading (bottom) on the total product yield (cyclohexanol and cyclohexanone) in C_6H_{12} oxidation with H_2O_2.

Results (Catalysis)

The obtained tetracopper(II) complexes **1**–**3** were applied as efficient and versatile homogeneous catalysts in the oxidative C–H functionalization of alkanes (propane and cycloalkanes) by aqueous H_2O_2 in acidic MeCN/H_2O medium at 50°C, showing a remarkable level of activity. Two different model reactions were explored: (1) mild oxidation of alkanes with hydrogen peroxide to give alcohols and ketones, and (2) mild carboxylation of alkanes in the presence of carbon monoxide, water, and potassium peroxodisulfate to give carboxylic acids. For these reactions, effects of different parameters (acid promoter effect, catalyst amount, loading of substrate, oxidant and catalyst, substrate scope, and effect of water), as well as mechanistic and selectivity characteristics, were studied (Figures 3, 4 and 5). The maximum product yields up to 46% were obtained.

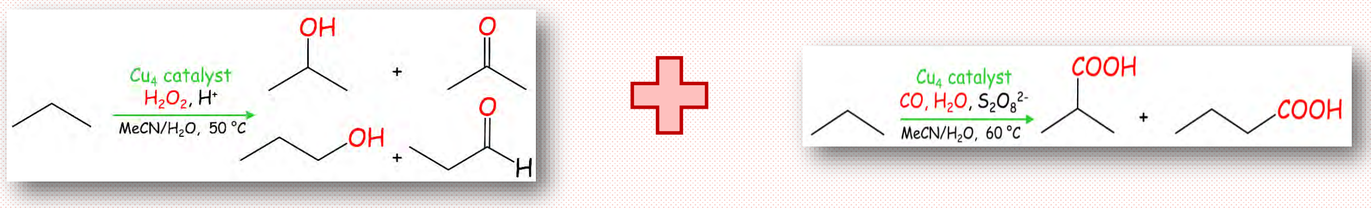

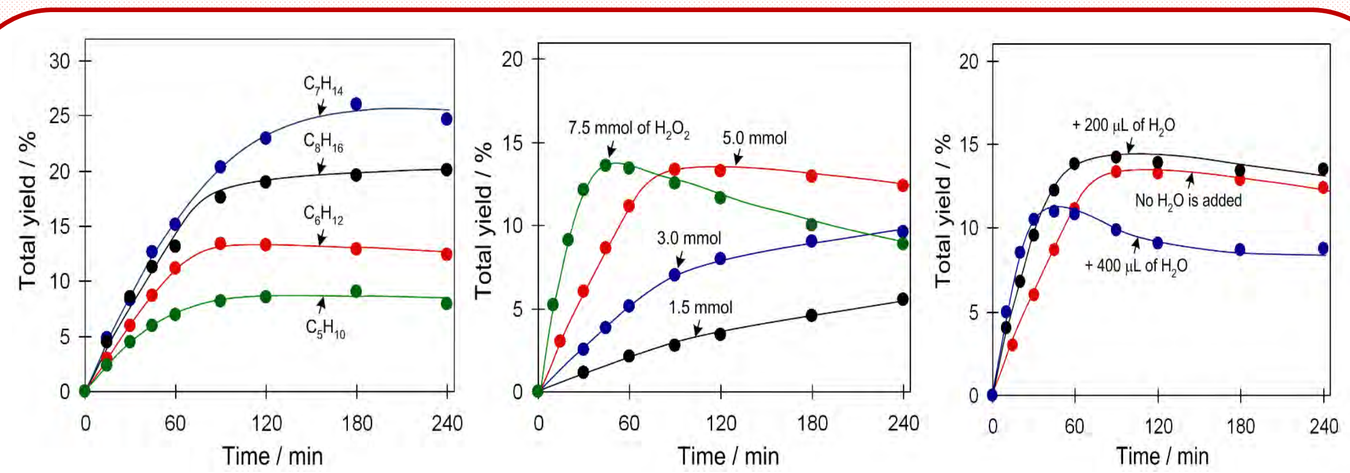

Figure 5. Substrate scope (left) and effect of H_2O_2 (center) and H_2O amount (right) on the total yield of products (cyclohexanol and cyclohexanone) in C_6H_{12} oxidation with H_2O_2.

05 Biomol

Funding:

Centro de Química Estrutural is funded by Fundação para a Ciência e Tecnologia – project UID/QUI/00100/2019.
Other funding:
IF/01395/2013/CP1163/CT005,
CEECIND/03708/2017,
UID/QUI/00100/2013,
LISBOA-01-0145-FEDER029697,
REM2013,
SFRH/BPD/119980/2016,
SFRH/BPD/78854/2011.

This research is based on MSc thesis of Inês F.M. Costa (2018, IST)

References:

[1]Costa, I. F. M., Kirillova, M.V., André, V.; Fernandes, T.A., Kirillov, A.M., *Catalysts*, 9, **2019**, 321.

[2]Kirillova, M.V.; Santos, C.I.M., Fernandes, T.A.; André, V.; Dias, S. S. P.; Kirillov, A.M.; *Inorg. Chem. Front.*, 4, **2017**, 968.

[3]Fernandes, T.A.; André, V.; Kłak, J.; Kirillov, A.M.; Kirillova, M.V., *J. Mol. Catal. A: Chem.* 426, **2017**, 357.

A New Calorimetric Cell for Studies of Co-Crystals Energetics

I.O. Feliciano[1], C.E.S. Bernardes[1], C. Naese[2], F. Emmerling[2], M.E. Minas da Piedade[1]

[1] Centro de Química e Bioquímica e Centro de Química Estrutural, Faculdade de Ciências, Universidade de Lisboa, Campo Grande, 1749-016 Lisboa, Portugal

[2] BAM Federal Institute for Materials Research and Testing, Richard-Willstaetter-Strasse 11, 12489 Berlin, Germany

idfeliciano@fc.ul.pt

CONTEXT

- Co-crystals are substances containing two or more different molecules (A_nB_m).
- The use of cocrystals has emerged in recent years as a very attractive strategy to tune the properties of new APIs and improve the performance of existing ones.
- A key aspect is to assess the stability those co-crystals relative to their co-formers.
- A good indicator of that stability is the standard molar enthalpy, $\Delta_r H^o_m$, of reaction:

$$nA(cr) + mB(cr) \rightarrow A_nB_m(cr)$$

A new cell has been developed for determination of $\Delta_r H^o_m$ with small amounts of sample

Calorimetric System and New Cell

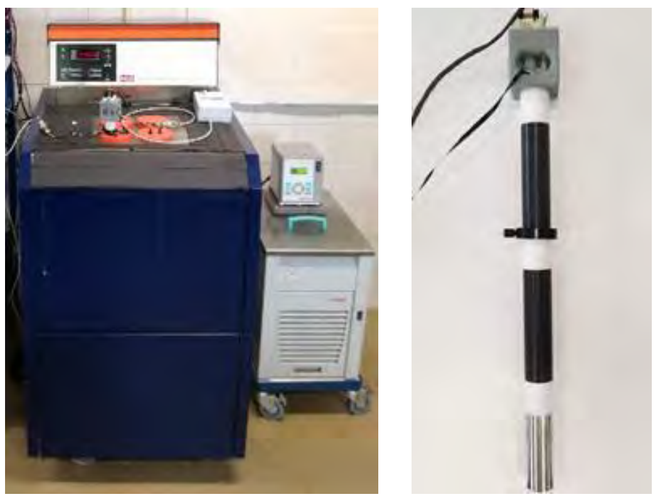

Fig.1- LKB 2277 Thermal Activity Monitor (left) and Calorimetric cell developed in this work (right)

PERFORMANCE

Quality of the calorimetric signal

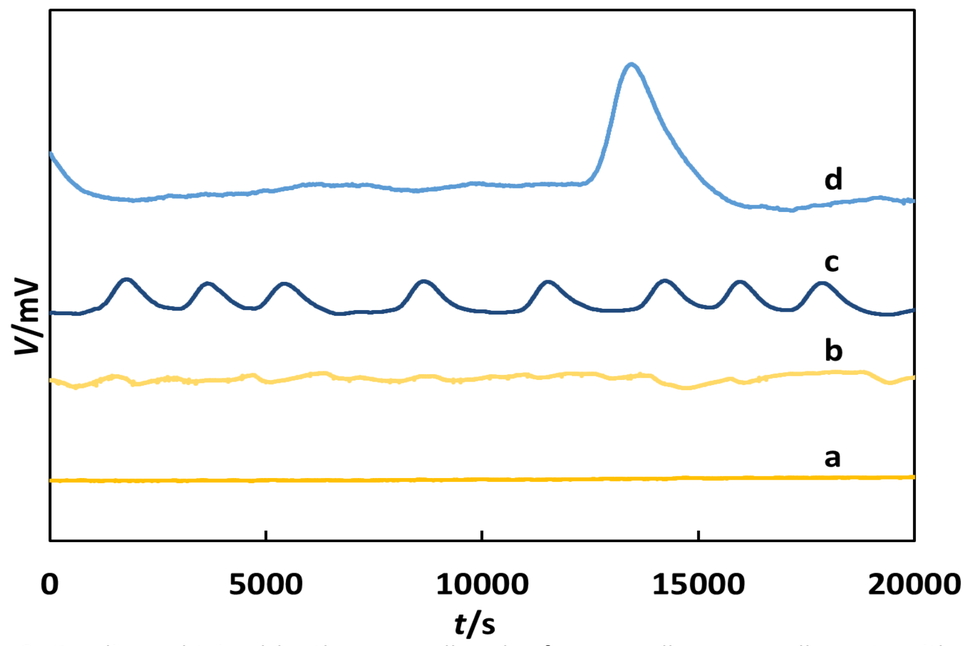

Fig.2- Baselines obtained by the new cell and reference cell: **a** new cell empty without stirring, **b** new cell fill with deionized water and stirring, **c** reference cell empty without stirring and **d** reference cell with deionized water and stirring.

Sensitivity of the calorimetric system

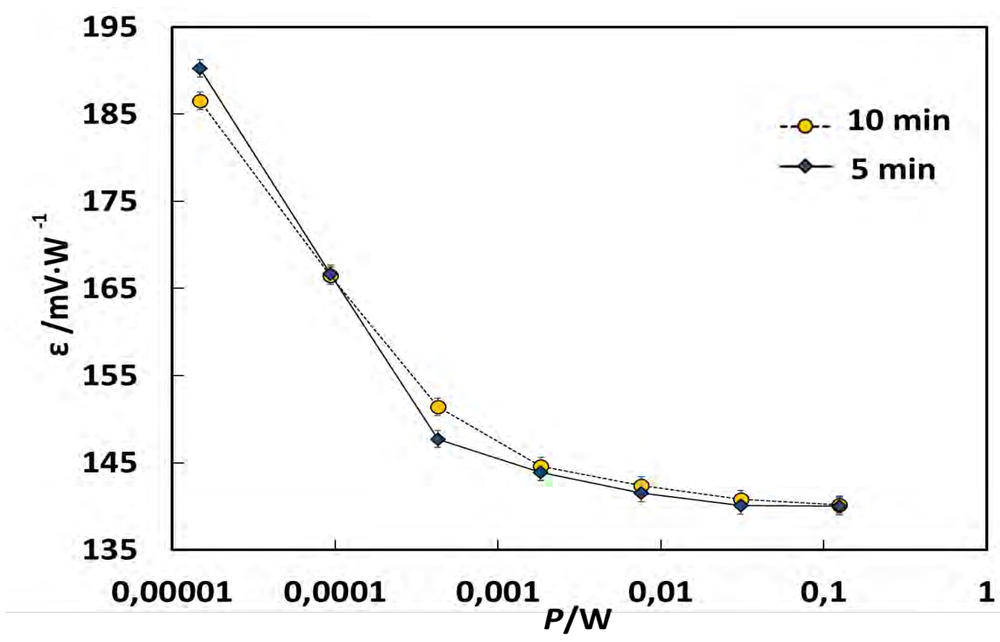

Fig.3- Relation between the calibration constant and the energy dissipated inside the calorimetric vessel per unit of time (power).

Dissolution tests: KCl and $Theo_2$:Oxa

$\Delta_{diss}H^o_m$ KCl

Obtained:
17,40±0,03 kJ·mol^{-1}

Expected:
17,40±0,11 kJ·mol^{-1}

Dissolution time:
~20 minutes

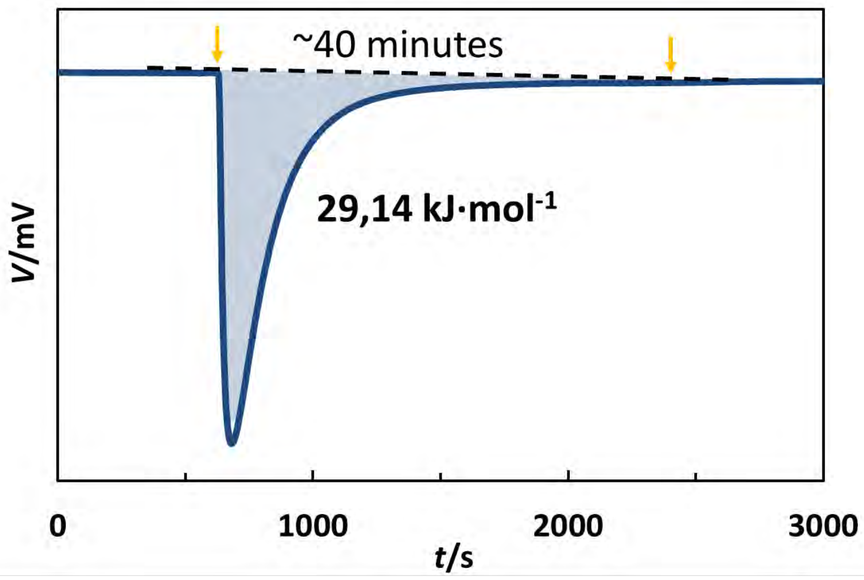

Fig.4- Solution calorimetry curve for the dissolution of the co-crystal $Theo_2$:Oxa

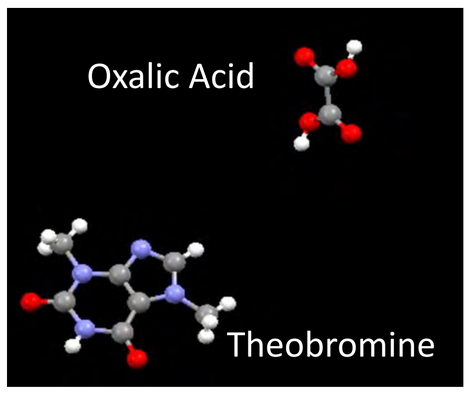

Fig.5- Molecular structure of Theobromine and Oxalic Acid, precursors of $Theo_2$:Oxa co-crystal

CONCLUSION

- The baseline noise is an order of magnitude smaller than that of a previous existing cell.
- The calibration constant was found to be stable if power P > 10^{-4} W.
- Validation through $\Delta_{diss}H^o_m$ (KCl, cr) measurements showed excellent accuracy and better precision than recommended reference data.
- Tests with $Theo_2$:Oxa showed excellent performance of the new cell for co-crystal stability studies with small amounts of sample.

09 MET

Funding:
Centro de Química Estrutural is funded by Fundação para a Ciência e Tecnologia – project UID/QUI/00100/2019. This work was supported by Fundação para a Ciência e a Tecnologia – project PTDC/QUI-OUT/28401/2017 (LISBOA-01-0145-FEDER-028401) and UID/MULTI/00612/2013.

References

For leading references see:
[1] Fischer, F. et al. Cryst Eng Comm 17, 824–829 (2015)
[2] De Araujo, G. L. B. et al. Cryst. Growth Des. 18, 2377–2386 (2018)
[3] A.O.L. Évora, C.E.S. Bernardes, M. Fátima M. Piedade,A.C.L. Conceição, M.E. Minas da Piedade; *Cryst. Growth Des*. 18 (2019), in press.

FCT Fundação para a Ciência e a Tecnologia

Lighting the mitochondria with Two-photon red-emitting cationic molecules

ines.mariz@tecnico.ulisboa.pt

Inês F. A. Mariz,[1] Sandra N. Pinto,[2] José M. G. Martinho,[1] Javier Recio,[3] Juan J. Vaquero,[3] Ana M. Cuadro[3] and Ermelinda M. S. Maçôas[1]

[1] *Centro de Química Estrutural, and IN-Institute of Nanoscience and Nanothecnology, Instituto Superior Técnico, Universidade de Lisboa, Av. Rovisco Pais, 1049-001 Lisboa, Portugal*

[2] *Institute for the Bioengeneering and Bioscienes, and IN-Institute of Nanoscience and Nanothecnology, Instituto Superior Técnico, Universidade de Lisboa, Av. Rovisco Pais, 1049-001 Lisboa, Portugal*

3 Departamento de Química Orgánica y Química Inorgánica, Universidad de Alcalá, 28871-Alcalá de Henares, Madrid, Spain

CQE Química Estrutural

08 MPPM

FCT Fundação para a Ciência e a Tecnologia

A set of fluorescent mitochondria target molecules based on dipolar and quadrupolar quinolizinium and benzimidazolium cations were developed. (Fig. 1) Some of the dipolar compounds could be excited in the Near-infrared due to a high two-photon brightness while exhibiting emission in the red part of the visible spectra (600-700 nm). Interaction with the mitochondria in living cells leads to an unexpected blue-shift of the emission of these compounds.

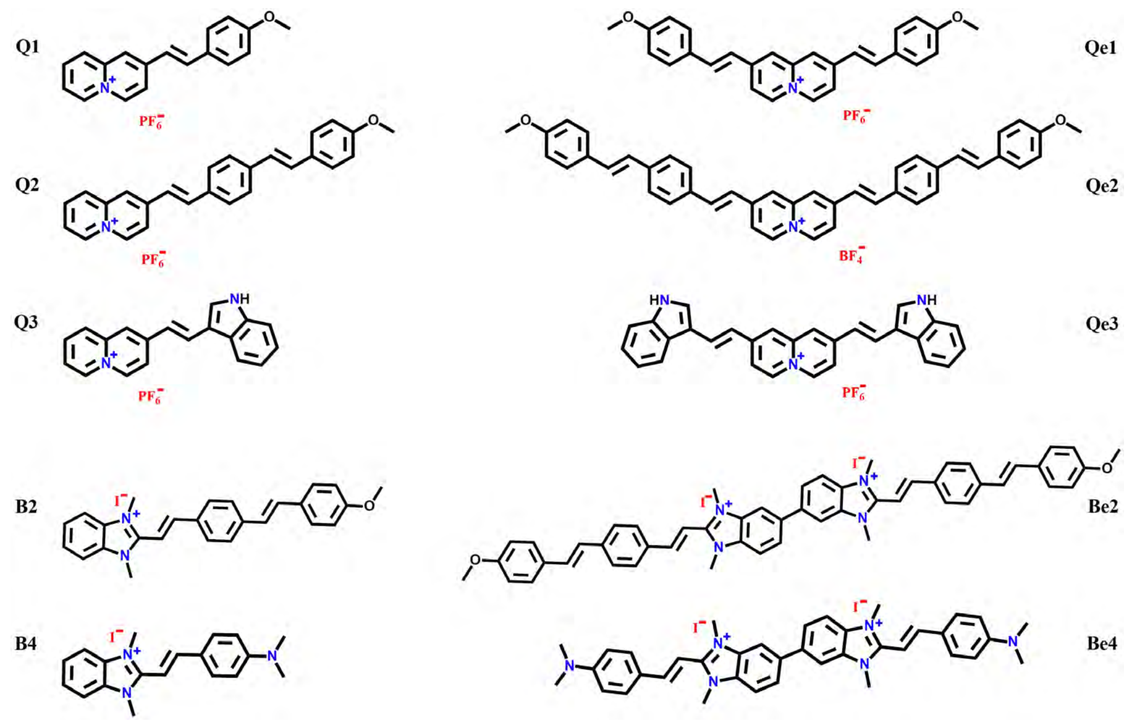

Fig. 1 - General structure of push-pull systems based on either the quinolizinium (**Q** and **Qe**) or benzimidazolium (**B** and **Be**) cations. Ten charged compounds where prepared by combining the different electron acceptor core with different electron donor groups.

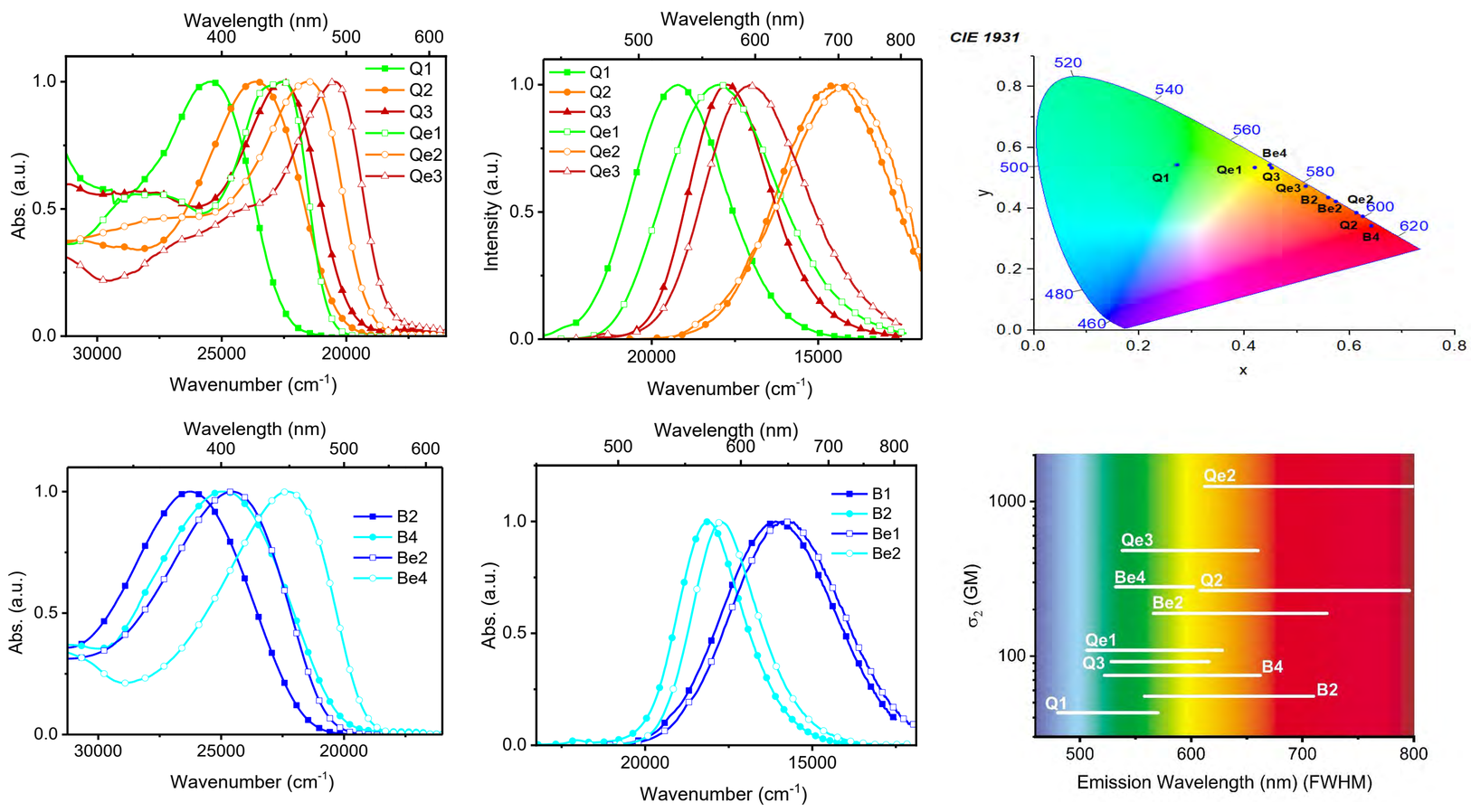

Fig. 2 – Absorption (left) and emission (middle) spectra for the Quinolizinium (top) and Benzimidazolium (bottom) compounds in DMSO; CIE 1931 colour space chromaticity diagram for their emission (right top) and TPA cross-section (σ2) against the full width at half maxima (FWHM) of the two-photon induced emission band for all the compounds.

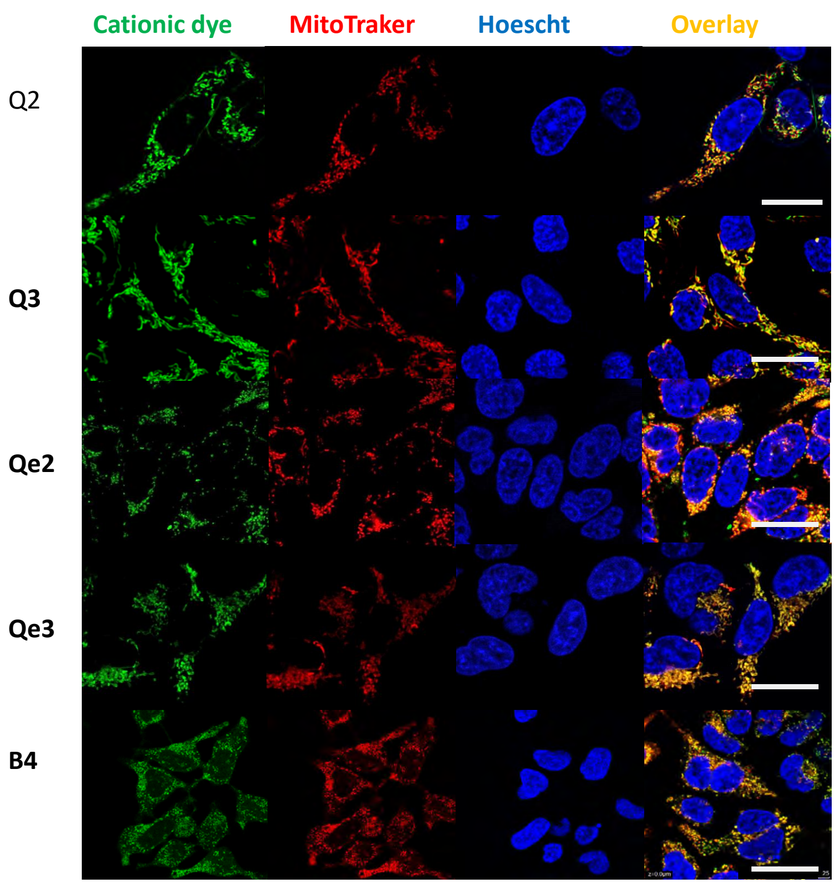

Fig. 3 - Fluorescence microscopy images of HEK 293 T cells co-stained with the compounds **Q2**, **Q3**, **Qe2, Qe3 and B4** (green), the MitoTracker Red (red) and the Hoechst 33342 (blue) and the overlay of the isolated channels showing the co-localization of the selected compounds with the MitoTracker. Scale bar common in all images: 10 µm.

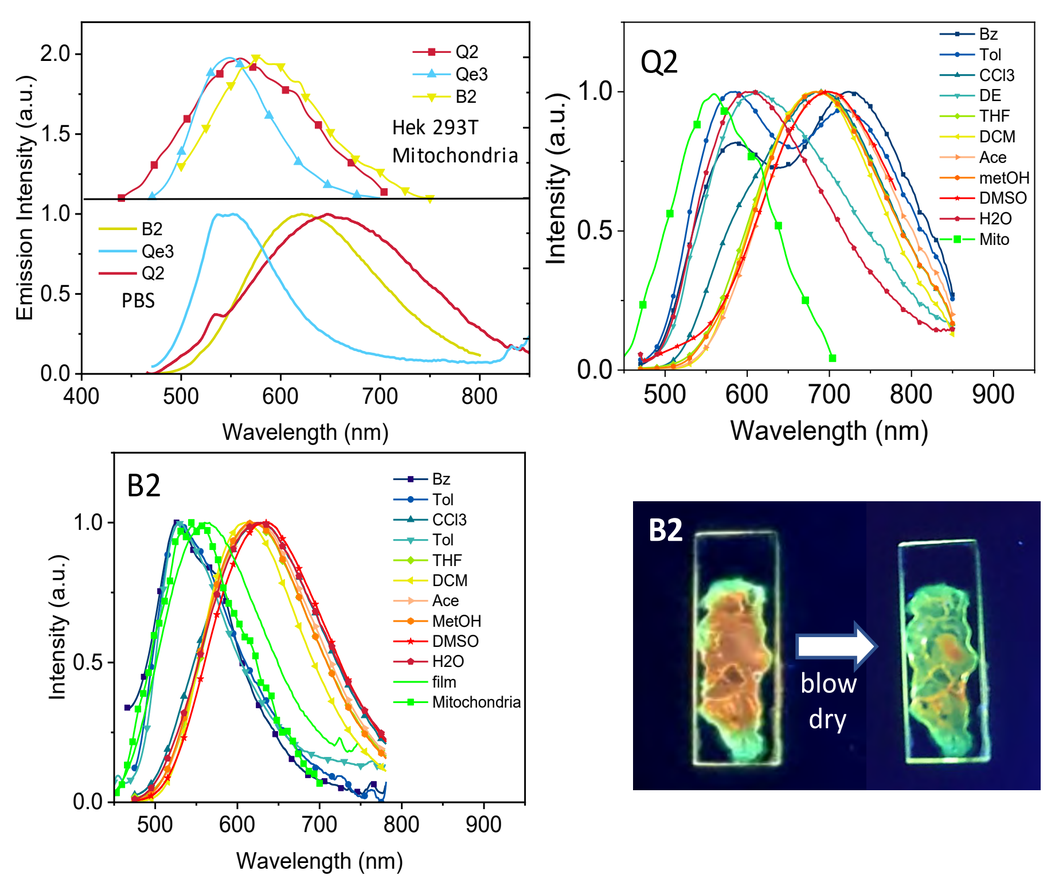

Fig. 4 - Emission spectra of **Q2**, **B2** and **Qe3** in HEK 293T cells and in PBS at pH7 solution (top left) and solvatochromic studies for the red emitting **Q2** (top right) and **B2** (bottom left) showing the blue-shift in emission in low polarity solvent. The photograph shows emission of a film of **B2** changing from orange to green while it dries.

Funding:
Centro de Química Estrutural is funded by Fundação para a Ciência e Tecnologia – project UID/QUI/00100/2019. This work was supported by Fundação para a Ciência e a Tecnologia (FCT) and by Programa Operacional Competitividade e Internacionalização via Fundos Europeus de Desenvolvimento Regional (FEDER/FNR) (projects PTDC/QUI-QFI/29319/2017 and PTDC/NAN-MAT/29317/2017)

References:

G. Marcelo, S. Pinto, T. Cañeque, I. F. A. Mariz, A. M. Cuadro, J. J. Vaquero, J. M. G. Martinho and E. M. S. Maçôas; *J. Phys. Chem. A* 2015, 119, 11, 2351-2362.

Catalytic activity of carbon supported Cu(I) complexes for the synthesis of 1,2,3-triazoles

Ivy L. Librando,[1] Abdallah G. Mahmoud,[1] Sónia A.C. Carabineiro,[1] Carlos F.G.C. Geraldes,[2] M. Fátima C. Guedes da Silva,[1] Armando J.L. Pombeiro[1]

[1] Centro de Química Estrutural, Instituto Superior Tecnico, Universidade de Lisboa, Av. Rovisco Pais, 1049-001 Lisboa, Portugal

[2] Faculdade de Ciencias e Tecnologia, Universidade de Coimbra, Calçada Martim de Freitas 3000-393 Coimbra, Portugal

CQE Days
Spring Meeting 2019

01 CCC

Funding:
Centro de Química Estrutural is funded by Fundação para a Ciência e Tecnologia – project UID/QUI/00100/2019. This work was supported by CATSUS PhD grant PD/BD 135555/2018 from Fundação para a Ciência e a Tecnologia and project UID/QUI/00100/2019.

INTRODUCTION

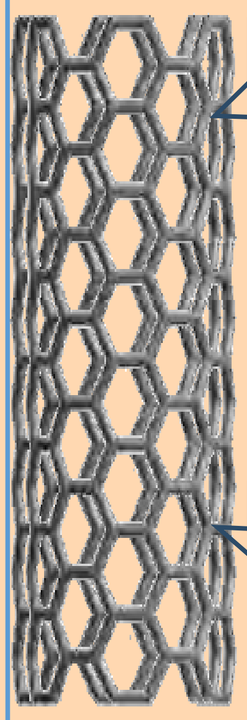

Metal catalysts supported by carbon materials[2-9]

- Reduced catalyst loading
- Improved efficiency and recovery
- High surface area
- Porous surface
- Thermal stability

Synthesis of 1,2,3-triazoles[1,8-9]

- Highly valuable organic scaffolds
- Use of inexpensive Cu-catalyst

OBJECTIVES

- To subject different carbon materials to pre-treatment methods (i.e., C-ox and C-oxNa)
- To immobilize Cu(I) complexes to commercially available and pre-treated supporting matrices (i.e., charcoal, carbon nanotubes)
- To synthesize disubstituted triazoles using carbon supported Cu(I) complexes
- To compare catalytic efficiency of supported catalysts versus the homogeneous counterparts.

METHODOLOGY

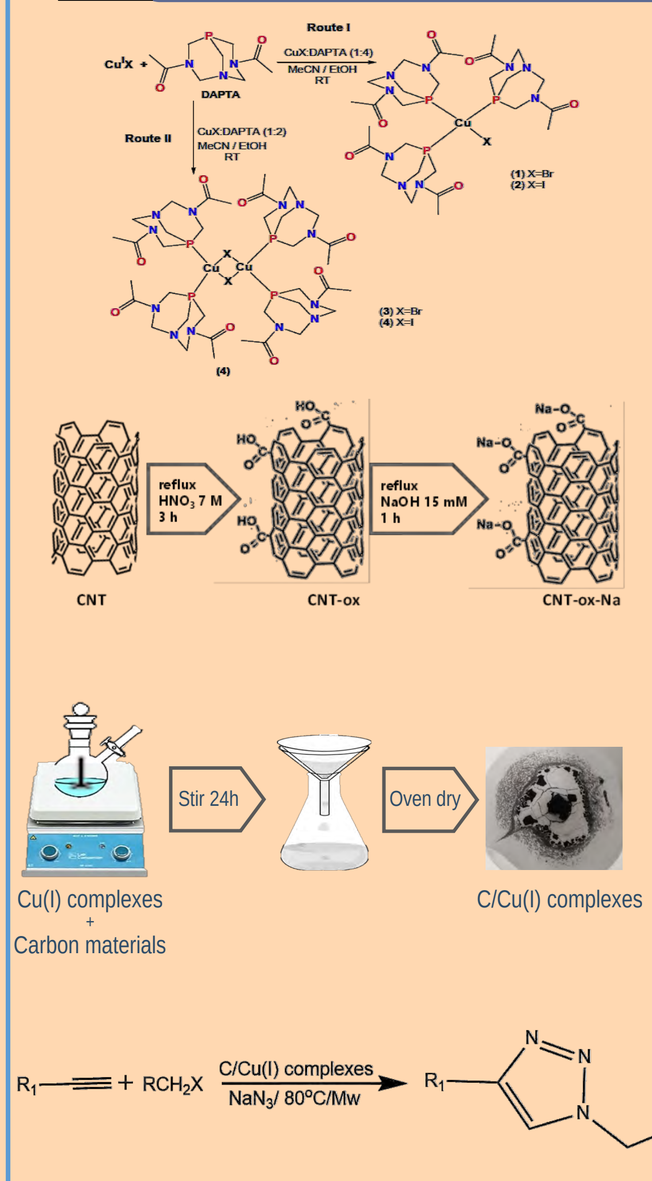

1. Cu(I) complexes preparation[1]
2. Carbon materials preparation[2-7]
3. Immobilization of Cu(I) complexes to carbon materials
4. Synthesis of 1,2,3-triazoles

RESULTS

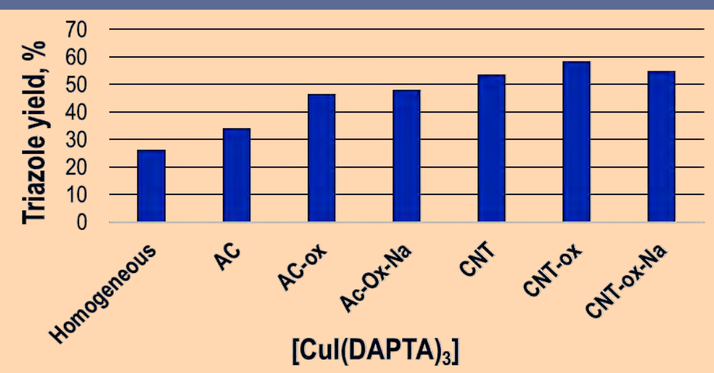

Figure 1. Yield of 1,2,3-triazole from MW-assisted three-component CuAAC click reaction.

- The figure above (Fig. 1) shows the comparison between the yields obtained from homogeneous versus supported catalysts.
- Higher yields were observed upon immobilization of Cu(I) complex and greatly increased upon the use of CNT (carbon nanotube) materials as support.

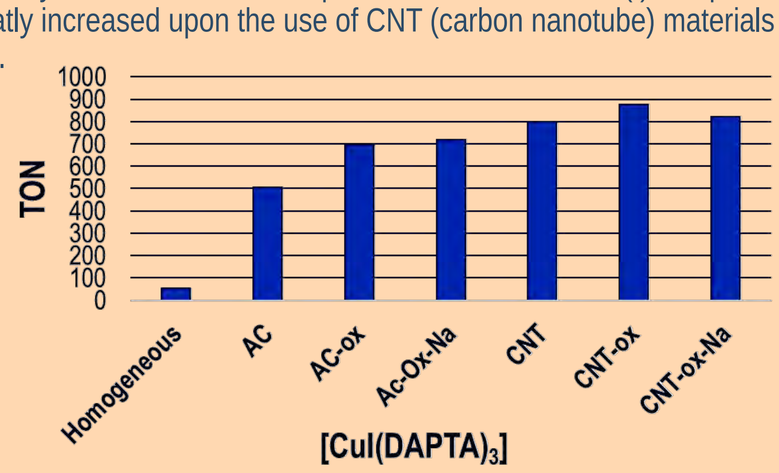

Figure 2. TON of Cu(I) complex as catalyst for the synthesis of 1,2,3-triazole under MW-irradiation for 15 min.

- Figure 2 shows the different TONs obtained by a specific Cu(I) complex when used as a homogeneous and heterogeneous catalysts.
- The TONs were greatly enhanced, from 26 using bulk catalyst to 800 upon immobilization to carbon materials.

CONCLUSION

Carbon supported Cu(I) complexes were used as catalyst for the synthesis of 1,2,3-triazole. The immobilized catalysts show higher TONs as compared to the homogeneous counterpart. Moreover, the reaction was performed under MW irradiation for 15 min at lower temperature (80 ⁰C) with very low catalyst loading of 0.067 mol %.

Acknowledgment:
The authors are grateful to the Laboratory of Analyses of IST for the assistance with the ICP experiments.

References :

1. Mahmoud AG, Guedes da Silva MFC, Sokolnicki J, Smolenski P, Pombeiro AJL. Dalton Trans. 47 (2018) 7290-7299.
2. de Almeida MP, Martins LMDRS, Carabineiro SAC, Lauterbach T, Rominger F, Hashmi ASK, Pombeiro AJL, Figueiredo JL., Catal. Sci. Technol. 3 (2013) 3056–3069.
3. Martins LMDRS, de Almeida MP, Carabineiro SAC, Figueiredo JL, Pombeiro AJL, ChemCatChem 5 (2013) 3847–3856.
4. Sutradhar M, Martins LMDRS, Carabineiro SAC, Guedes da Silva MFC, Buijnsters JC, Figueiredo JL, Pombeiro AJL, ChemCatChem 8 (2016) 2254–2266.
5. Wang J, Martins LMDRS, Ribeiro APC, Carabineiro SAC, Figueiredo JL, Pombeiro AJL, Chem. Asian J. 12 (2017) 1915–1919.
6. Carabineiro SAC, Martins LMDRS, Pombeiro AJL, Figueiredo JL, ChemCatChem 10 (2018) 1804–1813.
7. Martins LMDRS, Ribeiro APC, Carabineiro SAC, Figueiredo JL, Pombeiro AJL, Dalton Trans. 45 (2016) 6816–6819.
8. Nia et al. Chem. Eur. J. 21 (2015) 10763-10770.
9. Mahmoud N, Jaleh B, Fakhri P, Zahraei A, Ghadery E. RSC Adv. 5 (2015) 2785-2793.

Insights of Sorbent Selectivity and pH Effects on Bar Adsorptive Microextraction

J.M.M. Praça*, O.C. Gonçalves, S.M. Ahmad, N.R. Neng, J.M.F. Nogueira**
Centro de Química Estrutural, Centro de Química e Bioquímica, Faculdade de Ciências, Universidade de Lisboa, Campo Grande, 1749-016 Lisboa, Portugal
(*joanampraca@gmail.com, **ocgp98@gmail.com)

06 CE

Introduction

In the last few years, an alternative static microextraction technique, bar adsorptive microextraction, was proposed for trace analysis of polar to nonpolar analytes in aqueous media. This analytical approach, based on the floating sampling technology enrichment process, presents several advantages, including the possibility of selecting the most convenient sorbent coating (*e.g.* activated carbons (ACs), polymers (Ps), etc.) according to the target compounds involved, which has already shown high effectiveness in many applications [1-3].

In order to maximise the microextraction efficiency, several parameters used to be optimised, including sorbent selectivity, equilibrium time, agitation speed and matrix properties, such as, pH, polarity and ionic strength. Nevertheless, the matrix pH may have a significant influence on the recovery yields, once it decides the overall charge of the ionic compounds in the matrix and can also affect the surface charge of the sorbent phases.

Meanwhile, the interactions between the matrix pH, sorbent phase and compound polarity (Fig. 1) were never truly studied in detail by BAµE. The present contribution aims the evaluation of the performance of BAµE prior to high-performance liquid chromatography-diode array detection to understand the mechanisms behind those interactions by using several organic analytes with distinct polarity and p*K*a values as model compounds and different sorbent phases.

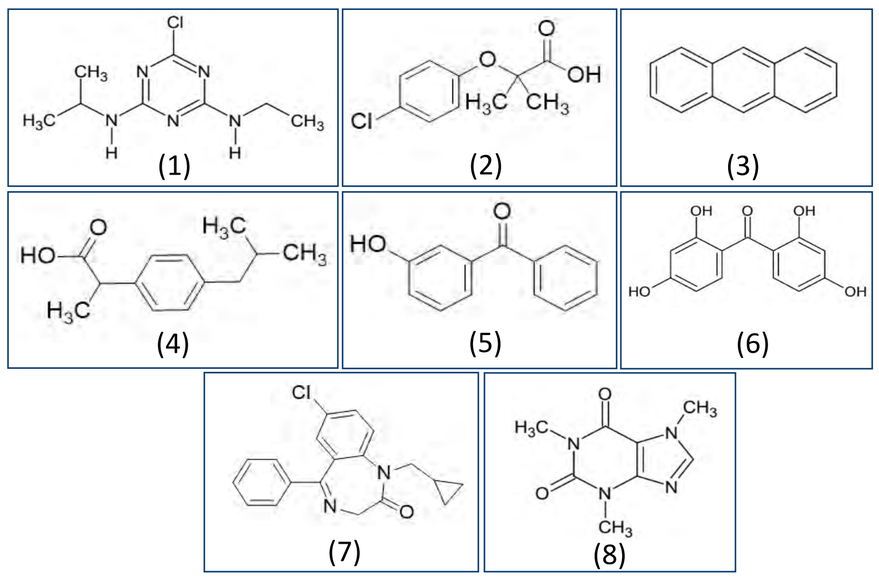

Figure 1: Chemical structures of the studied compounds studied. 1. Atrazine; 2. Clofibric Acid; 3. Anthracene; 4. Ibuprofen; 5. 3-hydroxybenzophenone; 6. 2,2',4,4'-tetrahydroxybenzophenone; 7. Prazepam; 8. Caffeine

Experimental Procedure

BAµE procedure:
- Equilibrium time: 16 h
- Stirring rate: 1000 rpm
- Sorbent selectivity

Back-extraction:
- Microliquid desorption
- 100 µL MeOH
- 30 min under sonification

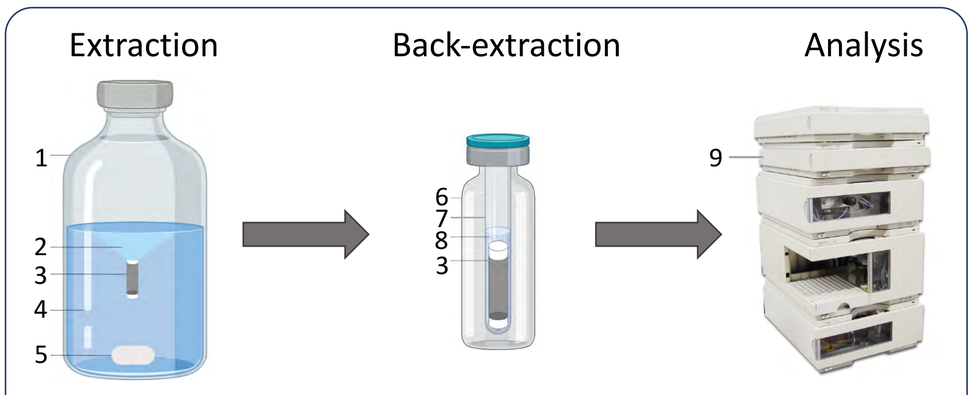

Figure 2: Schematic of the procedure for the microextraction methodologies. 1. Sample flask; 2. Vortex; 3. BAµE device; 4. Sample; 5. Teflon magnetic stir bar; 6. Injection vial;7. Insert; 8. Solvent; 9. HPLC-DAD.

Instrumental Analysis
- **HPLC-DAD:** Agilent 1100 Series (Agilent Technologies) equipped with a vacuum degasser (G1322A), autosampler (G1313A), thermostated column compartment (G1316A), quaternary pump (G1311A) and a diode array detector (G1315B);
- **Column**: Kinetex C18 column, 150 mm × 4.6 mm, 2.6 µm particle size (Phenomenex, U.S.A);
- **Mobile phase**: 0,1 % CHOOH : MeOH

Results

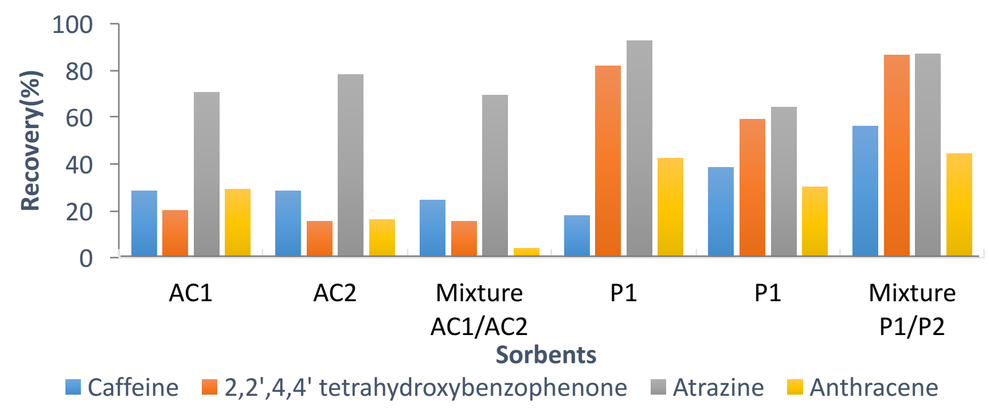

Figure 3: Mixture effect on the average yields obtained by BAµE-µLD/HPLC-DAD using different ACs and Ps sorbent phases for the microextraction of the different compounds.

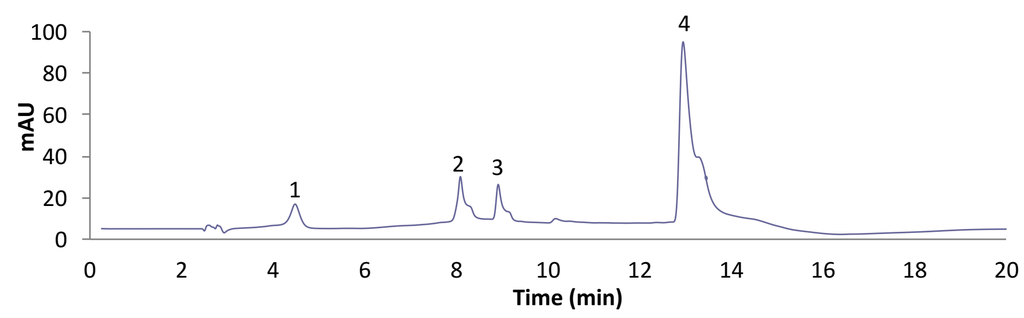

Figure 4: Chromatogram of a standard mixture of the four compounds (5 mg/L) obtained by HPLC/DAD at 254 nm. 1. Caffeine; 2. 2,2',4,4'-tetrahydroxybenzophenone; 3. Atrazine; 4. Anthracene.

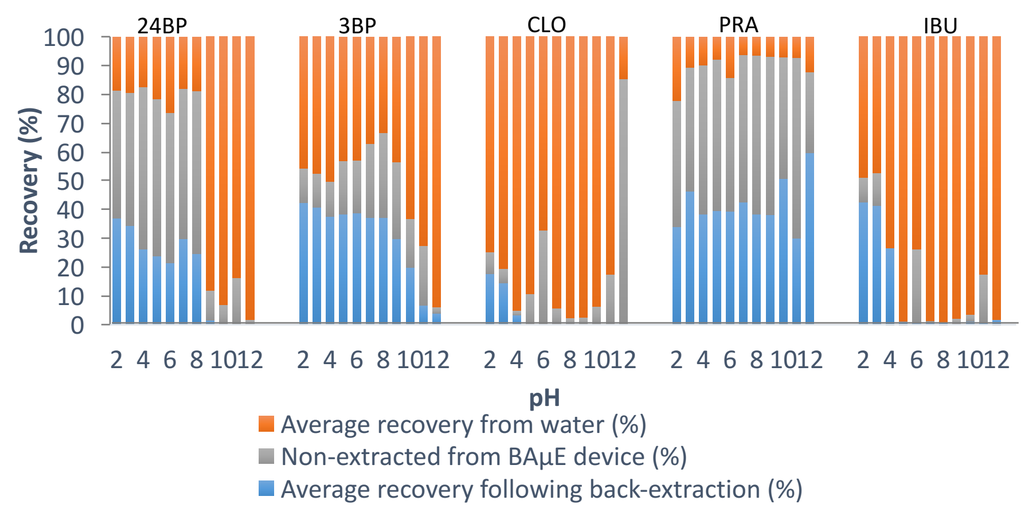

Figure 5: Average recovery following back-extraction, from ultrapure-water and non-extracted from BAµE device using AC1 as sorbent phase. 24BP: 2,2',4,4'-tetrahydroxybenzophenone; 3BP: 3-hydroxybenzophenone; CLO: clofibric acid; PRA: prazepam; IBU: ibuprofen.

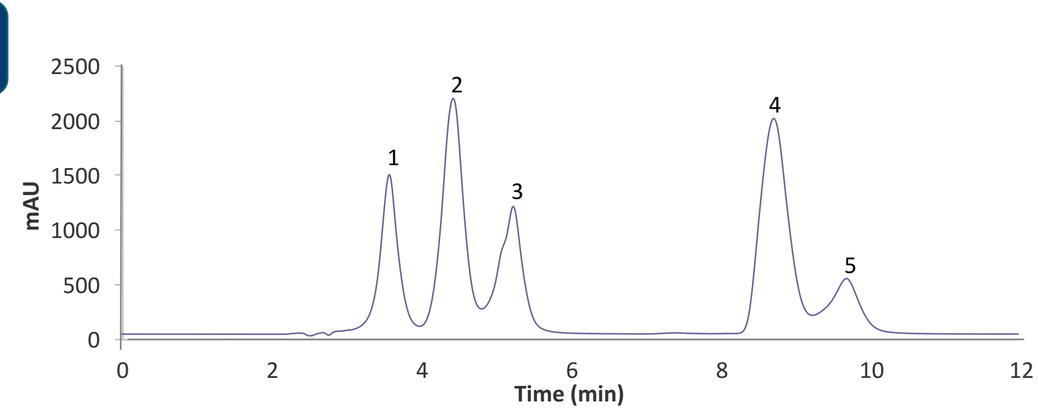

Figure 6: Chromatogram of a standard mixture of the four compounds (250 mg/L) obtained by HPLC/DAD at 226 nm. 1. 2,2',4,4'-tetrahydroxybenzophenone; 2. 3-hydroxybenzophenone; 3. Clofibric acid; 4. Prazepam; 5. Ibuprofen.

Conclusions

- The sorption mechanism of organic compounds in aqueous media using activated carbons and polymers is a very complex task;
- The main parameters involved are the polarity of the compounds, the physico-chemical characteristics of the sorbents as well as, the matrix pH;
- In general, the more alkaline are the matrix conditions the less favourable are for both the microextraction and back-extraction stages;
- The compounds polarity seems to have a strong influence on the enrichment process;
- By mixing some sorbent phases, better recovery yields are observed for some particular compounds.

Funding:
The authors thank Fundação para a Ciência e a Tecnologia (Portugal) for financial support through project UID/QUI/00100/2019 for CQE, UID/Multi/00612/2019 for CQB and for the post-Doc (SFRH/BPD/86071/2012) and PhD (SFRH/BD/107892/2015) grants.

References:

1. Neng, N.R., Silva, A.R., Nogueira, J.M.F., J. Chromatogr. A, 1217 (2010) 7303-7310.
2. Nogueira, J.M.F., Anal. Chem. Acta. 757 (2012) 1-10.
3. Nogueira, J.M.F., Trends Anal. Chem. 71 (2015) 214-223.

TÉCNICO LISBOA

Camphor complexes with antimicrobial and/or cytotoxic properties: design, synthesis and assessment of biological activity

Joana P. Costa, M Fernanda NN Carvalho*

Centro de Química Estrutural **Email: fcarvalho@tecnico.ulisboa.pt**

CQE Química Estrutural

05 BIOMOL

Introduction

This project aims at find new camphor derived complexes with antibacterial, antifungal and/or cytotoxic properties that may overcome the increasing fungi and bacteria resistance to antimicrobials in use. A particular focus is made in the search for active molecules that combine anti-cancer and antimicrobial properties to fight opportunistic infections during anti-cancer treatment.

The strategy is to design and synthesize camphor derivatives that react with metals to produce biological active complex. The variety of ligands provides different electronic and steric properties that can be tuned accordingly to the applications by changing the mono or bicamphor character and the substituents (Y or Z) at the imine group. Initially, the metal precursor chosen was silver nitrate. Good to excellent antimicrobial results were obtained although the toxicity of nitrate was a drawback that is tentatively beng faced by using acetate or chloride silver salts. The biological activity of all compounds was evaluated by calculation of MIC values.

Currently the project was extended to synthesis and biological assessment of Au(I) camphor derived complexes. Other metals of groups 10 and 11 will be screened.

Synthesis

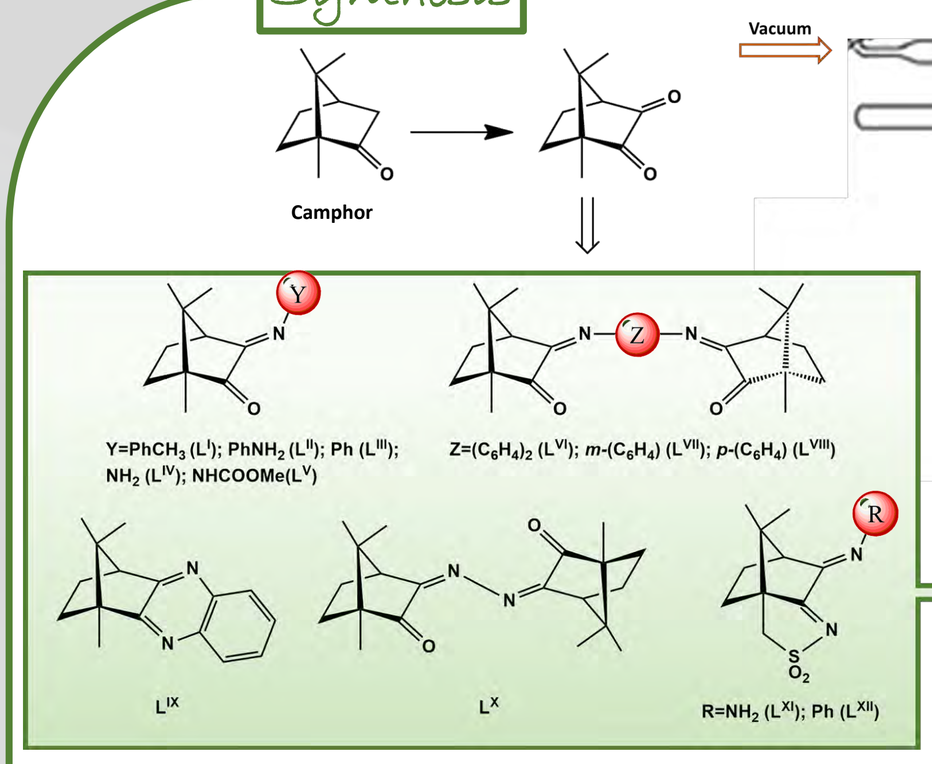

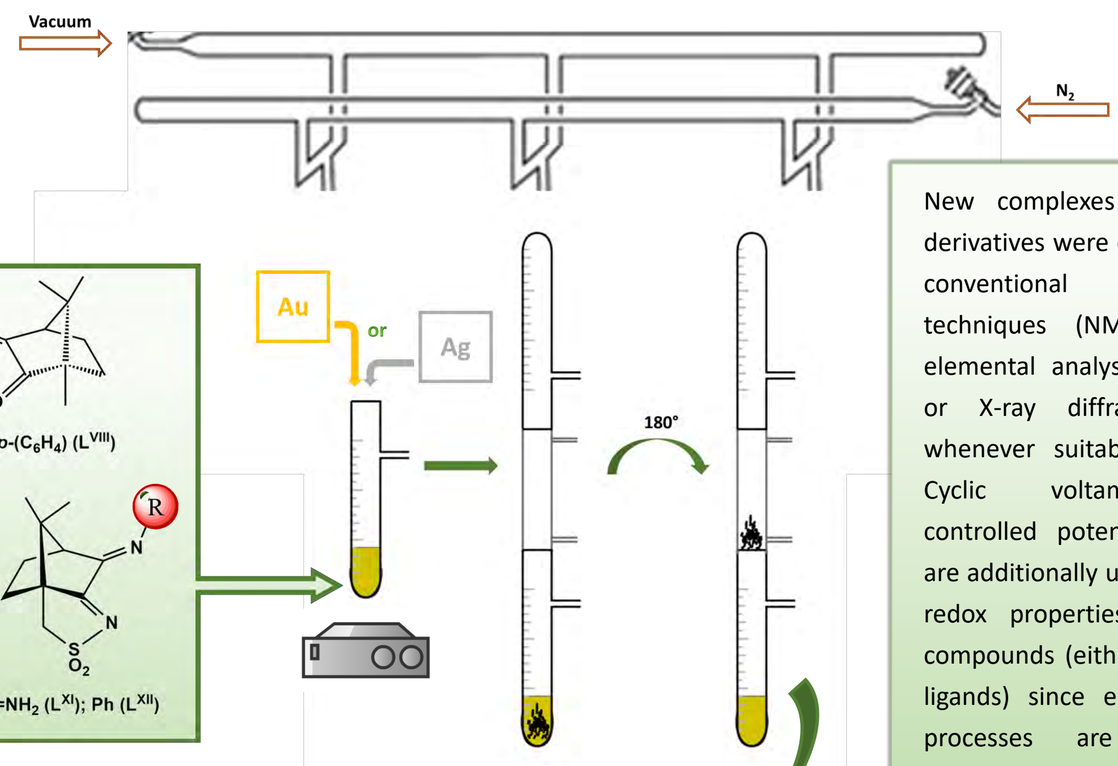

New complexes and camphor derivatives were characterized by conventional spectroscopic techniques (NMR, FTIR) and elemental analysis. ESI-MS, XPS or X-ray diffraction analysis whenever suitable or possible. Cyclic voltammetry and controlled potential electrolysis are additionally used to study the redox properties of the new compounds (either complexes or ligands) since electron transfer processes are of utmost relevance concerning biological processes.

Camphor imine complexes using Ag(I) or Au(I) metal precursors

Metal	Ligand	Complex
Ag(OAc)	L^{I}; Y=$PhCH_3$ L^{VI}; Z=$(C_6H_4)_2$	$[\{AgL^{I}\}_2(\mu\text{-}O)]$ $[Ag(OH)L^{VI}]$
AgCl	L^{II}; Y=$PhNH_2$ L^{III}; Y=Ph	$[\{AgL^{II}\}_2(\mu\text{-}O)]$ $[AgClL^{III}]$
$Ag(NO_3)$	L^{VII}; Y=m-(C_6H_4) L^{VIII}; Y=p-(C_6H_4)	$[Ag(NO_3)L^{VII}]$ $[Ag(NO_3)L^{VIII}]$
$KAu(CN)_2$	L^{I}; Y=$PhCH_3$ L^{VI}; Y=m-(C_6H_4)	$K[Au(CN)_2L^{I}]$ $[Au(CN)L^{VI}]\cdot CH_3CN$

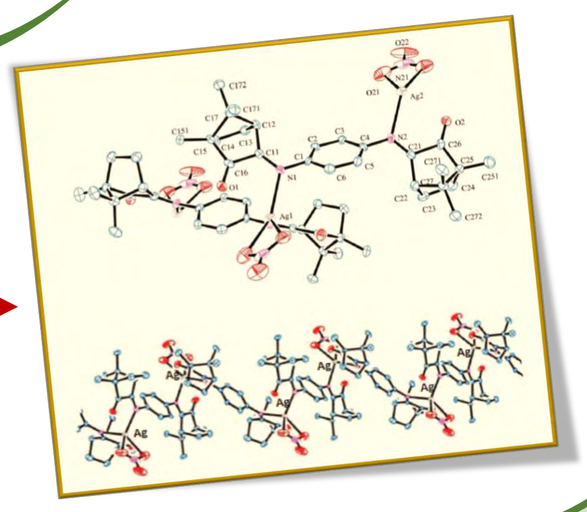

Antimicrobial activity

The MIC values of silver and gold compounds were calculated in order to assess their antimicrobiala activities. The silver compounds showed excellent antifungal (C. albicans, C. glabrata, C. parapsilosis and C. tropicalis) and antibacterial (S. aureus Newman, B. contaminans IST408, E. coli ATCC25922, P. aeruginosa 477) activities. Preliminary results from gold compounds point to low or no activity.

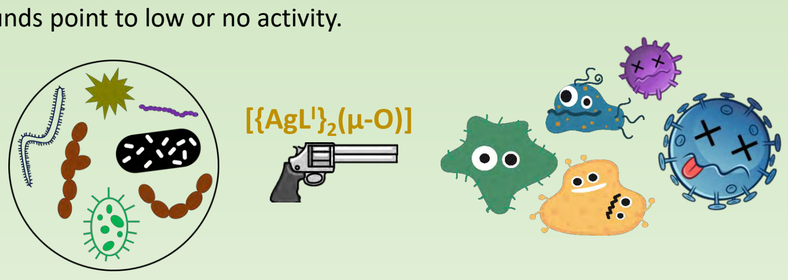

Evaluation of the antifungal activity of selected Ag (I) complexes in combination with hydroxyapatite (calcium phosphate similar to human hard tissues) showed that there is no lost of activity. Such data foresees Feasible medicinal applications (ex.protesis).

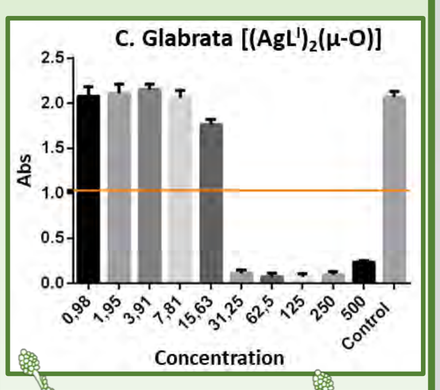

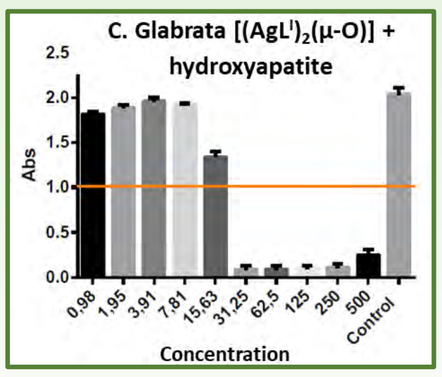

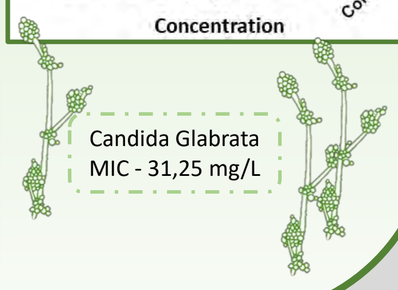

Cytotoxic activity

Selected complexes were probed through evaluation of the cytotoxic properties (IC_{50}) towards A2780 and A2780cisR cell lines.

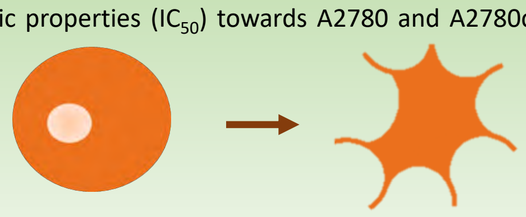

The toxicity of the complexes towards HEK 293 cell line was assessed to evaluate their toxicity towards human cells

Conclusions

- High active **antifungal and antibacterial silver complexes** were synthesized by design of the **camphor ligands**.
- The electronic and steric characteristics of the ligands are tuned through choice of the imine substituent (Y) at the camphor imine ligand. Such choice drives the biological activity towards fungi or bacteria and in some cases also combining cytotoxic activity.
- Preliminary results show that silver camphor imine complexes perform much better than the corresponding gold complexes in what concerns antimicrobial activity.
- Preliminary results show that applications in the area of medicinal materials are feasible.

Funding:

Project UID/QUI/00100/2019 Fundação para a Ciência e Tecnologia (FCT) and Grant BL-CQE/2018-013 - Fundação para a Ciência e a Tecnologia (FCT).

Collaborations:

1. Jorge Leitão (iBB-CBiol, IST)
2. Nuno Mira (iBB-CBiol IST)
3. Fernanda Marques (C2TN-BIOIN, IST)
4. Adelino Galvão (CQE-MPPM, IST)
5. Marta Alves (CQE-CSSE, IST)

References:

1. Leitão J.H., Sousa S.A., Leite S.A., Carvalho M.F.N.N. Antibiotics, 7(3) (2018) 65.
2. Cardoso J.M.S., Guerreiro S.I., Lourenço A., Alves M.M., Montemor M.F., Mira N.P, Leitão J.H., Carvalho M.F.N.N. PLOS ONE, (2017)
3. Cardoso J.M.S., Galvão A.M., Guerreiro S.I., Leitão J.H., Suarez A.C., Carvalho M.F.N.N., Dalton Trans., 45, (2016) 7114-7123.
4. Cardoso J.M.S., Correia I, Galvão A.M., Marques F., Carvalho M.F.N.N. J. Inorg. Biochem. 166 (2017) 55–63.

NEW SELECTIVE COPPER(I) COMPLEXES FOR PROSTATE CANCER CELLS

João Franco Machado[1,2,3], Fernanda Marques[3], M. Fátima M. Piedade[2,4], Maria J. Villa de Brito[1,2], M. Helena Garcia[1,2], Tânia S. Morais[1,2*]

[1] Centro de Química Estrutural, Faculdade de Ciências, Universidade de Lisboa, Portugal | [2] Departamento de Química e Bioquímica, Faculdade de Ciências, Universidade de Lisboa, Portugal | [3] Centro de Ciências e Tecnologias Nucleares, Instituto Superior Técnico, Universidade de Lisboa, Portugal | [4] Centro de Química Estrutural, Instituto Superior Técnico, Universidade de Lisboa, Portugal

E-mail: joaomachado@campus.ul.pt

INTRODUCTION

Prostate cancer is the second most common cancer in men (1.3 million new cases in 2018). Platinum-based drugs are one of the most used anticancer agents, however they show severe side effects and drug resistance.[1] **Copper complexes** are emerging as potential alternatives, as they are likely to be equally effective, less toxic, overcome platinum resistance, and be less expensive to produce.[2]

Recently, our group has been developing novel copper(I)-phosphane complexes for cancer therapy, showing **higher cytotoxicity than cisplatin** against ovarian and breast cancer cells.[3,4]

Herein, we report the synthesis, characterization and evaluation of the anticancer activity of a new family of complexes of general formula **[Cu(PP)(LL)][BF_4]**, in which PP represents several bi/monodentate phosphanes and LL different N,O-heteroaromatic ligands (Scheme 1).

STRUCTURAL CHARACTERIZATION

NMR analysis are in good agreement with the proposed structures for all the compounds. In general, upon coordination of the ligand, deshielding is observed from the ^{1}H NMR spectrum (Figure 1). No significative shift is observed for the ^{31}P resonance. Broad signals are characteristic of coordination with Cu(I).

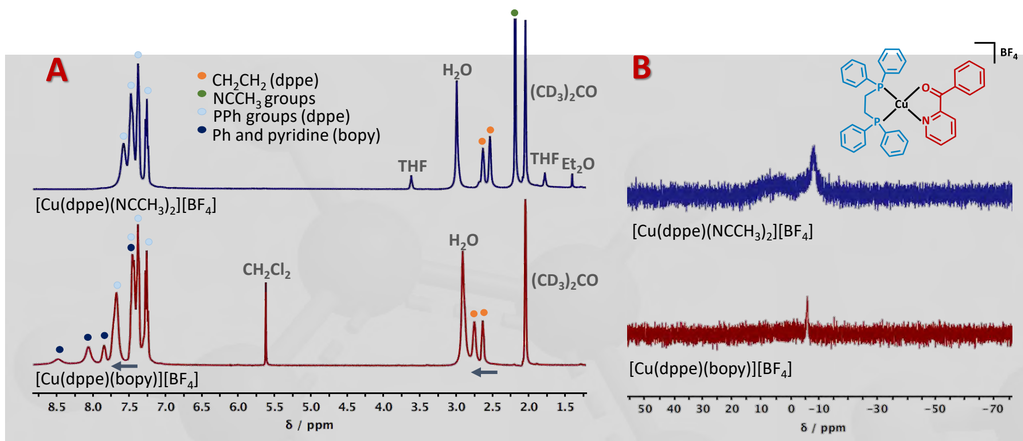

Figure 1. ^{1}H NMR (**A**) and ^{31}P{^{1}H} NMR (**B**) spectra of [Cu(dppe)(bopy)][BF_4] (red) and its precursor (blue) in acetone-d^6 (RT).

X-ray diffraction studies of **single crystals** were performed for 9 of the complexes. As example, [Cu(PPh_3)$_2$(2-ap)][BF_4] crystalized in monoclinic crystal system, space group P 21/n, with one cationic complex molecule and one BF_4^- as a counter ion in the asymmetric unit. The complex show a distorted tetrahedral coordination geometry (Figure 2).

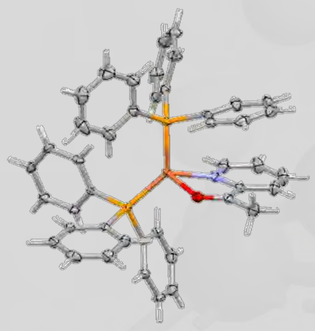

Figure 2. Molecular diagram depicting the cationic moiety of [Cu(PPh_3)$_2$(2-ap)][BF_4].

ANTI-CANCER ACTIVITY

The cytotoxicity of the complexes was evaluated by MTT assay in human LnCap **prostate cancer** and RWPE **healthy prostate** cells. All compounds revealed to be **highly active** and **selective** for cancer cells over healthy cells.

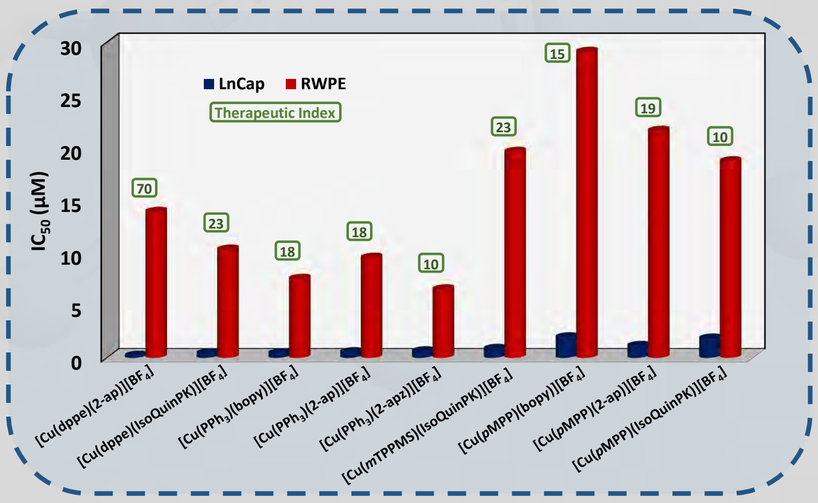

Figure 5. IC_{50} values found for the selected Cu(I) complexes in LnCap and RWPE cells (24h incubation). Therapeutic Index values are indicated in green.

SYNTHESIS

Cu(I) complexes were synthesized according to Scheme 1, with **34 to 96 %** yields.

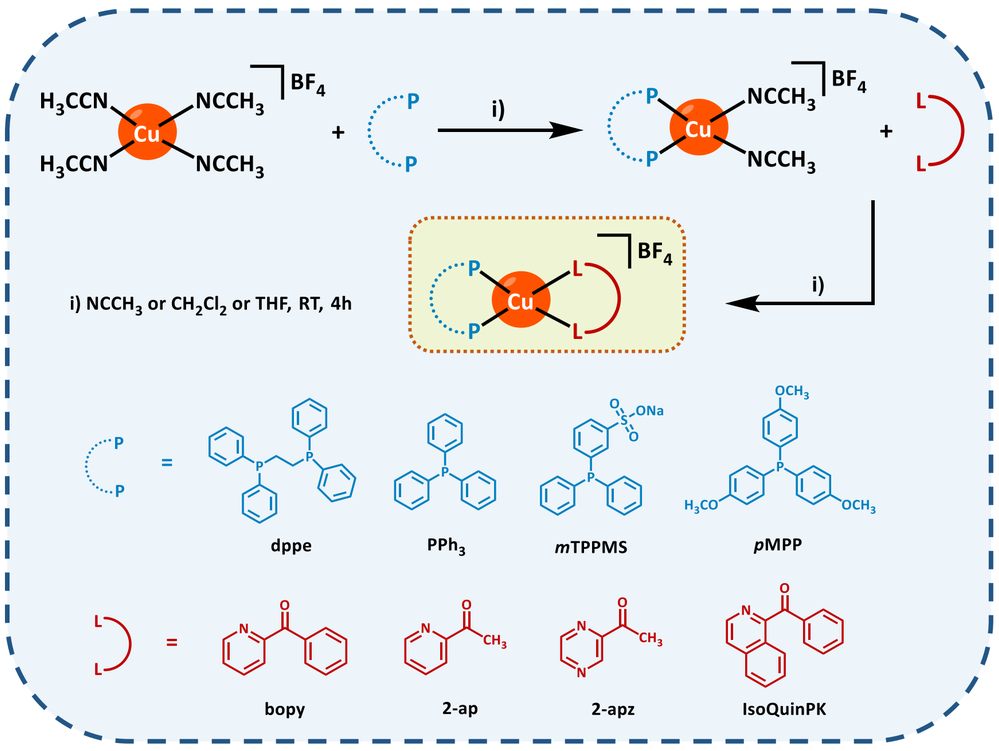

Scheme 1. Reaction scheme for the synthesis of [Cu(PP)(LL)][BF_4] complexes, where PP = bi/monodentate phosphanes (blue) and LL = N,O- heteroaromatic ligands (red).

ULTRAVIOLET-VISIBLE SPECTROSCOPIC STUDIES

The complexes show an intense absorption band in the UV region with maximum circa 240-270 nm (**π→π* transitions** of the aromatic fragments) and a second broad less intense band between 350 and 470 nm (**metal to ligand charge transfer band**).

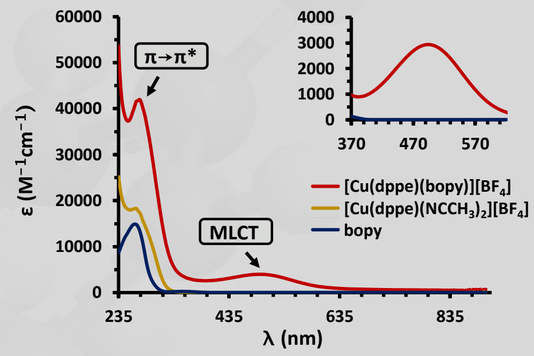

Figure 3. Electronic spectra of [Cu(dppe)(bopy)][BF_4], its precursor and free bopy in dichloromethane.

All compounds are **stable** in DMSO and DMSO/DMEM solution **over 24 hours**.

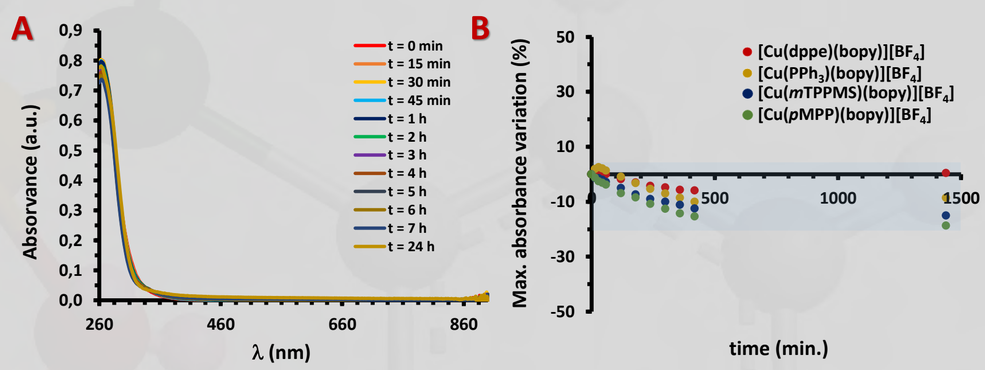

Figure 4. UV-Visible spectra of [Cu(*m*TPPMS)(bopy)][BF_4] in DMSO (2.5×10^{-5} M) recorded over 24h (**A**). Variation of the maximum absorbance in function of time (complexes concentration ranging from 2.5×10^{-5} M to 4.5×10^{-5} M in DMSO, **B**).

CONCLUSIONS

- A **new** family of **16** complexes of formula **[Cu(PP)(LL)][BF_4]** (PP = phosphanes; and LL = N,O-heteroaromatic ligands) was synthesized with high purity.
- All complexes were **structurally characterized** by elemental analysis, FT-IR, UV-Vis and multinuclear NMR techniques.
- **9** structures were determined by **single crystal X-ray diffraction** studies.
- All complexes are **stable over 24h in aqueous and organic solution**.
- The complexes showed **high activity** against **prostate cancer** cells (LnCap).
- All complexes are **selective** with therapeutic index values ranging from **10 to 70**.

04 BIOIN

Funding:

Centro de Química Estrutural is funded by Fundação para a Ciência e Tecnologia (FCT) – project UID/QUI/00100/2019.

T.S.Morais acknowledges the CEECIND 2017 Initiative for the project CEECIND/00630/2017 (acknowledging FCT, as well as POPH and FSE-European Social Fund).

J. F. Machado thanks FCT for his doctoral grant (SFRH/BD/135915/2018).

References:

[1] Oun R, Moussa YE, Wheate NJ, Dalton Trans. 19 (**2018**) 6645-6653.

[2] Santini C, Pellei M, Gandin V *et al.*, Chem. Rev. 114 (**2014**) 815-862.

[3] Lopes J, Alves D, Morais TS *et al.*, J. Inorg. Biochem. 169 (**2017**) 68-78.

[4] Morais TS, Jousseaume Y, Piedade MFM *et al.*, Dalton Trans. 47 (**2018**) 7819-7829.

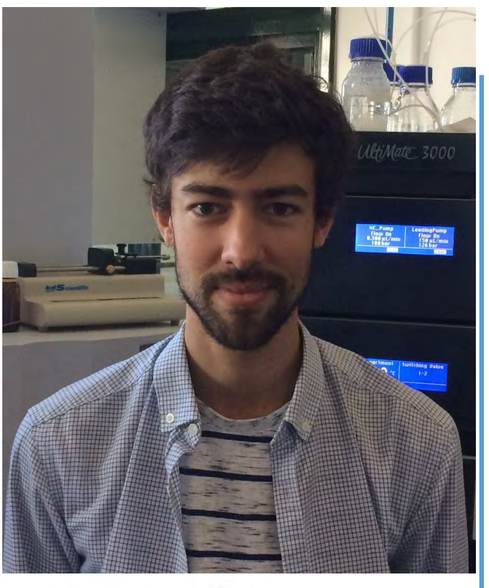

A Metabolomics-based Workflow to Identify Protein Covalent Modifications

João Nunes[1], Catarina Charneira[1], Sofia Gouveia-Fernandes[2,3], Jacinta Serpa[2,3], Judit Morello[1], Alexandra M. M. Antunes[1]

[1] *Instituto Superior Técnico, ULisboa, Centro de Química Estrutural, Lisboa, Portugal*
[2] *Faculdade de Ciências Médicas, Universidade Nova de Lisboa, Centro de Estudos de Doenças Crónicas (CEDOC), Lisboa, Portugal*
[3] *Instituto Português de Oncologia de Lisboa Francisco Gentil, Lisboa, Portugal*

CQE Química Estrutural

05 BIOMOL

FCT Fundação para a Ciência e a Tecnologia

Funding:
Centro de Química Estrutural is funded by Fundação para a Ciência e Tecnologia – project UID/QUI/00100/2019. Doctoral fellowships SFRH/BD/102846/2014 and SFRH/BD/140157/2018. RNEM-LISBOA-01-0145-FEDER-022125 postdoctoral fellowship.

Introduction

Identification of protein covalent modifications (covalent adducts) is a challenging task mainly due to the lack of data processing approaches for Adductomics studies. Despite the huge technological advances in mass spectrometry (MS) instrumentation and bioinformatics tools for proteomics studies, enabling the identification of several thousands of proteins in a single injection analysis, these methodologies have very limited success on the identification of low abundant covalent protein adducts.[1]

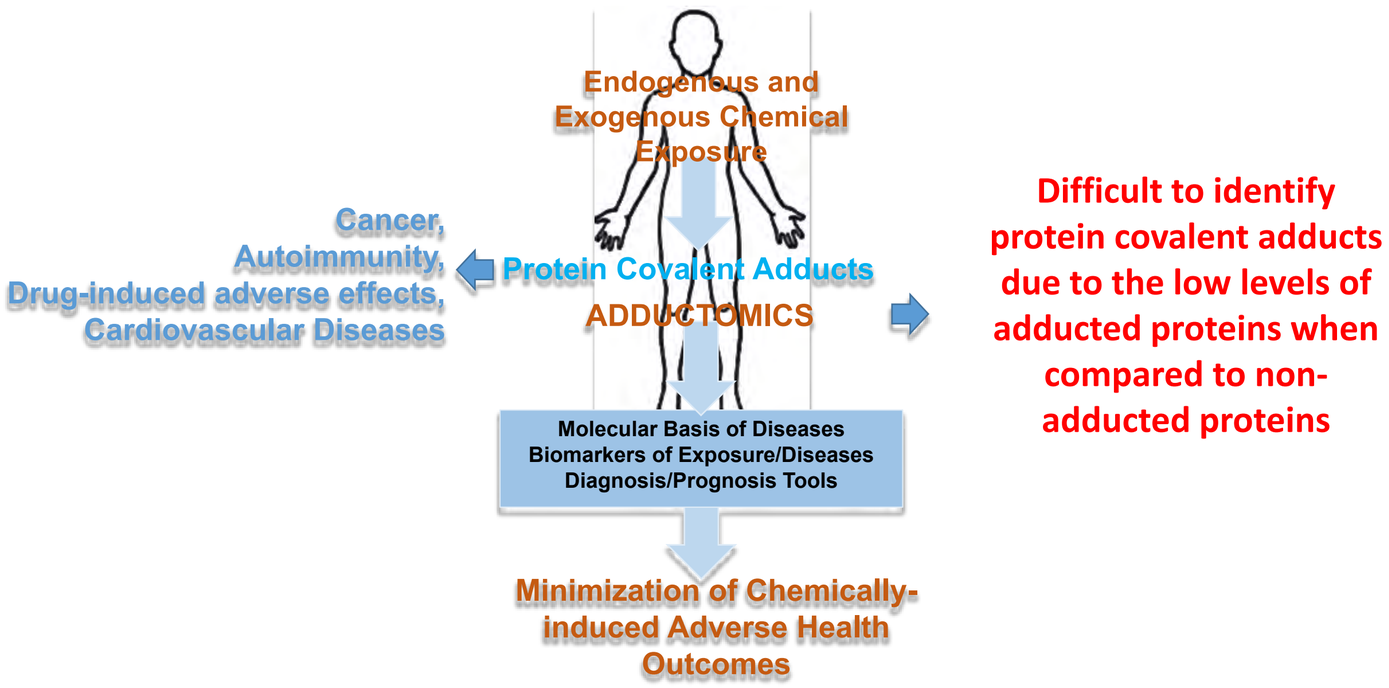

Figure 1: The key role of Adductomics towards the exposome assesment and the minimization of adverse health outcomes

Our Approach

Herein we present a novel strategy to identify protein covalent modifications inspired in metabolomics workflows that consists on LC-MS data pre-processing using the open source software MZmine followed by statistical analysis. Our workflow involves three steps: 1) data acquisition in full scan mode to maximize the sensitivity; 2) LC-MS data preprocessing followed by statistical analysis to reveal those ions (adducts) that differentiate negative samples from positive samples (non-exposed vs exposed or healthy vs disease); and 3) targeted MS/MS acquisition of the statistically significant ions for adduct identification.

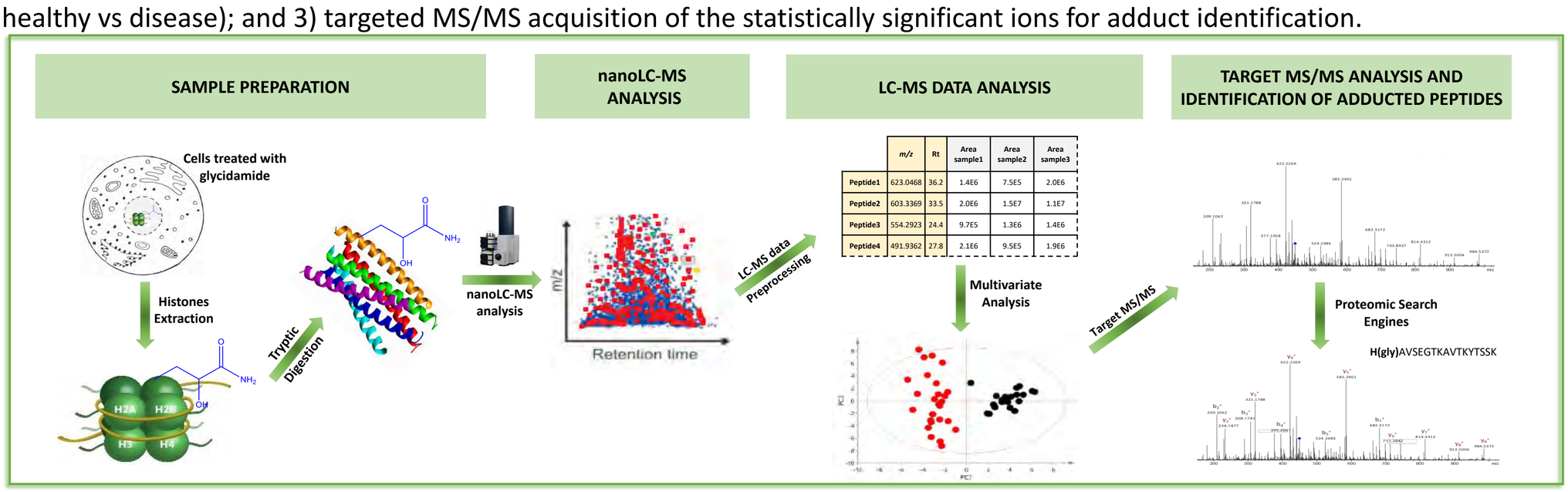

Figure 2: Workflow of our metabolomics-based approach to identify protein covalent modifications

Results

Table 1. Comparison of results obtained by our novel metabolomics-inspired strategy and the standard Adductomics strategies.

Cell Line	Glycidamide-modified peptide	*m/z* ± error (ppm) (charge)	Protein	Novel approach	GPM Fury	MaxQuant	MASCOT	MSFragger
HepG2	^{110}HAVSEGTKAVTKYTSSK^{126}	627.6670 ± -8.12 (+3)	Histone H2B					
	^{74}IAGEASRLAHYNKRSTITSR^{93}	580.3200 ± -11.03 (+4)	Histone H2B					
	^{2}TKIKADPDGPEAQAEACSGER^{22}	754.0300 ± -10.74 (+3) 565.7740 ± -10.25 (+4)	H/ACA ribonucleoprotein complex subunit 2					
THLE-2	^{110}HAVSEGTKAVTKYTSSK^{126}	627.6670 ± -8.12 (+3)	Histone H2B					
	^{110}HAVSEGTKAVTKYTSAK^{126}	467.0030 ± -7.49 (+4)	Histone H2B					
	^{74}IAGEASRLAHYNKRSTITSR^{93}	580.3200 ± -11.03 (+4)	Histone H2B					
	^{2}TKIKADPDGPEAQAEACSGER^{22}	754.0300 ± -10.74 (+3) 565.7740 ± -10.25 (+4)	H/ACA ribonucleoprotein complex subunit 2					

Using our novel metabolomics-inspired approach we were able to identify more glycidamide-modified peptides than the commonly used methodologies in proteomics studies.

Conclusions

We present a new metabolomics-inspired data processing approach for the identification of covalently-modified peptides that is fast, sensitive and allows to perform any statistical analysis. This methodology will increase the possiblity of identifying low abundant adducted peptides in biological samples and, thereby, enhancing the chances of identifying new biomarkers of exposure to carcinogens.

References:

1 - Nunes, J., Charneira, C., Morello, J., Rodrigues, J., Pereira, S.A., Antunes, A.M.M., High-Throughput. (**2019**), 8, 9.

Gamma Irradiation of Clove: Level of Trapped Radicals and Effects on Bioactive Composition

João P. Telo,[1] Elvira M. Gaspar,[2] José C. Santana,[2] Pedro M. P. Santos,[3] Abel J. S. C. Vieira[2]

[1] Centro de Química Estrutural, Instituto Superior Técnico, Lisboa, Portugal
[2] LAQV-REQUIMTE, Faculty of Science and Technology, Universidade NOVA de Lisboa, Caparica, Portugal
[3] Centro de Ciências e Tecnologias Nucleares, Instituto Superior Técnico, Bobadela, Portugal

Introduction

Food irradiation is a widely used technique for improving the safety and shelf-life of foods, including most spices. However, growing concerns by the consumers about this technique require further investigation on the effects of radiation, both on the safety of the food and on its organoleptic properties.

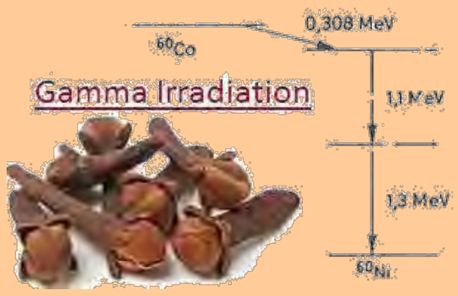

Cloves of diverse origins were submitted to different irradiation doses in a ^{60}Co source. Trapped radicals and their decay were assessed by EPR spectroscopy. The volatile bioactive composition and the clove oil were evaluated before and after irradiation GC-TOF-MS.

Results and Discussion

The central EPR line appears in most spices that were not exposed to radiation, and is due to semiquinone radicals produced by oxidation of phenolic groups in polyphenols or lignin. The weak triplet with a 30 G coupling constant arises from a C(5) carbon-centered cellulose radical, and these are the lines used to prove irradiation. These radicals decay fast and 120 days after irradiation they are practically undetectable by EPR.

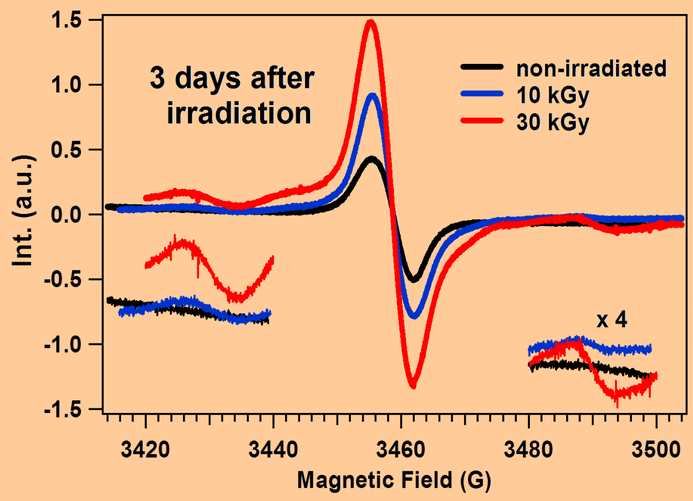

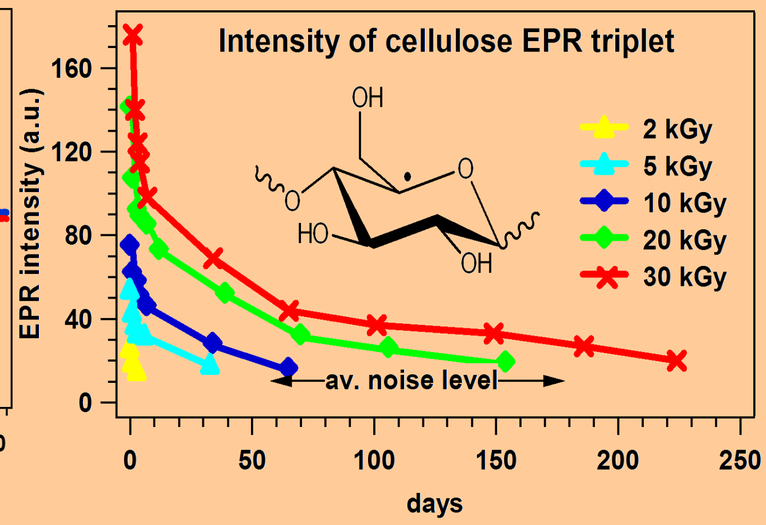

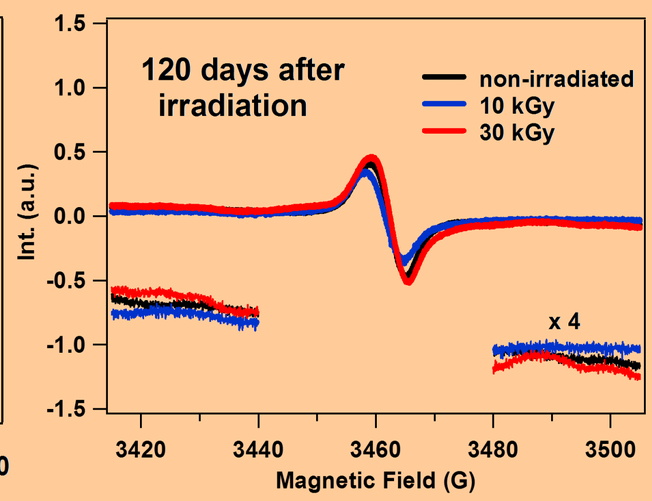

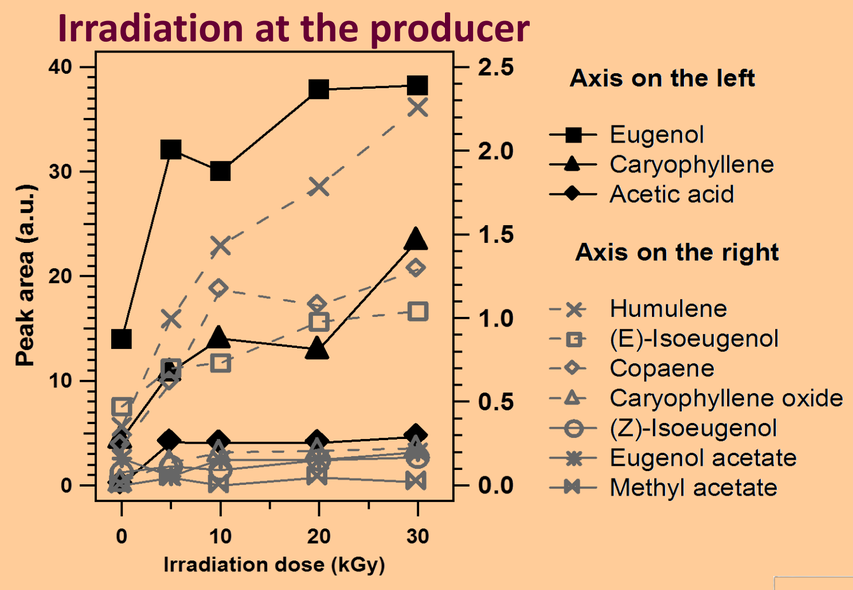

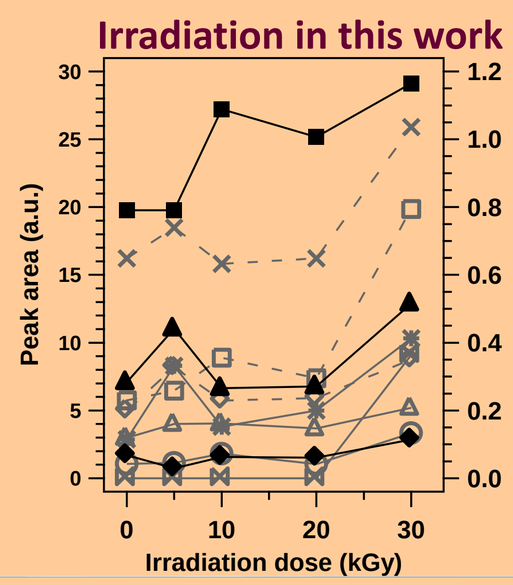

The gas chromatography results show an increase of the amount of volatiles collected after irradiation due to the break of cellulose cells. This means that irradiated clove has more aroma than non-irradiated. No new compound was detected after irradiation.

Change of the volatile and liquid (in the oil) composition relative to eugenol (100 in all) with the dose of irradiation:

1) caryophyllene contributes more to the clove aroma than its content in the oil would predict.
2) decrease of caryophyllene and an increase in caryophyllene oxide with the irradiation, although the latter is still a minor component.

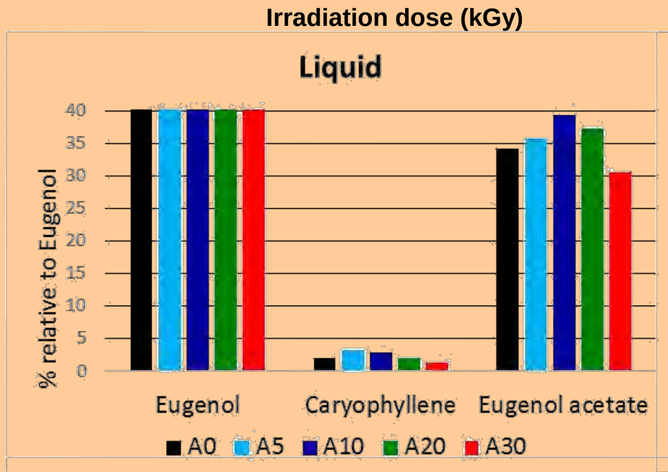

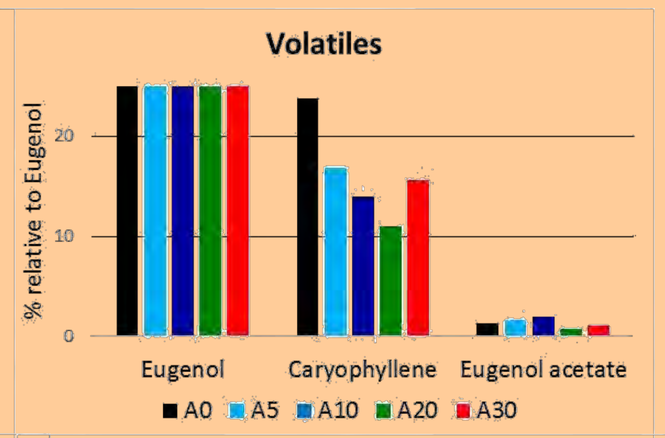

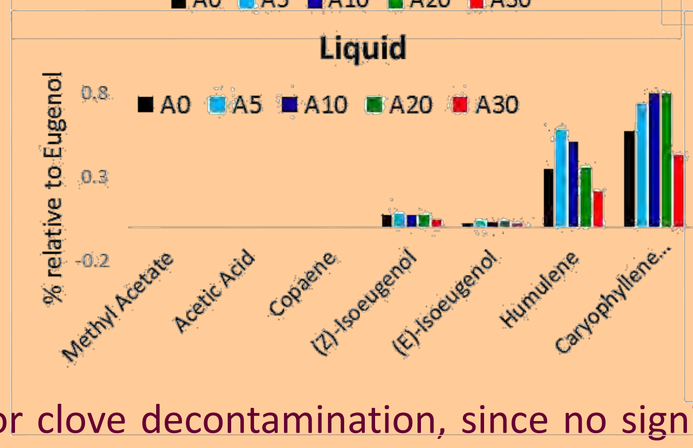

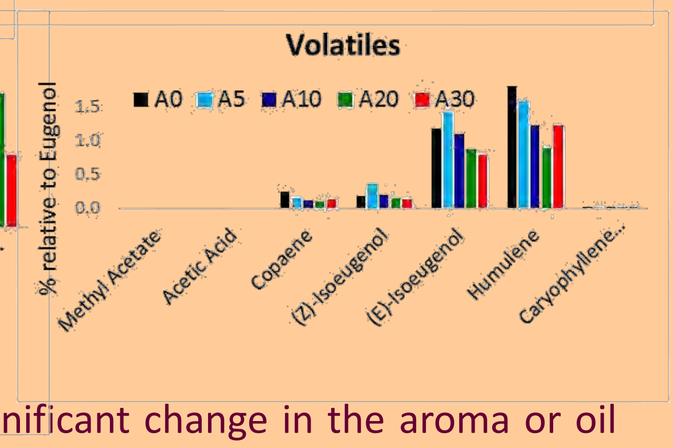

Conclusions

Gamma irradiation is a clean technique for clove decontamination, since no significant change in the aroma or oil compositions was found and low levels of trapped paramagnetic species, after the initial decay period, were detected upon irradiation. Furthermore, irradiation doses higher than the legally allowed are equally safe.

05 BIOMOL

Funding:
Centro de Química Estrutural is funded by Fundação para a Ciência e Tecnologia – project UID/QUI/00100/2019. PMP Santos acknowledges the FCT support through the UID/Multi/04349/2013 project. AJSC Vieira acknowledges COST Action CM1201.

References:
E. M. Gaspar, J. C. Santana, P. M. P. Santos, J. P. Telo, A. J. S. C. Vieira, *J. Sci. Food Agric.*, 99, 1668–1674 (2019)

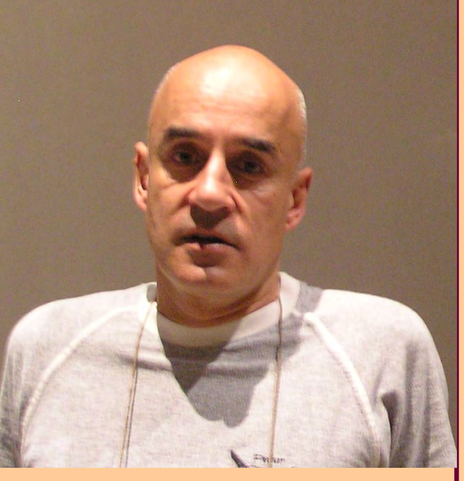

Mixed valence radical anions of 4,4”-dinitro-p-terphenyl and its aza-derivatives as models for electronic communication in conducting polymers

João P. Telo, M. Fernanda N. N. Carvalho

Centro de Química Estrutural, Instituto Superior Técnico, Lisboa, Portugal.

Introduction

Poly(*p*-phenylene) (**PPP**) is an aromatic polymer that is interesting in various areas of material science, such as conducting materials, molecular composites, nonlinear optics, or electroluminescence.[1,2]

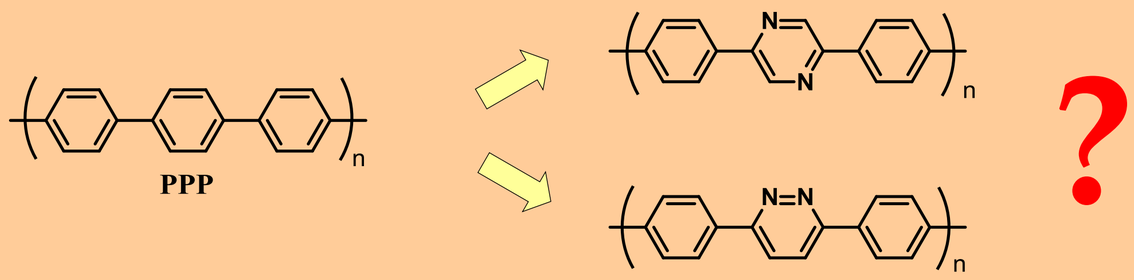

The Mixed Valence radical anions of **2**, **3** and **4** were prepared as models for electron conductance in poly(*p*-phenylene) polymers, to study how the increasing electron-accepting bridges influence their electronic properties.

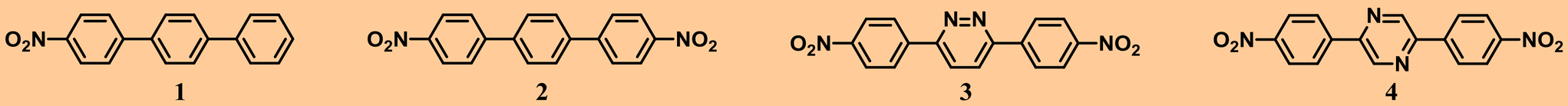

Results and Discussion

Optical spectra of **2** (0: neutral) upon reduction with Na (Hg) to the radical anion (-1) and dianion (-2) in NMP. (**Inset**: relative concentrations of the three species in equilibrium). Due to disproportionation, the NIR wide band of the radical anion is superimposed with the dianion. To have the NIR spectra of the “pure” radical anion, a fraction of the dianion spectra was subtracted from the maximum of radical anion.

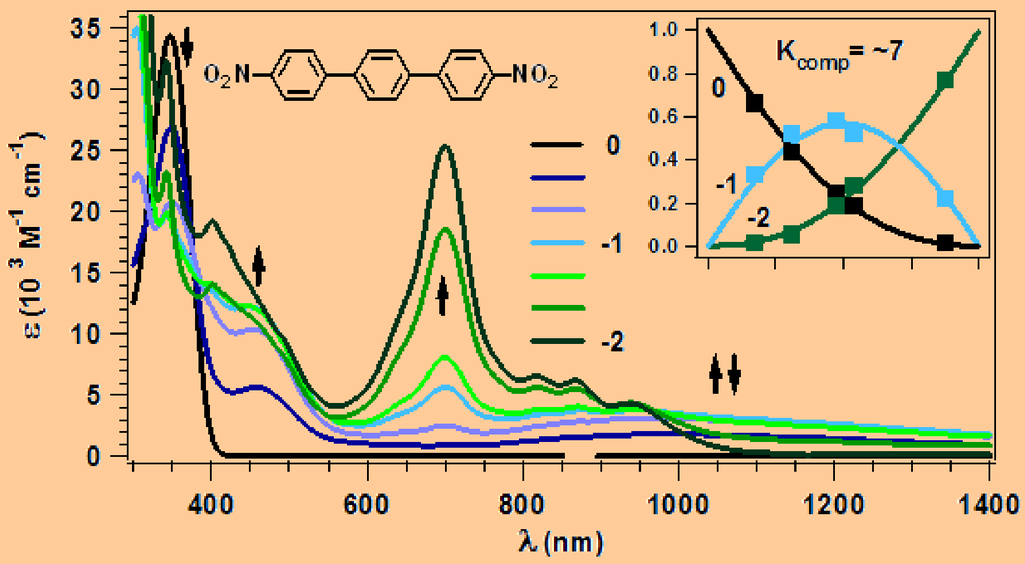

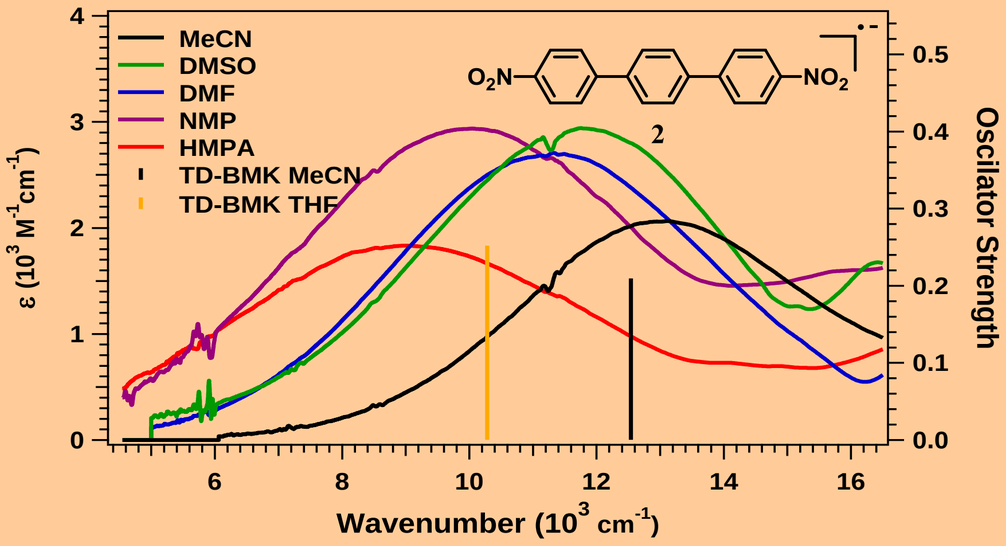

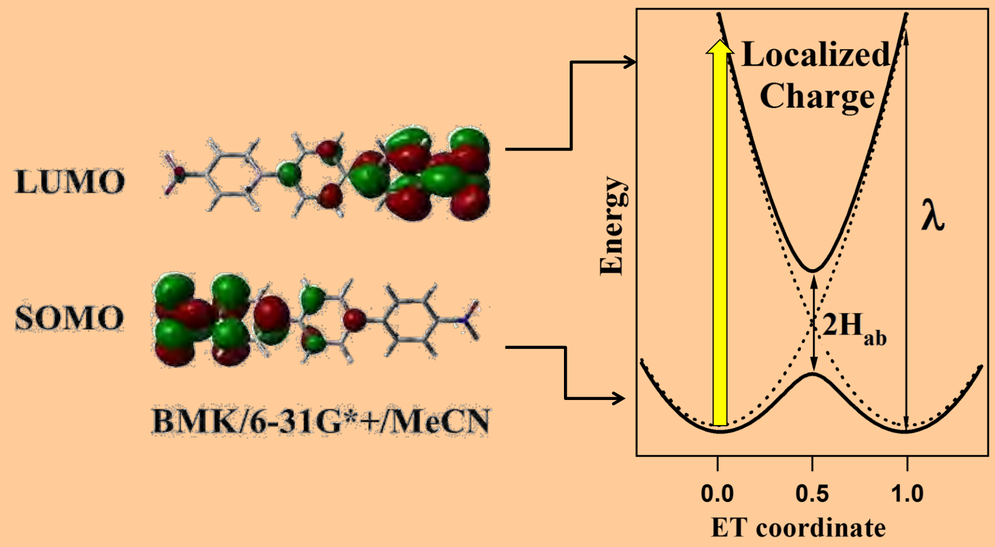

Marcus-Hush analysis of the charge-transfer band allows the calculation of the reorganization energy (λ) and the electronic coupling (H_{ab}), the latter being a measure of the conductivity of the bridge. Contrary to **2**, radical anion of **4** has a delocalized charge in THF, and so a smaller H_{ab}. **3** has an intermediate behavior (not shown).

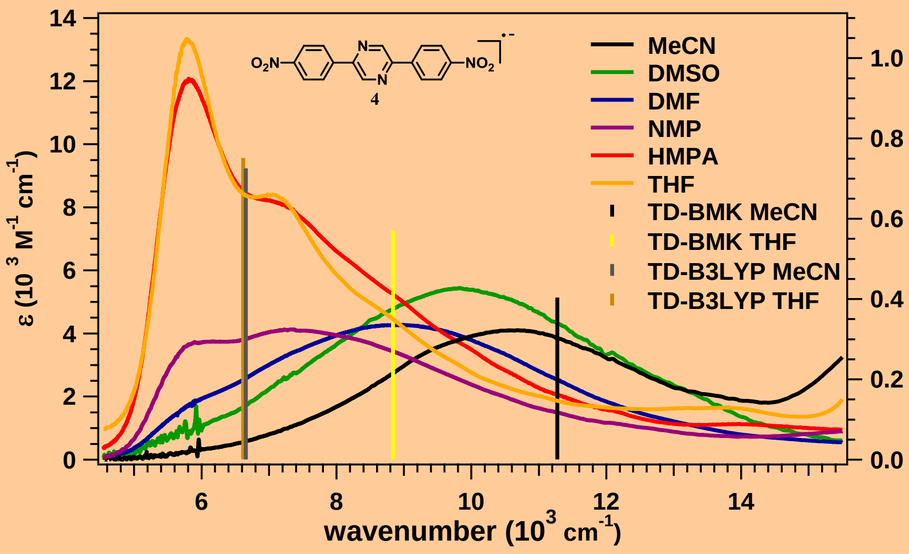

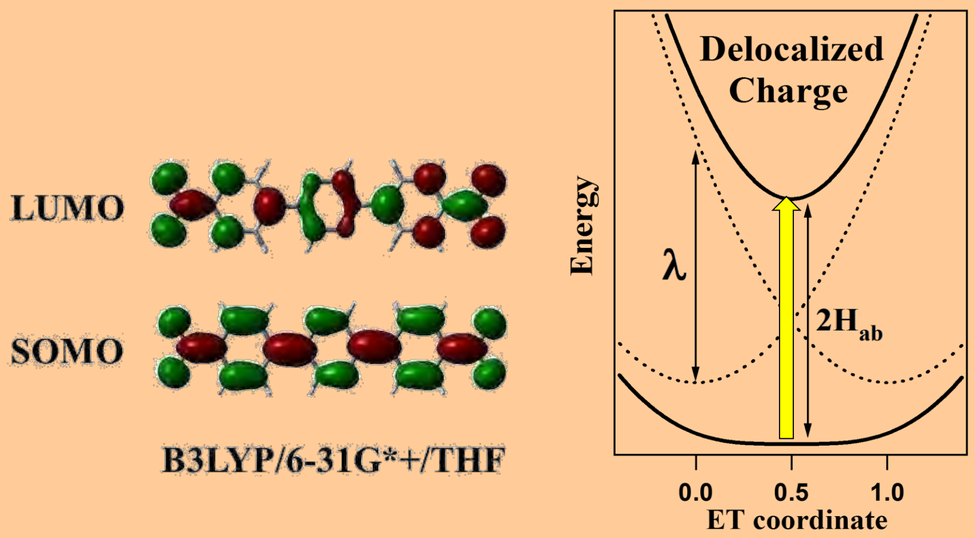

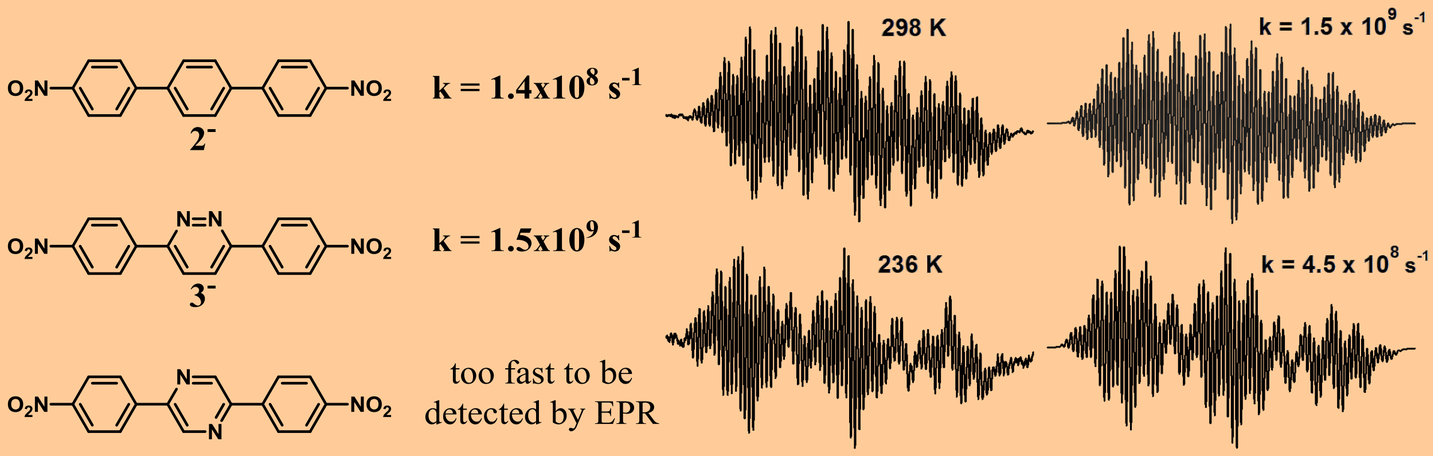

Conclusions

Rate of electron transfer (by EPR) and electronic coupling H_{ab} in the order **2** < **3** < **4** .

Inclusion of pyrazine or pyridazine units in poly-*p*-phenylene polymers may result in enhanced electrical properties and better condutivity due to a lower band gap and increased planarity

05 BIOMOL

Funding:

Centro de Química Estrutural is funded by Fundação para a Ciência e Tecnologia – project UID/QUI/00100/2019.

References:

1 V. Cimrová *et al.*, *Adv. Mater.* 8 (**1996**) 146-149.

2 G. Grem *et al.*, *Adv. Mater.* 4 (**1992**) 36-37.

3 J.P Telo, M.F.N.N. Carvalho, *J. Photochem. Photobiol. A: Chem.*, 376 (**2019**) , 140-145.

Gas-Phase Ion Chemistry Studies with *p*-, *d*- and *f*-Elements

Joaquim Marçalo,[1] Bernardo Monteiro,[1] João P. Leal,[1] Joaquim B. Branco,[1] José M. Carretas,[1] Leonor Maria,[1] Sandrina Oliveira[1]

[1] Centro de Química Estrutural & Centro de Ciências e Tecnologias Nucleares, Instituto Superior Técnico, Universidade de Lisboa, Bobadela

Introduction

For some years, we have been using FTICR and QIT mass spectrometry to examine the gas-phase ion chemistry of the lanthanides from La to Lu (except Pm), the actinides from Th to Cm, and several *d* transition elements.[1] We revealed new species, determined thermodynamic properties of neutral and ionic molecules, and, in the case of the actinides, probed the role of 5*f* electrons in bonding and the issue of covalence. Recently, we have also focused our attention on the chemistry of the noble gases,[2] particularly of Kr and Xe as a prelude to future experiments with highly radioactive and scarcely studied Rn.

Experimental details

ESI-QIT

The QIT-MS experiments were performed using a Bruker HCT equipped with an ESI interface and with MS^n collision induced dissociation (CID) capability. Stock solutions of $M(NO_3)_3(H_2O)_x$ (M = Sc, Y, Ln), $Th(NO_3)_4(H_2O)_x$ and $UO_2(NO_3)_2(H_2O)_x$ in water were diluted with ethanol to prepare 10^{-4} M solutions for ESI. The $Cu(CH_3COO)_2.H_2O$ solution was prepared in CH_3OH. The metal solutions were directly injected into the ESI source using a syringe pump. The helium buffer gas pressure in the trap was constant at $\sim 10^{-4}$ Torr. The background air and water pressure in the ion trap is estimated to be on the order of 10^{-6} Torr. Neutral reagents were introduced into the mass spectrometer through a leak valve to pressures on the order of 10^{-5} Torr. The MS^n capabilities of the QIT were used for isolation of ions with a specific *m/z* and subsequent CID of mass-selected ions, using helium buffer gas as the collision partner.

EI-FTICR

The FTICR-MS experiments were performed in an Extrel/Finnigan FTMS 2001-DT 3 Tesla spectrometer with an "internal" source design. The instrument was controlled by a system developed by BridgePoint (Portugal), based on National Instruments units and LabVIEW software. The reagent gases were introduced in the spectrometer through leak valves to pressures on the order of 10^{-7} Torr. The studied noble gases were Kr and Xe and as oxidizing and fluorinating agents we used N_2O and SF_6, respectively. The reagent ions were produced by electron ionization (EI) and mass spectra were acquired at various reaction time delays.

Results and discussion

d- and *f*-Elements — ESI-QIT Experiments

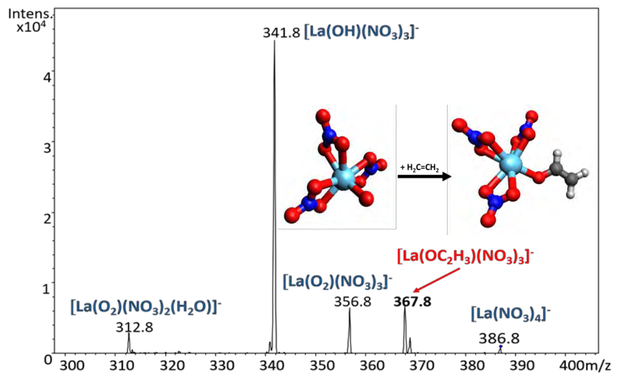

Fig. 1 – Mass spectrum showing activation of ethene by $[LaO(NO_3)_3]^-$ during CID of $[La(NO_3)_4]^-$.

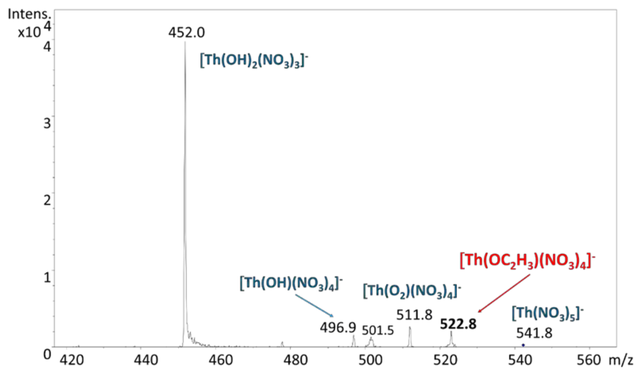

Fig. 2 – Mass spectrum showing activation of ethene by $[ThO(NO_3)_4]^-$ during CID of $[Th(NO_3)_5]^-$.

CID of $[M(NO_3)_4]^-$ gave rise to oxide nitrate anions, $[MO(NO_3)_3]^-$, that result from NO_2 elimination. CID in the presence of ethene (Fig 1), ethane and benzene showed the formation of $[M(OR)(NO_3)_3]^-$. These C-H activation reactions were also observed for $[ThO(NO_3)_4]^-$ anions (Fig. 2), which similarly to the case of the REs, are formed by CID of $[Th(NO_3)_5]^-$. Other reactive oxide nitrate anions can be obtained by nitrate CID, including for uranyl by starting with the precursor anion $[UO_2(NO_3)_3]^-$.

p- and *d*-Elements — ESI-QIT Experiments

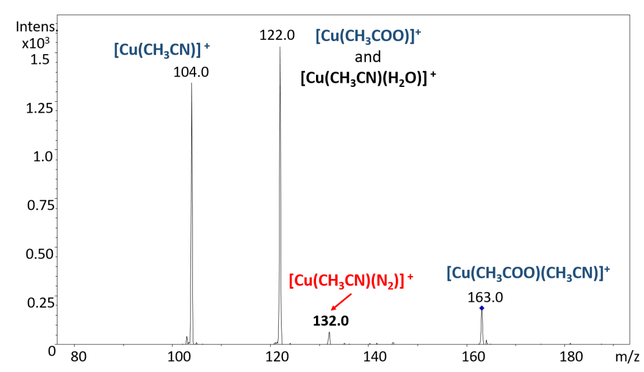

Fig. 3 : Mass spectrum showing coordination of dinitrogen to $[Cu(CH_3CN)]^+$ during CID of $[Cu(CH_3COO)(CH_3CN)]^+$.

CID of $[Cu(CH_3COO)(CH_3CN)]^+$ (Fig 3) showed the formation of $[Cu(CH_3CN)]^+$, which reacted with neutral N_2 present in the ion trap instigating the formation of $[Cu(CH_3CN)(N_2)]^+$. This coordination of a very soft ligand to Cu(I) encouraged some preliminary studies of potential coordination of noble gases (Kr and Xe) to this *d*-transition metal but no satisfactory results were obtained until now.

p-Elements — EI-FTICR Experiments

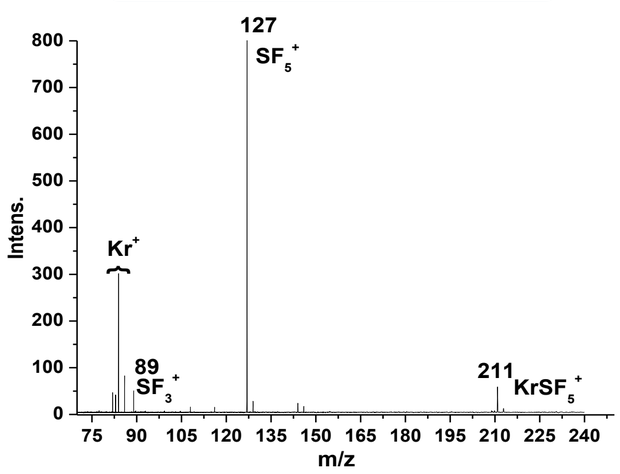

Fig. 4 – Mass spectrum of the reaction of Kr^+ with the fluorinating agent SF_6 .

The reaction of Kr^+ with SF_6 gave rise to the formation of SF_5^+ as well as to a $KrSF_5^+$ species at *m/z* 211 (Fig. 4). The origin of this species was confirmed by reacting isolated SF_5^+ with neutral Kr up to 5 s, with no observation of $KrSF_5^+$. These reactions were not observed with Xe^+, as shown in Fig. 5.

In the reaction of Kr^+ with N_2O only electron transfer to yield N_2O^+ was observed, while for Xe^+ no reaction occurred.

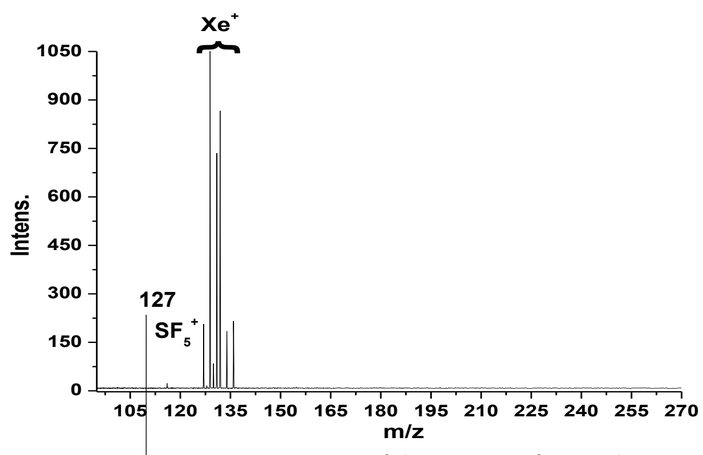

Fig. 5 – Mass spectrum of the reaction of Xe^+ with the fluorinating agent SF_6 .

Concluding remarks

We obtained experimental evidence that highly reactive rare earth and actinide oxide nitrate anions are capable of activating hydrocarbons in the gas phase. These ongoing experimental studies bear interest in the long-standing search for systems that are capable of activating methane.[3]

For the reactions involving the noble gases, evidence was obtained for the formation of an interesting $KrSF_5^+$ species. This result indicates that new gas-phase chemistry for the noble gases, including Rn, can be expected using these MS techniques.

CQE Química Estrutural

IOARC

Funding:

Centro de Química Estrutural is funded by Fundação para a Ciência e Tecnologia – project UID/QUI/00100/2019. This work was supported by FCT projects PTDC/QEQ-QFI/6430/2014, PTDC/QUI-QFI/31896/2017 and UID/Multi/04349/2019, and by RNEM – Portuguese Mass Spectrometry Network, ref. LISBOA-01-0145-FEDER-022125, supported by FCT and the Lisboa Regional Operational Programme (Lisboa2020), under the PT2020 Partnership Agreement, through the European Regional Development Fund (ERDF).

References:

1. Marçalo, J., Gibson, J. K., Gas-Phase Ion Chemistry of Rare Earths and Actinides, in *Handbook on the Physics and Chemistry of Rare Earths (Including Actinides)*, Bünzli, J.-C. G., Pecharsky, V. K., Eds., Elsevier, Amsterdam, 2014, Vol. 45, Ch. 263, pp. 1–110.
2. Grandinetti, F., *Noble Gas Chemistry - Structure, Bonding, and Gas-Phase Chemistry*, Wiley-VCH, Weinheim, 2018.
3. Schwarz, H., Shaik, S., Li, J., *J. Am. Chem. Soc.* 2017, 139, 17201.

FCT Fundação para a Ciência e a Tecnologia

RARE EARTH RECOVERY AND VALORIZATION PROTECTION OF ENVIRONMENT

José Carretas[1,2], Adelaide Cruz[1,2], Beatriz Bento[1,2], Bernardo Monteiro[1,2], Catarina Galinha[2], Isabel Paiva[2], João P. Leal[1,2], Joaquim Marçalo[1,2], Leonor Maria[1,2], M. Fátima Araújo[2], Susana S. Gomes[2]

[1] Centro de Química Estrutural, Instituto Superior Técnico, Universidade de Lisboa, Bobadela

[2] Centro de Ciências e Tecnologias Nucleares, Instituto Superior Técnico, Universidade de Lisboa, Bobadela

CQE Química Estrutural

02 IOARC

Funding:

— FCT projects UID/QUI/00100/2019, UID/MULTI/04349/2019, ENVIREE (ERA-MIN/0002/2014), and REEuse (PTDC/QEQ-EPR/1249/2014);

— PT2020 project RecValTR (03/SI/2017-I&DT Empresarial project in co-promotion nº 33576);

— RNEM – Portuguese Mass Spectrometry Network, ref. LISBOA-01-0145-FEDER-022125, supported by FCT and the Lisboa Regional Operational Programme (Lisboa2020), under the PT2020 Partnership Agreement, through the European Regional Development Fund.

FCT Fundação para a Ciência e a Tecnologia

Rare Earth Elements (REEs; lanthanides (Ln), scandium and yttrium) have become an important raw material in the industry, playing an essential role in modern electronic technologies, industrial and medical products and innovative environmental technologies. REEs are considered as being highly relevant for societal needs but there exists a significant risk of supply for actual demand. Therefore, the development of selective, efficient, economical and environmentally friendly separation processes of REEs from different materials is under intense development.(1) In our current work, ionic liquids (ILs) with only CHON elements in their composition, both already existent or newly synthesized, are being used for separation of REEs from other metals, as an alternative to more traditional methods.(2)

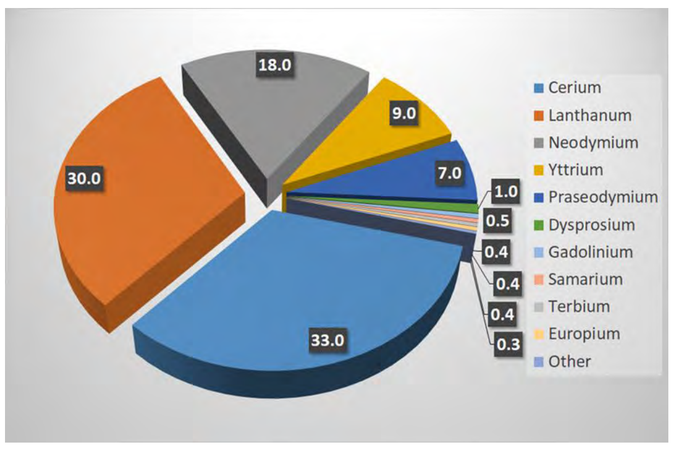

Fig 1 – Worldwide end use by element.

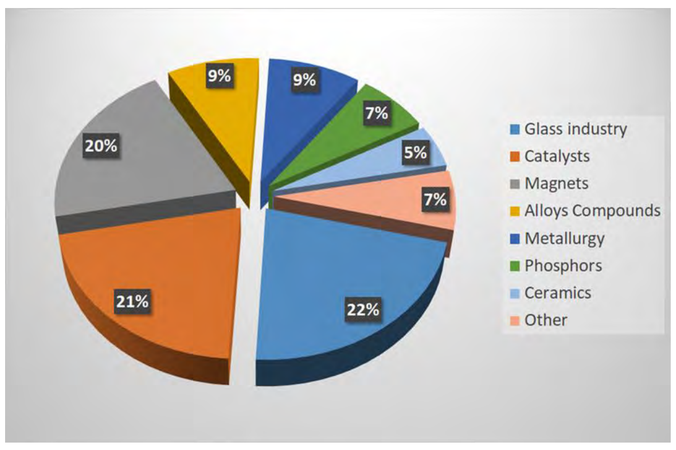

Fig 2 – Applications of REEs.

The experiments involved the combination of aqueous solutions of several lanthanides (Ln) in acidic media, at different pHs, with toluene solutions of ILs, in various molar ratios IL:metal and several extraction times. Metal concentrations in the aqueous phases, before and after extraction, were assessed by ICP-MS.

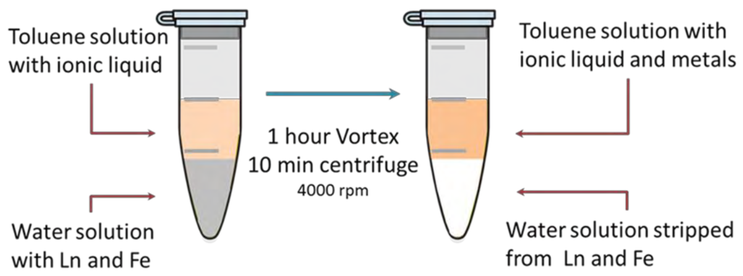

Fig 3 – Scheme of the extraction process.

Tetraoctylammonium oleate (IL1)(3), 1-butyl-3-methylimidazolium-di(2-ethylhexyl)-oxamate (IL2)(4), and the new tetraoctylammonium dioctyldiglycolamate (IL3) and tetraoctylammonium di(2-ethylhexyl)-oxamate (IL4) were the ILs under investigation. IL1 and IL4 displayed a significant differentiation between lanthanides and are adequate to selectively extract Ln among them. Results for IL1 are presented in Fig 4. In certain conditions, IL2 was able to separate Ln from other metals, as Fe(III) was partially extracted while Ln were not (Fig 5). Work is in progress for optimizing a selective extraction of REEs in the presence of other metals and an effective separation along the lanthanide series.

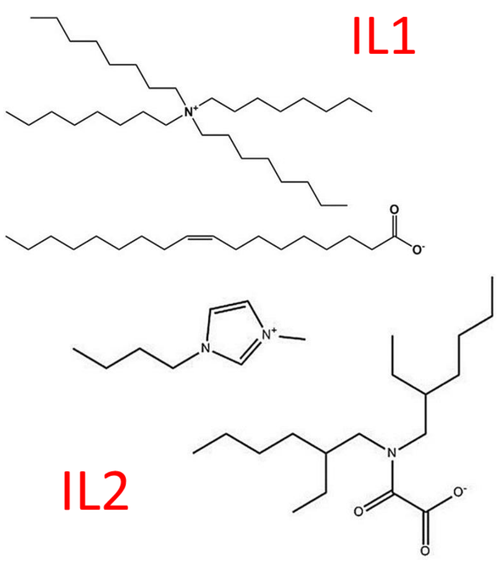

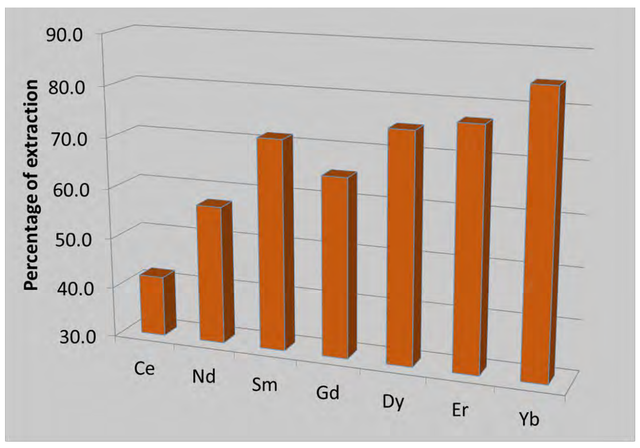

Fig 4 – Extraction with IL1.

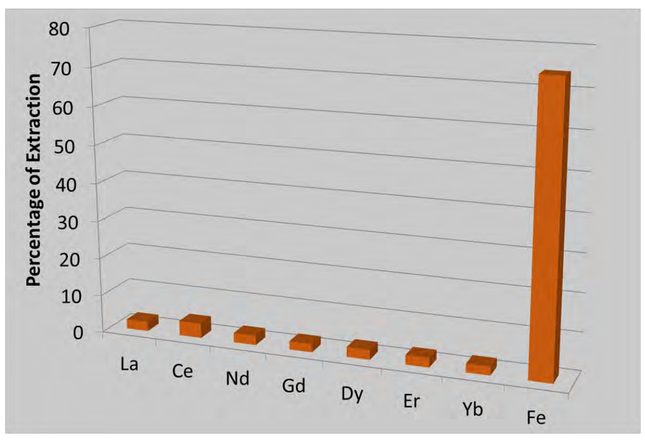

Fig 5 – Extraction with IL2.

References:

[1] Binnemans K, Jones PT, Blanpain B, Gerven TV, Yang Y, Walton A, Buchert M (2013) *J. Clean. Prod.* 51, 1-22.

[2] Makanyire T, Sanchez-Segado S, Jha A (2016) *Adv. Manuf.* 4, 33–46.

[3] Parmentier D, Metz SJ, Kroon MC (2013) *Green Chem.* 15, 205-209.

[4] Braam A, PhD Thesis, Philipps-Universitat Marburg, 2015.

Non-iridescent tunable spherical colloidal photonic pigments

Laurinda R. P. Areias, José Paulo S. Farinha

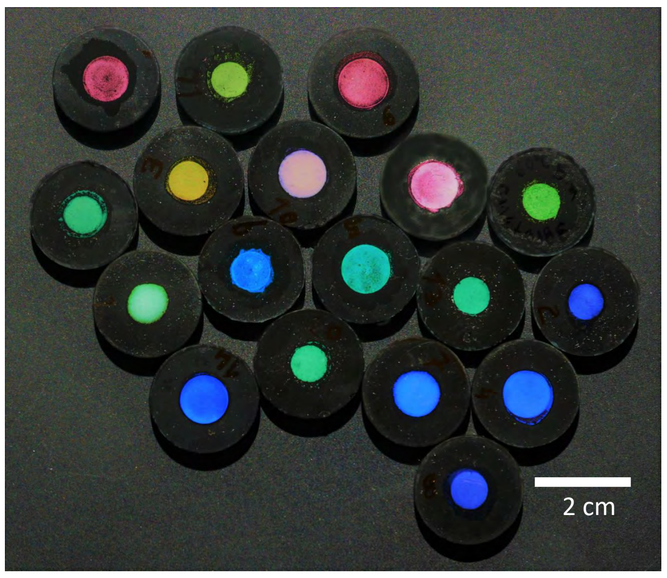

Overview

Synthetic colloidal photonic crystals consist of periodically arranged nanoparticles originating repeating regions of low and high dielectric constants that can be used to control the propagation of light. Their shining structural coloration arises from the modulation of electromagnetic waves by means of Bragg reflection from photonic band gaps. They can be used as waveguides in optoelectronic and photovoltaic applications, and as sensors or in structural color.

Experimental details

Colloidal building blocks

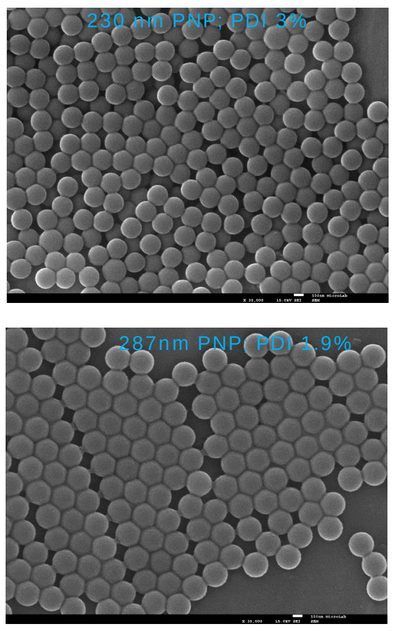

Soft- lithography

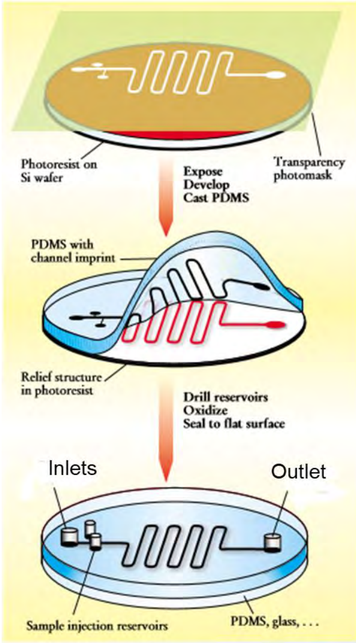

Microfluidic W/O emulsification followed by PNP assembly

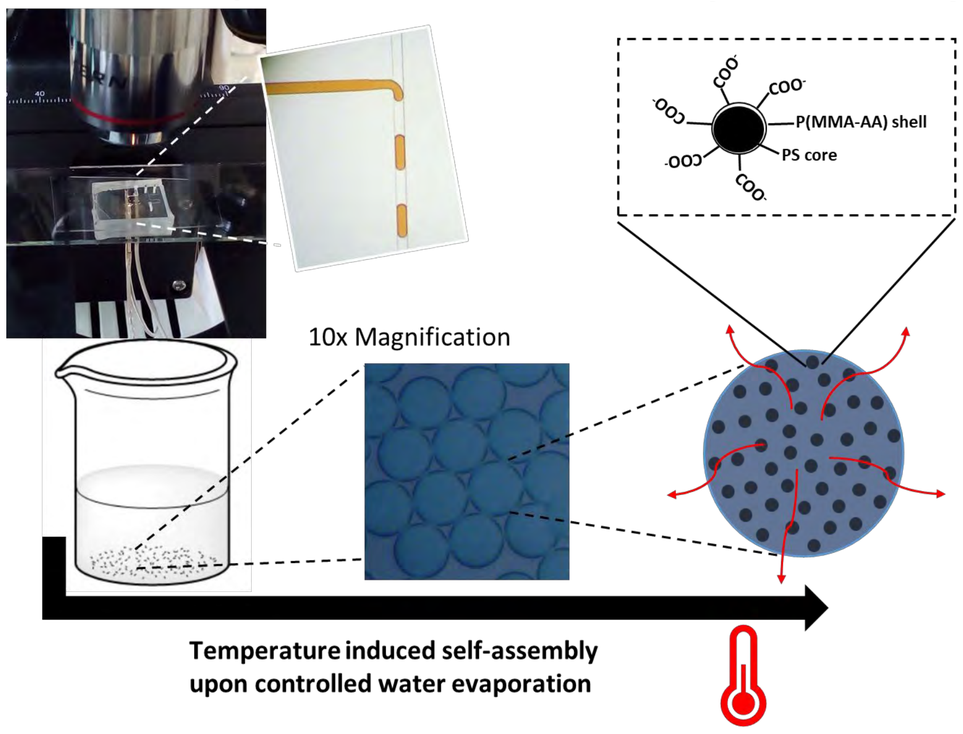

Optical characterization of spherical photonic pigments

FCC packing of PNP

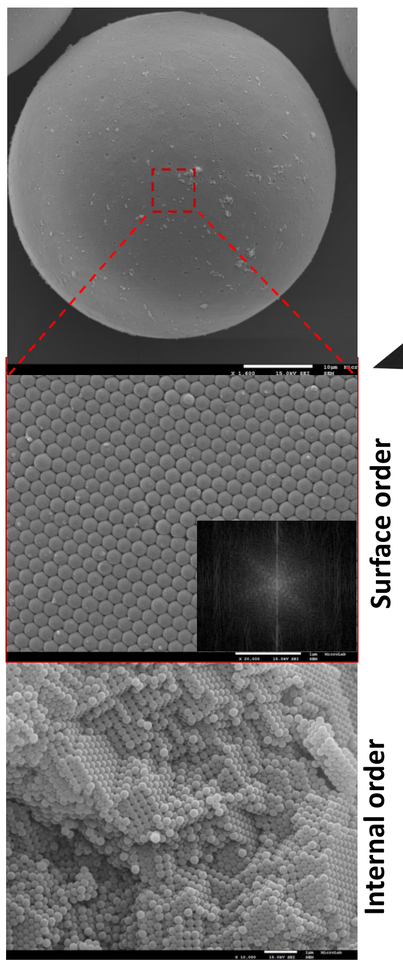

Angle-resolved reflectance measurements

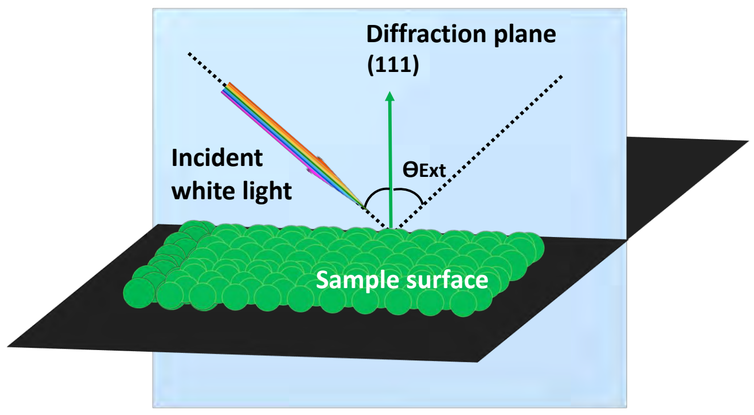

Non-iridescent photonic pigments

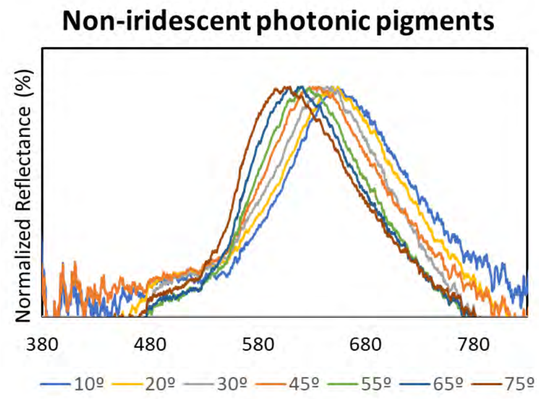

No angular dependence of photonic pigments

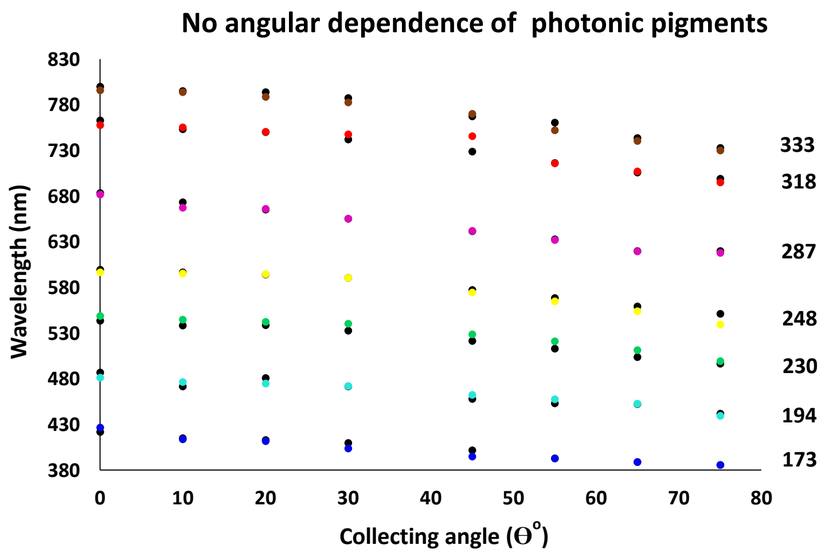

$$\lambda = \left(\frac{8}{3}\right)^{\frac{1}{2}} dp\left(np^2 0.74 + nA^2 0.26\right)^{\frac{1}{2}}$$

Vibrant and bright structural color

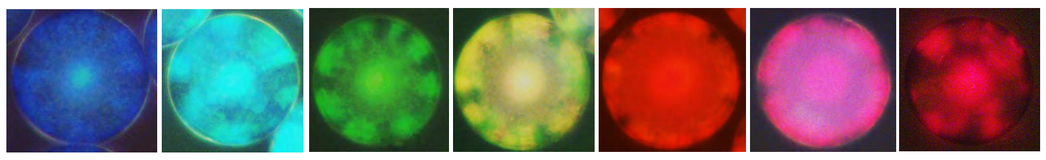

XY Coordenates in CIE 1931 Color map

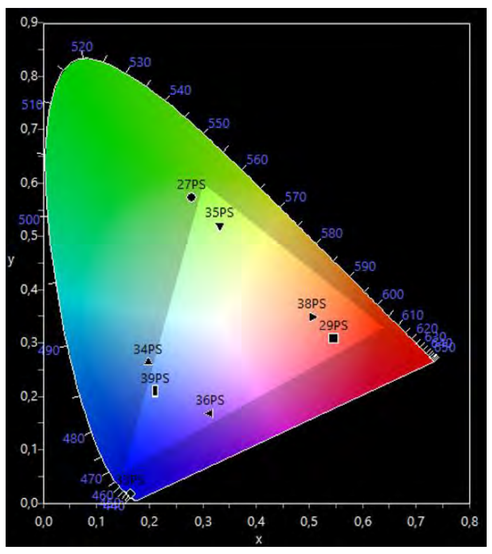

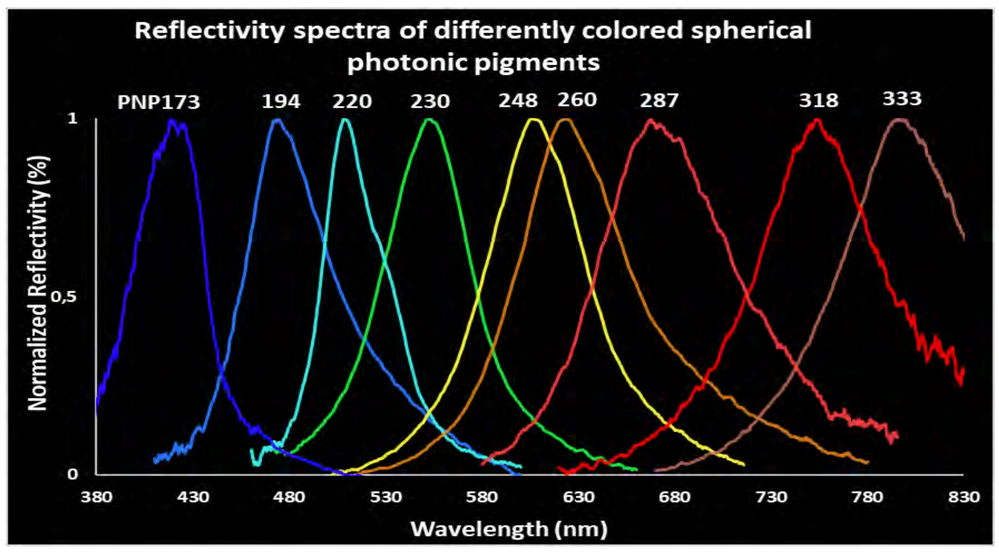

Conclusions

- Microfluidics yields highly monodispersed and homogeneous spherical photonic pigments;
- Spherical confinement breaks long range-order originating non-iridescent structural color;
- Vibrant and bright structural color from photonic pigments obtained using 170 - 333 nm diameter PNP, covering the entire visible light range

08 MPPM

Funding:
Centro de Química Estrutural is funded by Fundação para a Ciência e Tecnologia – project UID/QUI/00100/2019.
PhD grant: PD/BD/113533/2015;
FCT and COMPETE (FEDER) within projects UID/NAN/50024/2013 and PTDC/CTM-POL/3698/2014.

References:

J. Rep. Prog. Phys. 71, (2008) 076401;
Eur. Polym. Jour. 113, (2019) 349-356;
Adv. Mater. 25, (2013) 5314–5320.

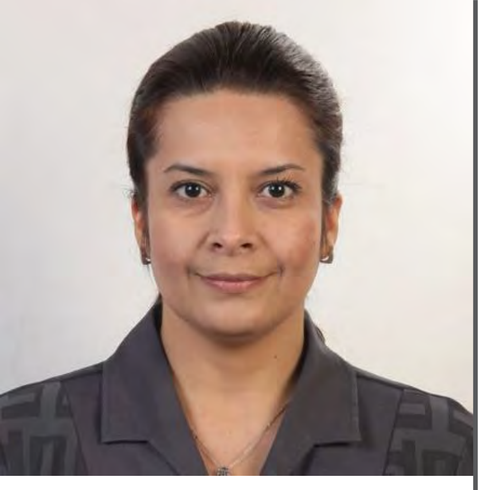

Novel Corrosion Inhibition Strategy for Mild Steel

M. Attaei[1*a], L. M. Calado[1*b], Y. Morozov[1], A. C. Marques[2], F. M. Montemor[1]

[1]CQE, Instituto Superior Técnico, Universidade de Lisboa, Av. Rovisco Pais 1, 1049-001 Lisbon, Portugal
[2]CERENA, Instituto Superior Técnico, Universidade de Lisboa, Av. Rovisco Pais 1, 1049-001 Lisbon, Portugal

*These authors contributed equally to this work
a) mahboobehattaei@tecnico.ulisboa.pt
b) leniacalado@tecnico.ulisboa.pt

Abstract

Efficient corrosion protection strategies are of great importance for most industries today, especially smart self-healing coating systems. In this work, microcapsules containing isocyanate-based polymerizable agent in their core were used in combination with cerium-based pH-sensitive corrosion inhibitor. The synergistic effect of both these additives was investigated. The barrier properties were studied using Electrochemical Impedance Spectroscopy (EIS). To assess the self-healing potential, Localized Electrochemical Impedance Spectroscopy (LEIS) was used. Results showed improved protection of the underlying mild steel substrate when the additive-modified coating system was used.

Experimental

EIS was performed during sample immersion in 0.05 M NaCl, using SCE as reference electrode. LEIS measurements were performed at 10 Hz, over artificial defect, during immersion in 0.005 M NaCl.

Results

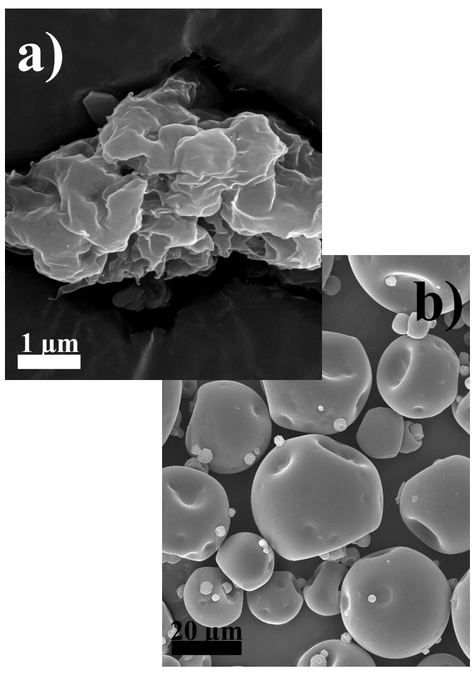

Fig. 1: FEG-SEM images of corrosion inhibitor (a) and self-healing microcapsules (b).

EIS

- Highly capacitive behavior
- Good barrier properties

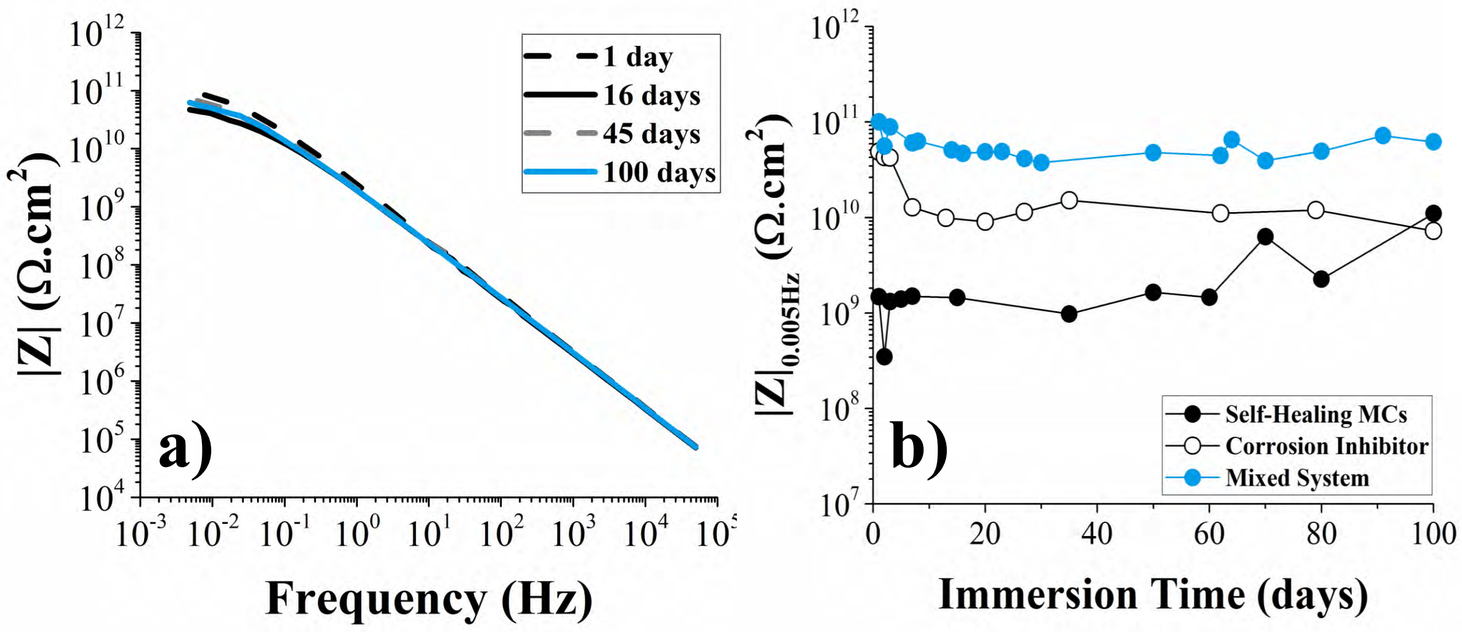

Fig. 2: Bode plot of coating modified with mixed additive-MCs system, applied on mild steel (a); and evolution of low frequency impedance modulus with the immersion time for coatings modified with the mixed additives, and coatings modified with each additive (corrosion inhibitor or MCs) (b).

LEIS

Suppression of corrosion propagation

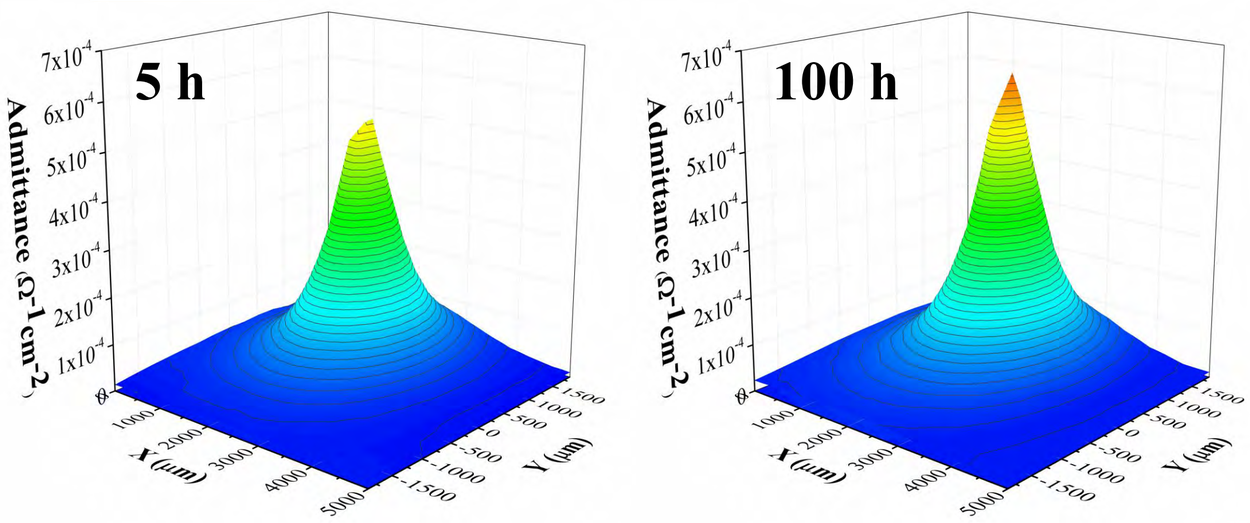

Fig. 3: LEIS maps obtained for coated samples with an artificial defect: coating with mixed additive-MCs system after 5 h and 100 h of immersion in 0.005 M NaCl .

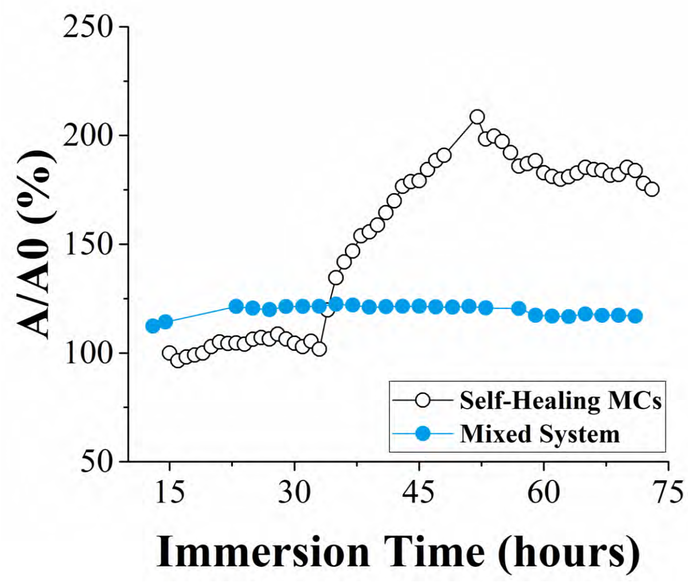

Fig. 4: Evolution of admittance for coated samples with an artificial defect: coating with self-healing microcapsules, and coating with mixed additive-MCs system.

Conclusions

In this work, the synergistic effect of two coating additives (corrosion inhibitor and self-healing microcapsules) was studied. The mixed coating system showed good barrier properties and a synergistic effect was found. Furthermore, the mixed coating system was able to continuously suppress the intensification of corrosion activity and its propagation. Thus, this work represents an important step towards the development of autonomous corrosion protection strategies.

CQE Química Estrutural

07 CSSE

FCT Fundação para a Ciência e a Tecnologia

Acknowledgements

Sherwin Williams for providing the model coating formulation; Shell Qatar (and Dr. Nick Laycock) as partner in the project SmartCoat (NPRP 9); L. M. Calado acknowledges FCT for PhD grant SFRH/BD/127341/2016 and M. J. Carmezim for scientific supervision.

Funding

This work was made possible with the funding granted by SmartCoat project (NPRP 9) – Grant no. 080-02-039 funded by QNRF. Centro de Química Estrutural is funded by Fundação para a Ciência e Tecnologia – project UID/QUI/00100/2019.

NON-AQUEOUS URANIUM COORDINATION CHEMISTRY: URANIUM COMPLEXES SUPPORTED BY HYDROBIS(MERCAPTOIMIDAZOLYL)BORATES

Leonor Maria,[1,2] Joaquim Marçalo,[1,2] Isabel C. Santos,[2] Adelaide Cruz[1,2]

[1]Centro de Química Estrutural, Instituto Superior Técnico, Universidade de Lisboa, Bobadela
[2]Centro de Ciências e Tecnologias Nucleares, Instituto Superior Técnico, Universidade de Lisboa, Bobadela

e-mail: leonorm@ctn.tecnico.ulisboa.pt

INTRODUCTION

Compared to d-block metals, **uranium chemistry** is less developed, and uranium-ligand bonding and reactivity remain puzzling and unpredictable. Insight into the fundamental chemistry of this *f*-element is crucial in many aspects of nuclear technology and in determining its mobility in the environment, as well in the search for new applications. The oxidation of a metal is a well-suited reaction to study the influence of the supporting ligand on reactivity. Since trivalent uranium has a high reducing power, its complexes are extremely reactive with oxidizing substrates. As such, studies of U(III) redox chemistry have been reported using diverse U(III)-systems leading to unprecedented transformations and structures, demonstrating the chemical potential and unique properties of uranium.[1]

Hydrobis(mercaptoimidazolyl)borate ligands are mono-anionic soft chelates, analogues to the $[N_2]$-donor hydrobis(pyrazolyl)borate ligands, that provide $[S_2]$-donor ligands. Previous results obtained by us demonstrated that the bis(mercaptoimidazolyl)borate ligands $[H(R)B(tim^{Me})_2]^-$ are able to stabilize uranium(III) cationic complexes.[2] Revisiting our studies with these [S2]-donor chelators, we verified that the neutral U(III) complex $[U\{\kappa^3\text{-}H,S,S'\text{-}H(Ph)B(tim^{Me})_2\}_2I(thf)_2]$ can be used as an U(III) precursor in electron-transfer reactions to access new tetravalent and hexavalent uranium complexes supported by soft bis(azolyl)borate ligands.[3]

SYNTHESIS AND CHARACTERIZATION

Oxidation of the U(III) complex $[UI\{\kappa^3\text{-}H,S,S'\text{-}H(Ph)B(tim^{Me})_2\}_2(thf)_2]$ with the one–electron oxidants $AgBPh_4$ or I_2 lead to the formation of the cationic U(IV) compounds $[U\{\kappa^3\text{-}H,S,S'\text{-}H(Ph)B(tim^{Me})_2\}_3][X]$ (X = BPh_4, I). The more sterically crowed U(IV) complexes probably resulted from ligand redistribution of the unstable U(IV) cation, $[UI\{\kappa^3\text{-}H,S,S'\text{-}H(Ph)B(tim^{Me})_2\}_2]^+$. The uranium complexes were characterized by multinuclear NMR, IR and UV-vis/NIR spectroscopies and by X-ray diffraction analysis.

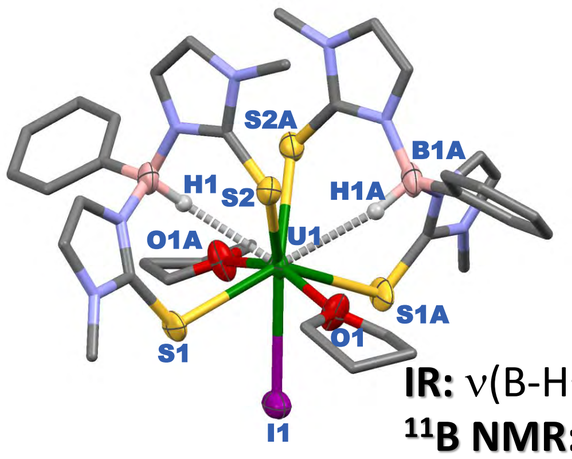

$[U^{III}(\kappa^3\text{-}L)_2I]$

IR: ν(B-H···U) 2360 cm^{-1}
^{11}B NMR: 57.44 ppm

$AgBPh_4$ or I_2
thf, r.t.

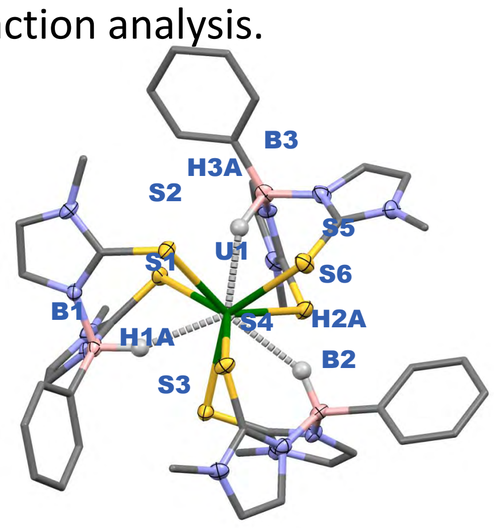

$[U^{IV}(\kappa^3\text{-}L)_3]^+$

UNPRECEDENTED ISOLATION OF A HOMOLEPTIC κ^3- H,S,S' -BASED *f*-ELEMENT COMPLEX

IR: ν(B-H···U) 2260 cm^{-1}
^{11}B NMR: -20.36 ppm

X-RDA: Distorted tricapped trigonal prismatic geometry
U-S_1 2.950(5), 2.81(1), 2.964(5) Å
S-U-S 83.6 Å
U···B 3.61 Å
U-O1 2.510(12); **U-I1** 3.275(2) Å

X-RDA: Distorted tricapped trigonal prismatic geometry
U-$S_{av.}$ 2.80(2), 2.81(1), 2.80(1) Å
S-U-S 84.88(3), 87.28(3), 85.29(3) Å
U···B 3.413(4), 3.425(5), 3.407(6) Å
U···H-B 2.36(4), 2.39(3), 2.30(3) Å

The reaction of the U(III) neutral precursor with O-atom transfer reagents, such as pyridine N-oxide led to the formation of the uranyl complex $[U\{\kappa^2\text{-}S,S'\text{-}H(Ph)B(tim^{Me})_2\}_2(O)_2]$ and of $[U\{\kappa^3\text{-}H,S,S'\text{-}H(Ph)B(tim^{Me})_2\}_3][I]$.

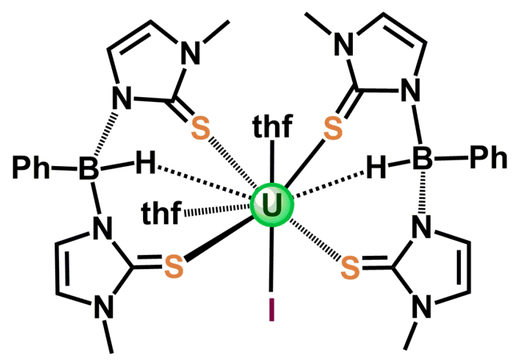

$[U^{III}(\kappa^3\text{-}L)_2I]$

1 equiv. pyridine N-oxide
CH_3CN, r.t.

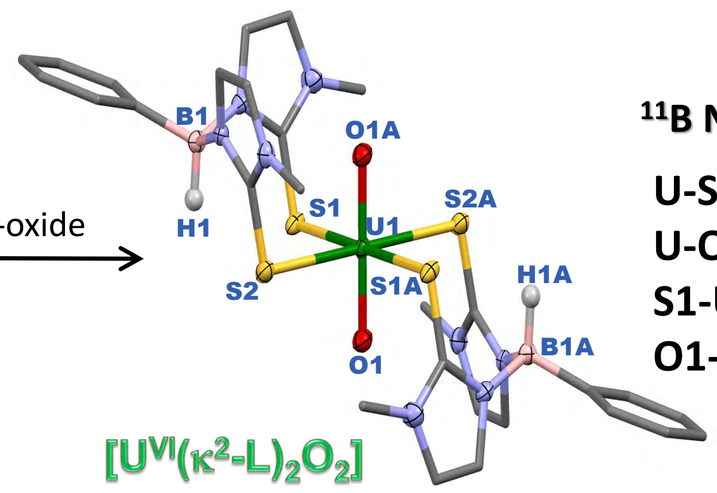

$[U^{VI}(\kappa^2\text{-}L)_2O_2]$

^{11}B NMR: 1.08 ppm
U-S 2.745(1), 2.753(1) Å
U-O1 1.780(3) Å
S1-U-S2 87.69(3)°
O1-U-O1A 180.0(1)°

CONCLUDING REMARKS

We have demonstrated that the soft donor ligand $[H(Ph)B(tim^{Me})_2]^{-1}$ is able to stabilize the **+3**, **+4** and **+6** uranium oxidation states. Oxidation reactions of the U(III) precursor allowed to isolated tetravalent and hexavalent uranium complexes. The U(III) and U(IV) complexes were stabilized by additional U···H-B three-center two-electron interactions.[3]

CQE Química Estrutural

02 IOARC

Funding:
- Centro de Química Estrutural is funded by Fundação para a Ciência e Tecnologia – project UID/QUI/00100/2019.
- Centro de Ciências e Tecnologias Nucleares is funded by FCT – project UID/MULTI/04349/2019

FCT Fundação para a Ciência e a Tecnologia

References:
1. Liddle, S. T., *Angew. Chem. Int.Ed.* 54, **2015**, 8604.
2. Maria, L.; Domingos, A; Santos, I. *Inorg. Chem.*, **2001**, 40, 6863.
3. Maria, L.; Santos, I. C.; Santos, I. *Dalton Trans.* **2018**, 47, 10601 (Invited article - New Talent: Europe).

Co-Crystals of Fumaric Acid Esters with Aminoacids

L. Pereira[1], M. F. M. Piedade, M. E. Minas da Piedade[1]

[1]Centro de Química e Bioquímica e Centro de Química Estrutural, Faculdade de Ciências, Universidade de Lisboa, 1749-016 Lisboa, Portugal

Email: fc49744@alunos.fc.ul.pt

Scope

Fumaric acid esters are one of the most commonly used active pharmaceutical ingredients (API) in the treatment of psoriasis vulgaris.[1] The **low solubility** of fumaric acid esters in aqueous media poses significant limitations to the development of pharmaceutical formulations with high bioavailability. An interesting strategy to improve this is based on the formation of **co-crystals**, multi-component substances combining two or more molecules in the same crystal lattice.

AIM

Produce co-crystals of methyl fumarate, ethyl fumarate and dimethyl fumarate through mechanochemistry with amino acids as co-formers, to increase the solubility of the APIs

Method

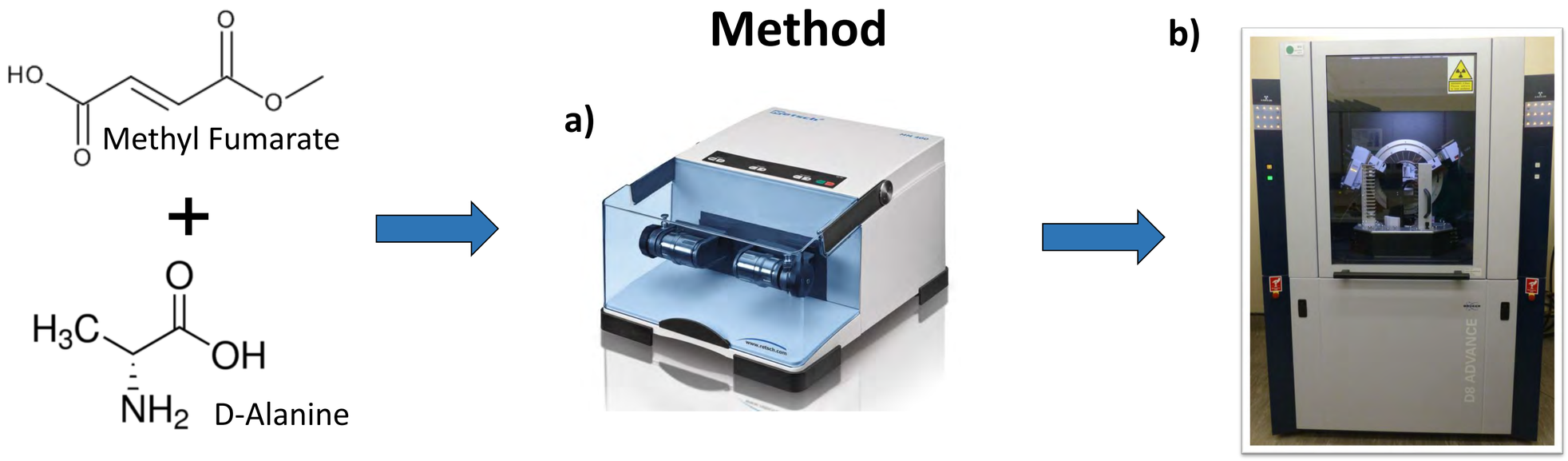

Figure 1. (a) Ball mill for mechanochemistry and **(b)** X-ray powder diffractometer.

Results

Table 1. Results for the compound mixtures utilized for the mechanochemical grinding. Every test was made with a 1:1 stoichiometry.

Compound	D-Alanine	L-Cysteine	DL-Serine	DL-Arginine	D-Aspartic Acid	L-Glutamic Acid	L-Phenylalanine
Methyl fumarate	✗	✗	✗	○	–	⊘	–
Dimethyl Fumarate	○	⊘	⊘	⊘	⊘	–	⊘
Ethyl Fumarate	✗	✗	–	○	–	–	○

○ → Reaction occured ✗ → Reaction did not occur ⊘ → Partial reaction occured – → Untested Mixture

Ethyl Fumarate + L-Phenylalanine as an example of a complete reaction

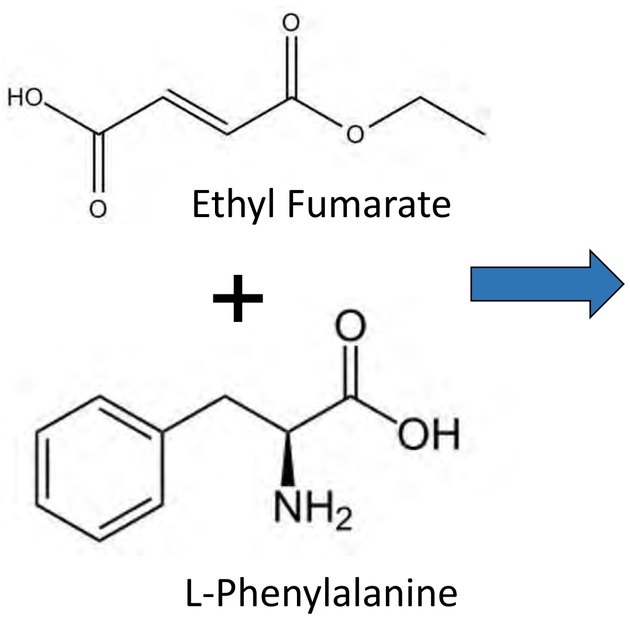

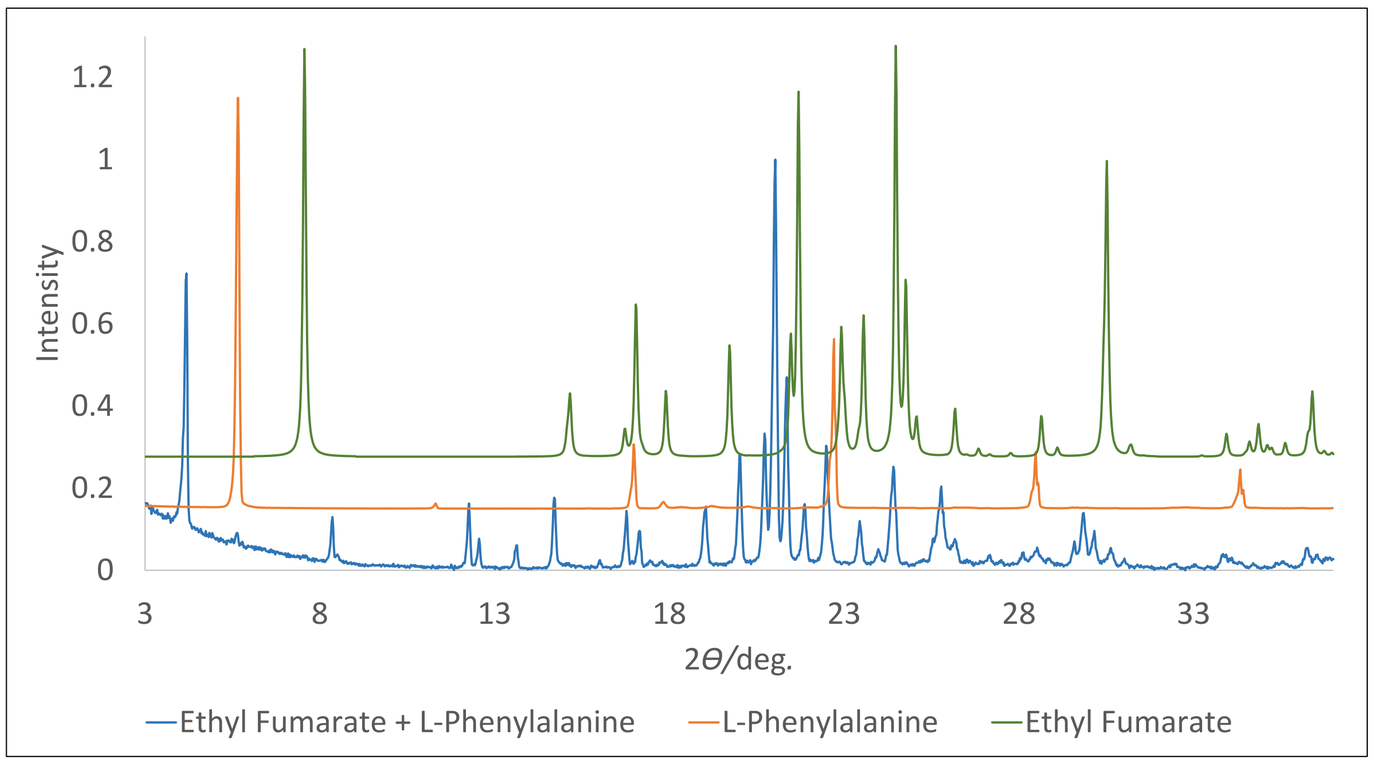

Figure 2. X-ray powder diffractograms (XRPD) of ethyl fumarate, L-phenylalanine, and the resulting mixture.

Conclusions:

- Out of all the tested systems, 4 achieved a complete reaction, yielding co-crystals.
- Formation of co-crystals was also suggested from the XRPD data for 6 mixtures. This, indicates that complete co-crystal formation may be achieved if the reaction conditions are changed (e.g. stoichiometry, type/quantity of solvent, and reaction time).

CQE Química Estrutural

09 MET

Funding:

Centro de Química Estrutural is funded by Fundação para a Ciência e Tecnologia – project UID/QUI/00100/2019.

This work was supported by Fundação para a Ciência e a Tecnologia (FCT), Portugal through Projects PTDC/QUI-OUT/28401/2017 (LISBOA-01-0145-FEDER-028401) and UID/MULTI/00612/2013.

FCT Fundação para a Ciência e a Tecnologia

References:

[1] H. A. Blair, Drugs 78 (2018) 123-130.

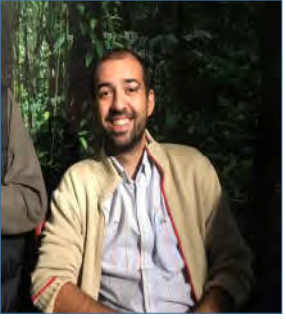

Supercritical Antisolvent Precipitation, a way to design particles

Luis C. S. Nobre, António M. F. Palavra, Mário J. F. Calvete, Carlos A. Nieto de Castro, Beatriz P. Nobre

The **Supercritical Antisolvent precipitation** (SAS) is a semi-continuous process that uses a supercritical fluid, or a compressed gas, as an antisolvent. The compound of interest to be precipitated is dissolved in an organic solvent and is fed to the precipitator, alongside the supercritical fluid that is, generally, CO_2 due to his characteristics (non flammability, low toxicity, low cost, abundant, with a critical point readily accessible: T=31.2ºC and P=7.38 MPa).

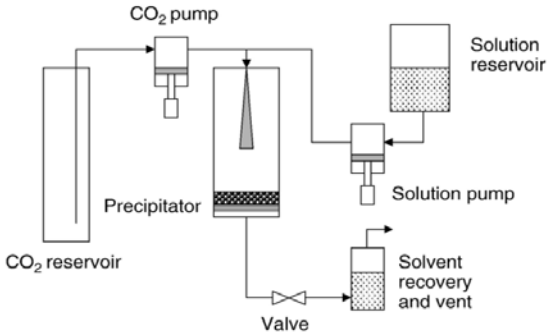

Fig 1. Schematic diagram of a semi continuous SAS apparatus

Through this technique was already proven the possibility to produce compounds, from catalysts to pharmaceutical principles. One advantage of this method is the possibility, by changing the operating conditions, to tune the morphology and particle size of the compounds, mainly temperature, pressure, concentration of the solute in the liquid solution and flow rate of the liquid solution.

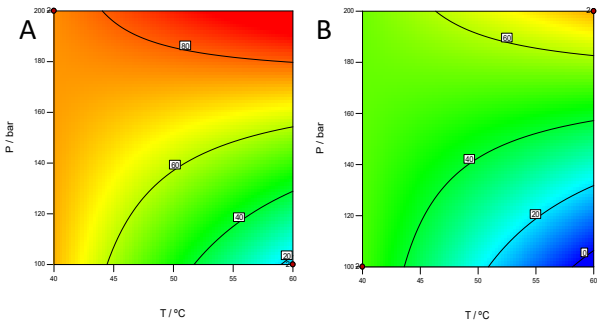

Fig 2. Example of the efficiency in function of temperature and pressure, at different flow rates, to the micronization of the Calcium Acetate: A – at 0.5 min.ml^{-1} and B – at 3 min.ml^{-1}

To study the effect of the different variables in the final product, usually it is used a fractional factorial design of experiment. This type of tool allows the statistical study of the effect of the variables over the characteristics of product or the efficiency of the process, with the reduction of the experiences (fig.2.).

The fig. 3 presents the effect of the conditions has on the obtained product, and the figure 4 shows other kind of materials treated with this technique.

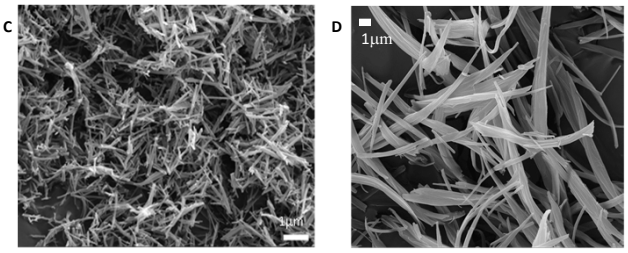

Fig. 3. Micronized calcium acetate at: **C**- P = 150 bar, and T = 323.15 K and **D** - P = 100 bar, and T = 313.15 K

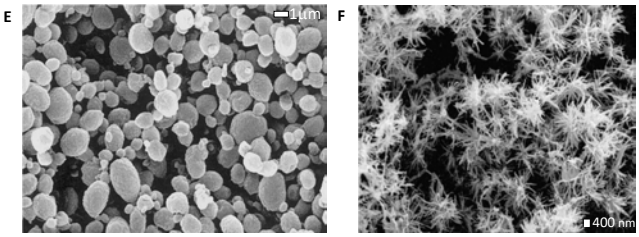

Fig. 4. Examples of treated products: **E** - Micronized Poly-L-Lactide at P = 120 bar, and T = 313.15 K and **F** - Micronized Salbutamol at P = 150 bar, and T = 313.15 K , both studies published by E. Reverchon *et all.*

In order to complete the studies, precipitated compounds must be very well characterised. Besides the morphology analysis using SEM imagens, others techniques are required like infrared spectroscopy, X-ray diffraction, thermogravimetry or isothermal adsorption.

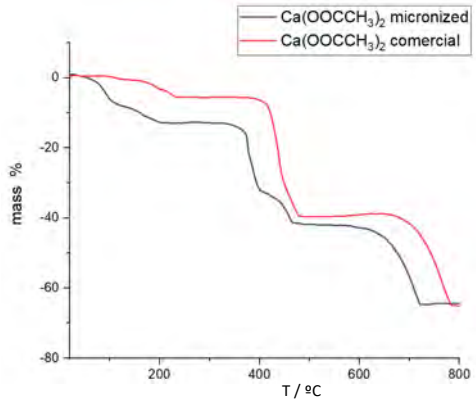

Fig 5. Example of thermogravimetry analysis comparing the calcium acetate micronized and the commercial

This is a versatile and environmental friendly technique. Through this, is possible to tune the physical characteristics of the materials by changing the operation conditions. The applicability of this technique is huge, with tested products from the pharmaceutical industry to the catalysts field, crossing the polymers area.

CQE Química Estrutural

09 MET
10 MTFT

Funding:
Centro de Química Estrutural is funded by Fundação para a Ciência e Tecnologia – project UID/QUI/00100/2019. The PhD grant of the author is also funded by Fundação para a Ciência e a Tecnologia- PD/BD/133309/2017

References:

1.Reverchon, E.; The Journal of Supercritical Fluids 1999, 15, 1-21.
2.Reverchon, E.; Adami, R. The Journal of Supercritical Fluids 2006, 37, 1-22.
3. Tenorio, A., Gordillo, M. D., Pereyra, C. M., & de la Ossa, E. J. M. The Journal of Supercritical Fluids, 2008, 44(2), 230–237.
4. Rueda, M.; Sanz-Moral, L. M.; Martín, Á. Crystal Growth & Design 2014, 14, 4768-4776.

FCT Fundação para a Ciência e a Tecnologia

C-dots based nanocomposites materials for the photodegradation of organic pollutants

Luísa D. Chiavassa,[1] A.J. Silvestre,[2,3] J.V. Prata,[4,5] O.C. Monteiro[1]

[1] Centro de Química Estrutural e Centro de Química e Bioquímica, Faculdade de Ciências, Universidade de Lisboa, Portugal.
[2]Departamento de Física, Instituto Superior de Engenharia de Lisboa, Instituto Politécnico de Lisboa, Portugal
[3]LSPL and CeFEMA, Departamento de Física, Faculdade de Ciências, Universidade de Lisboa, Portugal
[4] Departamento de Engenharia Química, Instituto Superior de Engenharia de Lisboa, Instituto Politécnico de Lisboa, Portugal.
[5]Centro de Química-Vila Real, Universidade de Trás-os-Montes e Alto Douro, Vila Real, Portugal.

INTRODUCTION

Although a wide variety of semiconductor materials have been studied as potential photocatalysts for the photodegradation of organic pollutants, the low efficiency of this class of materials in the visible region has been obstructing their largescale application. A possible way to achieve the foreseen visible-light-active photocatalysts with high efficiency can be addressed by hybrid nanostructured materials in which two or more units are combined together into a single nanocomposite material. This work involves the development of visible-light-active carbon dots (C-dots) based nanocomposites for the photodegradation of caffeine, being silica the inert matrix used. The C-dots were obtained using cork industry and olive mill wastewaters as C sources aiming at the valorization of these industrial wastes.

EXPERIMENTAL

- **Synthesis of SiO_2 microparticles (Stöber method)**

- **Synthesis of C-dots/SiO_2**

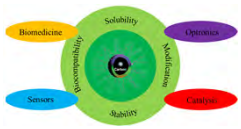

RESULTS AND DISCUSSION

ATR

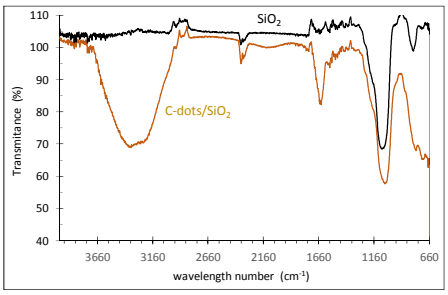

- The Attenuated Total Reflection (ATR) spectra indicates the immobilization of the C-dots nanoparticles in the SiO_2 surface.

DRS and UV-vis spetra

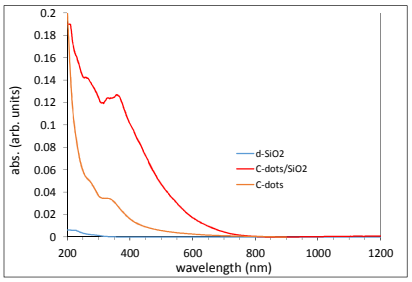

- The absorption spectrum of C-dots/SiO_2 confirms the immobilization of C-dots in the matrix surface;
- After C-dots incorporation, the nanocomposite starts to absorbs in the visible range.

Caffeine photocatalytic degradation under UV-vis radiation

Caffeine 20 ppm, 150 mL, 20 mg catalyst

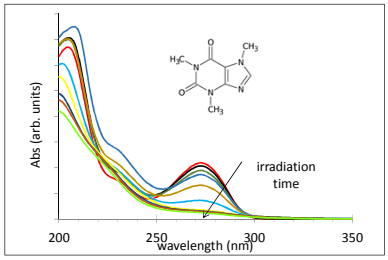

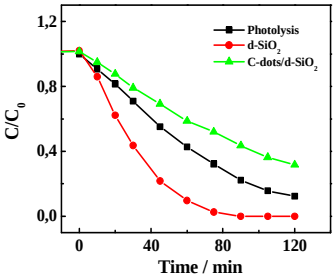

- The C-dots/d-SiO_2 were not catalytic for caffeine photo-assisted degradation;
- The positive results obtained with the d-SiO_2 sample should be do to adsorption of degradation intermediates in the SiO_2 surface;
- Possible degradation of C-dots.

CONCLUSIONS

- New C-dots/SiO_2 nanocomposite materials were successfull prepared;
- The C-dots/d-SiO_2 were not photocatalytic for caffeine degradation usingr UV-vis radiation, probably due to the degradation of C-dots;
- New applications for these C-dots/SiO_2 hybrid materials are currently in study.

06 Chem4Env Chemistry for the Environment -

Funding:
Centro de Química Estrutural is funded by Fundação para a Ciência e Tecnologia – project UID/QUI/00100/2019.
This work was also supported by projects:UID/MULTI/00612/2019, IF/01210/2014 (FCT) and by IPL under the project IPL/2018/VLA-NANOC/ISEL

References:

1. Sousa, D.A., Costa, A.I., Alexandre, M.R., Prata, J.V., *Sci Total Environ.* (2019) 647: 1097–1105.
2. Zhang, D., Wang, M., Ma, J. et al. *J Nanopart Res* (2014) 16: 2635.
3. Franco, A; Neves, MC; Carrott, MMLR; Mendonca, MH; Pereira, MI; Monteiro, OC. *J. Haz. Mat.* 161 (2009) 545–550.

Cu(II)-Aroylhdrazones: Syntheses and Catalytic C-H functionalization

***Manas Sutradhar*, M. Fátima C. Guedes da Silva, Armando J. L. Pombeiro**

[1]*Centro de Química Estrutural, Instituto Superior Técnico, Universidade de Lisboa, Av. Rovisco Pais, 1049-001 Lisboa, Portugal.*
email: manas@tecnico.ulisboa.pt

INTRODUCTION

The coordination chemistry of Cu(II) is very interesting. It exhibits a rich variety of distorted coordination geometries including tetragonal, tetrahedral, square planar, and trigonal bipyramidal. Due to the presence of single unpaired electron and flexible coordination behavior, Cu(II) complexes are widely explored for magnetic studies, with a growing interest on the synthesis of polynuclear complexes and clusters and their application in molecular magnetism.[1]

In this work, we are presenting the syntheses, characterizations and the catalytic activity of three tetranuclear Cu(II) aroylhydrazone complexes towards mild hydrocarboxylation of linear and cyclic alkanes into carboxylic acids in water/acetonitrile medium. The complexes **1–3** are shown to act as good catalytic precursors for the hydrocarboxylation of linear and cyclic C5–C8 alkanes, leading to carboxylic acid yields up to 26% based on the starting alkane. [2]

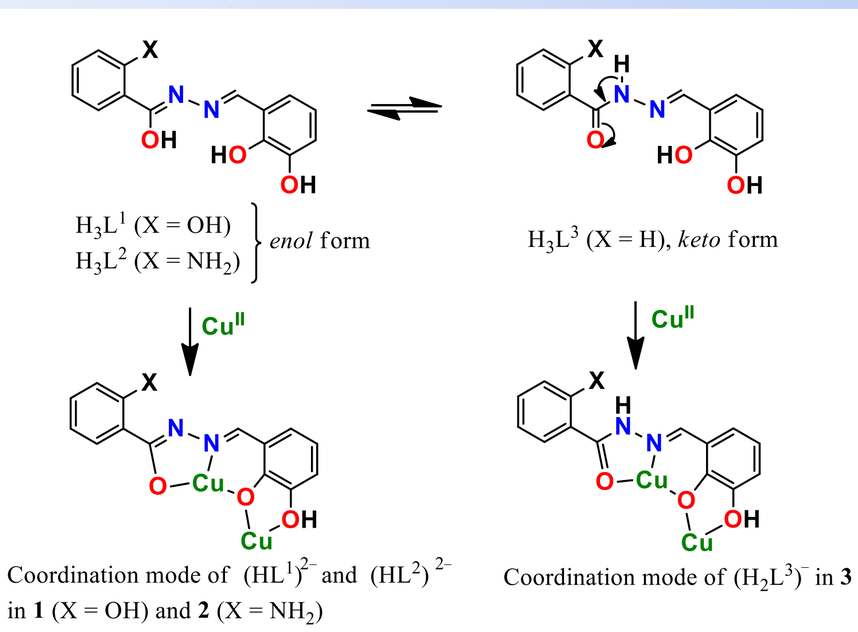

Scheme 1 Coordination behavior of the aroylhydrazone ligands in the tetranuclear Cu(II) complexes

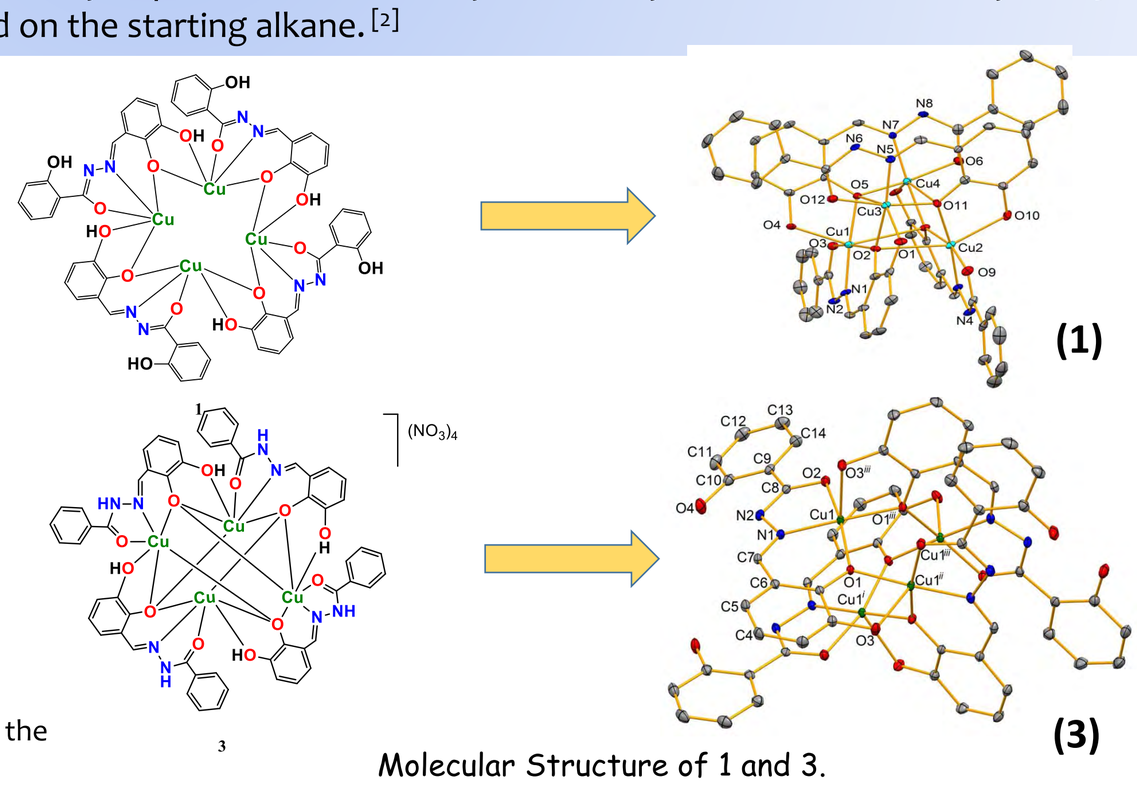

Molecular Structure of 1 and 3.

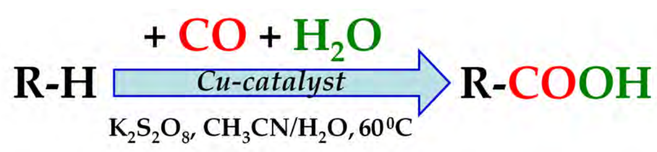

Mild single-pot hydrocarboxylation of Cn (n = 5–8) alkanes into Cn+1 carboxylic acids.

In this work we have reacted linear (n-pentane, n-hexane, n-heptane and n-octane) and cyclic (cyclopentane, cyclohexane, cycloheptane and cyclooctane) C5–C8 alkanes with CO and H2O in the presence of each of the Cu-complexes **1–3** and K2S2O8 (at 50–60° C, in 1:2 H2O/CH3CN medium) and have obtained the corresponding C6–C9 linear or cyclic carboxylic acids.

The three complexes **1–3** exhibit good catalytic activity towards the alkane hydrocarboxylation, leading to carboxylic acid yields up to 26% based on the starting alkane. The achieved herein activity is quite considerable taking into account the high inertness of alkanes and the rather mild reaction conditions (60° C, 4 h, aqueous medium). In general, the highest activity is shown by complex 1, followed by 3 and 2.

A free-radical mechanism of alkane hydrocarboxylation is proposed. Sulfate radicals SO4•- derived from thermolysis of K2S2O8 react with the alkanes, resulting in the formation of alkyl radicals R•. These rapidly react with CO forming the corresponding acyl radicals RCO•. The catalytic role of the Cu-complex consists in the oxidation of these acyl radicals RCO• to acyl cations RCO+ via the CuII/CuI redox couple. The RCO+ is further hydrolyzed by water to form the carboxylic acid RCOOH.

Entry	Alkane	Products	Catalyst	Product yield, %[b] (1)	(2)	(3)	(4)	Total[c]	Regioselectivity[d] C(1):C(2):C(3):C(n)
1	*n*-C_5H_{12}	$C_5H_{11}COOH$ (*1*)	**1**	0.8	12.1	6.4	–	19.3	1:23:24
2		$C_3H_7CH(COOH)CH_3$ (*2*)	**2**	0.7	10.2	5.0	–	15.9	1:22:21
3		$C_2H_5CH(COOH)C_2H_5$ (*3*)	**3**	1.0	14.8	7.2	–	23.0	1:22:22
4	*n*-C_6H_{14}	$C_6H_{13}COOH$ (*1*)	**1**	1.0	12.8	12.0	–	25.8	1:19:18
5		$C_4H_9CH(COOH)CH_3$ (*2*)	**2**	0.7	8.2	7.3	–	16.2	1:18:16
6		$C_3H_7CH(COOH)C_2H_5$ (*3*)	**3**	1.0	12.5	11.9	–	25.4	1:19:18
7	*n*-C_7H_{16}	$C_7H_{15}COOH$ (*1*)	**1**	0.7	8.0	8.1	3.6	20.4	1:17:17:15
8		$C_5H_{11}CH(COOH)CH_3$ (*2*)	**2**	0.4	4.3	4.3	2.0	11.0	1:16:16:15
9		$C_4H_9CH(COOH)C_2H_5$ (*3*) $C_3H_7CH(COOH)C_3H_7$ (*4*)	**3**	0.7	7.8	7.6	3.6	19.7	1:17:16:15
10	*n*-C_8H_{18}	$C_8H_{17}COOH$ (*1*)	**1**	0.6	8.0	7.6	7.5	23.1	1:20:19:19
11		$C_6H_{12}CH(COOH)CH_3$ (*2*)	**2**	0.3	4.0	3.8	3.8	11.9	1:20:19:19
12		$C_5H_{11}CH(COOH)C_2H_5$ (*3*) $C_4H_9CH(COOH)C_3H_7$ (*4*)	**3**	0.5	6.0	5.8	5.6	17.9	1:18:17:17
13	C_5H_{10}	C_5H_9COOH (*1*),	**1**	19.2	2.2	0.6	–	22.0	–
14		C_5H_8O (*2*), C_5H_9OH	**2**	15.0	1.6	0.9	–	17.5	–
15		(*3*)	**3**	15.2	2.4	0.9	–	18.5	–
16[e]	C_6H_{12}	$C_6H_{11}COOH$ (*1*),	**1**	19.6	1.0	0.5	–	21.1	–
17[e]		$C_6H_{10}O$ (*2*),	**2**	19.8	0.7	0.3	–	20.8	–
18[e]		$C_6H_{11}OH$ (*3*)	**3**	16.9	1.2	0.4	–	18.5	–
19	C_7H_{14}	$C_7H_{13}COOH$ (*1*),	**1**	22.1	6.5	4.7	–	33.2	–
20		$C_7H_{12}O$ (*2*),	**2**	9.8	6.3	2.0	–	18.1	–
21		$C_7H_{13}OH$ (*3*)	**3**	14.9	5.7	2.1	–	22.6	–
22	C_8H_{16}	$C_8H_{15}COOH$ (*1*),	**1**	6.1	7.4	4.6	–	18.1	–
23		$C_8H_{14}O$ (*2*),	**2**	5.0	4.5	2.5	–	12.0	–
24		$C_8H_{15}OH$ (*3*)	**3**	6.1	7.5	3.2	–	16.8	–

CONCLUSIONS

Three different hydrazone Schiff base ligands have been synthesized by condensation reactions of 2,3-dihydroxy benzaldehyde separately with 2-hydroxybenzohydrazide, 2-aminobenzohydrazide or benzohydrazide. The complexes **1–3** are shown to act as good catalytic precursors for the hydrocarboxylation of linear and cyclic C5–C8 alkanes, leading to carboxylic acid yields up to 26% based on the starting alkane. The achieved herein activity is quite considerable taking into account the high inertness of alkanes and the used rather mild reaction conditions (60 ° C, 4 h, aqueous medium).

Funding:
Centro de Química Estrutural is funded by Fundação para a Ciência e Tecnologia – project UID/QUI/00100/2019.

ACKNOWLEDGEMENTS
M.S. acknowledges the FCT and IST for a working contract "DL/57/2017" (Contract no. IST-ID/102/2018). We are thankful to Dr. Marina V. Kirillova for her help in the catalytic activity study.

References:

[1] D. Venegas-Yazigia, D. Aravenab, E. Spodineb, E. Ruizd, S. Alvarezd, *Coord. Chem. Rev.* **2010**, *254*, 2086

[2] M. Sutradhar, M. V. Kirillova, M. F. C. Guedes da Silva, C-M. Liu, A. J. L. Pombeiro, *Dalton Trans.* **2013**, *42*, 16578

Green methodologies in the preparation of new photoactive MOFs for energy applications

Márcia A. Ribeiro[1,2], **Hermenegildo Garcia**[2], **M. Teresa Duarte**[1], **Carlos Baleizão**[1]

[1]*Centro de Química Estrutural, Instituto Superior Técnico, Universidade de Lisboa, Portugal*

[2] *Instituto de Tecnologia Química/CSIC, Universidade Politécnica de Valência, Spain*

Email: marcia.ribeiro@tecnico.ulisboa.pt

▪This communication presents a new sustainable approach for the preparation of metal-organic frameworks (MOFs) with semiconductor behaviour. A large number of structural features makes these hybrid materials good candidates for energy conversion in electroluminescent devices [1].

▪The novelty is to introduce ligands and co-ligands with improved light harvesting properties in MOFs, and for that, the reactivity of unexplored functional ligands: diphenyl anthracene (DPA), naphthalene diimides (NDIs) and perylene diimides derivatives (PDIs).

Methods

Mechanosynthesis: Ball Mill Approach

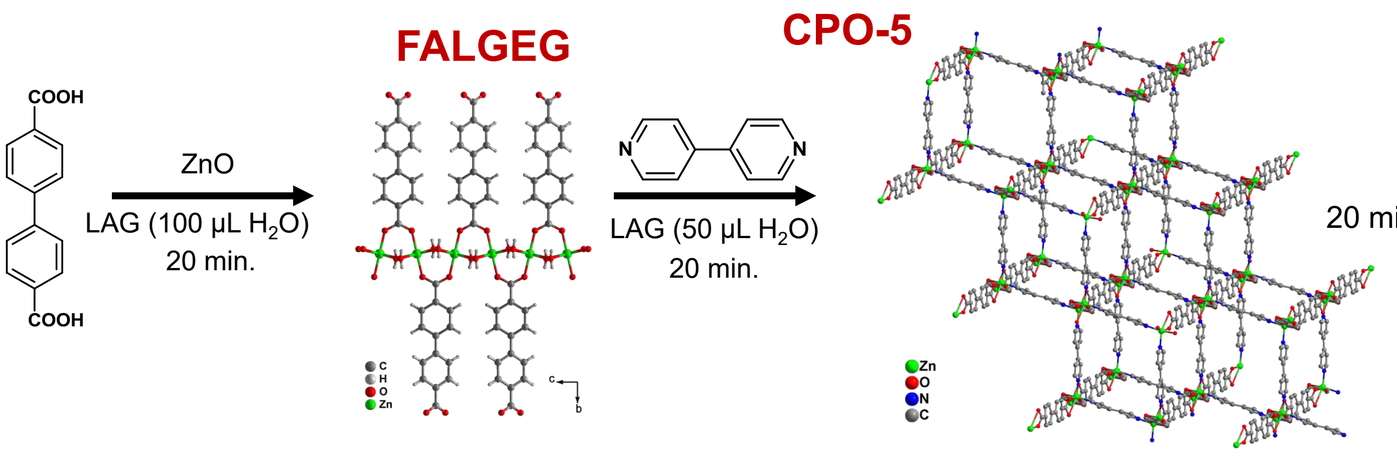

@RT

Microliters of deionized water (LAG)

20 min. + 20 min. reactions; powder dried in air at RT

η= 100 %

Scheme 1: *(left)* Schematic representation of the mechanosynthesis assisted methodology to obtain FALGEG. *(right)* Schematic representation of the mechanosynthesis assisted methodology to obtain CPO-5. **C**rystal packing of CPO-5 highlighting the 2-fold catenated structure.

Solid State Characterization

SEM/EDS

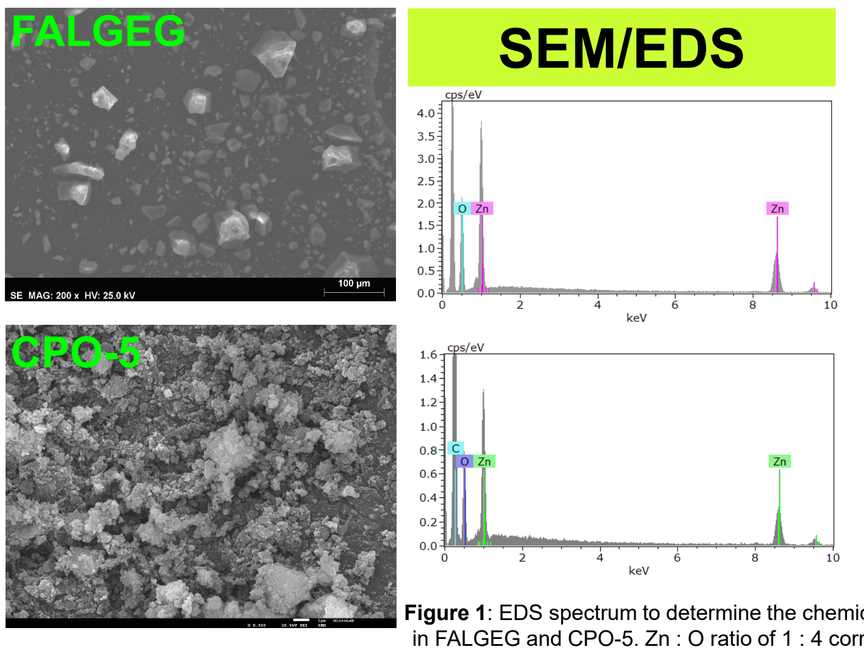

Figure 1: EDS spectrum to determine the chemical composition of elements in FALGEG and CPO-5. Zn : O ratio of 1 : 4 correlates with the proportions unveiled by single crystal X-ray diffraction studies (SCXRD).

Thermogravimetric Studies

CPO-5 synthesized by milling methodology

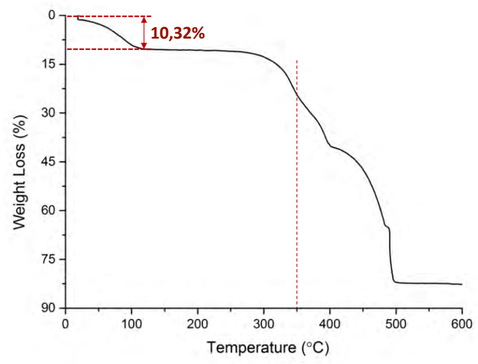

Figure 2: Thermogram of CPO-5 synthesized by milling. Analysis performed between ambient temperature and *ca.* 800 °C.

Variable-temperature Powder X-Ray Diffraction

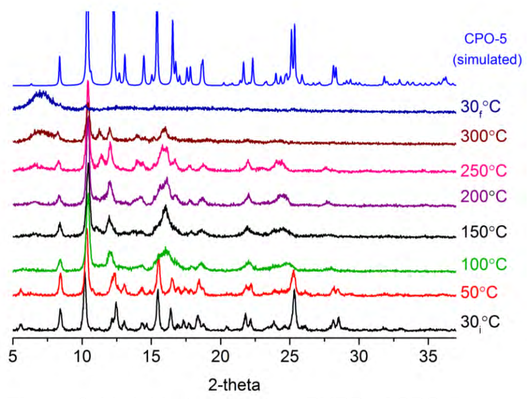

Figure 3: Variable-temperature PXRD of CPO-5.

The dehydration process of CPO-5 observed in the thermogram is also evident in the variable-temperature PXRD study. Until **200°C**, the MOF structure is maintained.

FT-IR Spectra

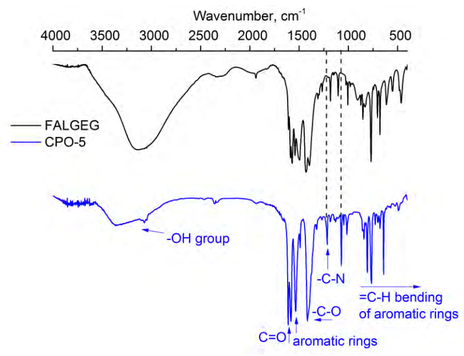

Figure 4: FT-IR Spectra of FALGEG and CPO-5 bulk materials.

On going studies

Ball Milling

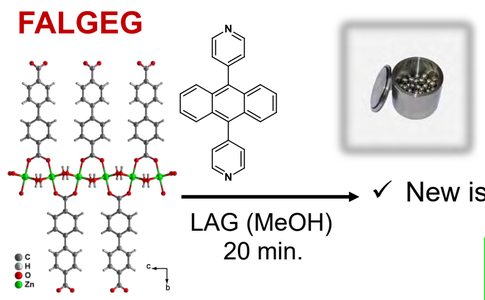

✓ New isolated MOF

Different crystalline structure

Microwave- Assisted procedures

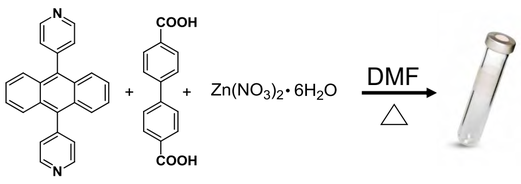

✓ New isolated MOF

Conclusions/Future Work

- ✓ A new, simple and sustainable synthetic route to obtain CPO-5 was developed, as well as its 1D MOF precursor.
- ✓ The obtained small particles are predictably advantageous to engineer these materials in the active layer of electroluminescent devices.
- ✓ Future studies to be performed on these materials include photoluminescent properties as well as cyclic voltammetry.
- ✓ Expand the methodology to other photoactive ligands (NDIs, PDIs).

08 MPPM

Funding:
Centro de Química Estrutural is funded by Fundação para a Ciência e Tecnologia – project UID/QUI/00100/2019. Fundação para a Ciência e Tecnologia (FCT-Portugal) is acknowledged for financial support within the Materials Chemistry PhD program (PD/BD/127983/2016). This work was partially supported by (FCT-Portugal) and COMPETE (FEDER) projects PTDC/CTM-NAN/6249/2014, RECI/QEQ-QIN/0189/2012, and UID/QUI/00100/2013.

References:

[1] V. Stavila, A. A. Talin, and M. D. Allendorf, *Chem. Soc. Rev.*, 2014, 43, 5994–6010.

Viscosity measurements of compressed ionic liquid EMIM OTf

Maria C. M. Sequeira[1], Helena M. N. T. Avelino[1,2], Fernando J. P. Caetano[1,3], João M. N. A. Fareleira[1]

1 Centro de Química Estrutural, Instituto Superior Técnico, Universidade de Lisboa. Av. Rovisco Pais, 1, 1049-001 Lisboa, Portugal
2 Área Departamental de Engenharia Química, Instituto Superior de Engenharia de Lisboa, Instituto Politécnico Lisboa, R. Conselheiro Emídio Navarro, 1, 1959-007 Lisboa, Portugal
3 Departamento de Ciências e Tecnologia, Universidade Aberta, Rua da Escola Politécnica, 141, Lisboa, Portugal

CQE Química Estrutural

09 MET

Background:

Properties for several Ionic Liquids such as viscosity, density, eletrical condutivity have been measured by our group [1 – 5]

1-Ethyl-3-methylimidazolium bis[(trifluoromethyl)sulfonyl]imide (**[C2mim][NTf2]**)
1-Ethyl-3-methylimidazolium ethyl sulfate (**[C2mim][EtSO4]**)
1-Ethyl-3-methylimidazolium trifluoromethanesulfonate (**[C2mim][OTf]**)
1-Hexyl-3-methylimidazolium bis[(trifluoromethyl)sulfonyl]imide (**[C6mim][NTf2]**)

Vibrating-wire viscosity measurements – the sensor has a tungsten wire subjected to a magnetic field (>4000 Gauss). A Lock-in amplifier is used to apply a current through a range of frequencies and measure the potential drop across the vibrating-wire.

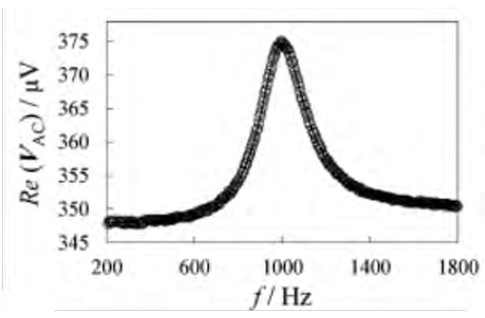

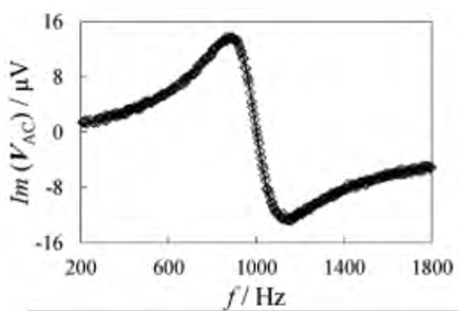

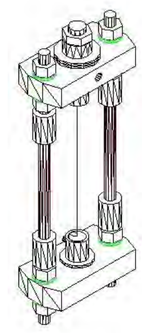

Electrical conductivity, κ, measurents of the ILs

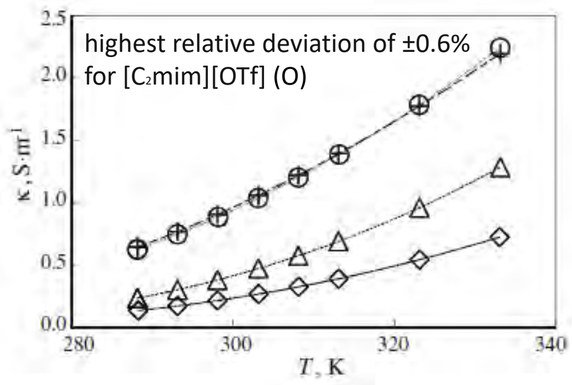

New and sustainable achievements

1-ethyl-3-methylimidazolium trifluoromethanesulfonate **([EMIM] [Otf])**

High-pressure / high-temperature density measurements

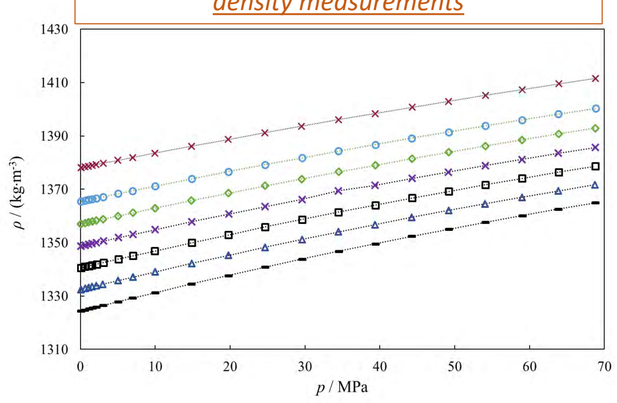

Experimental density data of EMIM OTf at temperatures: +298K; ○, 313 K; ◇, 323 K; ×, 333 K; □, 343 K; △, 353 K; ▫, 363 K

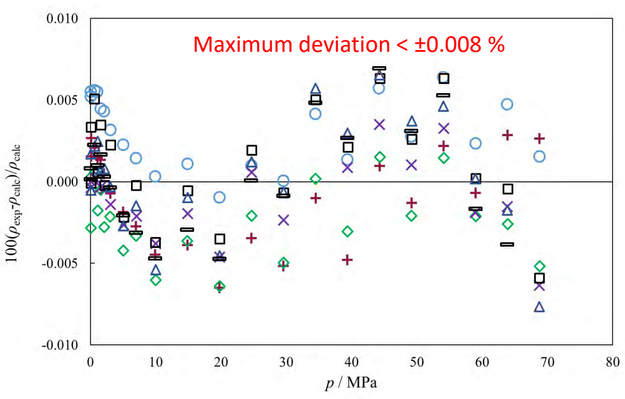

The **root mean square deviation** of the fitting is **0.003 %** and the **bias** is essentially **zero**

High-pressure / high-temperature - Viscosity measurements

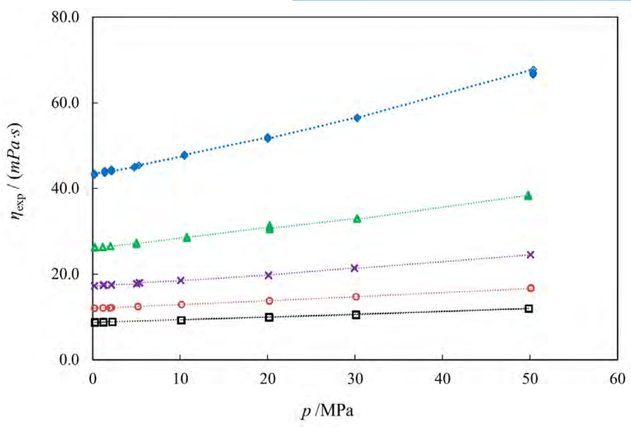

Experimental viscosity data of EMIM OTf at temperatures: ◇,298K; △, 313 K; ×, 328 K; ○, 343 K; □, 358 K.

Correlation for the viscosity data, η, obtained with the vibrating-wire viscometer.

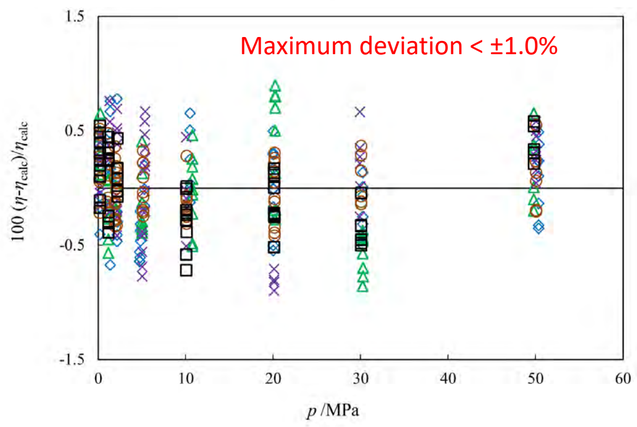

Deviations of the viscosity, η, of EMIM OTf obtained with a vibrating wire viscometer, from correlation: ◇, 298K; △, 313 K; ×, 328 K; ○, 343 K; □, 358 K.

$$\eta^* = 6.035 \times 10^8 \left(\frac{1}{MRT}\right)^{\frac{1}{2}} \eta\,(V_m)^{\frac{2}{3}}$$

$$\frac{1}{\eta^*} = \sum_{i=0}^{4} a_i \left(\frac{V_m}{V_0}\right)^i$$

$$V_0(T) = V_{0,ref} + l\,(T - T_{ref}) + m\,(T - T_{ref})^2$$

✓ *The **root mean square deviation** from the correlation is **0.48 %**, and the **bias** is essentially **zero***

$$|Z| = R_\infty + b \times f^{-1/2} \qquad \kappa = \frac{K}{R_\infty}$$

Deviation plot of the fitted values of the electrical conductivity, κ, in the temperature range 285 K (15 ºC) to 358 K (75 ºC)

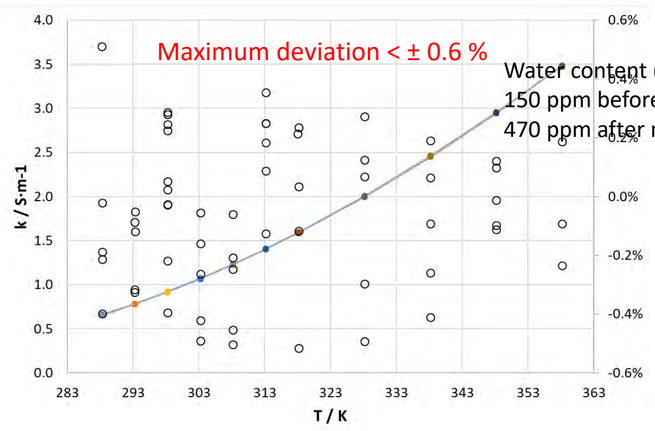

Electrical conductivity, κ, measurements

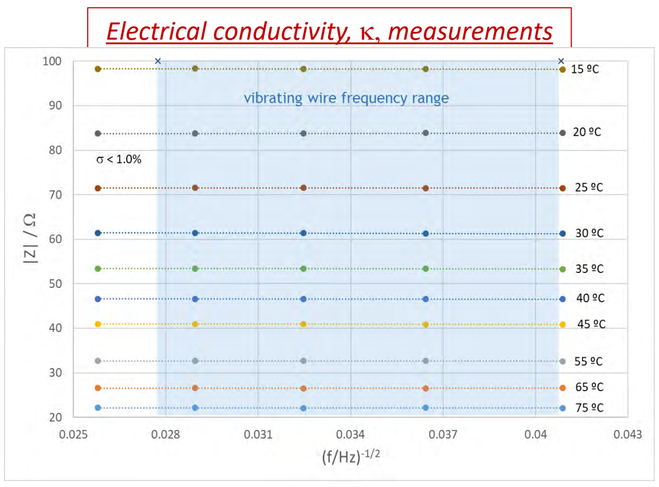

✓ Impedance measurements are **constant (σ < 1.0 %)** for the full working frequency range of the vibrating-wire measurements.

✓ *At each temperature, **viscosity measurements are not affected** by the electrical conductivity in the working frequency range.*

Walden plot - this IL ([EMIM] [Otf]) has the same logaritmic linear behavior as the reference, KCl, 1M

Empirically relation established by Walden

$$\Lambda_m^0 \times \eta^\alpha = C = constant$$

$$log(\Lambda_m^0) = log(C) + \alpha \times log(\eta^{-1})$$

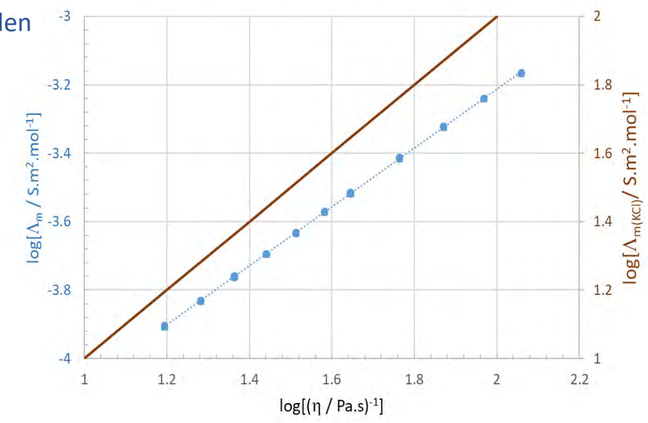

Outcomes:

- **High quality** determination of properties: (1) **viscosity** at *high temperatures* and *high pressures; (2)* **electrical conductivity**, of the ionic liquid **([EMIM] [Otf])**.
- Vibrating-wire viscosity technique may be applied ILs without any loss of its high accuracy.
- As far as the authors are aware these are the **only IL frequency-dependent electrical conductivity** measurements, extrapolated to infinite frequency, applied to ILs.

Funding:
Centro de Química Estrutural is funded by Fundação para a Ciência e Tecnologia – project UID/QUI/00100/2019.

References:

[1] Calado, Marta S., João C. F. Diogo, José L. Correia da Mata, Fernando J. P. Caetano, Zoran P. Visak, and João M. N. A. Fareleira. 2013. "Electrolytic Conductivity of Four Imidazolium-Based Ionic Liquids." International Journal of Thermophysics 34(7):1265–79.

[2] Diogo, João C F, Fernando J. P. Caetano, and João M. N. A. Fareleira. 2012. "DENSITY OF THE REFERENCE IONIC LIQUID [C6mim][NTf2] AT HIGH PRESSURES."

[3] Diogo, João C. F., Fernando J. P. Caetano, João M. N. A. Fareleira, and William A. Wakeham. 2013. "Viscosity Measurements of Three Ionic Liquids Using the Vibrating Wire Technique." Fluid Phase Equilibria 353:76–86.

[4] Diogo, João C. F., Fernando J. P. Caetano, João M. N. A. Fareleira, and William A. Wakeham. 2014. "Viscosity Measurements on Ionic Liquids: A Cautionary Tale." International Journal of Thermophysics 35(9–10):1615–35.

[5] Diogo, João C. F., Fernando J. P. Caetano, João M. N. A. Fareleira, William A. Wakeham, Carlos A. M. Afonso, and Carolina S. Marques. 2012. "Viscosity Measurements of the Ionic Liquid Trihexyl(Tetradecyl)Phosphonium Dicyanamide [P 6,6,6,14][Dca] Using the Vibrating Wire Technique." Journal of Chemical & Engineering Data 57(4):1015–25

FCT Fundação para a Ciência e a Tecnologia

05 BIOMOL

NMR in Strategic Areas of CQE's Research

Maria João Ferreira, José R. Ascenso

05 BIOMOL

J Marreiros, M Diaz-Couce, MJ Ferreira, PD Vaz, MJ Calhorda, CD Nunes "Synthesis and catalytic activity of Mo(II) complexes of alpha-diimines intercalated in layered double hydroxides" Inorganica Chimica Acta 2019, 486, 274-282.

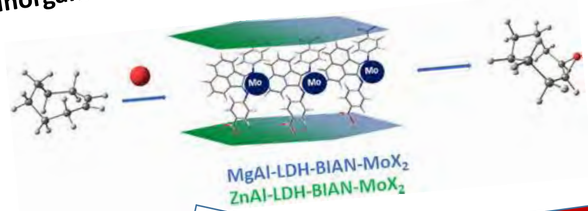

Ana S. Augusto, Alexandre S. Miranda, José R. Ascenso, Margarida Q. Miranda, Vítor Félix, Giovanna Brancatelli, Neal Hickey, Silvano Geremia, Paula M. Marcos" Anion Recognition by Partial Cone Dihomooxacalix[4]arene-Based Receptors Bearing Urea Groups: Remarkable Affinity for Benzoate Ion "EurJOC 2019, 41, 5657-5667.

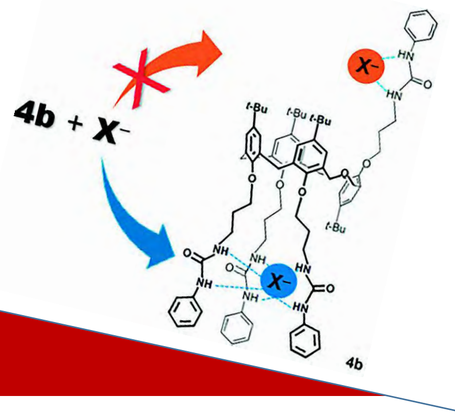

Sena da Fonseca, B.; Ferreira, M.J.; Taryba, M.G.; Piçarra, S.; Pinto, A.P.F.; Montemor, M.F. "Alkoxysilane-based sols for consolidation of carbonate stones: Impact of the carbonate medium in the sol-gel processes." Journal of Cultural Heritage 2019, 37, 63-72.

Lourenço, M. A. O.; Ferreira, M. J. G.; Sardo, M.; Mafra, L.; Gomes, J. R. B.; Ferreira, P. "Microwave-Assisted N,N-Dialkylation of Amine-Functionalized Periodic Mesoporous Phenylene-Silica: An Easy and Fast Way to Design Materials." Microporous and Mesoporous Materials 2017, 249, 10-15.

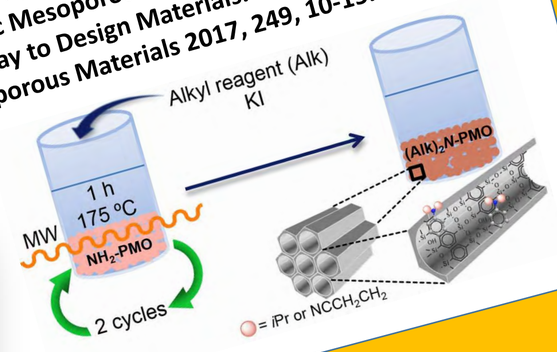

MJ Ferreira, T. Nunes, J. Canário, Permafrost – Soil Analysis by Solid-State NMR

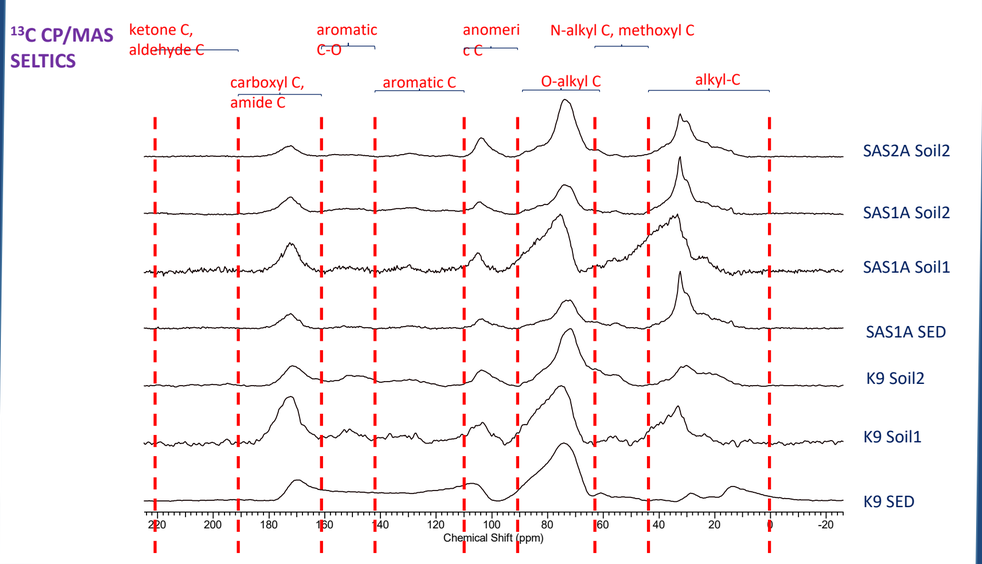

Emanuel D. Costa, Josefina Priotti, Silvina Orlandi, Darío Leonardi, María C. Lamas, Teresa G. Nunes, Hermínio P. Diogo, Claudio J. Salomon, M. João Ferreira*, "Unexpected solvent impact in the crystallinity of praziquantel/poly(vinylpyrrolidone) formulations. A solubility, DSC and solid-state NMR study" International Journal of Pharmaceutics 2016, 511, 983-993.

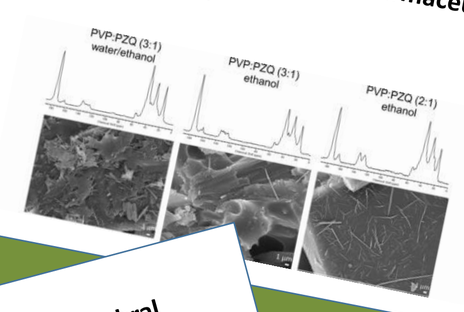

Francisco Silva, Ajit Zambre, Maria Paula Cabral Campello, Lurdes Gano, Isabel Santos, Ana Maria Ferraria, Maria João Ferreira, Amolak Singh, Anandhi Upendran, António Paulo, Raghuraman Kannan "Interrogating the Role of Receptor-Mediated Mechanisms: Biological Fate of Peptide-functionalized Radiolabeled Gold Nanoparticles in Tumor Mice" Bioconjugate Chem. 2016, 27, 1153-1164.

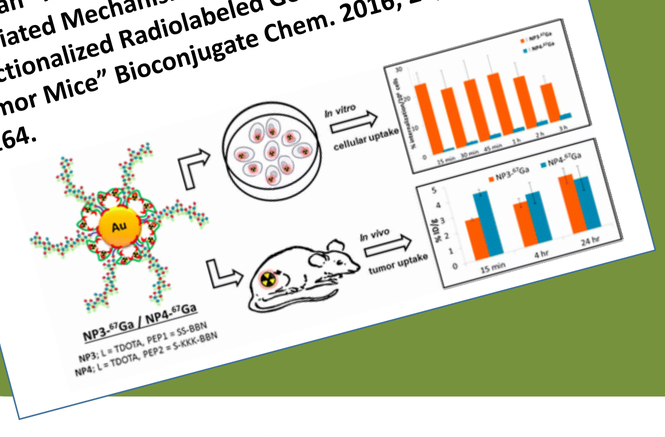

Acknowledgements: The NMR spectrometers are part of the National NMR Network (PTNMR) and are partially supported by Infrastructure Project No 022161 (co-financed by FEDER through COMPETE 2020, POCI and PORL and FCT through PIDDAC). Further financial aid comes from the FCT institution (Project number UID/QUI/00100/2019).

FCT Fundação para a Ciência e a Tecnologia

A UNIFIED pH SCALE FOR ALL SOLVENTS
Meaning and assessment of pH in solvents other than water

Filomena Camões,

Bárbara Anes, Cristina Oliveira, Ricardo Silva

The concept of pH is very well defined and routinely evaluated by means of potentiometric measurements valid in dilute aqueous solutions.

$$\mathrm{pH} = -\lg\left(a_{\mathrm{H}^+}\right)$$

Values of pH in different media are related through the proton Gibbs free energy of transfer between solvents

$$\mathrm{pHs} = -\lg\left(a_{\mathrm{H}^+,\mathrm{solv}}\right)$$

$$\mu = \delta G/\delta n = \mu^\circ + R\,T \ln a \qquad \mu(\mathrm{H}^+) = \mu^0(\mathrm{H}^+) + R\,T \ln a(\mathrm{H}^+) = \mu^0(\mathrm{H}^+) - R\,T\ \ln 10 \times \mathrm{pH_S}$$

The introduction of the unified acidity concept, $\mathrm{pH_{abs}}$, based on the protochemical potential, $\mu(\mathrm{H}^+)$, has enabled comparability of pH values between all phases.

$$\mu_{abs}(\mathrm{H}^+, \mathrm{solv}) = \Delta_{\mathrm{solv}} G^0(\mathrm{H}^+, \mathrm{S}) - R\,T \ln 10 \times \mathrm{pH_S}$$

Concept of a unified Brønsted acidity scale $\mathrm{pH_{abs}}$ defined on the basis of the chemical potential of the proton, $\mu(\mathrm{H}^+)$

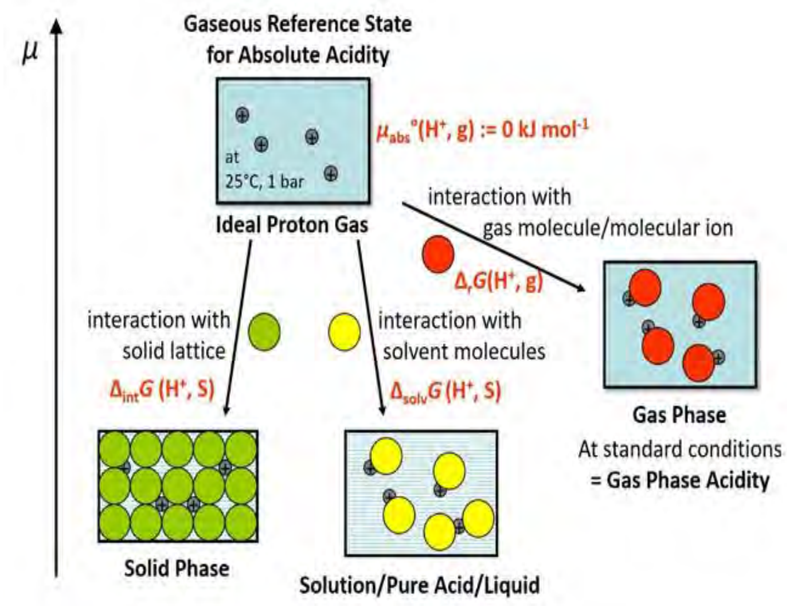

It is practical to link the absolute acidity to the aqueous pH scale via the Gibbs free energy of solvation of the proton in water

$$\mathrm{pH}_{\mathrm{abs}}^{\mathrm{H_2O}} = \mathrm{pH_{abs}} + \frac{\Delta_{\mathrm{solv}} G^0(\mathrm{H}^+, \mathrm{H_2O})}{5.71}$$

-193.5 pH at 25 °C

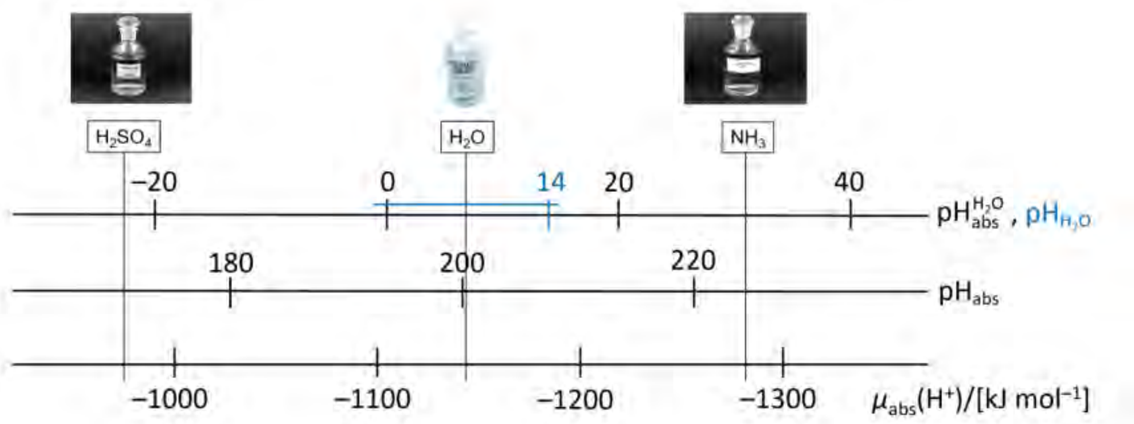

Indicator electrode ($\mathrm{Ind_1}$) | Solution 1 ($\mathrm{S_1}$) | Bridge solution (B) | Solution 2 ($\mathrm{S_2}$) | Indicator electrode 2 ($\mathrm{Ind_2}$)

$$\Delta G = -W_e = -\,n\,F\,E \qquad E = E^\circ - \frac{RT}{nF} \ln a$$

$$\Delta E = E(\mathrm{Ind_2}) - E(\mathrm{Ind_1}) = -\frac{RT\ln 10}{F}\left[\mathrm{pH}(\mathrm{S_2}) - \mathrm{pH}(\mathrm{S_1})\right]$$

$$\Delta E = \Delta E_{\mathrm{measured}} + \Delta E_{\mathrm{j}}(\mathrm{B}, \mathrm{S_1}) - \Delta E_{\mathrm{j}}(\mathrm{B}, \mathrm{S_2})$$

Glass electrode 1| Sol.A ¦¦ Pt in IL ¦¦ Sol.B | Glass Electrode 2

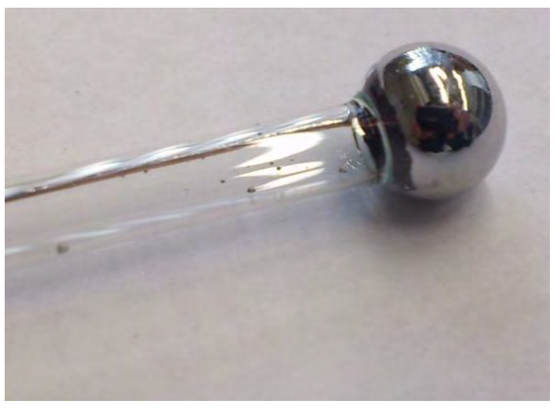

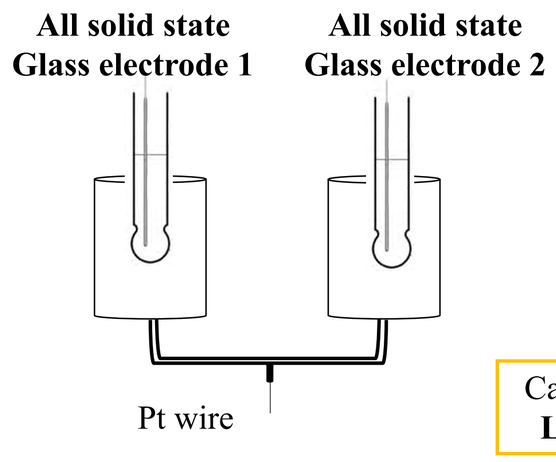

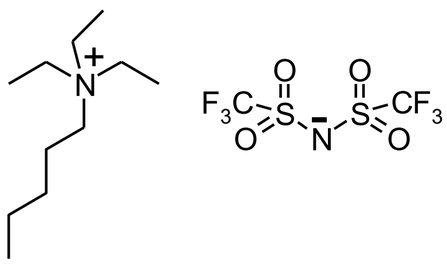

Capillary filled with **Ionic Liquid (IL) N225 ntF2**

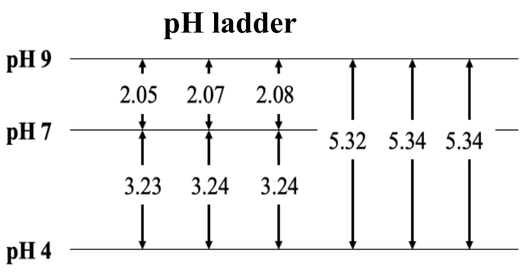

UnipHied cell with the ionic liquid

Solution	DIFF	ΔpH	Expected
pH 4 - pH 4	-23.8	0.44	0.00
	-22.6	0.42	0.00
	-22.6	0.42	0.00
pH 7 - pH 7	-22	0.40	0.00
	-22.1	0.41	0.00
	-19.9	0.37	0.00
pH 9 - pH 9	-19.5	0.36	0.00
	-20.4	0.37	0.00
	-20.5	0.38	0.00
pH 7 - pH 4	-198.8	3.23	3.00
	-199.4	3.24	3.00
	-199.3	3.24	3.00
pH 7 - pH 9	90.2	-2.05	-2.00
	91	-2.07	-2.00
	91.8	-2.08	-2.00
pH 9 - pH 4	-311.1	5.32	5.00
	-312.1	5.34	5.00
	-312.1	5.34	5.00
TRIS-TRIS HCl em H_2O -	-21.7	0.40	0.00
TRIS-TRIS HCl em H2O	-22	0.40	0.00
	-20.5	0.38	0.00
TRIS-TRIS HCl em ASW -	-20	0.37	0.00
TRIS-TRIS HCl em ASW	-21	0.39	0.00
	-21.6	0.40	0.00
TRIS-TRIS HCl em ASW -	-26.5	0.06	0.02
TRIS-TRIS HCl em H_2O	-28	0.09	0.02
	-28.2	0.10	0.02

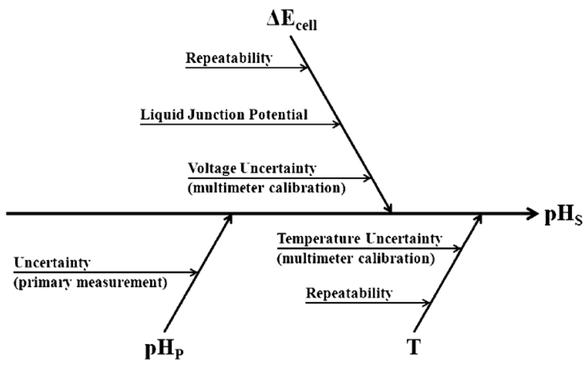

Pan-European Network of Fundamental pH Research: UnipHied, to further develop the practical realization of the $\mathrm{pH_{abs}}$ scale in a variety of solvents, on a strong metrological foundation, i.e., with the development of associated uncertainty budgets.

06 EC

UnipHied is funded from the EMPIR programme (project 17FUN09) co-financed by the Participating States and from the European Union's Horizon 2020 research and innovation programme.

Centro de Química Estrutural is funded by Fundação para a Ciência e Tecnologia – project UID/QUI/00100/2019.

References:

- D. Himmel, S. K. Goll, I. Leito, and I. Krossing, "Anchor Points for the Unified Brønsted Acidity Scale: The rCCC Model for the Calculation of Standard Gibbs Energies of Proton Solvation in Eleven Representative Liquid Media," *Chem. - A Eur. J.*, **17**, 5808–5826 (2011).
- K. Izutsu, "Liquid junction potentials between electrolyte solutions in different solvents," *Anal. Sci.*, **27**, 685 (2011)
- V. Radtke, A. Ermantraut, D. Himmel, T. Koslowski, I. Leito, and I. Krossing, "The Ideal Ionic Liquid Salt Bridge for the Direct Determination of Gibbs Energies of Transfer of Single Ions, Part I: The Concept," *Angew. Chemie Int. Ed.*, **57**, 2344–2347 (2018).

MS in Strategic Areas of CQE's Research

Maria da Conceição Oliveira

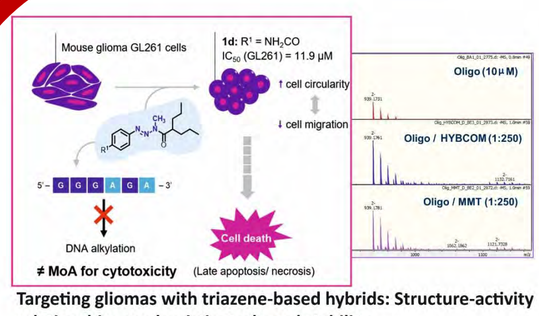

Targeting gliomas with triazene-based hybrids: Structure-activity relationship, mechanistic study and stability.
Claudia Braga *et al.* Eur J. Med. Chem. 2019

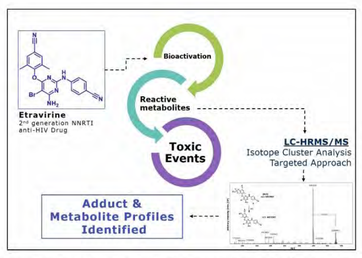

HRMS-based methodologies for identification of Etravirine bioactivation to reactive metabolites: *In vitro* and *in vivo* approaches.
Ana Godinho *et al.* Eur. J. Pharm. Sc. 2018

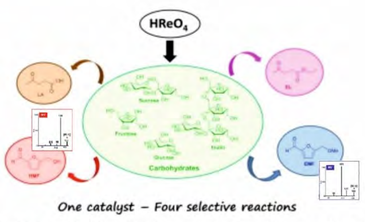

HReO4 as highly efficient and selective catalyst for the conversion of carbohydrates into value added chemicals.
Joana R. Bernardo *et al.* Molecular Catalysis 2019

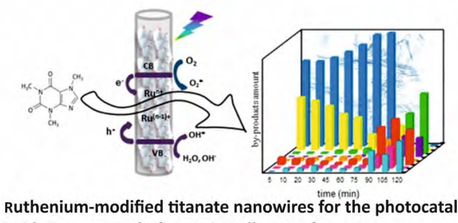

Ruthenium-modified titanate nanowires for the photocatalytic oxidative removal of organic pollutants from water.
Beatriz T. Barrocas *et al.* ACS Appl. Nano Mater. 2019.

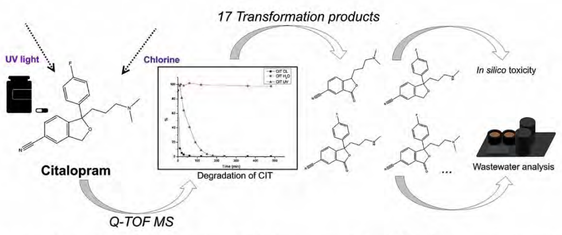

Transformation products of citalopram: Identification, wastewater analysis and *in silico* toxicological assessment.
Rodrigo A. Osawa *et al.* Chemosphere, 2017.

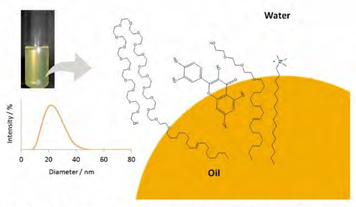

A high loaded cationic nanoemulsion for quercetin delivery obtained by sub-PIT method.
Michelli F. Dario *et al.* Colloids and Surfaces A: Physicochem. Eng. Aspects 2016.

Identification of *Contaminants of Emerging Concern (CEC)* in surface waters

CEC (as human and veterinary pharmaceuticals, pesticides, and various industrial additives) belong to the most important chemical contaminants currently found in the environment . These analysis is really challenging because of the diversity in chemical properties, the complexity of matrices, and generally the very low concentrations at which *CEC* are found.

UHPLC-ESI(+/-)TOF MS and Suspected Target Analysis

- ✓ An in-house accurate mass library was constructed for 64 standards plus 650 suspected substances (drugs and pesticides and care)
- ✓ Screening using Find Compounds-Chromatogram via SigmaFiT™ with Target Analysis Software (Bruker).
- ✓ Values with a mass deviation lower than 5 ppm and mSigma lower than 100 (match factor between the measured isotopic pattern and the theoretical pattern for a given chemical formula) were considered acceptable for positive confirmation (mSigma <100 acceptable, <50 good, and <25 excellent).
- ✓ After screening with the Target Analysis software the results were manualy validated, using the Data Analysis software (accurate mass, isotopic and MS/MS profiles)

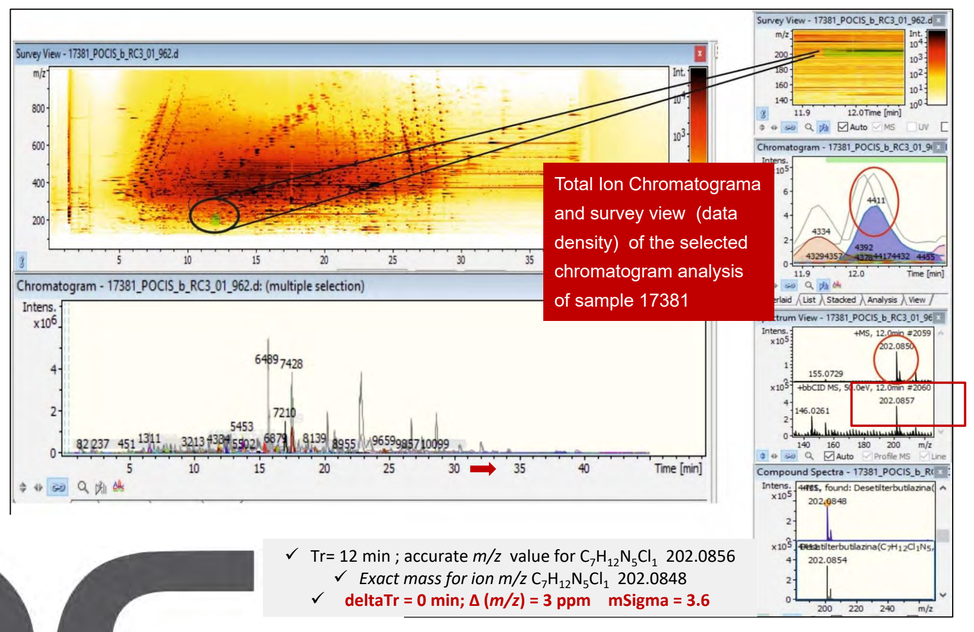

At retention time betwen **11.9 e 12.1 min**

↓

Peak nº 4411 (Tr = 12 min)

↓

ESI(+)/MS and ESI(+)-MS/MS *Spectra*

↓

***m/z* 202.0856 (isotopic profile and MS/MS spectrum)**

↓

Comparison with standard (Data Base)

- ✓ Tr= 12 min ; accurate *m/z* value for $C_7H_{12}N_5Cl_1$ 202.0856
- ✓ *Exact mass for ion m/z* $C_7H_{12}N_5Cl_1$ 202.0848
- ✓ **deltaTr = 0 min; Δ (*m/z*) = 3 ppm mSigma = 3.6**

Validation accept ; contaminant identified ⟶ Simazine CAS 122-34-9

MASS SPECTROMETRY

ESI(+)/HRMS: *m/z* calcd. for $[C_{10}H_6N_4O_2+H]^+$: 215.0564; found 215.0548.

A Sustainable Synthesis of Asymmetric Phenazines and Phenoxazinones Mediated by CotA-Laccase.
Ana Catarina Sousa et al., Adv. Synthesis & Catalysis, 2018.

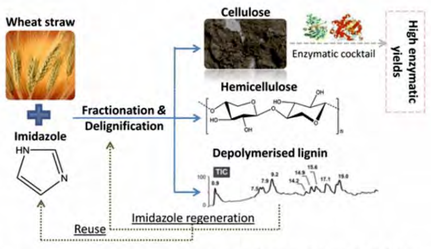

Imidazole: Prospect solvent for lignocellulosic biomass fractionation and delignification.
Ana Rita Morais *et al.* ACS Sustainable Chem. Eng. 2016

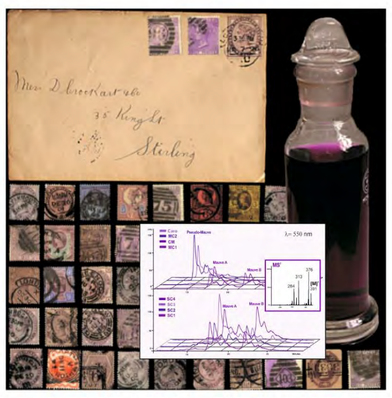

Perkin´s and Caro Mauveine in Queen Victoria Lilac postage stamps: A Chemical Analysis
M. Conceição Oliveira *et al.* Chem. Eur. J. 2014

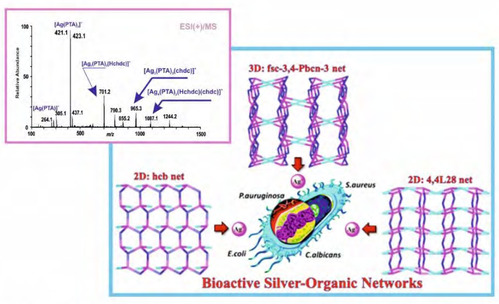

Bioactive Silver-Organic Networks assembled from1,3,5-Triaza-7--phosphaadamantane and flexible Cyclohexanecarboxylate blocks.
Sabina W. Jaros *et al.* Inorganic Chemistry 2016.

Biodegradation products of a sulfonated azo dye in aerobic granular sludge sequencing batch reactors treating a simulated wastewater

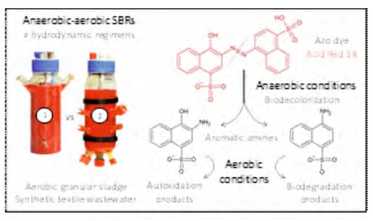

Rita D.G. Franca, TEA 2018
(PhD Programma in Biotechnology and Biosciences)

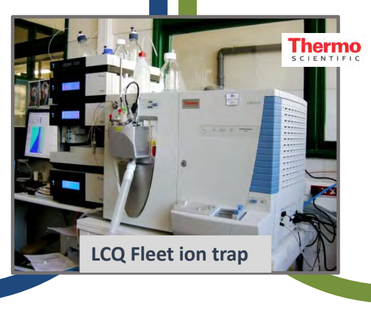

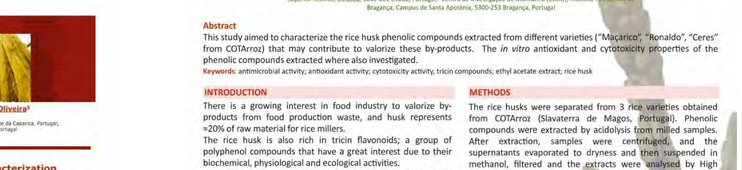

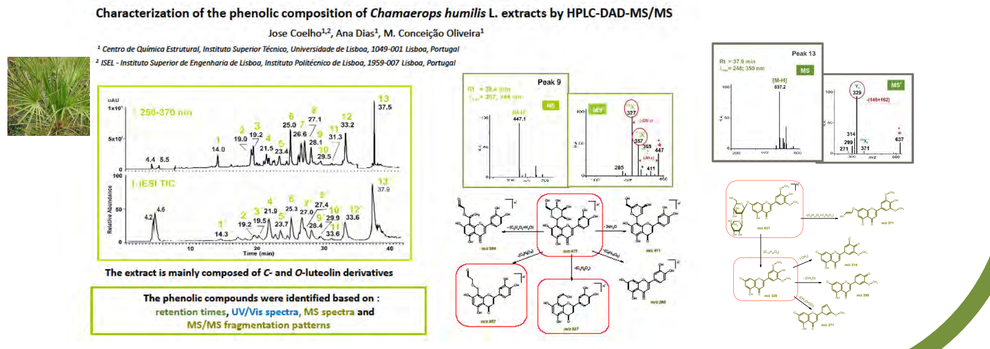

Funding:

Centro de Química Estrutural is funded by Fundação para a Ciência e Tecnologia – project UID/QUI/00100/2019.

Rede Nacional de Espectrometria de Massa, ref. LISBOA-01-0145-FEDER-022125

FCT Fundação para a Ciência e a Tecnologia · Lisb@20 20 · Portugal 2020 · União Europeia Fundo Europeu de Desenvolvimento Regional · RNEM Portuguese Mass Spectrometry Network

Development of an Analytical Method for the Determination of 6 Tricyclic Antidepressants in Biological Matrices

M.N. Oliveira*, S.M. Ahmad, N.R. Neng, J.M.F. Nogueira

Centro de Química Estrutural, Centro de Química e Bioquímica

Faculdade de Ciências, Universidade de Lisboa, Campo Grande, 1749-016 Lisboa, Portugal

(*mariananetoliveira@hotmail.com)

06 CE

Introduction

Depression affects around 300 million people globally. It substantially impairs people's life. It can even lead to suicide. Antidepressants are used as an effective form of treatment[1].

Patients with a record of depressive disorders, dementia and anxiety disorders in Portugal have increased over recent years[2].

Tricyclic antidepressants (TCAs) are an important class of psychoactive drugs, however they can dangerously lead to an overdose due to the TCAs' relatively narrow therapeutic/toxic index. The determination of TCAs in biological matrices is compulsory for emergency toxicological screening, drug abuse testing, forensic medical examinations for probable fatality caused through overdose, therapy monitoring, and for pharmacokinetics studies[3].

In this contribution, we propose an analytical methodology for the determination of 6 common TCAs (figure 1) using bar adsorptive microextraction[4] followed by microliquid desorption in combination with large volume injection-gas chromatography coupled to mass spectrometry operating in the selected-ion monitoring acquisition mode (BAµE-µLD/LVI-GC-MS(SIM)).

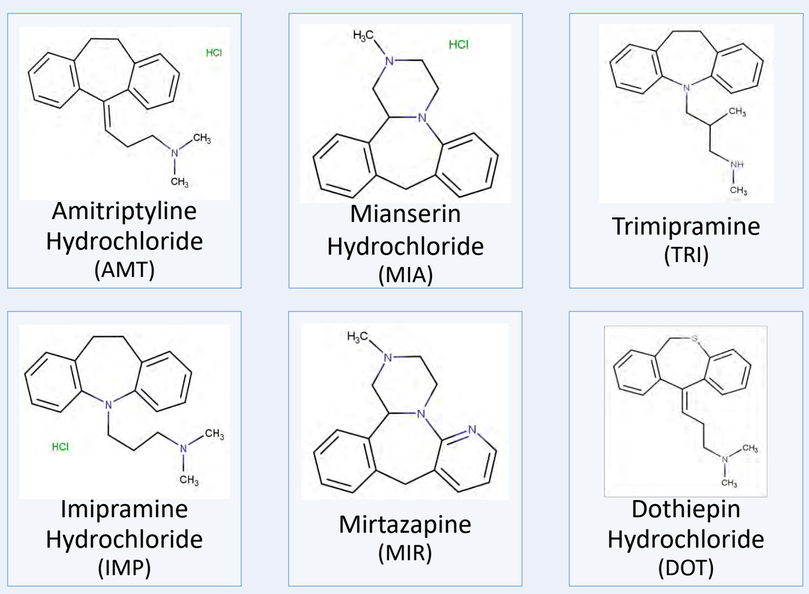

Figure 1 - Chemical structures of the studied TCAs.

Experimental Procedure

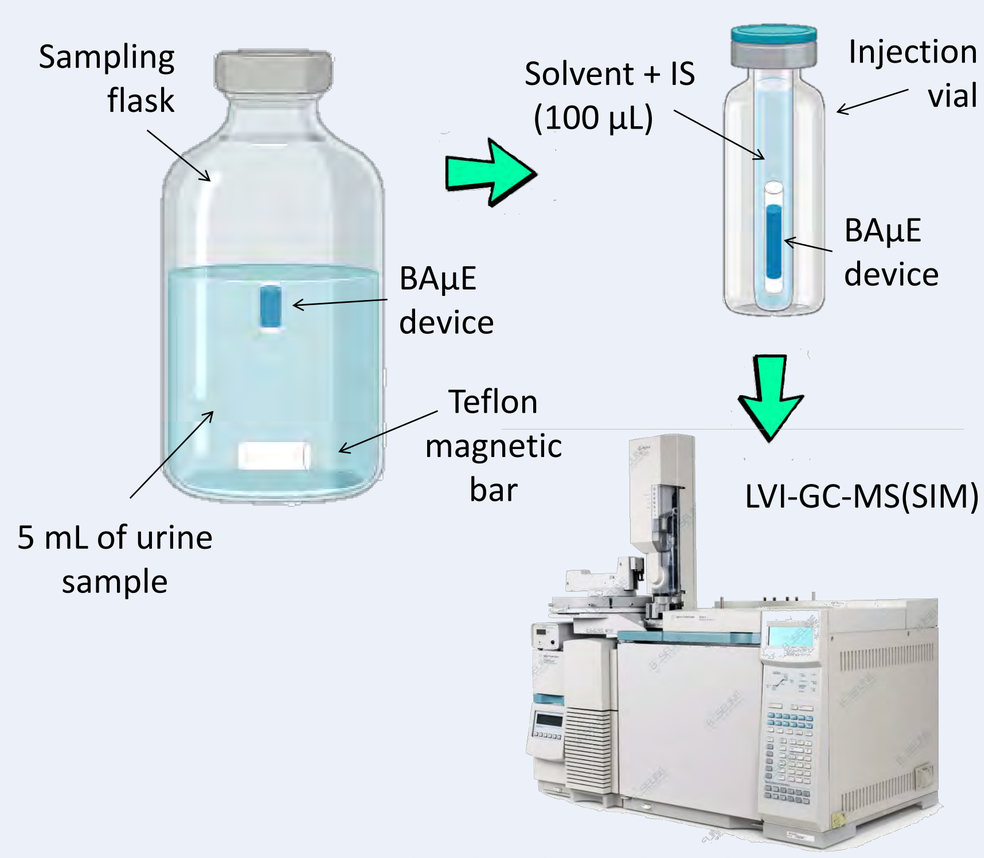

Figure 2 - Proposed analytical procedure scheme.

Instrumental Analysis

GC conditions

- Gas Chromatograph: 6890 Agilent Technologies System
- Column: Zebron ZB-5 (30m × 0.25mm × 0.25µm) (Phenomenex)
- Software: MSD ChemStation (version C.00.00);
- Injection Mode: Solvent vent (10 µL)
- Injector Temperature: 80 ˚C (0.45 min) to 280 ˚C at a rate of 600 ˚C min^{-1}
- Oven: 80 ˚C (held 1 min) and then at 20 ˚C min^{-1} to 240 ˚C (hold for 5 min); 1 ˚C min^{-1} to 245 ˚C; 20 ˚C min^{-1} to 300 ˚C;
- Mobile Phase: Helium, at constant pressure mode

MS conditions

- Mass detector: 5973*N* Agilent Technologies
- Transfer Line: 280 ˚C
- Quadrupole: 150 ˚C
- Ion source temperature: 230 ˚C
- Ionization mode: Electronic ionization (70 eV)

Results

Method optimization

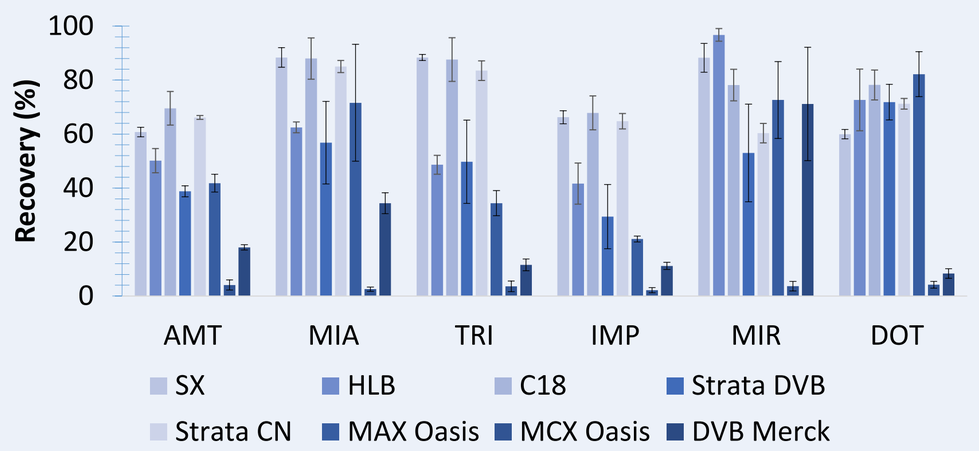

Figure 3 - Selectivity effect on the average yields obtained by BAµE-µLD/LVI-GC-MS(SIM) using diferente polymeric based sorbent phases for the microextraction of the target TCAs in aqueous matrices.

Optimized experimental conditions

Microextraction

- Sorbent: C18
- Equilibrium time: 16 h
- Stirring rate: 990 rpm
- Matrix pH: 12
- Organic modifier (MeOH): 0%
- Ionic strength (NaCl): 5%

Back-extraction

- Desorption solvent: MeOH:ACN (50:50, v:v, 90µL)
- 30 min under sonication

Application to urine matrices

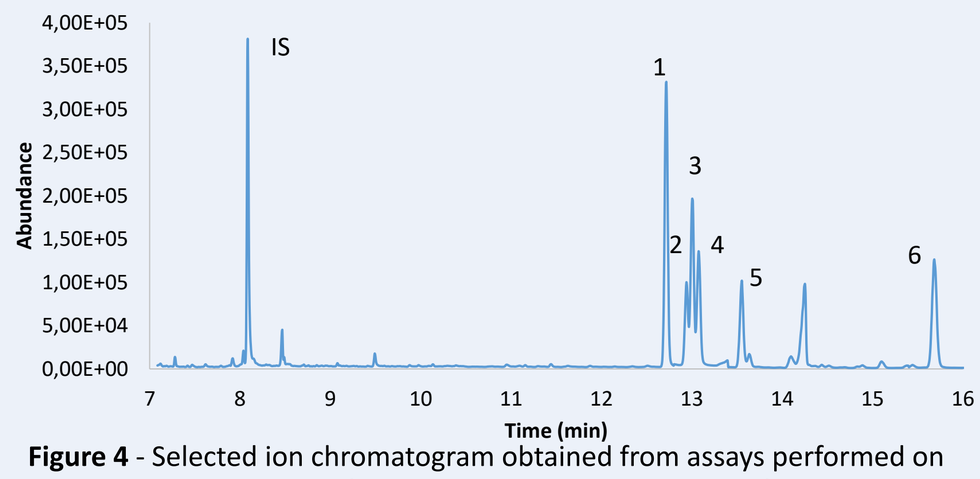

Figure 4 - Selected ion chromatogram obtained from assays performed on spiked urine sample (0.1 µg/L), performed by BAµE(C18)-µLD/LVI-GC-MS(SIM), under optimized experimental conditions. 1 - AMT; 2 - MIA; 3 - TRI; 4 - IMP; 5 - MIR; 6 - DOT.

Table 1 - Validation data obtained for the present study, including average recovery yields, limits of detection (LOD), lower limits of quantification (LLOQ), linear range and determination coeficientes (r^2), obtained by BAµE(C18)-µLD/LVI-GC-MS(SIM), under optimized experimental conditions.

Compounds	Recovery Yields ± RSD (%)	LOD (µg/L)	LLOQ (µg/L)	Linear range (µg/L)	r^2
AMT	103.0 ± 6.8	0.1953	12.5	12.5 - 100.0	0.9991
MIA	93.0 ± 1.2	0.1953	1.6	1.6 - 100.0	0.9994
TRI	94.6 ± 2.0	0.1953	12.5	12.5 - 100.0	0.9989
IMP	97.3 ± 5.7	0.1953	12.5	12.5 - 100.0	0.9987
MIR	99.7 ± 4.4	0.3906	1.6	1.6 - 100.0	0.9997
DOT	100.9 ± 4.9	1.5625	1.6	1.6 - 100.0	0.9976

The linear model proved to be suitable for the analysis of the 6 target TCAs from urine samples ($r^2 > 0.99$).

Very soon intra and inter-day accuracy and precision assays will also be performed, as well as matrix effects and average recovery yield assays at different spiking levels. Different biological matrices (such as plasma) will also be studied.

Conclusions

- A novel methodolgy (BAµE(C18)-µLD/LVI-GC-MS(SIM)) is proposed for trace analysis of six TCAs in urine matrices.
- The analytical data shows remarkable performance, indicating to be a good alternative over other established microextraction techniques.

Funding:

The authors thank Fundação para a Ciência e Tecnologia (Portugal) for financial support through project UID/QUI/00100/2019 for CQE, UID/Multi/00612/2019 for CQB and for the post-Doc (SFRH/BPD/86071/2012) and PhD (SFRH/BD/107892/2015) grants.

References:

1. Web page about Mental Disorders from World Health Organization. http://www.who.int/en/news-room/fact-sheets/detail/mental-disorders. Published on April 9th, 2018. (Consulted on April 4th, 2018).
2. Relatório do Programa Nacional para a Saúde Mental 2017 from Direção-geral de Saúde.
3. Farajzadeh, M. A.; Abbaspour, M. Biomed. Chromatogr. 32 (8) (2018) e4251.
4. Nogueira, J. M. F. Anal. Chim. Acta 757 (2012) 1–10

NEW DONEPEZIL MIMETIC HYBRIDS AS POTENTIAL MULTI-TARGET ANTI-ALZHEIMER´S DISEASE AGENTS

Marina Costa[a], Federica Rinaldo[a,b], Romane Josselin[a], Luca Piemontese[b], Diana Silva[c], Sandra M. Cardoso[c,d], Sílvia Chaves[a], M. Amélia Santos[a]

[a]Centro de Química Estrutural, Instituto Superior Técnico, Universidade de Lisboa, Av. Rovisco Pais 1, 1049-001 Lisboa, Portugal; [b]Dipartimento di Farmacia–Scienze del Farmaco, Università degli Studi di Bari "Aldo Moro", Via E. Orabona 4, 70125 Bari, Italy; [c]CNC – Center for Neuroscience and Cell Biology, University of Coimbra, Coimbra, Portugal; [d]Institute of Molecular and Cell Biology, Faculty of Medicine, University of Coimbra, Coimbra, Portugal

Email:masantos@tecnico.ulisboa.pt

CQE Química Estrutural

04 BIOIN

Introduction

Alzheimer's Disease (AD)

- **AD is a complex neurodegenerative disorder characterized by progressive deterioration in memory, cognition and behavior.**
- **Main pathological hallmarks of AD brains:**
  Amyloid plaques; Neurofibrillary tangles; Cholinergic deficit
- **Current symptomatic treatment (no cure):**
  Inhibitors of AChE; NMDA receptor antagonist
- ***AD* Multifactorial nature ⟹ *Multi-target approach*** [1]:
  Inhibition of AChE; Inhibition of Aβ aggregation; Control of ROS ; Modulation of metal dyshomeostasis.

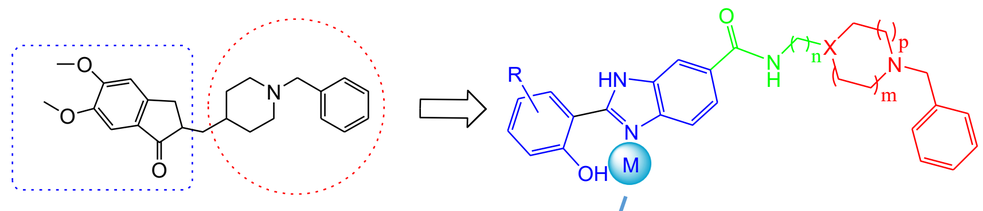

Scheme 1. Donepezil (DNP) and design of hybrid DNP mimetics

Aims. To pursue our interest on the engineering of new multitargeting drug candidates[2,3], aimed to combat both the symptoms and the causes of Alzheimer´s disease (AD), Donepezil (DNP) templates (for cholinesterase inhibitory capacity) are hybridized with hydroxyphenylbenzimidazole-based units to provide the conjugates with other important pharmacological responses, namely through the inhibition of Aβ aggregation and the control of related features as metal dysregulation of AD patient brains.
Methods. The polyfunctional compounds are firstly designed on the basis of computational simulation and then selected compounds are prepared by standard methods of organic synthesis. The new compounds are evaluated in aqueous solution for their biological activity, namely for the inhibition of AChE and Aβ aggregation, under the co-effect of metal ions, using standard spectroscopic techniques. Effects of these compounds in cell viability and neuroprotection are also assessed in neuroblastoma cells after $A\beta_{1-42}$ induced toxicity.

Molecular Modelling

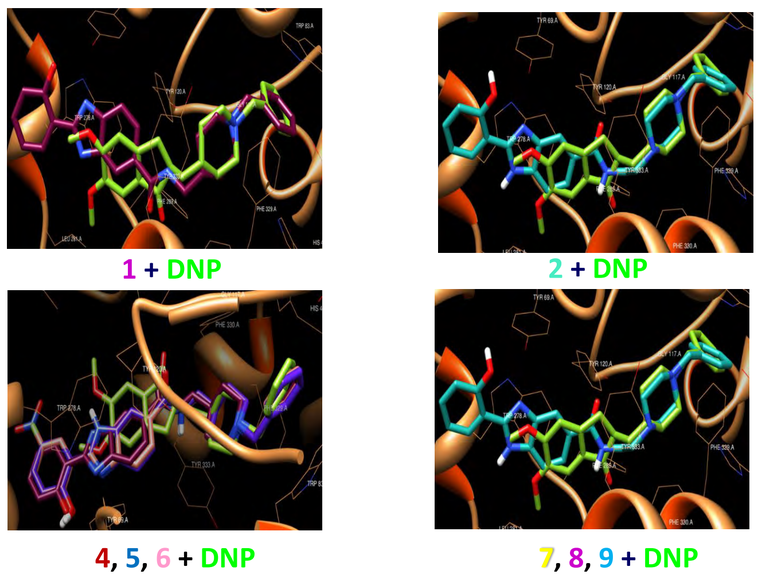

Fig1. Docking models of ligands superimposed with DNP (1ODC, green) within the *Tc*AChE active site[4,5].

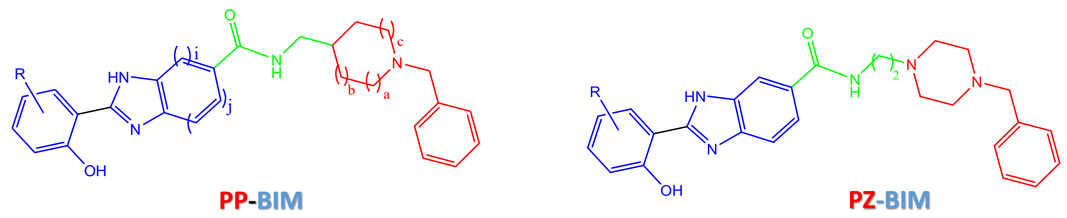

L (PP, BIM)c	a/b/c	i/j	R	clog P	log BB
1 (p,p)	1/1/1	1/1	H	4.39	-0.73
3 (m,p)	0/1/2	1/1	H	4.12	-0.83
4 (o,p)	0/0/3	1/1	H	4.22	-0.54
5 (p,o)	1/1/1	3/0	H	3.98	-0.73
6 (p,p)	1/1/1	1/1	F	4.14	-0.36

L	R	clog P	log BB
2	H	2.59	-0.10
7	NO_2	2.42	-1.15
8	F	3.49	-0.15
9	OMe	2.84	-0.03

Scheme 2. Structural parameters of the hybrid DNP mimetics: Benzylpiperidine-Benzimidole (**PP-BIM**) and Benzylpiperazine-Benzimidazole (**PZ-BIM**). Calculated *c*Log *P* and log *BB* (*QikProp* prog.)

Inhibition of Aβ aggregation

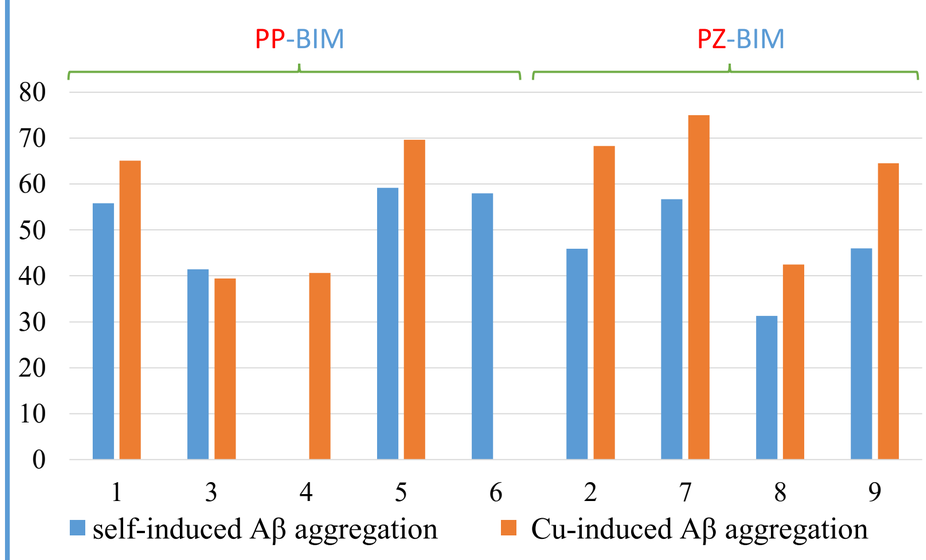

Fig. 2 % Inhibition of self- & Cu^{2+}-induced $A\beta_{42}$ aggregation (ThT fluoresc. method)[3]

AChE Inhibition

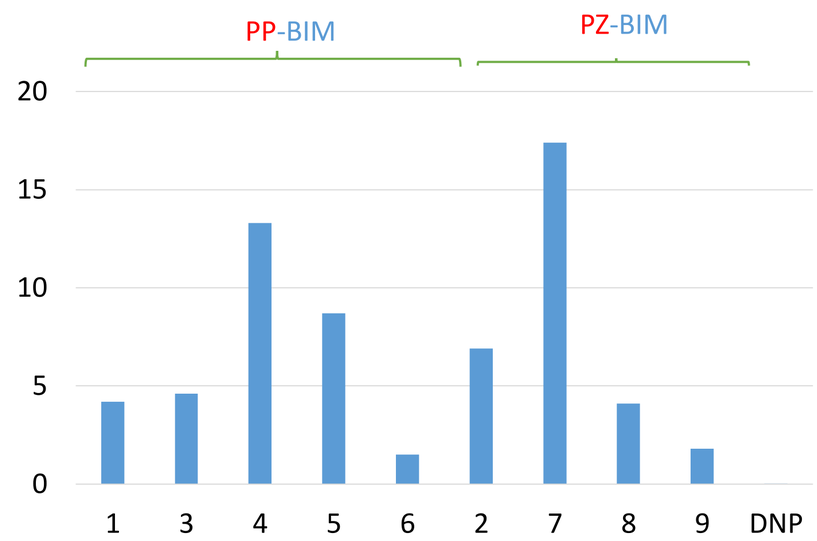

Fig. 3. AChE (*Electric eel*) inhibition (IC_{50}, μM). (Adap. Ellman's method)[3]

Neuroprotective Effect

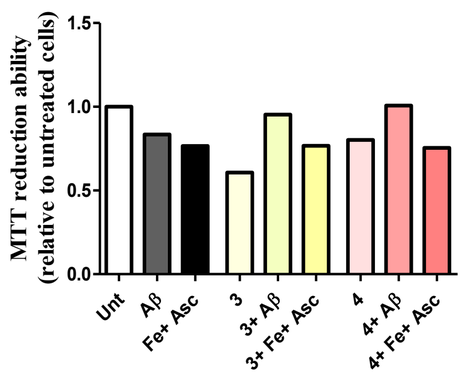

Fig. 4. Potential of compounds **3** and **4** to rescue cell viability after treatment with AD stressors (amyloid peptide and oxidative stress). SHSY-5Y cells were pre-treated for 1h with the compounds and then $A\beta_{42}$ or Iron/Ascorbate were added. After 24h, MTT cell viability assay was performed. Results are expressed against untreated cells.

Conclusions

- The compounds present a moderate-high (31-75%) Aβ-aggregation inhibition with apparent dependence both on the intercalating ability of the compound inside the fibrils and on its copper chelating capacity due to the **BIM** chelating moiety. For the benzylpiperidine-bearing hybrids (**PP-BIM**), the positional isomerization in the **BIM** moiety is not determinant for activity, in opposition to the **PP** moiety for which the *para* position is favored. Regarding the benzylpiperazine hybrids (**PZ-BIM**) , there is dependence on the **BIM** substituent with best activity for the nitro-derivative (less lipophilic).
- The AChE inhibition showed activity in low micromolar range, evidencing some structure-activity relationships, mostly supported by docking simulations. The **PP-BIM** hybrids present better activity than the corresponding **PZ-BIM** analogues (**1/2**; **6/8**); the positional isomers of PP-BIM hybrids evidenced activity increase with the distance between amine group of piperidine (**1**, **3**, **4**) (and also of benzimidazole(**1**, **5**)) and the corresponding carbon of derivatization. Substitution on the **BIM** unit affects the AChE inhibitory activity: the best (+) effects were found for the fluoro-derivatives (**6/1** and **9/2**), while a (-) effect was observed for the nitro- derivative (**7/2**).
- The neuroprotective effects were accomplished for a selection of PP-BIMs (**3**,**4**) by preventing Aβ-induced cell toxicity, but the cell protection from Asc/Fe-induced oxidative stress was not evidenced (preliminary results).

Funding:
This work was supported by FCT/MEC financing CQE (FCT UID/QUI/0100/2019)) from IST-ID and also Erasmus Programs (F.R., R.J.).

FCT Fundação para a Ciência e a Tecnologia

References:

[1] a) A. Cavalli, M.L. Bolognesi, C. Melchiorre et al, *J. Med. Chem.* 2008, 51, 347; b) M.A. Santos, K. Chand, S. Chaves, *Future Med. Chem*. 2016, 8, 2113.
[2] A. Hiremathad, R.S. Keri, A.R. Esteves, S.M. Cardoso, S. Chaves, M.A. Santos, *Eur. J. Med. Chem.* 2018, 148, 255-267.
[3] L. Piemontese, D. Tomás, A. Hiremathad, V. Capriati, E. Candeias, S.M. Cardoso, S. Chaves, M.A. Santos, *J. Enz. Inhib. Med. Chem.* 2018, 33, 1212.
[4] RCSB Protein Data Bank (PDB, entry 1ODC).
[5] GOLD software v. 5.2. G. Jones, P. Willett, R.C. Glen, A.R. Leach, R. Taylor, *J. Mol. Biol.* 1997, 267, 727.

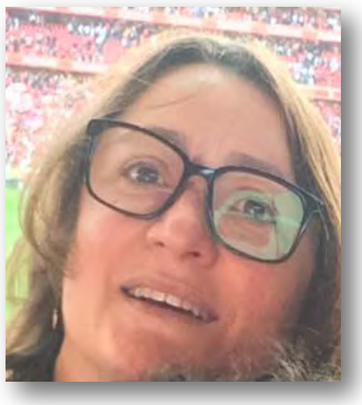

SYNTHESIS AND CHARACTERIZATION OF LOW-COST ADSORBENT MATERIALS FROM GLYCEROL

Mary Batista[1,2], Isabel Fonseca[2], Ana Carvalho[1]

[1] Faculdade de Ciências da Universidade de Lisboa
[2]Faculdade de Ciências da Universidade Nova de Lisboa

INTRODUCTION

- In the search for alternative fuels to petroleum, biodiesel has gained expression in the market and its production has been increasing steadily.
- Sustainable biodiesel production requires optimization of the production process and drastic increase in the utilization of glycerol, the principal by-product of the process.
- With the introduction of large volumes of glycerol coming from biodiesel production, it is imperious to find new applications for this chemical; otherwise the economic feasibility of the biodiesel as a renewable fuel can be impaired.[1,2]Recent studies report the use of glycerol for the production of chars.[3,4]
- This present study is focused on the synthesize glycerol-based activated carbons *via* a two-step: (1) procedure involving carbonization and (2) chemical activation or thermal activation.

ACARBONS PRODUCTION

Carbonization
- Glycerol (Iberol-Portugal)
- Glycerol:H_2SO_4; 180 °C for 6 h

Chemical Activation
- Char:K_2CO_3
- N_2 flow of 5 $cm^3\ min^{-1}$
- 700 °C for 1h

Thermal Activation
- 500 °C, 600 °C and 700 °C for 1h
- N_2 flow of 5 $cm^3\ min^{-1}$

CHARACTERIZATION TECHNIQUES

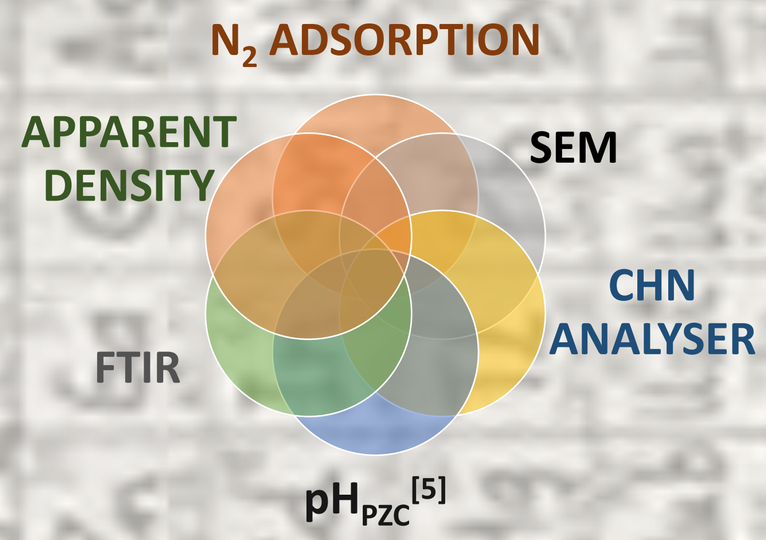

CHARACTERIZATION OF MATERIALS

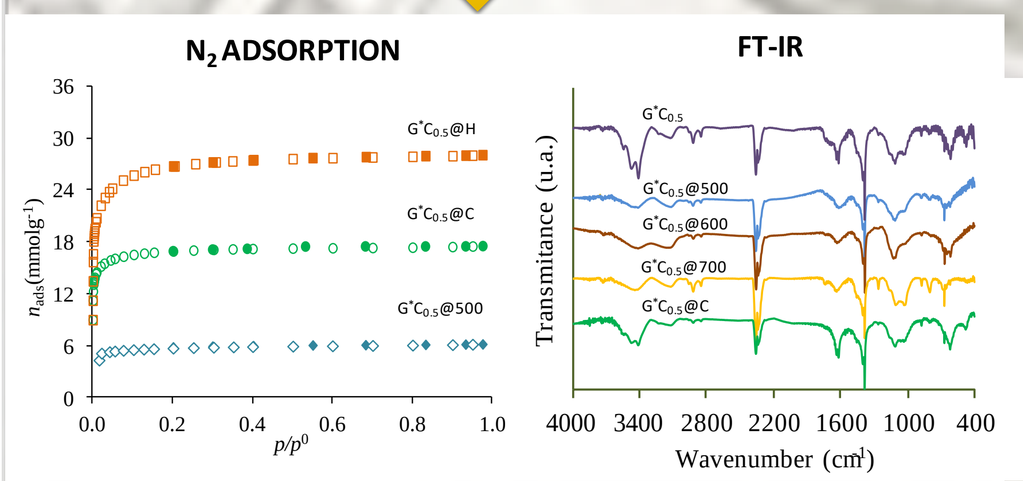

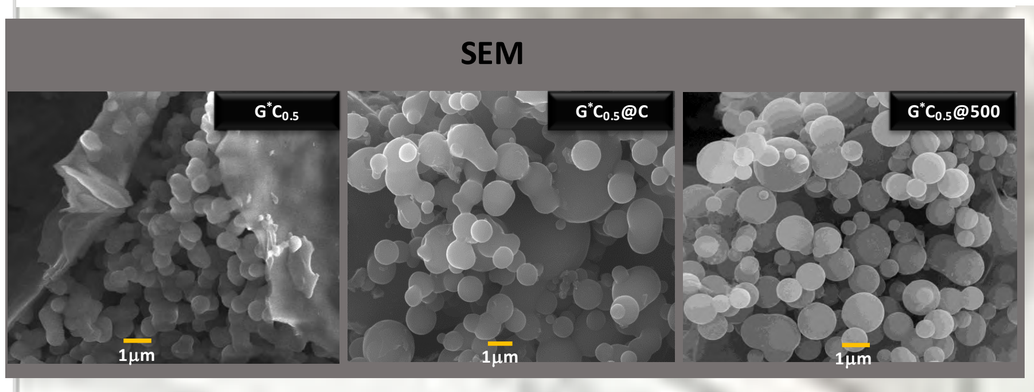

TEXTURAL PROPERTIESAND PREPARATION YIELD (%) OF GLYCEROL-BASED *MATERIALS*

Sample	A_{BET} ($m^2\ g^{-1}$)	V_{TOTAL}[a] ($cm^3\ g^{-1}$)	V_{MESO}[b] ($cm^3\ g^{-1}$)	α_s method $V_{\alpha\ TOTAL}$ ($cm^3 g^{-1}$)	$V_{\alpha\ ULTRA}$ ($cm^3\ g^{-1}$)	$V_{\alpha\ SUPER}$ ($cm^3\ g^{-1}$)	Apparent density (kgm^{-3})	Yield [c](%)
Samples from industrial glycerol								
$G^{\gamma}C_1$	5	-	-	-	-	-	196	49
$G^{\gamma}C_1$@C	1805	0.75	0.06	0.69	0.39	0.30	368	42
$G^{\gamma}C_1$@H	2097	0.99	0.08	0.95	0.09	0.86	122	15
$G^{\gamma}C_{0.5}$	12	0.01	-	-	-	-	437	49
Activation with K_2CO_3								
$G^{\gamma}C_{0.5}$@C	1111	0.44	0.01	0.43	0.26	0.17	493	23
Activation with KOH								
$G^{\gamma}C_{0.5}$@H	2157	0.99	0.08	0.91	0.09	0.82	125	10
Thermal activation								
$G^{\gamma}C_{0.5}$@500	523	0.22	0.02	0.20	0.11	0.09	442	28
$G^{\gamma}C_{0.5}$@600	474	0.19	0.01	0.18	0.13	0.05	501	26
$G^{\gamma}C_{0.5}$@700	467	0.19	0.01	0.18	0.12	0.06	525	23

[a]Evaluated by the amount adsorbed at p/p^0 = 0.95 in the N_2 adsorption isotherm. [b] Calculated by the difference between V_{TOTAL} and $V_{\alpha TOTAL}$. [c]The yield glycerol-char calculated by eq. (1): Yield (%) = $(w_f/w_0) \times 10$ (1), were w_f and w_0 (g) are the weights of glycerol-based activated carbons and glycerol-char, respectively.

CHEMICAL AND PHYSICAL PROPERTIES OF GLYCEROL-BASED *MATERIALS*

Sample	Ash (%)	C (%)	H (%)	N (%)	S (%)	O (%)	pHpzc
$G^*C_{0.5}$	0.2	69.1	4.4	n.d.	1.1	25.0	2.0
$G^*C_{0.5}$@C	3.1	82.1	0.7	0.07	1.1	9.8	3.8
$G^*C_{0.5}$@500	2.3	80.8	2.8	0.02	3.3	8.5	4.1

n.d. = not detected

FINAL REMARKS AND FUTURE WORK

- Chemical activation of acid carbonized glycerol allowed the preparation of an activated carbon with a developed micropore network. Regardless the temperature used, thermal activation promoted a smaller porosity development, composed practically only by micropores.
- SEM micrographs show that the materials are constituted by interconnected spheres with diameters of ≈ 1-2 µm.
- The FTIR and pH_{PZC} data reveal the acidic nature of the surface functional groups, which is in line with the high amounts of sulfur and oxygen detected in the elemental analysis.
- Considering all the above facts, glycerol-derived activated carbons will be tested as adsorbent materials. Moreover, the high acidity of the samples allow us to foreseen their use as catalysts.

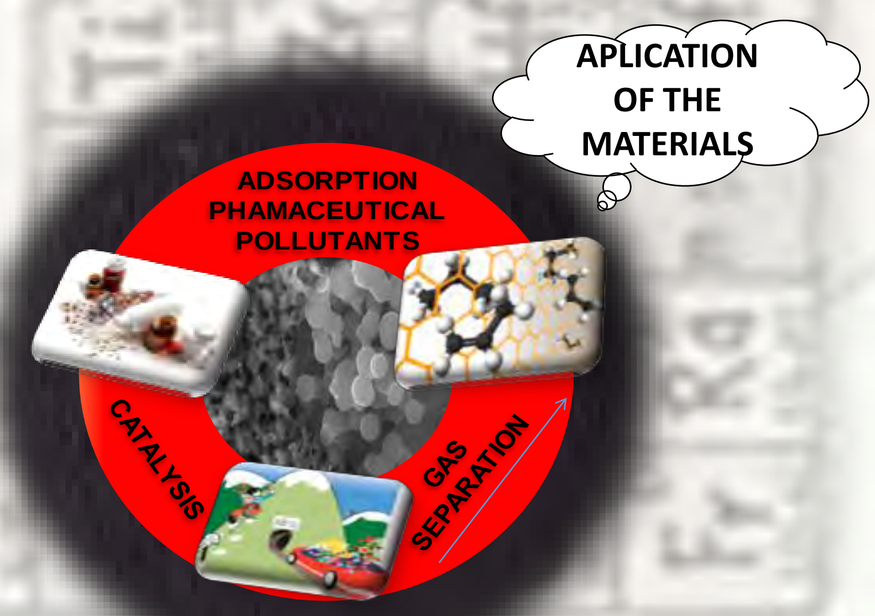

06 CE

Funding:
Fundação para a Ciência e Tecnologia (FCT) funds Centro de Química Estrutural by project UID/QUI/00100/2019; Centro de Química e Bioquímica by project UID/Multi/00612/2019. Mary Batista thanks FCT by Post-doc grant (SFRH/PBD/84542/2012) and IBEROL for supplying the glycerol.

References:
[1]M.A. Betiha *et al.* Appl. Catal. B: Environ. 182 (2016) 15-25.
[2]B.P. Pinto et al. C.J.A. Mota, Fuel 168 (2016) 76-80.
[3]S. Álvarez-Torrellas *et al*. Chem. Eng. J. 296 (2016) 277.
[4]M.K.S. Batista *et al.* RSC Adv. 6 (2016) 45419-45 427.
[5] J. S. Noh, J.A. Schwarz, Colloid Interface Sci. 130 (1989) 157-167.

In-situ electrochemical and fiber-optic micro-sensors: traditional and novel applications, limitations, challenges

Maryna Taryba, Alberto Adán-Más, M.F. Montemor

CQE Química Estrutural

CSSE

Funding:
Centro de Química Estrutural is funded by Fundação para a Ciência e Tecnologia – project UID/QUI/00100/2019. M-ERA.NET/0004/2014

FCT Fundação para a Ciência e a Tecnologia

Equipment:

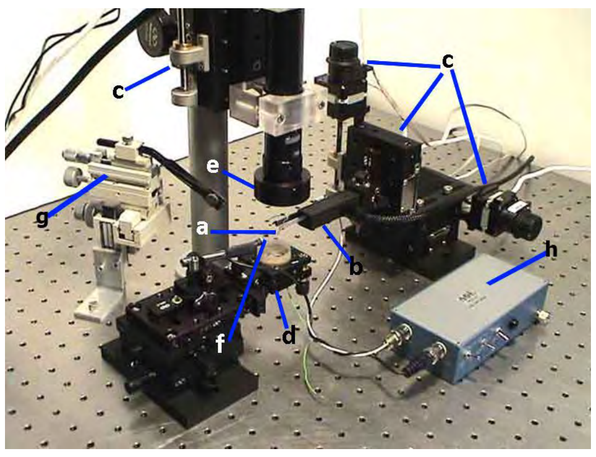

a) vibrating probe;
b) 2D vibrating linkage (preamplifier);
c) 3D computerized stepper-motors system;
d) movable holder;
e) video camera, with a long-distance lens, providing magnification up to 400 times;
f) two pin set of reference electrode and ground electrode;
g) 3D micro-manipulator, used for calibration or probe positioning in advanced multi-electrode setup;
h) SVET preamplifier

Advanced sensors combinations, examples:

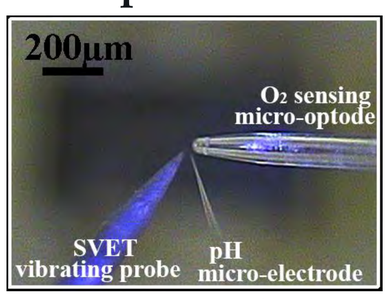

Assembled cell for triple simultaneous measurements:

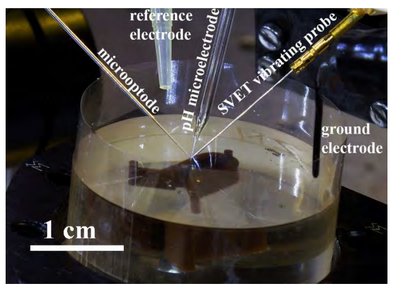

Tools/Techniques:

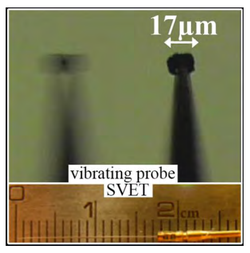

SVET measures the potential difference between extreme points of the probe vibration. The measured potential difference is being converted into current density using cunductivity/resistivity of the immersion solution. The probe is vibrating in the vertical (Z) and horizontal (X) planes. →Current density distribution is registered.

SIET - potentiometry with microprobes. Glass-capillary ion-selective microelectrode are prepared using the silanized capillaries that are tip-filled with a selective membrane and back-filled with an inner reference solution (membrane length ~ 60 µm). →ion (e.g. pH) distribution is registered.

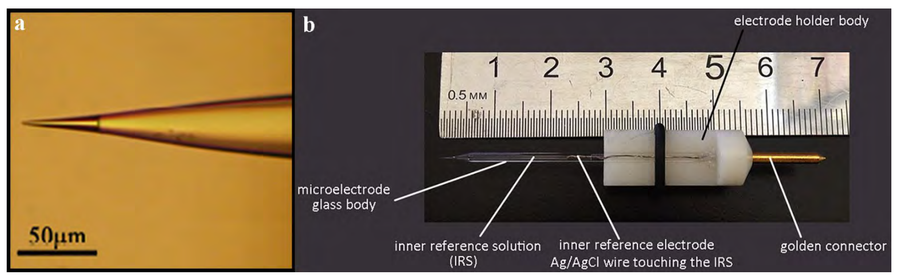

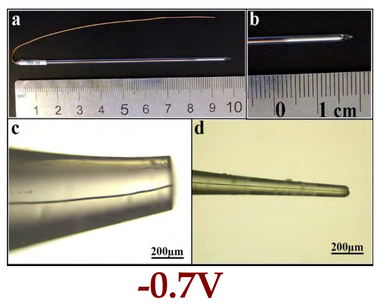

-0.7V

SPET: Various sensors can be used as micro-amperometric probes:
(1) Pt disk probes (d=5-100) µm. Disadvantage - fast fouling
(2) Boron doped nano-crystaline diamond (B-NCD) amperometric micro-sensor (radii < 100nm) [1]. Calibration of microsensor is recorded using N_2 and air saturated solutions. →Dissolved oxygen distribution is registered.

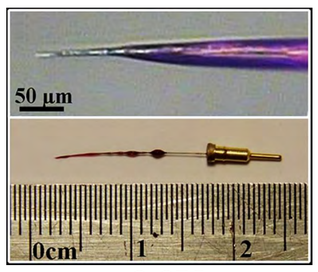

-0.9V

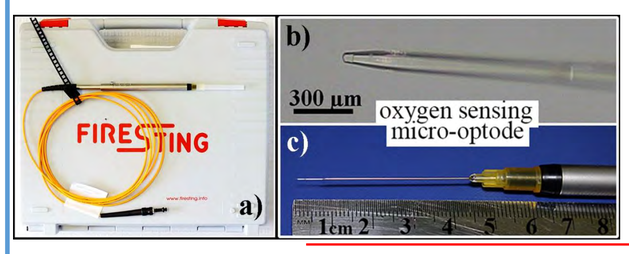

Fiber-optic micro-sensor employs an O2-sensitive luminescent indicator, immobilized on the tip. The indicator is excitable with orange-red light at a wavelength of 610-630nm and demonstrates an oxygen dependent luminescence at 760-790nm. The detection limit of the micro-optode is 0.01 ppm.

Examples

Energy storage

pNa measurements during charge-discharge of mixed Ni-Co hydroxide electrodes in 0.05M Na_2SO_4

Na^+

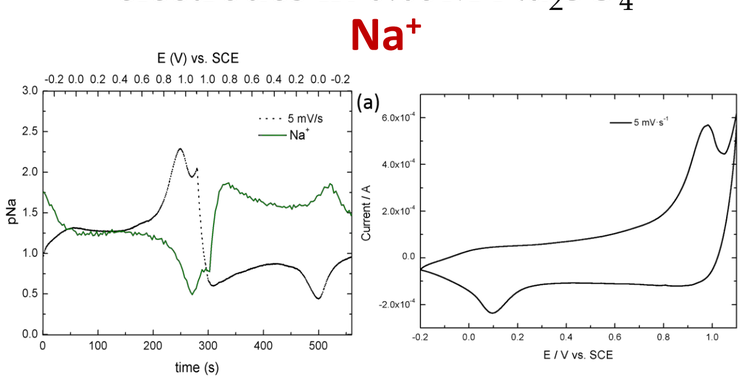

Na_2SO_4 0.05M

Correlation between pH, pNa and dissolved O_2 distributions and cyclic voltammetry provided relevant information concerning the charge-discharge reaction mechanism. Results reinforce the solid-state proton diffusion model and confirms the effect of oxygen evolution reaction as parasitic reaction [2].

Corrosion studies

Simultaneous current density, pH and dissolved oxygen monitoring of the epoxy-coated steel substrate with 2 artificial defects during 24h of non-stop immersion in 0.05M

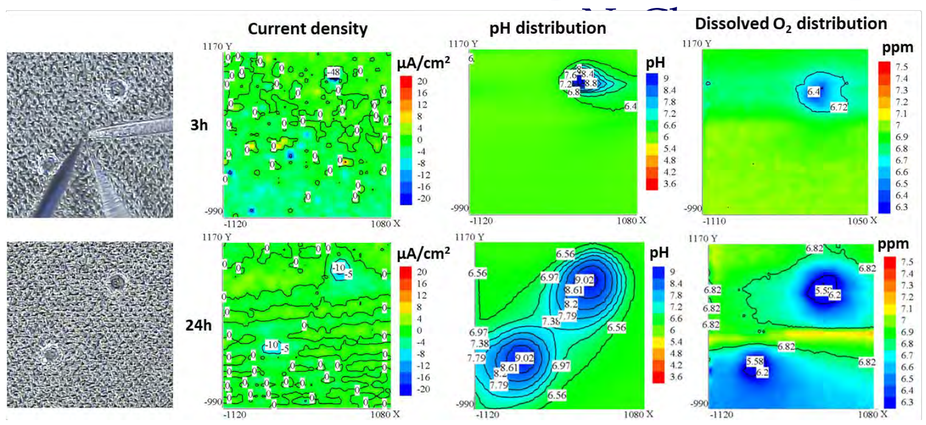

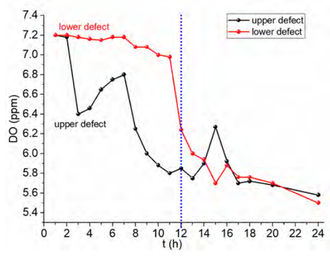

DO: distinguishing cathodic activity and flow of negatively charged species from the coating in absence of cathodic activity

Cathodic process: $O_2 + 2H_2O + 4\bar{e} \rightarrow 4OH^-$

Anodic process: $Me - n\bar{e} \rightarrow Me^{n+}$

Following hydrolysis Process (1st stage): $Me^{n+} + H_2O \rightarrow Me(OH)^{(n-1)+} + OH^-$

Conclusions

- **Micro-scale processes of different nature can be assesses employing micro-sensors with various principles of detection.**
- **Quasi-simultaneous data acquisition allows for obtaining highly reliable correlations**
- **Complementation of the results obtained using localized techniques with physico-chemical analysis can provides additional information for confirmation and clarification of the proposed clues (mechanisms, reactions involved, corrosion products formed)**
- **The process of oxygen reduction can show important signs of degradation for both, energy storage and corrosion science applications. Such signs sometimes are not detectable by other techniques.**
- **Localized electrochemical and fiber-optic micro-sensors successfully demonstrate their efficiency for already known applications (i.e. corrosion science, physiology) and for integration into new challenging fields with extreme importance for modern society (e.g. energy storage)**

References:

[1] E.L. Silva, A.C. Bastos, M.A.Neto, R.F. Silva, M.L. Zheludkevich, M.G.S. Ferreira, F.J. Oliveira. "Boron doped nanocrystaline diamond microelectrodes for the detection of Zn2+ and dissolved O2". Electrochim. Acta 76 (2012) 487-494.

[2] Alberto Adán-Más, Maryna G. Taryba, Teresa M. Silva, Liliane Guerlou-Demourgues, M. F. Montemor, "In-situ localized pH, pNa and dissolved O2 measurements during charge-discharge of mixed Ni-Co hydroxide electrodes". Submitted.

Natural Deep Eutectic Mixtures-Based Aqueous Biphasic Systems For Extraction Of Virus-Like Particles

Mateusz Marchel, Ana S. Coroadinha, Isabel M. Marrucho

CQE Química Estrutural

09 MET

Introduction

Due to their unique properties, virus-like particles (VLPs) have been portrayed as a promising high-value biopharmaceutical in VLP-based vaccination and cancer therapy. Nevertheless, due to the limited physical and economical capabilities of the current downstream processing of VLPs, their production is still difficult and seen as major problem that needs to be tackled.

Aqueous biphasic systems (ABS) have shown to be an alternative unit operation in purification of various biomolecules, because they are versatile, biocompatible and easy to scale-up. Especially the introduction of adjuvants, such as ionic liquids (ILs), in ABS implementation showed that it is possible to fine tune the properties of the aqueous phases in equilibrium, offering new separation schemes characterized by high effectiveness, high yield and high purity degree [1]. In the last years, deep eutectic solvents (DES) have emerged and gained a lot of attention in several fields and different applications, including the ABS implementation, where they have been proposed as a cheaper, versatile and very often more readily biodegradable substitute of ILs [2].

Results

Phase diagrams of PPG 425 + carbohydrate or DES + H_2O

T=25°C

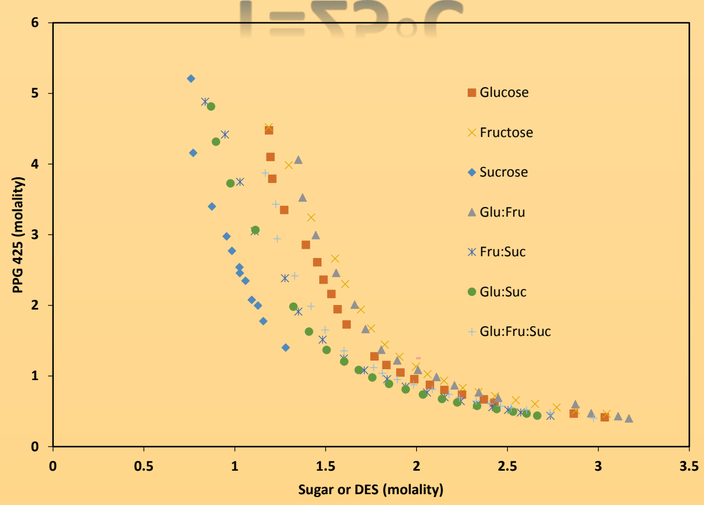

T=37°C

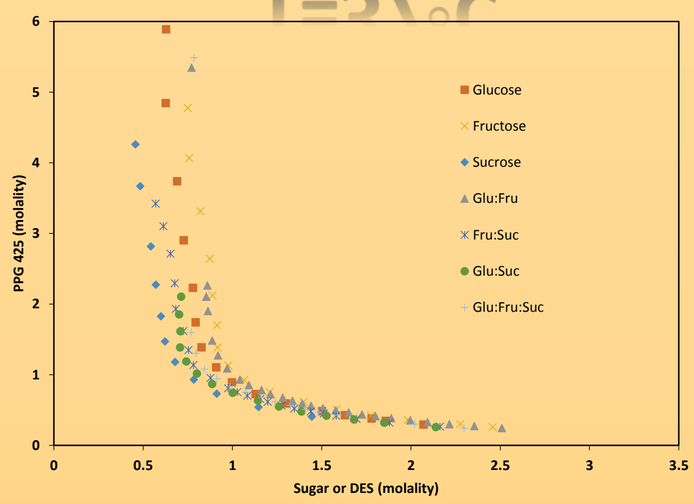

Sucrose > Glu:Suc ≈ Fru:Suc > Glu:Fru:Suc > Glucose > Glu:Fru ≈ Fructose

Decreasing trend order of the ability of studied carbohydrates and DES to promote a biphasic system

Thermoreversible ABS

Increase in binodal phase diagram with increase of temperature

Representation of the binodal curves as a function of carbohydrate concentration

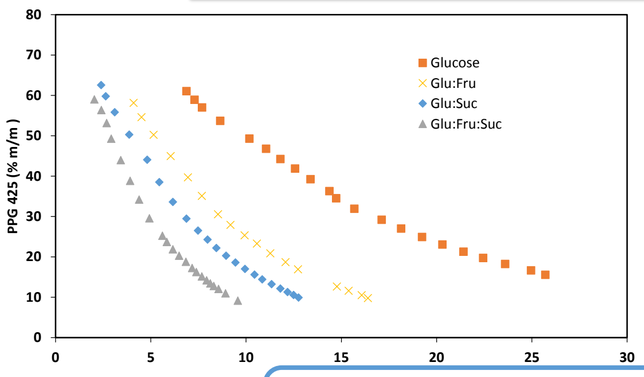

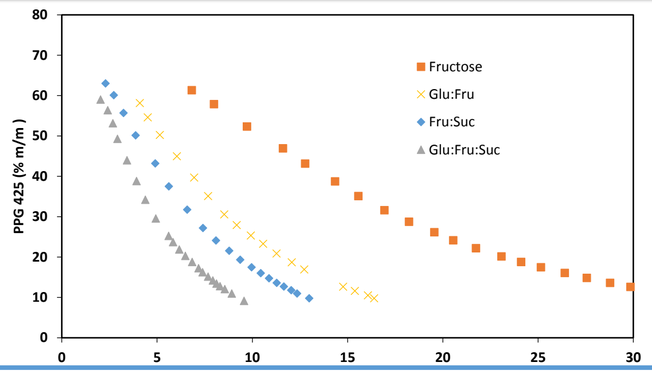

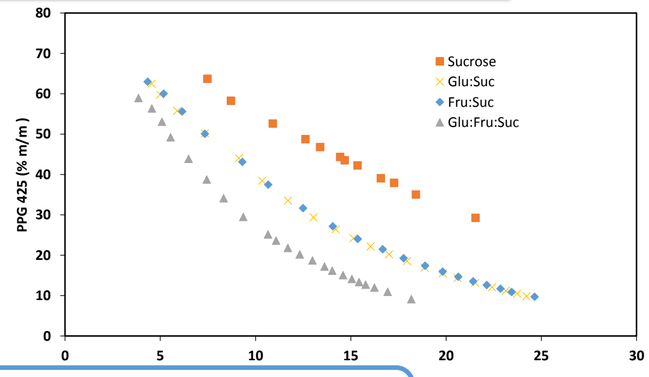

Decrease of concentrations of carbohydrates needed for the liquid-liquid demixing

Cytotoxicity profile:

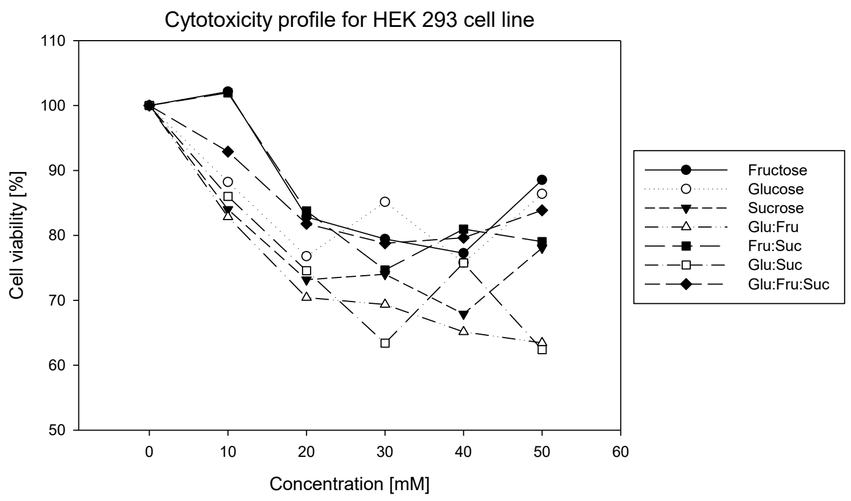

- Good biocompatibility of all tested carbohydrates and DES for HEK 293 cells
- Low concentrations of fructose and Fru:Suc increase cell viability in HEK 293 cells

Conclusions

- Novel thermoreversible ABS composed of carbohydrates and its deep eutectic mixtures were developed and characterized
- The use of DES leads to a decrease of concentrations of compounds needed for the liquid-liquid demixing, when compared with systems composed by only one of the DES components
- The studied carbohydrates and DES show good biocompatibility for the cells and therefore their use in ABS implementation for extraction of VLPs is very promising

Funding:
Centro de Química Estrutural is funded by Fundação para a Ciência e Tecnologia – project UID/QUI/00100/2019. This work was supported by PhD grant PD/BD/114041/2015 from Fundação para a Ciência e a Tecnologia (FCT)

FCT Fundação para a Ciência e a Tecnologia

References:

1. Freire, M.G.; Cláudio, A.F.; Araújo, J.M.; Coutinho, J.A; Marrucho, I.M.; Canongia Lopes, J.N.; Rebelo, L.P. Chem Soc Rev. 2012, 41 (14), 4966-95.
2. Zeng, Q.; Wang, Y.; Huang, Y.; Ding, X.; Chen, J.; Xu, K. Analyst 2014, 139 (10), 2565-2573.

Ionic Liquids Incorporating Nitrogen Units as Novel Lubricants or Oil Additives

Antunes[1,2], A.S. Campinhas[3,4], M. Sá Freire[1,2], P. M. Amorim[1,2], R. Colaço[4], B. Saramago[1], L. C. Branco[2]

[1] Centro de Química Estrutural, Instituto Superior Técnico, Universidade de Lisboa, Av. Rovisco Pais, 1049-001 Lisboa, Portugal,
[2] LAQV-REQUIMTE, Faculdade de Ciências e Tecnologia, Universidade Nova de Lisboa Campus da Caparica, 2829-516 Caparica, Portugal,
[3] Institut Supérieur de BioSciences de Paris, Université Paris XII, Créteil, France,
[4] IDMEC-Instituto de Engenharia Mecânica, Departamento de Engenharia Mecânica, Instituto Superior Técnico, Universidade de Lisboa, Av. Rovisco Pais, 1049-001 Lisboa, Portugal.

Introduction

Lubrication of microelectromechanical and nanoelectromechanical systems are in high demand since the rise of the development of this kind of materials and the need to improve its efficiency. [1] Ionic Liquids (ILs) have been studied for this purpose in Si substrates.

In the present study, the ILs [(C_4SO_3H)MIM][TfO][2], [C_2MIM][S-CSA], [C_2MIM][R-CSA], [C_1-3-pic][$MeSO_4$]; [C_2MIM][TfO][3], and [C_2MIM][$EtSO_4$] [3] were characterized as 2% wt additives to commercial lubricant PEG 200 while the ILs [C_1-3-pic][$MeSO_4$] and [C_2-3-pic][$EtSO_4$][4] were characterized as pure lubricants. Also, the application of Deep Eutectic Solvents (DES as formed by combination of Hydrogen bond donors and acceptors) as lubricants have been tested (DES based on [C_1-3-pic][$MeSO_4$]:PEG 200 (1:4) and [C_2MIM][S-CSA]: PEG 200 (1:4)).

ANIONS

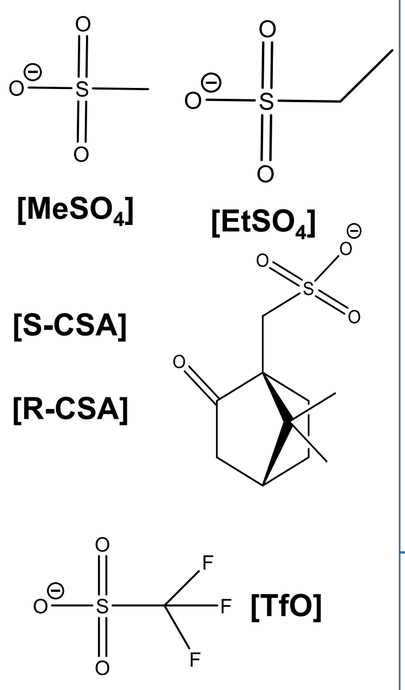

CATIONS

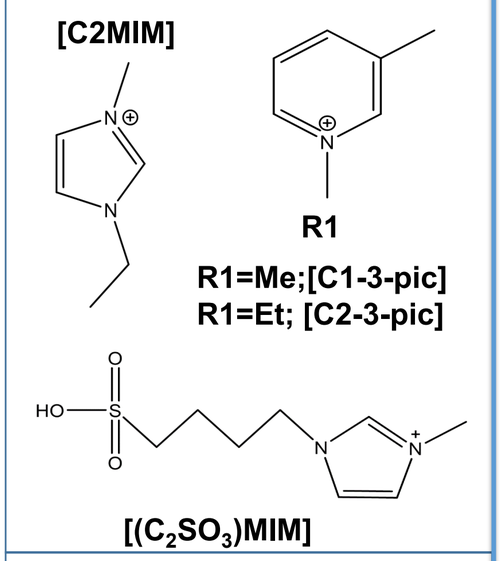

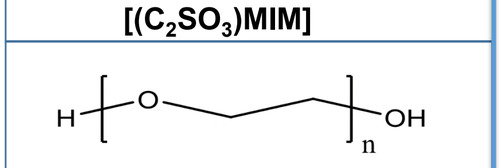

Synthesis of ILs

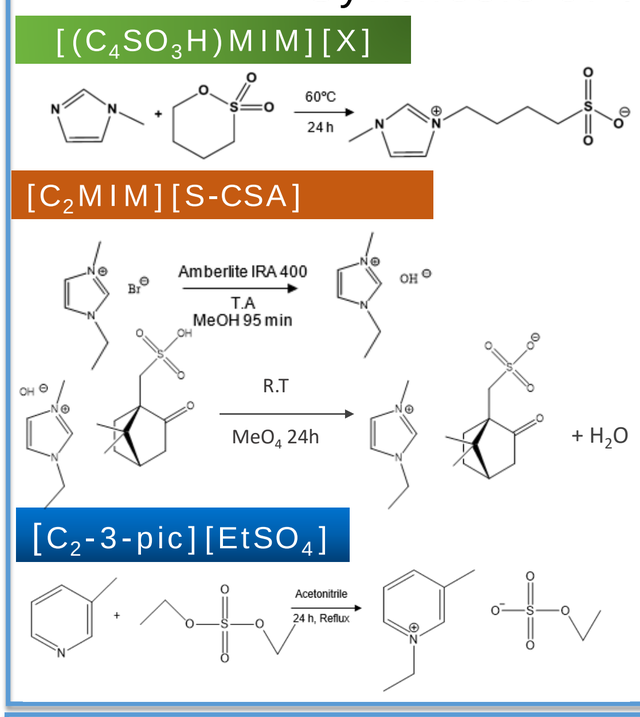

- Higher Yields and Purity levels
- NMR and FTIR Characterization
- Sustainable Synthesis

Contact Angles and Viscosity

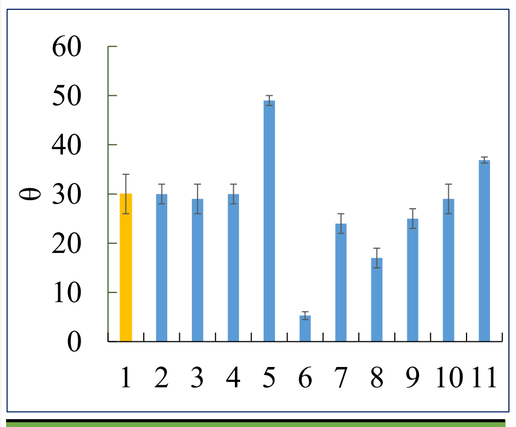

Lubricant	Viscosity (mPa.s) (25 ºC)
1	48
2	51
3	50
4	61
5	938
6	79
7	53
8	53
9	74
10	94
11	135

Legend *1 - PEG; 2-(S) [C_2MIM] [CSA]2%; 3-(R) [C_2MIM] [CSA]2%; 4-[C_1-3-pic][$MeSO_4$] 2%; 5- [C_1-3-pic][$MeSO_4$] ; 6- [(C_4SO_3H)MIM] [TfO] 2% ; 7- [C_2MIM][TfO] 2%; 8- [C_2MIM][$EtSO_4$] 2%; 9- [C_2-3-pic][$EtSO_4$]; 10- (S)[C2MIM][CSA]: PEG 200; 11- [C_1-3-pic][$MeSO_4$]:PEG 200*

- Low contact angles (5º to 49º)
- In general the PEG200 viscosity is increased between 4 to 10% by adding 2% wt of the ILs.
- DES based on [C_2MIM][S-CSA]: PEG is significantly more viscous than PEG 200, with a rise of viscosity of 95%.

Tribological tests

Friction coeficient (CoF) as a function of sliding velocity

PURE ILs

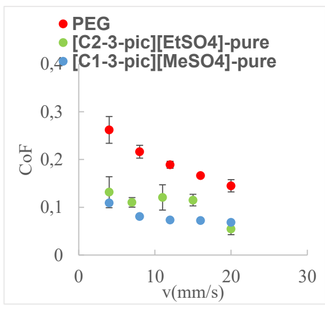

PURE DES

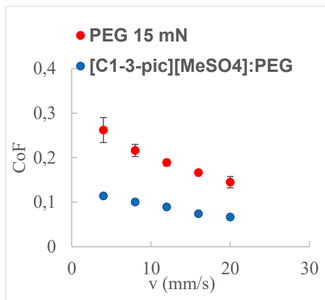

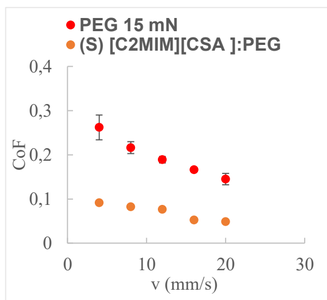

ILs AS ADDITIVES

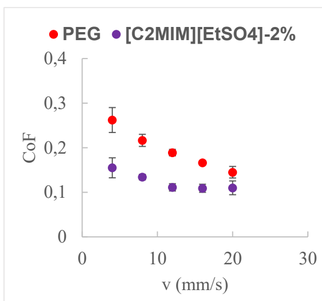

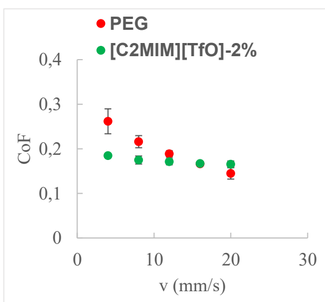

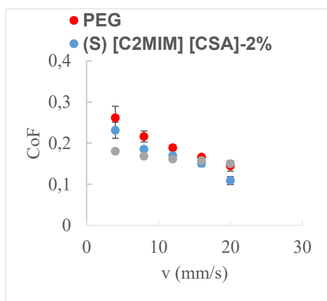

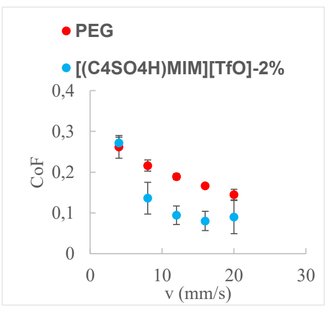

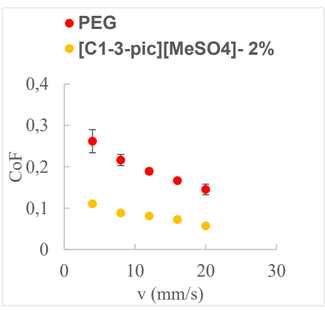

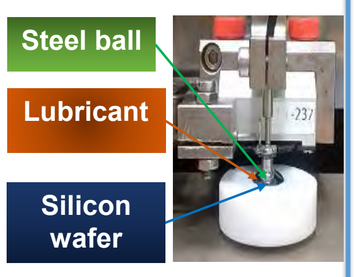

- All lubricants led to similar or smaller CoFs than PEG 200, whose values are between 0.15 and 0.26.
- The CoF values of the ILs based on the cation [C_2MIM] are similar, independently of the anion.
- Furthermore, the similar CoF values of 0.11-0.08 obtained with pure [C_2-3-pic][$EtSO_4$] and [C_1-3-pic][$MeSO_4$] demonstrate that increasing the length of the alkyl group in the cation and the anion had no significant effect. The CoF lubricant [C_1-3-pic][$MeSO_4$], in its pure and additive 2% form, are similar.
- The DES showed very good results, with a CoF of 0.11-0.05.

Conclusions

- ✓ Novel RTILs based on pyridinium and methylimidazolium cations have been developed
- ✓ In general, ILs additives showed lower or similar contact angles on Si surfaces than PEG (commercial model lubricant) without significant viscosity variation as well as lower CoF values (good lubrification attributed to strong interaction between the IL and the surface).
- ✓ Pure ILs and DES are effective as lubricants with promising performances

CQE Química Estrutural

09 MET

Funding:
Centro de Química Estrutural is funded by Fundação para a Ciência e Tecnologia – project UID/QUI/00100/2019. COMPETE (FEDER), within projects UID/NAN/50024/2013 and PTDC/CTM-POL/3698/2014

References:

1-Bhushan, B. *Microeletr. Eng.* 84. 387-412 (2007).; **2**-Freire, M MSc Thesis IST 2017.**3**-Cosme *et al., ChemistrySelect* 1, 3612-3617 (2016); **4**-Amorim *et al, Beilstein J. Nanotechnol* 8, 1961-1971 (2017);

FCT Fundação para a Ciência e a Tecnologia

Characterization and interaction with Albumin of 3-hydroxyl-2-naphthoylhydrazones oxidovanadium(IV) complexes

Nádia Ribeiro, Filipa Ramilo-Gomes, Adelino M. Galvão, Clara Gomes, João Costa Pessoa, Isabel Correia

INTRODUCTION

The use of metallodrugs has been a subject of interest for several years, especially after the discovery of powerful anti-cancer agents. It is known that metal ions play crucial roles in the living organisms and, therefore, biology has found control mechanisms by developing dedicated biomolecules to transport and store these elements, namely proteins. In the last decades, there was an increasing need for developing techniques and assays that provide insight over the metallodrugs-proteins relationships, for it is known that this phenomena can help explain experimental results. Biospeciation is an emergent area of research and spectroscopic techniques associated with computational studies are indispensable tools for a bioinorganic chemist.

In this work we have synthesised and characterized three ligands and their oxidovanadium(IV) complexes, as well as several spectroscopic experiments which provided us with an overview of how they interact with albumins. Computational docking studies were used to validate the experimental results. Aroylhydrazones have already proven their value on the pharmaceutical application, as well as vanadium compounds and therefore were chosen for biological evaluation.

SYNTHESIS AND CHARACTERIZATION

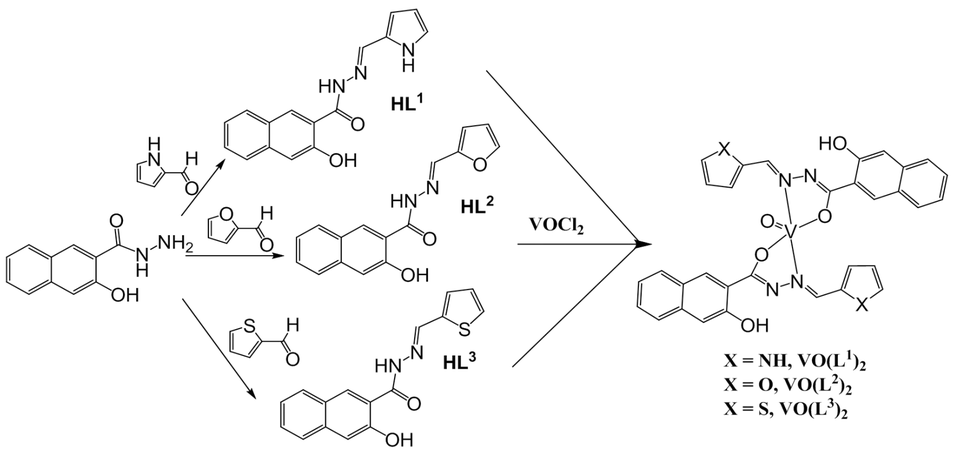

Scheme I – Synthetic pathway for the ligands and corresponding $V^{IV}O$ complexes.

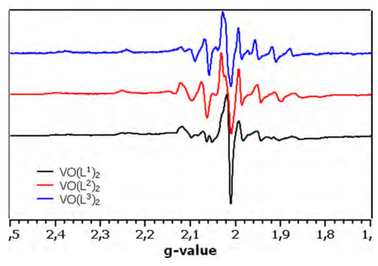

Figure 1 – First derivative X-band EPR spectra of the $V^{IV}O$ complexes measured at *ca.* 100 K in DMF. Concentration *ca.* 3 mM.

The EPR characterization shows the presence of two species, which were simulated for $VO(L^1)_2$. One should correspond to the hydrazine moiety (N_{im} and $C\text{-}O^-$) of both ligand molecules binding in the equatorial plane, Az *ca.* 159×10^{-4} cm^{-1} and the other to the binding of one ligand in equatorial/equatorial and the other in equatorial/axial and one DMF molecule completing the equatorial plane ($2xN_{im}$, $1xC\text{-}O^-$ and 1xDMF): Az *ca.* 165×10^{-4} cm^{-1}.

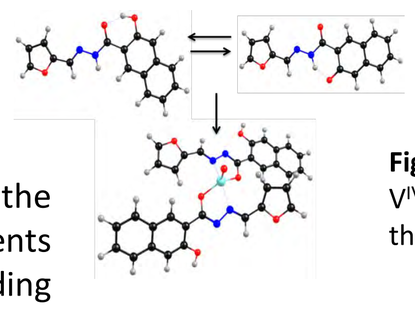

Figure 2 – DFT optimized structures of HL^2 and its $V^{IV}O$ complex based on the obtained structure for the ligand using single crystal X-ray diffraction.

SPECTROSCOPIC TECHNIQUES

Spectroscopic techniques were used to follow the interaction of the compounds with BSA. Far UV-Vis circular dichroism (CD) experiments showed an increase in the α-helix content of BSA, due to H-bonding interactions of BSA with the free hydroxyl groups of the compounds; UV-Vis absorption revealed strong interaction with the protein, mainly affecting the aromatic amino-acid residues. Fluorescence quenching experiments also revealed the interaction of the compounds within the hydrophobic binding site I where Trp213 is located.

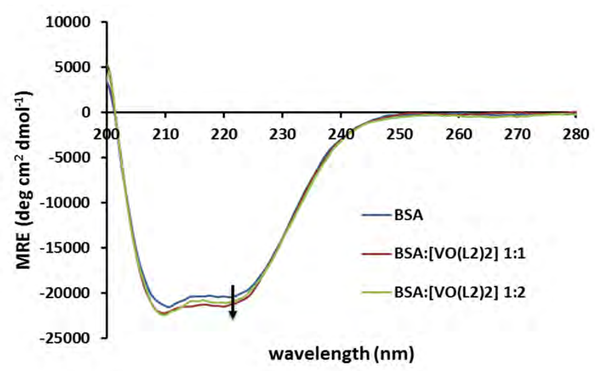

Figure 3 – Far-UV CD spectra measured for solutions containing BSA (*ca.* 1 μM) and molar ratios of $BSA:VO(L^2)_2$ of 1 or 2 for. MRE is the mean residue elipticity.

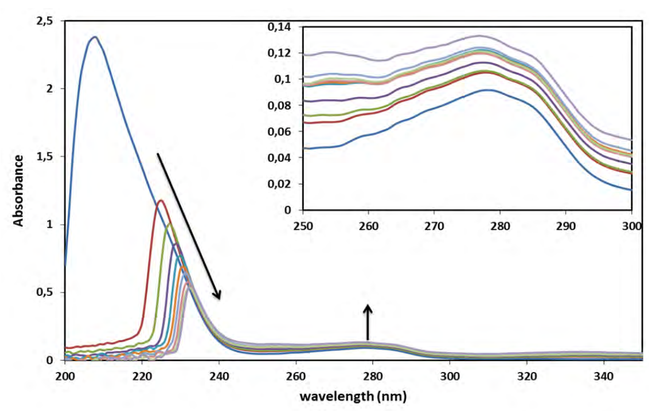

Figure 4 - UV absorption spectra of solutions containing BSA (*ca.* 3μM) and molar ratios of $VO(L^2)_2$:BSA from 0 to 4.

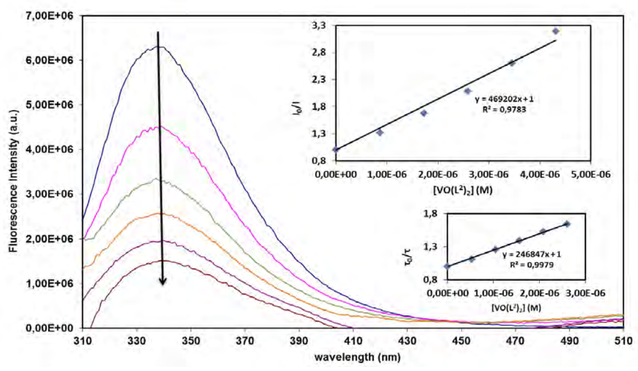

Figure 5 - Emission spectra (λ_{ex}= 295 nm) of BSA (1.5 μM) in the absence and in the presence of increasing concentrations of $VO(L^2)_2$ in 0.3% DMSO/ PBS aqueous buffer pH 7.4 (arrow indicates the variation observed with increasing concentration of the metal compound). Insets: Stern-Volmer plots at 340 nm obtained from steady-state (I_0/I) and lifetime (τ_o/τ) measurements.

DOCKING STUDIES

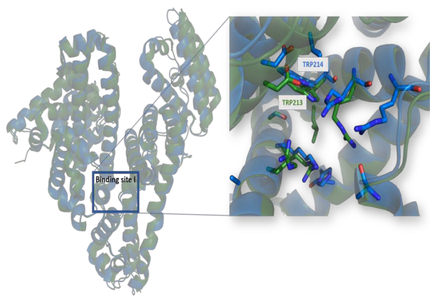

Figure 6 - Superimposed chains of Bovine Serum Albumin and Human Serum Albumin. BSA (PDB-ID:4JK4-A) is represented in green and HSA (PDB-ID:3LU6-A) represented in blue. Zoom of Binding site I, of sub-domain IIA for BSA (green) and HSA (blue), superimposed. The amino acids represented in sticks are the most relevant for interactions with the ligands.

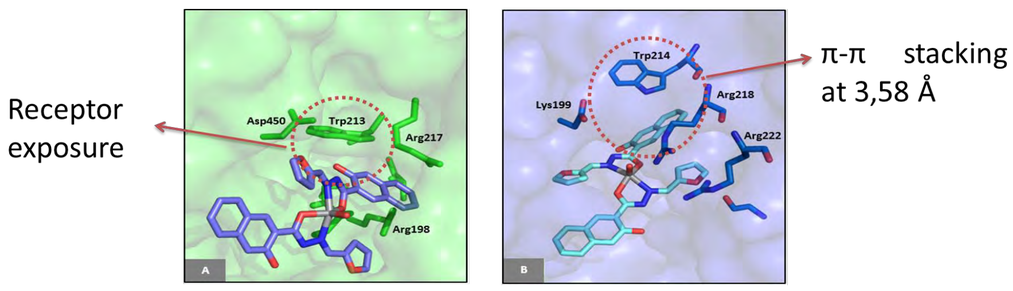

Figure 7- **A.** Proposed interaction of $VO(L^2)_2$ inside the pocket of BSA (PDB-ID: 4JK4). **B.** Proposed binding mode of $VO(L^2)_2$ with HSA (PDB-ID: 3LU6).

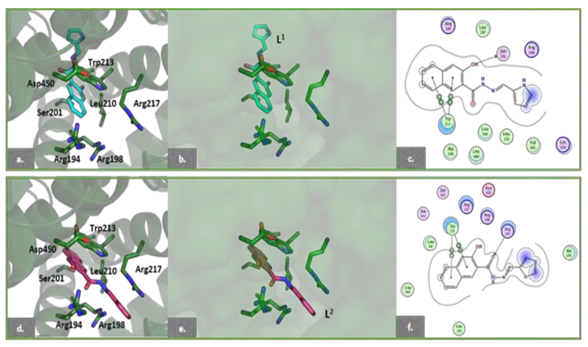

Figure 8 - Docking binding modes for HL^1 and HL^2 with BSA (PDB-ID:4JK4) where a stacking with Trp213 is observed. Similar results were obtained for HL^3.

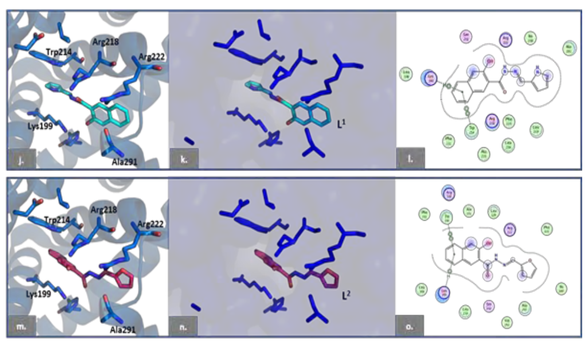

Figure 9 - Docking binding modes for HL^1 and HL^2 with HSA (PDB-ID: 3LU6) where a stacking with Trp214 is observed. Similar results were obtained for HL^3.

CONCLUSION

Three new $V^{IV}O$ complexes were prepared from naphthoylhydrazones ligand precursors with a ML_2 stoichiometry, all presenting a distorted square pyramidal geometry, also predicted by DFT theoretical calculations. Spectroscopic studies conducted with bovine serum albumin showed strong interactions with all compounds, resulting in high conditional binding constants, an increase of the α-helix content of the protein and aromatic amino-acid residues exposure, also corroborated by molecular docking studies for both bovine and human serum albumins.

04 BIOIN

Funding:
Centro de Química Estrutural is funded by Fundação para a Ciência e Tecnologia – project UID/QUI/00100/2019. Fundação para a Ciência e Tecnologia (FCT) is acknowledged for UID/MULTI/04349/2013, UID/BIO/04565/2013, RECI/QEQ-QIN/0189/2012, RECI/QEQ-MED/0330/2012, UID/DTP/04567/2016, UID/04138/2019, SAICTPAC/0019/2015, PTDC/QUI-QAN/32242/2017, PD/BD/128320/2017 , SFRH/BD/135797/2018 and SFRH/BPD/107834/2015. The Portuguese NMR and Mass Spectrometry IST–UL Centers are acknowledged for the access to the equipment.

Exploring the catalytic behavior of hierarchical BEA zeolite in Friedel-Crafts Acylations

Leonor Borbinha[1,2], Catarina Marranita[3], Angela Martins[1-3], Nelson Nunes[1-3], Ruben Leitão[1-3], Filomena Martins[1,2]

[1]Centro de Química e Bioquímica, Faculdade de Ciências, Universidade de Lisboa, Edif. C8, Campo Grande 1749-016 Lisboa, Portugal.
[2]Centro de Química Estrutural, Faculdade de Ciências, Universidade de Lisboa, Edif. C8, Campo Grande 1749-016 Lisboa, Portugal.
[3]ADEQ, ISEL-IPL, Rua Conselheiro Emídio Navarro, 1959-007 Lisboa, Portugal

E-mail : leonor.b.97@hotmail.com

CQE Química Estrutural

9 MET

FCT Fundação para a Ciência e a Tecnologia

Centro de Química e Bioquímica is funded by Fundação para a Ciência e Tecnologia – project UID/QUI/00612/2019.

Introduction

Friedel-Crafts acylation is an organic synthesis widely used reaction to acylate compounds. However, this reaction requires, in general, the use of non-reusable and environmentally harmful catalysts. In the last 20 years several studies have been reported in which zeolites replace classical catalysts, making it easier the regeneration and separation processes, while leading to less toxic and corrosive residues [1].

In the sequence of a previous work,[2] we present here some preliminary results of the systematic study of the catalytic behavior of hierarchical BEA zeolite (**Fig. 1**), modified by alkaline treatment followed by acid leaching, in Friedel-Crafts acylations using environmentally friendly reaction conditions.

Figure 1

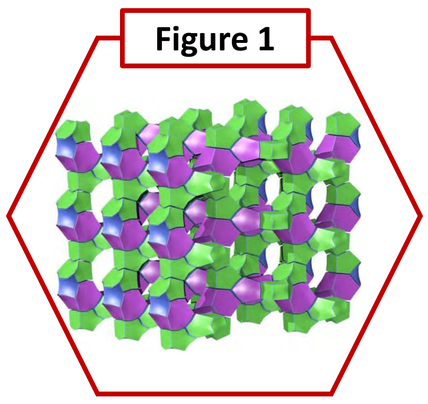

Figure 2

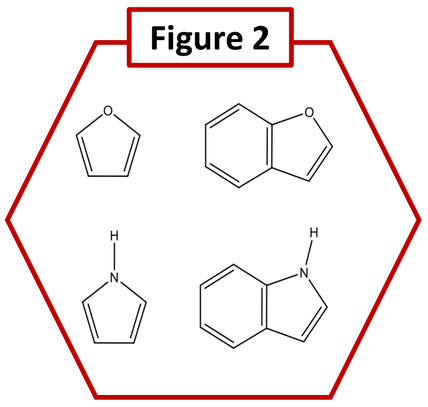

Methodology

Substrates **(Fig. 2)** (0.0105 mol) and acetic anhydride (0.0529 mol) were mixed and subsequently a zeolite sample (150 mg) was added.

The mixture was stirred and heated at 60 ° C or 120ºC on a heating and stirring plate **(Fig. 3)**.

The samples were removed using a hypodermic syringe and filtered using a Millipore Swinnex to separate the catalyst from the remaining reaction mixture.

The reaction progress was analyzed by gas chromatography on a Perkin Elmer GC, equipped with a DB-5MS capillary column and a flame ionization detector **(Fig. 4)**.

Figure 3

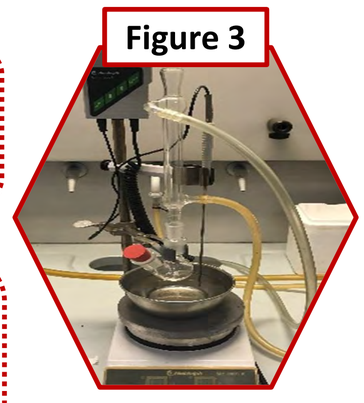

Figure 4

Results and Discussion

Figure 5

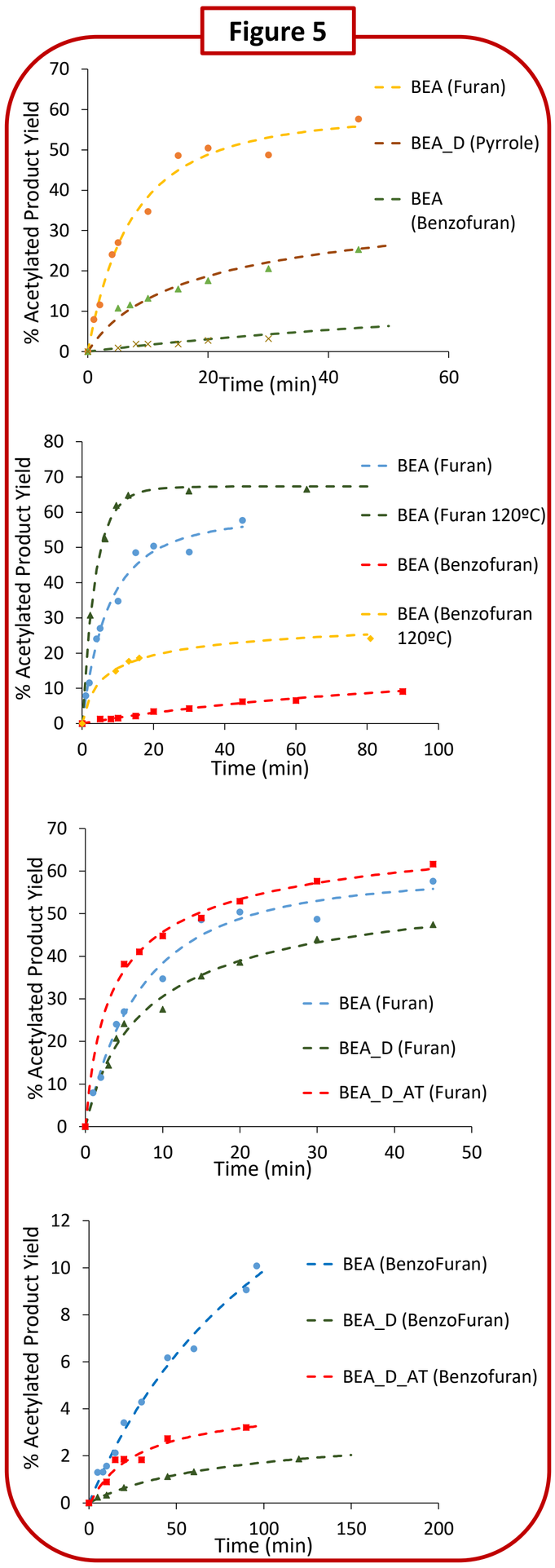

Equation 1

Langmuir-Hinshelwood simplified model equation[2]

$$Rate \cong k\frac{[A][S]}{[A]+[S]+K_r[P]^2}$$

[A] - concentrations of acetic anhydride
[S] - concentrations of substrate
[P] - concentrations of acylated product
k - rate constant
K_r - ratio between the adsorption equilibrium constants.

Table 1

Catalyst	Substrate	Temp. (°C)	k (mmol min^{-1} g^{-1})	K_r
BEA	Furan	60	60	6
BEA	Furan	120	132	2
BEA_D	Furan	60	58	12
BEA_D_AT	Furan	60	164	14
BEA	Pyrrole	60	17	20
BEA	Benzofuran	60	1.34	26
BEA	Benzofuran	120	39	53
BEA_D	Benzofuran	60	0.31	240
BEA_D_AT	Benzofuran	60	1.15	201
BEA	Indole	60	Conversion < 1.5%	

BEA : Commercial Beta zeolite ; BEA_D : NaOH desilicated zeolite
BEA_D_AT : NaOH desilicated zeolite + acid treatment

The simplified model **(Eq. 1)** was applied to all kinetic data **(Fig. 5)** and results are summarized in **Table 1**.

- In the case of furan, the increase in temperature leads to a significant increase in the rate constant. At 60 °C, the rate constant remains approximately unchanged when the zeolite suffers only desilication (BEA_D) but shows a major increase upon acid treatment (BEA_D_AT).
- On the other hand, with benzofuran the acylation rate constant, even after desilication and acid treatment at 60 °C, is rather low, which is probably related with its chemical structure (bigger size and fewer acylation positions). However, when the temperature is doubled, a 30-fold increase in the rate constant is observed.
- As regards to pyrrole and indole, additional experiments are needed to compare the substrates' behavior under different zeolite treatment conditions. However, indole shows already a very small reactivity at 60 °C which might render further analysis pointless.
- The analysis of the equilibrium constants shows that when the zeolite suffers desilication, K_r increases significantly, suggesting an accumulation of products inside the pores, but this result is much less important or even slightly reversed upon acid leaching due to pores obstruction by Si debris.
- As a final note, one can say that, in the case of furan, desilication + acid treatment increase both rate and equilibrium constants, whereas for benzofuran this effect is only observed in K_r.

References:

1. R. Maggi, G. Sartori, Advances in Friedel-Crafts Acylation Reactions: Catalytic and Green Processes, 1st Ed., CRC Press, 2009.
2. R. Aleixo, R. Elvas-Leitão, F. Martins, A.P. Carvalho, A. Brigas, A. Martins, N. Nunes, Mol. Catal. 434 (2017) 175–183.

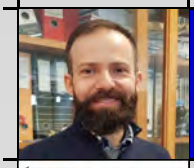

An electrochemical biosensor for toxic amides determination in food and environmental samples: Optimizing the bioreceptor immobilization procedure and materials

Nelson A. F. Silva[1,2], Maria M. Rocha[2], Amin Karmali[1], Hugo Silva[1,2], Manuel J. Matos[1,3]

CQE Days Spring Meeting 2019

1 ISEL ADEQ Área Departamental de Engenharia Química
2 CQE Química Estrutural
3 it instituto de telecomunicações

INTRODUCTION 1

In this work different electrochemical biosensors, with potentiometric and conductometric transduction, were developed aiming at the determination of toxic amides, such as acrylamide and formamide, in foodstuff [1] as well as in drinking water and wastewater [2]. The biological recognition element consisted of whole cells of ***Pseudomonas aeruginosa*** containing intracellular amidase (EC 3.5.1.4) activity. The biosensors' detection mechanism relied on the monitorization of the potential difference or conductivity changes due to the formation of ammonium and hydroxide ions, resulting from acrylamide hydrolysis catalyzed by amidase, either using an ammonium ion selective electrode, or several interdigital conductometric devices developed by our group. These interdigital devices were constructed with different designs and electrode materials, namely graphite, silver, aluminum and gold. The electrodes were deposited by ink-jet printing or from metallic vapor consisting of different interdigital fingers and relative distance, thus resulting in different sensitive areas (0.13 cm^2, 0.16 cm^2, 0.17 cm^2 and 0.21 cm^2). One of the most important aspects regarding the development and assembly of a biosensor, relies on the procedure and materials used for the immobilization of the biological recognition element or bioreceptor. An adequate immobilization of the biological material may have a crucial impact on the overall analytical performance of the biosensor [3-5]. In the present study, the bioreceptor was immobilized on the surface of several types of polymeric membranes, such as polyethersulphone, polycarbonate, nylon, polyvinylidene fluoride, nitrocellulose, cellulose acetate and biocellulose, using glutaraldehyde as a crosslinking agent or physically confined. As an alternative to the use of polymeric membranes, several bioreceptor immobilization matrices were tested, based on natural polymers, such as gelatin and agarose, crosslinking agents, such as glutaraldehyde and bovine serum albumin, charge exclusion polymers, such as nafion and encapsulation media such as inorganic and organic sol-gel. Several figures of merit as well as other biosensors performance characteristics arising form these several immobilization procedures were evaluated.

Immobilization using polymeric membranes 2

- Polyethersulphone
- Nylon
- Polyvinylidene Fluoride
- Nitrocellulose
- Polycarbonate
- Cellulose Acetate
- Biocellulose

Polymeric membranes used for *Pseudomonas aeruginosa* cells immobilization

General procedure for whole cells immobilization onto the potentiometric transducer using polymeric membranes

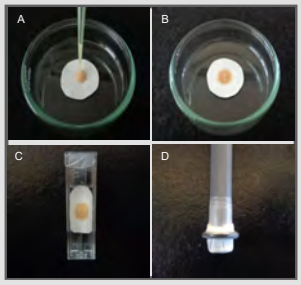

Immobilization sequence: A) Deposition of 60µL cell suspension; B) Incubation at room temperature; c) Membrane washing; D) Attachment to the transducer.

Special case: Biocellulose membrane produced by *Gluconacetobacter xylinus*

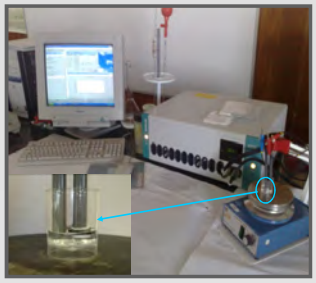

Experimental setup used for the assays performed with the potentiometric biosensors

Immobilization using different material matrices 3

- Glutaraldheyde
- Gelatin
- Bovine serum albumine (BSA)
- Nafion
- Agarose
- Sodium silicate
- Tetraethyl orthosilicate (TEOS)

Different matrices used for *Pseudomonas aeruginosa* cells immobilization

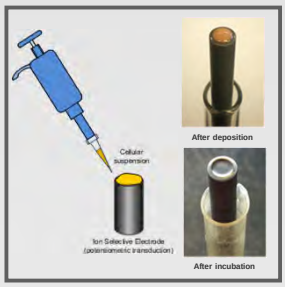

General procedure for whole cells immobilization onto the potentiometric transducer using different material matrices

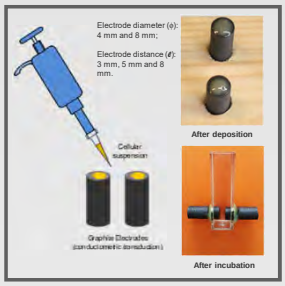

Whole cells immobilization onto the surface of graphite electrodes used to assemble a conductometric cell type biosensor

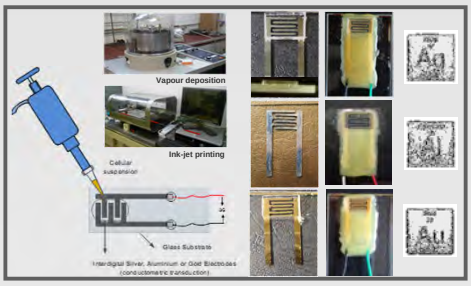

Whole cells immobilization onto the sensitive area of different interdigital electrodes used to assemble a conductometric biosensor

Comparative results 4

Polymeric membranes

Preliminary evaluation

Membrane	Incubation time	Attachement to the transducer	Typical response (mV)	Membrane regeneration
Polyethersulphone	20 min	suitable	120 – 140	45 min
Nylon	30 min	suitable	80 – 100	50 min
Polyvinylidene Fluoride	> 60 min	not suitable	n.d.	n.d.
Nitrocellulose	> 60 min	not sutiable	n.d.	n.d.
Polycarbonate	> 60 min	suitable	100 – 120	25
Cellulose Acetate	> 60 min	not suitable	n.d.	n.d.
Biocellulose	*	suitable	60 - 80	10 min

** Biocellulose membrane preparation was aprox. 2 days corresponding to the cells growth period; n.d. – not determined.*

Analytical performance

Figures of merit	Polyethersulphone membrane	Polycarbonate membrane	Biocellulose membrane
Linear response interval (M)	5×10^{-4} - 1×10^{-1}	5×10^{-4} - 1×10^{-1}	5×10^{-4} - 5×10^{-2}
Sensitivity (mv/decade)	45.03±1.70	48.04±1.14	30.65±2.76
Correlation coefficient	0.998	0.998	0.988
Typical response (mV)	120 - 140	100 - 120	60 - 80
Limit of detection (M)	4.90×10^{-4}	2.29×10^{-4}	5.28×10^{-4}
Limit of quantification (M)	5.66×10^{-4}	4.00×10^{-4}	1.05×10^{-4}
Membrane regeneration time (min)	45	27	10
Response time (min)	3.4±0.2	2.3±0.2	3.9±0.9
Incubation time (min)	20	> 60	---
Half-life time (days)	30	14	12

Immobilization matrices

Preliminary evaluation

Material	Physical consistency	Stability towards agitation	Typical response (mV)	Biolayer regeneration
Glutaraldheyde	High	High	120 – 140	10 min
Gelatin	High	Low	20 – 30	n.d.
BSA	Low	n.d.	n.d.	n.d.
Nafion	High	Low	30 – 40	25 min
Agarose	High	Low	80 – 100	n.d.
Sodium silicate	High	Low	60 – 100	30 min
TEOS	High	High	80 - 100	> 60 min

n.d. – not determined.

Analytical performance

Figures of merit	Potentiometric biosensor	Ag interdigital biosensor	Al interdigital biosensor	Au interdigital biosensor
Linear response interval (M)	5×10^{-4} - 1×10^{-1}	2×10^{-4} - 5×10^{-2}	2×10^{-4}- 3×10^{-2}	2×10^{-4} - 5×10^{-2}
Sensitivity ((mv or mS)/decade)	56.60±1.78	123.52±2.03	40.20±1.53	51.02±1.30
Correlation coefficient	0.998	0.988	0.996	0.995
Typical response (mV or mS)	120-140	6.30	1.30	2.70
Limit of detection (M)	3.35×10^{-4}	1.34×10^{-4}	4.10×10^{-4}	3.23×10^{-4}
Limit of quantification (M)	5.28×10^{-4}	4.45×10^{-4}	1.37×10^{-4}	1.08×10^{-3}
Biolayer regeneration time (min)	45	continous	continous	continous
Response time (min)	3.1±0.2	1.8±0.3	1.8±0.3	1.8±0.3
Incubation time (min)	60	overnight	overnight	overnight
Half-life time (days)	100	disposable	disposable	disposable

FINAL COMMENTS 5

- Regarding the use of polymeric membranes for whole cells of ***Pseudomonas aeruginosa*** immobilization, both polyethersulphone and polycarbonate proved to be most adequate.
- In fact, the biosensor assembled with the polycarbonate membrane exhibited lower limits of detection and quantification and higher sensitivity;
- However the device using polyethersulphone membrane showed a higher response, a lower incubation time and a longer period of reusability, thus allowing a reduction in costs, bearing in mind effective savings resulting from the reduction of cells suspension and polymeric membrane utilization.
- In what the alternative immobilization materials it concerns, the use of glutaraldehyde as an immobilization matrix exhibited the most suitable results.
- Almost all the materials were able to produce biolayers with significant physical consistency. However only glutaraldehyde and TEOS resisted well to solution agitation, where the former exhibited a higher response and a significant reduction in the biolayer regeneration time.
- When comparing materials it can be seen that the use glutaraldehyde as an immobilization matrix allowed the development of biosensors with better figures of merit, namely sensitivity, limits of detection and quantification and half-life time, thus increasing its reusability.

06 CE

Centro de Química Estrutural is funded by Fundação para a Ciência e Tecnologia – project UID/QUI/00100/2019.

FCT Fundação para a Ciência e a Tecnologia

REFERENCES:

[1] Tareke, E., Rydnerg, P., Karlsson, P., Eriksson, S., Tornqvist, M, J Agric Food Chem. (**2002**) 4998-5006.

[2] Smith, E., A., Oehme, F., W, Rev. Environ. Health 9 (**2011**) 215-228.

[3] Nguyen, H. H, Lee, S. H, Lee, U. J, Fermin, C. D, Kim, M, Materials 12, 121 (**2019**) 1-34.

[4] Asal, M., Ozen, O., Sahinler, M., Baysal, H. T., Polatoglu, I, Sens. Rev. (**2018**).

[5] Bhardwaj, T, IJERT 3 (**2014**) 294-298.

nsilva@deq.isel.pt

On the preparation of metallic Co foams based nanocomposites as electrodes for energy storage devices

Arévalo-Cid P.[1], Adán-Más A.[1], Montemor M.F.[1], Silva T. M.[1,2]

1 Centro de Química Estrutural-CQE, DEQ, Instituto Superior Técnico, Universidade de Lisboa, 1049-001, Lisboa, Portugal
2 ADEM, GI-MOSM, ISEL-Instituto Superior de Engenharia de Lisboa, Instituto Polit ecnico de Lisboa, Lisboa, Portugal

CQE Química Estrutural

07 CSSE

FCT Fundação para a Ciência e a Tecnologia

Obtention of Co foams

Highly porous Co nanofoams were prepared by using the Dynamic Hydrogen Bubbling Template (DHBT) method. This process is based on the application of high negative potentials to simultaneously propitiate both hydrogen evolution and the reduction of Co^{2+} ions contained in the electrolyte. Metallic cobalt deposition is influenced by hydrogen release, which acts as a template, leading to a porous material that is controlled by the bubbles' shape and pathway.

Electrolyte: $CoCl_2$ 0.1 M, NH_4Cl 2 M **Counter electrode:** Pt **Applied current** = -1.8 A·cm^{-2}

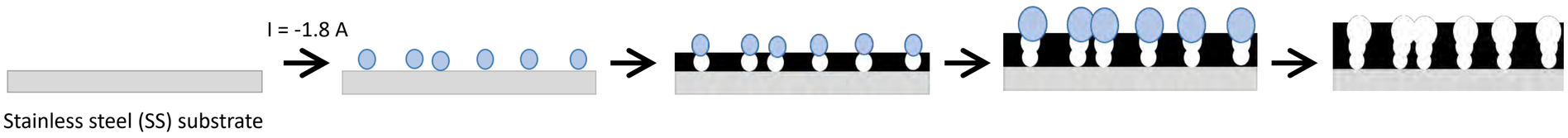

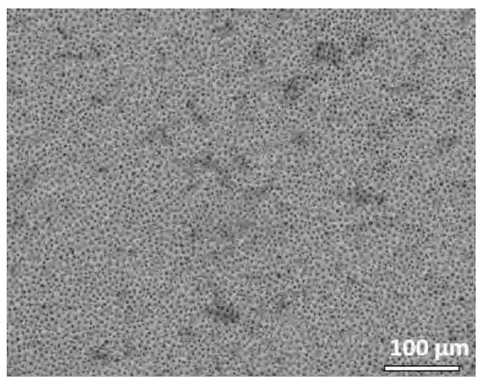

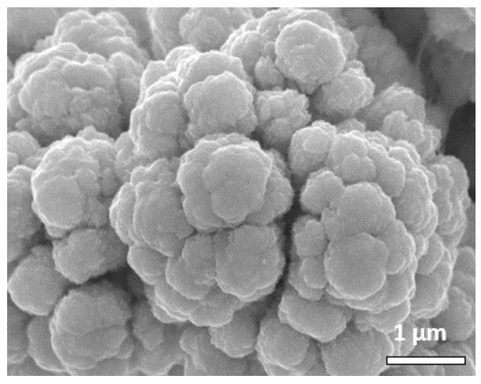

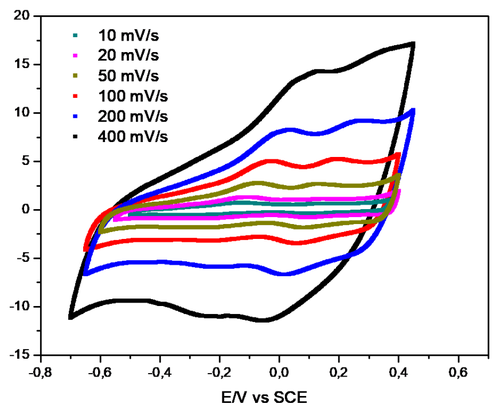

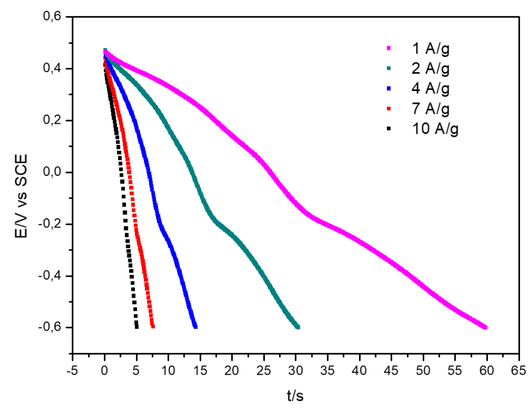

Number of pores	Average pore area / µm²	Median pore area / µm²
3617	229.55	188.16

Electrolyte: KOH 1M
Counter electrode: Pt

Co foam: 21 mA·h·g^{-1}

Functionalization of foams: $NiCo(OH)_x$@Co

Co nanofoams were used as improved substrates for the deposition of Ni-Co hydroxide, used as positive electrode for energy storage devices. To prove the enhancement of its electrochemical response, a thin-film of the same material was directly deposited onto stainless steel and is electrochemical response evaluated in KOH 1M.

Electrolyte: $Co(NO_3)_2$ 0.1 M, $Ni(NO_3)_2$ 0.1 M **Counter electrode**: Pt **Pulsed deposition**: -1.1V/0V for 1s/1s during 200 cycles

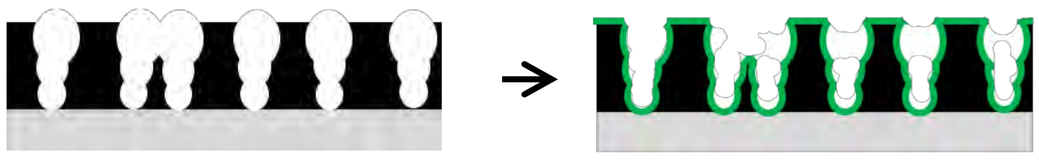

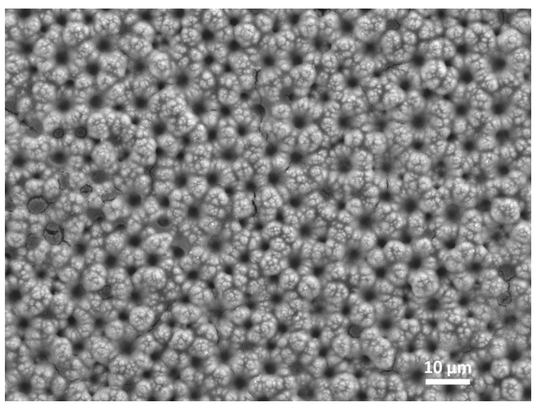

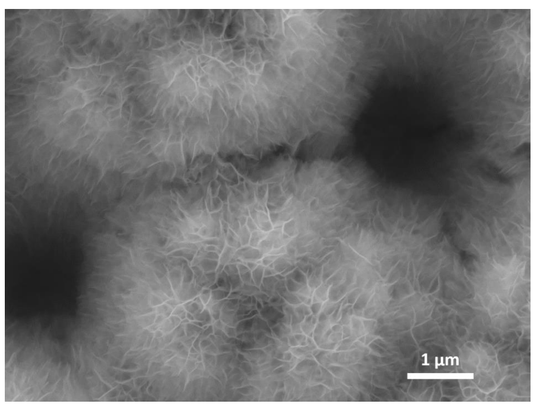

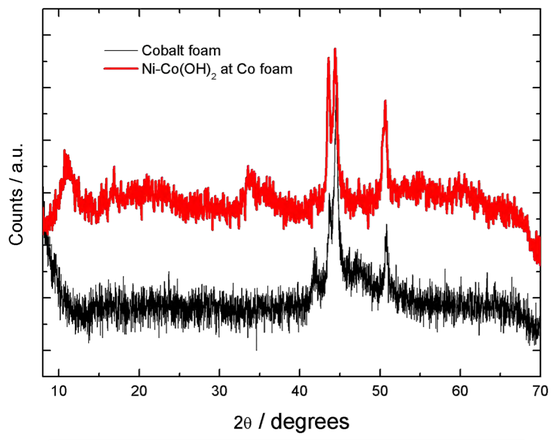

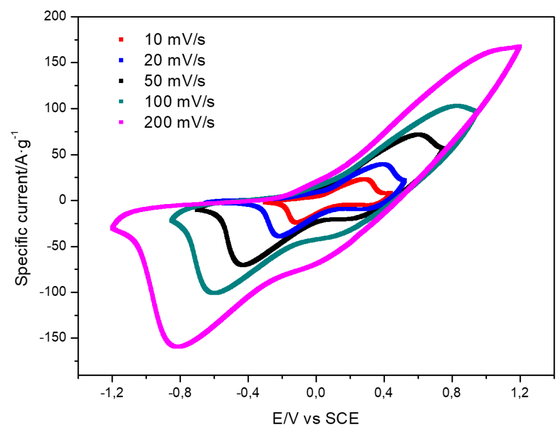

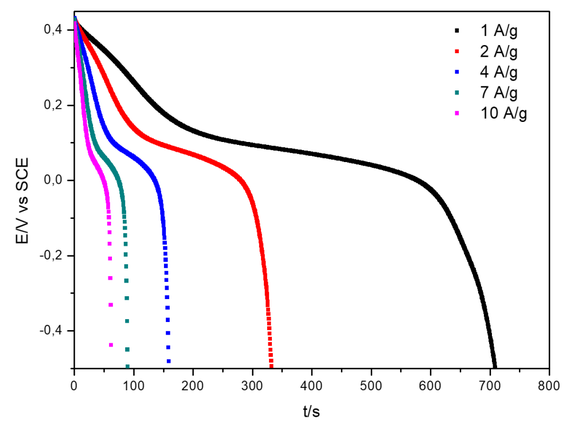

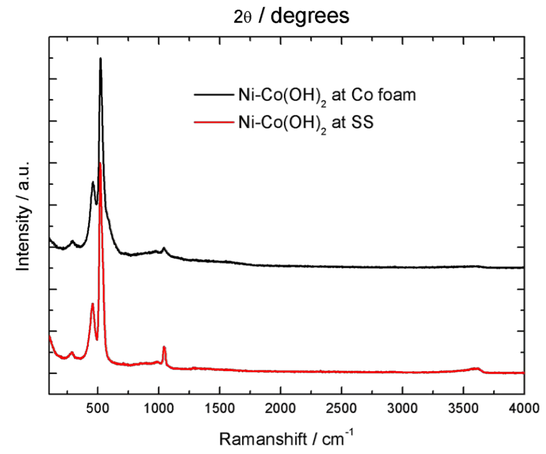

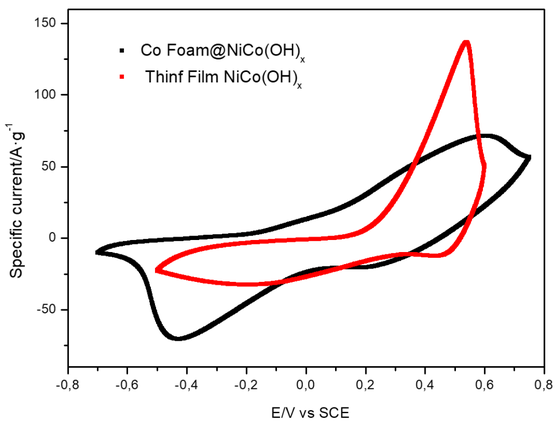

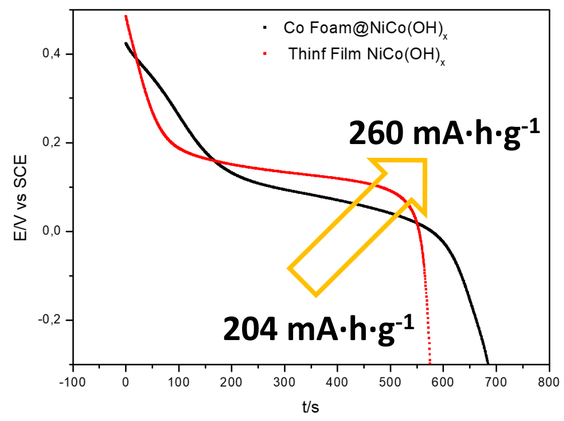

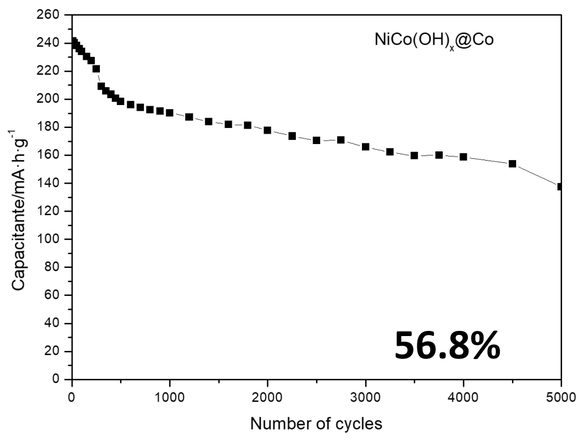

Conclusion

$Ni\text{-}Co(OH)_x$ thin-films have been electrodeposited on top of Co foams prepared by using DHBT method. The introduction of a cobalt-based porous structure leads to a 22% improvement of capacitance when compared to the analogous thin-film obtained under the same conditions. This result can be directly correlated to a larger active area caused by the porous microstructure.

Funding:
Centro de Química Estrutural is funded by Fundação para a Ciência e Tecnologia – project UID/QUI/00100/2019.
This work was supported by grant PTDC/QUI-ELT/28299/2017 and M-ERA-NET/0004/2014.
from Fundação para a Ciência e a Tecnologia.

References:

1. K.I. Siwek, S. Eugenio, D.M.F. Santos, M.T. Silva, M.F. Montemor, Int. J. Hydrogen Energ. 44 (2019) 1701–1709.

Inducing the activity of NK cells with NKp30 small organic ligands

Pedro F. Pinheiro, Gonçalo C. Justino, Joana P. Miranda, M. Matilde Marques

Centro de Química Estrutural – Instituto Superior Técnico
iMed.UL Instituto de Investigação do Medicamento – Faculdade de Farmácia

NATURAL KILLER CELLS AND IMMUNOSURVEILANCE

Natural killer (NK) cells are a type of cytotoxic lymphocyte critical to the innate immune system. NK cells provide rapid responses to viral-infected cells and respond to tumor formation as they can kill tumor cells without previous sensitization [1].

NK-mediated cancer immunosurveillance is prompted by the recognition of surface ligands on tumor cells that trigger the activation of cytotoxic responses [2]. In humans, NKp30, NKp44, and NKp46 are major activating NK receptors [3].

Amongst the known natural cytotoxicity receptors (NCRs), NKp30 is the one for which a ligand (B7-H6) has been identified and whose structure has been resolved in both free and bound forms. B7-H6 is selectively expressed on tumor cells and its interaction with NKp30 results in NK cell activation [5].

The comparison between the two 3D structures revealed important conformational changes that may be a key-factor for the NK-response activation by B7-H6.

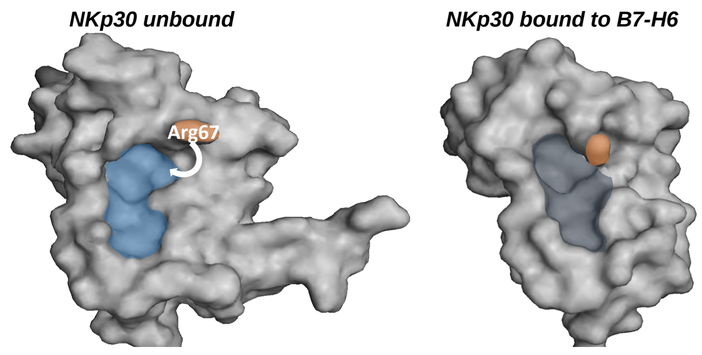

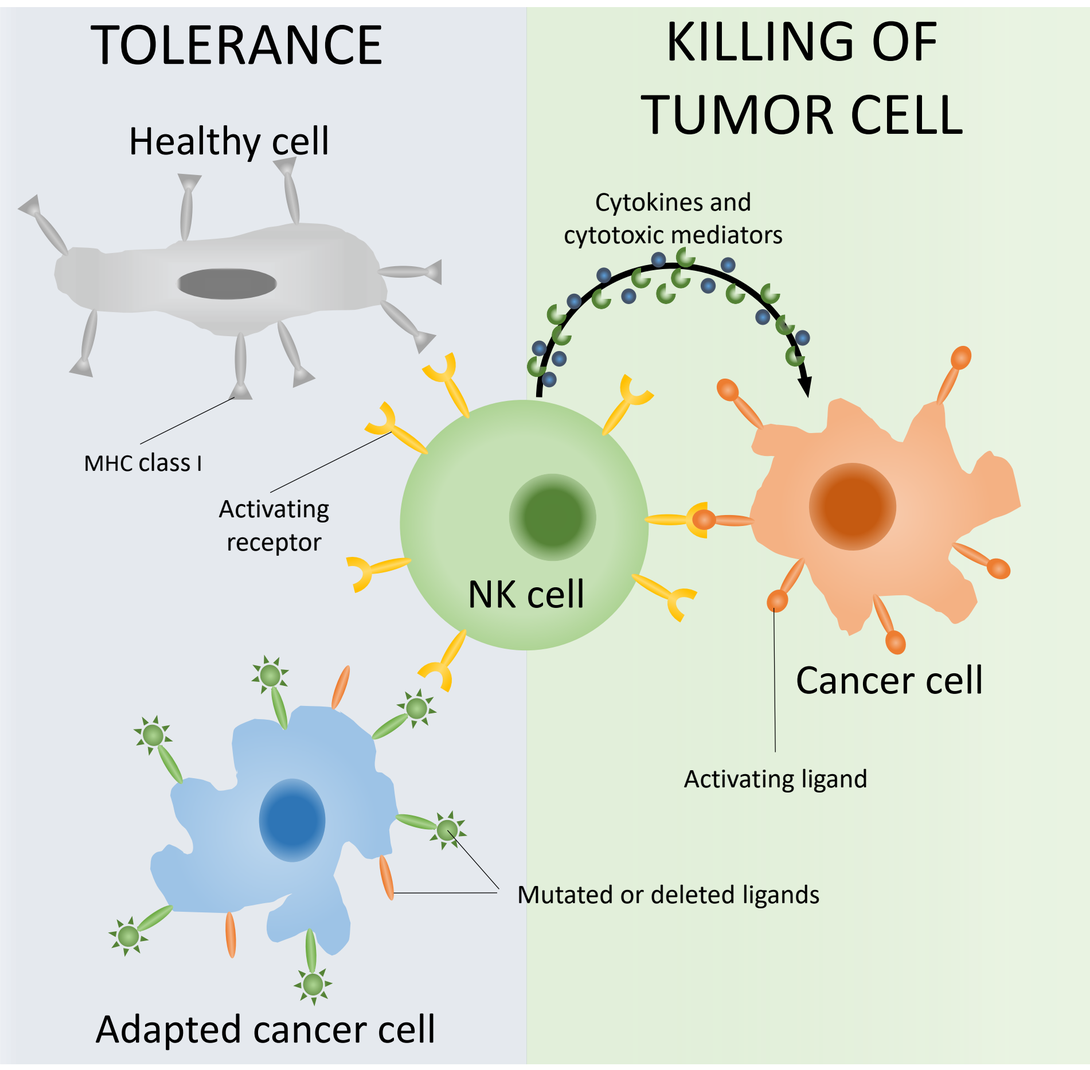

However, tumor cells employ many strategies to evade immunosurveillance by NK cells through over-expression of histocompatibility receptors or by suppressing the expression of NK-activation receptors, *masking* the malignant cells [4].

By building an artificial NK-activation ligand it should be possible to induce the cytotoxic activity of these cells against a desired target.

A combined computational docking and molecular dynamics approach was used to screen a wide library of ligands to find the ones establishing stronger interactions with the NKp30 ligand bay in its bound form (PDB 3PV6).

AutoDock Vina was used in docking routines, using several restriction boxes centered in the ligand bay, to dock ligand structures obtained from *ChemBank*. The results were filtered, by selection of the best candidates for refining using *GROMACS* in molecular dynamics simulations. Finally, all the hits were docked against NKP30's unbound conformation (PDB 3NOI), probing the ability of the designed ligands to interact with the native protein. This yielded a family of ligands for the NKp30 receptor.

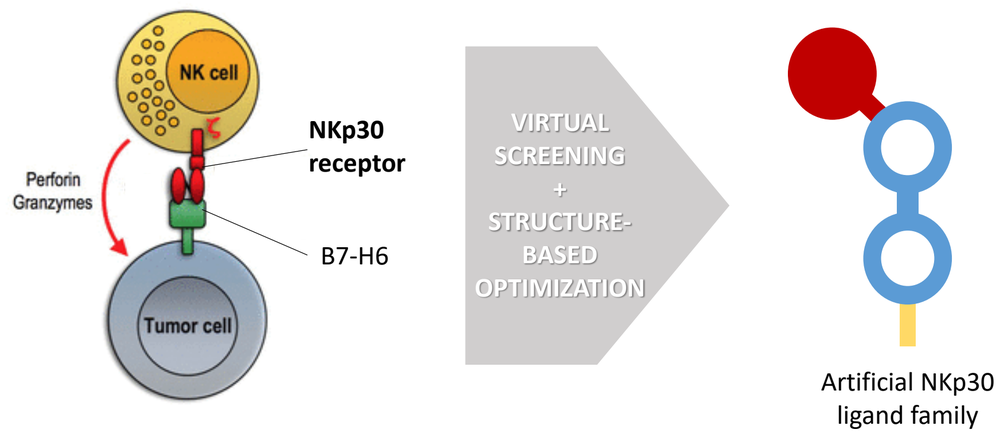

SYNTHESIS AND TESTING OF THE ARTIFICIAL NKp30 LIGANDS

Fifteen new molecules were obtained from the same core structure. These were fully characterized by NMR and MS.

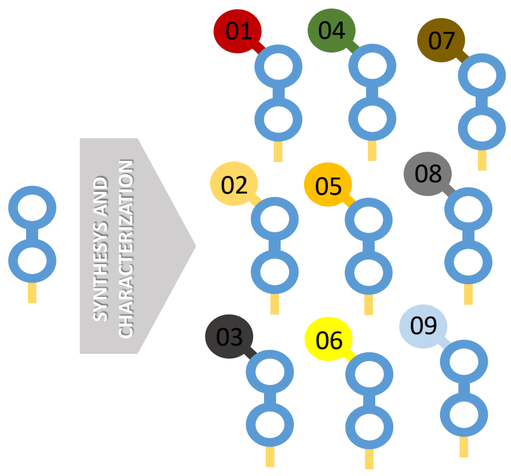

FAMILY OF ca. 10 NEW COMPOUNDS

Binding affinity towards the NKp30 receptor (recombinant protein) was determined by an MS-based technique. Six of the 10 ligands tested showed positive interaction with the receptor.

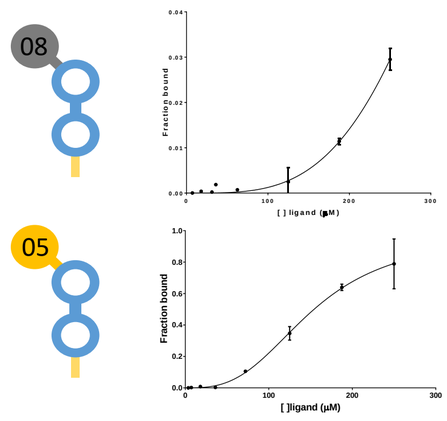

LIGAND 05 PRESENTED A EC_{50} OF 19.2 μM

The ligation of ligand 05 with the recombinant receptor was confirmed by NMR.

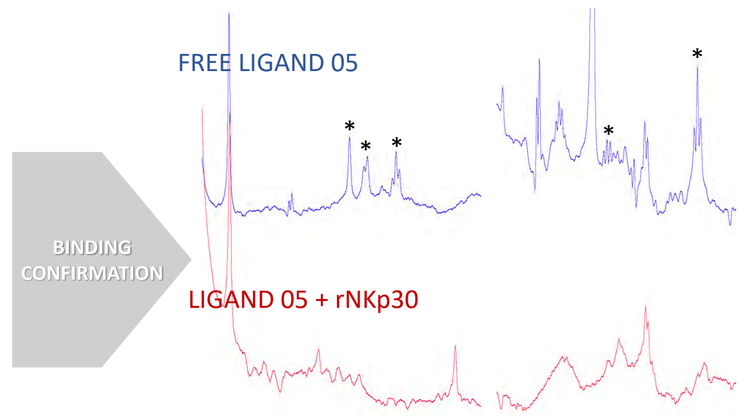

LIGAND 05 SPECIFIC SIGNALS (*). LIGAND LINE-WIDTH (T_2) CHANGES UPON PROTEIN BINDING

ACTIVATION OF NK CELLS WITH LIGAND 05

Human peripheral blood mononuclear cells (PBMCs) were isolated from 5 healthy donors and exposed for 24h to Ligand 05. Secretion of the cytokines TNF-α and IFN-γ was determined by ELISA.

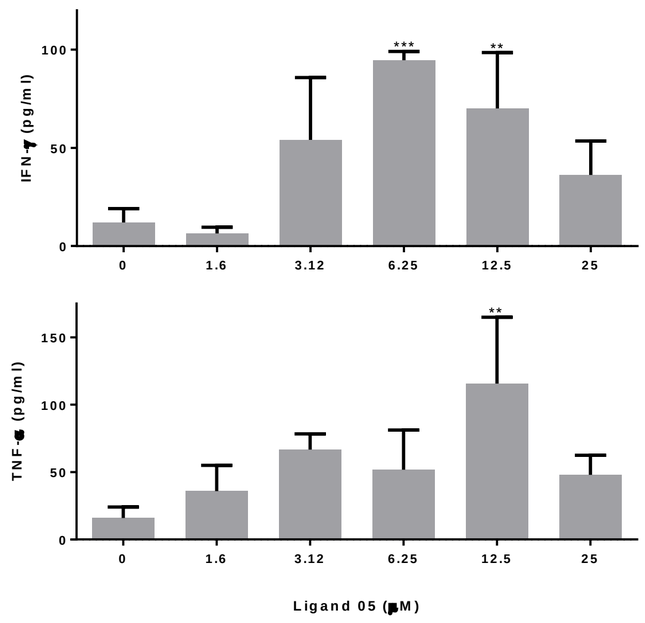

The capacity of Ligand 05 to induce the cytotoxic responses of NK cells was also probed. A culture of target cells (HepG2 cell line) was exposed to PBMCs isolated from 3 donors in the presence or absence of 10 μM of Ligand 05. After 24h the viability of the target cells was determined.

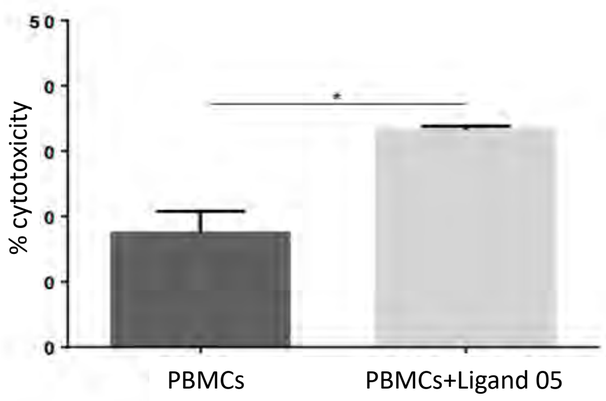

LIGAND 05 INCREASES THE CYTOTOXIC POTENTIAL OF PBMCs BY ca. 2 FOLD

The cytotoxicity of Ligand 05 was tested in the same target cells (HepG2) and no evidence of cell death was found after 24h of exposure.

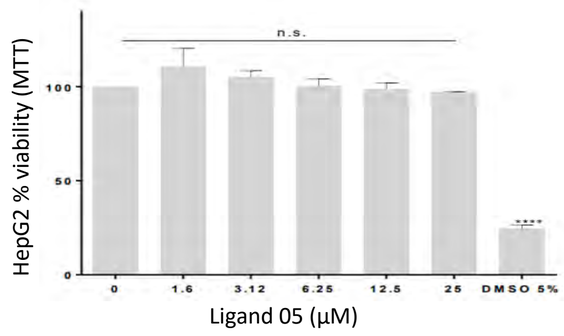

CONCLUSIONS

LIGAND 05 is a non-toxic potent NKp30 agonist that induces cytotoxic response of NK cells.

New experiments are being designed to further characterize the responses elicited by this molecule. Future work will aim at directing the triggered activity towards cancer cells as part of a new therapeutic strategy.

05 BIOMOL

Funding:

Centro de Química Estrutural is funded by Fundação para a Ciência e Tecnologia – project UID/QUI/00100/2019. This work was supported by grant LPCC/NRS –Terry Fox 2015-17 from Liga Portguesa Contra o Cancro, grant SFRH/BD/110945/2015 from Fundação para a Ciência e a Tecnologia (FCT), and projects SAICTPAC/0019/2015 and PTDC/QUI-QAN/32242/2017, funded by national funds through FCT and when appropriate co-financed by FEDER under the PT2020 Partnership Agreement.

References:

1. I Waldhauer and A Seinle, *Oncogene* **2008**, *27*, 5932-5943
2. K Imai, S Matsuyama, *et al.*, *Lancet* **2000**, *356*, 1795-1799
3. A Moretta, C Bottino, *et al.*, *Annu. Rev. Immunol.* **2001**, *19*, 197-223
4. C Classen, C Falk, *et al.*, *Haematologica* **2003**, *88*, 509-521
5. C Brandt, M Baratin, *et al.*, *J. Exp. Med.* **2009**, *206*, 1795-1503
6. X Chen, S Qin, *et al., Sci. Rep.* **2015**, *5*, 8361

plmelo@fc.ulisboa.pt

Theoretical Study of Low Temperature Solid-Solid Phase Transitions in 4'-Hydroxyacetophenone

P. Tomaz Melo, C. E. S. Bernardes, M. E. Minas da Piedade

Centro de Química e Bioquímica e Centro de Química Estrutural, Faculdade de Ciências, Universidade de Lisboa, Campo Grande, 1749-016, Portugal

Scope

Polymorphism, the ability of a substance to crystallize in more than one lattice arrangement, is currently a major concern for the manufacture of organic products, since each crystal form can exhibit significant differences in physicochemical properties (e.g. fusion temperature, solubility/dissolution rate).

4'-Hydroxyacetophenone (HAP; Figure 1) is a compound with significant commercial applications and additional potential end uses. Two polymorphs of HAP (Form I and Form II) have been reported up to now [1].

A new phase transition in both polymorphs at ~79 K was recently identified from adiabatic calorimetry studies [2].

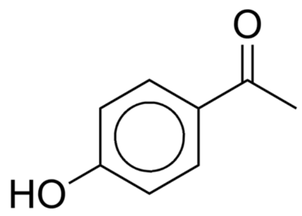

Figure 1. Molecular structure of 4′-Hydroxyacetophenone (HAP)

AIM. Use molecular dynamics simulations to investigate the nature of the low-temperature phases transitions of HAP.

Results

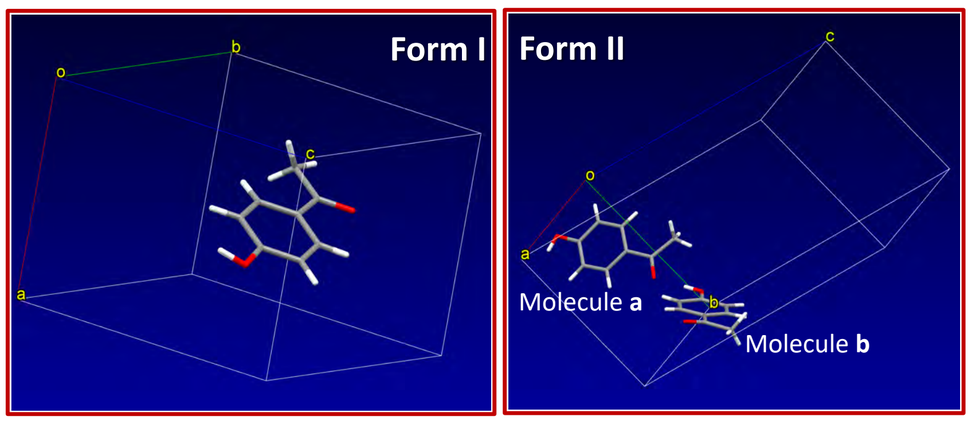

Figure 2. Single crystal X-ray structures of HAP exhibiting one and two molecules in the unit cell asymmetry unit of HAP in form I and II, respectively.

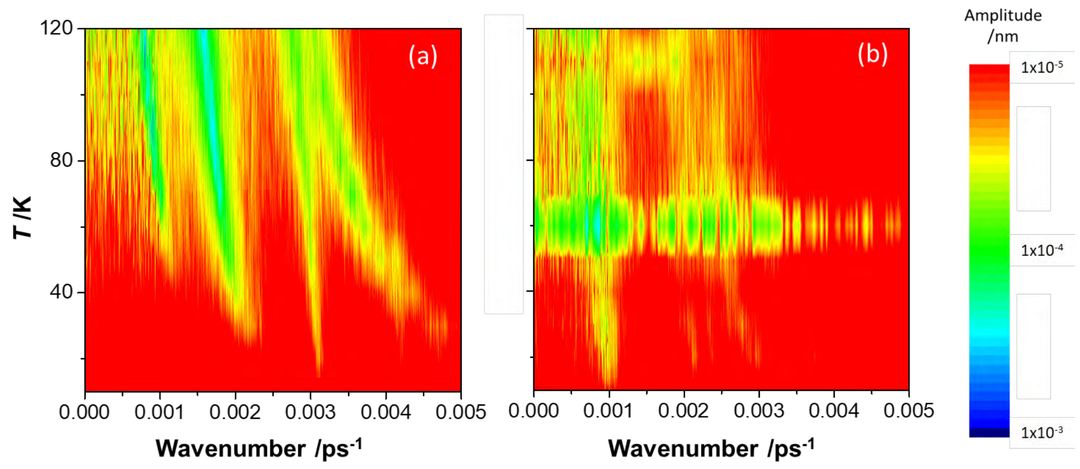

Figure 3. Resonance vibration frequencies of the crystal simulation box computed for (a) Form I and (b) Form II, as a function of the temperature.

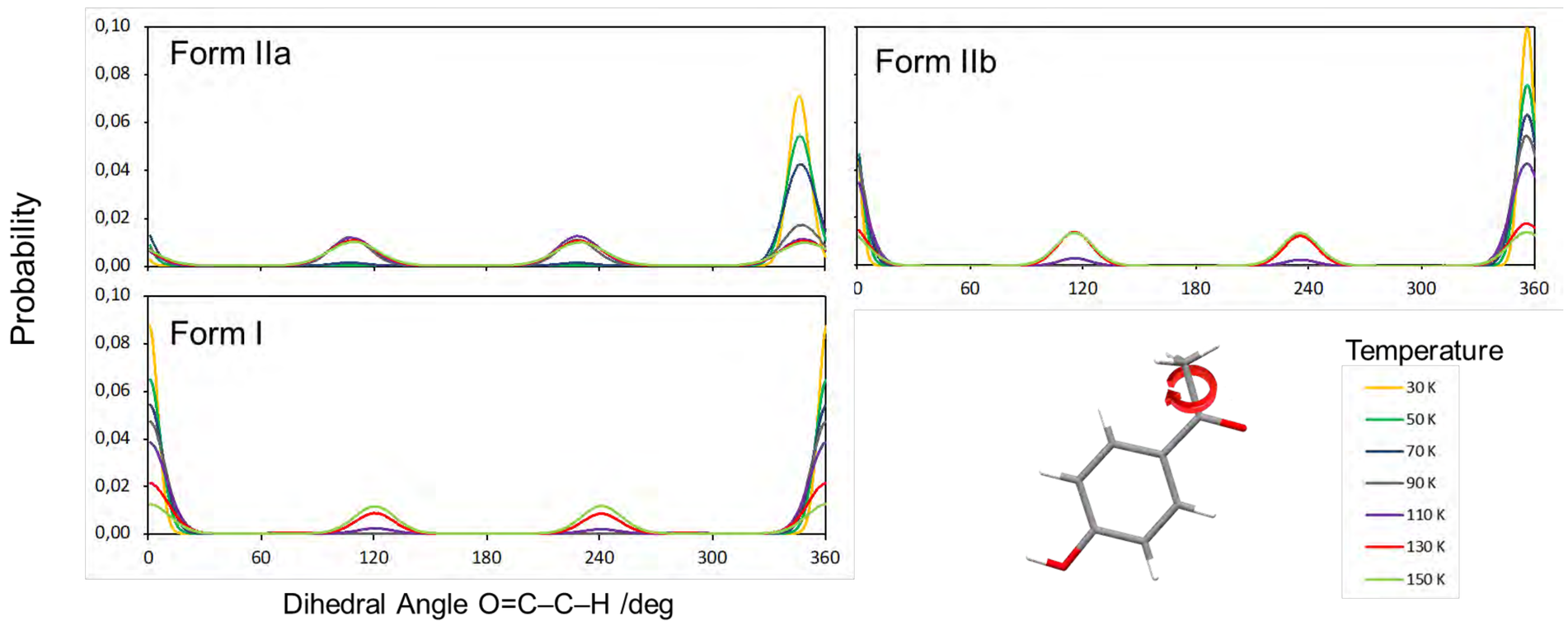

Figure 4. Probability distribution of the HAP dihedral angle O=C–C–H as a function of temperature, determined to the different molecules in the asymmetric unit of the two polymorphs of HAP.

Conclusion

- A modulation effect seems to occur in the case of HAP Form II around 60 K (Figure 3).
- The MD simulation results suggest that the experimentally observed phase transition at ~79 K may be related to a variation in the mobility of the HAP methyl group with temperature (Figure 4).
- The activation process for the rotation of the methyl groups is different in both polymorphs, and in the case of form II, is different in the two molecules in the asymmetric unit.

09 MET

Funding:

Centro de Química Estrutural is funded by Fundação para a Ciência e Tecnologia – project UID/QUI/00100/2019. This work was supported by Fundação para a Ciência e a Tecnologia (FCT), Portugal through Projects PTDC/QUIOUT/28401/2017(LISBOA-01-0145FEDER-028401) and UID/MULTI/00612/2013. A Post-Doctoral grant from FCT is also gratefully acknowledged by C. E. S. Bernardes (SFRH/BPD/101505/2014).

References:

[1] CES Bernardes, M.E. Minas da Piedade; *Cryst. Growth Des.* **2008**, *8*, 2419

[2] C.E.S. Bernardes, D.Y. Ilin, VA. Lukyanova, A.I. Druzhinina, M.E. Minas da Piedade; Unpublished Results.

Adaptation to nutrient-limited media remains accurate at the cost of an increased energy dissipation

R. N. Bento, C. E. S. Bernardes, M. E. Minas da Piedade, F. Antunes

CQE Química Estrutural

09 MET

Scope

Adaption is a fundamental biological process by which organisms adjust internal molecular mechanisms to achieve a better fitting to environmental conditions[1], having implications in health and disease, underlying processes such as acquired resistance to antimicrobials. Recently the existence of a trade-off between the energetic resource usage for adaptation and the speed and accuracy of the adaptive process has been proposed (**ESA**)[2], supported by the observation that (1) a high energy dissipation is necessary for an accurate and fast adaptation response[2] and (2) when the energy source in the medium decreases, the speed of adaptation of *E. coli* to a chemical stress also decreases with little effect on the accuracy of adaptation[2]. But while the speed and accuracy of adaptation were experimentally determined, energy dissipation was estimated.

Aim

Aim: Understand how the energy cost of adaptation is affected by nutrient availability.

Approach: Use of **microcalorimetry** to follow metabolic activity of *Saccharomyces cerevisiae* (*S. cerevisiae*) cells in real time during growth in Yeast Petone Dextrose (YPD) and Synthetic Complete (SC) media, which are nutrient **rich and poor media**, respectively.

Calorimetric data is coupled with results from cell concentration and other auxiliary measurements.

Figure 1. Experimental apparatus consisting of a modified LKB 10700-1 flow calorimeter coupled to cell count, ethanol and CO_2 sensors.

Results

1. Adaptation is faster in the poorer medium, but its accuracy is similar in the poor and rich media

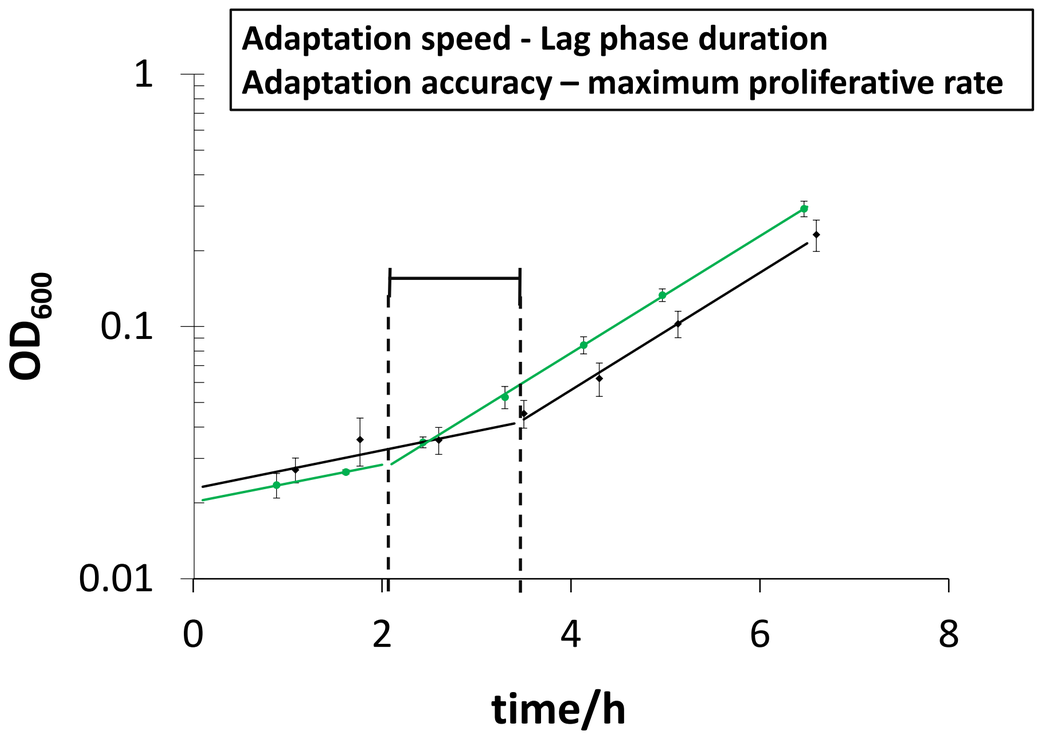

Figure 2. The growth of *S. cerevisiae* cells in YPD (in black) and SC (in green) media was followed by optical density at 600 nm.

2. Energy dissipation increases to compensate for nutrient limitations in the poor medium

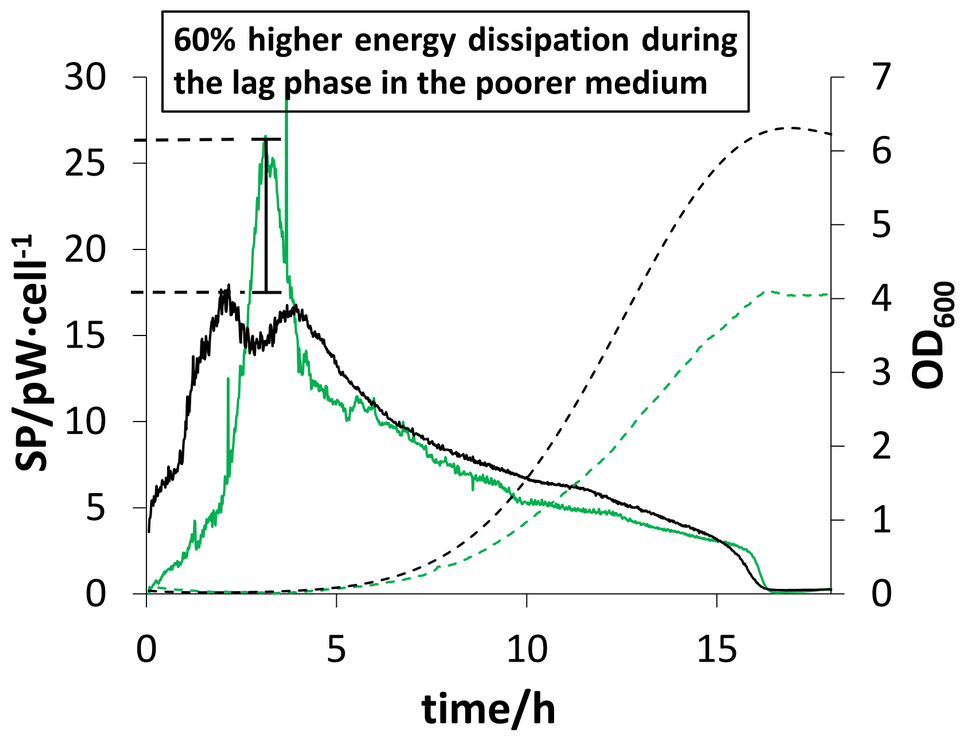

Figure 3. The specific power (*SP*, continuous lines) and optical density measurements at 600 nm (dashed lines) are presented for cultures grown in SC and YPD media (in green and black, respectively).

Conclusions

- 60% **higher energy dissipation** in the nutrient-limited (Synthetic Complete) medium during the lag phase **compensates** for the **nutrient constraint** to **maintain the adaptation accuracy** (measured by the maximal proliferation rate) and **increases the adaptation speed** (measured by the duration of the lag phase)
- This work provides the experimental evidence necessary to validate the ESA hypothesis
- The detection of an enhanced energy dissipation is a potential biomarker for metabolic deficiencies

Funding:
Centro de Química Estrutural is funded by Fundação para a Ciência e Tecnologia – project UID/QUI/00100/2019.
This work was supported by Fundação para a Ciência e a Tecnologia (FCT), Portugal through Project UID/MULTI/00612/2013.
PhD and Post-Doctoral grants from FCT are also gratefully acknowledged by R. N. Bento (SFRH/BD/117787/2016) and C. E. S. Bernardes (SFRH/BPD/101505/2014), respectively.

FCT Fundação para a Ciência e a Tecnologia

1. Schiraldi, A., Pure Appl. Chem. 67 (1995) 1873-1878.
2. Lan, G., Sartori, P., Neumann, S., Sourjik, V., Tu, Y. H., Nat. Phys. 8 (2012) 422-428.

Emulsions Based on Hydrophobic Eutectic Mixtures

Ricardo J. Nunes[1,2], Benilde Saramago[1], Filomena Martins[2], Isabel M. Marrucho[1]

[1] Centro de Química e Bioquímica, Faculdade de Ciências, Universidade de Lisboa, Ed. C8, Campo Grande 1749-016 Lisboa, Portugal.
[2] Centro de Química Estrutural, Instituto Superior Técnico, Universidade de Lisboa, Avenida Rovisco Pais, 1049-001 Lisboa, Portugal.

Email: ricardojgrn@gmail.com

CQE Química Estrutural

09 MET

Introduction

Up until recently, the study of eutectic solvents has been mostly focused on hydrophilic mixtures. However, mixtures composed of hydrophobic components such as terpenes, organic acids, and ammonium salts, among other classes of compounds, have been shown to have eutectic ratios as well, and thus can also be used as solvents.

Being hydrophobic, these mixtures present excellent dissolution properties for added value hydrophobic compounds such as pharmaceuticals, for example. Thus, the study and understanding of hydrophobic eutectic solvents surface properties is of utmost importance for these applications.

Starting compounds

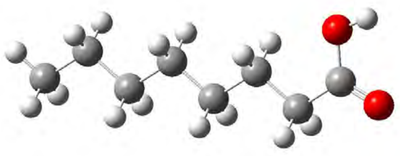

Octanoic Acid (C8)

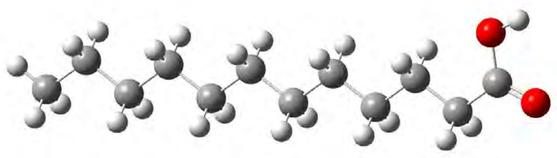

Dodecanoic Acid (C12)

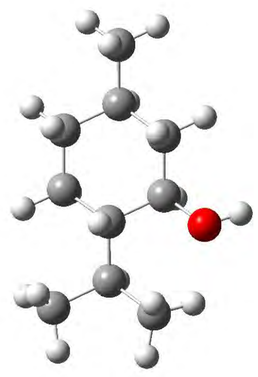

Menthol (M)

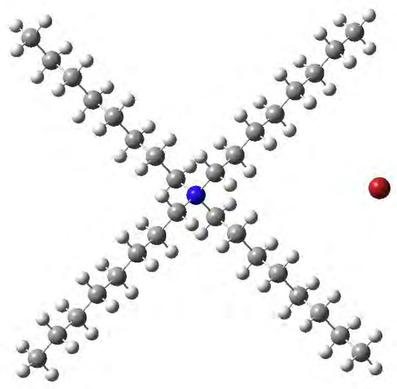

Tetraoctylammonium Bromide (N8888)

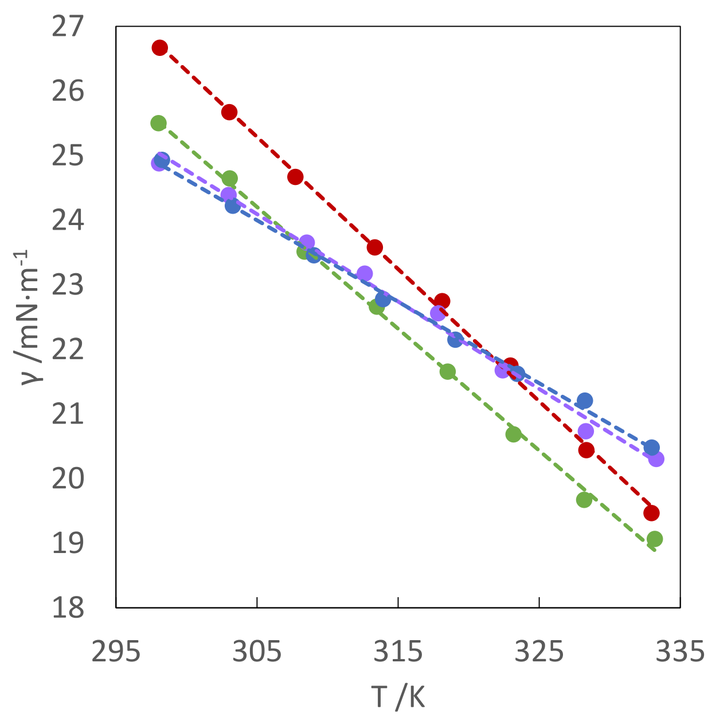

Figure 1 Surface tension of hydrophobic eutectic solvents: MC8 (1:1) (●), MC12 (2:1) (●), C8C12 (3:1) (●), N8888C8 (1:2) (●).

Surface tension

- Measure of the liquid-air interface energy.
- Typical values for hydrophilic eutectic systems: 40 to 65 $mN \cdot m^{-1}$
- Values for studied hydrophobic eutectic systems: 20 to 30 $mN \cdot m^{-1}$
- Linear trend with temperature

Emulsions

Typical case:

- Two unmixable phases
- Addition of surfactant leads to micelle formation
- Micelles dispersed in one of the phases
- Stability controlled by temperature: heat leads to separation.

Ouzo effect[1]:

- Uses a third solvent
- Exploits solubility of both phases in the third solvent.
- Three possible stages: solution, emulsion and microemulsion
- Stability controlled by temperature: cold leads to separation.

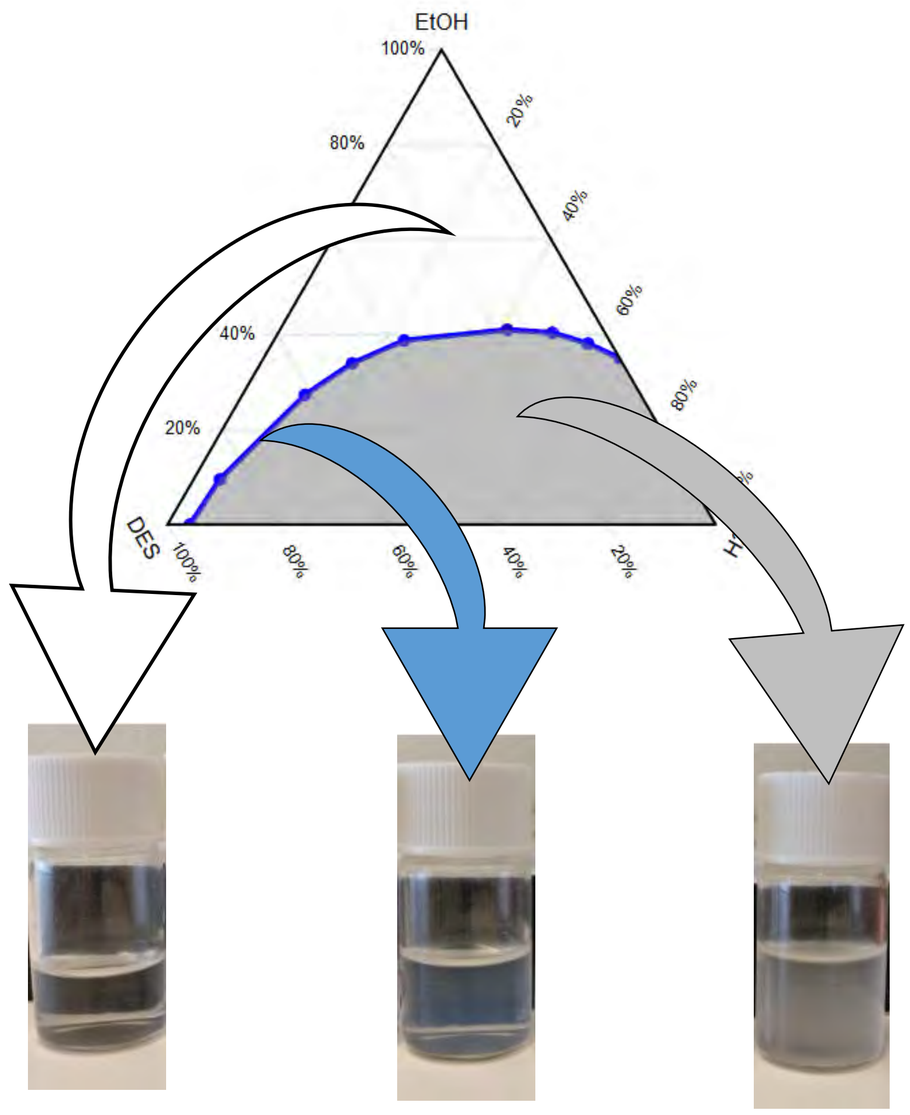

Figure 2 Phase diagram of the ternary system MC8/EtOH/H_2O

Conclusion

Hydrophobic eutectic solvents have the potential to be used extraction of pharmaceuticals, drug delivery and cosmetics. In addition to being cheap to prepare, their low surface tension, as well as low viscosity, makes them easy to use in an industrial setting.

Funding:
Centro de Química Estrutural is funded by Fundação para a Ciência e Tecnologia – project UID/QUI/00100/2019.

FCT Fundação para a Ciência e a Tecnologia

1. Ganachaud, F., Katz, J. L., *ChemPhysChem* 6 (2005) 209–216.

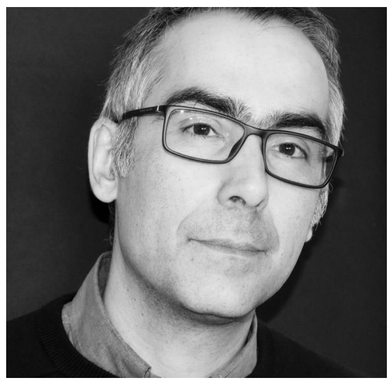

Extracting more information from research in chemistry: The multidisciplinary evaluation of data uncertainty

Ricardo Bettencourt da Silva (rjsilva@fc.ul.pt)

All research in chemistry involves comparing and/or reporting qualitative and/or quantitative chemical information. The quality of the research depends on the quality of the information and of their interpretation. The sciences of qualitative and quantitative chemical analysis are Examinology and Metrology in Chemistry, respectively.

When small trends or differences of chemical systems need to be distinguished, it is necessary to manage all evaluation steps and effects that affect the result to guarantee information will be fit for the intended use. If qualitative and quantitative information is reported with uncertainty, it can be quantified the probability of their interpretation being correct. For instance, the presence of trace-levels of a compound in a urine sample can be reported with a probability of 99.993 % of being correct and the reduction of a contaminant in the water of a river after improving wastewaters treatment can be determined with a risk of 0.03 % of wrongly concluding that the reduction is meaningful.

Our research group have been developing novel strategies for extracting objective and more information from complex and vast chemical systems and is willing to collaborate in new challenges for producing sound chemical information.

We recently developed strategies for evaluating the uncertainty of kinetic constants that quantify the efficiency of photodegradation catalysts[1], strategies for the objective detection of trends of vast environmental areas[2], and reliable criteria for identifying trace levels of compounds in complex matrices by GC-MS/MS or LC-MS/MS[3]. All these achievements are supported on publications in the highest impact factors journals.

Determination of kinetic constants with uncertainty:

The first assessments of kinetic constants uncertainty were applied to the determination of methylene-blue photodegradation by UV/Vis spectroscopy[1]. Methylene-blue is a frequently used photodegradation marker. This publication aimed at discussing how calibrators quality and the lack of linearity of the instrumental response can affect the uncertainty of kinetic constants quantification. At this moment, a flexible tool for determining the uncertainty of kinetic constants have been developed that can be used regardless of calibrators uncertainty value. Monte Carlo simulations were implemented in a user-friendly spreadsheet to allow the evaluation of kinetic constants uncertainty by non-experts in metrology.

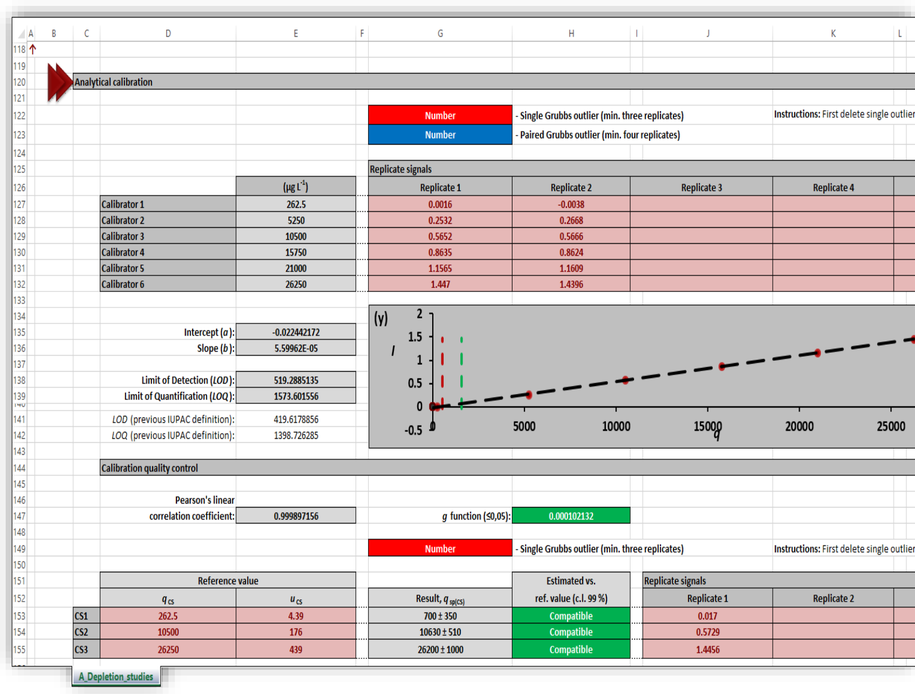

Determination of environmental pollution trends:

One of the more demanding challenge in environmental chemistry research is the objective assessment of the status or trends of a vast environmental compartment. Our research group developed an innovative tool for estimating the mean value of a chemical parameter, and the respective uncertainty, in a vast environmental compartment by modelling the available information of the spatial distribution of the parameter[2]. The modelling considers the uncertainty of the GPS coordinates and of the estimated chemical parameter on analysed samples. This modelling allows the optimization and objective determination of small trends of the environmental system.

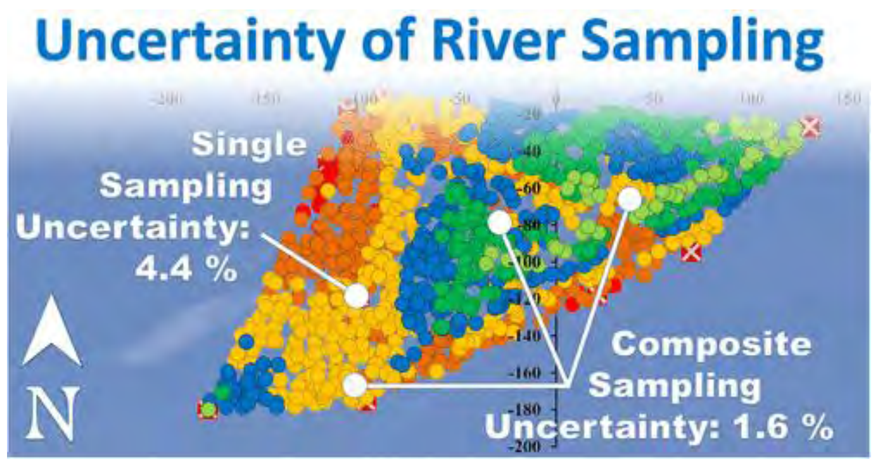

Reliable identification of trace-levels of compounds:

The false identification of trace levels of compounds in complex matrices by low-resolution GC-MS/MS or LC-MS/MS is frequent due to the inadequate interpretation of the analytical data. Our research group develop statistically sound criteria for identifying compounds using these instrumental methods of analysis that proved official doping analysis are affected by high rates of false negative results[3]. That technology can be used in many other research fields.

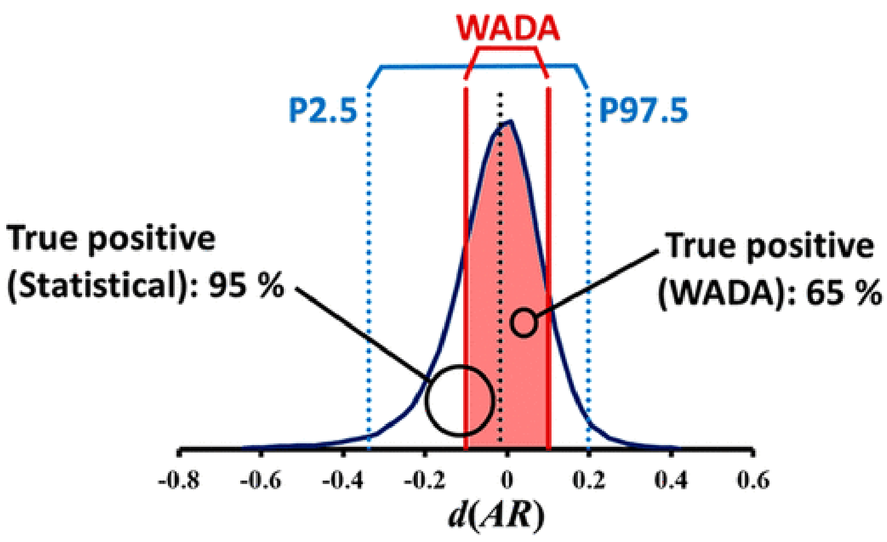

CQE Química Estrutural

06 CE

Funding:
Fundacão para a Ciência e Tecnologia

Projects UID/QUI/00100/2019 and SFRH/BPD/110186/2015

FCT Fundação para a Ciência e a Tecnologia

References:

1. Rosa, NF, Monteiro, OC, Camões, MF, Silva, RB, Accred. Qual. Assur. 22 (2017) 217–226.

2. Borges, C, Palma, C, Silva, RB, Anal. Chem. (2019) In press (DOI 10.1021/acs.analchem.8b05781)

3. Narciso, J, Luz, S, Silva, RB, Anal. Chem. (2019) In press (DOI 10.1021/acs.analchem.9b00560)

Conformational Polymorphism in Molecular Organic Crystals: 4'-Hydroxyvalerophenone, as a Case Study

Ricardo G. Simões,[1] Cátia S. D. Lopes,[1] Carlos E.S. Bernardes,[1] M. Fátima M. Piedade,[1,2] Hermínio P. Diogo,[2] and Manuel E. Minas da Piedade[1]

[1] Centro de Química e Bioquímica e Centro de Química Estrutural, Faculdade de Ciências, Universidade de Lisboa, 1749-016 Lisboa, Portugal

[2] Centro de Química Estrutural, Complexo Interdisciplinar, Instituto Superior Técnico, 1049-001, Lisboa, Portugal.

CQE Química Estrutural

09 MET

Scope

- Many compounds can crystallize in more than one solid structure, a phenomenon known as polymorphism.
- Different polymorphs often display different properties (e.g. melting point, solubility), and thus represent a challenge for the production of solid materials with highly reproducible properties.
- Polymorphic studies in families of structurally related molecules can offer insights into how small variations in the molecular structure can lead to alterations in the packing architecture and relative stability of different crystals.
- In this work, the polymorphic behavior of 4'-hydroxyvalerophenone (HVP, Figure 1) was analyzed. This molecule is part of a family of compounds with the general formula ($HOC_6H_4C(O)R$, with R=H, n-alkyl), and where conformational and packing polymorphism have previously been identified [1,2].

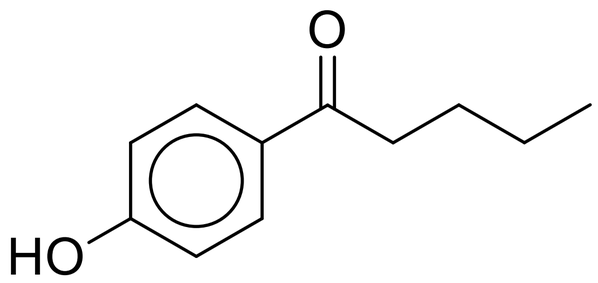

Figure 1. Molecular structure of HVP.

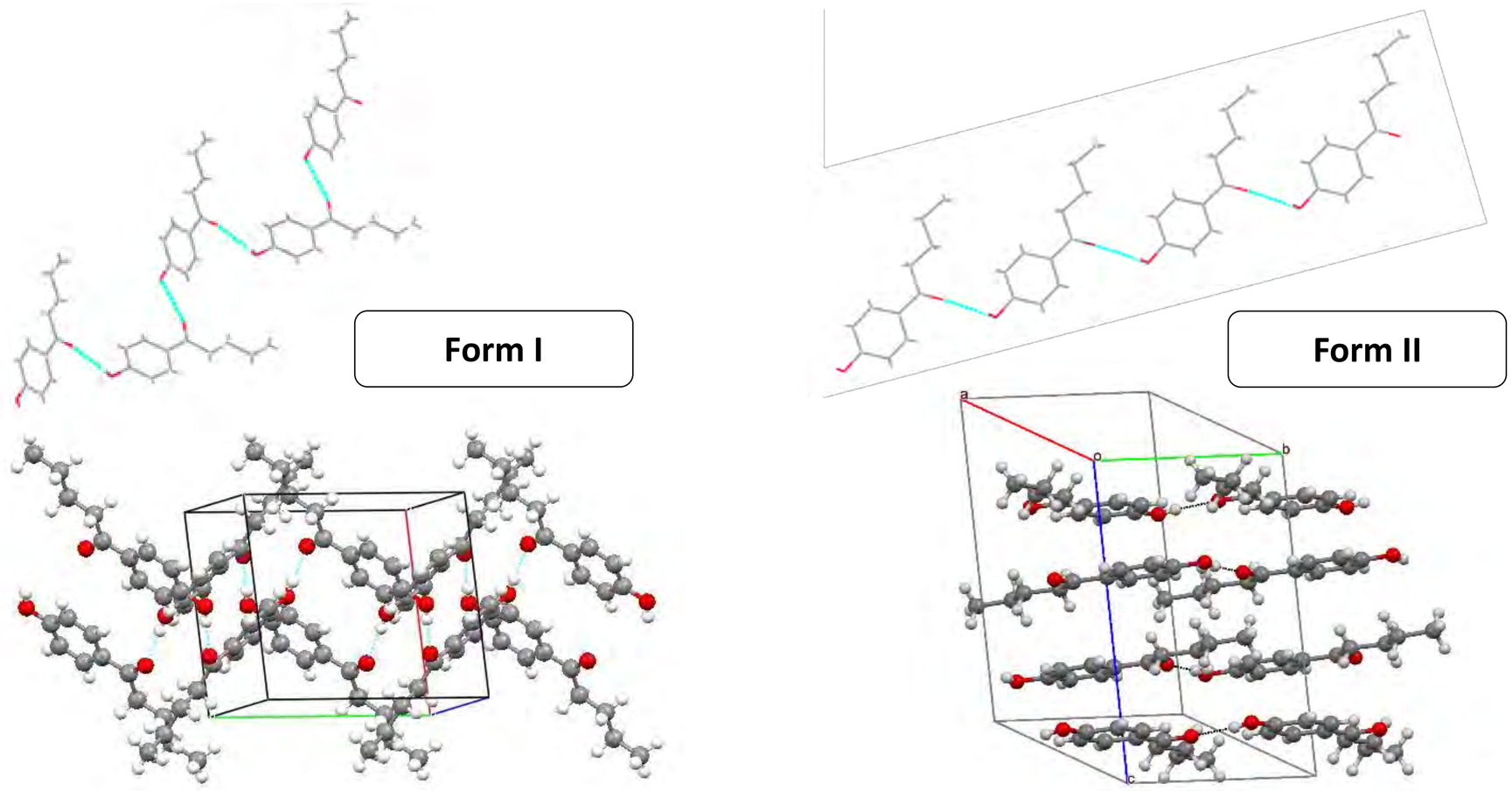

Figure 2. Crystal structures of HVP Forms I and II. Molecular chains (above) and the crystal packing (bellow).

Table 1. Crystal data for the two polymorphic forms of HVP.

	Form I	Form II
Space group	$P2_1/c$	$C2/c$
Crystal System	monoclinic	monoclinic
a (Å)	9.990(2)	8.4860(16)
b (Å)	10.454(2)	14.976(3)
c (Å)	9.882(2)	12.045(13)
β (°)	107.46(3)	111.054(13)
Z/*Z'*	4/1	8/1
ρ (g·cm^{-3})	1.202	1.145

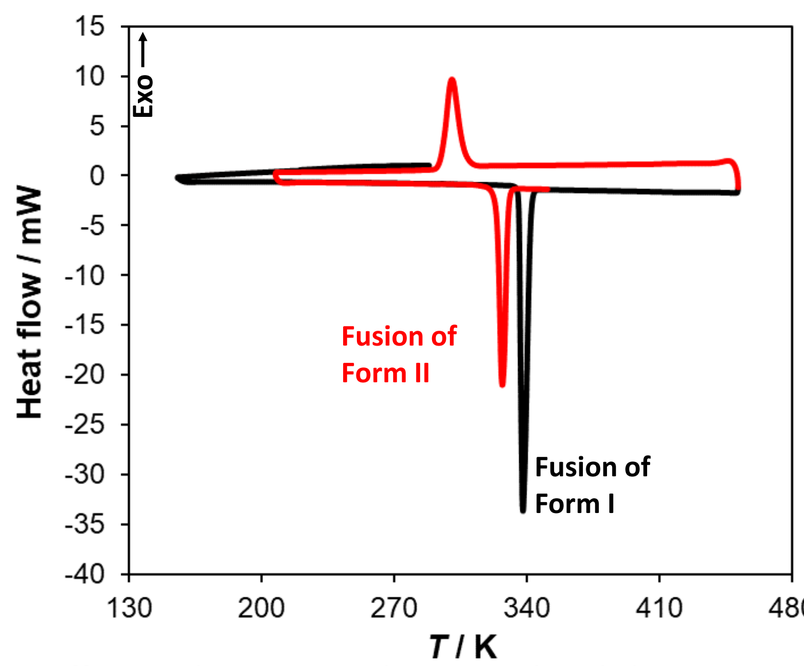

Figure 3. Differential scanning calorimetry (DSC) thermogram of HVP Form I. Temperature program: cooling to 153 K, heating to 453 K (black line), cooling to 212 K, heating to 453 K (red line). The heating/cooling runs were conducted at 10 K·min^{-1}.

Conclusions:

The crystal structure of a new polymorph of HVP was determined, and compared with the previously published form [3]. The molecular conformation was different in the two structures (*Z* in Form I and *E* in Form II, Figure 2), revealing a case of conformational polymorphism in this compound.

The melting temperature and enthalpy of fusion determined for Form II (T_{fus}=324.3±0.2K, $\Delta_{fus}H_m$=18.14±0.18 kJ·mol^{-1}), was significantly lower than what was observed for Form I (T_{fus}=335.6±0.7K, $\Delta_{fus}H_m$=26.67±0.04 kJ·mol^{-1}), as seen in Figure 3, while changes to the space group, cell parameters and density of the crystals were also noted between the two polymorphs (Table 1). The decrease in density and the DSC results suggest that Form II is less stable than Form I, and that the system is monotropic.

Funding:
Centro de Química Estrutural is funded by Fundação para a Ciência e Tecnologia – project UID/QUI/00100/2019.
Projects:
PTDC/QUI-OUT/28401/2017 (LISBOA-01-0145-FEDER-028401) and UID/MULTI/00612/2013.
Post-doctoral grants:
R. G. Simões (SFRH/BPD/118771/2016)
C. E. S. Bernardes (SFRH/BPD/101505 /2014)
Doctoral grants:
C. S. D. Lopes (SFRH/BD/128794/2017).
We also acknowledge the COST Action CM1402.

FCT Fundação para a Ciência e a Tecnologia

References:

[1] C.E.S Bernardes, M.F.M. Piedade, M.E. Minas da Piedade, Cryst. Growth Des. 8 (2008) 2419-2430
[2] R.G. Simões, C.E.S. Bernardes, M.E. Minas da Piedade, Cryst. Growth Des. 13 (2013) 2803-2814.
[3] Z. Luo, H. Zhu, S. Liu, Acta Cryst. E 62 (2006) o5054.

Synthesis of half-sandwich ruthenacarboranes complexes incorporating *N*-donor ligands as eminent candidates for Boron Neutron Capture Therapy

Ricardo G. Teixeira,[1] Xavier F. Gubau,[2] Fernanda Marques,[3] M. Paula Robalo,[4,5] M. Helena Garcia,[1] Clara Viñas,[6] Andreia Valente[1]

[1] Centro de Química Estrutural, Faculdade de Ciências da Universidade de Lisboa, Campo Grande, 1749-016 Lisboa, Portugal. [2] Unitat d'Anàlisi Química i Estructural, Parc Científic i Tecnològic de la UdG, 15, 17003 Girona, Spain. [3] Universidade de Ciências Químicas e Radiofarmacêuticas, Instituto Superior Técnico, Campus Tecnológico e Nuclear, Estrada Nacional 10, 2686-953 Sacavém, Portugal. [4] Área Departamental de Engenharia Química, Instituto Superior de Engenharia de Lisboa, Rua Conselheiro Emídio Navarro, 1, 1959-007 Lisboa, Portugal.[5] Centro de Química Estrutural, Complexo I, Instituto Superior Técnico, Universidade de Lisboa, Av. Rovisco Pais, 1049-001 Lisboa, Portugal. [6] Institut de Ciència de Materials de Barcelona (ICMAB-CSIC), Campus U.A.B., 08193 Bellaterra, Spain.

rjteixeira@fc.ul.pt

CQE Química Estrutural

04 BIOIN

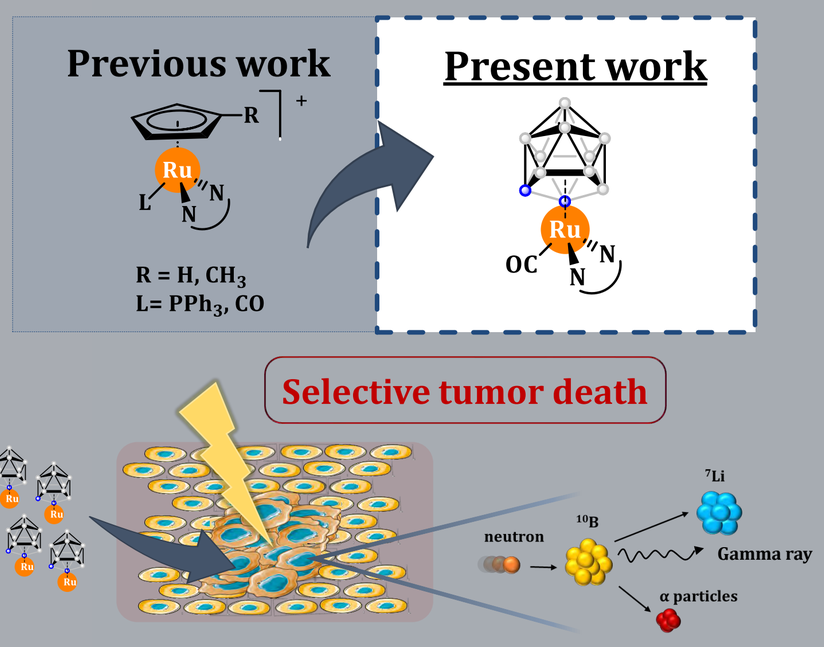

Figure 1. Scheme for Boron Neutron Capture Therapy (**BNCT**). BNCT is based on non-reactive isotope ^{10}B atom that absorbs low energy neutrons and disintegrates into α particles and ^{7}Li nucleus causing nonreparable damages to the cell where they were generated while sparing the healthy tissues.

INTRODUCTION

One of our newer approaches in the design of novel antitumor agents involves the replacement of the monoanionic cyclopentadienyl ($[\eta^5\text{-}C_5H_5]^-$) moiety by a highly boronated dianionic *nido*-carborane cluster ($[C_2B_9H_{11}]^{2-}$) in order to amplify the action of our ruthenium-based complexes (Figure 1). This rationale modification would amplify the antitumoral potential of our Ru compounds since a combinatory therapy can be envisaged this way (traditional chemotherapy and Boron Neutron Caption Therapy, BNCT).

Therefore, in this communication, we reveal the synthesis and characterization of a new family of ruthenacarboranes complexes of general formula [3-CO-3,3-{κ^2-4,4´-R_2-2,2'-$(NC_5H_3)_2$}-*closo*-3,2,1-$RuC_2B_9H_{11}$] comprising 2,2´-bipyridyl ligands. All complexes were screened against the highly metastatic human melanoma cell line (A375) and human primary glioblastoma cell line (U87) and the irradiation reaction of the boron cluster conjugate is currently under evaluation.

CHARACTERIZATION

NMR spectroscopy

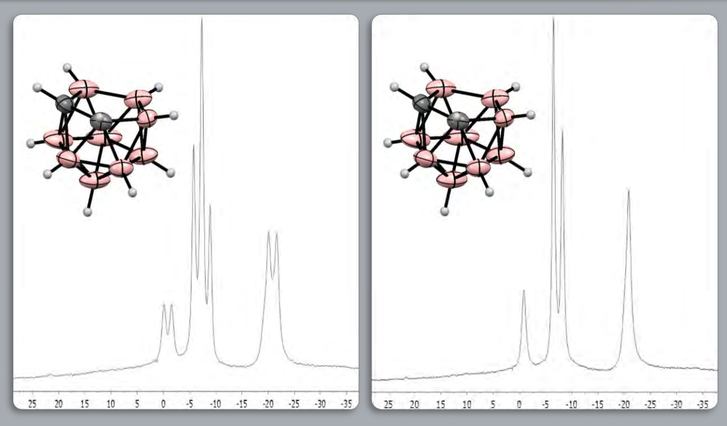

Figure 2. ^{11}B and $^{11}B\{^1H\}$ NMR spectrum of **Ru1** in acetone-d_6.

UV-visible spectroscopy

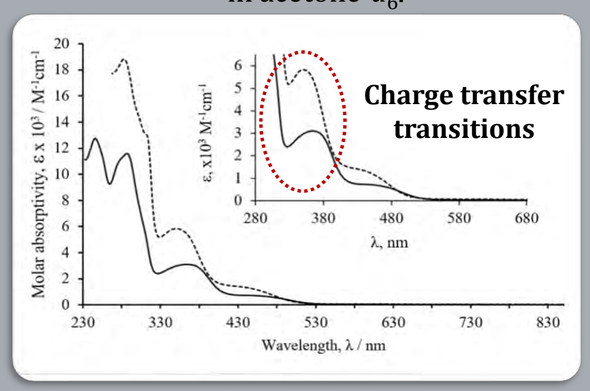

Figure 3. Absorption spectrum of **Ru1** in CH_2Cl_2(—) and DMSO (- - -).

Cyclic voltammetry

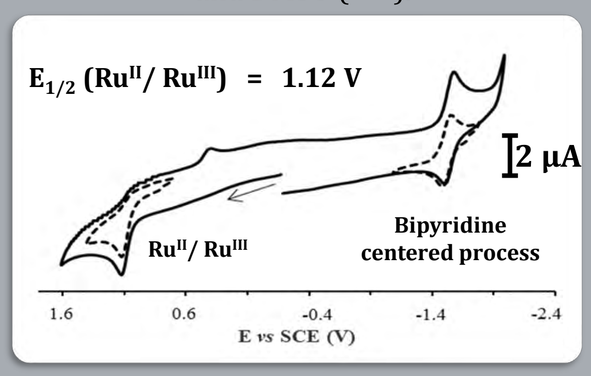

Figure 4. Cyclic voltammogram of **Ru1** in CH_2Cl_2 at scan rate of 200 mVs^{-1}.

SYNTHESIS AND STRUCTURE

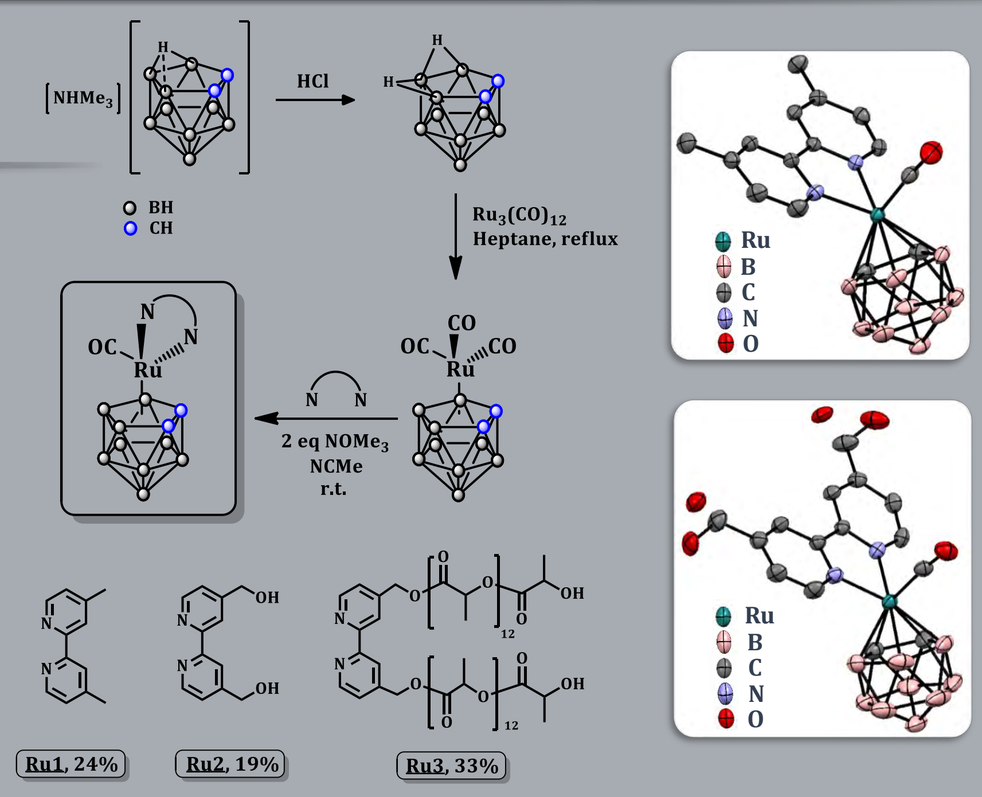

Ru1–Ru3 are stable in aqueous solution over 24 h period.

Figure 5. IC_{50} values (half-inhibitory concentrations) of **Ru1–Ru3** against **human melanoma** cell line (**A375**) and **human primary glioblastoma** cell line (**U87**) within a period of exposure of 24 h (left) and cellular distribution of **Ru1-Ru3** in **A375** cells determined by ICP-MS analysis (right).

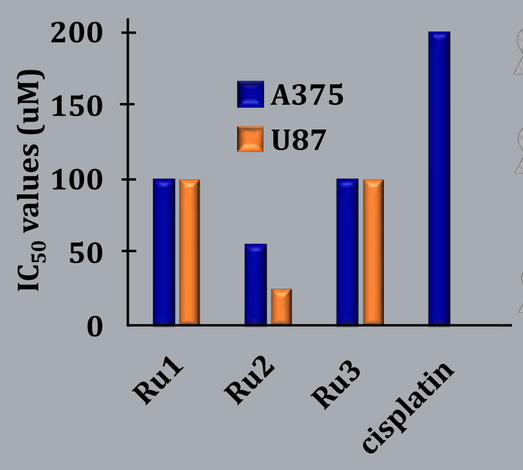

- **Ru1** and **Ru3** show low cytotoxic activity in both cancer cell lines studied;
- **Ru2** presents moderate cytotoxic activity against highly aggressive **A375** and **U87** cancer cell lines;
- Different mechanisms of action for **Ru1** and **Ru3** *vs* **Ru2**, leading to different IC_{50} values and intracellular distribution.

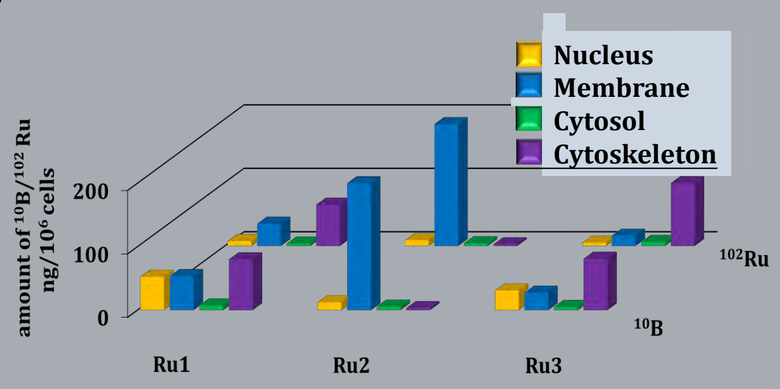

Ru1 and Ru3 accumulate at the cytoskeleton whereas Ru2 accumulates preferentially at the membrane.

CONCLUSIONS

- **Three new ruthenacarboranes complexes with bipyridyl ligands were successfully synthesized and proposed for BNCT;**
- **Ru1-Ru3 were the first complexes of Ru-carboranyl-bipyridyl conjugates been biological evaluated. All compounds showed promising cytotoxic profile against the A375 and U87 cancer cell lines for BNCT reaction;**
- **The irradiation with neutrons of Ru1-Ru3 is currently on-going to further explore the potential of these compounds in BNCT.**

Funding:
Centro de Química Estrutural is funded by Fundação para a Ciência e Tecnologia – project UID/QUI/00100/2019. Financial support was also provided by FCT through PTDC/QUI-QIN/28662/2017; Andreia Valente acknowledges CEEC-IND/01974/2017 (acknowledging FCT, as well as POPH and FSE - European Social Fund).
Ricardo G. Teixeira thanks FCT for his Ph.D. Grant (SFRH/BD/135830/2018).

GOVERNO DE PORTUGAL · POPH · IF INVESTIGADOR FCT · FCT Fundação para a Ciência e a Tecnologia · UNIÃO EUROPEIA Fundo Social Europeu

References:
[1] T.S. Morais, A. Valente, A.I. Tomaz, F. Marques, M.H. Garcia, Future Medicinal Chemistry (**2016**) 8(25), 527-544.
[2] M.H. Garcia, A. Valente, T. Morais, A.I. Tomaz, Macromolecular Transition Metal Complexes for Treatment of Cancer and Process for Their Preparation, PCT/IB2015/002312; WO 2016/087932.
[3] A. Valente, M.H. Garcia, F. Marques, Y. Miao, C. Rousseau, P. Zinck, J. Inorg. Biochem. (**2013**) 127, 79-81.

Exploring Solvent Properties of Hydrophobic Eutectic Mixtures

Ricardo J. Nunes[1-3], Isabel Marrucho[2], Filomena Martins[1,3]

[1] Centro de Química e Bioquímica, Faculdade de Ciências, Universidade de Lisboa, Ed. C8, Campo Grande 1749-016 Lisboa, Portugal.
[2] Centro de Química Estrutural, Instituto Superior Técnico, Universidade de Lisboa, Avenida Rovisco Pais, 1049-001 Lisboa, Portugal.
[3] Centro de Química Estrutural, Faculdade de Ciências, Universidade de Lisboa, Edif. C8, Campo Grande 1749-016 Lisboa, Portugal.

Email: ricardojgrn@gmail.com

CQE Química Estrutural

09 MET

Introduction

Kamlet-Taft parameters (α, β, and π^*) which are a measure of solute-solvent interactions, are usually determined through solvatochromic probes (A to E – **Fig. 1**) resorting to some known mathematical relations – **Fig. 2**. In some cases, however, probe A characteristic band, which allows the calculation of α, can appear partially or fully masked by other bands, making its determination by UV-Vis hard or even impossible. On the other hand, it has been shown that rate constant for tertiary alkyl halides solvolyses correlate well with Kamlet-Taft parameters[1], in pure organic solvents. For the solvolysis of *t*-BuBr, the correlation is as follows:

$$\log k = 6.91\pi^* + 3.39\alpha + 0.67\beta - 12.48 \qquad N = 21,\ r^2 = 0.99$$

Thus, by using this correlation, it is possible to extract α for a given system if β, π^* and k are known.

In recent years, there has been a growing interest in hydrophobic eutectic mixtures that can be used in various water sensitive applications[2]. Yet, for these mixtures it is often difficult to determine α by spectrophotometry. In this work, a kinetic-based approach was used to compute α for DL-menthol:octanoic acid and octanoic acid:dodecanoic acid eutectic mixtures - **Table 1**.

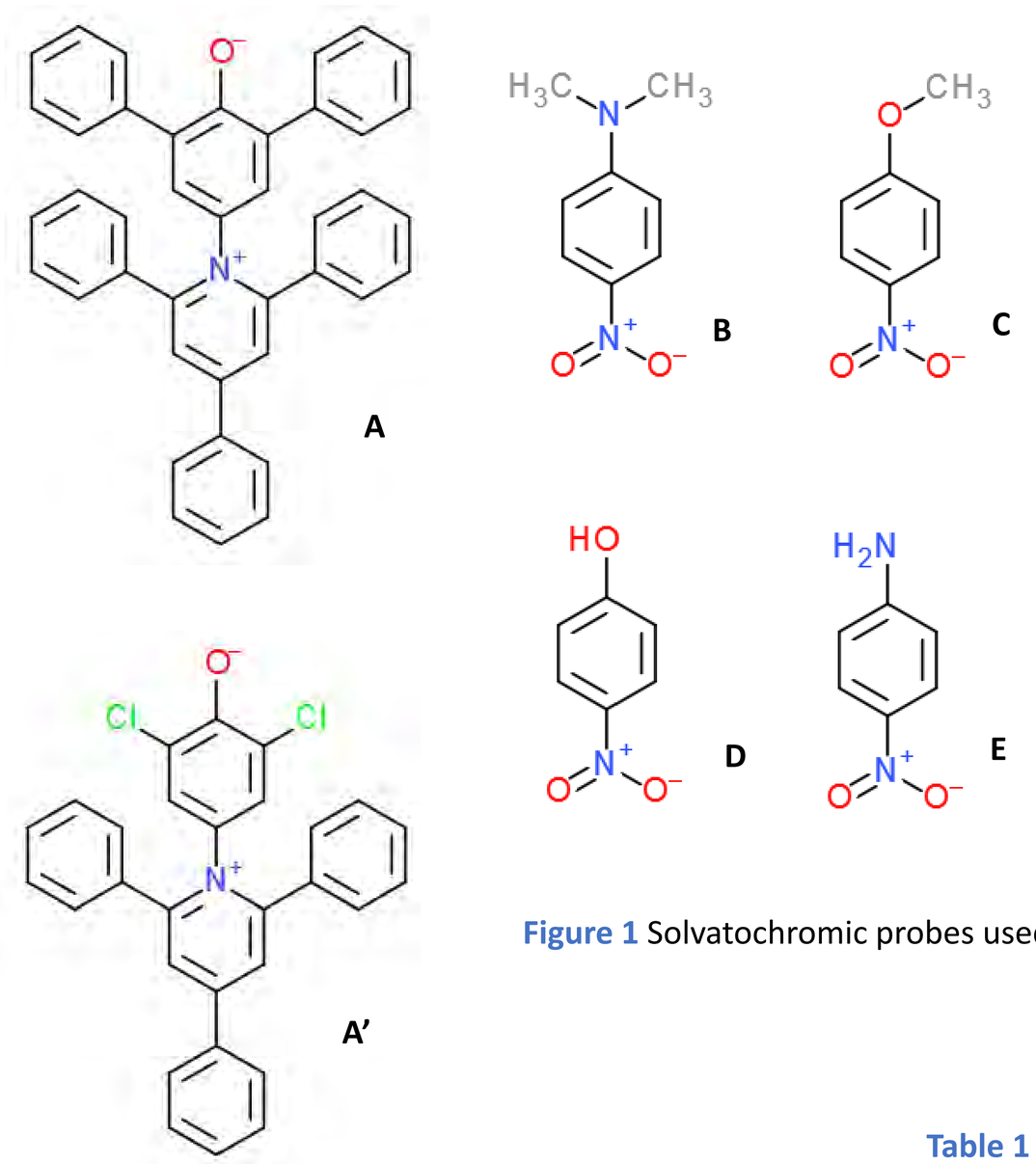

Figure 1 Solvatochromic probes used

$$\pi^*_{OMe} = \frac{[\overline{\sigma}_{Probe\ C} - 34.12]}{[31.72 - 34.12]}$$

$$\pi^*_{NMe_2} = \frac{[\overline{\sigma}_{Probe\ B} - 28.18]}{[24.66 - 28.18]}$$

$$\alpha_{OMe} = \frac{[1.873\overline{\sigma}_{Probe\ C} - 74.58] + \overline{\sigma}_{Probe\ A}}{6.24}$$

$$\alpha_{NMe_2} = \frac{[1.318\overline{\sigma}_{Probe\ B} - 47.70] + \overline{\sigma}_{Probe\ A}}{5.47}$$

$$\beta_{OH} = \frac{[1.0434\overline{\sigma}_{Probe\ C} - 0.57] - \overline{\sigma}_{Probe\ D}}{2.00}$$

$$\beta_{NH_2} = \frac{[0.9841\overline{\sigma}_{Probe\ B} + 3.49] - \overline{\sigma}_{Probe\ E}}{2.759}$$

Figure 2 Eqs to determine α, β, and π^*, using both O- and N- scales

Table 1 Composition of the studied eutectic mixtures

Systems	*HBA*	*HBD*	*Ratio*
DES1	DL-Menthol	Octanoic Acid	1:1
DES2	Octanoic Acid	Dodecanoic Acid	3:1

Table 2 Results obtained for α using both approaches

Systems	π^*	β	$k \times 10^4$ /s^{-1}	α_{Probes}	$\alpha_{Kinetics}$
DES1	0.70	0.63	2.64	1.07	1.04
DES2	0.71	0.20	8.13	1.25	1.29

Results

- π^* and β values were determined experimentally and agree with literature values[2].
- k values were determined experimentally for these systems for the first time, from the kinetics of *t*-butyl bromide in the referred solvent mixtures.
- Values of α were determined experimentally using probe A' to overcome probe A solubility and reactivity problems and from the referred correlation.

Conclusion

This work validates the use of a combined spectroscopic and kinetics approach to determine the value of α, in cases where the use of probe A is not possible, thus extending the span of log *k vs.* (α, β, and π^*) correlation from pure solvents to hydrophobic eutectic mixtures.

Funding:
Centro de Química Estrutural is funded by Fundação para a Ciência e Tecnologia – project UID/QUI/00100/2019. Centro de Química e Bioquímica is funded by Fundação para a Ciência e Tecnologia – projects UID/QUI/00612/2013 and UID/QUI/00612/2019.

FCT Fundação para a Ciência e a Tecnologia

References:

1. Abraham, M. H., Doherty, R. M., Kamlet, M. J., Harris, J. M., Taft, R. W., *J. Chem. Soc., Perkin Trans.* 2 (7) (1987) 913–920.

2. Ribeiro, B. D., Florindo, C., Iff, L. C., Coelho, M. A. Z., Marrucho, I. M., *ACS Sustainable Chemistry & Engineering* 3(10) (2015) 2469–2477.

Hydrogen transfer reactions of nitro compounds using MoS_2 / titanate nanotubes as catalyst

Rita Sales, Carla D. Nunes, Olinda C. Monteiro

Centro de Química e Bioquímica and Centro de Química Estrutural, Faculdade de Ciências, Universidade de Lisboa, Campo Grande, 1749-016 Lisboa, Portugal

CQE Química Estrutural

06 CE

Introduction

It is known that nitroarenes are vital chemicals for living organisms and environment. Not only nitro compounds, but also their reduction products, like amino compounds are essential in several industries such as dyes, pigments, agrochemicals, herbicides, pharmaceuticals, rubber manufacturing, chelating agents and textile. [1]

This work focused on the synthesis of nanostructured titanate nanotubes (TNT) modified with molydenum disulfide nanoparticles (MoS_2/TNT) and its application in catalytic reduction reactions of nitro compounds. The titanate nanotubular sample was prepared by a hydrothermal approach, using an amorphous precursor. [2] Using the same method, the molydenum disulphide nanoparticles were produced in the presence of the TNT particles. [3]

Hydrogen transfer reactions of several nitroarenes were studied to evaluate the MoS_2/TNT catalytic activity. The results indicate that the reaction is only possible in the presence of the MoS_2/TNT and the obtained reaction products were the wanted amino compounds.

Catalyst synthesis & characterization

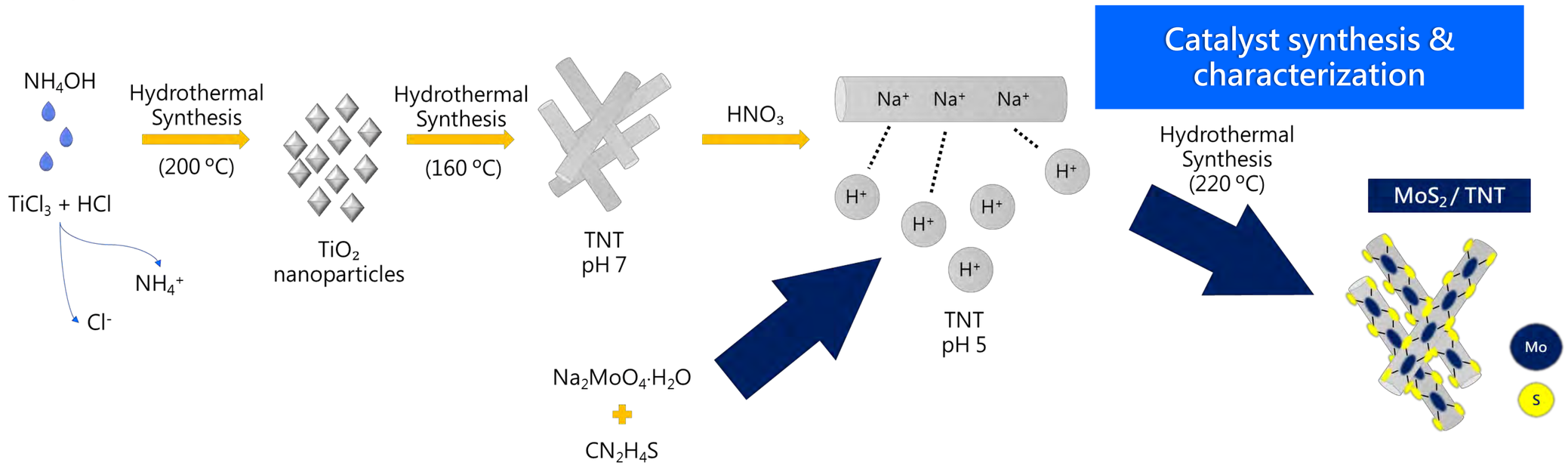

Powder X-Ray diffraction

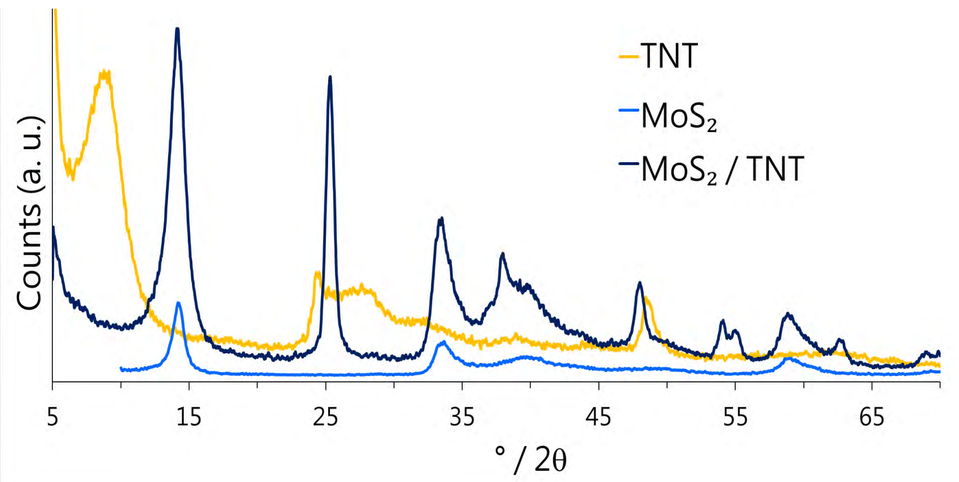

Scanning electronic microscopy of MoS_2

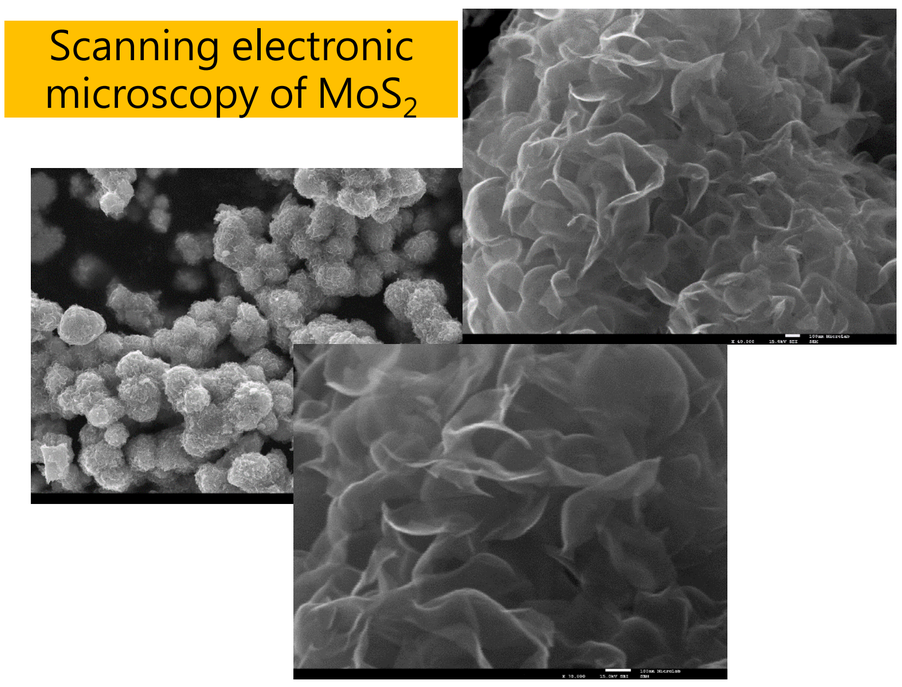

Catalytic results

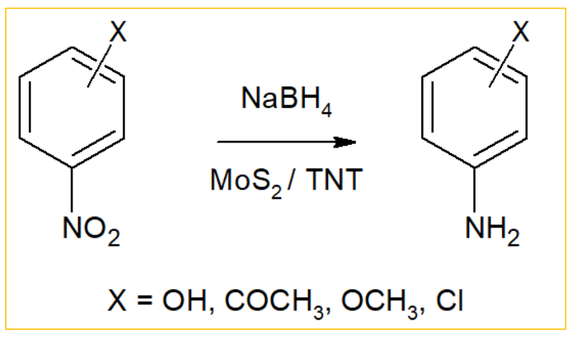

Hydrogen transfer reaction of nitro compounds.

Substrate	Reaction time (min)
p-nitrophenol	50
methyl-*p*-nitrobenzoate	5
m-nitrophenol	30
1-chloro-*p*-nitrobenzene	30
p-nitroanisole	40
p-nitrotoluene	3

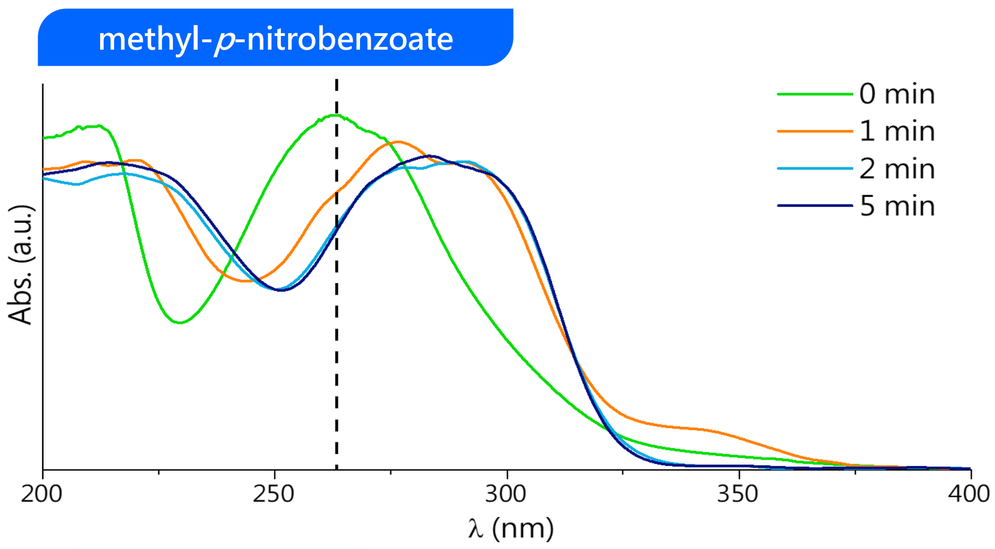

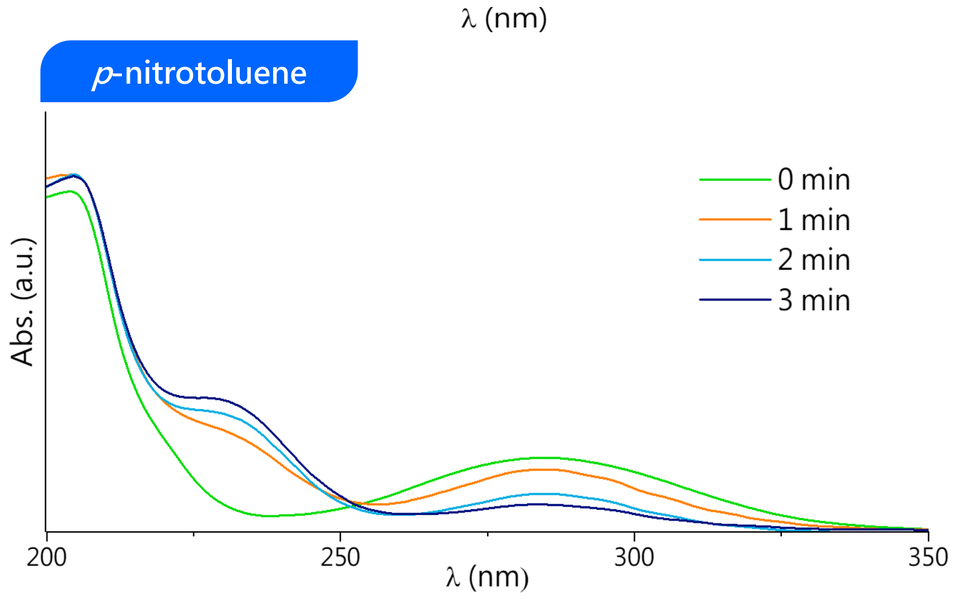

Conclusions

The results indicate that the hydrogen transfer processes are only possible in the presence of the MoS_2/TNT and the obtained reaction products were the expected amino compounds. All substrates were successfully reduced, being methyl-*p*-nitrobenzoate and *p*-nitrotoluene the fastest ones.

Funding:
Centro de Química Estrutural is funded by Fundação para a Ciência e Tecnologia (FCT) project UID/QUI/00100/2019. This work was also funded by FCT through the projects UID/MULTI/00612/2019 and IF/01210/2014.

References:

1. Mali M, Synth Catal. 2 (2017) 2.
2. Barrocas B, Neves M C, Conceição O M, Monteiro O C, Environ. Sci. Nano. 5 (2018) 350.
3. Li A, Xu W, Wang G, Wang X, J. Appl. Polym. Sci. 46064 (2018) 1.

Ciências ULisboa · FCT Fundação para a Ciência e a Tecnologia · ULISBOA Universidade de Lisboa

Mercury cycling in a Portuguese mesotidal ecosystem, Tagus estuary: Water column chemistry and transport

Rute Cesário[1,*], João Canário[1], Marta Nogueira[2]

[1]Centro de Química Estrutural, Instituto Superior Técnico, Universidade de Lisboa, Av. Rovisco Pais, 1, 1049-001 Lisboa, PORTUGAL

[2]IPMA I.P. - Instituto Português do Mar e Atmosfera, R. Alfredo Magalhães Ramalho, 6, 1495 - 006, Lisboa, PORTUGAL

rute.cesario@tecnico.ulisboa.pt

Química Estrutural

06 CE SUSCHEM

Introduction and aims

The data set emphasizes the importance of examining the complex site-to-site variation within a system, in order to understand estuary wide mercury (Hg) and methylmercury (MMHg) dynamics, and demonstrates that processes driving MMHg fate may be distinct in different regions of the same system. Six sampling campaigns were performed bimonthly during one year covering the North Channel (NC) and the adjacent areas of Tagus estuary to better understand transport and fate of mercury species in the water column. The association of Hg species with organic matter and the evaluation of other processes that governs Hg methylation were also studied.

Study Area

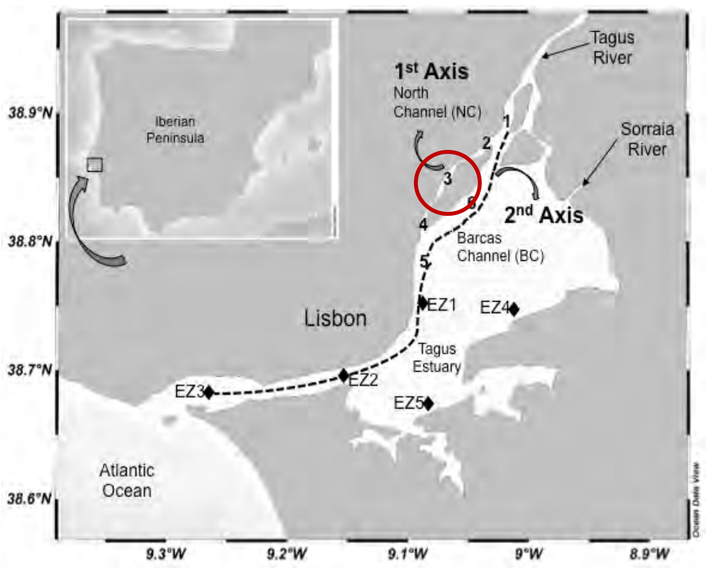

- North Channel - NC (#2; #3; #4) (1st axis)– anthropogenic Hg inputs
- Barcas channel - BC (#1; #6; #5)
- Middle and lower estuarine zones - EZ (#1EZ - #5EZ)

} 2nd Axis

Sampling strategy and Analysis

Samples were collected enclosed different tide conditions and also a tidal cycle of 13 hours was made with samples collected hourly. Mercury species (Hg, MMHg), organic carbon in both dissolved and particulate fractions (POC, DOC), suspended particulate matter (SPM), salinity and other interpretative parameters were determined.

Salinity, pH, Temperature, DO

- THg_D → CV-AFS
- Hg_P → CV-AAS
- $MeHg_D$, $MeHg_P$ → GC-CV-AFS
- DOC → HTCO
- POC → E.A.

Major Findings

MMHg inside the NC

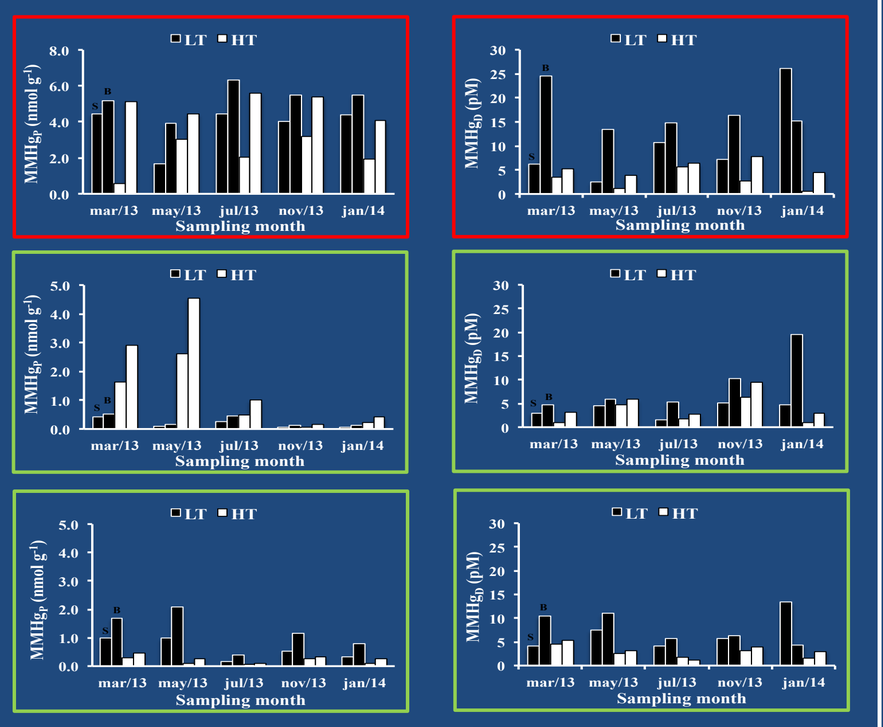

$MMHg_P$ exports from NC to BC from both entrances depending on tidal excursion

$MMHg_P$ exports mainly by downstream entrance (#4)

Semi diurnal tidal cycle

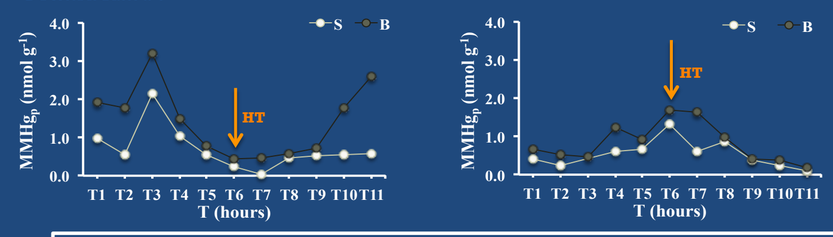

Tidally driven transport of $MMHg_P$ inside the NC (mainly associated to particles) is confirmed by the semi-diurnal tidal cycle

$MMHg_P$ in the BC

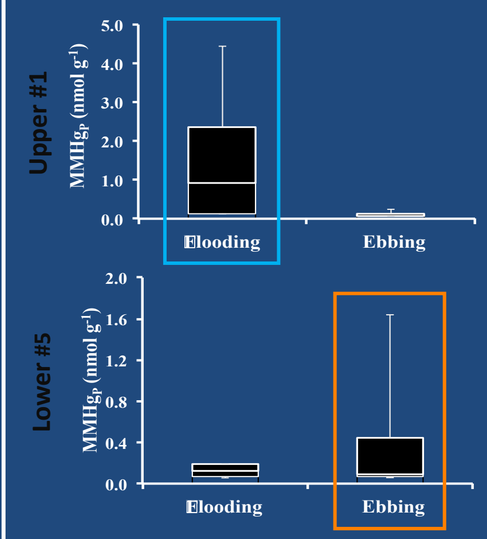

Higher [$MMHg_P$] in #1 in flood tide suggest the export of $MMHg_P$ from NC to BC mainly from the upstream (#2) entrance

Ebbing data in #5 proved the export of $MMHg_P$ from #4 of NC in LT conditions, although in a lesser extent

$MMHg_P$ in the EZ stations

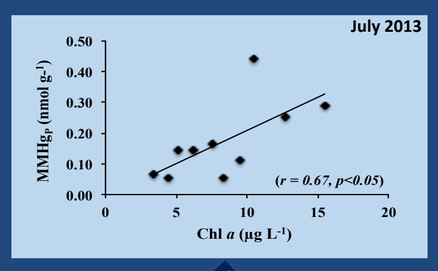

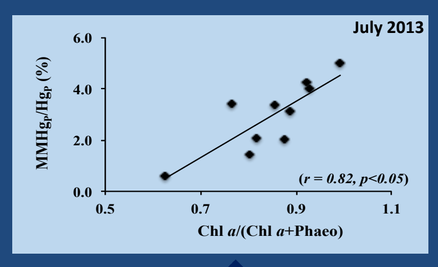

Potential affinity between phytoplankton biomass and the $MMHg_P$ in the water column

Preferential uptake or sorption of MMHg by phytoplankton species with active Chl *a*

$MMHg_P$ is more associated with active Chl *a* than detrital or non-organic particles

Final Remarks

- The MMHgP export from NC is clearly influenced by tidal excursion.
- The transport of mercury species is mainly associated with SPM.

Sediments are important sources of MMHg to the water column although phytoplankton role must also be considered

Future Perspectives

- MMHg production and transport in this estuary must be clarified MAINLY IN THE DISSOLVED FRACTION. A detailed hydrodynamic modeling to study methylmercury speciation would be useful.
- Determination of residence times in specific regions to obtain an accurate mass balance between MMHg loading from the water column and from the sediment will also be necessary.
- Application of Hg stable isotope techniques to evaluate simultaneously the methylation/demethylation rates in the water column should be performed.

FCT Fundação para a Ciência e a Tecnologia

Funding:

- Centro de Química Estrutural is funded by Fundação para a Ciência e Tecnologia – project UID/QUI/00100/2019.
- Rute Cesário PhD grant (SFRH/BD/86441/2012) funded by the Portuguese Foundation for Science and Technology (FCT)
- Projects financed by FCT:
  I. PROFLUX - Processes and fluxes of mercury and methylmercury in a contaminated coastal ecosystem, Tagus estuary, Portugal (PTDC/MAR/102748/2008)
  II. PLANTA - Effect of salt-marsh plants on mercury methylation, transport and volatilization to the atmosphere (PTDC/AAC-AMB/115798/2009).

High Throughput Bar Adsorptive Microextraction (HT-BAµE) – Application for monitoring nicotine and cotinine in large number of urine samples

S.M. Ahmad*, J.M.F. Nogueira

Centro de Química e Bioquímica e Centro de Química Estrutural, Faculdade de Ciências, Universidade de Lisboa

Campo Grande 1749-016 Lisbon, Portugal (* smahmad@fc.ul.pt)

Introduction

Tobacco consumption is the leading cause of cancer death worldwide. Nicotine (the main component of tabacco) poses several health hazards [1]. For this reason, there is a need to monitor levels of nicotine and its main biomarker (cotinine) in biological fluids, *e.g.*, urine.

In this contribution, A simple, effective, convenient and environmentally friendly methodology using high throughput bar adsorptive microextraction (HT-BAµE [2]) with microliquid desorption (µLD) in combination with large volume injection-gas chromatography–mass spectrometry operating in the selected-ion monitoring acquisition mode (LVI-GC-MS(SIM)) was applied for the determination of nicotine and cotinine in urine samples. The target compounds were extracted in a HT-BAµE apparatus, which allows for simultaneous microextraction and subsequent back-extraction of up to 100 samples, resulting in a sample preparation time of 1.8 min/sample, with average recovery yields of 61.7-67.5 % and 53.9-57.8 % for nicotine and cotine, respectively. The developed methodology was applied for the analysis of 86 samples, belonging to various volunteers having different smoking habits, where the target compunds were quantified in the ranging from 23.6 to 2612.6 µg L^{-1}.

Experimental procedure

1. HT-BAµE extraction procedure (Sorbent selectivity, Stirring rate, Equilibrium time, Matrix pH, Organic modifier, Ionic strength)
2. Back-extraction step (Solvent type, Sonification time)
3. Method validation (linearity, accuracy, precision, recovery, matrix effects, limits of detection and quantification)
4. Application to real urine samples

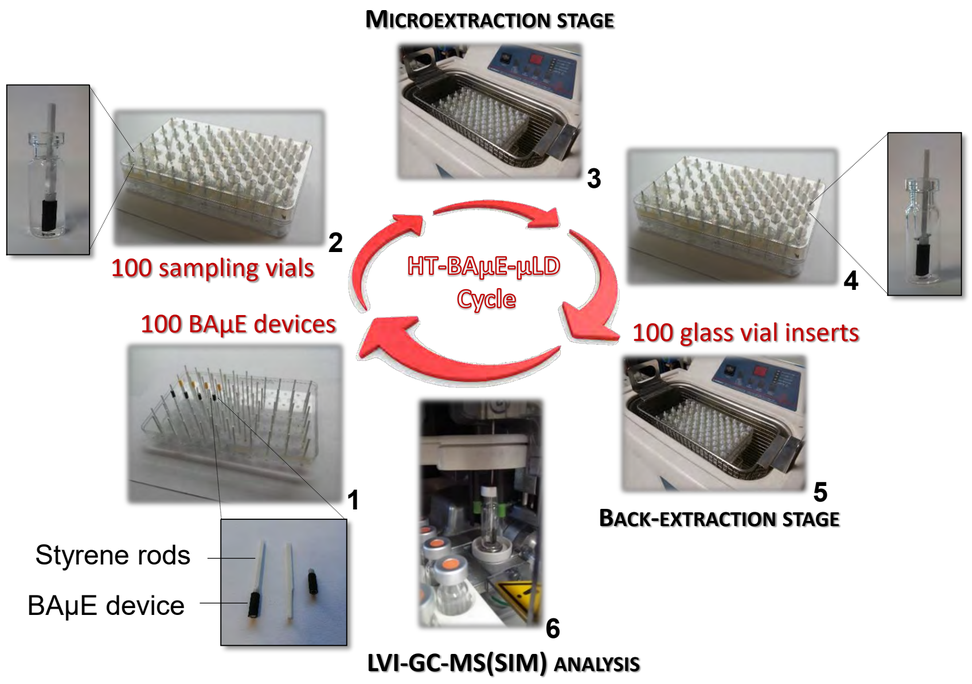

Figure 1 – Proposed HT-BAµE-µLD cycle. 1 - Apparatus with the possibility of accommodating 100 BAµE devices; 2 - Apparatus closed and containing 100 vials ready for the microextraction stage; 3 - 100 simultaneous microextractions *via* cavitation in an ultrasonic bath; 4 - Apparatus closed and containing 100 glass vial inserts for µLD; 5 - 100 simultaneous µLD *via* cavitation in an ultrasonic bath; 6 - The vials are closed and ready for LVI-GC-MS(SIM) analysis analysis, where the HT-BAµE-µLD apparatus can be reused after being rinsed.

Results

Method development

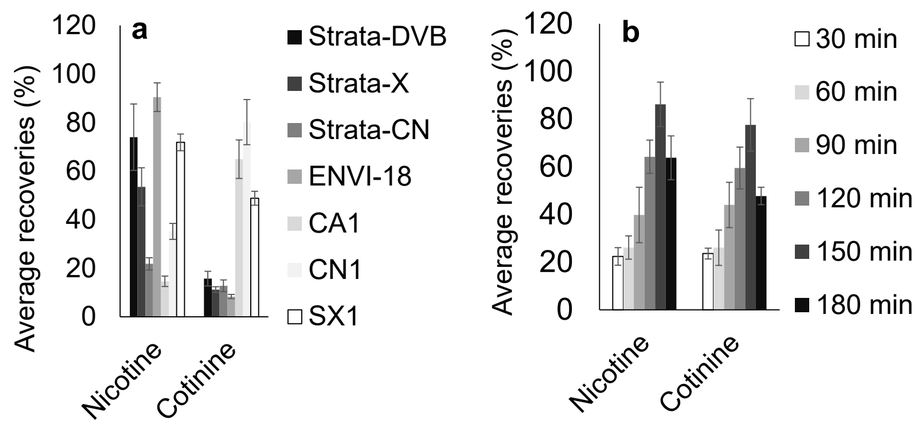

Figure 2 - Effect of polymeric sorbent selectivity (a), as well as microextraction time (b) on the enrichment of nicotine and cotinine from aqueous media, obtained by HT-BAµE-µLD/LVI-GC-MS(SIM). The error bars represent the standard deviation of three replicates.

Table 1 – Optimized experimental conditions using HT-BAµE-µLD/LVI-GC-MS(SIM).

Condition	Desorption solvent	Back extraction time	Equilibrium time	Matrix pH
Optimized parameter	MeOH (100µL)	30 min	2.5 h	11.0

Application to real samples

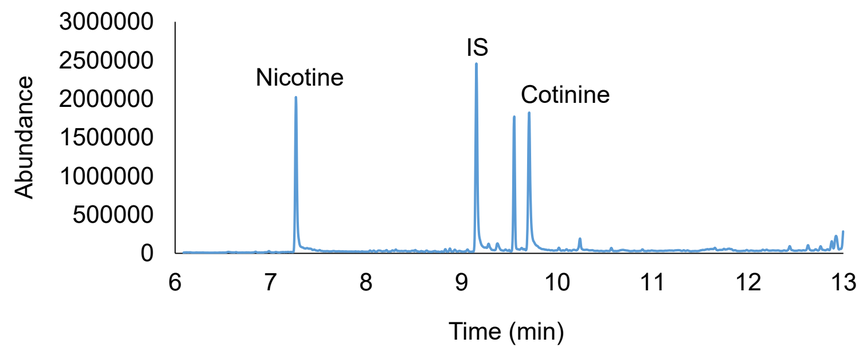

Figure 3 – Total ion chromatogram achieved from an assay performed on a real urine sample, obtained by HT-BAµE-µLD/LVI-GC-MS(SIM), under optimized experimental conditions.

There were 86 subjects, ages 18-53, which were divided in three groups: non-smokers and not exposed to ETS for at least a week before sampling (*n*=1; group #1), non-smokers and exposed to ETS in the week of sample collection (*n*=64; group #2), and smokers (*n*=6; group #3).

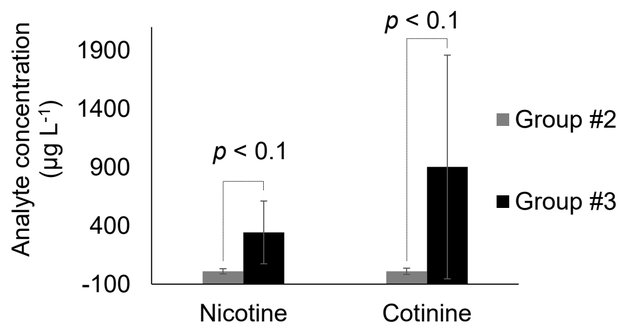

Figure 4 –Student's *t* test performed on the mean values of nicotine and cotinine present in the urine belonging to groups #2 and #3. The error bars represent the standard deviation.

Conclusions

- Method successfully optimized, validated and applied for the analysis of nicotine and cotinine in urine samples using a convenient HT-BAµE apparatus,
- The proposed HT-BAµE-µLD cycle proved to be simple, cost-effective and environmentaly friendly, without compromising performance

06 Chem4Env

Funding:
Centro de Química Estrutural and Centro de Química e Bioquímica are funded by Fundação para a Ciência e Tecnologia (FCT) – projects UID/QUI/00100/2019 and UID/Multi/00612/2019, respectively.
The authors also thank FCT for funding S.M. Ahmad PhD grant (SFRH/BD/107892/2015).

References:

[1] WHO, Gender, Women and the Tobacco Epidemic - Addiction to Nicotine (2010) 137–150.

[3] S.M. Ahmad, J.M.F. Nogueira, Talanta 199 (2019) 195-202.

FCT Fundação para a Ciência e a Tecnologia
MINISTÉRIO DA CIÊNCIA, TECNOLOGIA E ENSINO SUPERIOR

Photoimmunoconjugates to treat Cancer and Age-related Macular Degeneration by Photodynamic Therapy

Sandra Beirão,[1,2,3] **Sara R. G. Fernandes,**[1,4,5] **Bruno Sarmento,**[4,5,6] **Rosa Fernandes,**[2,3] **João P. C. Tomé**[1]

[1]CQE, Departamento de Engenharia Química, Instituto Superior Técnico, Universidade de Lisboa, Lisboa, Portugal
[2]iCBR, Faculty of Medicine, University of Coimbra, Coimbra, Portugal
[3]CNC.IBILI Consortium, University of Coimbra, Coimbra, Portugal
[4]INEB - Instituto de Engenharia Biomédica, University of Porto, Porto, Portugal
[5]i3S - Instituto de Investigação e Inovação em Saúde, University of Porto, Porto, Portugal
[6]CESPU, Instituto de Investigação e Formação Avançada em Ciências e Tecnologias da Saúde, Instituto Universitário de Ciências da Saúde, Gandra, Portugal

CQE Química Estrutural

01 CCC

A key component of the PhotoDynamic Therapy (PDT) is a photosensitizer (PS)[1] and its choice is critical for a successful PDT treatment.[2]

Since the approval of the PDT, several photoactive molecules of the first and second generation, such as porphyrin, chlorin and phthalocyanine derivatives are promising PS candidates for the PDT treatment to various medical diseases and conditions.[3] This strategy has been widely studied for the treatment of various types of tumors[4] and, more recently, for the treatment of Age-related Macular Degeneration (AMD), a painless eye condition that affects the macular region of the retina.[5]

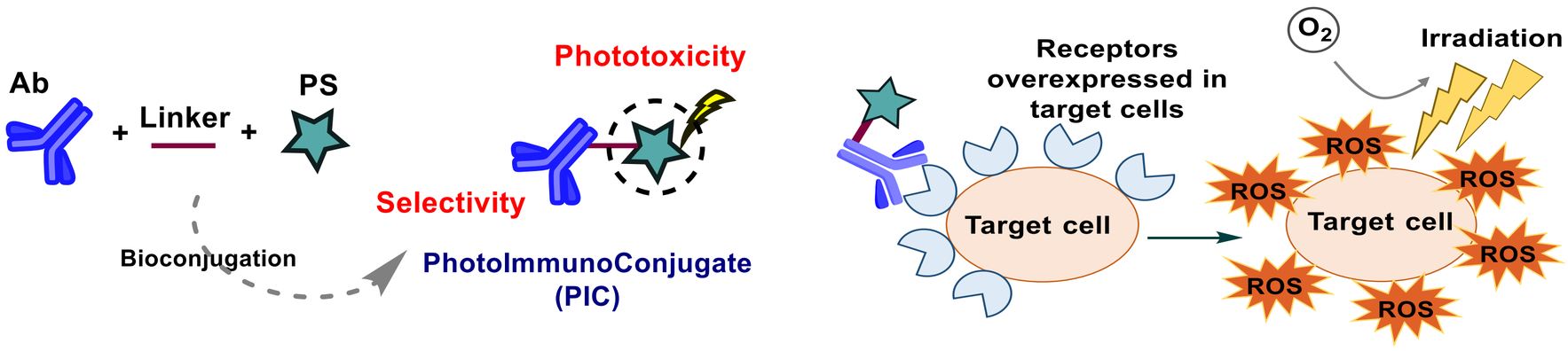

Figure 1: Schematic representation of a PIC and its photodynamic action.

Targeted PhotoDynamic Therapy (tPDT) appeared as a more selective PDT approach and uses third generation PSs to reduce the side effects.[6] The design strategy of these compounds includes the conjugation of first or second generation PSs with a biomolecule or a targeting agent, for example antibodies (Abs), which selectively bind to target cell receptors and improve the selectivity and efficiency of the photobioconjugates (Figure 1).[7]

The main objective of these two works is the synthesis of new PSs (Figure 2) for the preparation of PICs to target tumor cells and endothelial cells of choroidal neovessels and their validation in photodynamic activity.

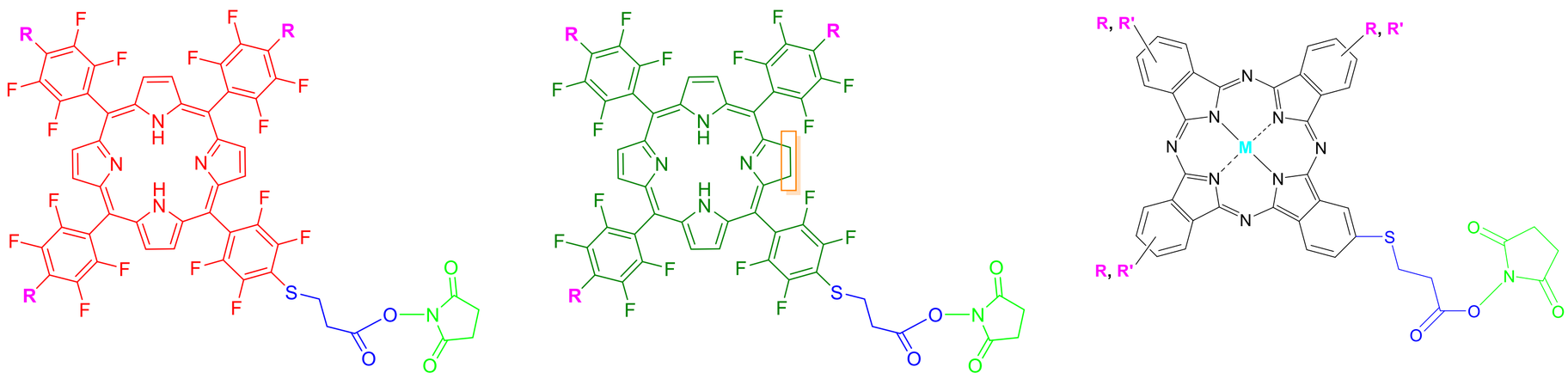

Figure 2: Chemical structures of PICs precursors.

tPDT using PICs promises to bring the benefits of conventional PDT combined with the specificity and potency of antibody therapy. It is expected that in the next few years PDT can be frequently used in the fight against oncological and ophthalmologic diseases and thus to contribute to a better quality of life of the patients.

Funding:
Centro de Química Estrutural is funded by Fundação para a Ciência e Tecnologia – project UID/QUI/00100/2019, CNC.IBILI (FCT UID/NEU/04539/2013) and INEB (POCI-01-0145-FEDER-007274) research units, through national founds (PIDDAC) and where applicable co-financed by the FEDER-Operational Thematic Program for Competitiveness and Internationalization-COMPETE 2020, within the PT2020 Partnership Agreement. S. Beirão and S. Fernandes have been funded by the FCT PhD grants SFRH/BD/140098/2018 and SFRH/BD/129200/2017, respectively.

References:
[1]A. Kawczyk-Krupka, A.M. Bugaj, W. Latos, K. Zaremba, K. Wawrzyniec, M. Kucharzewski, A. Sierón, Photodiagnosis Photodyn. Ther. 13 (2016) 158-174.
[2]G.M.F. Calixto, J. Bernegossi, L.M. Freitas, C.R. Fontana, M. Chorilli, Molecules 21 (2016) 342.
[3]B.L. Josefsen, W.R. Boyle, Metal-Based Drugs 11 (2008) 1-24.
[4]J. Bazak, J.M. Fahey, K. Wawak, W. Korytowski, A.W. Girotti, Cancer Cell Microenviron. 4 (2017) e1511.
[5]H. Deng, T. Li, J. Xie, N. Huang, Y. Gu, J. Zhao, Dye Pigm. 99 (2013) 930-939.
[6]P.M.R. Pereira, B. Korsak, B. Sarmento, R.J. Schneider, R. Fernandes, J.P.C. Tomé, Org. Biomol. Chem. 13(9) (2015) 2518-2529.
[7]S.R.G. Fernandes, R. Fernandes, B. Sarmento, P.M.R. Pereira, J.P.C. Tomé, Org. Biomol. Chem. 17(10) (2019) 2579-2593.

FCT Fundação para a Ciência e a Tecnologia
MINISTÉRIO DA EDUCAÇÃO E CIÊNCIA

Structure-based virtual screening toward Hexokinase 2 inhibitors: targeting metabolism and apoptosis signaling in cancer cells

Sara N Garcia[1,2], Rita C Guedes[2], M Matilde Marques[1]

[1]Centro de Química Estrutural, Instituto Superior Técnico, Universidade de Lisboa, Av. Rovisco Pais, 1049-001 Lisboa, Portugal

[2]iMed.ULisboa, Faculdade de Farmácia, Universidade de Lisboa, Av. Prof. Gama Pinto, 1649-003 Lisboa, Portugal

sara.garcia@tecnico.ulisboa.pt

Background

Glucose metabolism is a potential target pathway to be explored for cancer treatment. Hexokinase 2 (HK2) is overexpressed in different types of cancer cells[1]. HK2 is involved in the first and most determinant step of glycolysis, as well as in mitochondria-induced apoptosis. HK2 binds to voltage-dependent anion channel (VDAC) blocking the action of pro-apoptoic proteins (e.g. Bax).

Inhibition of the HK2 catalytic pocket has shown to be effective in both reducing glycolysis and detaching HK2 from VDAC, reducing the main source of energy to cancer cells and enhancing apoptosis[2,1].

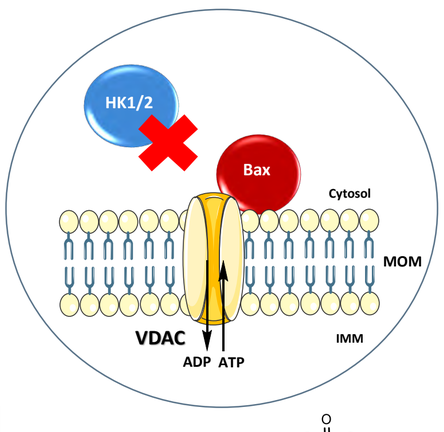

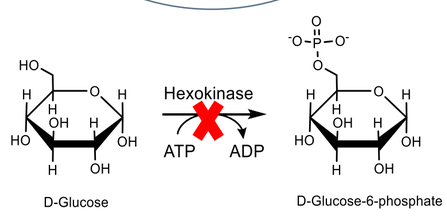

Aim

Finding hit compounds for HK2 inhibition:

→ Defining an accurate molecular docking protocol suitable to be used for structure-based virtual screening (SBVS)

→ Screening different databases to find hit compounds

Molecular Docking calculations

Defining the protocol

Testing...

- ✓ Available 3D structures
- ✓ Protein's energy minimization
- ✓ Water influence
- ✓ Centre and flexibility of the catalytic pocket
- ✓ Different software, scoring functions and searching algorithms

Final protocol

- PDB:5HG1[3]
- Gold 5.20
- GoldScore
- Glu742
- r=15 Å
- No H_2O
- No flexible residues

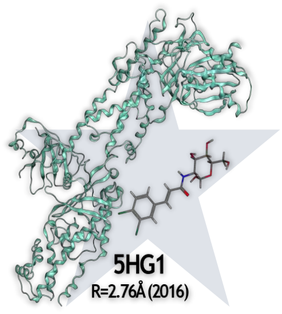

Protocol Validation

Chosen protocol possesses:

→ Lowest RMSDs between docked and crystallographic structures

→ Best correlation between experimental and *in silico* data

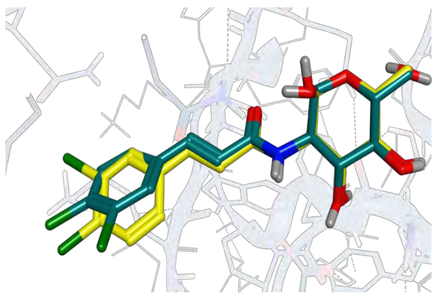

Figure 1 – Overlap of crystallized compound 1[3] (yellow) with its docked conformation (blue) RMSD= 0.45 – image from MOE2016.0802.

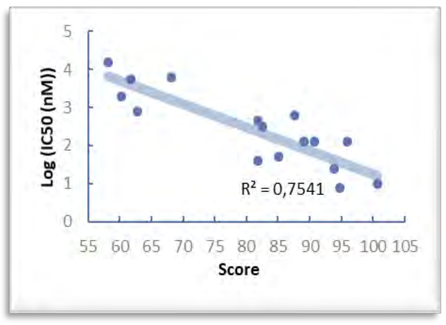

Figure 2 – Best correlation between experimental data (Log[IC_{50}]) and score (*in silico* results) of 16 known HKII inhibitors – pdb:5HG1, centre: Glu742m r=15, with goldscore scoring function of Gold 5.20 software.

SBVS

Synthetic and Natural Product-focused databases

- 23 databases -

Pre-selection, remove:

- MW>800
- Isolated atoms
- Polymers
- Small inorganic molecules

↓

Protonation (pH=7.4) | Energy minimization (Amber12) |Moe2016 0802|

↓

Molecular Docking - Gold 5.20

Genetic algorithm runs- 50

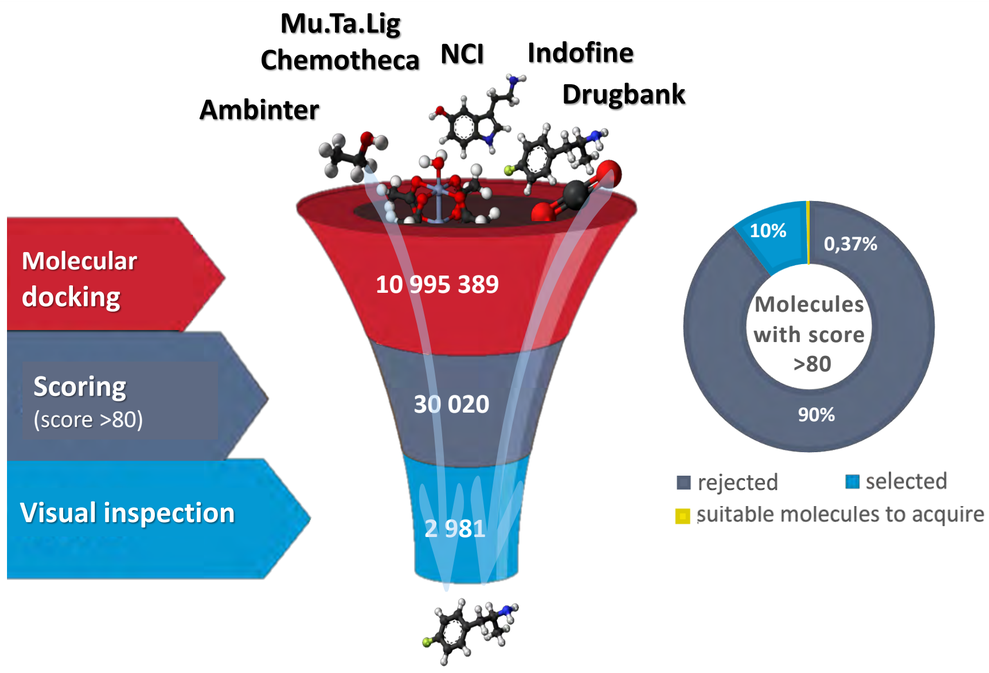

Characteristics Prevision of drug-like properties

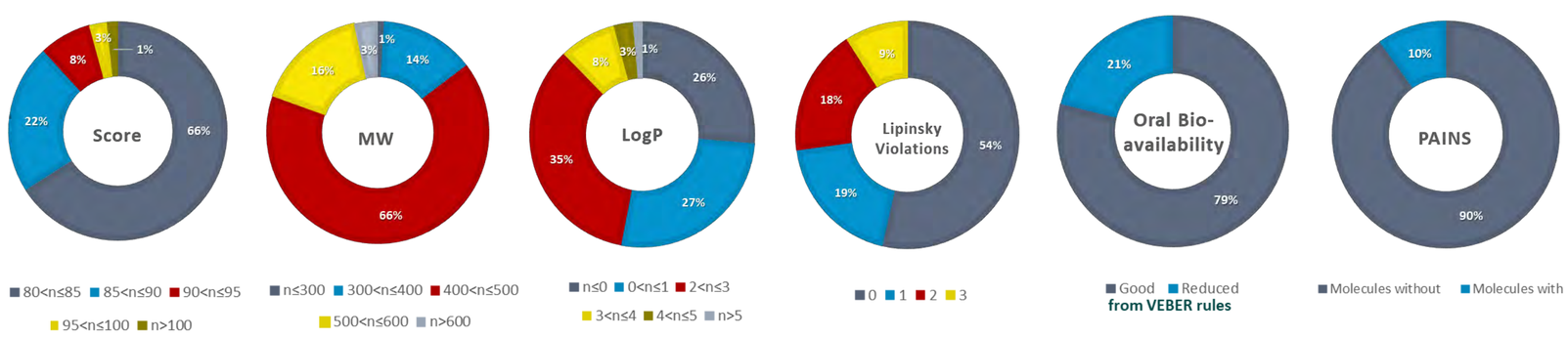

*Previsions performed with FAFdrugs4

- Docking results
- Drug-like properties
- Commercial reasons

2981 → 111 suitable molecules for testing

Conclusions and Future work

- ✓ An *in silico* protocol for virtual screening of HK2 inhibitors was generated.
- ✓ 2981 potential HK2 inhibitors were selected from docking results
- ✓ SBVS results were filtered based on drug-like properties and 111 molecules were selected as suitable for testing.
- ✓ 64 selected molecules are being used to validate the SBVS with biochemical assays.

G5 BIOMOL

Funding:
Centro de Química Estrutural is funded by Fundação para a Ciência e Tecnologia – project UID/QUI/00100/2019.
We also thank Fundação para a Ciência e a Tecnologia for financial support (PD/BD/135284/2017, UID/DTP/04138/2019, SAICTPAC/0019/2015, PTDC/QUI-QAN/32242/2017).

References:

(1) Hay, N. Nat. Rev. Cancer 2016, 16 (10), 635–649.
(2) Martinez-Outschoorn, U. E.; Peiris-Pagès, M.; Pestell, R. G.; Sotgia, F.; Lisanti, M. P. Nat. Rev. Clin. Oncol. 2017, 14 (1), 11–31.
(3) Lin, H. et al. ACS Med. Chem. Lett. 2016, 7, 217–222.

Boron: Optical Detection and Scavenging Materials for Wastewater Remediation

Sérgio Alves, Laurinda Areias, Federica Albertini, Tânia Ribeiro, José Paulo S. Farinha, Carlos Baleizão

INTRODUCTION

Boron

5
B
10.81

- Beneficial for life in trace amounts
- Toxic in high concentrations
- Drinking water: Usually below 0.5 ppm
  World Health Org. guidelines [1]: < 2.4 ppm

High boron contents in water may result from [1]

- Boron containing rocks 
- Industrial wastewaters 
  Detergents and soaps, Glass and ceramics, Pesticides, Fertilizers, Semiconductors, Flame retardants , Pharmaceutical
- Urban and agricultural activities 

BOREON DETECTION

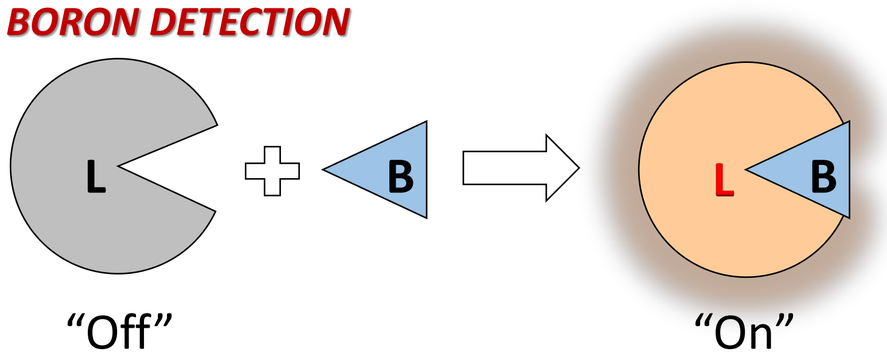

Detection based on hexahydroxytriphenylene [2,3]

We proposed 2,3,6,7,10,11-hexahydroxytriphenylene as an optical sensor for boron, using spectrofluorimetry or UV-visible spectrophotometry detection.[2,3]

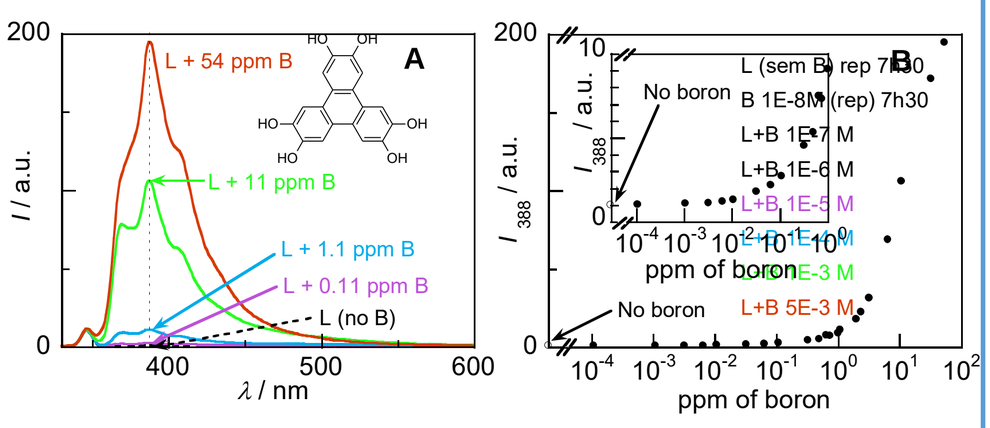

Complexation of our sensor with boron at pH ≈ 9 leads to an increase in emission intensity.

Limits of detection	Fluorimetry	Absorption
Boric acid	10 ppb B	5 ppm B
Phenylboronic acid	6 ppb B	0.3 ppm B

Polymeric Hydroxytriphenylene Derivatives [4]

Polymeric fluorescent boron sensor

- Excellent water solubility
- High boron sensitivity
- Easy to handle
- Can be easily recovered after use [4]

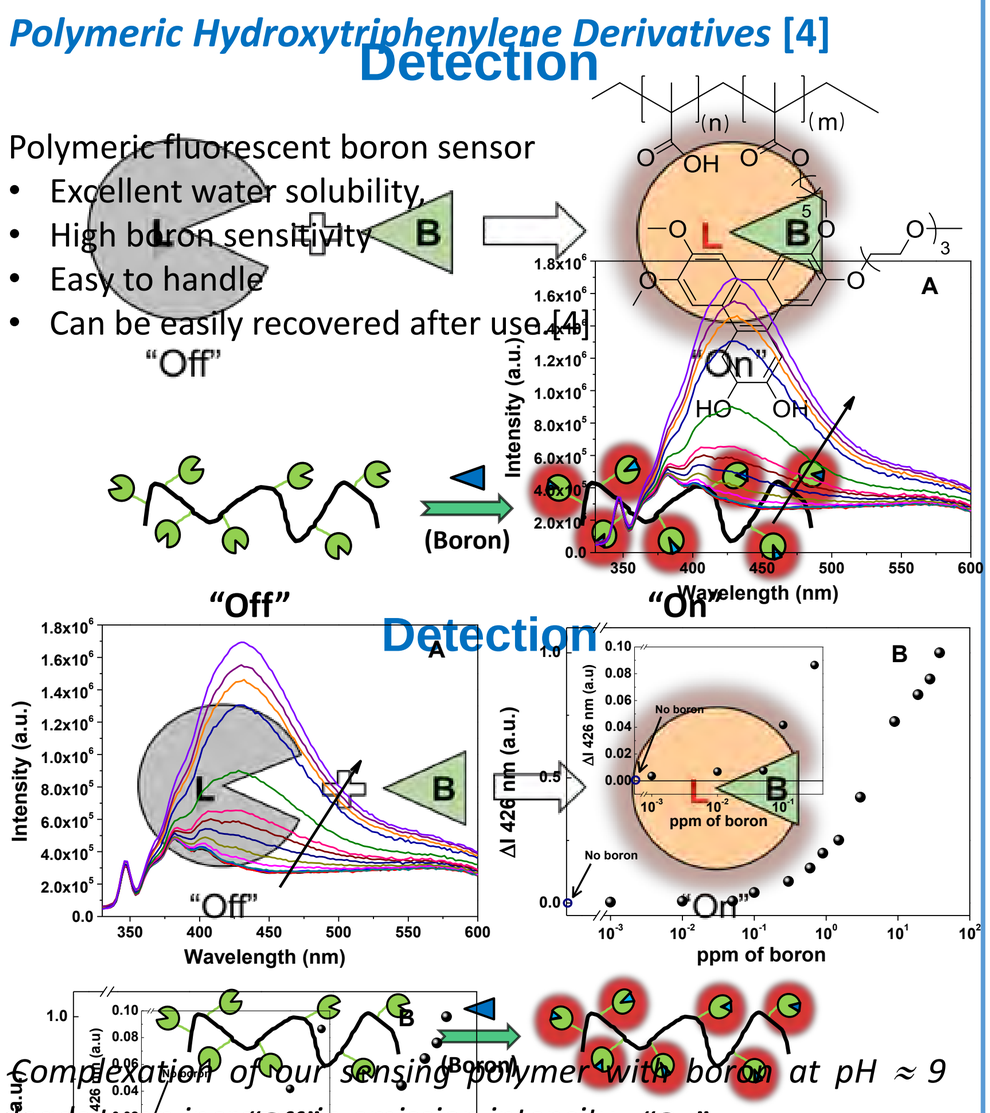

Complexation of our sensing polymer with boron at pH ≈ 9 leads to an increase in emission intensity.

Limits of detection	Fluorimetry
Boric acid	10 ppb B
Phenylboronic acid	10 ppb B

BOREON SCAVENGING

Smart Polymeric Nanoparticles [5]

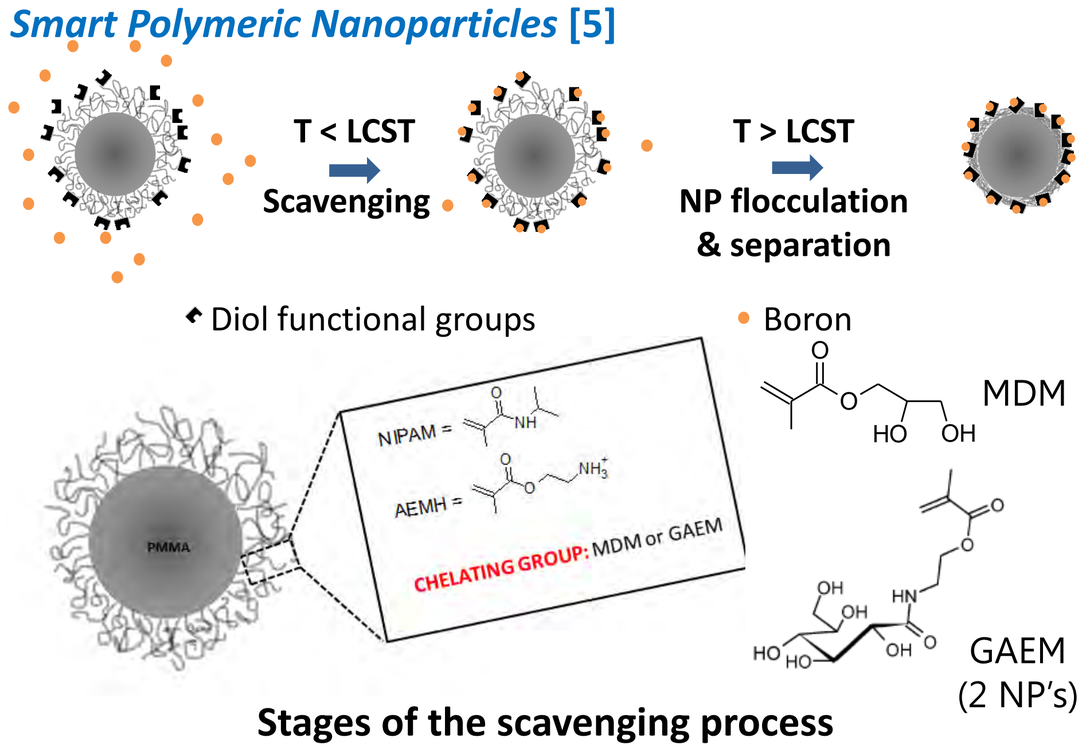

Stages of the scavenging process

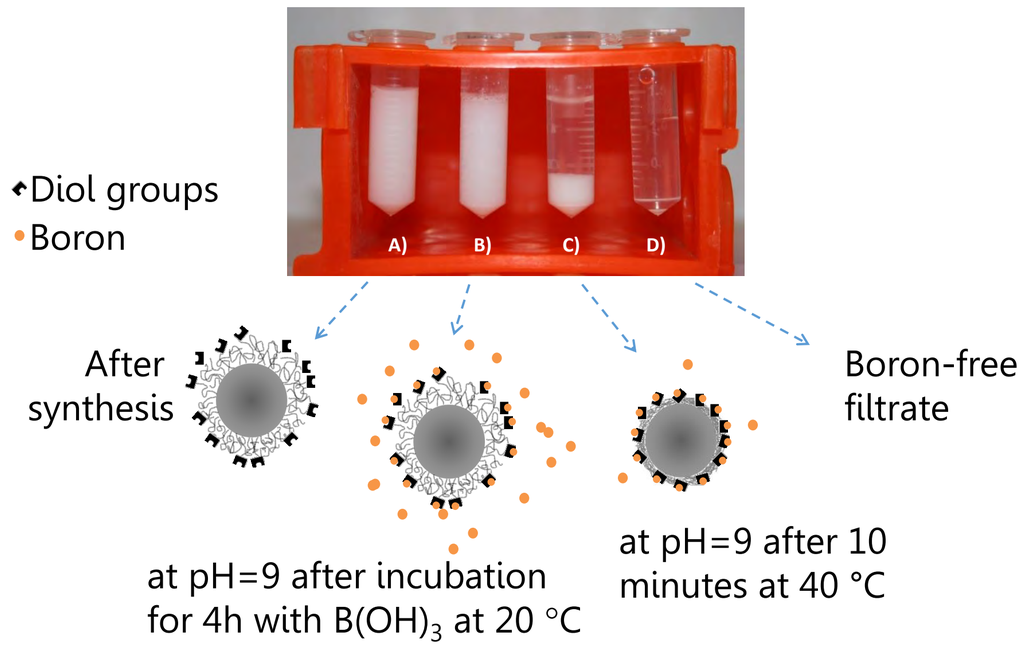

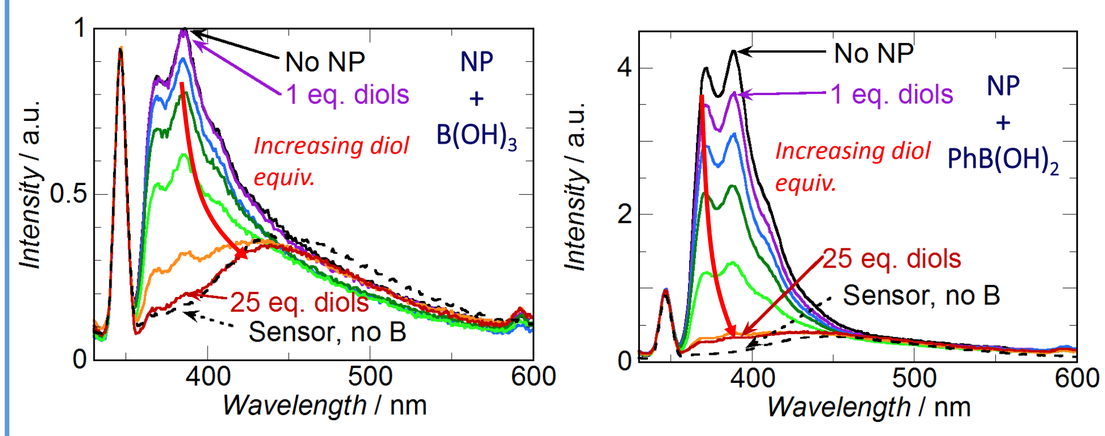

Fluorescence decreases with increasing diol (NP) concentration as less boron remains in water. Of the three NP types tested, the smallest ones bearing GAEM groups were the most efficient in boron scavenging.

Boron-chelating membranes based in hybrid mesoporous silica NP [6]

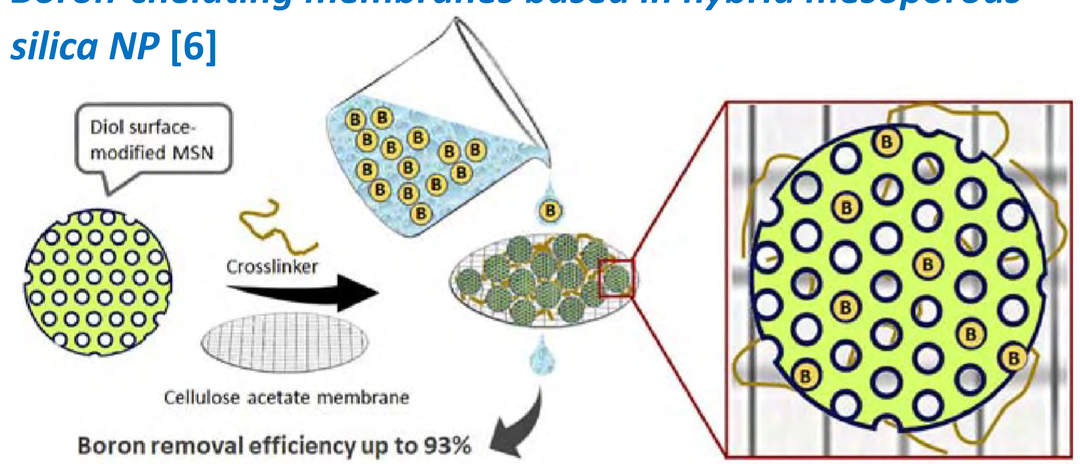

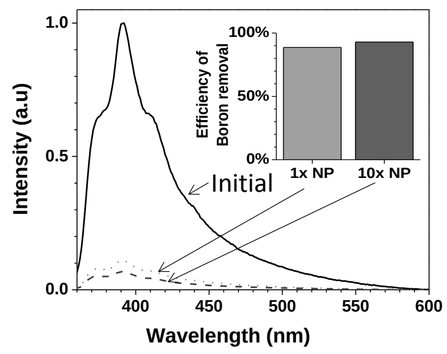

- *NPs able to remove up to 93% of the initial boron concentration*
- *Hybrid membranes reduce boron to 70% of initial value in a single filtration step.*

08 MPPM

Funding:
Centro de Química Estrutural is funded by Fundação para a Ciência e Tecnologia – project UID/QUI/00100/2019.
This work was also supported by project PTDC/CTM-POL/3698/2014 and grants SFRH/BPD/74654/2010 (S.A.), SFRH/BPD/96707/2013 (T.R.), PD/BD/113533/2015 (L.A.).

References:

1. World Health Organization. Guidelines for drinking-water quality. 4th ed. (2011), World Health Organization.
2. Farinha, J.P.S.; Baleizão, C.; Alves, S. WO2014123436 (2014).
3. Alves, S.; Baleizão, C.; Farinha, J.P.S., *Anal. Methods* 6 (2014), 5450.
4. Areias, L.; Costa, A.; Alves, S.; Baleizão, C.; Farinha, J.P.S., *RSC Advances*, 7 (2017), 4627.
5. Alves, S.P.C; Santos, C.; Costa, A.P.; Silva, M.; Baleizão, C.; Farinha, J.P.S., *Chem. Eng. J.*, 319 (2017), 31.
6. Albertini, F.; Ribeiro, T.; Alves, S.P.C.; Baleizão, C.; Farinha, J.P.S., *Materials and Design*, 141 (2018), 407.

Mechanochemically built bio-inspired metalorganic frameworks as a tool to improve drugs' efficiency

Sílvia Quaresma, Vânia André, Catarina Bravo, Paula Marques, Filipa Galego, André Ramires Ferreira da Silva, Marta Martins, M. Teresa Duarte

silvia.quaresma@tecnico.ulisboa.pt

Química Estrutural

05 BIOMOL

INTRODUCTION

The interest on metalorganic frameworks (MOFs) towards pharmacological applications has been increasing, especially for controlled drug delivery and release. Our group has been designing novel bio-inspired MOFs (BioMOFs) exploring the possibility of using active pharmaceutical ingredients (APIs) as ligands. This approach presents several benefits over the traditional methodology of encapsulating APIs in the pores of MOFs built with safe organic ligands: i) porosity is no longer required as the release of the API or bioactive molecules is achieved by degradation of the compound; ii) no multistep synthesis is required as the molecules are part of the matrix; iii) synergetic effects between the active molecule and the metal may be explored; iv) the co-delivery of drugs may be possible if a porous network is built with one and the incorporation of a second one is feasible.[1,2]

Here we present some of the most successful examples:

Seventeen new BioMOFs of gabapentin, a neuroleptic drug, with Y(III), Mn(II) and several lanthanides were prepared. These have shown potential luminescent properties that can be further explored for theranostic applications.[3]

BioMOFs with azelaic acid have also been explored. The well-known antibacterial and antimicrobial activities of this API have been enhanced opening new routes for its dermal application.

The development of novel coordination frameworks with nalidixic acid, a quinolone antibiotic, using safe metals has proven to affect the solubility of the API. Furthermore, the BioMOFs show increased antimicrobial activity while exhibiting adequate cytotoxicity.[4,5]

In these studies we recurred to mechanosynthesis as the main synthetic pathway. This environment-friendly technique drastically reduces the amount of solvents and time, proving to be very efficient in different areas, including MOFs' synthesis.[6]

To conclude, we have been proving that BioMOFs are promising candidates for the development of more effective therapies.

Synthesis

API
Gabapentin
Azelaic acid
Nalidixic acid

+

Safe metal

or

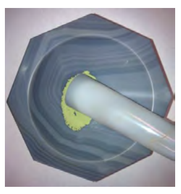

→ BioMOF → Biological/Pharmaceutical application

Gabapentin

+

La (III)
Y (III)
Ce (III)
Er (III)
Nd (III)
Mn (II)

- 17 new metal coordination networks
- Fully characterized

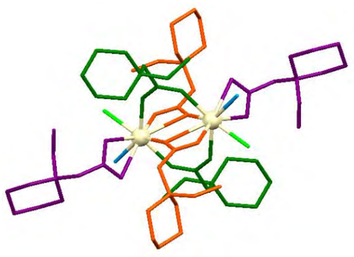

GBP:Er1, ***GBP:Nd2*** and ***GBP:Y2*** networks, $[Ln_2GBP_6(H_2O)_2Cl_2]Cl_4.8H_2O$, based on dimers.

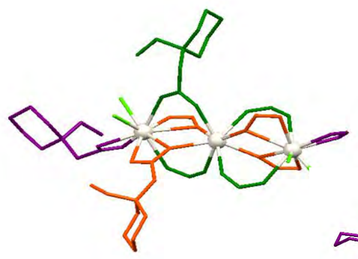

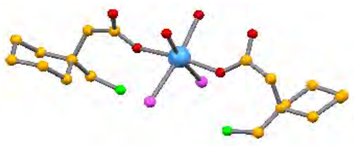

GBP:Mn1 and ***GBP:Mn6*** networks, $[MnGBP_2(H_2O)_2Cl_2]$, based on monomers

GBP:La2 and ***GBP:Ce2*** networks, $[Ln_6GBP_{16}(H_2O)_{10}Cl_4]Cl_{14}.20H_2O$, based on trimers.

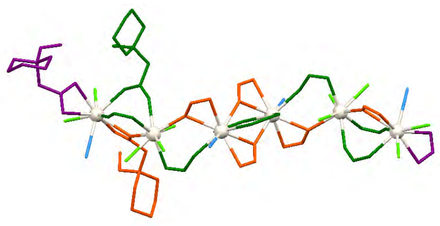

GBP:Ce1 and ***GBP:La1*** networks, $[Ln_6GBP_{16}(H_2O)_{10}Cl_4]Cl_{14}.20H_2O$, based on hexamers. GBP moieties are only fully shown once for each mode

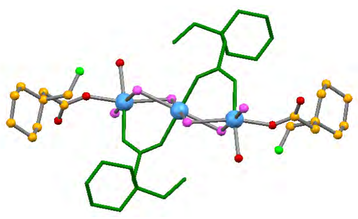

GBP:Mn5 network, $[[Mn_3GBP_4(H_2O)_2Cl_6]$, based on trimers

Azelaic acid

+

Mg (II)
K (I)
Na (I)

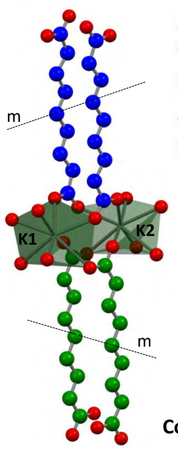

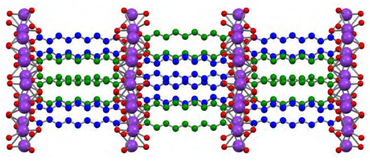

Polyhedral representation of K1 and K2 coordination sphere; Crystal packing of **AZE:K** in a view along *c*.

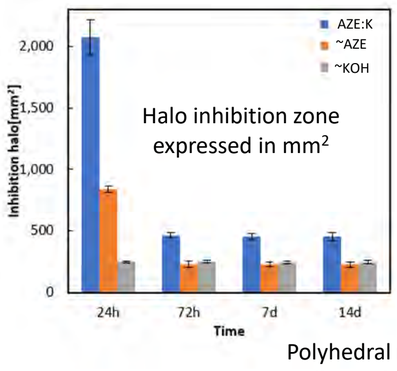

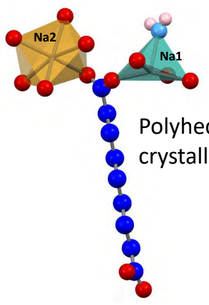

Polyhedral representation of the two crystallographic independent Na centres

Polyhedral representation of the octahedral geometry around the Mg metal centres

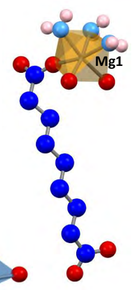

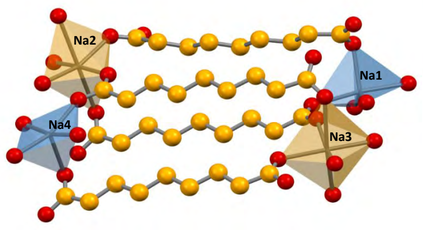

Polyhedral representation of the four crystallographic independent Na centres

Color code: K^+, purple; C atoms of AZE^{2-}, blue; C atoms of AZE, green; C atoms of AZE^-, yellow; O_{COOH}, O_{COO^-} red; Ow, cyan; H, white square antiprismatic polyhedral representation, pale green; octahedral polyhedral representation, pale yellow; square-pyramidal polyhedral representation, pale blue and trigonal bipyramidal polyhedral representation, greenish blue. H atoms of carbons were omitted for clarity

- 7 new BioMOFs
- Fully characterized
- Solubility studies
- Antimicrobial activity

Nalidixic acid

+

Zn (II)
Mn (II)
Mg (II)
Cu (II)

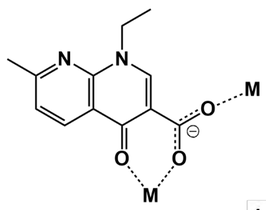

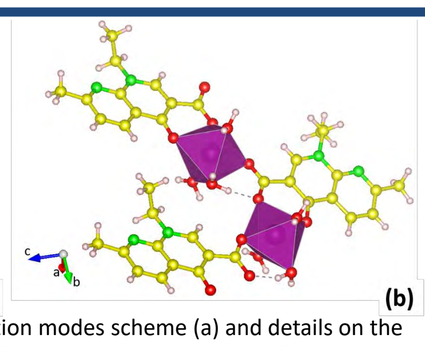

Nalidixic acid coordination modes scheme (a) and details on the octahedral geometry in the coordination sphere of the metal centers (b) characteristic of Mn, Mg and Zn MOFs

Minimum Inhibitory and Bactericidal Concentrations, MIC and MBC (or minimum fungicidal concentration, MFC) values, of the Mn and Mg-MOFs against Gram-negative and Gram-positive bacteria and yeasts strains (µg/mL)

	S. aureus		*E. faecalis*		*P. aeruginosa*		*E. coli*		*C. albicans*		*S. cerevisiae*	
Compound	MIC	MBC	MIC	MBC	MIC	MBC	MIC	MBC	MIC	MBC	MIC	MBC
NA	125	500	125	500	125	500	3.91	31.2	62.5	62.5	125	125
Mg-MOF	31.3	500	31.3	250	125	500	0.98	1.95	62.5	250	31.3	250
Mn-MOF	31.3	250	31.3	250	250	500	0.98	7.81	31.3	125	31.3	125
Positive	7.82	Nt	1.95	nt	<0.48	nt	0.98	nt	0.98	nt	0.98	nt
Control	VAN				NOR				NYS			

NA – Nalidixic Acid; nt– not tested; VAN – Vancomycin; NOR – Norfloxacin; NYS – Nystatin.

- 8 new metal coordination frameworks and complexes
- Stability and solubility studies
- Improved antimicrobial activity

Supramolecular packing of nalidixic acid:oxalic acid:Zn complex depicting the complex formed (right), and the 14.5% VOID of the unit cell volume (237.62Å³) (left)

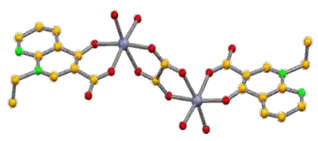

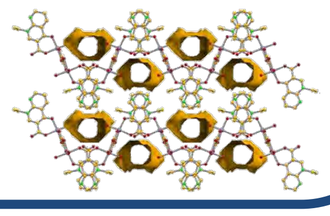

Funding:
Centro de Química Estrutural is funded by Fundação para a Ciência e Tecnologia (FCT) – project UID/QUI/00100/2019.
Authors further acknowledge FCT and FEDER for funding - project PTDC/QUI-OUT/30988/2017 and PhD grant SFRH/BD/100029/2014).
Dr. Alexandra Antunes, Dr. Auguste Fernandes, and Dr. Patrícia Rijo are acknowledged for HPLC, DSC-TGA and antimicrobial experiments, respectively.

FCT Fundação para a Ciência e a Tecnologia

References:
1. Quaresma, S; André, V; Fernandes, A; Duarte, MT, Inorganica Chimica Acta, 455 (2017) 309-318.
2. Domingos, S; André, V; Quaresma, S; Martins, ICB.; Minas da Piedade, MF; Duarte, MT, Journal of Pharmacy and Pharmacology, 67(6) (2015) 830-846.
3. Quaresma, S; André, V; Antunes, AMM; Cunha-Silva, L; Duarte, MT, Crystal Growth & Design, 13(11) (2013) 5007-5017.
4. André, V; Galego, F; Martins, M, Crystal Growth & Design, 18(4) (2018) 2067-2081.
5. André, V; Ferreira da Silva, AR; Fernandes, A; Frade, R; Garcia, C; Rijo, P; Antunes, AMM; Rocha, J, Duarte, MT, ACS Applied Biomaterials (2019) ASAP
6. André, V; Quaresma, S; da Silva, J LF; Duarte, MT, Beilstein Journal of Organic Chemistry, 13 (2017) 2416-2427.

Analysis of the Aroma Profile of Wines Samples by Headspace using Novel Microextraction Techniques

Ciências ULisboa — Faculdade de Ciências da Universidade de Lisboa

S.C.F. Amorim*, S.M. Ahmad, N.R. Neng, J.M.F. Nogueira

Centro de Química Estrutural, Centro de Química e Bioquímica, Faculdade de Ciências, Universidade de Lisboa
Campo Grande, 1749-016 Lisboa, Portugal
(*susy.scfa.1997@gmail.com)

CQE Química Estrutural

06 CE

Introduction

Bar adsorptive microextraction (BAµE) technique was introduced in 2010 as an alternative cost-effective enrichment process for trace analysis of polar to nonpolar compounds in aqueous media. This solid-based microextraction approach, presents several advantages, including the possibility of selecting the most convenient sorbent coating (e.g. activated carbons (ACs), polymers (Ps), etc.), according to the target compounds involved [1-2].

More recently, hollow fiber microextraction (HFµE) was proposed as an alternative liquid-based microextraction approach [3]. Nevertheless, both BAµE and HFµE were never applied for the analysis of the organic compounds in gas phase.

Figure 1: HS-BAµE and HS-HFµE analysis of the aroma profile in wines samples.

In this work, BAµE and HFµE prior to gas chromatography-mass spectrometry were applied for the first time in headspace (HS) analysis to characterize the aroma profile of wine samples. Several assays were performed, including the study of different type of wines using several sorbent phases at various extraction temperatures and equilibrium times. For comparison purposed, stir bar sorptive extraction (SBSE) was also tested.

Experimental Procedure

1 Extraction procedure
HS-SBSE, HS-BAµE (Sorbent selectivity, Equilibrium time and Ionic strength) and HS-HFµE (Solvent selectivity, Equilibrium time and Ionic strength)
2 Back-extraction step (Solvent type, Sonification time)

Microextraction

- HS analysis
- Porto, Madeira and red wine samples
- 3h and 1000 rpm

Back-extraction

- Microliquid desorption
- 100 and 200 µL of solvent
- 30 minutes under sonication

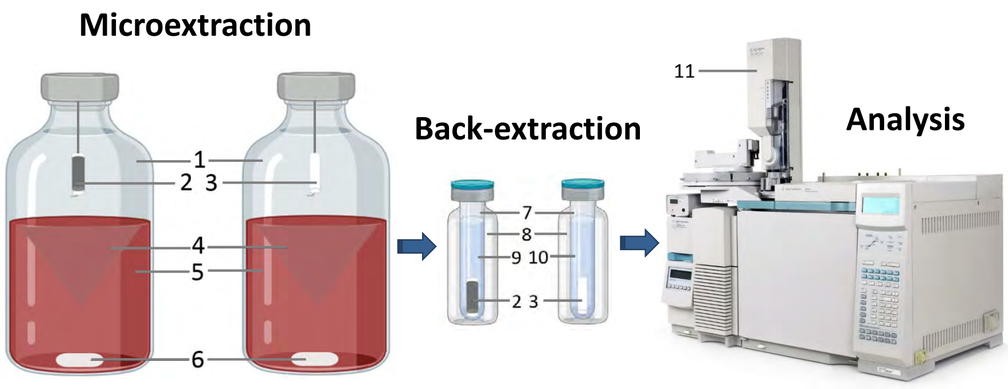

Figure 2: Schematic of the procedure for the microextraction methodologies. 1. Sample flask; 2. BAµE device; 3. HFµE device; 4. Vortex; 5. Sample (wine); 6. Teflon magnetic stir bar; 7. Insert; 8. Injection vial; 9. Solvent (MeOH); 10. Solvent (soaked solvent); 11. GC-MS.

Instrumental analysis

GC

Gas chromatograph: 6890 Agilent Technologies System (U.S.A)
Column: Zebron ZB-5 (30m × 0.25mm × 0.25µm) (Phenomenex)
Software: MSD ChemStation (versão C.00.00);
Injection Mode: Splitless (1 µL)
Injector Temperature: 260 ºC (held 1 min)
Oven: 40 ºC (held 1 min) and then at 10 ºC min^{-1} to 300 ºC (hold for 10 min)
Mobile Phase: Helium, at constant pressure mode

MS

Mass detector: 5793*N* Agilent Technologies (U.S.A.)
Transfer line: 280ºC
Quadrupole: 150ºC
Ion source temperature: 230ºC
Ionization mode: Electronic Impact (70 eV)

Results

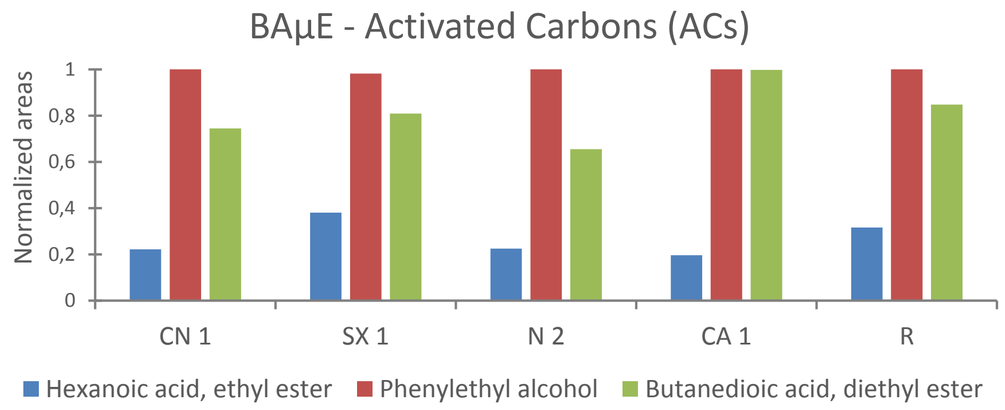

Figure 3: Data obtained using HS-BAµE(ACs)-µLD/LVI-GC-MS, for the three major compounds.

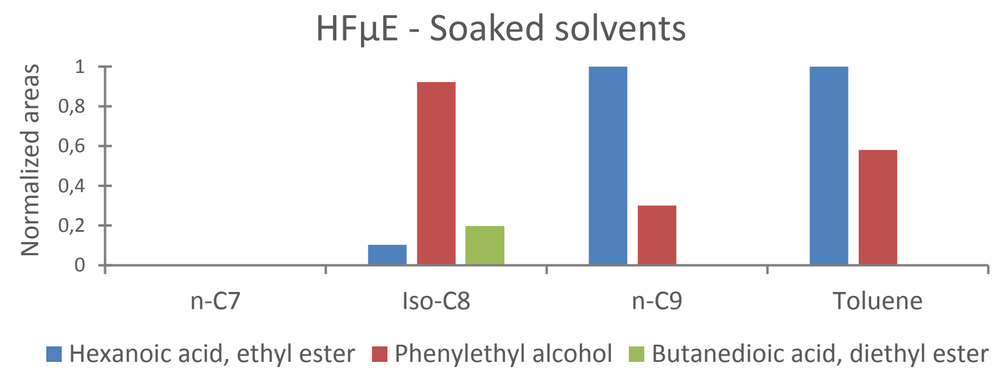

Figure 4: Data obtained using HS-HFµE-µLD/LVI-GC-MS, for the three major compounds.

Table 1: Optimized experimental conditions for HS-BAµE(CN 1)-µLD/LVI-GC-MS and HS-HFµE(Iso-C8)-µLD/LVI-GC-MS used for wine samples.

Condition	Equilibrium time	Stirring rate	Temperature	Ionic strenght (NaCl)	Desorption solvent	Back extraction time
BAµE	3 h	1000 rpm	30 °C	20 %	MeOH (200 µL)	30 min
HFµE			40 °C		Iso-C8 (100 µL)	

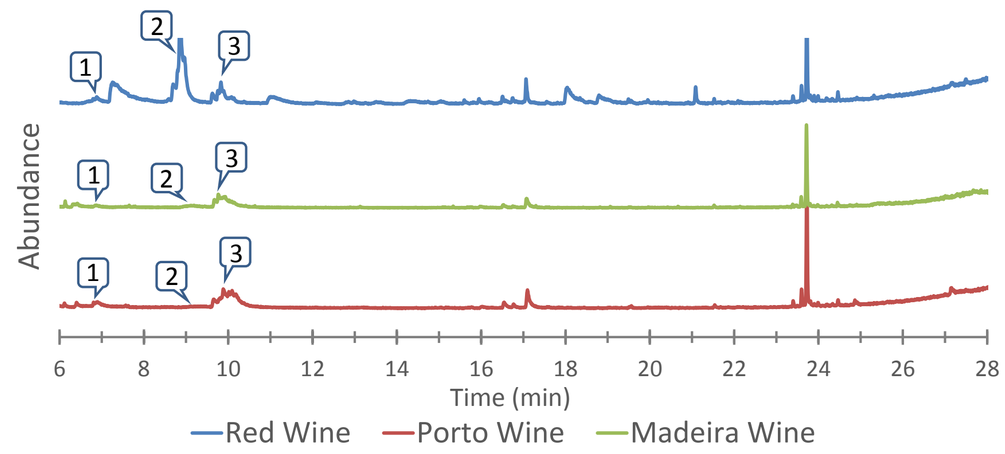

Figure 5: Total ion chromatogram using HS-BAµE(CN 1)-µLD/LVI-GC-MS for red, Porto and Madeira wine samples. 1. Hexanoic acid, ethyl ester; 2. Phenylethyl alcohol; 3. Butanedioic acid, diethyl ester.

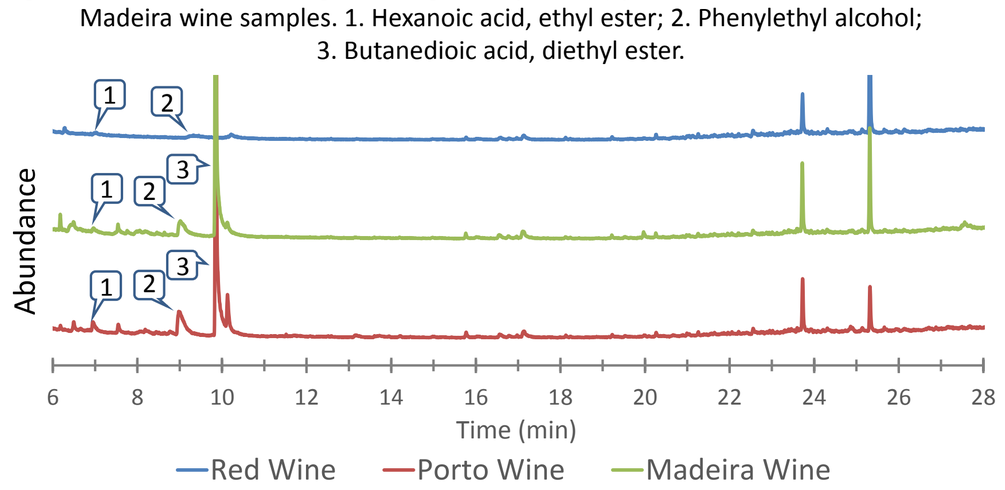

Figure 6: Total ion chromatogram using HS-HFµE(Iso-8)-µLD/LVI-GC-MS for red, Porto and Madeira wine samples. 1. Hexanoic acid, ethyl ester; 2. Phenylethyl alcohol; 3. Butanedioic acid, diethyl ester.

Conclusions

- HS-BAµE coated with ACs and HS-HFµE soaked with convenient solvents, showed for the first time, good performance for the HS analysis.
- HS-HFµE(Iso-C8) and HS-BAµE(CN 1) showed better response when compared with well-established microextraction techniques (e.g. HS-SBSE).
- The applied techniques showed remarkable performance for the analysis of the aroma profiles from red, Porto and Madeira wines.

Funding:
The authors thank Fundação para a Ciência e a Tecnologia (Portugal) for financial support through project UID/00100/2019 for CQE, UID/Multi/00612/2019 for CQB and for the post-Doc (SFRH/BPD/86071/2012) and PhD (SFRH/BD/107892/2015) grants.

FCT Fundação para a Ciência e a Tecnologia

References:

1. Neng, N.R., Silva, A.R., Nogueira, J.M.F., J. Chromatogr. A, 1217 (2010) 7303-7310.

2. Nogueira, J.M.F., Trends Anal. Chem. 71 (2015) 214-223.

3. Ide, A.H., Nogueira, J.M.F., Anal. Bioanal. Chem. 410 (2018) 2911-2920.

Bioinspired polymers for the development of optical immunosensors

Frade, T,[1] Almeida, LC,[1] Niu, Y,[2] Jin, G,[2] Correia, JP,[1] Viana, AS[1]

[1]Centro de Química e Bioquímica, Centro de Química Estrutural, Faculdade de Ciências da Universidade de Lisboa, Campo Grande, 1749-016 Lisboa

[2]NML, Institute of Mechanics, Chinese Academy of Sciences, Beijing, 100190, China

Email: tcfrade@fc.ul.pt
anaviana@fc.ul.pt

Ciências ULisboa

06 CE

Introduction

- The efficient linkage of functional proteins to biocompatible films is crucial when developing **BIOSENSORS**.
- **Polydopamine** (**PDA**) films are inspired on the mussel-foot proteins and have been used in many biomedical applications, due to their biocompatibility and adhesive properties, provided by the catechol groups [1,2].
- Electrochemical synthesis is an alternative route to chemical methods to prepare PDA with defined physico-chemical properties (e.g. thickness, wettability and available functional groups) for a reproducible attachment of proteins [3].
- Herewith, potentiodynamically grown PDA films on gold electrodes are used as platforms for the sensitive detection of **antigen-antibody interactions**. Immunoglobulin G (**IgG**) or **protein A**, for an improved orientation of the antibody, are directly adsorbed on PDA matrices. A post-modification of PDA/IgG or PDA/Protein A with **ethanolamine** (**ETA**) is proposed to inhibit the non-specific protein adsorption and increase the selectivity.
- This platform is versatile and can be tailored into any trial of interest, including the construction of sandwich-type architectures for the detection of small target molecules, such as toxins.

Methods

Potentiodynamic growth of polydopamine (PDA)

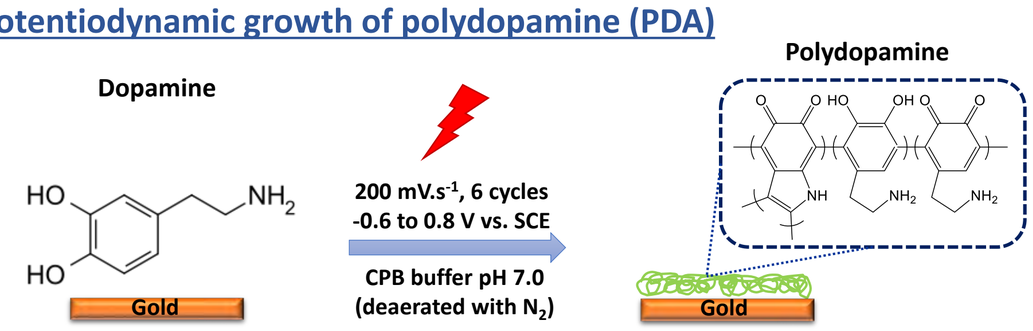

Biosensor platform based on PDA films

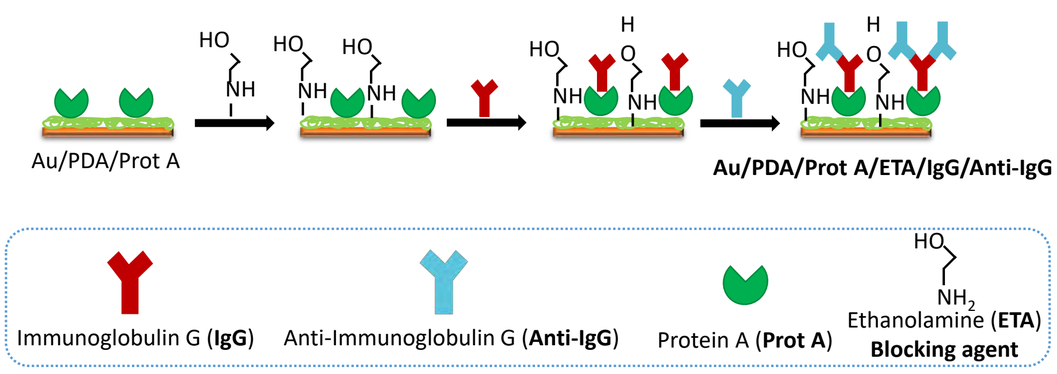

Electropolymerization and characterization of PDA films

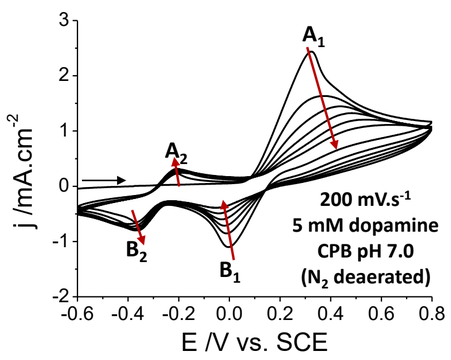

Decrease in the current of the main redox processes (dopamine/ dopaminequinone, A_1/B_1) of polydopamine reveals the formation of a poorly conducting polymer [4].

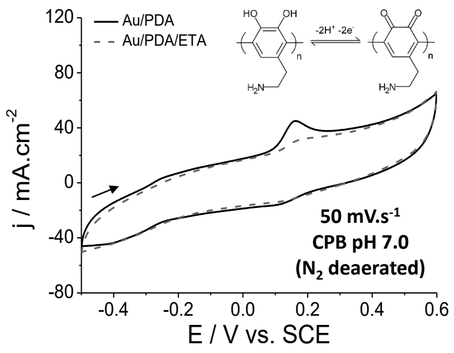

Decrease of the number of electroactive sites upon ETA incubation

Binding of ETA, possibly through NH_2 groups to the available quinone moieties at PDA surface

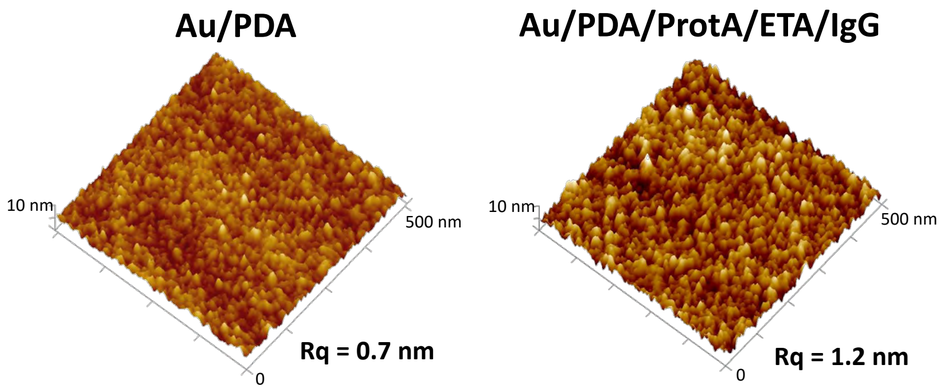

- Uniform and highly adherent PDA thin films were obtained by electrochemical synthesis.
- AFM imaging of **Au/PDA/ProtA/ETA/IgG** clearly shows the presence of an even distribution of individual proteins on the surface, also confirmed by the small increase of the root-mean square (Rq).

PDA-modified film biossensor performance

Surface Plasmon Resonance (SPR)

Real-time SPR are carried out to evaluate the performance of the new bottom-up approach regarding the specific **immunosensor biorecognition reactions** (IgG-Anti/IgG)

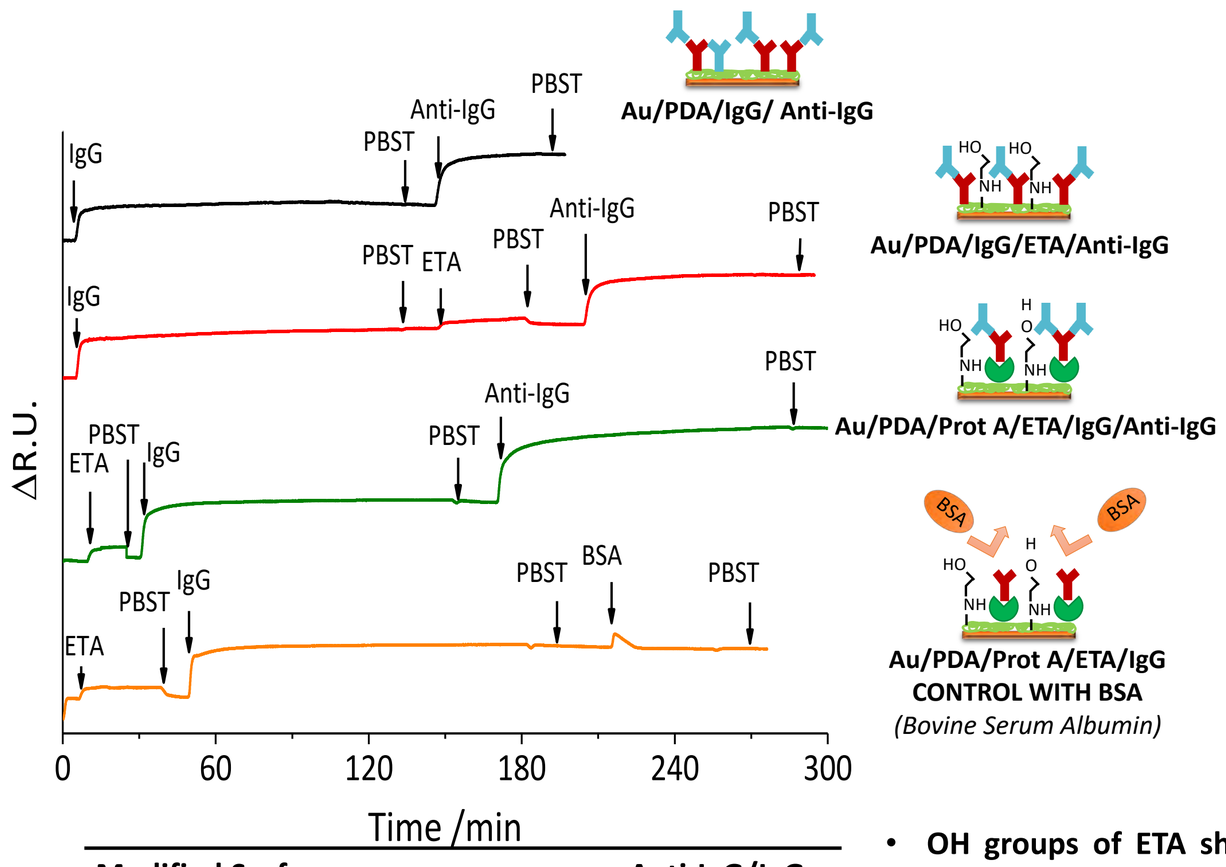

Modified Surfaces	Anti-IgG/IgG
Au/PDA/IgG/Anti-IgG	1.52 ± 0.05
Au/PDA/IgG/ETA/Anti-IgG	1.24 ± 0.03
Au/PDA/Prot A/ETA/IgG/Anti-IgG	1.39 ± 0.04

- **OH groups of ETA should be responsible non-specific adsorption biomolecule inhibition**
- **Higher Anti-IgG/IgG ratio when using Protein A**

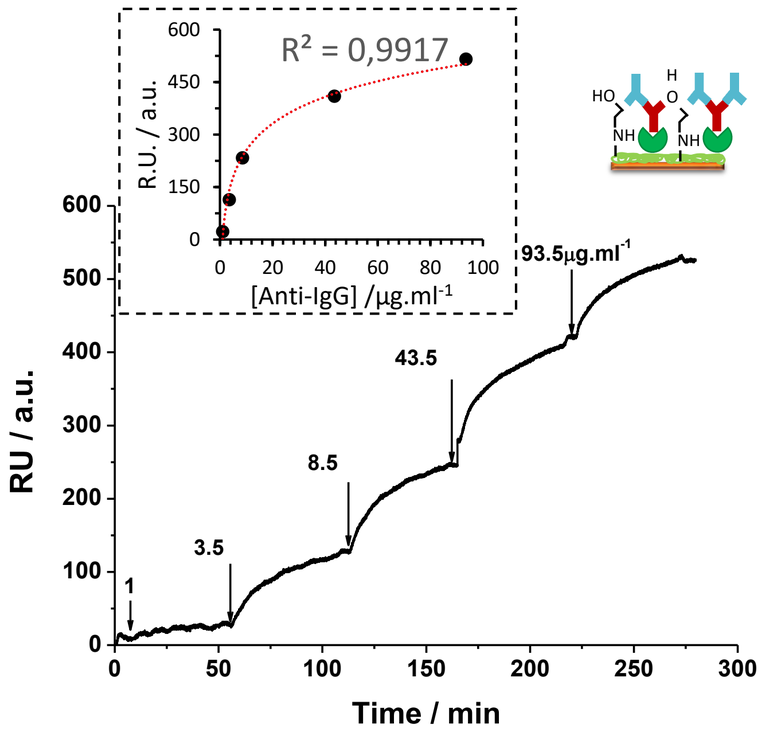

Ellipsometry

Highly sensitive **spectroscopic ellipsometry** measurements is used to corroborate all the modification steps and Biosensor performance.

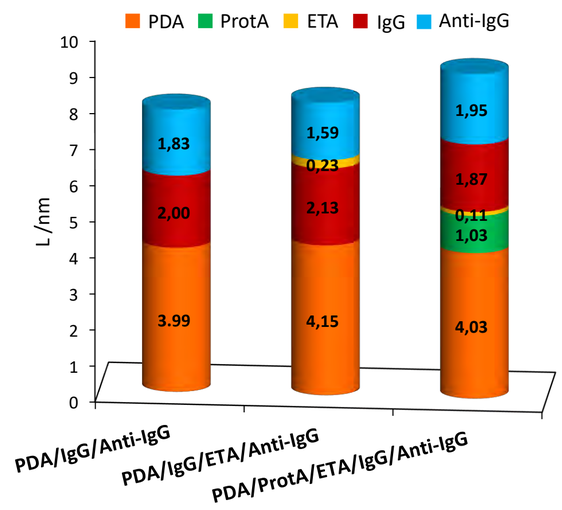

Conclusions

- **Biocompatible and uniform PDA films** can be formed by potentiodynamic control.
- Successful immobilization of ETA on PDA-modified films allow to inhibit the **non-specific biomolecule interactions, not affecting the bioaffinity reaction** – High potential to be employed in optical **IMMUNOSENSORS.**

Funding:
Centro de Química Estrutural is funded by Fundação para a Ciência e Tecnologia (FCT) – project UID/QUI/00100/2019. This work was supported by FCT through the projects IF/00808/2013/CP1159/ CT0003 (POPH, UE-FSE), PTDC/CTM-NAN/0994/2014 and UID/MULTI/00612/2013.

FCT Fundação para a Ciência e a Tecnologia
MINISTÉRIO DA CIÊNCIA, TECNOLOGIA E ENSINO SUPERIOR

References:

1. **Niu, Y, Matos, AI, Abrantes, LM, Viana, AS, Jin, G, Langmuir 28 (2012) 17718-17725.**
2. **Ryu, JH, Messersmith, PB, Lee, H, ACS Appl. Mater. Interfaces 10 (2018) 7523–7540.**
3. **Paiva, TO, Almeida, I, Marquês, JT, Liu, W, Niu, Y, Jin, G, Viana, AS, App. Surf. Sci. 412 (2017) 455-463.**
4. **Almeida, LC, Correia, RD, Marta, A, Squillaci, G, Morana, A, Cara, FL, Correia, JP, Viana, AS, App. Surf. Sci. 480 (2019) 979-989.**

Catalytic applications of Cu(II) complexes towards microwave-assisted peroxidative oxidation of toluene and 1-phenylethanol

Tannistha Roy Barman,[a] Manas Sutradhar,[a] Elisabete C.B.A. Alegria,[a,b] Francesco Scorcelletti,[a] M. Fátima C. Guedes da Silva,[a] Armando J. L. Pombeiro[a]

[a]Centro de Química Estrutural, Instituto Superior Técnico, Universidade de Lisboa, Av. Rovisco Pais, 1049-001 Lisboa.
[b]Chemical Engineering Departament, ISEL-Instituto Superior de Engenharia de Lisboa, Instituto Politécnico de Lisboa, 1959-007 Lisboa.
email: roybarman@tecnico.ulisboa.pt

Abstract: Two Cu(II) complexes in two different tautomeric forms (keto and enol) derived from the aroylhydrazone Schiff base 2-hydroxy(2-hydroxybenzylidene)benzohydrazide (H_2L) have been synthesized (**Scheme 1**) and characterized by elemental analysis, IR spectroscopy, ESI-MS and single crystal X-ray crystallography. Compound **1** with the enol form of the ligand exists as the 1D polymer but compound **2** with the keto form of the ligand exists as the monomer. Both **1** and **2** act as good catalysts towards the microwave-assisted peroxidative oxidation of toluene and 1-phenylethanol with tert-butyl hydroperoxide. **2** exhibits the highest activity in both catalytic reactions, leading selectively to a maximum product yield of 39 and 92%, respectively [1].

Syntheses

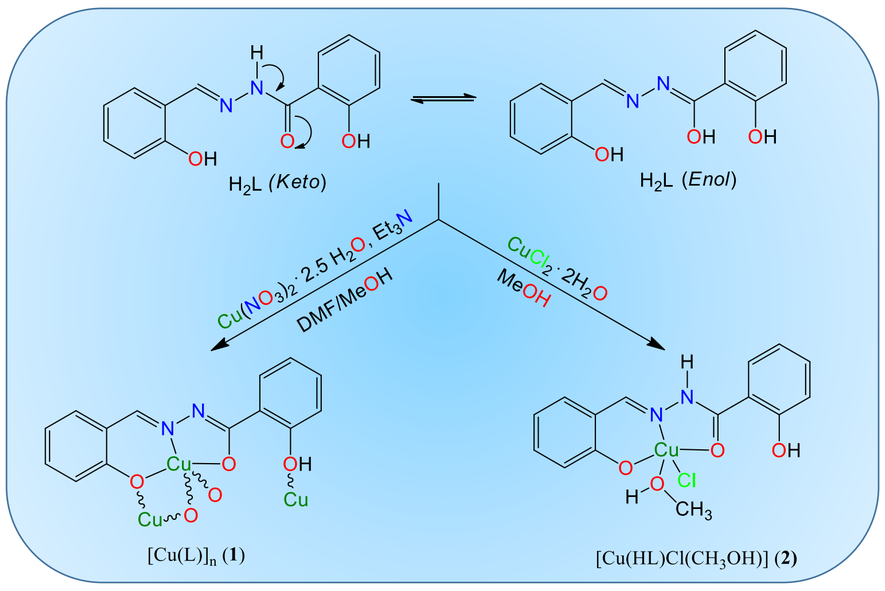

X-ray structures

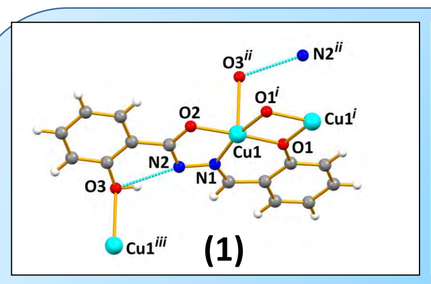

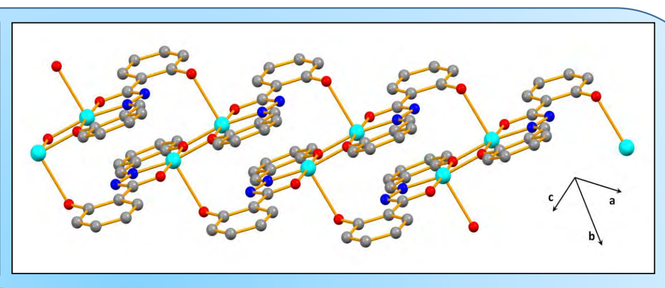

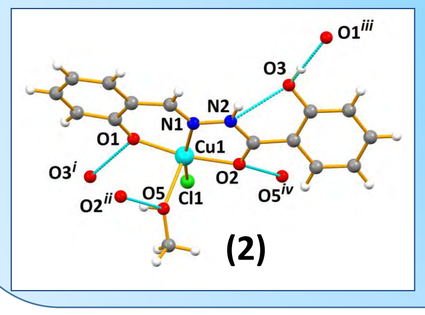

The infinite 1D chain of **1** running along the crystallographic a axis

Figure 1

Catalysis

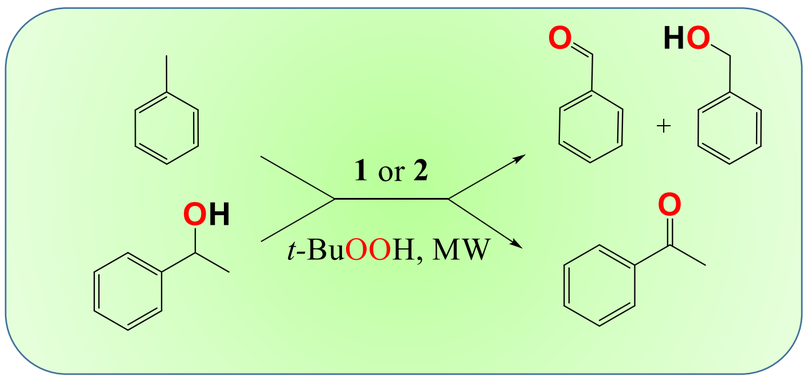

Microwave-assisted peroxidative oxidation of toluene and 1-phenyl ethanol

Entry	Catalyst	Additive (mol% *vs.* substrate)	Yield (%)			Selectivity to benzylaldehyde (%)
			Benzaldehyde	Benzyl alcohol	Total[b]	
1	1	-	4.3	1.4	5.7	75.4
2[c]		-	1.9	0.8	2.7	70.4
3		TEMPO (0.6)	1.4	0.5	1.9	73.7
4		HNO_3 (0.2)	12.5	0.2	12.7	98.4
5		HNO_3 (0.7)	7.4	0.4	7.8	94.8
6	2	-	38.1	0.6	38.7	98.5
7[c]		-	29.3	0.5	29.8	98.3
8		TEMPO (0.6)	1.6	0.6	2.2	72.7
9		HNO_3 (0.2)	0.8	0.4	1.2	66.7
10		HNO_3 (0.7)	0.3	0.2	0.5	60.0
11[d,e]		-	2.4	2.1	4.4	52.3
12[d,f]		-	3.7	3.0	6.7	55.2
13[d,g]		-	5.9	3.4	9.3	63.4
14[d,h]		-	7.4	3.6	11.0	67.3
15	$Cu(NO_3)_2$	-	2.8	0.8	3.6	77.8
16	H_2L	-	-	-	-	-

[a]Reaction conditions unless stated otherwise: toluene (1.67 M), catalyst precursor **1** or **2** (3.3×10^{-3} M), TBHP (70% aq, 3.3 M), NCMe (3 mL), 50 ºC, 1 h, MW (5W). [b]Moles of products [benzaldehyde + benzyl alcohol]/100 mol of toluene, determined by GC. [c]Solvent-free. [d]Reaction performed using conventional heating. [e]1 h. [f]6 h. [g]12 h. [h]24 h.

A possible mechanism of the catalytic reaction may involve the metal-assisted generation of *t*-BuOO• and *t*-BuO• radicals [2], upon oxidation or reduction of *t*-BuOOH by a Cu^{II} or Cu^{I} centre, respectively. The *t*-BuOO• radical can undergo dismutation to the *t*-BuO• radical and O_2, and the *t*-BuO• radical can abstract an H atom from toluene (RH) to form the benzyl radical R• which upon reaction with O_2 forms the benzyl peroxyl radical ROO•. Dismutation of the latter radical leads to ROH (benzyl alcohol) and benzaldehyde (plus O_2). Moreover, H-abstraction from toluene (RH) by ROO• forms ROOH (plus R•) which upon reduction by a Cu^{I} centre, forms the benzyloxyl RO• radical (plus hydroxide) that leads to benzyl alcohol (plus R•) by H-abstraction from toluene [2].

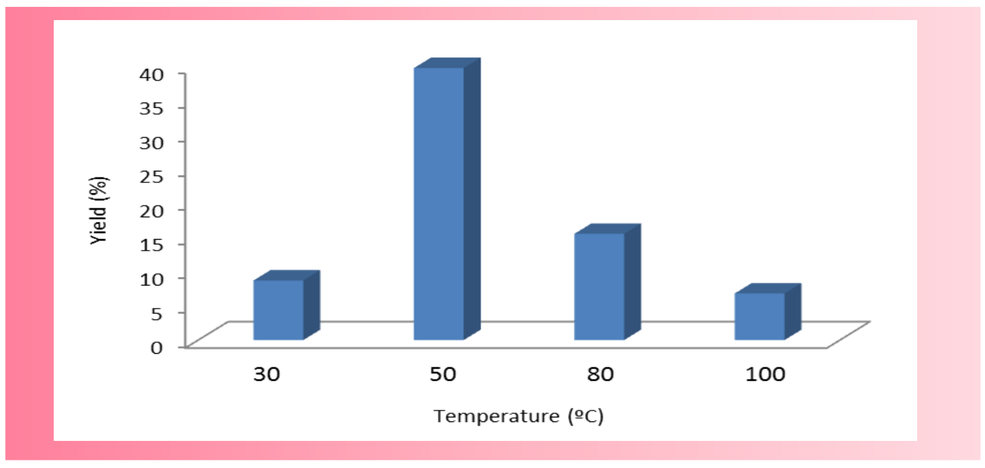

Effect of temperature on the catalytic oxidation of toluene in the presence of **2**. Reaction conditions: [toluene] = 1.67 M; [**2**] = 3.3×10^{-3} M; [TBHP] = 3.3 M, in NCMe, during 1 h under MW-irradiation (5 W).

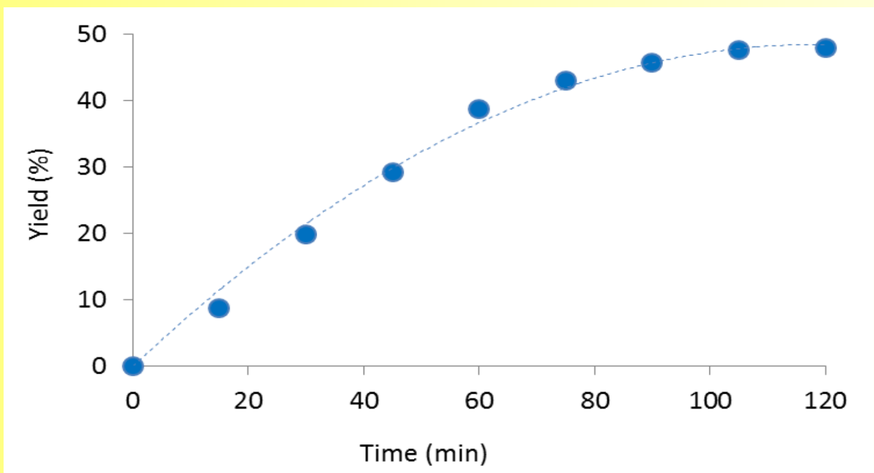

Dependence of total benzaldehyde + benzyl alcohol product yield on the reaction time, catalyzed by **2**. Reaction conditions: [toluene] = 1.67 M; [**2**] = 3.3×10^{-3} M; [TBHP] = 3.3 M, in NCMe, under MW-irradiation (5 W) during 0-120 min.

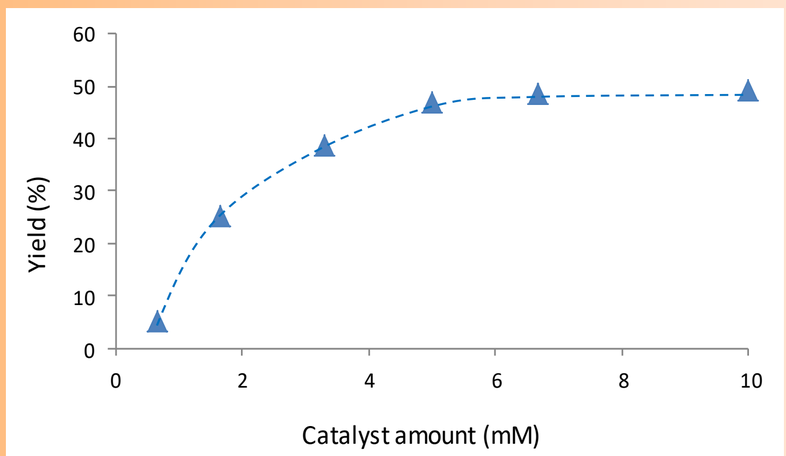

Dependence of total benzaldehyde + benzyl alcohol product yield on the catalyst concentration (0.67-10 mM), catalyzed by **2**. Reaction conditions: [toluene] = 1.67 M; [TBHP] = 3.3 M, in NCMe at 50ºC during 1 h under MW-irradiation (5 W).

Syncat

Funding:
Centro de Química Estrutural is funded by Fundação para a Ciência e Tecnologia – project UID/QUI/00100/2019.

ACKNOWLEDGEMENTS
M.S. acknowledges the FCT and IST for a working contract "DL/57/2017" (Contract no. IST-ID/102/2018).

References:

[1] M. Sutradhar, E.C.B.A. Alegria, T. Roy Barman, F. Scorcelletti, M.F.C. Guedes da Silva, A.J.L. Pombeiro, Molecular Catalysis 439 (2017) 224–232.
[2] T.C.O. Mac Leod, M.V. Kirillova, A.J.L. Pombeiro, M.A. Schiavon, M.D. Assis, Appl. Catal. A: Gen. 372 (2010) 191-198.

Bioinspired Copper(II) Aminoalcohol Complexes and Coordination Polymers: Self-assembly Synthesis, Structural Features and Catalysis

Tiago A. Fernandes, Marina V. Kirillova, Carla I. M. Santos, Vânia André, Alexander M. Kirillov

Introduction

As a continuation of our research on the synthesis and catalytic application of bioinspired multicopper(II) cores,[1-5] the main aim of the current work consisted in the self-assembly generation of new water-soluble copper(II) compounds bearing aminoalcohols as principal N,O-ligands. The solubility of coordination polymers (CPs) in aqueous medium can be achieved by introducing into the structure at least one organic building block that is soluble in water. Aminoalcohols are particularly attractive examples of such ligands owing to their coordination flexibility, low toxicity, high stability and solubility, and low cost.[1,2]

Results

N-benzylethanolamine (Hbea), triisopropanolamine (H_3tipa), *N*,*N*-dimethylethanolamine (Hdmea), *N*-methyldiethanolamine (H_2mdea) or *N*-ethyldiethanolamine (H_2edea) were applied as *N*,*O*-building blocks for the self-assembly generation of seven novel copper(II) compounds: $[Cu_2(\mu\text{-bea})_2(Hbea)_2](NO_3)_2$ (**1**), $[Cu_2(H_3tipa)_2(\mu\text{-pma})]\cdot 7H_2O$ (**2**), $[\{Cu_2(\mu\text{-dmea})_2(H_2O)\}_2(\mu_4\text{-pma})]_n\cdot 4nH_2O$ (**3**), $[\{Cu_2(\mu\text{-Hedea})_2\}_2(\mu_4\text{-pma})]_n\cdot 4nH_2O$ (**4**), $[\{Cu(bea)(Hbea)\}_4(\mu_4\text{-pma})]_n\cdot 2nH_2O$ (**5**), $[Cu(H_{1.5}mdea)_2]_2(H_2pma)$ (**6**), and $[\{Cu_2(\mu\text{-Hmdea})_2\}_2(\mu_4\text{-pma})]_n\cdot 2nH_2O$ (**7**) {H_4pma = pyromellitic acid}.

All products were isolated in good yields and fully characterized by IR spectroscopy, ESI–MS(±), elemental analysis, and single-crystal X-ray diffraction.

Figure 1 - Crystal structures of discrete complexes **1**, **2** and **6** and 2D coordination polymers **3-5** and **7**.

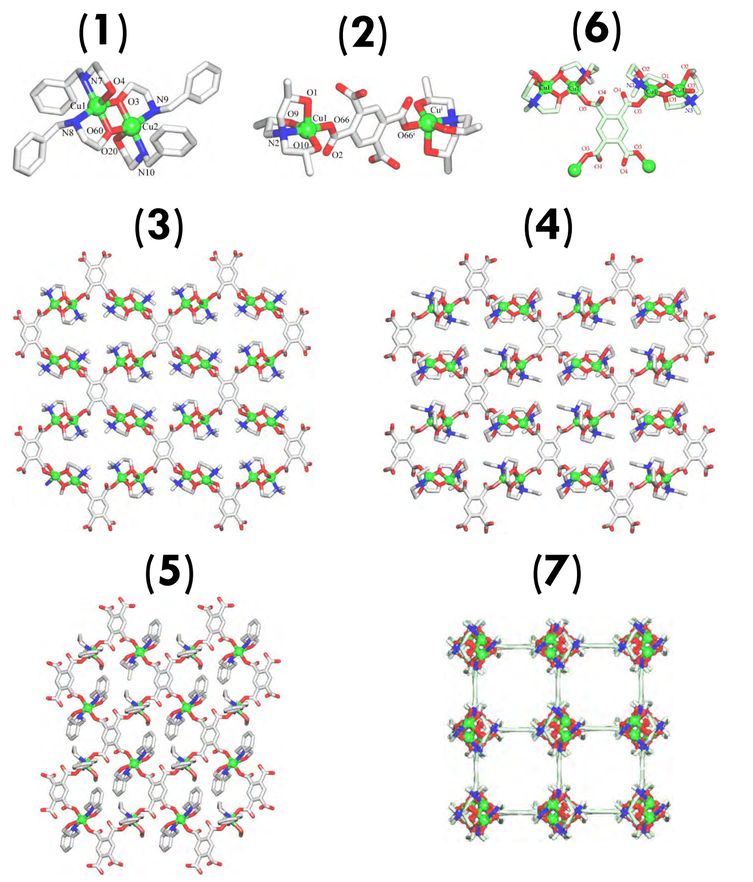

Cu (green balls), N (blue), O (red), C (gray or pale green).

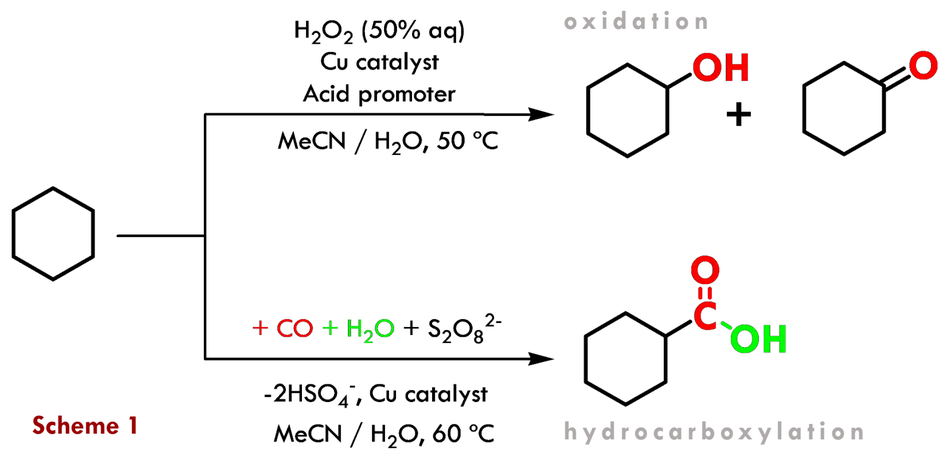

Scheme 1

Catalysis

Catalytic activity of the obtained compounds was also investigated in the **mild homogeneous oxidation** (Table 1, Figure 2) or **hydrocarboxylation of cycloalkanes** (Table 2) to give the corresponding cyclic alcohols and ketones or carboxylic acids.

Tested copper(II) compounds act as **highly efficient catalysts** for the mild homogeneous oxidation, by aqueous H_2O_2 in acidic MeCN/H_2O medium at 50 °C, of C5–C8 cycloalkanes to the corresponding alcohols and ketones (Scheme 1). Based on cycloalkane, overall product yields up to 45% were achieved and the effects of various reaction parameters were investigated: type and loading of pre-catalyst, amount and kind of acid promoter (HNO_3, H_2SO_4, HCl, or CF_3COOH), influence of water, and the substrate scope (Scheme 1, Figure 2).[4,5]

TOPICS FOR POTENCIAL COLLABORATION

Library of diverse Cu catalysts (complexes, MOFs, for C-H activation reactions

Library of Ag, Fe, Co, Mn, and Co MOFs as potential catalysts for C-H activation reactions

Synthesis and crystallization of new coordination compounds on demand

Topological analysis

Evaluation of new catalysts in our model reactions:

- *Oxidation of alkanes, alkenes, alcohols*
- *Reduction of alcohols, ketones, sulfoxides*

Figure 2 – Studied effects for mild oxidation of cycloalkanes.

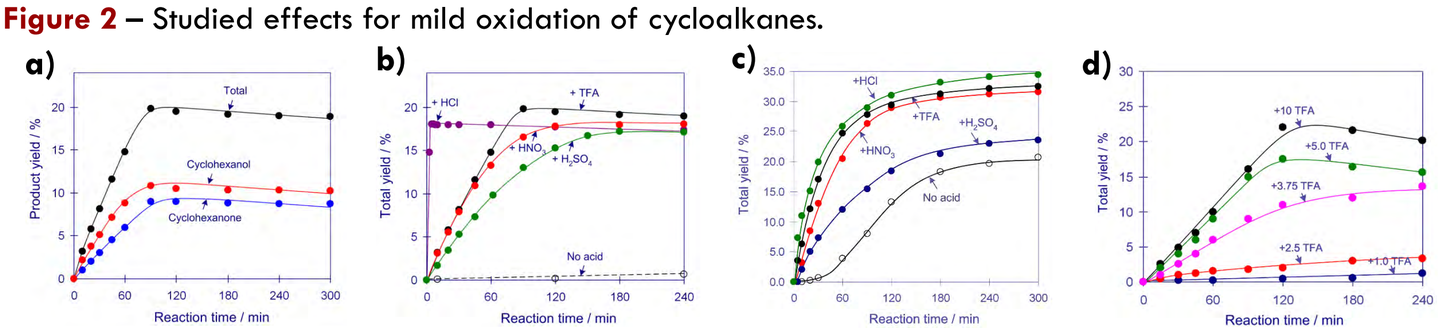

a) Kinetic curves of product accumulation in the cyclohexane oxidation by H_2O_2 catalyzed by **1**. Effect of the type of acid promoter on the total yield of the products in the cyclohexane oxidation with H_2O_2 catalyzed by **b) 1** and **c) 5**. **d)** Effect of catalyst amount on the total product yield in the cyclooctane oxidation with H_2O_2 catalyzed by **6**. Reaction conditions: catalyst (5 μmol), TFA (0.05 mmol), C_6H_{12} (1.0 mmol), H_2O_2 (5.0 mmol), CH_3CN (up to 2.5 mL of the total volume), 50 °C.

Figure 3 - H_2O effect on the total product yield in cyclohexane oxidation

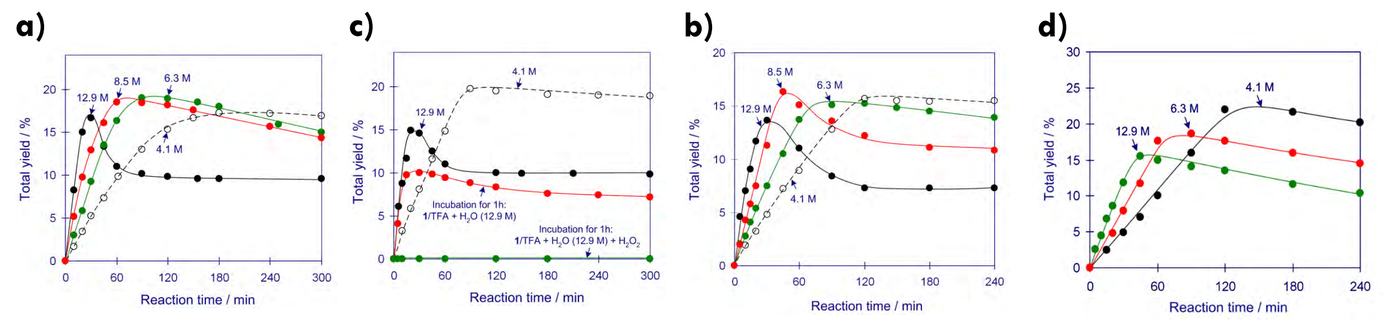

The effect of the H_2O amount on the total product yield in the cyclohexane oxidation with H_2O_2 catalyzed by **a) 1**/H_2SO_4, **b) 1**/TFA, **c) 2**/TFA systems and **d) 6**/TFA systems. Reaction conditions: catalyst (0.01 mmol), acid promoter (0.1 mmol), C_6H_{12} (2.0 mmol), H_2O_2 (10.0 mmol), added H_2O (up to 0.8 mL), CH_3CN (up to 5.0 mL total volume), 50 °C.

Table 1. Oxidation of cycloalkanes by H_2O_2 catalyzed by **1–6**

Cycloalkane	Total product yield (alcohol + ketone), %[a]					
	1	**2**	**3**	**4**	**5**	**6**
C_5	9	6	17	36	26	8
C_6	19	15	24	30	33	15
C_7	23	23	21	36	34	19
C_8	18	22	26	36	32	18

Table 2. Hydrocarboxylation of cycloalkanes by H_2O_2 catalyzed by **1**,**2** and **6**

Cycloalkane	Catalyst	Product Yield, %[a]			
		Acid	Ketone	Alcohol	Total[b]
C_5	**1**	27	<1	<1	27
	2	21	<1	<1	21
	6	30	<1	<1	30
C_6	**1**	38	2	<1	40
	2	38	2	<1	41
	6	43	2	<1	45
C_7	**1**	24	10	2	36
	2	26	8	2	37
	6	23	7	2	32
C_8	**1**	13	12	5	30
	2	10	10	4	24
	6	9	13	6	28

Although water typically strongly inhibits alkane oxidations due to the reduction of H_2O_2 concentration and lowering of the alkane solubility, in some catalytic systems we observed a significant growth of an initial reaction rate in the cyclohexane oxidation on increasing the amount of H_2O in the reaction mixture. H_2O showed a remarkable promoting behavior in some related Cu-containing catalytic systems as well as acted as unusual hydroxylating reagent and solvent component in mild copper-catalyzed alkane hydrocarboxylations.

Such promoting role of water is still uncommon but may open a possibility of applying diluted in situ generated aqueous solutions of H_2O_2 as a green oxidant in alkane oxidation processes.

CQE Química Estrutural

05 BIOMOL

Funding:

Centro de Química Estrutural is funded by Fundação para a Ciência e Tecnologia (FCT) – project UID/QUI/00100/2019. We thank FCT for support: IF/01395/2013/CP1163/CT005, SFRH/BPD/119980/2016, SFRH/BPD/78854/2011, CEECIND/03708/2017, LISBOA-01-0145-FEDER-029697, REM2013.

FCT Fundação para a Ciência e a Tecnologia
MINISTÉRIO DA CIÊNCIA E DO ENSINO SUPERIOR

References:

1. Fernandes, T.A., Kirillova, M.V., André, V., Kirillov, A.M., *Dalton Trans.*, 47 (2018) 16674–16683.
2. Kirillova, M.V., Santos, C.I.M., André, V., Fernandes, T.A., Dias, S.S.P., Kirillov, A.M., *Inorg. Chem. Front.*, 4 (2017) 968-977.
3. Fernandes, T.A., Santos,C.I.M., André, V., Dias, S.S.P., Kirillova, M.V., Kirillov, A.M., *Catal. Sci. Technol.*, 6 (2016) 4584-4593.
4. Fernandes, T.A., Santos, C.I.M., André, V., Kłak, J., Kirillova, M.V., Kirillov, A.M., *Inorg. Chem.*, 55 (2016) 125-135.
5. Fernandes, T.A., André, V., Kirillov, A.M., Kirillova, M.V., *J. Mol. Catal. A: Chem.*, 426 (2017) 357-367.

To see this poster in augmented reality:

GET ZAPPAR
ZAP THE CODE
App Store Google play

Water-borne smart polymer nanoparticles for high-performance applications

Tiago D. Martins, Carlos Baleizão, José Paulo S. Farinha

GOALS

- Here, we aimed the synthesis of functionalized polymer nanoparticles that can covalently bond for high-performance self-healing materials.
- A combination of dynamic covalent chemistry with BMA allow us to obtain a formulation where the low T_g of BMA increase the mobility of the macromolecules at low temperatures and facilitating the reversible reaction.
- The combination of aldehyde and amino functionalized monomers into core-shell nanoparticle structure allow a reversible covalent bond between different nanoparticles

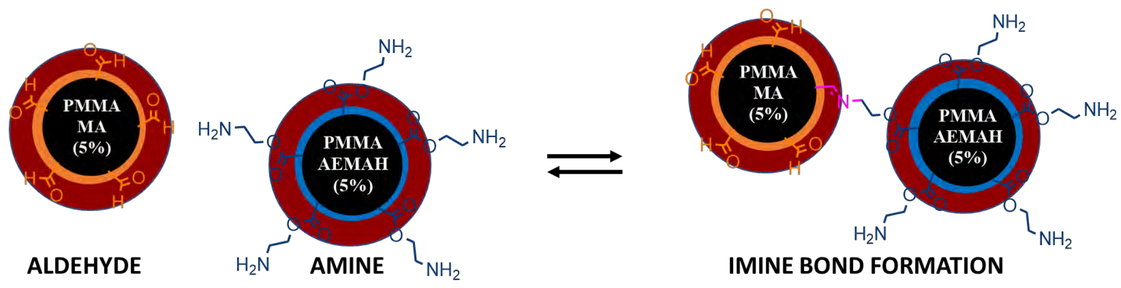

✓ Growth of the core-shell nanoparticles followed by dynamic light scattering (**DLS**).

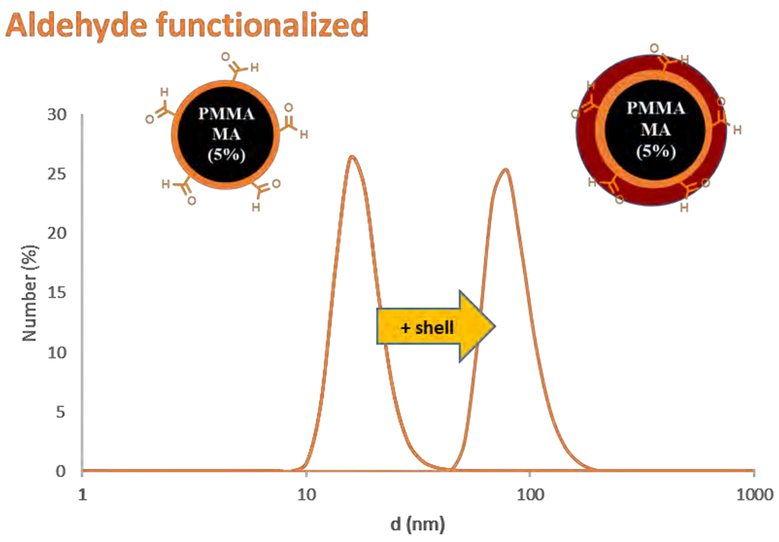

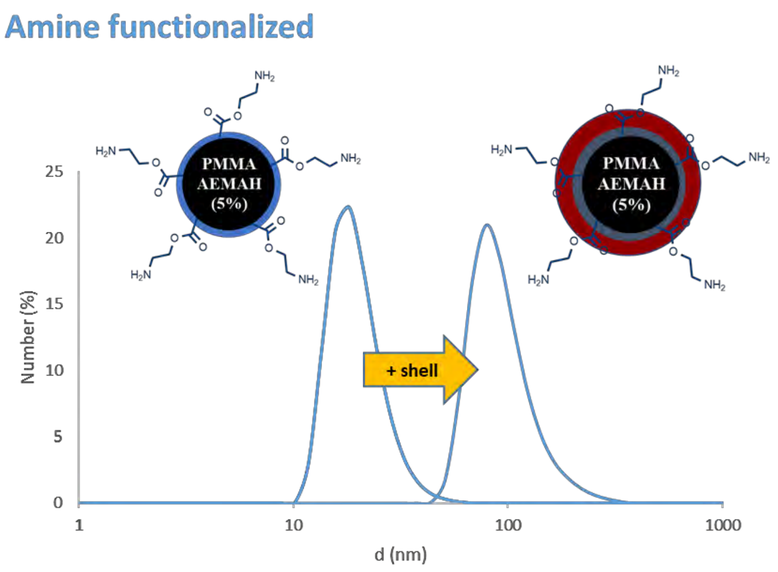

✓ Polymerization followed by **^{1}H-NMR**.

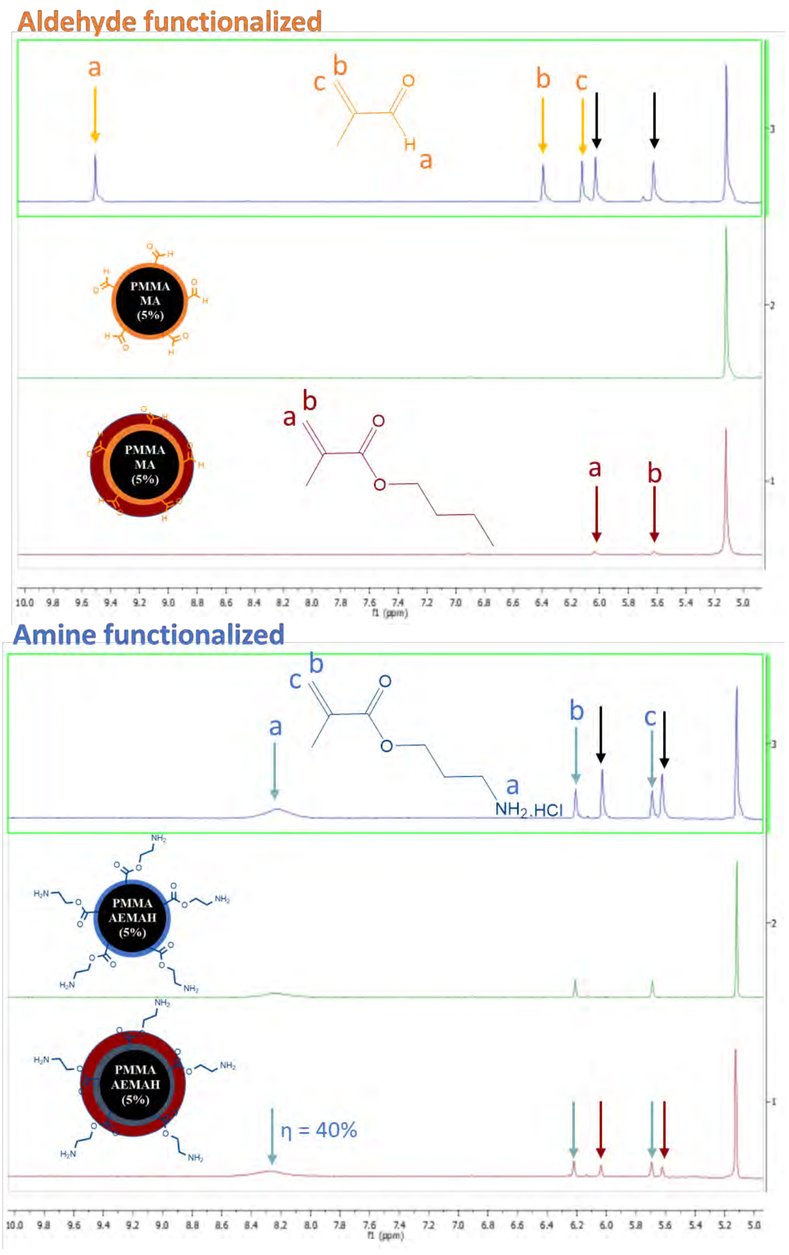

✓ Final product was analyzed by diffuse reflectance infra-red Fourier transform (**DRIFT**).

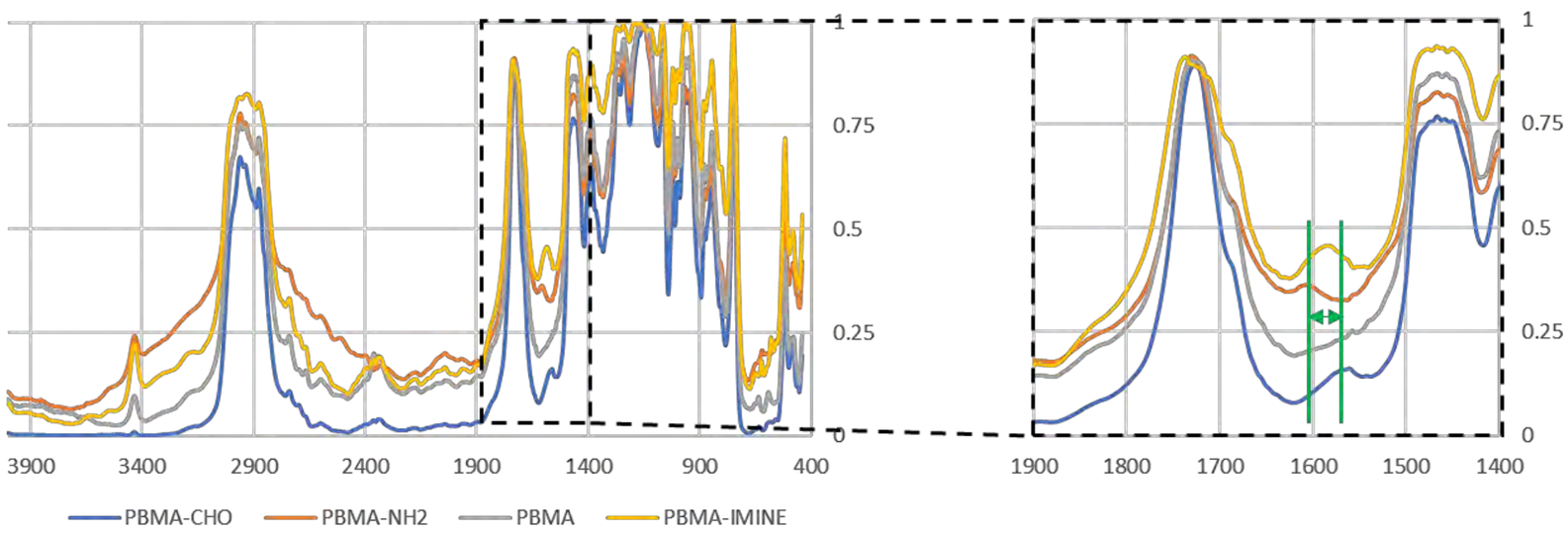

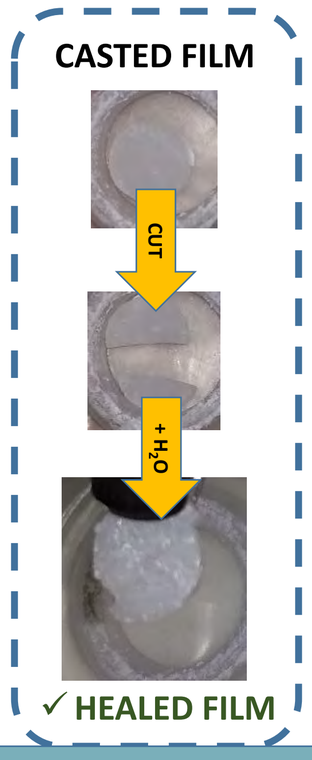

Outlook

- Functionalized core-shell nanoparticles were successfully synthesized and characterized.
- DLS measurements show the formation of a core and the growth of its shell
- NMR spectra show the monomer consumption due to the efficient polymerization reaction
- FTIR-DRIFT shows the formation of a new band due to imine bond formation, when the two nanoparticles are mixed.

08 MPPM

Funding:
Centro de Química Estrutural is funded by Fundação para a Ciência e Tecnologia – project UID/QUI/00100/2019. This work was supported by PhD grant SFRH/BD/132486/2017 and project UID/NAN/50024/2013 and PTDC/CTM-POL/3698/2014 from Fundação para a Ciência e a Tecnologia (FCT).

References:

1. Alves S, Santos C, da Costa AP, Silva M, Baleizão C, Farinha JPS. *Chem Eng J*. 319 (**2017**) 31-38. doi:10.1016/j.cej.2017.02.139
2. Marcelo G, Areias LRP, Viciosa MT, Martinho JMG, Farinha JPS. *Polymer (Guildf)*. 116 (**2017**) 261-267. doi:10.1016/j.polymer.2017.03.071
3. Piçarra S, Fidalgo A, Fedorov A, Martinho JMG, Farinha JPS. *Langmuir*. 30 (**2014**) 12345-12353. doi:10.1021/la502826r
4. Ribeiro T, Baleizão C, Farinha JPS. *Materials (Basel)*. 7 (**2014**) 3881-3900. doi:10.3390/ma7053881
5. Thakur VK, Kessler MR. *Polym (United Kingdom)*. 69 (**2015**) 369-383. doi:10.1016/j.polymer.2015.04.086
6. Engel T, Kickelbick G. *Polym Int*. 63 (**2014**) 915-923. doi:10.1002/pi.4642
7. Martinho JMG, Farinha JPS. *CoatingsTech*. 10 (**2013**) 42-49.

Microplastics in the marine environment: Raise awareness and challenges

Vanessa Morgado,[1,2] Carla Palma,[2] Ricardo B. Silva[1]

[1]Centro de Química Estrutural da Faculdade de Ciências da Universidade de Lisboa – Campo Grande, 1749-016 Lisboa
[2]Instituto Hidrográfico, Rua das Trinas, 49, 1249-093 Lisboa

CONTEXTUALIZING

Even the firsts scientific reports are dated from the 70s years, the plastic pollution in marine environment stood out as a serious problem only after the discovery of "The Great Pacific Garbage Patch" – the largest of five offshore plastic accumulation zones in the oceans – 90s years. Currently, the plastic debris can account over than 60 % of marine litter.

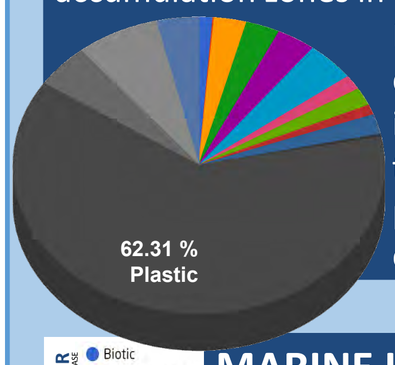

Microplastics – plastic pieces less than 5 millimeters long – have been studied from the last decade to present, due to their accelerated increase and widespread in the environment. These SMALL contaminants are released into the environment as manufactured particles with a microscopic size (*i.e.* less than 5 mm) or as a result of the fragmentation and degradation of large plastic products (*e.g.* macro plastic debris). As such, these small pieces are classified as primary and secondary, respectively. Actually, microplastics can reach already concentrations of 100 000 particles per m^3 in water or sediments (Wright, 2013; Conkle, 2018).

MARINE LITTER

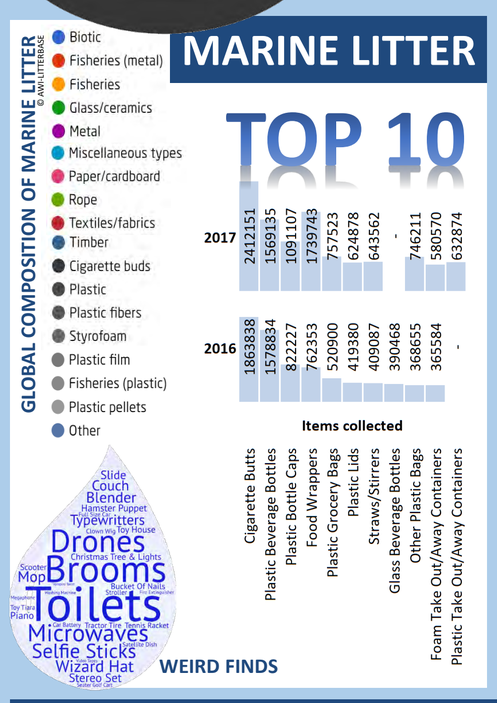

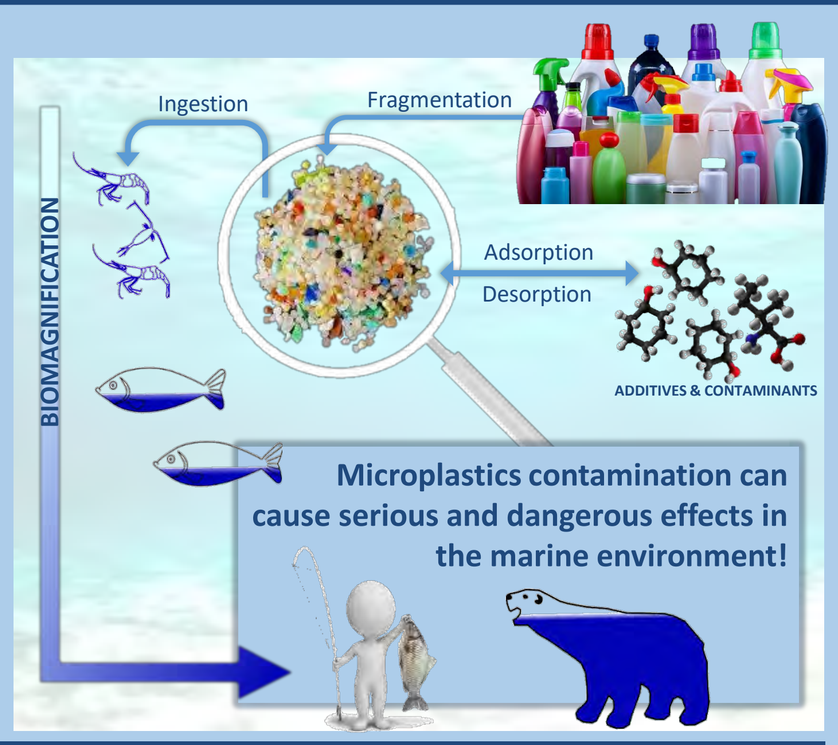

MICRO LITTER (< 5 mm)

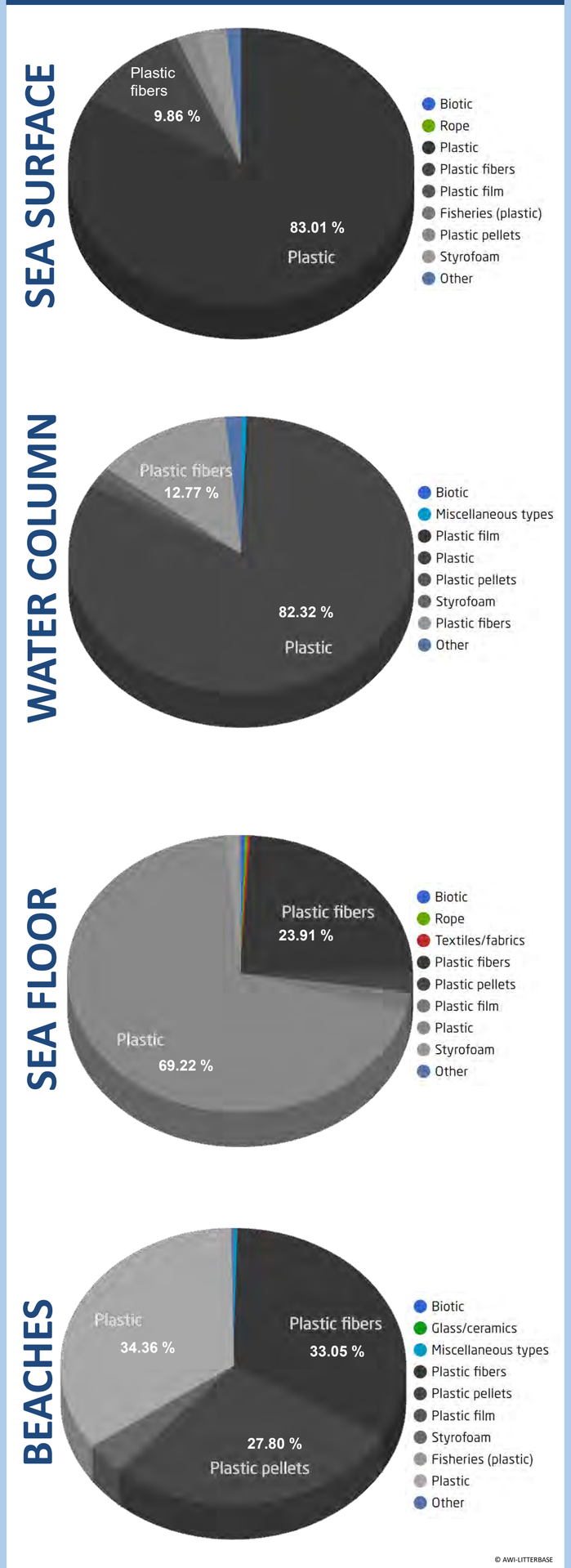

CHALLENGES

EUR-Lex

25.6.2008 EN Official Journal of the European Union L 164/19

DIRECTIVE 2008/56/EC OF THE EUROPEAN PARLIAMENT AND OF THE COUNCIL

of 17 June 2008

establishing a framework for community action in the field of marine environmental policy (Marine Strategy Framework Directive)

(Text with EEA relevance)

Annex I, Descriptor 10

"Properties and quantities of marine litter do not cause harm to the coastal and marine environment."

Convenção Internacional para a Prevenção da Poluição por Navios

(MARPOL 73/78)

PROTOCOLO DE 1978 RELATIVO À CONVENÇÃO INTERNACIONAL PARA A PREVENÇÃO DA POLUIÇÃO POR NAVIOS, 1973

The reliable determination of microplastic pollution trends in large environmental compartments allows understanding which contamination sources are threatening the environment and **must** be controlled.

OUR PURPOSE

- Assessing the impact of analytical steps on the uncertainty of microplastic contamination determination.
- Development of tools for the objective determination of microplastics pollution trends of vast environmental compartments (*i.e.* trends with quantified uncertainty).
- Determination of microplastic pollution trends in relevant environmental resources of Portugal (size, number and type).

Next work:

Microplastics in the marine environment: a rigorous analysis by FTIR

06 CE

Funding:

Centro de Química Estrutural is funded by Fundação para a Ciência e Tecnologia – project UID/QUI/00100/2019.

This work was supported by a doctoral grant from Universidade de Lisboa (UL), 2018.

References:

AWI-LITTERBASE©, (https://litterbase.awi.de/).

Conkle, J., et al., Environmental Management 61:1 (2018) 1–8.

International Coastal Cleanup, Together for out Ocean, 2017 Report.

International Coastal Cleanup, Building a Clean Swell, 2018 Report.

Wright, S., et al., Environmental Pollution 178 (2013) 438–492.

Exploring crystal engineering to revive old drugs

Vânia André, Fátima Minas da Piedade, João Luís Ferreira da Silva, Inês Martins, Sofia Domingos, Mariama Djaló, Martin Zabransky, Merve Arpacioglu, M. Teresa Duarte

INTRODUCTION

Crystal engineering (CE) has been widely used over the last years in the discovery of new crystal forms of active pharmaceutical ingredients (API). One of CE most important applications is the rational design and arrangement of molecular packing, which affects and controls the API properties, such as stability, solubility and bioavailability. The new crystal forms enclose not only polymorphs, hydrates and solvates but also co-crystals and molecular salts and even though solution techniques were traditionally used in their synthesis, mechanochemistry has been assuming an important role in the screening and preparation of these new crystal forms.

As important as the synthesis of these new compounds is the injunction of their structure-properties relationships. Solubility is a major factor that is known to strongly affect API's performance and therefore its correlation with structural and thermal data is of upmost importance.

In the last decade a large part of our group's research has been oriented for the synthesis and characterization of polymorphs, co-crystals and salts of APIS using mechanochemistry as primary synthetic technique. We targeted different APIs, such as gabapentin,[1,2] gabapentin-lactam,[3] 4-aminosalicylic acid,[4,5] dapsone,[6] sulfadimethoxine,[7] sparfloxacin, pipemidic acid and azelaic acid.[8] The new crystal forms obtained are overall stable and, in most cases, their effect in solubility has been studied revealing promising results.

MECHANOCHEMISTRY

Consists on grinding together the reactants to promote a reaction

Why?

- Straightforward and clean
- Desired products are obtained in high purity and high quantitative yield
- It is environmental-friendly, combining high reaction efficiency and minimal input of energy and solvent
- It is rapidly becoming a method of choice in different areas of chemical and materials synthesis

Mortar and pestle

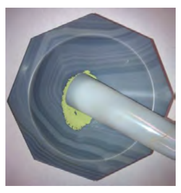

Ball mill

SUSChem

MEDLife

CRYSTAL ENGINEERING

CE is the design of molecular solids with specific physico-chemical properties through the understanding and manipulation of intermolecular interactions, such as hydrogen bonds, halogen bonds and π-π interactions.

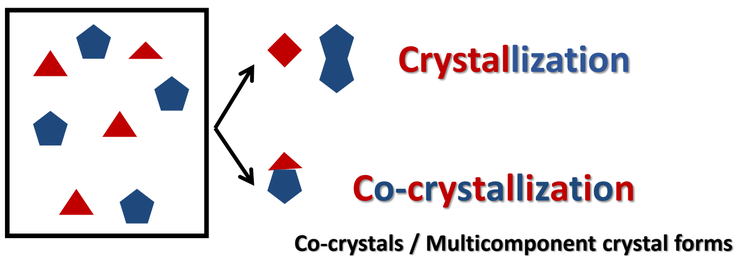

APIs = multiple functional groups =
Multiple pathways to give rise to new forms exploring CE principles

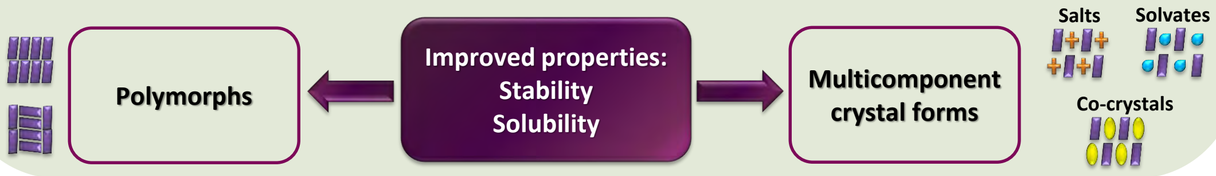

SUMMARY OF THE MOST RELEVANT RESULTS

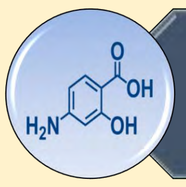

4-Aminosalicylic acid

- 9 multicomponent crystal forms
- 3 concomitant polymorhic salts

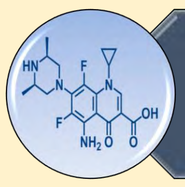

Sparfloxacin

- 12 multicomponent crystal forms
- 3 solvates
- Solubility studies

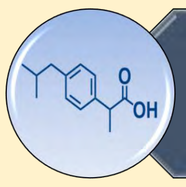

Ibuprofen

- 2 multicomponent crystal forms
- Chiral resolution studies

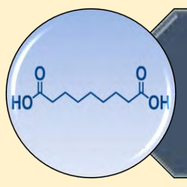

Azelaic acid

- 5 multicomponent crystal forms
- Preliminary solubility studies

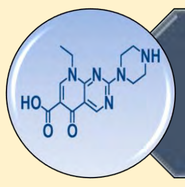

Pipemidic acid

- 5 multicomponent crystal forms
- Solubility studies

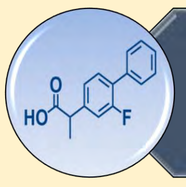

Flurbiprofen

- 10 multicomponent crystal forms
- Chiral resolution studies

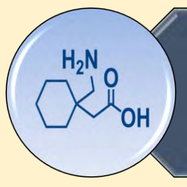

Gabapentin

- 2 new polymorphic forms and 1 ester derivative
- 2 multicomponent crystal forms

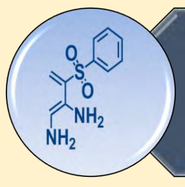

Dapsone

- 2 co-crystals
- 1 solvate

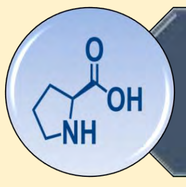

Proline

- 13 multicomponent crystal forms
- Chiral resolution studies

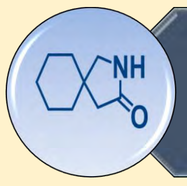

Gabapentin-lactam

- 5 multicomponent crystal forms
- Solubility studies and development of mathematical models

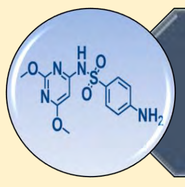

Sulfadimethoxine

- 8 multicompnent crystal forms
- Solubility studies

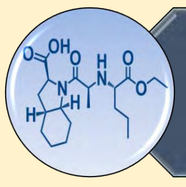

Perindopril Erbumine

- First crystal structure determined
- New hydrated form
- Dissolution studies

Gabapentin-lactam

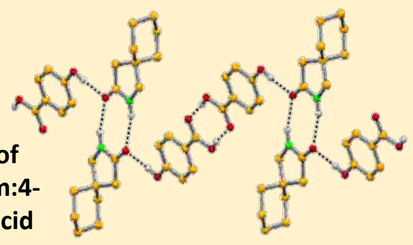

Crystal packing of gabapentin-lactam:4-hydroxybenzoic acid co-crystal

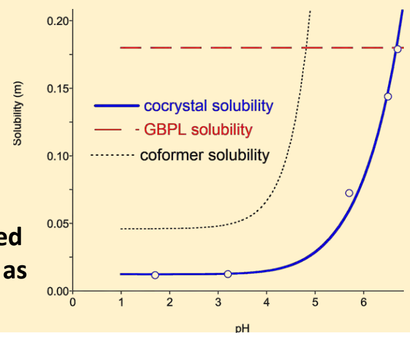

Mathematical models developed for the solubility as function of pH

Sulfadimethoxine

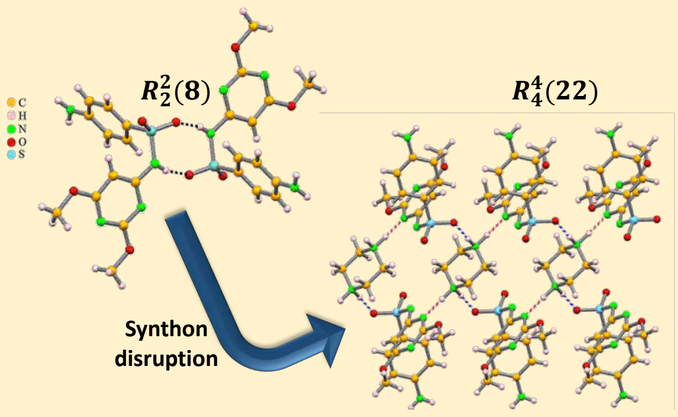

Crystal packing of sulfadimethoxine (left) and sulfadimethoxine:piperazine salt (right)

Sulfadimethoxine salts more soluble than co-crystals

Perindopril erbumine

Chirality is maintained in the new perindopril hydrate

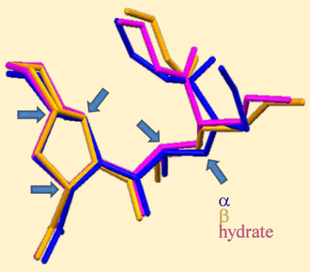

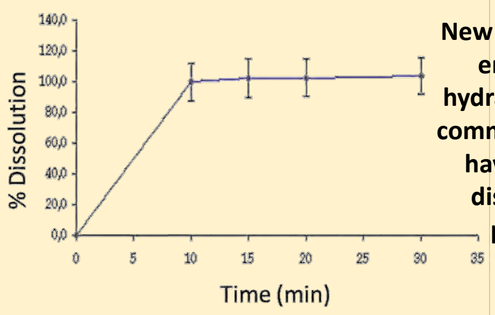

New perindopril erbumine hydrate and the commercial form have similar dissolution profiles

05 BIOMOL

Funding:

Centro de Química Estrutural is funded by Fundação para a Ciência e Tecnologia – project UID/QUI/00100/2019.

Authors further acknowledge FCT and FEDER for funding - project PTDC/QUI-OUT/30988/2017.

References:

1. Braga, D; Grepioni, F; Maini, L; Rubini, K; Polito, M; Brescello, R; Cotarca, L; Duarte, MT; André, V; Piedade, MFM, New Journal of Chemistry, 32 (2008) 1788-1795.
2. Martins, ICB; Gomes, JRB; Duarte, MT; Mafra, L, Crystal Growth & Design, 17 (**2017**) 428-432.
3. Maheshwari, C; André, V; Reddy, S; Roy, L; Duarte, MT; Rodríguez-Hornedo, N, CrystEngComm, 14 (**2012**) 4801-4811.
4. André, V; Shemchuk, O; Grepioni, F; Braga, D: Duarte, MT, Crystal Growth & Design, 17 (**2017**), 6417-6425.
5. André, V; Braga, D; Grepioni, F; Duarte, MT, Crystal Growth & Design, 9(12) (**2009**) 5108-5116.
6. Martins, I; Martins, M; Fernandes, A; André, V; Duarte, MT, CrystEngComm, 15 (**2013**) 8173-8179.
7. Domingos, S; Fernandes, A; Duarte MT; Piedade, MFM, Crystal Growth & Design, 16 (**2016**) 1879-1892.
8. Martins, ICB; Sardo, M; Santos, SM; Fernandes, A; Antunes, A; André, V; Mafra, L; Duarte, MT, Crystal Growth & Design 16(1) (**2016**) 154-166.

Hydrogen peroxide as a key player in bystander effects

Pinto V [1,2], Carmona B[1,2,3], Antunes F[1,2], Marinho HS[1,2], Vieira L[3,4] and Soares H[1,2,3]

[1] Centro de Química Estrutural, Faculdade de Ciências da Universidade de Lisboa; [2] Centro de Química e Bioquímica, Faculdade de Ciências da Universidade de Lisboa; [3] Escola Superior de Tecnologia da Saúde de Lisboa, Instituto Politécnico de Lisboa; [4] Instituto de Biofísica e Engenharia Biomédica, Faculdade de Ciências da Universidade de Lisboa

BACKGROUND

During radiotherapy for cancer treatment protocols, cells that were not directly exposed to ionizing radiation (IR) show similar phenotypes, as for example DNA damage, to the ones directly irradiated, a phenomenon denominated bystander effect (BE). Investigating the molecular mechanisms underlying the BE has impact in several clinical applications, such as undermining the resistance to radiotherapy and adapting sensitization to BE in order to improve treatment efficacy, and is the focus of our research[1,2,3].

Bystander effect

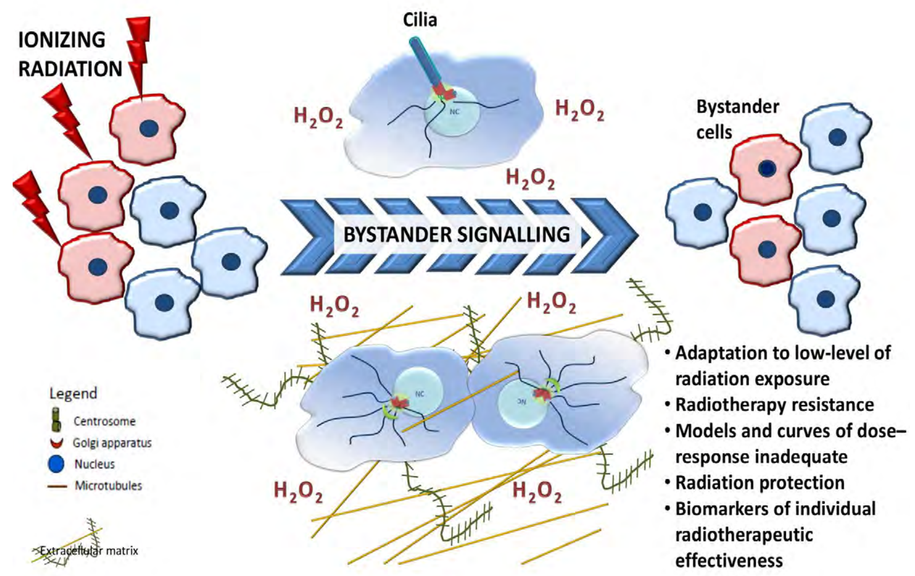

WORKING HYPOTHESIS

Hydrogen peroxide (H_2O_2) has the potential to be a key molecule responsible for this cell-cell communication, on the account of being one of the chemical species generated by H_2O radiolysis when cells are exposed IR and easily defuses through biological membranes. Also, H_2O_2 has emerged as a key regulatory molecule involved in a variety of distinct biological processes. Nowadays, the essential regulating role played in vivo by H_2O_2 is unquestionable and has important implications in health and disease[4].

AIMS

The specific aim of this work is to identify dose-response relationships that correlate H_2O_2 with the onset of BE in exposed cells to IR. In a first step we established a setup in which tumor (HeLa cells) and non-tumor cells (hTERT-RPE1) were exposed to different regimens of H_2O_2 doses (continuous and single dose by bolus addition), that were able to produce DNA damage - double-strand breaks (DSB), quantified by changes in γH2AX foci numbers, mimicking cell exposition to IR.

RESULTS

Setup A: recovery time course after exposure to 50 μM and 250 μM H_2O_2 during 5 min

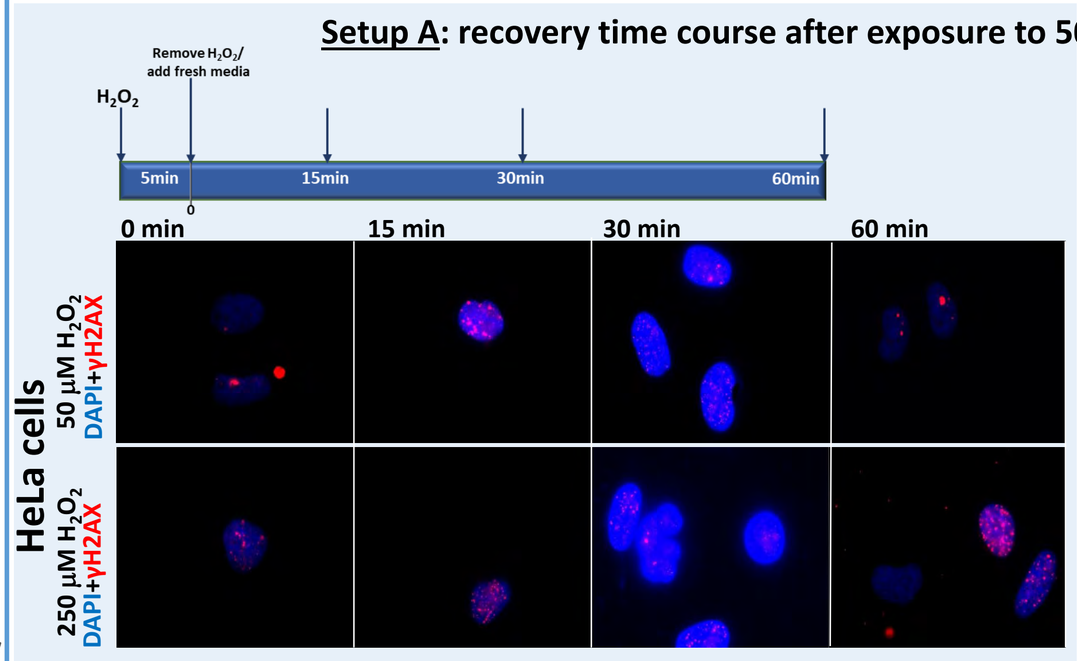

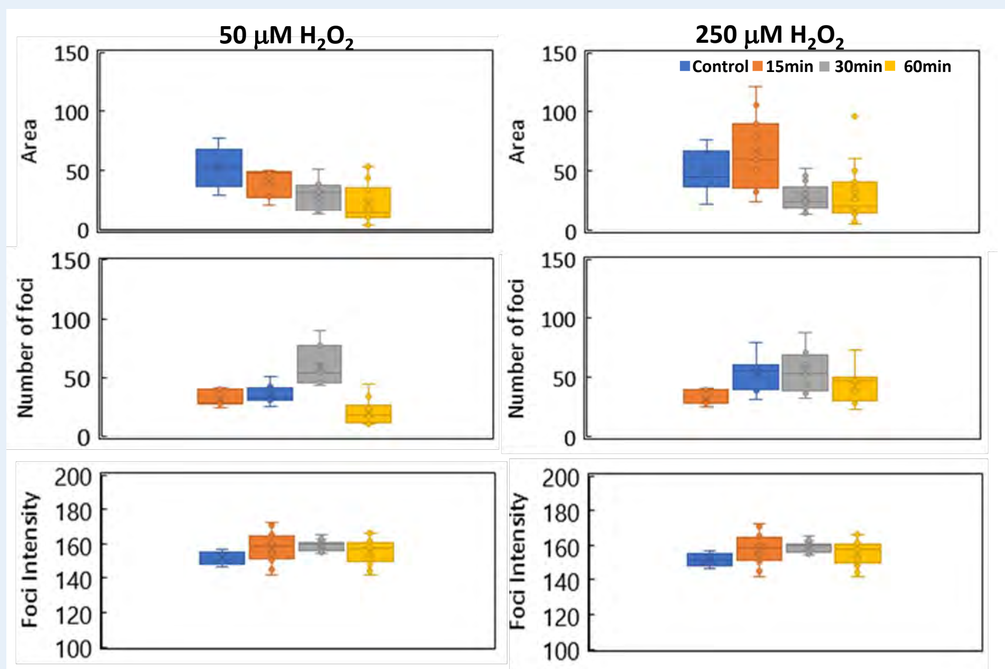

In HeLa cells, the exposure to 50 μM and 250 μM of H_2O_2 during 5 min followed by a recover in fresh media for different times causes a transient increase in the number of γH2AX foci that is also accompanied by an increase in their intensity. The increase in foci number is faster in cells recovering from an exposure to 250 μM of H_2O_2 in comparison to those exposed to 50 μM of H_2O_2. In both cases the average area of foci decreases during time.

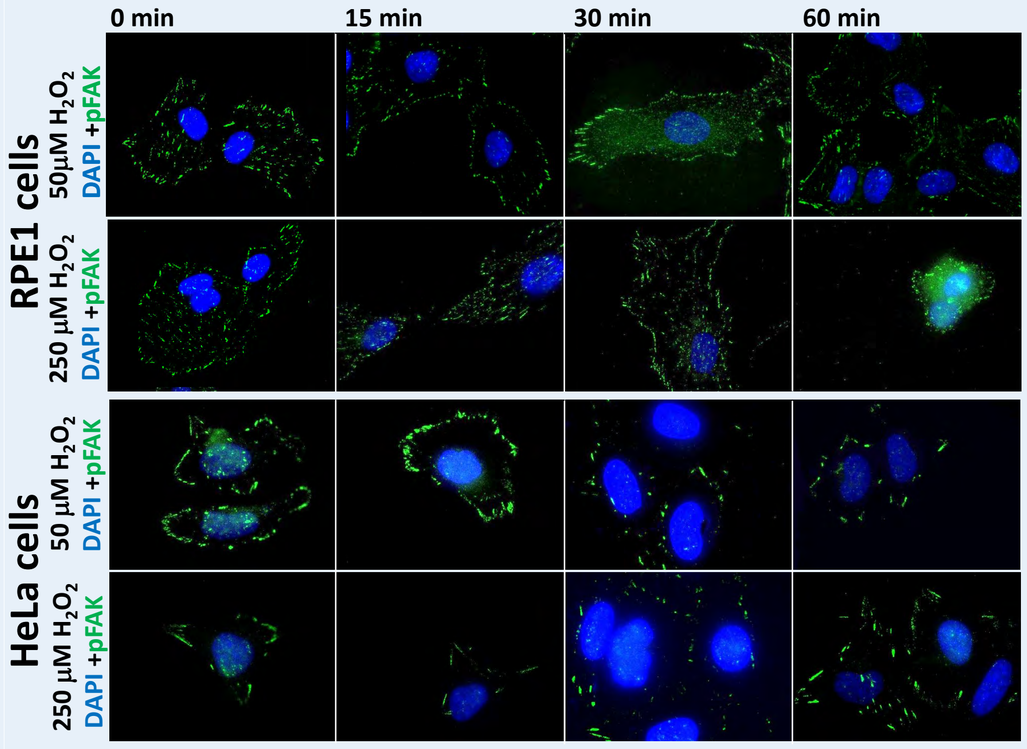

FAK is a non-receptor tyrosine kinase that is critical in signaling networks arising from focal adhesions that mediate cell-extracellular matrix interactions and transduce signals from cells microenvironment to the cytoplasm. For both concentrations of H_2O_2 we have observed that although the number of pFAK foci tends to decrease since 15 min of recovery, the intensity increases. The response is faster for 50 μM H_2O_2 in comparison to that of 250 μM H_2O_2.

Setup B: exposure time course after bolus addition of 50 μM and 250 μM of H_2O_2.

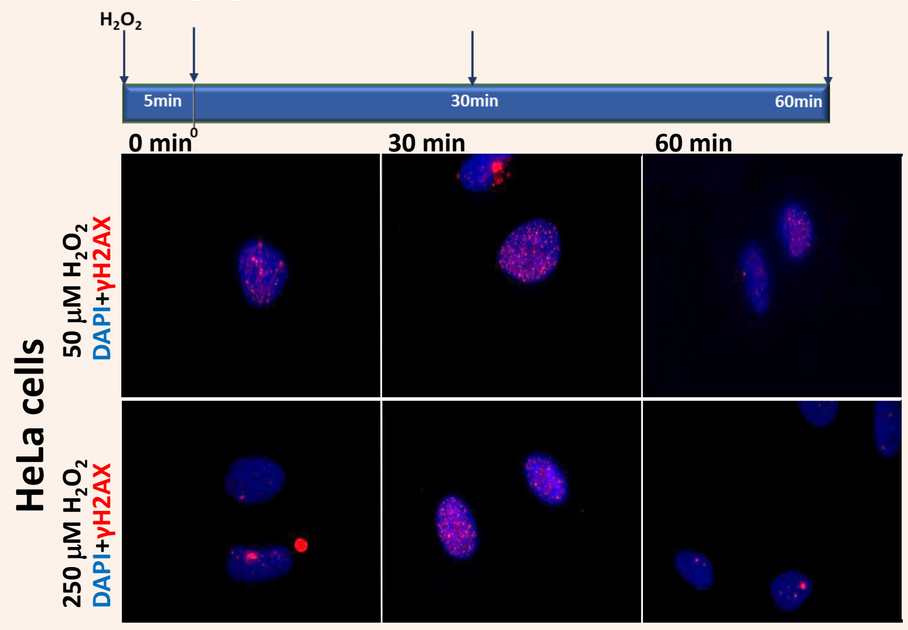

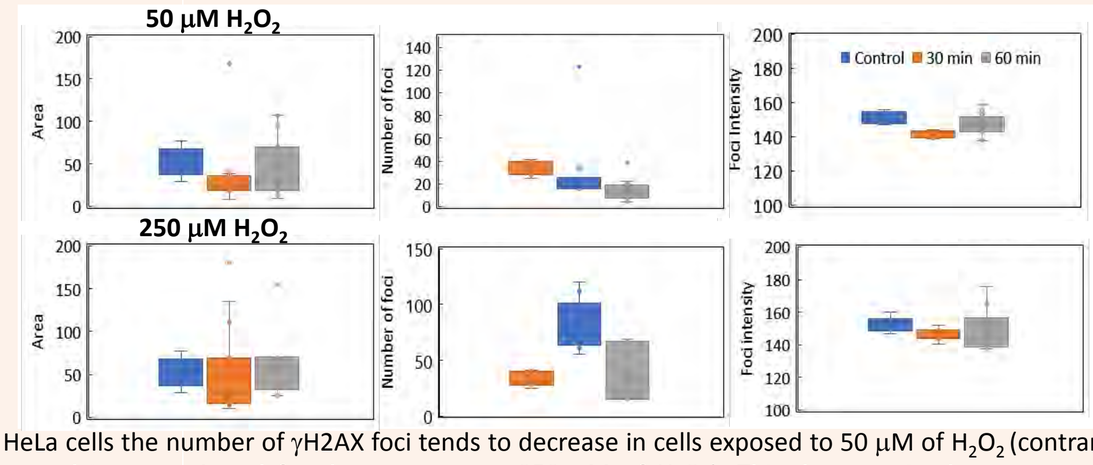

In HeLa cells the number of γH2AX foci tends to decrease in cells exposed to 50 μM of H_2O_2 (contrary to what observed in setup A and for the exposure to 250 μM of H_2O_2). This decrease is also accompanied by a decrease in γH2AX foci intensity.

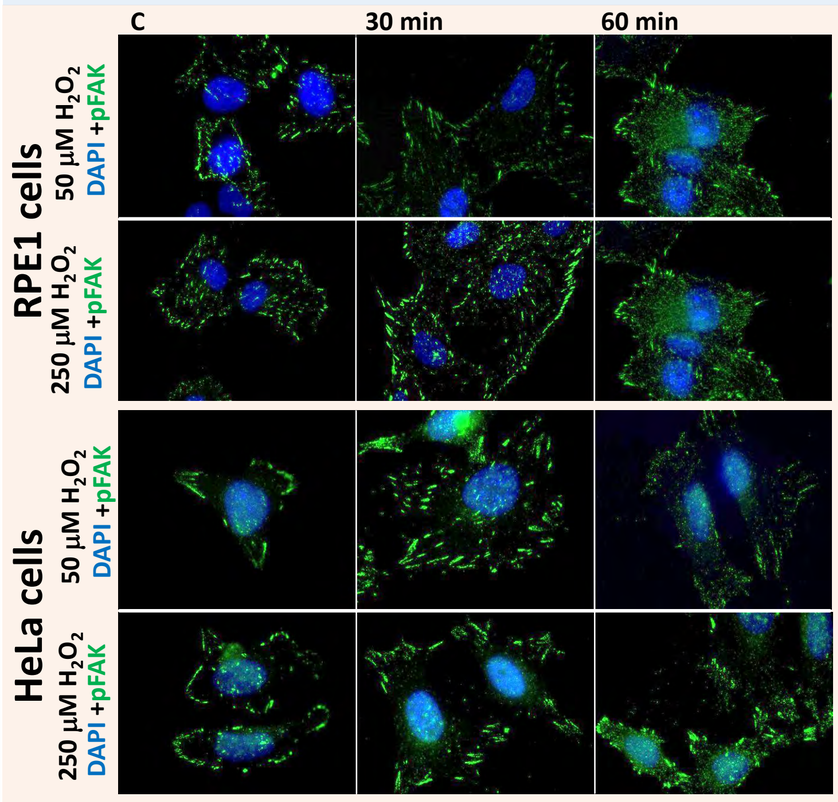

The number of pFAK foci tends to increase. A clear peak is observable for cells exposed during 30 min to 50 μM of H_2O_2. However, this peak is accompanied by a decrease in intensity.

CONCLUSIONS: H_2O_2 is able to produce DNA damage - double-strand breaks (DSB)-which was quantified by changes in γH2AX foci numbers/intensity/area. H_2O_2 effects are dependent on the distinct regimens of exposing cells to H_2O_2 doses; both strategies of exposure to H_2O_2 seems to affect pFAK pattern of staining. We have established two set ups to compare the obtained results to those that will be obtained in cells exposed to radiation that allow testing whether H_2O_2 is a key signaling molecule responsible for BE.

05 BIOMOL

Funding:

CQE (Centro de Química Estrutural) is funded by Fundação Fundação para a Ciência e Tecnologia (FCT, Portugal) – project UID/QUI/00100/2019 and CQB PEst-OE/QUI/UI0612/2013, Fundação para a Ciência e a Tecnologia; IPL/2018/OxByStand, Instituto Politécnico de Lisboa (to HS).

References:

1-Aravindan, N., Aravindan, S., Pandian, V., et al. (2014). Acquired tumor cell radiation resistance at the treatment site is mediated through radiation-orchestrated intercellular communication. Int. J. Radiat. Oncol. Biol. Phys, 88(3), 677–685.

2-Burtt, J. J., Thompson, P. A., & Lafrenie, R. M. (2016). Non-targeted effects and radiation-induced carcinogenesis: a review. J. of Rad. Protec., 36(1), R23–R35.

3-Morgan, W. F. (2012). Non-targeted and delayed effects of exposure to ionizing radiation: I. Radiation-induced genomic instability and bystander effects in vitro. 2003. Radiation Research, 178(2), AV223-36.

4-Marinho, H. S., Real, C., Cyrne, L., Soares, H., & Antunes, F. (2014). Hydrogen peroxide sensing, signaling and regulation of transcription factors. Redox Biology, 2, 535–562.

FCT
Fundação para a Ciência e a Tecnologia

Natural fibers modification with metal chalcogenides nanoparticles with photocatalytic properties for pollutants degradation

Inês Ferreira, O.C. Monteiro, V.C. Ferreira
Centro de Química Estrutural e Centro de Química e Bioquímica, Faculdade de Ciências, Universidade de Lisboa, Campo Grande, 1749-016 Lisboa, Portugal

Ciências ULisboa | CQB Centro de Química e Bioquímica

CQE Química Estrutural

06 Chemistry for the Environment - Chem4Env

Introduction

Throughout the years the modification of fibers caught the scientists' special attention, in particular due to the possibility of using nanoparticles (NPs) to improve their characteristics and impart new properties.[1] Examples include antimicrobial/antibacterial, self-cleaning and photocatalytic properties being the later relevant for pollutants degradation processes. [2,3]

In this work, Bi_2S_3 and ZnS NPs were used to modify cotton, the natural fiber. The photocatalytic performance was then evaluated towards the degradation of pollutants using a dye molecule.

Experimental details

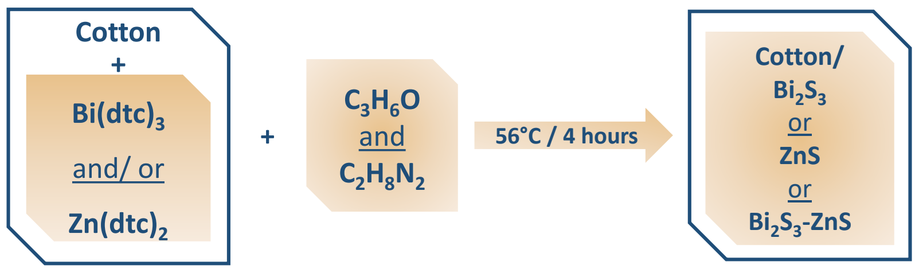

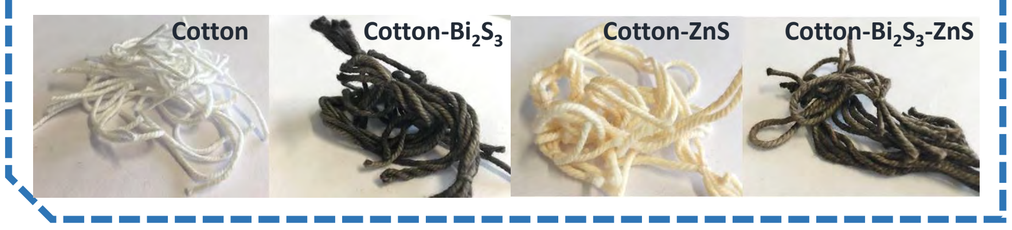

Optical characterization

DRS

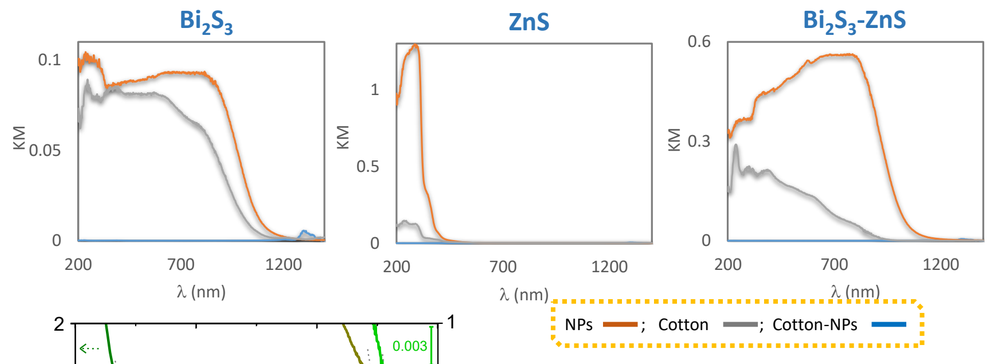

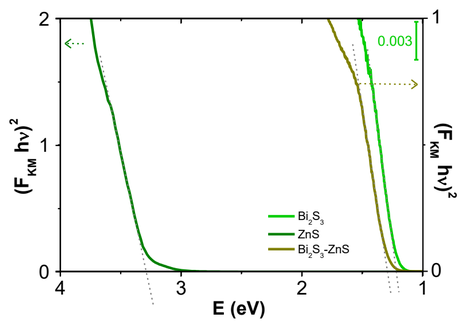

Sample	NPs	Cotton-NPs
	E_g (eV)	
Bi_2S_3	1.21	1.29
ZnS	3.84	3.84
Bi_2S_3-ZnS	1.29	1.37

- DRS shows the **successful modification** of the fibers with NPs
- Bi_2S_3 **band edge** in the visible range and ZnS in the UV range
- Presence of small amount of ZnS in the mixture ⇒ **E_g shift** to higher values than pure Bi_2S_3
- **Blue shift** for the Bi_2S_3 and Bi_2S_3-ZnS NPs synthesised in the presence of fibers ⇒ **smaller size** NPs produced

Structural and morphological characterization

DRX

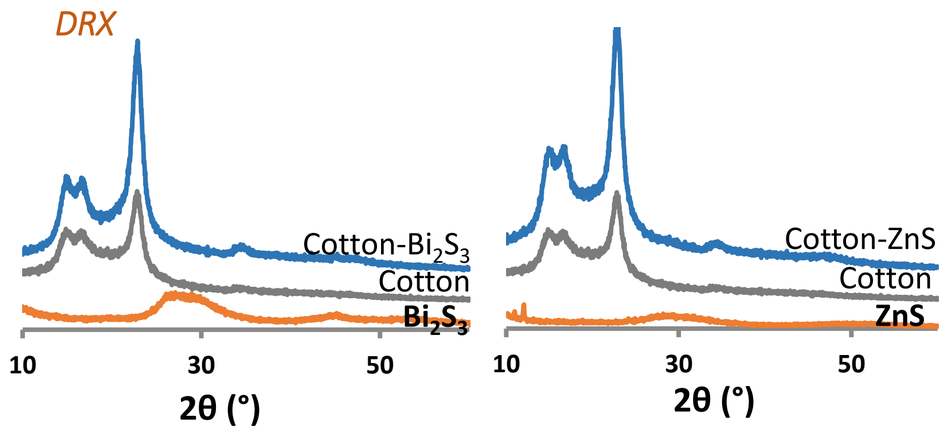

- NPs present a non-crystalline structure or/and have a very small size
- It is not possible to confirm that NPs are attached to cotton by XRD

Sample	A (m^2/g)	Sample	A (m^2/g)
Cotton	6.725	ZnS	17.191
Bi_2S_3	15.679	Cotton-ZnS	6.330
Cotton-Bi_2S_3	8.800	Bi_2S_3 e ZnS	18.909
		Cotton-Bi_2S_3-ZnS	6.552

Surface area:
- Bi_2S_3-ZnS > ZnS > Bi_2S_3
- Cotton-Bi_2S_3 > Bi_2S_3-ZnS > Cotton-ZnS

TEM and SEM

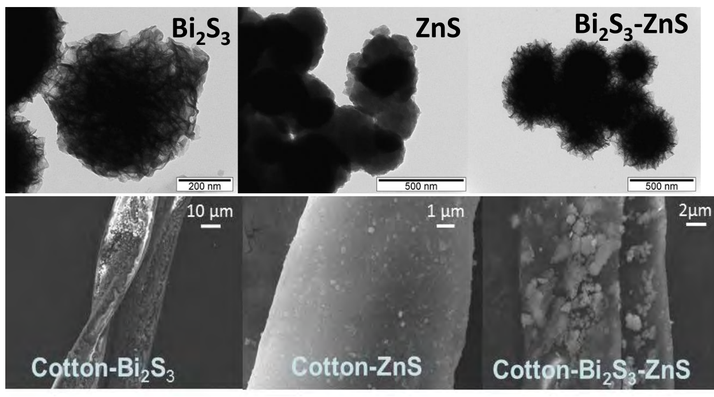

EDS

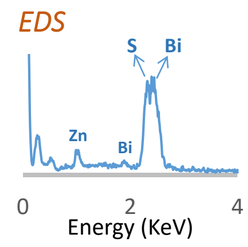

- Bi_2S_3 NPs present a sheet-like morphology
- Aggregates of small size ZnS NPs
- Bi_2S_3-ZnS mixture similar to Bi_2S_3
- SEM confirms the successful modification of Cotton fibers with NPs
- Presence of ZnS in the Cotton-Bi_2S_3-ZnS confirmed by EDS

Photocatalytic degradation

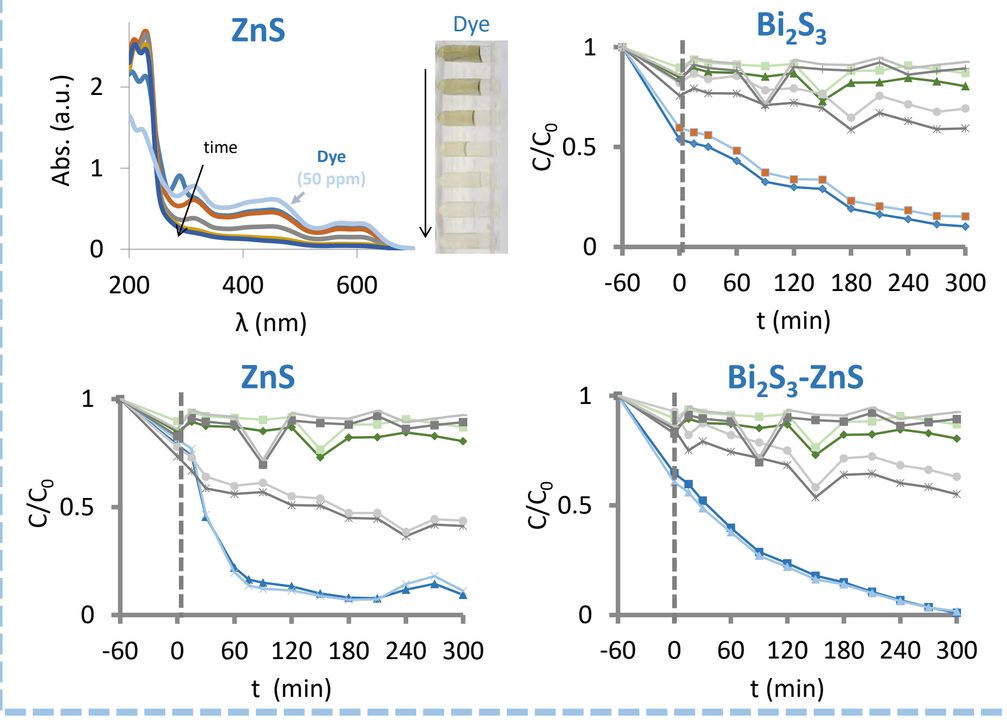

Sample	Adsorption (%)		Removal (%)	
	452 nm	572 nm	452 nm	572 nm
Bi_2S_3	46	40	90	85
ZnS	22	19	91	89
Bi_2S_3-ZnS	35	40	99	99
Cotton-Bi_2S_3	24	18	40	31
Cotton-ZnS	27	23	59	57
Cotton-Bi_2S_3-ZnS	15	8	45	37
Cotton	15	11	20	14

- *Adsorption ability:*
  - Bi_2S_3 > Bi_2S_3-ZnS > ZnS
  - Cotton-ZnS > Cotton-Bi_2S_3 > Cotton > Cotton- Bi_2S_3-ZnS
- *Dye removal ability:*
  - Bi_2S_3-ZnS > ZnS > Bi_2S_3
  - Cotton-ZNS > Cotton-Bi_2S_3-ZnS > Cotton-Bi_2S_3> Cotton

Photolysis; Cotton; NPs; Cotton-NPs

(dark line): 452 nm; (light line): 572 nm

Conclusions

The successful modification of the fibers was confirmed by DRS and SEM analysis. It could not be confirmed by XDR, due the small size of crystallites and /or the non-crystalline structure. The mixture of both NPs presents a higher superficial area than the pristine NPs, although the XRD analysis did not allowed the ZnS identification, it was confirmed by EDS analysis. The complete degradation of a dye from the leather industry was attained using Bi_2S_3-ZnS NPs under visible light irradiation for 5 hours. Encouraging results were also obtained for NPs-modified cotton fibers, with ca. 60 % degradation achieved with the Cotton-ZnS composite.

Funding:
Support for this work was provided by FCT through UID/MULTI/00612/2019.
V.C. Ferreira acknowledges financial support from Fundação para a Ciência e a Tecnologia, scholarship: SFRH/BPD/77404/2011
Centro de Química Estrutural is funded by FCT project UID/QUI/00100/2019.

FCT Fundação para a Ciência e a Tecnologia

References:
1. A.K. Yetisen, H. Qu, A. Manbachi, H. Butt, M.R. Dokmeci, J.P. Hinestroza, M. Skorobogatiy, A. Khademhosseini, S.H. Yun, ACS Nano 10 (2016) 3042–3068.
2. S.T. Dubas, P. Kumlangdudsana, P. Potiyaraj, Colloid Surface A 289 (2006) 105-109.
3. M. Rastgoo, M. Montazer, R.M.A. Malek, T. Harifi, M.M. Rad, Ultrason. Sonochem. 31 (2016) 257-266.